



N°d'ordre NNT 2023ISAL0044

## **THESE de DOCTORAT DE L'INSA LYON, membre de l'Université de Lyon**

**Ecole Doctorale N° accréditation  
Ecole Doctorale Matériaux de Lyon**

**Spécialité/ discipline de doctorat** : Matériaux

Soutenue publiquement le 03/07/2023, par :  
**Gabriel Perli**

---

**From the Design of Second-Generation Epoxy Monomers  
Based on Ionic Liquids to the End-of-Life of Degradable Multi-  
functional Thermosets**

---

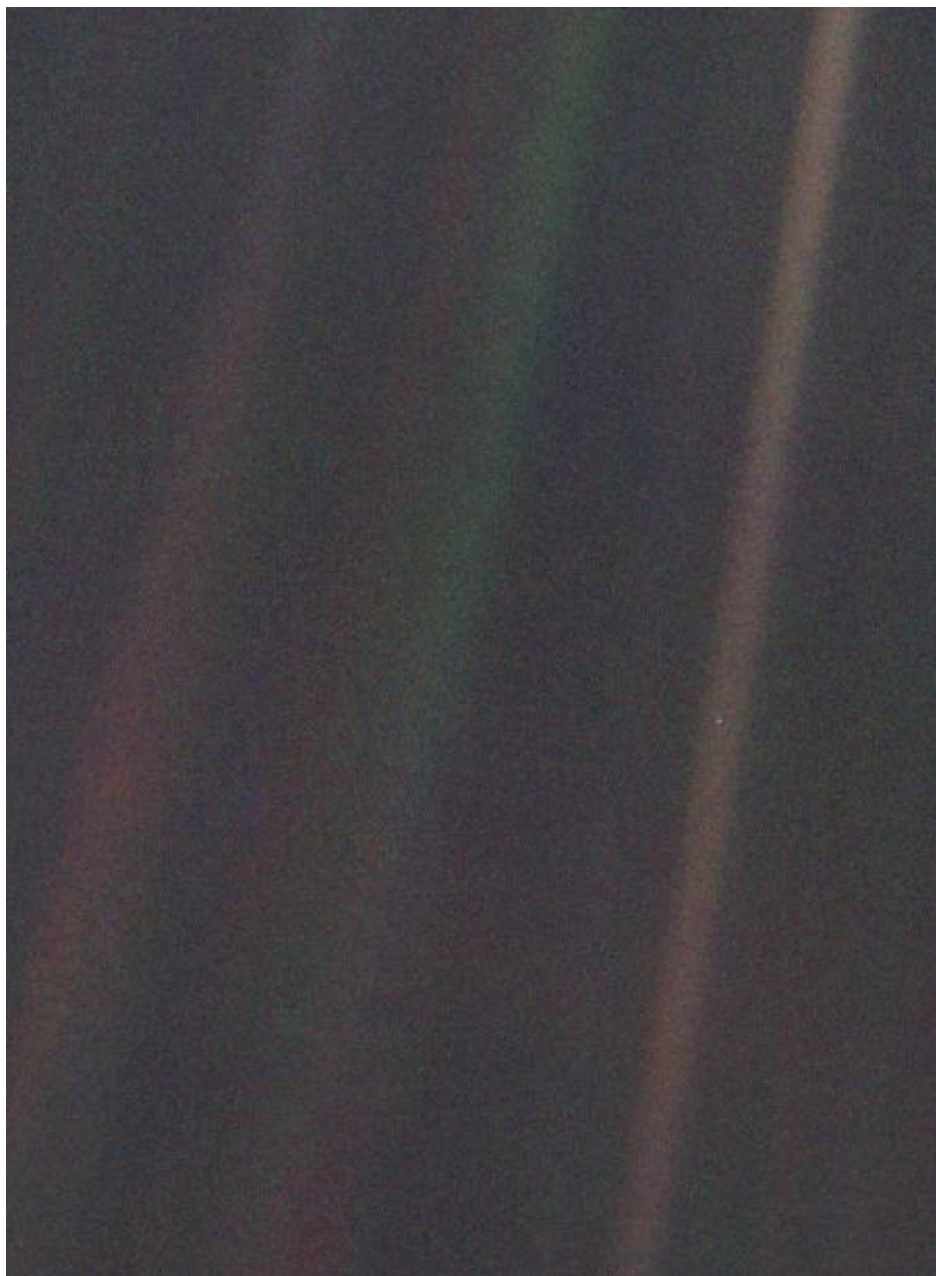
Devant le jury composé de :

LUTZ, Jean-François	Directeur de Recherche (CNRS), Institut de Science et d'Ingénierie Supramoléculaires (ISIS)	Rapporteur
GRANDE, Daniel	Directeur de Recherche (CNRS), Institut de Chimie et des Matériaux Paris-Est	Rapporteur
GARDETTE, Jean-Luc	Professeur, Institut de Chimie de Clermont- Ferrand	Examineur
Gérard, Jean-François	Professeur, (INSA LYON)	Examineur
DUCHET-RUMEAU, Jannick	Professeur, (INSA LYON)	Directrice de thèse
LIVI, Sébastien	Professeur, (INSA LYON)	Co-directeur de thèse

**Département FEDORA – INSA Lyon - Ecoles Doctorales**

<b>SIGLE</b>	<b>ECOLE DOCTORALE</b>	<b>NOM ET COORDONNEES DU RESPONSABLE</b>
<b>CHIMIE</b>	<b>CHIMIE DE LYON</b> <a href="https://www.edchimie-lyon.fr">https://www.edchimie-lyon.fr</a> Sec. : Renée EL MELHEM Bât. Blaise PASCAL, 3e étage secretariat@edchimie-lyon.fr	<b>M. Stéphane DANIELE</b> C2P2-CPE LYON-UMR 5265 Bâtiment F308, BP 2077 43 Boulevard du 11 novembre 1918 69616 Villeurbanne directeur@edchimie-lyon.fr
<b>E.E.A.</b>	<b>ÉLECTRONIQUE, ÉLECTROTECHNIQUE, AUTOMATIQUE</b> <a href="https://edeea.universite-lyon.fr">https://edeea.universite-lyon.fr</a> Sec. : Stéphanie CAUVIN Bâtiment Direction INSA Lyon Tél : 04.72.43.71.70 secretariat.edeea@insa-lyon.fr	<b>M. Philippe DELACHARTRE</b> INSA LYON Laboratoire CREATIS Bâtiment Blaise Pascal, 7 avenue Jean Capelle 69621 Villeurbanne CEDEX Tél : 04.72.43.88.63 philippe.delachartre@insa-lyon.fr
<b>E2M2</b>	<b>ÉVOLUTION ÉCOSYSTÈME, MICROBIOLOGIE, MODELISATION</b> <a href="http://e2m2.universite-lyon.fr">http://e2m2.universite-lyon.fr</a> Sec. : Bénédicte LANZA Bât. Atrium, UCB Lyon 1 Tél : 04.72.44.83.62 secretariat.e2m2@univ-lyon1.fr	<b>Mme Sandrine CHARLES</b> Université Claude Bernard Lyon 1 UFR Biosciences Bâtiment Mendel 43, boulevard du 11 Novembre 1918 69622 Villeurbanne CEDEX sandrine.charles@univ-lyon1.fr
<b>EDISS</b>	<b>INTERDISCIPLINAIRE SCIENCES-SANTÉ</b> <a href="http://ediss.universite-lyon.fr">http://ediss.universite-lyon.fr</a> Sec. : Bénédicte LANZA Bât. Atrium, UCB Lyon 1 Tél : 04.72.44.83.62 secretariat.ediss@univ-lyon1.fr	<b>Mme Sylvie RICARD-BLUM</b> Institut de Chimie et Biochimie Moléculaires et Supramoléculaires (ICBMS) - UMR 5246 CNRS - Université Lyon 1 Bâtiment Raulin - 2ème étage Nord 43 Boulevard du 11 novembre 1918 69622 Villeurbanne Cedex Tél : +33(0)4 72 44 82 32 sylvie.ricard-blum@univ-lyon1.fr
<b>INFOMATHS</b>	<b>INFORMATIQUE ET MATHÉMATIQUES</b> <a href="http://edinfomaths.universite-lyon.fr">http://edinfomaths.universite-lyon.fr</a> Sec. : Renée EL MELHEM Bât. Blaise PASCAL, 3e étage Tél : 04.72.43.80.46 infomaths@univ-lyon1.fr	<b>M. Hamamache KHEDDOUCI</b> Université Claude Bernard Lyon 1 Bât. Nautibus 43, Boulevard du 11 novembre 1918 69 622 Villeurbanne Cedex France Tél : 04.72.44.83.69 hamamache.kheddouci@univ-lyon1.fr
<b>Matériaux</b>	<b>MATÉRIAUX DE LYON</b> <a href="http://ed34.universite-lyon.fr">http://ed34.universite-lyon.fr</a> Sec. : Yann DE ORDENANA Tél : 04.72.18.62.44 yann.de-ordenana@ec-lyon.fr	<b>M. Stéphane BENAYOUN</b> Ecole Centrale de Lyon Laboratoire LTDS 36 avenue Guy de Collongue 69134 Ecully CEDEX Tél : 04.72.18.64.37 stephane.benayoun@ec-lyon.fr
<b>MEGA</b>	<b>MÉCANIQUE, ÉNERGÉTIQUE, GENIE CIVIL, ACOUSTIQUE</b> <a href="http://edmega.universite-lyon.fr">http://edmega.universite-lyon.fr</a> Sec. : Stéphanie CAUVIN Tél : 04.72.43.71.70 Bâtiment Direction INSA Lyon mega@insa-lyon.fr	<b>M. Jocelyn BONJOUR</b> INSA Lyon Laboratoire CETHIL Bâtiment Sadi-Carnot 9, rue de la Physique 69621 Villeurbanne CEDEX jocelyn.bonjour@insa-lyon.fr
<b>ScSo</b>	<b>ScSo*</b> <a href="https://edsciences sociales.universite-lyon.fr">https://edsciences sociales.universite-lyon.fr</a> Sec. : Mélina FAVETON INSA : J.Y. TOUSSAINT Tél : 04.78.69.77.79 melina.faveton@univ-lyon2.fr	<b>M. Bruno MILLY</b> Université Lumière Lyon 2 86 Rue Pasteur 69365 Lyon CEDEX 07 bruno.milly@univ-lyon2.fr

\*ScSo : Histoire, Géographie, Aménagement, Urbanisme, Archéologie, Science politique, Sociologie, Anthropologie



**THE PALE BLUE DOT OF EARTH** "That's here. That's Home. That's us."Image: NASA / JPL

“Look again at that dot. That’s here. That’s home. That’s us. On it everyone you love, everyone you know, everyone you ever heard of, every human being who ever was, lived out their lives. The aggregate of our joy and suffering, thousands of confident religions, ideologies, and economic doctrines, every hunter and forager, every hero and coward, every creator and destroyer of civilization, every king and peasant, every young couple in love, every mother and father, hopeful child, inventor and explorer, every teacher of morals, every corrupt politician, every ‘*superstar*,’ every ‘*supreme leader*,’ every saint and sinner in the history of our species lived there-on a mote of dust suspended in a sunbeam.

The Earth is a very small stage in a vast cosmic arena. Think of the rivers of blood spilled by all those generals and emperors so that, in glory and triumph, they could become the momentary masters of a fraction of a dot. Think of the endless cruelties visited by the inhabitants of one corner of this pixel on the scarcely distinguishable inhabitants of some other corner, how frequent their misunderstandings, how eager they are to kill one another, how fervent their hatreds.

Our posturings, our imagined self-importance, the delusion that we have some privileged position in the Universe, are challenged by this point of pale light. Our planet is a lonely speck in the great enveloping cosmic dark. In our obscurity, in all this vastness, there is no hint that help will come from elsewhere to save us from ourselves.

The Earth is the only world known so far to harbor life. There is nowhere else, at least in the near future, to which our species could migrate. Visit, yes. Settle, not yet. Like it or not, for the moment the Earth is where we make our stand.

It has been said that astronomy is a humbling and character-building experience. There is perhaps no better demonstration of the folly of human conceits than this distant image of our tiny world. To me, it underscores our responsibility to deal more kindly with one another, and to preserve and cherish the pale blue dot, the only home we’ve ever known.”

— Carl Sagan, *Pale Blue Dot*, 1994

Copyright © 1994 by Carl Sagan, Copyright © 2006 by Democritus Properties, LLC.



## Acknowledgments

Expressing gratitude appear as a prospect for failure and unfairness. Therefore, I express my gratitude to all those who have shared their knowledge with me throughout my life. Intimately, I thank Chemistry and Polymer Science, whose existences are perfect on all levels and lend men their properties to save and improve lives.

I thank the institutions that best introduced me to Polymer Science, namely the INSA de Lyon, Université de Lyon I, and more precisely the Laboratoire de Ingénierie des Matériaux Polymères (IMP, UMR CNRS 5223).

Additionally, I want to express my gratitude to my family, my parents, Ana, and Jair, for their continuous teachings on love, altruism, and respect. Equally, I extend my thanks to my brother Rafael for his unwavering support and encouragement.

I am immensely grateful to Prof. Jannick Duchet-Rummeau for the opportunities, guidance, trust, and kindness. Without a doubt, you are the finest leader I have ever encountered. Thank you.

I express my gratitude to Prof. Jean-François Gérard for being an exemplary professor and researcher. I aspire to one day possess even small fraction of your knowledge in the field of Polymer Science.

I thank Prof. Sébastien Livi for being a mentor in both my professional and, at times, personal life. You have been instrumental in assisting me in various aspects of my life, and your guidance has also deepened my understanding of Polymers, Ionic Liquids, and French culture.

*'Ironman, people think it's an obsession. A compulsion. As if there were an irresistible impulse to act. It's never been like that. I chose this life. I know what I'm doing. And on any given day, I could stop doing it. Today, however, isn't that day. And tomorrow won't be either.'*

*Batman*

I am thankful for the priceless corrections, scientific insights, and engaging discussions offered by the board of examiners, namely Prof. Jean-François Lutz, Prof. Daniel Grande, Prof. Jean-Luc Gardette, and Prof. Jean-François Gérard.

I extend my thanks to Liuyun Jiang for the enriching discussions and enjoyable moments we shared, which have solidified a friendship that will bring throughout my life. I am also grate-

ful to Alexei Radchecko for generously sharing knowledge and making significant contributions to this project with valuable suggestions. Additionally, I express my appreciation to Celso Yassuo for his friendship, patience, and wealth of knowledge he shared.

I thank Eva Laureys, Sarah Buisson and my advisors for kindly correcting my French. Obviously, they are *innocent* of my mistakes.

I express my gratitude to the entire academic staff and professors at IMP, including Prof. Sébastien Pruvost, Isabelle Polo, Prof. Catherine Marestin, Raphael Brunel, Patrick Goetick, Marie Rouault, Laura Courty, and Vivien Truchot.

I also extend my thanks to the individuals who take care of the common areas and services, ensuring the well-functioning of IMP, which allows us to carry out our activities with greater well-being and tranquility.

Furthermore, I am immensely grateful to the team of nuclear magnetic resonance, electronic microscopy, and multiuser laboratory laboratories. Their support and expertise were crucial for the conclusion of this work.

I thank all my friends and colleagues from IMP for the delightful moments that I have shared during my time in France: Eva Laureys, Adrien Topalian, Younes El Omari, Ting Shi, Xavier Morelle, Martin Jégou, Matheus Nachbar, Amélie Teissoniere, Raouhi Sanaa, Mathieu Vangrevelinghe, Valentina Cavallo, Carolina Franzon, Victor Haddad, Camille Villard, Yiping Chen, Loup Mambré, Okba Mostefaoui, Giovanni Parente, Virginie Lacotte, Charlotte Michelin, Théophile Ienn, Mathieu Madau, and Taha Chabbah.

To the person who most supported me at the end of this journey, Eva, in the vastness of space and the immensity of time, it is my joy to share a planet and an epoch with you.

I thank you, dear reader, for the attention dedicated to reading this work, I hope you can find something helpful.

This work was carried out with the financial support of the IDEXLYON Project from the University of Lyon as part of the Programme Investissements d'Avenir (ANR-16-IDEX-0005).

## Abstract

Extensive research has been conducted on epoxy polymers, which are recognized as an important class of thermosetting materials. These polymers exhibit exceptional qualities such as versatile curing methods, minimal shrinkage, electrical insulation, and thermal and chemical stability. Due to their outstanding qualities, epoxy thermosets have been utilized in a wide range of industries, including construction, high-end sports equipment, aerospace, and automotive manufacturing. Despite the remarkable properties and numerous potential applications of epoxy thermosets, they tend to be brittle and unrecyclable. To address the brittleness issue, researchers have explored different fillers to adjust the mechanical properties of the thermoset networks. Ionic Liquids (ILs) emerge as a promising platform among the fillers. ILs are organic salts with melting temperatures below 100 °C. Because of the various combination possibilities of cations and anions, a wide range of properties can be achieved by incorporating ILs into epoxy materials. Indeed, ILs exhibit exceptional properties that make them highly valuable in material science, including high thermal stability, low volatility, wide liquid temperature range, compatibilizing ability, and tunable physical and chemical properties. To attain advanced multifunctional properties in thermosets, we integrated the remarkable attributes of both epoxy and ILs into a single molecule, introducing a new class of epoxy resins referred to as the second generation. Furthermore, to address the limited recyclability of epoxy thermosets, we incorporated cleavable ester groups to ensure the selective solvolysis of the networks. This approach enables the recovery of IL derivatives and offers a more sustainable end-of-life solution for thermosets, presenting an alternative to landfilling and pyrolysis. Herein, we have designed a small library of epoxidized-IL monomers that can be categorized into two families. The first family incorporates imidazolium-moiety, cleavable ester groups and multiple oxirane groups. The second family features monomers with imidazolium and benzyl moieties and two cycloaliphatic epoxy groups. This approach allowed building materials with fine-tuned mechanical properties and emerging features, such as increased thermal stability, shape memory, hydrophobicity, and tailored degradability. Fundamentally, our objective was to systematically design and synthesize a library of second-generation epoxy resins to construct thermosets and composites that exhibit exceptional performance and multi-functionality. Additionally, we aimed to enhance the sustainability of these thermosets at their end-of-life, aligning with the principles of the circular economy.

## Résumé

De nombreuses recherches ont été menées sur les polymères époxy, reconnus comme une classe importante de matériaux thermodurcissables. Ces polymères présentent des qualités exceptionnelles telles que des méthodes de reticulations polyvalentes, une rétraction minimale, une isolation électrique, ainsi qu'une stabilité thermique et chimique. Grâce à leurs propriétés remarquables, les thermosets époxy ont été utilisés dans de nombreux secteurs industriels, notamment la construction, les équipements sportifs haut de gamme, l'aérospatiale et l'industrie automobile. Malgré leurs propriétés exceptionnelles et leurs nombreuses applications potentielles, les thermosets époxy ont tendance à être fragiles et non recyclables. Pour remédier à la fragilité, les chercheurs ont exploré différentes charges afin d'ajuster les propriétés mécaniques des réseaux thermosets. Les liquides ioniques (LI) se présentent comme une plateforme prometteuse parmi ces charges. Les LI sont des sels organiques avec des températures de fusion inférieures à 100 °C. En raison des diverses combinaisons possibles de cations et d'anions, une large gamme de propriétés peut être obtenue en incorporant des LI dans les matériaux époxy. En effet, les LI présentent des propriétés exceptionnelles qui les rendent extrêmement précieux en science des matériaux, notamment une stabilité thermique élevée, une faible volatilité, une large plage de température liquide, une capacité de compatibilisation et des propriétés physiques et chimiques ajustables. Afin d'obtenir des propriétés multifonctionnelles avancées dans les thermosets, nous avons intégré les caractéristiques remarquables de l'époxy et des LI dans une seule molécule, introduisant ainsi une nouvelle classe de résines époxy appelée "deuxième génération". De plus, pour remédier à la recyclabilité limitée des thermosets époxy, nous avons incorporé des groupes ester clivables permettant la solvolysé sélective des réseaux. Cette approche permet de récupérer des dérivés de LI et offre une solution plus durable en fin de vie pour les thermosets, constituant une alternative à l'enfouissement et à la pyrolyse. Dans cette étude, nous avons conçu une petite bibliothèque de monomères époxydés-LI qui peuvent être classés en deux familles. La première famille intègre des groupes imidazolium, des groupes ester clivables et plusieurs groupes oxirane. La deuxième famille comprend des monomères avec des groupes imidazolium et benzyl, ainsi que deux groupes époxy cycloaliphatiques. Cette approche a permis de construire des matériaux avec des propriétés mécaniques ajustées et des caractéristiques émergentes telles qu'une stabilité thermique accrue, une mémoire de forme, une hydrophobicité et une dégradabilité adaptées. Fondamentalement, notre objectif était de concevoir et de synthétiser systématiquement une bibliothèque de résines époxy de deuxième génération afin de construire des thermosets.



## List of Published Scientific Articles

- (1) **Perli, G.**; Yassuo, C.; El Omari, Y.; Michelin, C.; Gérard, J.F.; Duchet-Rumeau, J.; Livi, S. Design for Disassembly of Composites and Thermoset by Using Cleavable Ionic Liquid Monomers as Molecular Building Blocks. *Composites Part B – Engineering* **2023**, *264* (2023) 110899. <https://doi.org/10.1016/j.compositesb.2023.110899>.
- (2) **Perli, G.**; Demir, B.; Pruvost, S.; Duchet-Rumeau, J.; Baudoux, J.; Livi, S. From the Design of Multifunctional Degradable Epoxy Thermosets to Their End of Life. *ACS Sustainable Chemistry and Engineering* **2022**, *10* (33), 11004–11015. <https://doi.org/10.1021/acssuschemeng.2c03326>.
- (3) **Perli, G.**; Wylie, L.; Demir, B.; Gerard, J. F.; Pádua, A. A. H.; Gomes, M. C.; Duchet-Rumeau, J.; Baudoux, J.; Livi, S. From the Design of Novel Tri- and Tetra-Epoxidized Ionic Liquid Monomers to the End-of-Life of Multifunctional Degradable Epoxy Thermosets. *ACS Sustainable Chemistry and Engineering* **2022**, *10* (47), 15450–15466. <https://doi.org/10.1021/acssuschemeng.2c04499>.
- (4) **Perli, G.**; Soares, M. C. P.; Cabral, T. D.; Bertuzzi, D. L.; Bartoli, J. R.; Livi, S.; Duchet-Rumeau, J.; Cordeiro, C. M. B.; Fujiwara, E.; Ornelas, C. Synthesis of Carbon Nanodots from Sugarcane Syrup, and Their Incorporation into a Hydrogel-Based Composite to Fabricate Innovative Fluorescent Microstructured Polymer Optical Fibers. *Gels* **2022**, *8* (9). <https://doi.org/10.3390/gels8090553>.
- (5) Demir, B.; **Perli, G.**; Chan, K.-Y.; Duchet-Rumeau, J.; Livi, S. Molecular-Level Investigation of Cycloaliphatic Epoxidised Ionic Liquids as a New Generation of Monomers for Versatile Poly(Ionic Liquids). *Polymers* **2021**, *13* (9), 1–15. <https://doi.org/10.3390/polym13091512>.
- (6) Wylie, L.; **Perli, G.**; Avila, J.; Livi, S.; Duchet-Rumeau, J.; Costa Gomes, M.; Padua, A. Theoretical Analysis of Physical and Chemical CO<sub>2</sub> Absorption by Tri- and Tetraepoxidized Imidazolium Ionic Liquids. *The Journal of Physical Chemistry B* **2022**, *126* (47), 9901–9910. <https://doi.org/10.1021/acs.jpcc.2c06630>.
- (7) Merlini, C.; Oliveira Castro, V.; **Perli, G.**; el Omari, Y.; Livi, S. Epoxidized Ionic Liquids as Processing Auxiliaries of Poly(Lactic Acid) Matrix: Influence on the Manufacture, Structural and Physical Properties. *Nanomaterials* **2023**, *13* (9), 1476. <https://doi.org/10.3390/nano13091476>.



## Summary

<i>Note to the Reader</i>	<i>1</i>
<i>Chapter I - Historical Introduction</i>	<i>3</i>
1. Les époxydes à travers le temps : Une activité de recherche historique au cœur du laboratoire d'Ingénierie des Matériaux Polymères (IMP-UMR CNRS 5223)	4
2. Objectifs à long terme	20
3. Références	21
4. Long-Term Goals	24
<i>Chapter II - Literature Review</i>	<i>26</i>
1. The Promising Synergy Between Ionic Liquids and Thermosetting Polymers	27
1.1. A Concise Introduction on Ionic Liquids	27
1.2. ILs as Reactive Additives to Tailor Thermoset Properties	28
1.3. Monoepoxidized ILs: The First Proposals	31
1.4. Bifunctional-Epoxy-Functionalized ILs	40
1.5. Epoxidized ILs With Multiple Epoxy Groups	47
2. Potential and Limitations of Recycling Thermosets and Composites	49
2.1. General Aspects & Environmental Regulations	49
2.2. Conventional Recycling Methodologies for Thermosets and Composites	50
2.3. Mechanical Recycling	51
2.4. Thermal Waste Management	52
2.5. Chemical Recycling	53
2.6. Designing Stimuli-Triggered Degradable Networks	53
2.7. Thermal Reworkable Networks	55
2.8. Cleavable Networks: Designing to Degrade	56
2.9. Cleavable Networks: <i>Design to Recycle</i>	58
3. Cleavable Linkages in Thermosets: Opportunities and Applications	62
3.1. Removable Adhesives	62
3.2. Electronic Packaging: Degrading Thermosets to Recycle Electronics	63
3.3. Affording a More Sustainable End-Of-Life for Composites and Nanocomposites	65
4. Exploring the Potential of Photopolymerization: An Overview of Techniques and Applications	71

4.1.	Cationic Photo- & Thermal-Induced Polymerization	72
4.2.	Cationically Photopolymerizable Monomers	74
4.3.	Ionic Liquids & Light: A Possible Wedding?	81
<b>5.</b>	<b>Conclusion of Chapter II</b>	<b>87</b>
<b>6.</b>	<b>References</b>	<b>88</b>
 <i>Chapter III - From the Design of Novel Tri- and Tetra-Epoxidized Ionic Liquid Monomers to the End-of-Life of Multifunctional Degradable Epoxy Thermosets</i>		
		<b>123</b>
<b>1.</b>	<b>De la conception de nouveaux monomères liquides ioniques tri- et tétra-époxydés à la fin de vie des thermodurcissables époxy multifonctionnels dégradables</b>	<b>124</b>
1.1.	Résumé	124
<b>2.</b>	<b>From the Design of Novel Tri- and Tetra-Epoxidized Ionic Liquid Monomers to the End-of-Life of Multifunctional Degradable Epoxy Thermosets</b>	<b>125</b>
2.1.	Abstract	125
<b>3.</b>	<b>Introduction</b>	<b>126</b>
<b>4.</b>	<b>Experimental section</b>	<b>128</b>
4.1.	Materials	128
4.2.	Synthesis of tri- and tetra-epoxidized IL monomers	128
4.3.	Epoxy Network Preparation	130
4.4.	Characterization methods	131
<b>5.</b>	<b>Results and Discussion</b>	<b>136</b>
5.1.	Design and Synthesis of Degradable Multifunctional Networks	136
5.2.	Polymerization of the Epoxy-Amine Systems: Investigation of Molecular Interactions and Reactivity Study (DSC)	136
5.3.	Network Tailoring and Thermal Stability	143
5.4.	Investigation of the Network Morphology	144
5.5.	Theoretical and Experimental Investigation of Networks' Preliminary Physicochemical Properties.	145
5.6.	Thermo-Mechanical Properties of the Networks and Shape Memory Behavior	147
5.7.	IL-based Green Methodology and Degradation Studies	150
<b>6.</b>	<b>Conclusion</b>	<b>154</b>
<b>7.</b>	<b>References</b>	<b>154</b>

**Chapter IV- Design for Disassembly of Composites and Thermoset by Using  
Cleavable Ionic Liquid Monomers as Molecular Building Blocks \_\_\_\_\_ 164**

<b>1. Conception pour le démontage des composites et des thermoset par utilisation des monomères liquides ioniques clivables comme éléments constitutifs moléculaires _____</b>	<b>165</b>
1.1. Résumé _____	165
<b>2. Design for Disassembly of Composites and Thermoset by Using Cleavable Ionic Liquid Monomers as Molecular Building Blocks _____</b>	<b>166</b>
2.1. Abstract _____	166
<b>3. Introduction _____</b>	<b>167</b>
<b>4. Materials and Characterization Methods _____</b>	<b>169</b>
4.1. Materials. _____	169
4.2. Synthesis of Tetra-Epoxidized IL Monomer (Tetra-IL) _____	169
4.3. Design and Curing of the Thermoset Networks. _____	170
4.4. Composite Manufacture _____	171
4.5. Characterization Methods _____	171
<b>5. Results and Discussion _____</b>	<b>173</b>
5.1. Design of Degradable Epoxy Networks and Fiber-Reinforced Epoxy Composites _____	173
5.2. Reactivity Study and Thermomechanical Property Investigation _____	174
5.3. Transesterification-Assisted Solvolysis _____	179
5.4. Composite Manufacture, Surface Properties, Morphological Structure, and CF Compatibility _____	180
5.5. Composite Deconstruction _____	182
5.6. Degradable Epoxy Thermoset Adhesives _____	184
5.7. Using Tetra-IL to Tailor Physical Properties of Epoxy-Amine Networks. _____	185
<b>6. Conclusion _____</b>	<b>186</b>
<b>7. References _____</b>	<b>187</b>

**Chapter V - Activated Cycloaliphatic Epoxidized Ionic Liquids as New Versatile Monomers for the Construction of Multifunctional Degradable Thermosets \_\_\_\_\_ 197**

<b>1. Liquides ioniques époxydés cycloaliphatiques activés comme nouveaux monomères pour le développement de thermoset multifonctionnels dégradables _____</b>	<b>198</b>
1.1. Résumé _____	198

<b>2. Activated Cycloaliphatic Epoxidized Ionic Liquids as New Versatile Monomers for the Construction of Multifunctional Degradable Thermosets</b>	<b>199</b>
2.1. Abstract	199
<b>3. Introduction</b>	<b>200</b>
<b>4. Materials and Methods</b>	<b>202</b>
4.1. Materials	202
4.2. Synthesis of Cycloaliphatic Epoxidized Ionic Liquid (CEIL)	202
4.3. Epoxy Network Preparation	203
4.4. Characterization Methods	204
4.5. Chemical Recycling Methodology	205
4.6. Simulation Methods	205
<b>5. Results and Discussion</b>	<b>205</b>
5.1. Development of Networks and Preliminary Thermal Characterizations	205
5.2. Morphological Investigation of Networks	208
5.3. Thermomechanical and Shape Memory Behavior of the Epoxy Networks	209
5.4. Sustainable Treatment and Chemical Recycling	213
<b>Chapter VI - Conclusion and Perspectives</b>	<b>234</b>
<b>Appendix I - From the Design of Novel Tri- and Tetra-epoxidized Ionic Liquid Monomers to the End-of-Life of Multifunctional Degradable Epoxy Thermosets</b>	<b>243</b>
<b>Appendix II - Design for Disassembly of Composites and Thermosets by Using Cleavable Ionic Liquid Monomers as Molecular Building Blocks</b>	<b>275</b>
<b>Appendix III - Activated Cycloaliphatic Epoxidized Ionic Liquids as New Versatile Monomers for the Construction of Multifunctional Degradable Thermosets</b>	<b>288</b>

## List of Abbreviations

AcOEt	<i>Ethyl Acetate</i>
AFM	<i>Atomic Force Microscope</i>
AHEW	<i>Amine Hydrogen Equivalent Weight</i>
ATR	<i>Attenuated Total Reflection</i>
<i>b</i>	<i>Broad Signal</i>
BP	<i>Benzophenone</i>
BSE	<i>Bifunctional Silyl Ether</i>
CEIL	<i>Cycloaliphatic Epoxidized Ionic Liquid</i>
CF	<i>Carbon-Fiber</i>
CFRPs	<i>Carbon-Fiber-Reinforced Polymers</i>
CHELPG	<i>Charges from Electrostatic Potentials using a Grid-Based</i>
CNTR	<i>Cresol Novolak-Type Phenolic Resin</i>
CVTE	<i>Coefficient of Volumetric Thermal Expansion</i>
<i>d</i>	<i>Doublet</i>
D230	<i>Jeffamine D230</i>
DCM	<i>Dichloromethane</i>
DCPD	<i>Dynamic Dicyclopentadiene</i>
<i>dd</i>	<i>Doublet of Doublets</i>
DDM	<i>4,4'-Diaminodiphenylmethane</i>
DDS	<i>4-Aminophenyl Sulfone</i>
DGEBA	<i>Bisphenol A diglycidyl ether</i>
DMA	<i>Dynamic Mechanical Analysis</i>
DMDO	<i>Dimethyldioxirane</i>
DOC	<i>Degree of Cross-Linking</i>
DSC	<i>Differential Scanning Calorimetry</i>
DVB	<i>Divinylbenzene</i>
ECC	<i>4-Epoxycyclohexylmethyl-3,4-Epoxycyclohexane Carboxylate</i>
EEW	<i>Epoxide Equivalent Weight</i>
EG	<i>Ethylene Glycol</i>
ESI	<i>Electron Spray Ionization</i>
ESO	<i>Epoxidized Oil</i>
FAP	<i>Tris(Pentafluoroethyl)Trifluorophosphate</i>

FDCA	<i>2,5-Furandicarboxylic Acid</i>
FT-IR	<i>Fourier Transform Infrared Spectroscopy</i>
G	<i>Storage Modulus</i>
G <sub>g</sub>	<i>Storage Modulus at Glassy State</i>
GlyMe <sub>3</sub> NCl	<i>2,3-epoxypropyltrimethylammonium chloride</i>
GlyMe <sub>3</sub> NNTf <sub>2</sub>	<i>Glycidyl trimethylammonium Bis(trifluoromethanesulfonyl) imide</i>
GMA	<i>Glycidyl methacrylate</i>
G <sub>r</sub>	<i>Storage Modulus at Glassy Rubbery</i>
HDCNs	<i>Hemiaminal Dynamic Covalent Networks</i>
HRMS	<i>High-Resolution Mass Spectrometry</i>
IBOA	<i>Isobornyl Acrylate</i>
IL	<i>Ionic Liquid</i>
IL104	<i>Trihexyltetradecylphosphonium bis(2,4,4-trimethylpentyl)phosphinate</i>
IOC	<i>4-octyloxyphenyl)phenyliodonium Hexafluoroantimonate</i>
IPDA	<i>3-(Aminomethyl)-3,5,5-trimethylcyclohexan-1-amine</i>
<i>m</i>	<i>Multiplet</i>
<i>m</i> CPBA	<i>meta-Chloroperoxybenzoic Acid</i>
MD	<i>Molecular Dynamics</i>
MeCN	<i>Acetonitrile</i>
MMA	<i>Methyl Methacrylate</i>
NMR	<i>Nuclear Magnetic Resonance</i>
NVP	<i>N-vinylpyrrolidone</i>
OA-POSS	<i>Octa-Aminopropyl Polyhedral Oligomeric Silsesquioxane</i>
ODA	<i>4,4'-Oxydianiline</i>
PACM	<i>4,4-Diaminodicyclohexylmethane</i>
PBCs	<i>Periodic Boundary Conditions</i>
pDCPD	<i>Poly(dicyclopentadiene)</i>
PHT	<i>Poly(hexahydrotriazine)</i>
<i>q</i>	<i>Quartets</i>
<i>qt</i>	<i>Quintets</i>
QTOF	<i>Quadrupole Time-of-Flight</i>
RDFs	<i>Radial Distribution Functions</i>
R <sub>f</sub>	<i>Shape Fixity</i>



ROMP	<i>Ring-Opening Metathesis Polymerization</i>
$R_r$	<i>Shape Recovery Ratio</i>
$s$	<i>Singlet</i>
S7MS	<i>(7-methoxy-4-methylcoumarin-3-yl)phenyliodonium hexafluoroantimonate (Sylanto 7M-S)</i>
SAA	<i>Sulfanilamide</i>
SAXS	<i>Small-Angle X-ray Scattering</i>
SDFs	<i>Spatial Distribution Functions</i>
SEM	<i>Scanning Electron Microscopy</i>
SM	<i>Shape Memory</i>
$t$	<i>Triplets</i>
Tan $\delta$	<i>Loss Factor</i>
TBD	<i>1,5,7-triazabicyclo[4,4,0]dec-5-ene</i>
$T_{df}$	<i>Deformation Temperature</i>
$T_{d5\%}$	<i>Degradation Temperature for 5% Weight Loss</i>
TEGDMA	<i>Triethylene glycol dimethacrylate</i>
TEM	<i>Transmission Electron Microscopy</i>
TERs	<i>Thermoset Epoxy Resins</i>
Tetra-IL	<i>Tetra-Epoxidized Imidazolium Ionic Liquid</i>
Tetra-N	<i>4,4'-Methylenebis(N,N - diglycidylaniline)</i>
TFA	<i>Trifluoroacetate</i>
TFI	<i>Triflate</i>
TGA	<i>Thermogravimetric Analyses</i>
$T_{max}$	<i>Maximal Degradation Temperature</i>
TMHMD	<i>Methyltetrahydrophthalic Anhydride</i>
TMPTA	<i>Trimethylolpropane Triacrylate</i>
$T_\alpha$	<i>Alpha Transition Temperature</i>

## **Note to the Reader**

The dissertation is organized into chapters, as specified below. The results were presented in a format similar to research papers, except for the fact that we provided additional information to aid the reader to further understand our work.

### **Chapter I – Historical Introduction: A Brief Time-lapse on Epoxy Research at IMP**

This chapter exposes an overview of the epoxy research conducted at IMP INSA Lyon. It is an integral part of the attempt to understand the importance of this manuscript for our local research and, more broadly, for material science. This section describes the main findings from the first publication on epoxy prepolymers in our lab to this present moment. The purpose of this section is not to delve into all the advancements made in the area of epoxy-based thermosets but rather to link the prior research conducted in our laboratory to the present. The final part of this chapter highlights the long-term goals of this research.

### **Chapter II – State of Art**

In state-of-the-art, we endeavored to situate the reader concerning the main topics addressed in this manuscript. Initially, we presented an overview about the synthesis of various epoxidized monomers bearing ionic liquid (IL) moieties of different natures to develop thermosets. Subsequently, we introduced the conventional recycling methodologies on thermoset materials and the recent advances regarding incorporating cleavable bonds to degrade, depolymerize or reprocess these crosslinked materials. Finally, we reviewed the main aspects of cationic photopolymerization and several works that combined photo-induced reactions and ionic liquid-based precursors.

### **Chapter III – From the Design of Novel Tri- and Tetra-Epoxidized Ionic Liquid Monomers to the End-of-Life of Multifunctional Degradable Epoxy Thermosets**

Chapter III comprises three distinct parts: an abstract in French, the main findings, and supplementary information in the Appendix. In the results and discussion, we presented the molecular design of two novel monomers bearing cleavable ester groups, an imidazolium-based IL moiety, and adjacent epoxy groups. Using these new epoxidized ILs, we created six different epoxy thermosets that were later degraded, leading to an eco-friendlier and more sustainable end-of-life for the thermosets.

### **Chapter IV - Design for Disassembly of Composites and Thermoset by Using Cleavable Ionic Liquid Monomers as Molecular Building Blocks**

This chapter is structured similarly to the previous one, consisting of an abstract in French, the main findings, and the supplementary information in the Appendix. Building on our prior work, we optimized and scaled up the synthesis of an epoxidized IL. In addition, we investigated this molecule as a comonomer, utilizing a commercial monomer as the main component of the newly designed networks. Our goal was to evaluate the influence of this new IL monomer on the thermoset properties and, more crucially, to design more sustainable carbon-fiber (CF) composites. Our findings indicated that when employed as a cleavable building block, the synthesised monomer confers degradability to the thermoset matrices under mild conditions. This, in turn, allows for the recovery of CFs in their original condition. Furthermore, we explored the potential of using these synthetic IL monomers to develop degradable adhesives, ensuring their degradation to facilitate the recovery of the composites' adherends.

## **Chapter V – Activated Cycloaliphatic Epoxidized Ionic Liquids as New Versatile Monomers for the Construction of Multifunctional Degradable Thermosets**

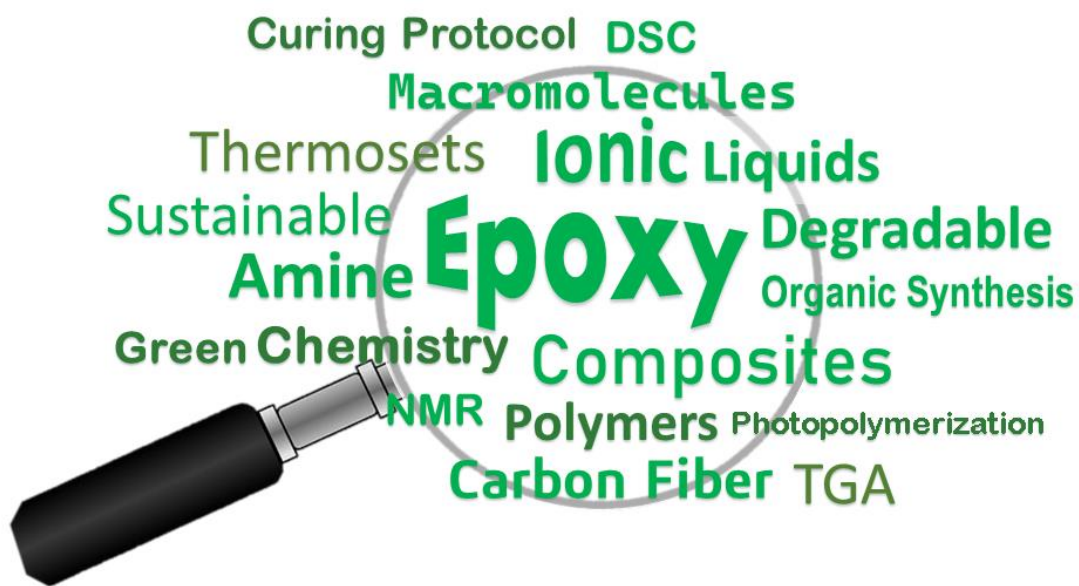
The chapter is divided into four main sections, including an abstract in French, major findings, perspectives on synthesizing cationic photopolymerizable monomers, and supplementary information found in the Appendix. It is worth noting that this project was initially aimed at synthesizing ILs for the development of 3D printing resins based on ILs. However, we discovered that the cationic photopolymerization of the cycloaliphatic epoxidized ILs (CEILs) did not proceed as we had anticipated. Therefore, the polymerization of these new monomers was carried out via thermally-activated curing. We examined the CEIL monomer as a molecular building block and discovered that this comonomer could afford various novel properties, including higher homogeneity, excellent thermal stability, and shape memory. At the end of this chapter, we detailed our efforts to synthesize multiple cycloaliphatic epoxidized ILs and provide a comprehensive examination of the ionic exchange reactions that we found to be crucial for advancing this project.

## **Chapter VI – General Conclusions & Perspectives**

The last chapter addresses the primary inquiries raised throughout this study and offers some insights into potential future research or applications associated with our main outcomes.

# 01

## Historical Introduction



## Chapter I - Historical Introduction

### 1. Les époxydes à travers le temps : Une activité de recherche historique au cœur du laboratoire d'Ingénierie des Matériaux Polymères (IMP-UMR CNRS 5223)

Lors de l'écriture de notre manuscrit de thèse, une question essentielle s'impose à nous :

*Quelle est la contribution de ma thèse sur cette thématique ?*

Deux sous-questions se posent :

(I) Comment nos recherches actuelles s'inscrivent-elles dans les objectifs du Laboratoire d'Ingénierie des Matériaux Polymères (IMP) ?

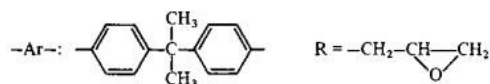
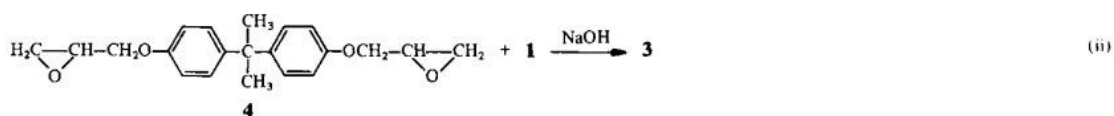
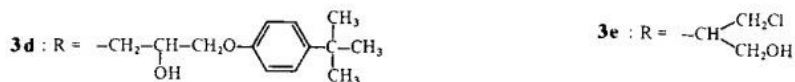
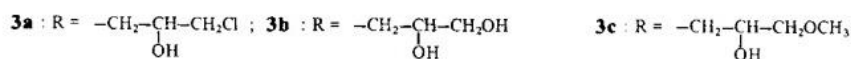
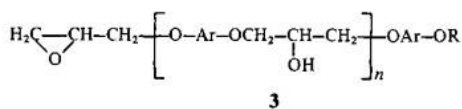
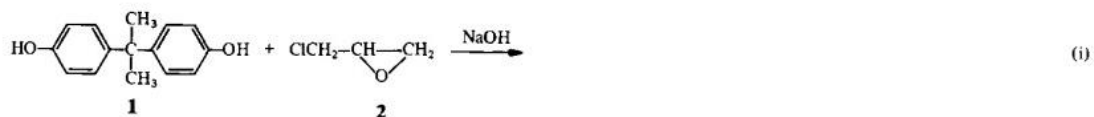
(II) Quelle est la réelle valeur ajoutée de notre contribution au domaine des polymères ?

Comme premier élément de réponse, cette partie introductive retrace l'histoire de cette thématique au sein du laboratoire IMP.

#### Professeur Quang Tho Pham – 1983

**Principales contributions :** Compréhension des mécanismes de polymérisation des époxy-amine et de l'influence de la structure chimique des monomères époxy dans le développement des réseaux.<sup>1</sup>

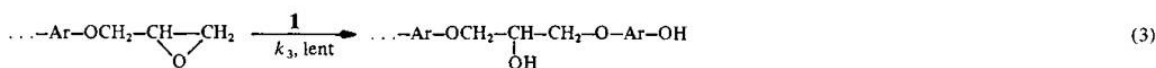
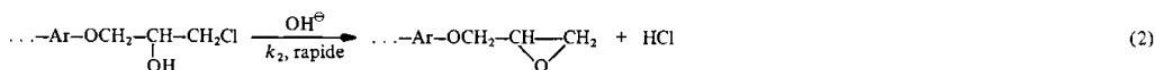
La première recherche sur les prépolymères époxy a été publiée en 1982 et s'intitule "*Étude des prépolymères époxydes par chromatographie et  $^1\text{H}$  RMN à 350 MHz*" et a comme auteur correspondant le Professeur Quang Tho Pham. Dans ce travail, les auteurs ont porté une attention particulière sur la composition exacte des prépolymères époxyde ainsi que sur leur caractérisation. En particulier, ils ont étudié différents prépolymères commerciaux synthétisés par le procédé Taffy et possédant différents équivalents époxyde (EE). D'après la littérature, le *procédé taffy* est la méthode de synthèse du prépolymère le plus communément utilisé de nos jours, c'est-à-dire le diglycidyl éther de bisphénol A (DGEBA). Dans cette réaction, le bisphénol A réagit avec le 2-(chlorométhyl)oxirane (épichlorhydrine) dans des proportions appropriées pour obtenir des résines époxyde (DGEBA) de différentes masses molaires. Les monomères époxyde sont obtenus selon une distribution statistique puisque les premiers monomères primaires peuvent continuer à réagir pour générer des oligomères. Les auteurs ont illustré la voie de synthèse et ont étudié les molécules probablement formées au cours de la synthèse (**Schéma I-1**).<sup>1</sup>



**Schéma I-1.** Synthèse de monomères et d'oligomères à base de DGEBA proposée par le professeur Quang Tho Pham.<sup>1</sup>

Les auteurs ont proposé :

- Les différentes structures possibles résultantes de la réaction d'ouverture du cycle époxy par les composants du mélange réactionnel.
- Une compréhension globale de la synthèse pour favoriser la formation d'oligomères de masse molaire plus élevée (**Schéma I-2**).



**Schéma I-2.** Brève compréhension de la cinétique des réactions.<sup>1</sup>

Selon les auteurs, une compétition a lieu entre les réactions **(1)** et **(3)**. Comme l'épichlorhydrine **2** est beaucoup trop réactive avec le Bisphénol A **1**, la formation d'oligomères de masse molaire plus élevée est empêchée. Ainsi, il est nécessaire de diminuer la quantité de **2** par rapport à **1**.<sup>1</sup>



Les prépolymères époxyde obtenus ne sont pas terminés uniquement par des groupes époxyde; ils peuvent être terminés par des groupes de nature différente. Ces groupes secondaires peuvent avoir une grande influence sur les réactions de durcissement. De ce fait, plusieurs auteurs ont cherché à caractériser complètement ces molécules. Les techniques utilisées sont généralement la chromatographie par perméation de gel (GPC), la chromatographie liquide haute pression (HPLC), ou la chromatographie sur couche mince. Elles sont souvent couplées à d'autres techniques comme la spectrométrie de masse, l'infrarouge ou la résonance magnétique nucléaire (RMN).<sup>1</sup>

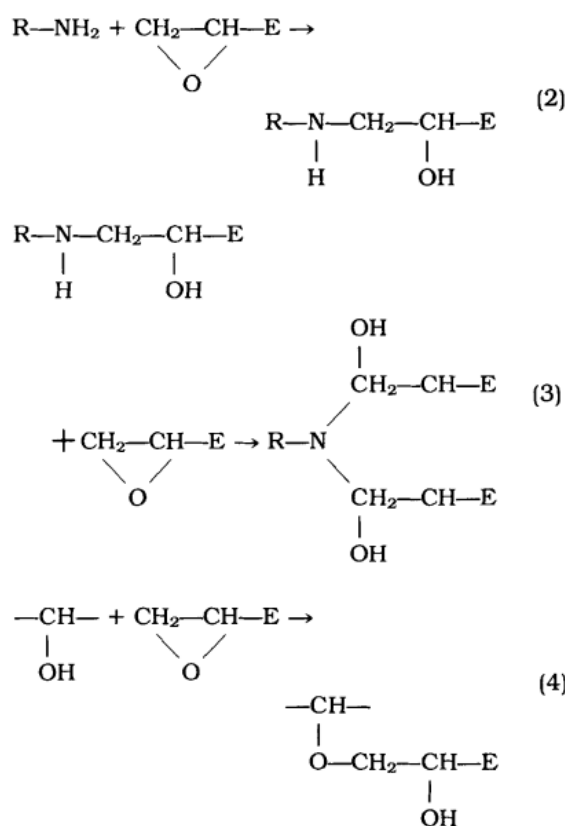
Dans ce travail développé à l'IMP, la composition des prépolymères a pu être déduite par GPC et par HPLC couplée à un détecteur UV-vis. Pour compléter la caractérisation, les auteurs ont réalisé des analyses RMN <sup>1</sup>H dans lesquelles ils ont observé la présence de groupements hydroxyle terminaux. Par la suite, ils ont fait réagir ces monomères porteurs de groupes hydroxyle terminaux avec du monoisocyanate. Ils ont observé trois environnements chimiques distincts pour les groupes hydroxyle suggérant qu'il existait trois natures différentes de ces groupes.<sup>1</sup>

En conclusion, les auteurs ont montré la possibilité d'obtenir une bonne estimation de la composition des prépolymères DGEBA par HPLC avec gradient d'élution. Ces résultats sont d'autant plus probants qu'ils sont accompagnés d'une analyse du produit modifié par un monoisocyanate réactif vis-à-vis des fonctions hydroxyles. L'étude approfondie par RMN <sup>1</sup>H leur ont permis d'accéder à la fonctionnalité des oligomères et de mettre en évidence la structure des extrémités de chaînes anormales.

Les fonctions hydroxyle primaires et secondaires attachées à ces extrémités de chaînes peuvent jouer un rôle important lors de la polycondensation ultérieure de ces prépolymères avec des diamines.<sup>1</sup> La compréhension de la structure des monomères et des propriétés physiques des matériaux a été un aspect crucial de ces recherches depuis le début des travaux de l'IMP. Cela continue d'être un point central dans nos recherches actuelles.

**Principales contributions :** Étude du comportement thermique par DSC et influence de l'utilisation d'un catalyseur pour des systèmes époxy-amine et époxy-anhydride pour le développement de réseaux thermodurcissables.<sup>2</sup>

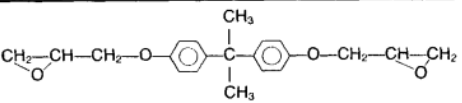
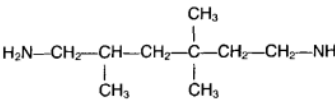
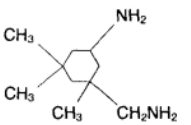
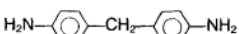
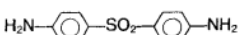
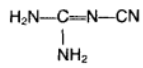
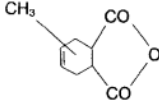
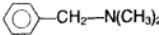
Dans ce travail, les auteurs ont comme objectif de comprendre le mécanisme de polymérisation d'une réaction époxy-amine (**Schéma I-3**). Ils ont émis l'hypothèse que la seule réaction notable en l'absence de catalyseur concerne les hydrogènes actifs de l'amine comme le montrent les équations **2 et 3**. Les auteurs ont suggéré que l'amine tertiaire créée dans la deuxième réaction (**3**) est trop encombrée stériquement pour permettre la troisième réaction correspondant à l'étherification (**4**). Cependant, lorsqu'un catalyseur est utilisé, des réactions peuvent compliquer la polyaddition ; par exemple l'oligomérisation impliquant l'hydroxyle et l'époxy par un processus ionique (**Schéma I-3**).<sup>2</sup>



**Schéma I-3.** Différentes voies possibles de réaction d'addition époxy-amine.<sup>2</sup>

Les auteurs ont étudié les aspects thermodynamiques de cette réaction de polymérisation et les propriétés résultantes des différents durcisseurs utilisés ; amines et anhydrides. L'enthalpie de réaction et les températures de transition vitreuse ( $T_g$ ) ont été évaluées et reliées à la structure du durcisseur pour les systèmes époxy-diamine. Une technique a également été mise au point pour déterminer l'énergie d'activation.<sup>2</sup>

**Tableau I-1.** Précurseurs de réseaux époxy.<sup>2</sup>

Name		Molecular Weight	Structure	Functionality	State/ Mixing
Diglycidyl ether of bisphenol A	a) DGEBA	342		2 or 4	$T_g = RT$
Trimethyl hexamethylene diamine	TMHMD	158		4	liq/RT <sup>ci</sup>
Isophorone diamine	b) IPD	170		4	liq/RT
4-4'-diamino diphenyl methane	DDM	193		4	solid/80°C
4-4'-diamino diphenyl sulfone	DDS	248		4	solid/130°C
Cyanoguanidine (or Dicyanodiamide)	DDA	84		4 (ref. 17 to 19)	solid/RT
Methyl tetra hydrophthalic anhydride	MTHPA	166		2	liq/RT
Benzyl dimethylamine	BDMA	135		catalytic agent	

Les auteurs ont également étudié le rapport stoechiométrique amine-époxy ( $r$ ) en considérant les quatre hydrogènes actifs des amines et les deux sites réactifs des prépolymères époxydes. Les  $T_g$  plus élevées ont été observées pour  $r = 1$ . En effet, les auteurs précisent que l'excès d'amines peut jouer un rôle de plastifiant. De plus, faire varier  $r$  impacte significativement la structure des réseaux. Cet aspect est essentiel pour la conception de réseaux homogènes bien maîtrisés. Pour ces raisons, les réseaux développés au cours de cette thèse ont toujours considéré un rapport stoechiométrique de  $r = 1$  (**Tableau I-2**).<sup>2</sup>

**Tableau I-2.** Composants et structures formés en fonction du rapport époxy-amine.<sup>2</sup>

Component	Structure	Conditions
1. Prepolymer repeat unit	$\begin{array}{c} \text{OH} \qquad \qquad \text{CH}_3 \\   \qquad \qquad   \\ \leftarrow \text{CH}_2 - \text{CH} - \text{CH}_2 - \text{O} - \text{C}_6\text{H}_4 - \text{C} - \text{C}_6\text{H}_4 - \text{O} \rightarrow \\   \\ \text{CH}_3 \end{array}$	Always
2. Fully reacted hardener unit	$\begin{array}{c} \nearrow \text{N} - \text{X} - \text{N} \searrow \\ \nearrow \text{HN} - \text{X} - \text{N} \searrow \\ \nearrow \text{HN} - \text{X} - \text{NH} \searrow \end{array}$	$r \leq 1$
3. Partly reacted hardener unit	$\begin{array}{c} \nearrow \text{HN} - \text{X} - \text{N} \searrow \\ \nearrow \text{HN} - \text{X} - \text{NH} \searrow \end{array}$	$1 < r < 1.5$ $1.5 < r < 2.0$
4. Unreacted epoxy ends	$\leftarrow \text{CH}_2 - \text{CH} - \text{CH}_2 \rightarrow$ $\quad \quad \quad \diagup \quad \diagdown$ $\quad \quad \quad \text{O}$	$r < 1$
5. Ether unit	$\leftarrow \text{CH}_2 - \text{CH} - \text{O} - \text{CH}_2 - \text{CH} - \text{O} \rightarrow$ $\quad \quad \quad   \qquad \quad  $ $\quad \quad \quad \text{R} \qquad \quad \text{R}$	$r < 1$ and catalyst

Comme mentionné précédemment, l'influence de la benzyldiméthylamine, en tant que catalyseur, dans les systèmes DGEBA/anhydride et DGEBA/diamine a été étudié. En utilisant différents types de durcisseur, les auteurs ont démontré un lien entre la nature de ce dernier et les propriétés physiques des réseaux époxy. En modifiant la nature chimique des durcisseurs amines, d'aliphatique (TMHMD), de cycloaliphatique (IPD) à aromatique (DDM ou DDS), les  $T_g$  évoluent fortement. En effet, les réseaux à base d'amines aliphatiques conduisent à des réseaux de plus faible  $T_g$  (105 °C pour la TMHMD) tandis que l'utilisation d'amines cycloaliphatiques et aromatiques, plus encombrés stériquement mènent à une réduction de la mobilité des réseaux et par conséquent à des  $T_g$  plus élevées.<sup>2</sup>

**Tableau I-3.** Évaluation des températures de polymérisation et vitreuse des réseaux à stœchiométrie en fonction de la nature de l'amine.<sup>2</sup>

Curing Agent	$T_1(^{\circ}\text{C})$	$T_p(^{\circ}\text{C})$	$T_2(^{\circ}\text{C})$	$T_g(^{\circ}\text{C})$
TMHMD	40	100	200	105
IPD	45	118	214	155
DDM	100	170	210	165
DDS	135	222	340	190
DDA	170	—	300	125

\*  $T_1$ ,  $T_p$  et  $T_2$  correspondent au pic exothermique observé au DSC.  $T_1$  indique le début du pic de polymérisation,  $T_p$  sa valeur maximale, et  $T_2$  la fin du pic de polymérisation exothermique.

En se basant sur les travaux menés par Jean Pierre Pascault, nous avons également étudié les propriétés des réseaux époxy-amine en fonction du type de durcisseurs et de monomères utilisés. Ainsi, dans le troisième chapitre de ce travail, vous verrez que de nouveaux réseaux époxy-amine ont été développés à partir de nouveaux monomères liquides ioniques époxydés et des amines aliphatiques, cycloaliphatiques et aromatiques comme durcisseurs.

**Professeur Jean François Gérard – 1996**

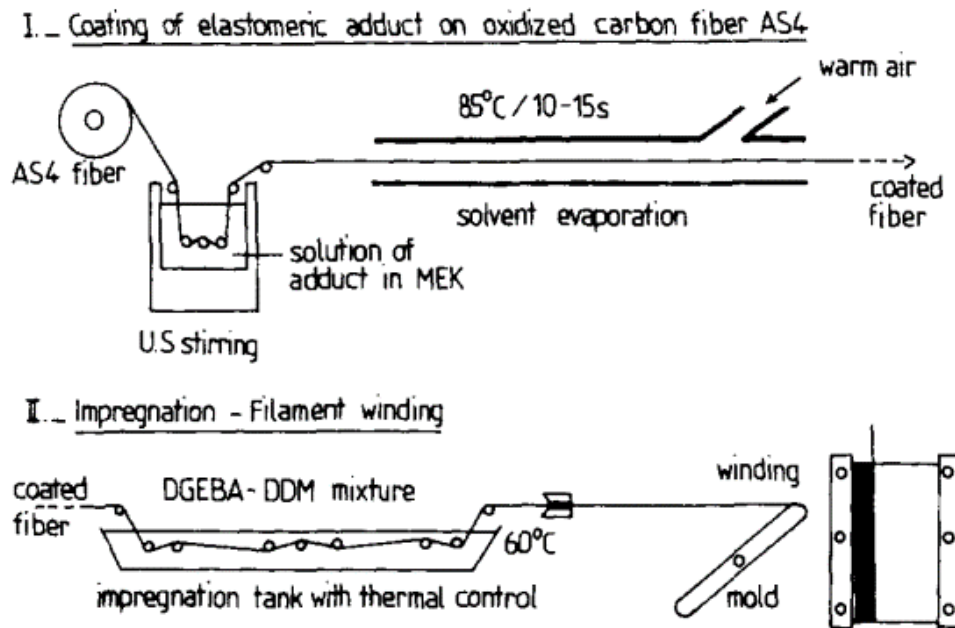
**Principales contributions :** Développement et caractérisation de réseaux multi-composants afin d'améliorer les performances mécaniques des matériaux époxy.<sup>3,4</sup>

Après avoir étudié et caractérisé de nombreux systèmes epoxydes en termes de réactivité, influence du rapport stoechiométrique, étude des réactions de polymérisation et d'identification des réactions secondaires, notre laboratoire a travaillé sur le développement de mélanges multicomposants pour améliorer les performances des matériaux époxy-amine. Cela impliquait l'introduction de charges (particules cœur-coquille, fibres de carbone) et le développement de systèmes multi-composants complexes susceptibles d'améliorer leurs propriétés. L'objectif était de mieux comprendre les relations structure-propriété liées à l'ajout de ces composants dans ces réseaux.<sup>3</sup>

Dans le premier travail dirigé par le Professeur Jean François Gérard, les auteurs ont construit différents réseaux époxy en introduisant des particules *cœur-coquille* constituées de copolymères à blocs pour améliorer les propriétés mécaniques et étudier le comportement à la rupture.<sup>3</sup> Les mélanges ont été obtenus dans des conditions de mise en œuvre parfaitement définies afin de moduler l'état de dispersion des particules dans la matrice. Dans ce cas-présent, l'utilisation d'une extrudeuse comme mélangeur conventionnellement utilisé pour la mise en œuvre des thermoplastiques a permis de conduire à une excellente dispersion des particules de copolymère à blocs dans la matrice époxy. Ainsi, ces travaux ont mis en évidence que l'incorporation de ces particules réduit de façon significative l'initiation et la propagation de la fissure.

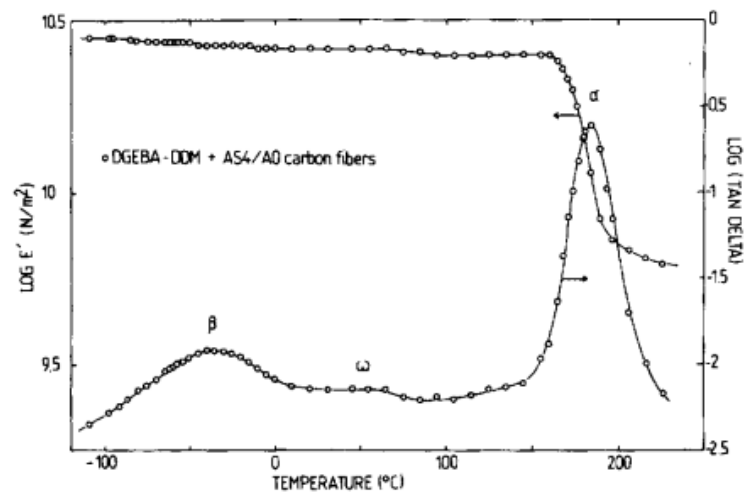
Les auteurs ont émis l'hypothèse que les mécanismes de réticulation sont liés à la cavitation et à l'apparition de bandes de cisaillement au sein du matériau. Les résultats ont également démontré que la formation d'interfaces et/ou d'interphases affectent l'adhésion entre les phases et influencent les propriétés de ténacité à la rupture. Parallèlement, l'adhésion est contrôlée et assurée par les fonctionnalités présentes sur les particules de copolymère à blocs.

Dans un autre travail, les auteurs ont proposé l'utilisation d'un élastomère réticulable à base de copolymère butadiène acrylonitrile à terminaison carboxy.<sup>5</sup> L'ajout de cet élément améliore les propriétés de la matrice époxy et renforce les fibres de carbone. En utilisant un processus d'enroulement filamentaire, les charges d'élastomères ont été adsorbées sur les fibres de carbone oxydées puis enduites dans la matrice époxy comme décrit sur la **Fig. I-1**.



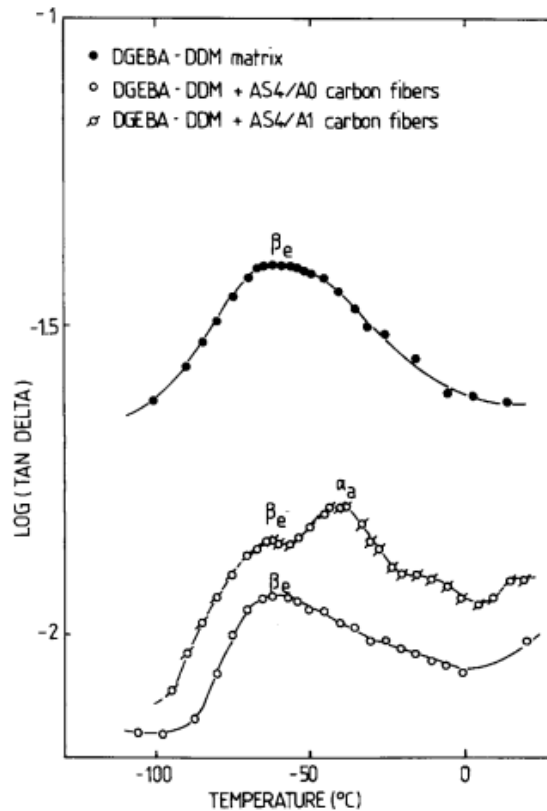
**Figure I-1.** Traitement de surface des enroulements fibres-filaments.<sup>5</sup>

Les réseaux époxy modifiés et les composites renforcés de fibres de carbone ont été étudiés par analyse mécanique dynamique (AMD). Ces résultats ont permis de mettre en œuvre les différentes relaxations mécaniques et les attribuer aux différents composants (Fig. I-2 et I-3).<sup>4</sup>



**Figure I-2.** Évaluation des relaxations au sein d'un composite DGEBA-DDM-fibre de carbone.<sup>4</sup>





**Figure I-3.**  $\beta_e$  relaxation du réseau époxy et  $\alpha_a$  transition de charge d'élastomère à  $3,3 \cdot 10^{-2}$  Hz.<sup>4</sup>

L'introduction des fibres de carbone et des copolymères à base d'élastomères décale la température des transitions  $\beta$ , sans induire de transitions séparées. Cette observation est importante car elle montre que, premièrement, les systèmes sont homogènes et deuxièmement, les charges ont bien été introduites dans le composite. La seule transition induite observée concernait le composite utilisant la fibre de carbone A1.

Le matériau composite résultant peut être décrit comme un système triphasé composé : d'un réseau époxy servant de matrice, de fibres de carbone et d'une couche intermédiaire souple, jouant le rôle d'interphase. Les propriétés mécaniques des matériaux composites unidirectionnels ont été évaluées par flexion et par tests aux chocs. Ces analyses révèlent une forte dépendance par rapport à l'épaisseur de l'interphase à la surface des fibres de carbone.<sup>4</sup>

La stratégie d'utiliser des charges pour ajuster les propriétés mécaniques des matériaux époxy, considérés trop cassants, est encore exploitée à l'IMP. Parmi les différentes charges qui ont été étudiées, les liquides ioniques ont suscité une attention particulière dans notre laboratoire. Dans ce travail de thèse, nous avons conçu des monomères liquides ioniques époxydés afin de développer des composites à fibres de carbone potentiellement

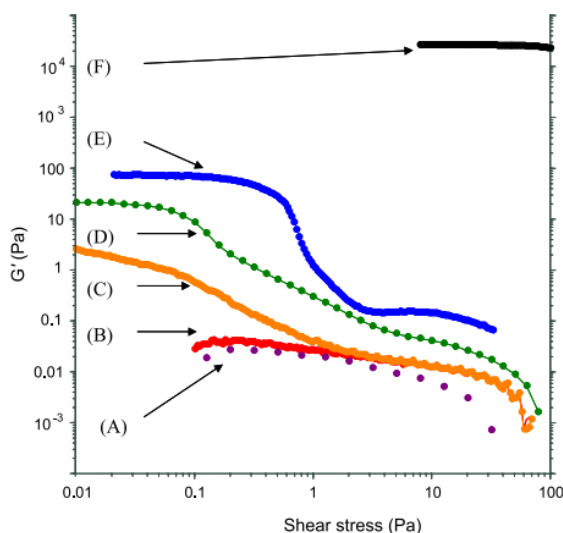
plus durables et dégradables permettant par exemple la récupération des fibres de carbone afin d'être réutiliser.

### Professeure Jannick Duchet-Rumeau – 2000

**Principales contributions :** Développements et caractérisations de nanocomposites époxy structurés.<sup>6,7</sup>

Dans ce travail, la professeure Jannick Duchet-Rumeau a étudié la modification chimique de charges lamellaires, en particulier des argiles puis la dispersion des montmorillonites modifiées organiquement (MMTM) dans systèmes époxy-amine. Plus précisément, l'étude a porté sur l'utilisation de la DGEBA utilisée comme prépolymère époxy et sur un durcisseur de type amine aliphatique à squelette polyoxypropylène (notée Jeffamine D2000). la morphologie de ces systèmes a été étudiée à différentes échelles (du nano vers le macro) par diffraction des rayons X, par diffusion des rayons X aux petit angles (SAXS) et par rhéologie.

Les propriétés mécaniques des gels résultants et la viscosité à haut taux de cisaillement sont liées à l'état de dispersion à l'échelle nanométrique de la MMTM. Cela révèle l'existence de deux organisations différentes; basées sur les interactions entre l'argile organique et le prépolymère DGEBA. Pour obtenir une caractérisation plus précise de la solidité des gels, le module de conservation a été analysé en faisant varier la quantité de MMTM introduite dans la DGEBA (**Fig. I-4**).



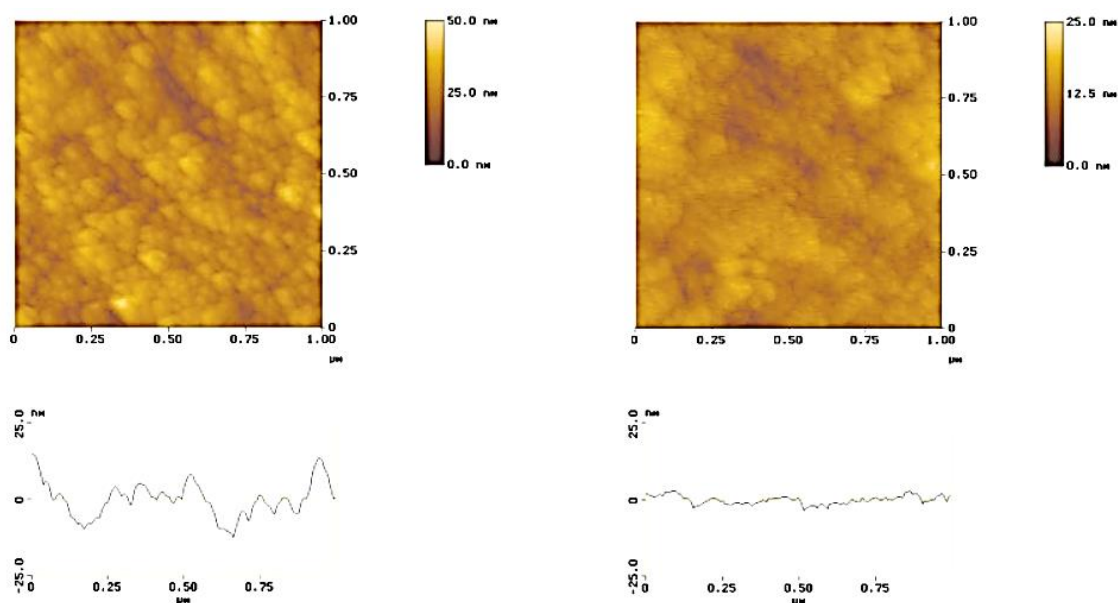
**Figure I-4.** Variations du module de conservation à 80 °C des suspensions MMTM/DGEBA pour différentes quantités de MMTM: **(A)** 0 phr, **(B)** 1 phr, **(C)** 2 phr, **(D)** 5 phr, **(E)** 10 phr , et **(F)** 30 phr.<sup>6</sup>

Pour un taux de montmorillonite faible ( $< 2$  phr), aucun changement dans le module mécanique n'a été observé. Pour des taux plus élevés ( $> 10$  phr), la réponse viscoélastique prouve la formation de gels.<sup>6</sup>

Afin de comprendre le comportement des mélanges réactifs et la structure des réseaux époxy-amine, les Professeurs Duchet-Rumeau et Pascault ont étudié leur homogénéité par microscopie à force atomique (AFM pour *atomic force microscope*). En effet, l'homogénéité de ces réseaux reste toujours aujourd'hui un sujet à débat.<sup>7</sup>

En utilisant l'AFM, en mode *tapping*, la morphologie a pu être examinée selon la nature du durcisseur et la stoechiométrie du mélange réactif. Une topographie homogène du réseau époxy, similaire à celle d'un thermoplastique amorphe, a été obtenue.<sup>7</sup>

Les auteurs ont précisé que, pour pouvoir observer les surfaces à une échelle nanométrique, deux précautions doivent être prises : (1) conserver la résolution nanométrique des pointes pour éviter la distorsion de l'image et (2) vérifier que les surfaces soient suffisamment planes pour éviter une influence sur le contraste de phase (**Fig. I-5**).<sup>7</sup>



**Figure I-5.** Images AFM en mode *tapping* d'une surface fracturée DGEBA-IPD : images et profils de hauteur (à gauche) réalisés avec une pointe au rayon de courbure élargi ( $RA = 37^\circ$ ) et (à droite) réalisés avec une pointe neuve ( $RA = 17^\circ$ ).<sup>7</sup>

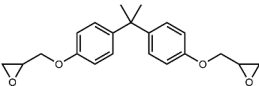
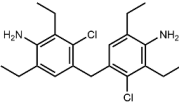

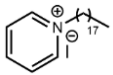
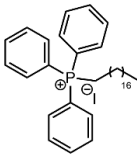
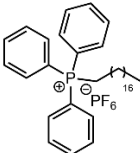
Cette étude a fourni les lignes directrices de l'utilisation de l'AFM, en mode *tapping*, pour caractériser les réseaux époxy-amine et discuter de leur homogénéité.

**Principales contributions :** Conceptions et développement de réseaux époxy modifiés par des liquides ioniques (LIs), employés comme des amorceurs de polymérisation/durcisseur soit comme nouveaux monomères époxydés.<sup>8,9</sup>

Un liquide ionique (LI) est un sel organique constitué d'un cation et d'un anion, sous forme de liquide pour des températures inférieures à 100°C.<sup>10</sup> Les LIs jouent un rôle de plus en plus important dans le domaine des matériaux polymères pouvant servir d'agents surfactants de charges lamellaires, d'agents plastifiants, de compatibilisants de mélanges polymères, d'électrolytes et d'agents de durcissement.<sup>11</sup>

En 2011, Professeur Sébastien Livi a étudié l'influence et l'impact des liquides ioniques pyridinium, imidazolium et phosphonium sur les diverses propriétés physiques des réseaux époxy-amine (**Tableau I-4**).<sup>8</sup>

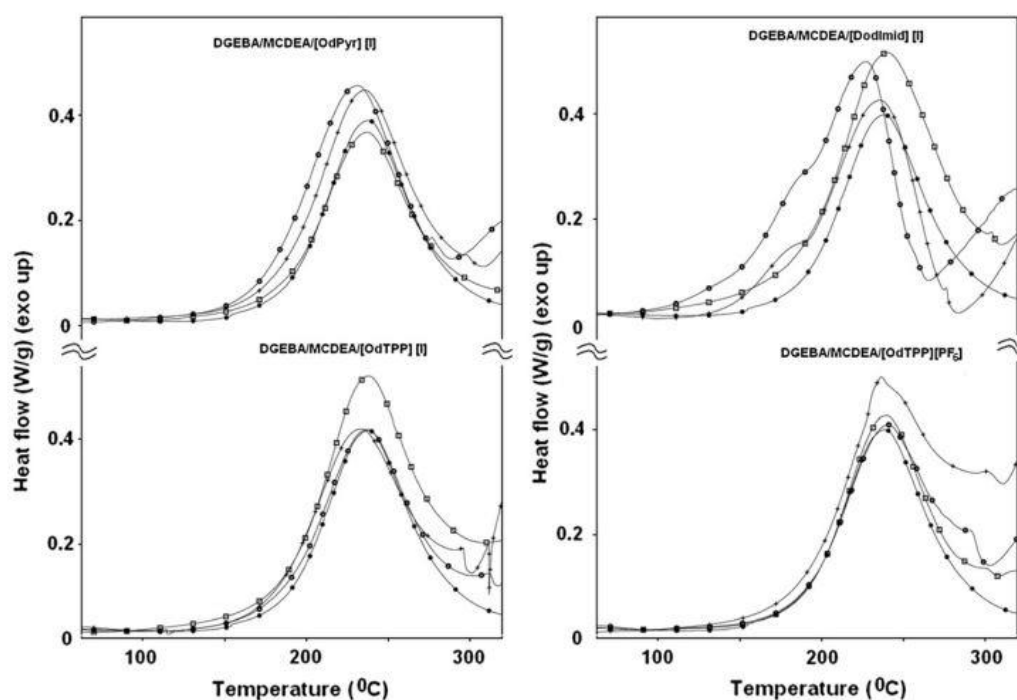
**Tableau I-4.** Structure des prépolymères utilisés pour l'élaboration de réseaux époxy modifiés.<sup>8</sup>

Name	Structure	Characteristics
DGEBA		Epon 827 from shell chemistry; 177-188 g/eq
MCDEA		Supplied by Lonza, Molar mass = 380 g/mol
1,3-bis Octadecylimidazolium iodide [DodImid][I]		Prepared according to the literature. Molar mass = 699.9 g/mol, mp = 64 °C
Octadecylpyridinium iodide [OdPyr] [I]		Molar mass = 459 g/mol, mp = 102 °C
Octadecyltriphenyl phosphonium iodide [OdTPP] [I]		Molar mass = 641.9 g/mol, mp = 86 °C
Octadecyltriphenyl phosphonium hexafluorophosphate [OdTPP][PF <sub>6</sub> ]		Molar mass = 660 g/mol, mp = 80 °C

Les quatre LIs ont été introduits, en proportions variables, dans le système DGEBA/MCDEA.

Il a été observé que :

- Les LIs à base d'imidazolium et de pyridinium jouent un rôle d'amorceurs de polymérisation anionique. En effet, leur dégradation à haute température (durant le protocole de cuisson) mène à la formation de complexes epoxy-imidazole et epoxy-pyridine servant d'amorceurs.
- Les LIs à base de phosphonium n'ont pas eu d'impact significatif sur la réticulation du réseau epoxy-amine comme l'ont démontré les analyses DSC dynamique et FTIR (**voir Figure I-7**).
- L'ajout de LI a entraîné une diminution de la température de transition vitreuse du système. Ainsi, l'utilisation de quantités de l'ordre de 5 phr ont conduit à un effet plastifiant. L'effet est moins prononcé dans les systèmes contenant [OdTPP] [PF<sub>6</sub>].



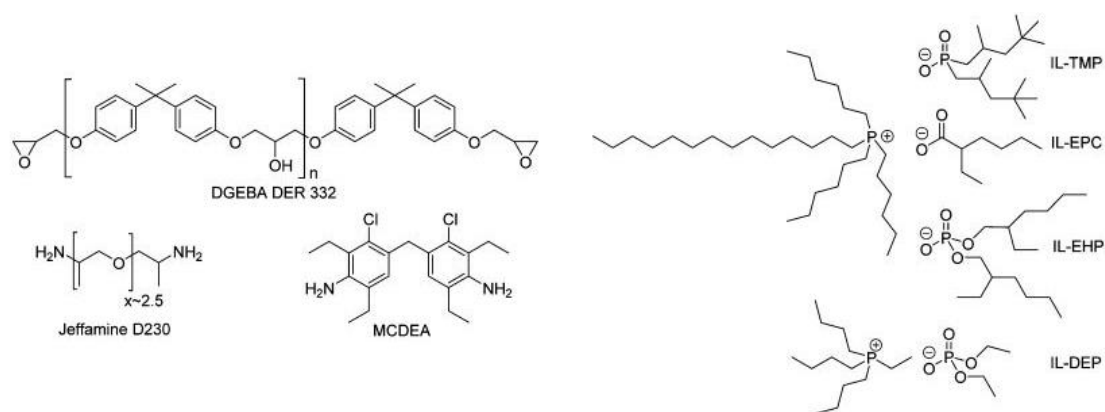
**Figure I-7.** Thermogrammes DSC pour balayage dynamique de DGEBA/MCDEA en fonction de la nature LI. (•) 0, (□) 1, (+) 2,5 et (○) 5,0 phr d'LI.<sup>8</sup>

Les LIs à base de phosphonium se sont avérés mieux confinés dans le réseau époxy. De plus, l'inclusion d'un contre-anion iodure avec le cation phosphonium a permis d'obtenir une meilleure stabilité thermique, se rapprochant de celle pouvant être obtenue pour des réseaux époxy-amine.

À partir de ces résultats, les auteurs ont conclu que l'utilisation de LIs à base de phosphonium était préférable pour limiter les nombreuses réactions de polymérisation possibles que peuvent induire les liquides ioniques imidazolium par exemple, avec la formation de carbène, lors de la dégradation du liquide ionique et initié initialement par l'anion. Ainsi, ils représentent la meilleure alternative pour obtenir de nouveaux réseaux époxy présentant une bonne stabilité thermique, un haut module mécanique et une température de transition vitreuse élevée.<sup>8</sup>

Ce travail a suggéré qu'il existait un potentiel dans le développement de nouveaux réseaux thermodurcissables à haut module et haute température de transition vitreuse.<sup>8</sup>

Dans un travail plus récent, le professeur Sébastien Livi et ses co-auteurs ont rapporté une nouvelle façon de développer des réseaux époxy en utilisant des LIs à base de phosphonium combinés à des contre-ions phosphinate, carboxylate et phosphate (**Fig. I-8**).<sup>9</sup>



**Figure I-8.** Structures chimiques des DGEBA, Jeffamine D230, MCDEA et liquides ioniques à cation phosphonium et anion phosphinate (IL-TMP), phosphate (IL-EHP et DEP) et carboxylate (IL-EPC).<sup>9</sup>

Ils ont montré qu'une petite quantité de LIs (de 10 à 30 phr) pouvait conduire à la formation de réseaux époxy-LI avec des propriétés physiques finales améliorées. L'influence de la nature chimique des anions a été étudiée sur la cinétique de polymérisation des systèmes époxy ainsi que sur les propriétés thermiques et mécaniques des réseaux époxy-LI. Dans tous les cas, les LIs ont montré une forte réactivité vis-à-vis du prépolymère et ont conduit à la formation de réseaux avec une conversion des groupes époxy pouvant aller jusqu'à 96 %.<sup>9</sup>

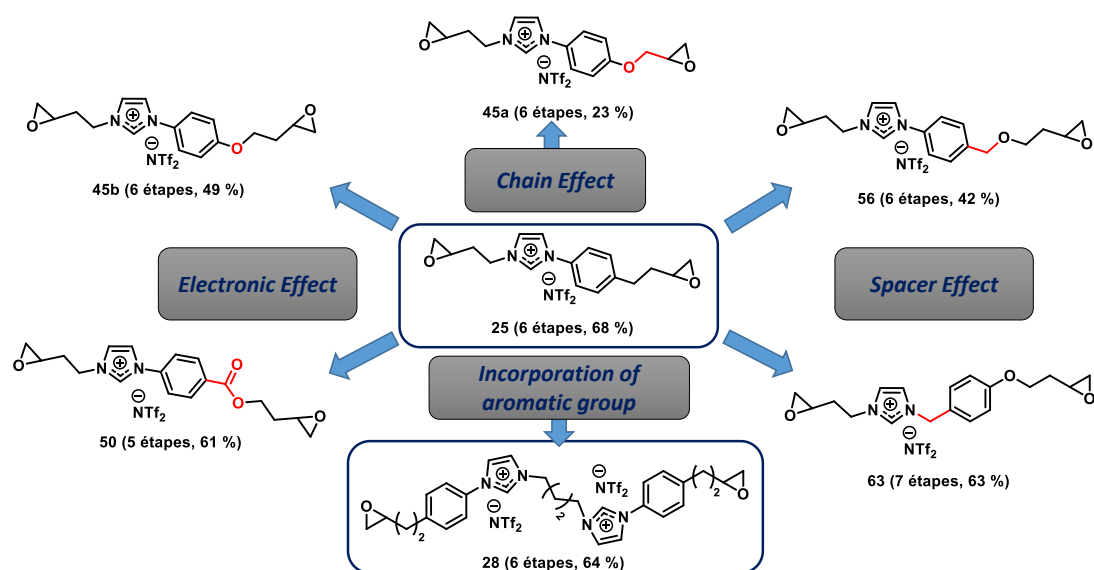
Par rapport aux systèmes époxy-amine classiques, les réseaux amorcés par des LIs ont obtenu des valeurs de température de transition alpha et de module mécanique similaires ou supérieurs. Ces premiers résultats sont encourageants et ont montré le potentiel des LIs comme comme amorceurs de polymérisation.<sup>9</sup>

**Tableau I-5.** Comportement thermomécanique des réseaux époxy polymérisés par différents durcisseurs.<sup>9</sup>

curing agent	$T_{\alpha}^a$ (°C)	$E'_R{}^b$ (MPa)	$\nu_e^c$ (mol·m <sup>-3</sup> )
MCDEA	160	16	1385
D230	100	16	1591
IL-TMP	140	104	9412
IL-EPC	144	124	11 121
IL-DEP	117	16	1527
IL-EHP	98	14	1399

En effet, les réseaux époxy-LI ont montré un comportement hydrophobe et une excellente stabilité thermique (supérieure à 350 °C) sous azote avec des  $T_g$  allant de 90 à 150 °C selon la structure chimique du LI. Les propriétés mécaniques en flexion ont été évaluées ainsi que la ténacité à la rupture de ces réseaux a également été étudiée. Les valeurs obtenues sont comparables à celles des réseaux epoxy-amine conventionnels. Ces travaux ont ouvert la voie au développement de réseaux époxy en utilisant, comme additifs réactifs, les LIs.<sup>9</sup>

Plus tard, des réseaux epoxy-amine ont été mis au point à partir de liquides ioniques diépoxydés en collaboration avec le laboratoire de Chimie Moléculaire et Thiorganique (LCMT).<sup>12-15</sup> Ainsi, une quarantaine de nouveaux monomères ont été mis au point et utilisés comme co-monomères (**Figure I-9**). Ces réseaux ont montré de nouvelles propriétés intéressantes et ont conduit à des réseaux possédant des  $T_g$  de l'ordre de 50°C à 130°C dépendant la nature chimique du durcisseur utilisé (aliphatique versus cycloaliphatique ou aromatique).



**Figure I-9.** Plateforme des monomères liquide ionique synthétisés.

Notre travail s'inscrit dans la continuité de la synthèse de nouveaux monomères liquide ioniques pouvant mener à des réseaux à plus hautes  $T_g$  pour des applications potentielles dans l'automobile et l'aéronautique. La circularité de ces nouveaux réseaux polyepoxydes ioniques est une caractéristique importante que nous souhaitons intégrer en y insérant des liaisons clivables témoignant de notre engagement continu dans ce domaine scientifique et de la durabilité des nouveaux matériaux. Finalement, ce manuscrit bien qu'il soit modeste, représente une contribution à ces travaux de recherche et s'inscrit dans la continuité de cette thématique.



## 2. Objectifs à long terme

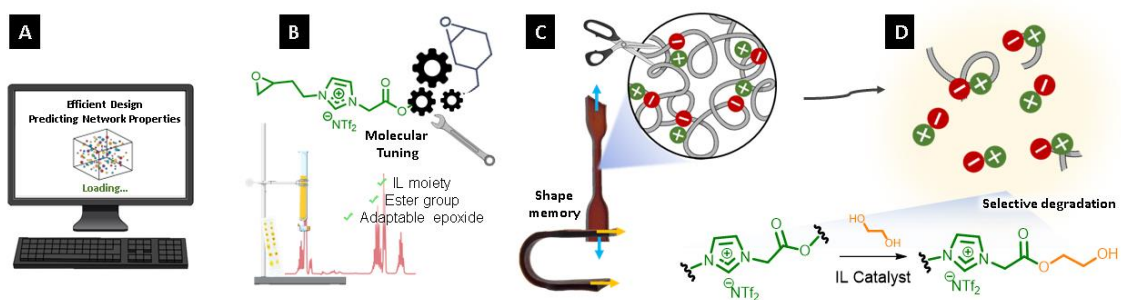
L'objectif à long terme de cette recherche est d'ouvrir la voie à la création d'une bibliothèque de monomères liquides ioniques époxydés pour développer des thermodurcissables et des composites multifonctionnels, performants et durables.

Cette recherche consiste en trois projets principaux : **(1)** Conception et synthèse de monomères LIs tri- et tétra-époxydés pour construire des thermodurcissables multifonctionnels et dégradables ; **(2)** Exploration d'un monomère LI clivable pour adapter le développement, le désassemblage et le recyclage de thermodurcissables et composites de hautes performances et **(3)** Recherche et synthèse de LIs photopolymérisables à base de monomères époxy cycloaliphatiques.

Concernant le développement du projet **(1)**, les étapes suivantes ont été cruciales : **(1a)** Etude des interactions intermoléculaires et des propriétés résultantes des réseaux par modélisation ; **(1b)** conception stratégique des voies de synthèse, suivie de l'optimisation de la synthèse et du *scale-up* ; **(1c)** élaboration des réseaux époxy-amines, évaluation de leurs caractéristiques et gestion des déchets.

Pour aborder la production des composites **(2)**, le procédé a impliqué **(2a)** la synthèse d'un LI époxydé clivable et la conception des réseaux thermodurcissables ; **(2b)** suivi du développement des composites et de leurs caractérisations et **(2c)** dégradation sélective de la matrice thermodule pour récupérer les fibres de carbone.

Le défi de la synthèse des LIs photopolymérisables **(3)** a été relevé par **(3a)** la conception de LIs époxydés cycloaliphatiques et leurs voies de synthèses correspondantes, **(3b)** l'étude de la photopolymérisation ou de la polymérisation thermique de ces composés, et **(3c)** la caractérisation complète des matériaux afin d'obtenir un scénario de fin de vie plus respectueux de l'environnement ont été menés.



**Schéma I-4.** Déroulement de cette recherche doctorale. La première étape **(A)** concerne, à moindre coût énergétique, économie d'atome et d'effort. L'étape correspond à **(B)** ingénierie moléculaire en introduisant des fragments de LIs, des groupes clivables et des groupes époxy classique ou cyclo-aliphatique. La troisième étape, **(C)** développement de matériaux multifonctionnels et leurs caractérisations, en essayant de comprendre les relations structure-propriétés. L'étape **(D)** est l'étape de solvolysé sélective de la matrice de thermodures, récupération des dérivés LIs ou des composants des composites.

En résumé, dans ce travail de thèse, nous nous sommes efforcés de concevoir de nouvelles résines époxy-amine de deuxième génération qui ont des performances élevées et satisferont également les prérequis de l'économie circulaire.

Tout au long de notre rétrospective, nous avons abordé la première sous-question **(I)**, et nous allons essayer de répondre à la deuxième sous-question **(II)** - à savoir, *quelle est la plus value de ces travaux par rapport au domaine des matériaux polymères ?* - dans la section dédiée aux perspectives et conclusions.

### 3. Références

- (1) Gulino, D.; Galy, J.; Pascault, J. P.; Tho Pham, Q. Etude Du Prépolymère Époxyde Par Chromatographie et 1H NMR à MHz, 2. *Makromol. Chemie. Macromol. Symp.* **1984**, 316, 297–316.
- (2) Galy, J.; Sabra, A.; Pascault, J.-P. Characterization of Epoxy Thermosetting Systems by Differential Scanning Calorimetry. *Polym. Eng. Sci.* **1986**, 26 (21), 1514–1523. <https://doi.org/10.1002/pen.760262108>.
- (3) Maazouz, A.; Becu, L.; Sauterau, H.; Gerard, J.-F. Fracture Toughness of Core-Shell Particles Modified Polyepoxy Networks. In *Deformation, Yield and Fracture of polymers*; **1997**; p 574.
- (4) Gerard, J.-F. Characterization and Role of an Elastomeric Interphase on Carbon Fibers Reinforcing an Epoxy Matrix. *Polym. Eng. Sci.* **1988**, 28 (9), 568–577. <https://doi.org/10.1002/pen.760280905>.

- (5) Perret, P.; Gerard, J. F.; Chabert, B.; Lyon, S. A. De; Cedex, V.; Claude, U.; Lyon, B.; Cedex, V. A New Method to Study the Fiber-Matrix Interface in Unidirectional Composite Materials: Application for Carbon Fiber-Epoxy Composites. *Polym. Test.* **1987**, *7*, 405–418.
- (6) Le Pluart, L.; Duchet, J.; Sautereau, H.; Halley, P.; Gerard, J.-F. Rheological Properties of Organoclay Suspensions in Epoxy Network Precursors. *Appl. Clay Sci.* **2004**, *25* (3–4), 207–219. <https://doi.org/10.1016/j.clay.2003.11.004>.
- (7) Duchet, J.; Pascault, J. P. Do Epoxy-Amine Networks Become Inhomogeneous at the Nanometric Scale? *J. Polym. Sci. Part B Polym. Phys.* **2003**, *41* (20), 2422–2432. <https://doi.org/10.1002/polb.10585>.
- (8) Guenther Soares, B.; Livi, S.; Duchet-Rumeau, J.; Gerard, J. F. F. Preparation of Epoxy/MCDEA Networks Modified with Ionic Liquids. *Polymer (Guildf)*. **2012**, *53* (1), 60–66. <https://doi.org/10.1016/j.polymer.2011.11.043>.
- (9) Nguyen, T. K. L.; Livi, S.; Soares, B. G.; Pruvost, S.; Duchet-Rumeau, J.; Gérard, J.-F. F. Ionic Liquids: A New Route for the Design of Epoxy Networks. *ACS Sustain. Chem. Eng.* **2016**, *4* (2), 481–490. <https://doi.org/10.1021/acssuschemeng.5b00953>.
- (10) Siriwardana, A. I. Industrial Applications of Ionic Liquids. In *Electrochemistry in Ionic Liquids*; Springer International Publishing: Cham, **2015**; pp 563–603. [https://doi.org/10.1007/978-3-319-15132-8\\_20](https://doi.org/10.1007/978-3-319-15132-8_20).
- (11) Lei, Z.; Chen, B.; Koo, Y. M.; Macfarlane, D. R. Introduction: Ionic Liquids. *Chem. Rev.* **2017**, *117* (10), 6633–6635. <https://doi.org/10.1021/acs.chemrev.7b00246>.
- (12) Chardin, C.; Rouden, J.; Livi, S.; Baudoux, J. 3-[2-(Oxiran-2-Yl)Ethyl]-1-{4-[(2-Oxiran-2-Yl)Ethoxy]Benzyl}imidazolium Bis(Trifluoromethane)Sulfonimide. *Molbank* **2018**, *2018* (1), 9–74. <https://doi.org/10.3390/M974>.
- (13) Radchenko, A. V.; Duchet-Rumeau, J.; Gérard, J.-F. F.; Baudoux, J.; Livi, S. Cycloaliphatic Epoxidized Ionic Liquids as New Versatile Monomers for the Development of Shape Memory PIL Networks by 3D Printing. *Polym. Chem.* **2020**, *11* (34), 5475–5483. <https://doi.org/10.1039/D0PY00704H>.
- (14) Chardin, C.; Durand, A.; Jarsalé, K.; Rouden, J.; Livi, S.; Baudoux, J. Sulfonimides versus Ketosulfonamides as Epoxidized Imidazolium Counterions: Towards a New Generation of Ionic Liquid Monomers. *New J. Chem.* **2021**, *45* (6), 2953–2957. <https://doi.org/10.1039/D0NJ05126H>.
- (15) Chardin, C.; Rouden, J.; Livi, S.; Baudoux, J. Dimethyldioxirane (DMDO) as a Valuable

Oxidant for the Synthesis of Polyfunctional Aromatic Imidazolium Monomers Bearing Epoxides. *Green Chem.* **2017**, *19* (21), 5054–5059.  
<https://doi.org/10.1039/C7GC02372C>.

#### 4. Long-Term Goals

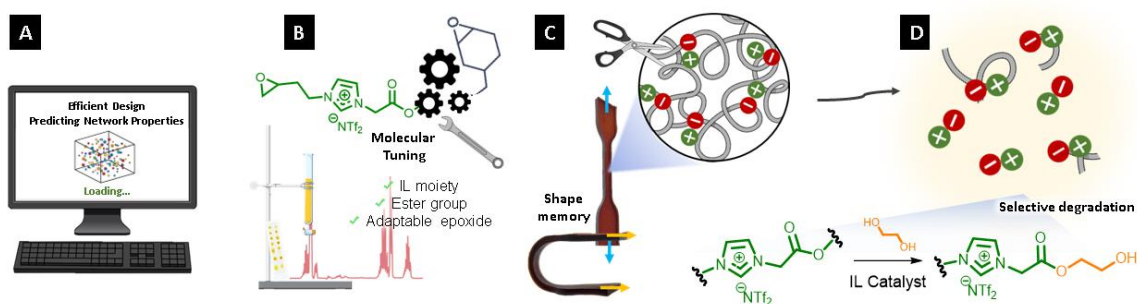
This research aims to pave the way to create a library of second-generation epoxy monomers to manufacture multifunctional, performing and sustainable thermosets and composites.

This research consists of three main projects: **(1)** Efficient design and synthesis of tri- and tetra-epoxidized IL monomers to build multifunctional and degradable thermosets; **(2)** Exploring a cleavable IL monomer for tailoring the manufacture, disassembly, and recycling of high-performance thermosets and composites and **(3)** Investigation and synthesis of photopolymerizable ILs based on cycloaliphatic epoxy monomers.

Concerning the development of the project **(1)**, the following steps were crucial: **(1a)** prediction of intermolecular interactions and resulting network properties by a computational-assisted methodology; **(1b)** strategic designing of the synthetic routes, followed by the optimization, synthesis, and scale up; **(1c)** creation the epoxy-amine networks, assessing their characteristics, and managing waste.

To tackle the production of composites **(2)**, the process involved **(2a)** the synthesis of a cleavable epoxidized IL and the design of the thermoset networks; **(2b)** followed by the manufacture of the composites and their characterization and **(2c)** selectively degradation of the thermoset matrix to recover the CFs.

The challenge of synthesizing photopolymerizable ILs **(3)** was attended through **(3a)** designing cycloaliphatic epoxidized ILs and their corresponding synthetic routes, **(3b)** studying the photopolymerization or thermal polymerization of these compounds, and **(3c)** thoroughly characterizing the materials to achieve a more environmentally friendly end-of-life scenario for them.



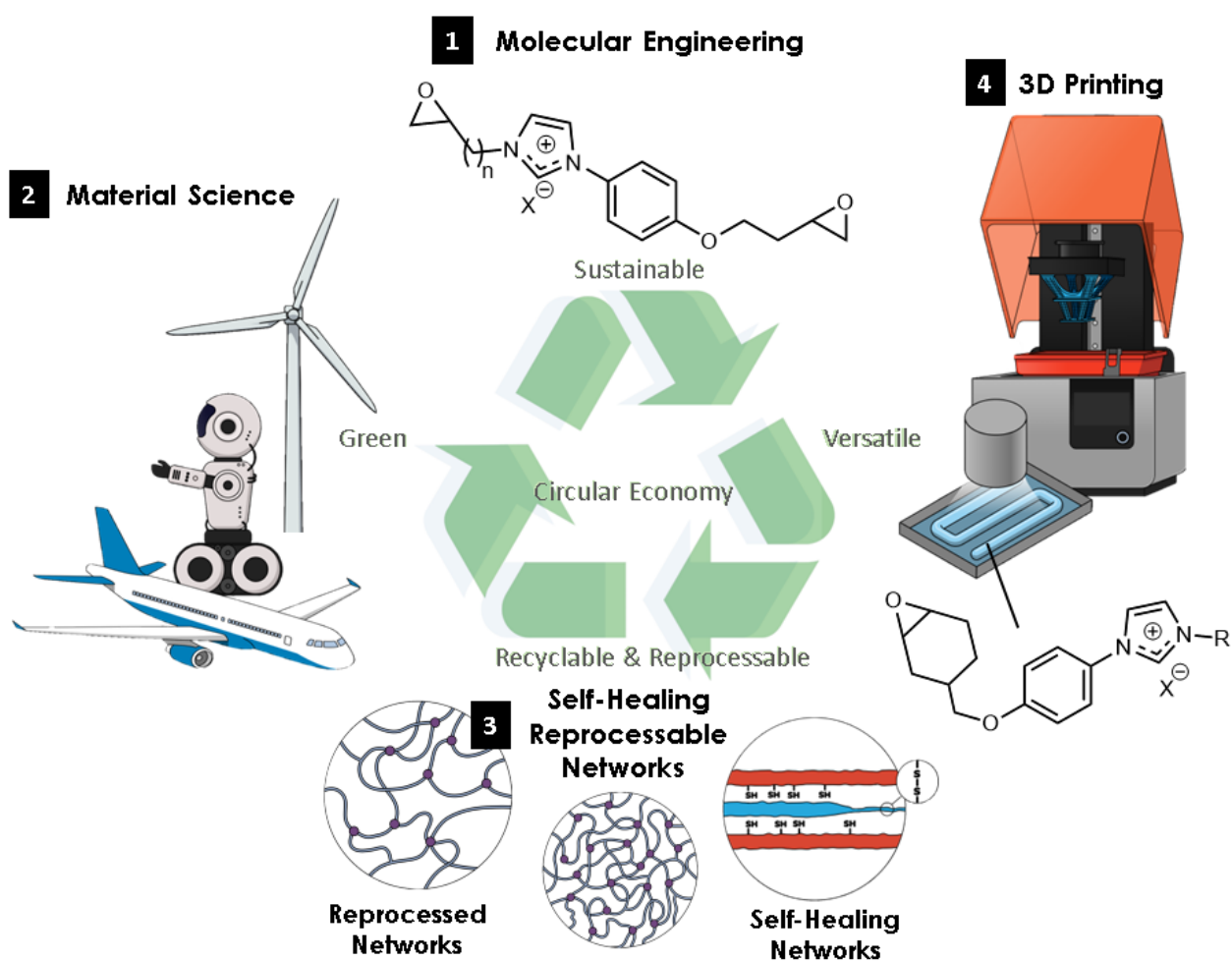
**Scheme I-4.** Workflow of this doctorate research. In **(A)** efficient design to conserve energy, resource and effort by predicting the maximum information about the new monomers and networks. **(B)** Molecular engineering by introducing IL moieties, cleavable groups and regular or cyclo-aliphatic epoxy groups. **(C)** Development of multifunctional materials and their characterization, trying to understand the structure-properties relationships. **(D)** Selective solvolysis of the thermoset matrix, recovering IL derivatives or composites' components.

In summary, in this doctorate research, we endeavored to utilize computational chemistry to efficiently design second-generation of epoxy resins, then synthesize these molecules and craft materials that achieve high performance and satisfy the prerequisites of a circular economy.

Throughout our historical overview, we strove to tackle the first subquestion (I), and we have plans to re-visit the significance of (II) - namely, *what actual value does it add to Polymer and Material Science?* - in the section dedicated to conclusions and perspectives.

# 02

## Literature Review







of quaternary ammonium salts in liquid form as processing aids for cellulose.<sup>15</sup> Their capacity to dissolve diverse organic substances and be employed in liquid-liquid extraction has made them a favorable option for processing poorly soluble biopolymers.<sup>16-23</sup>

The main protagonists of this doctorate research, *i.e.* imidazolium salts, came to the forefront only in the 1980s, when Wilkes and other researchers explored the potential of ILs as electrolytes in batteries.<sup>4,24-26</sup> At this moment, ILs are a widely accepted choice for electrolytes in the electrodeposition of metals onto conductive materials.<sup>27-31</sup> Their primary benefit stems from their exceptional electrochemical stability, which enables the reduction of numerous metals at room temperature. ILs have also been employed as polymerization media in numerous pathways, such as free-radical, living radical, cationic, anionic, and condensation polymerizations.<sup>32-37</sup>

In addition, ILs find application as additives for modifying polymers, including serving as plasticizers for PMMA and PVC to replace phthalate esters, which are known to have adverse effects on human health. These studies aimed to propose new, potentially safe plasticizers while utilizing the versatility of ILs.<sup>38-42</sup> More recently, ILs have been highlighted to be a promising alternative to conventional compatibilizers for polymer blends, such as starch/zein, PP/PA, and polyesters, resulting in polymer materials with improved properties, such as enhanced water barrier or mechanical performances.<sup>43-49</sup> In recent times, ILs have also been studied as lubricants, surfactants, and templates for porous polymers.<sup>49-53</sup>

Furthermore, ILs have since garnered increasing interest in the field of thermosetting polymers. Consequently, new approaches to designing epoxy networks utilizing ILs as either unreactive or reactive functional additives have recently been reported.<sup>54-59</sup> Two primary approaches have been examined to merge epoxy thermosets and ILs: i) the use of ILs as functional or reactive additives in traditional epoxy prepolymers to either initiate the polymerization pathway or to tailor the polymer features and ii) synthesizing IL molecules that bear epoxy termini groups that can polymerize to build different crosslinked polymers.<sup>60,61</sup>

## **1.2. ILs as Reactive Additives to Tailor Thermoset Properties**

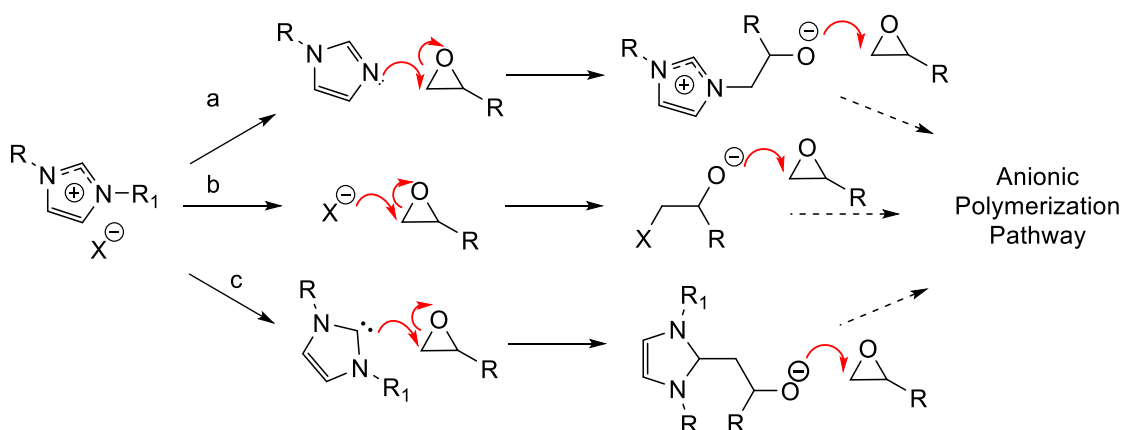
Multiple studies have explored the role of imidazole in initiating and catalyzing polymerization in epoxy thermosets. As a result of their comparable chemical structure, imidazolium ILs were initially described in the literature as potential new initiators for anionic polymerization in 2003.<sup>55,62-66</sup> The use of 1-butyl-3-methylimidazolium tetrafluoroborate as a latent hardener for epoxy prepolymer was first reported by Kowalczyk *et al.*<sup>67</sup> These researchers incorporated varying amounts of the IL (ranging from 0.5 to 5 phr) and studied

its effect on the crosslinking of the epoxy prepolymer at 190°C using FT-IR and DSC analyses. The imidazolium IL epoxy reactive mixture was stable at room temperature for up to six months without gelation phenomena. The polymerization mechanisms were not fully explained, leading to further research in this area by other investigators.<sup>62-65</sup>

Rahmathullah *et al.* were the first to demonstrate in 2009 the use of an imidazolium-based IL as an initiator for bisphenol-A diglycidyl ether (DGEBA) and to investigate the mechanisms of the crosslinking reactions.<sup>63</sup> The authors showed that the IL exhibited excellent miscibility with the epoxy precursors and that IL/epoxy mixtures remained stable at room temperature for extended periods.<sup>63,68,69</sup> Additionally, the authors revealed that the heat of reaction normalized by mole of epoxy groups was similar to the 100 kJ mol<sup>-1</sup> value reported in other studies for chain polymerization of DGEBA prepolymer. They observed two exothermic polymerization peaks suggesting a bimodal character corresponding to two mechanisms of polymerization. They argued that the first one could be started from the anion dicyanamide and the other by the eventual presence of imidazole resulting from the N-dealkylation of imidazolium.<sup>63</sup>

In 2012, Maka and colleagues explored the reactivity of epoxy prepolymer using various counter anions, including chloride, dicyanamide, and tetrafluoroborate, in combination with 1-butyl-3-methylimidazolium and 1-decyl-3-methylimidazolium ILs.<sup>68,69</sup> They also considered the mechanisms initiated by the anions and the imidazole resulting from the N-dealkylation pathway. They also proposed that the imidazolium could undergo deprotonation to form a carbene that could attack an epoxy, leading to the polymerization of the epoxy monomers.<sup>68</sup>

Thus, multiple reaction mechanisms for anionic polymerization have been proposed, as depicted in **Scheme II-1**. These include: **a)** the imidazole route resulting from the degradation of the imidazolium-IL into dealkylated products, **b)** the impact of the counter anion due to its nucleophilicity character, and **c)** the carbene route generated from the deprotonation of imidazolium.



**Scheme II-1.** Three reaction pathways to initiate the epoxy polymerization reaction from imidazolium-based IL: In **a**) the imidazole route derived from the dealkylating degradation reaction, **b**) nucleophilic attack from the anion and finally, **c**) the nucleophilic attack of the carbene generated by the deprotonation of imidazolium derivatives.

The various authors have emphasized that the different reaction mechanisms are frequently intertwined. This involves considering several parameters, such as: **i**) the concentration of the ILs, **ii**) the nucleophilic and steric-hindrance character of the anions, **iii**) the possibility of forming reactive species during the heating, and **iv**) the curing conditions.

Although numerous studies have reported the preparation of epoxy networks based on imidazolium ILs, very few works have investigated the resulting properties and the morphologies of these new networks.<sup>68–72</sup> This investigation into the physicochemical aspects of the resulting networks, including thermal stability, homogeneity, and mechanical properties, was pioneered by Maka's group.<sup>68,69,71,73</sup> They conducted several studies into reactive curing agents, which involved examining imidazolium ILs combined with chloride, dicyanamide, and tetrafluoroborate counter anions.

They investigated, for instance, the influence of 1-ethyl-3-methylimidazolium chloride (1,3 and 9 phr) on the final properties of epoxy networks prepared from low molar mass, based on bisphenol A Epdian 6.<sup>73</sup> Authors evaluated glass transition temperatures that fall between 90°C to 110°C. The mechanical performances were then evaluated using tensile, 3-point bending, and shear tests. The results showed that an increase in the amount of ILs led to significant plasticization of the resulting epoxy networks, significantly reducing the tensile, flexural, and shear strengths.<sup>73</sup> They concluded that adding 3 phr of imidazolium-IL led to optimal properties. This is likely because 3 phr represents a good compromise between the catalyst and plasticizer effects in the resulting epoxy networks.<sup>73</sup>

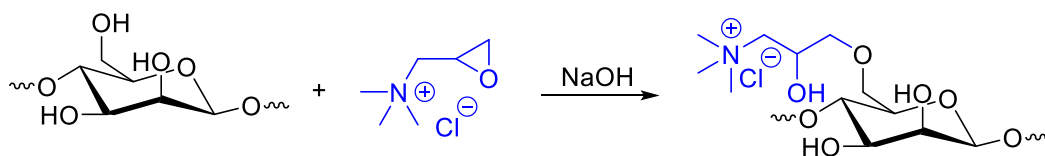
That year, the authors released a publication examining the impact of two different cations, specifically 1-butyl-3-methylimidazolium and 1-decyl-3-methylimidazolium with three different anions: chloride, dicyanamide, and tetrafluoroborate. The concentration of ILs and their reactivities were also investigated in terms of the thermomechanical properties.<sup>68</sup> They observed that the combination of imidazolium IL with dicyanamide counter anion demonstrated higher reactivity and led to a viscosity rise in the temperature range of 125-150 °C. In contrast, the same ILs combined with tetrafluoroborate anion exhibited the same effect at higher temperatures (200-240 °C).

Interestingly, no difference was observed in the reactivity of the systems based on the cation's chemical nature.<sup>68</sup> The epoxy networks were built with a  $T_g$  range of 55 to 180°C, and it was demonstrated that an IL concentration of 3 phr is optimal for achieving the highest crosslinking density.

### 1.3. Monoepoxidized ILs: The First Proposals

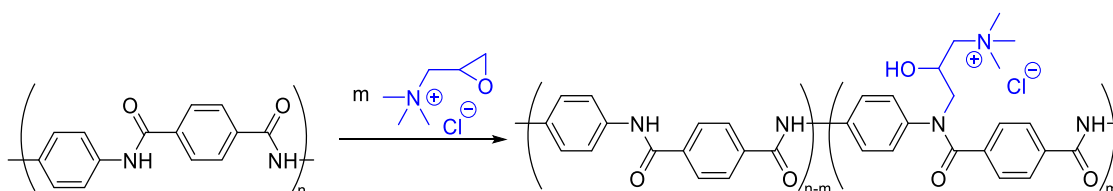
During the latter half of the 20th century, multiple research groups reported the production of an epoxy group-containing quaternary ammonium salt through amine alkylation using epichlorohydrin.<sup>74,75</sup> Subsequently, these salts were utilized to introduce the cationic group into various organic compounds owing to the high reactivity of the epoxy group.

For instance, GlyMe<sub>3</sub>NCl (2,3-epoxypropyltrimethylammonium chloride) was extensively employed to cationize diverse polysaccharides. **Scheme II-2** illustrates an example of this reaction.<sup>76,77</sup> Materials modified in this manner have been used in various industries such as food, cosmetics, petroleum, paper-making, and water treatment, and the publications concerning these materials have already been reviewed.<sup>76,78-80</sup>



**Scheme II-2.** Introducing ammonium-moieties in polysaccharide backbone through reaction with GlyMe<sub>3</sub>NCl.<sup>77</sup>

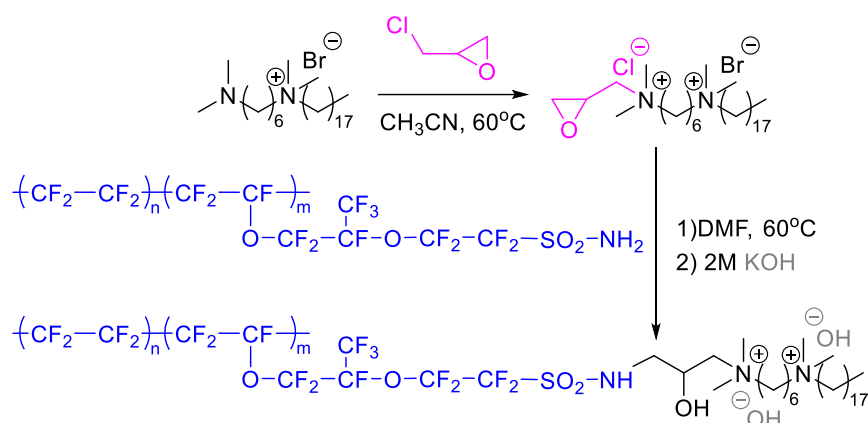
More recently, Ciejka *et al.* reported the functionalization of nano/microspheres of chitosan with GlyMe<sub>3</sub>NCl turning this biopolymer cationic.<sup>81</sup> Studies demonstrated that these particles have the ability to absorb human coronavirus (HCoV-NL63) and mouse hepatitis virus in a reversible manner. The same modification technique was also utilized on a synthetic polymer, poly(*p*-phenylene terephthalamide), to obtain ion exchange membranes resistant to organic solvent **Scheme II-3**.<sup>82</sup>



**Scheme II-3.** Modification of poly(*p*-phenylene terephthalamide) backbone through reaction with GlyMe<sub>3</sub>NCl.<sup>82</sup>

Endo *et al.* also used GlyMe<sub>3</sub>NCl followed by an ion exchange reaction with LiNTf<sub>2</sub> to obtain an ionic liquid at room temperature glycidyl trimethylammonium bis(trifluoromethanesulfonyl) imide (GlyMe<sub>3</sub>NNTf<sub>2</sub>).<sup>83</sup> Subsequently, the IL precursor was incorporated into a copolymerization process with amino-terminated polyethers and epoxy. The resulting networks exhibited low crystallinity and a *T<sub>g</sub>* of approximately -60 °C. Including quaternary ammonium groups slightly decreased the material's thermal stability. However, it resulted in an increase in ionic conductivity up to 2.8×10<sup>-3</sup> S/m at room temperature.<sup>83,84</sup>

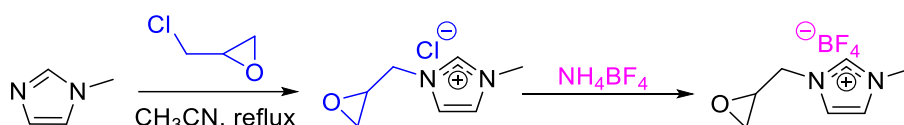
In a recent study, Liu *et al.* developed a new epoxy di-ammonium salt and used it to introduce hydrophilic ionic functionality into a perfluorinated polymer, as illustrated in **Scheme II-4**.<sup>85</sup> This innovative material was proposed for the production of ion exchange membranes used in fuel cells. Results demonstrated that the membrane exhibited an ion conductivity of 88.6 mS cm<sup>-1</sup> at 80°C and considerable alkali resistance.



**Scheme II-4.** Synthesis of epoxy di-ammonium salt and its subsequently reaction with poly(tetrafluoroethylene-co-perfluorovinyl ether sulfonamide).<sup>85</sup>

Essentially, epoxy-containing ammonium salts are valuable reagents for introducing cationic groups into polymer materials. However, their usage is limited by the requirement of toxic epichlorohydrin during synthesis and the relatively low thermal stability of quaternary ammonium, which restricts their application on an industrial scale.

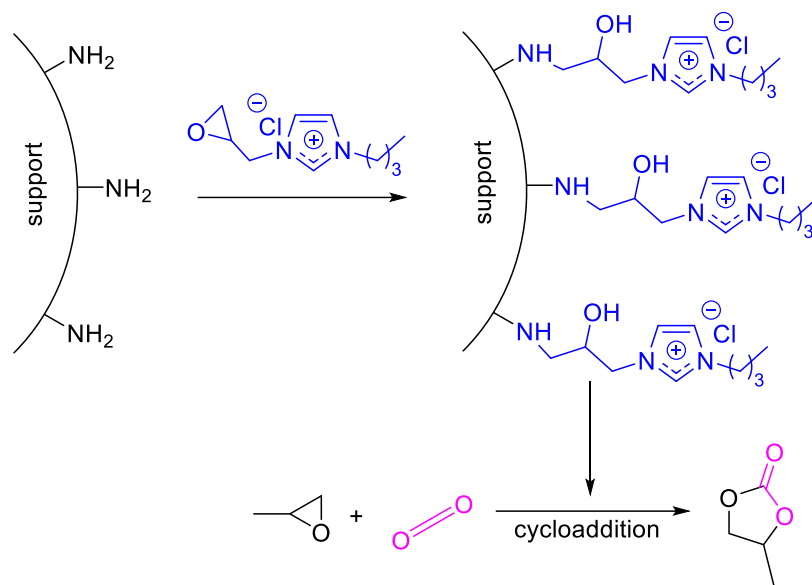
Demberelnyamba *et al.* devised a method for synthesizing various epoxy ILs, such as 1-glycidyl-3-methylimidazolium tetrafluoroborate, in order to introduce novel functionalities to room temperature ILs. **(Scheme II-5).**<sup>86</sup> To produce 1-glycidyl-3-methylimidazolium tetrafluoroborate, methylimidazole was reacted with epichlorohydrin, forming an imidazolium salt that was subsequently subjected to ion exchange with NH<sub>4</sub>BF<sub>4</sub>. However, the available characterization data for this compound is limited, with the authors only indicating that its T<sub>g</sub> is below -33.4°C without providing an exact value. Despite this, several subsequent studies have suggested various applications for this compound.



**Scheme II-5.** Epichlorohydrin-derived route to synthesize 1-glycidyl-3-methylimidazolium tetrafluoroborate.<sup>86</sup>

Xie *et al.* utilized this method to obtain 1-glycidyl-3-butylimidazolium chloride (GBIMCl) and used it to create supported catalysts for CO<sub>2</sub> cycloaddition reaction, as illustrated in **Scheme II-6.**<sup>87</sup> The researchers used the reaction between the amino groups present on the surface of modified silica or polymer spheres and the epoxy group in GBIMCl to connect the imidazolium group to the particles. These supported catalysts were then evaluated for their efficacy in facilitating the cycloaddition reaction between propylene oxide

and CO<sub>2</sub>. The findings revealed that the polymer-supported catalyst was even more efficient than free GBIMCl, and could be recycled up to 10 times without reducing its activity.



**Scheme II-6.** Synthesis of supported imidazolium catalyst and its application for cycloaddition reaction.<sup>87</sup>

Guo *et al.* have proposed an alternative method to produce a supported catalyst for the CO<sub>2</sub> cycloaddition reaction.<sup>88</sup> The researchers created a crosslinked copolymer by combining di-vinylbenzene with either 1-vinyl-3-epoxy imidazolium chloride or bromide, followed by hydrolyzing the epoxy groups to produce vicinal hydroxy groups. Results indicated that these networks containing imidazolium groups were effective catalysts for the CO<sub>2</sub> cycloaddition reaction with various epoxides (such as styrene oxide, epichlorohydrin, and cyclohexene oxide) and could be conveniently recycled.

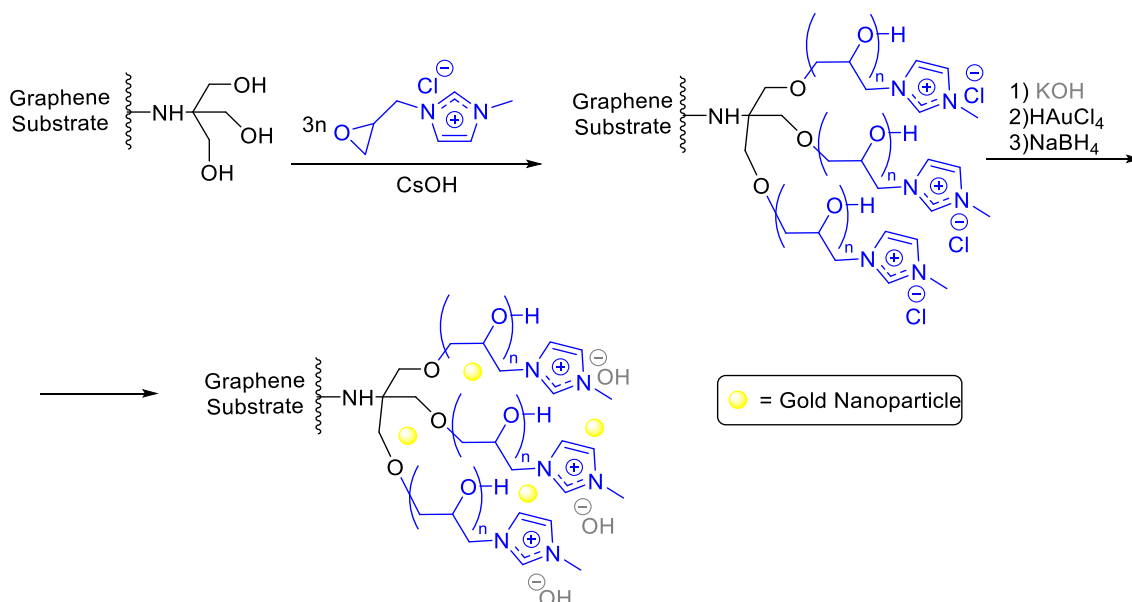
Eftekhari-Sis's group employed a method similar to the previously reported synthesis of supported catalysts using 1-glycidyl-3-methylimidazolium chloride to introduce ionic groups onto octa-aminopropyl polyhedral oligomeric silsesquioxane (OA-POSS).<sup>89</sup> The hybrids obtained were utilized to immobilize Cu or Ag nanoparticles, which were then utilized as catalysts for Cu-catalyzed click reactions and nitrophenol reduction, respectively. However, these supported catalysts experienced a partial activity loss after each recycling.

Xu *et al.* modified graphene using an epoxy imidazolium-IL.<sup>90</sup> They fixed 1-glycidyl-3-vinylimidazolium tetrafluoroborate on the surface of graphene through  $\pi - \pi$  stacking and polymerized it through the vinylic bond. The resulting modified graphene was then used to produce hybrid materials with 2,2-bis(4-cyanatophenyl) propane through thermal

curing. Including poly(IL) improved the dispersion of graphene in the resin matrix and enhanced the interaction between the resin and the nanofiller.

Liu's group, previously mentioned for their work on ammonium-perfluorinated polymer hybrids (**Scheme II-4**),<sup>85</sup> employed a similar approach to produce perfluorinated polymers with imidazolium functionality.<sup>91</sup> They also synthesized IL-functionalized graphene nanoribbons by reacting amino group-containing modified graphene with 1-glycidyl-3-methylimidazolium chloride. These two ionic hybrids were utilized to create a novel composite anion exchange membrane.

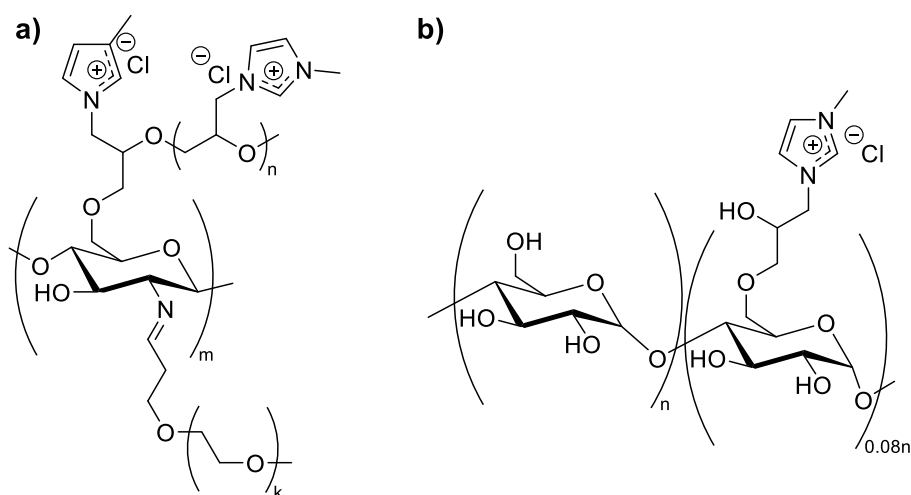
Gold's research team utilized epoxy IL to modify graphene, as well.<sup>92</sup> In their study, they utilized 1-glycidyl-3-methylimidazolium chloride to obtain gold nanoparticles supported on graphene that was grafted with a supramolecular IL. First, hydroxy groups that were present on the modified graphene were activated with cesium hydroxide to initiate the epoxide polymerization (**Scheme II-7**). Next, the obtained grafted poly(ionic liquid) was utilized to capture gold cations, which were then reduced to produce gold nanoparticles. This final compound was demonstrated to be an excellent catalyst for the selective aerobic oxidation reaction of primary and secondary alcohols into their corresponding aldehydes and ketones. A very similar approach was subsequently used to create Cu(I)@Fe<sub>3</sub>O<sub>4</sub> nanoparticles that were supported on imidazolium-based IL-grafted cellulose for N-sulfonylamidines and N-sulfonylacrylamidines synthesis.<sup>93,94</sup>



**Scheme II-7.** Synthesis of gold nanoparticles supported on supramolecular ionic liquid grafted graphene substrate.<sup>92</sup>



Two recent studies describe the modification of chitosan using epoxy imidazolium salt.<sup>95,96</sup> In one study, Lou *et al.* reacted the amino groups of chitosan with epoxy imidazolium salts, similar to the method shown in **Scheme II-1**.<sup>95</sup> However, the analysis provided was insufficient to confirm the suggested product structure. Nevertheless, the modified chitosan was shown to absorb Re(VII) selectively in the presence of other metal ions. In another study, Rahimi *et al.* modified chitosan using 1-glycidyl-3-methylimidazolium chloride.<sup>96</sup> Instead of using chitosan's amino groups, the OH groups in the C-6 position were activated with sodium methoxide to initiate epoxy ring-opening polymerization and graft the poly(imidazolium) chain. The remaining amino groups were used to link polyethylene glycol. The structure of the product is shown in **Fig. II-2**. Magnetic nanocarriers were added to the structure, and the compound was tested for targeted drug delivery, demonstrating promising results.



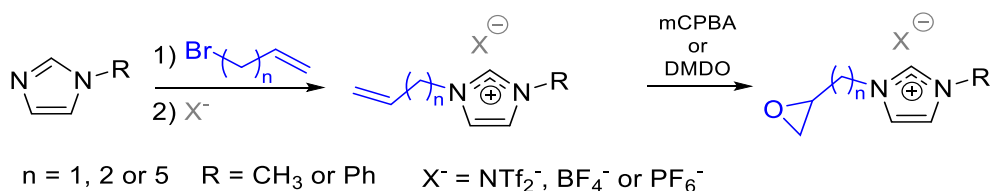
**Figure II-2.** Polysaccharide hybrids reported by Rahimi *et al.*<sup>96</sup> **a)** and by Lobregas *et al.*<sup>97</sup> **b)**

Cationic starch was obtained by Lobregas *et al.* through a reaction between 1-glycidyl-3-methylimidazolium chloride and the OH-group of starch, as depicted in **Fig. II-2b**.<sup>97</sup> The modified starch was used to create gels in DMSO along with additional free 1-glycidyl-3-methylimidazolium chloride as a plasticizer, which was then used to manufacture dye-sensitized solar cells. Likewise, Zhang *et al.* modified corn stalk polysaccharide by reacting it with 1-glycidyl-3-methylimidazolium chloride, resulting in a cationic polysaccharide that exhibited steel corrosion inhibition properties.<sup>98</sup>

Liao *et al.* proposed a method for synthesizing carbonaceous materials with a high surface area of 595 m<sup>2</sup> g<sup>-1</sup> using poly(1-glycidyl-2,3-dimethylimidazolium chloride) based on the knowledge that ILs and poly(IL)s serve as effective precursors for such materials.<sup>99</sup>

The authors suggested that the polymerization of 1-glycidyl-2,3-dimethylimidazolium chloride leads to the simultaneous synthesis and formation of poly(IL), which can subsequently be carbonized.<sup>100</sup> However, no empirical or analytical evidence was presented to validate this synthetic process.

In order to synthesize the aforementioned epoxy imidazolium-based ILs, the use of toxic and carcinogenic epichlorohydrin was required, limiting the practical applications of these methods in industry. To address this issue, our research group developed a clean and effective methodology for producing epoxidized imidazolium salts without the need for epichlorohydrin.<sup>101</sup> These monomers were suggested as an alternative to Bisphenol A diglycidyl ether (DGEBA), which is widely recognized for its endocrine-disrupting action. Initially, the authors developed methods for obtaining various imidazolium salts containing a vinylic function via the alkylation of commercially available N-methyl- or N-phenyl-imidazole using alkenyl bromide (as shown in **Scheme II-8**). They then thoroughly investigated the epoxidation reaction and found that dimethyldioxirane (DMDO) was a more efficient oxidizing agent than *m*CPBA, resulting in high yields of epoxides at room temperature in a shorter amount of time. Additionally, the only by-product produced in the reaction with DMDO is acetone, which can be easily removed through evaporation.

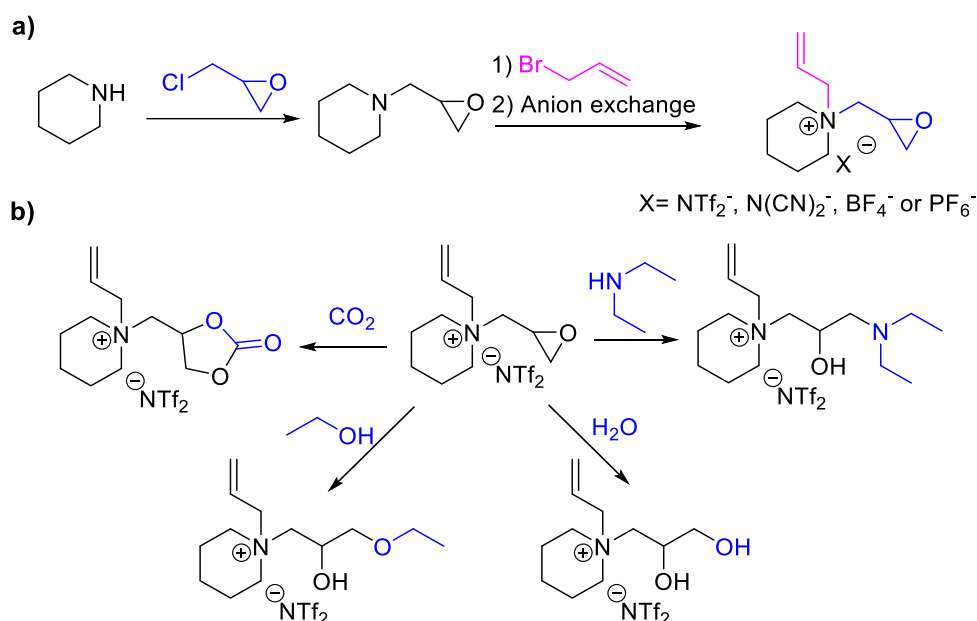


**Scheme II-8.** Synthesis of epoxy IL monomers suggested by Livi and Baudoux *et al.*<sup>101</sup>

While ammonium- and imidazolium-based epoxy-ILs have received the most attention in the literature, there have been some reports on the synthesis and application of epoxy pyridinium, piperidinium, pyrrolidonium, and triazolium salts. For example, Demberelnyamba *et al.* first reported the synthesis of pyridinium-based IL under the same conditions as the synthesis of 1-glycidyl-3-methylimidazolium tetrafluoroborate (as shown in **Scheme II-5**).<sup>86</sup> Later, Wang *et al.* used this reaction to obtain N-glycidylpyridinium chloride, which they then reacted with a primary amine to produce an ionic amino-alcohol. This compound was used to synthesize a hybrid with sodium phosphotungstate ( $\text{Na}_3\text{PW}_{12}\text{O}_{40}$ ), which demonstrated excellent catalytic activity in the Knoevenagel condensation reaction.<sup>102</sup>

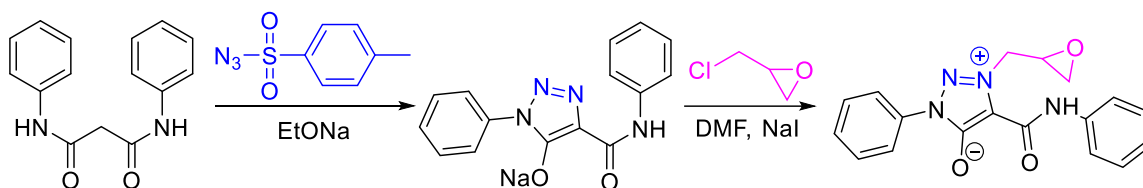
Tsuda *et al.* described the synthesis of ILs based on 1-allyl-1-glycidylpiperidinium (**Scheme II-9a**) and explored the potential for modifying these salts through the reactivity

of the epoxy group (**Scheme II-9b**).<sup>103</sup> The physical properties of the resulting epoxy ILs were thoroughly investigated, revealing that most of them exhibited a  $T_g$  within the range of -55 to -32°C. Only the IL containing the  $\text{PF}_6^-$  anion was solid at room temperature, melting at 90.5°C. Additionally, the IL with the  $\text{NTf}_2^-$  anion was the most thermostable, experiencing only 1% weight loss at 258°C. Notably, only the salts with  $\text{N}(\text{CN})_2^-$  and  $\text{BF}_4^-$  anions were soluble in water.



**Scheme II-9.** Synthesis of epoxy piperidinium salts **a)** and the reaction with one of them **b)** reported by Tsuda *et al.*<sup>103</sup>

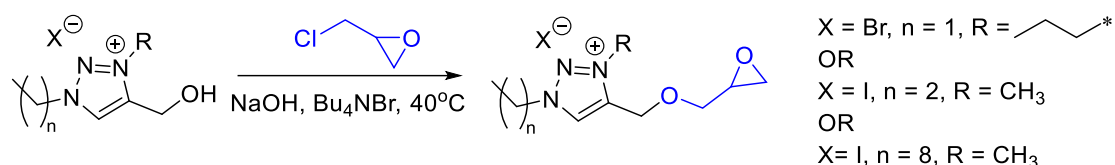
Nein *et al.* reported a noteworthy example of a triazolium-based epoxy salt.<sup>104</sup> They proposed synthesising a zwitterionic salt containing an epoxy group (**Scheme II-10**).



**Scheme II-10.** Synthesis of epoxy triazolium salt reported by Nein *et al.*<sup>104</sup>

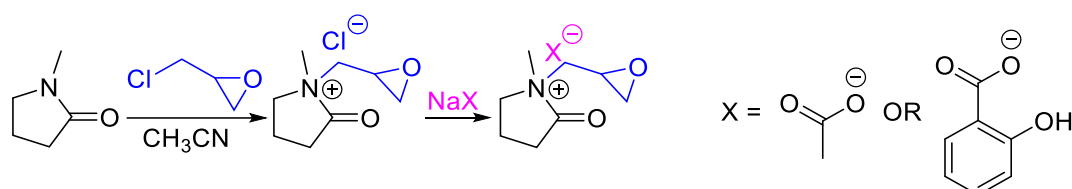
Although the melting point of this salt was reported to be 162°C, it cannot be strictly considered as an IL. However, Meinel *et al.* recently synthesized liquid epoxy-containing triazolium salts at room temperature (**Scheme II-11**).<sup>105</sup> The author employed the reaction between a triazolium salt containing an OH-group and epichlorohydrin to introduce an epoxy group. The ILs' biological activity against *Leishmania* parasites was examined, and it

was discovered that the IL with a long aliphatic chain (**n = 8, Scheme II-11**) exhibited the most pronounced effect while demonstrating negligible toxicity on murine macrophage.



**Scheme II-11.** Synthesis of epoxy triazolium ILs reported by Meinel *et al.*<sup>105</sup>

Vasanthakumar and colleagues have published a series of studies in which they demonstrated the synthesis of N-glycidyl-N-methyl-2-oxopyrrolidinium ILs with three different anions (as shown in **Scheme II-11**).<sup>106–110</sup> These ILs were then characterized by measuring their density, speed of sound, viscosity, and refractive index, both individually and in binary mixtures with various alcohols and acids such as methanol, ethanol, acetic acid, propanoic acid, and butanoic acid. Furthermore, the authors utilized N-glycidyl-N-methyl-2-oxopyrrolidinium chloride as a liquid phase in gas-liquid chromatography to determine the activity coefficients at infinite dilution for 30 organic compounds and water.<sup>110,111</sup>



**Scheme II-12.** Synthesis of epoxy oxopyrrolidinium ILs reported by Vasanthakumar *et al.*<sup>106–111</sup>

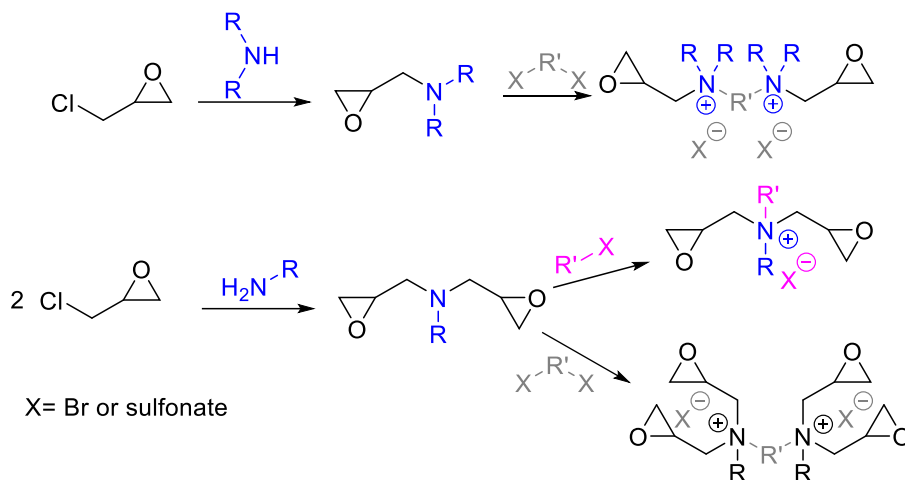
Various methods exist for obtaining mono-epoxy ILs with different characteristics. Among these, imidazolium-based epoxides have gained widespread use due to the availability of starting materials and the superior properties of the resulting compounds. Additionally, new techniques for synthesizing epoxy imidazolium salts enable the production of tailored ILs without using toxic or carcinogenic reagents.

#### 1.4. Bifunctional-Epoxy-Functionalized ILs

In 1963, Burness and Bayer synthesized organic salts with two epoxy-groups. They started by alkylating primary or secondary amines with epichlorohydrin to create tertiary amines with epoxide groups, as depicted in **Scheme II-13**. Then, they quaternized the amines with a mono- or di-functional alkylating agent to produce mono- or di-ammonium salts, respectively, containing two or even four epoxy groups (**Scheme II-13**).

The melting temperatures of the salts were reported by the authors to be between 48 to 242°C. However, some of the salts could not crystallize and were reported as *not isolated*. It should be noted that due to the early time of the study, analytical techniques were

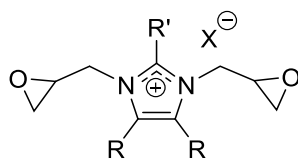
limited, and it could not be determined with accuracy whether the non-crystalline compounds were impure or not.



**Scheme II-13.** Synthesis of di- and tetra-epoxy imidazolium salts reported by Burness *et al.*<sup>75</sup>

The initial reference to an imidazolium salt containing two epoxide functions can be traced back to a publication from the mid-1980s.<sup>112</sup> The authors recommended employing 1,3-diglycidylimidazolium chloride to enhance the affinity of textiles to acidic dyestuffs. However, neither the synthesis of the salts nor its properties were described in the publication.

It wasn't until 1996 that the synthesis of diepoxy imidazolium salts was documented in scientific literature.<sup>113</sup> The authors conducted the alkylation of imidazole or one of its derivatives with epichlorohydrin in the presence of  $\text{NaClO}_4$  or  $\text{NaBF}_4$  to obtain the diepoxy imidazolium salts shown in **Fig. II-3**. The melting temperature of 1,3-diglycidylimidazolium perchlorate was reportedly around  $85^\circ\text{C}$ , indicating its status as an IL. Notably, salts that were 4,5-diphenyl-substituted demonstrated self-curing behavior at  $100\text{--}130^\circ\text{C}$ , although the properties of the cured materials were not examined. Later, Demberelnyamba *et al.* described a similar approach for synthesizing 1,3-diglycidylimidazolium tetrafluoroborate (also shown in **Fig. II-3**) by means of imidazole alkylation with epichlorohydrin and subsequent ion metathesis reactions with  $\text{NH}_4\text{BF}_4$ .<sup>86</sup>

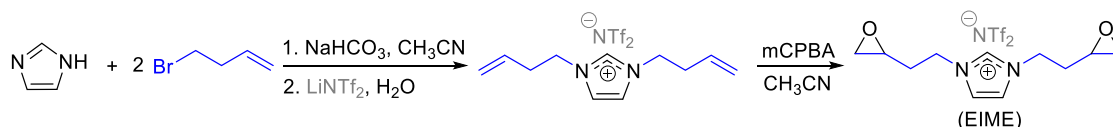


**Figure II-3.** The structure of diepoxy imidazolium salts: ref.<sup>112</sup>  $\text{X}=\text{Cl}$ ,  $\text{R}=\text{R}'=\text{H}$ ; ref.<sup>113</sup>  $\text{X}=\text{ClO}_4$  or  $\text{BF}_4$ ,  $\text{R}=\text{R}'=\text{H}$  or  $\text{R}=\text{R}'=\text{Ph}$  or  $\text{R}=\text{Ph}$ ,  $\text{R}'=\text{H}$ ; ref.<sup>86</sup>  $\text{X}=\text{BF}_4$ ,  $\text{R}=\text{R}'=\text{H}$ ;

Ten years later, Gin and Noble. investigated a novel synthetic method to obtain the diepoxidized IL-monomer and react it with an amine hardener.<sup>114</sup> Their research revealed that the methodology employed was unable to achieve high purity synthesis of the monomer, and it was also dependent on the use of hazardous epichlorohydrin.

Afterwards, they proposed a two-step route without using toxic and cancerogenic epichlorohydrin to overcome this challenge (**Scheme II-14**). The first step involved alkylation of imidazole by 4-bromobutene, followed by an anion exchange to obtain di-olefin imidazolium. The di-olefin imidazolium was then oxidized using *meta*-chloroperoxybenzoic acid (*m*CPBA) to produce the resulting diepoxy imidazolium IL (EIME).

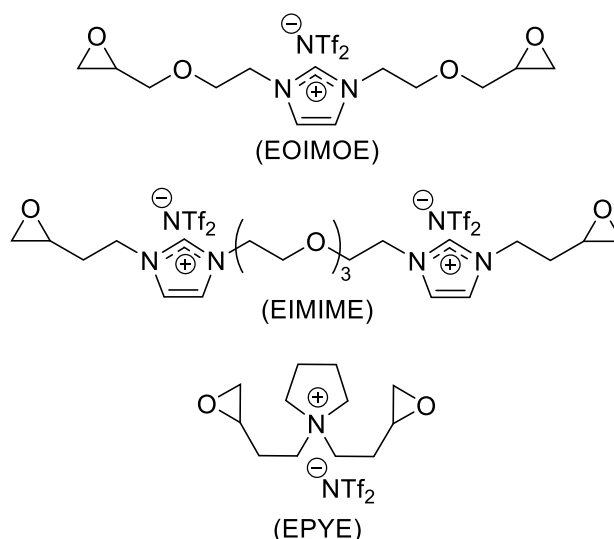
The synthesized EIME was used in a crosslinking reaction with tris(2-aminoethyl)amine (TAEA) at monomer ratios of 3:1 and 3:2 (EIME:TAEA), as well as in the presence of free IL up to 60 wt% to obtain neat networks or ion-gels, respectively. The reaction was conducted at 50°C, and the final conversion rate was approximately 70-80% for neat networks, decreasing to 40% at the maximal content of free IL. The networks were subjected to CO<sub>2</sub> sorption testing, and it was observed that the material with the 3:1 monomer ratio had a CO<sub>2</sub> uptake of 0.14 mmol g<sup>-1</sup>, while the 3:2 ratio led to 1.0 mmol g<sup>-1</sup> CO<sub>2</sub> uptake. This difference was attributed to the higher concentration of primary and secondary amines in the first network, which can interact with carbon dioxide. Ion-gels with free IL were used to produce gas separation membranes, and it was demonstrated that an increase in the concentration of free IL led to an increase in gas permeability while maintaining selectivity similar to that of previously described membranes.<sup>114-116</sup>



**Scheme II-14.** Synthesis of diepoxy IL monomer suggested by Gin *et al.*<sup>114</sup>

The same research team examined the impact of amine's nature on the crosslinking process of EIME and the characteristics of the obtained network.<sup>117</sup> As per their findings, the substitution of tris(2-aminoethyl)amine with tris[2-(methylamino)ethyl]amine resulted in a slower curing process but a rise in CO<sub>2</sub> permeability. The same approach used previously established methods to create three additional diepoxy IL monomers (**Fig. II-4**)<sup>117</sup>. These monomers were then used to investigate the impact of monomer structure on the resulting crosslinked material when cured with TAEA. The researchers discovered that EOIMOE and EIMIME (**Fig. II-4**) took longer to achieve high epoxide conversion than EIME. This was attributed to diffusion limitations for the larger molecular weight molecules.

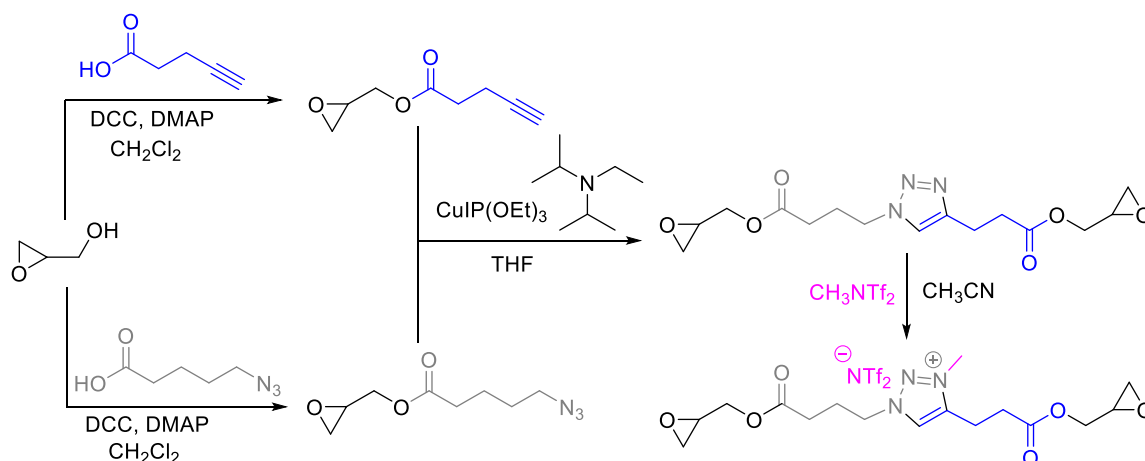
It was demonstrated that as the molecular weight of the monomer increased, the glass transition temperature ( $T_g$ ) of the crosslinked networks produced with TAEA decreased:  $T_g(\text{EIME}/\text{TAEA})=9^\circ\text{C}$ ,  $T_g(\text{EOIMOE}/\text{TAEA})=5^\circ\text{C}$ ,  $T_g(\text{EIMIME}/\text{TAEA})=-27^\circ\text{C}$ . The molecular weights of EIME and EPYE were nearly identical (489 and 492  $\text{g mol}^{-1}$ , respectively), yet the  $T_g$  of the EPYE/TAEA network was slightly lower ( $5^\circ\text{C}$ ). The authors explained this phenomenon as an increase in physical interactions resulting from hydrogen bonding and  $\pi$ - $\pi$  stacking forces of the imidazolium ring that are absent in the pyrrolidinium system. The  $\text{CO}_2$  permeability of the resulting materials depended on the number of amino-groups in the network, while the chemical structure of the epoxy monomer did not significantly impact the outcome. Briefly, this study involved the synthesis of three new diepoxy IL monomers, and the curing of these new monomers with TAEA was assessed to evaluate the effect of monomer structure on the properties of the crosslinked materials. EOIMOE and EIMIME required more time to achieve high epoxide conversion than EIME, ascribed to diffusion limitations for the higher molecular weight molecules.



**Figure II-4.** The structures of the diepoxy IL monomers.<sup>117</sup>

Drockenmuller and Duchet-Rumeau reported a new type of diepoxy IL and investigated its epoxy-amino networks.<sup>118</sup> The synthesis involved using glycidol as a starting material for Steglich esterification reaction to incorporate alkyne and azide functionalities (**Scheme II-15**). The two esters underwent copper-catalyzed alkyne-azide cycloaddition to form a 1,2,3-triazole containing two epoxy groups. Subsequent alkylation of the triazole with N-methyl-bis(trifluoromethylsulfon)imide yielded 1,2,3-triazolium-based diepoxy IL in high yield (**Scheme II-15**).

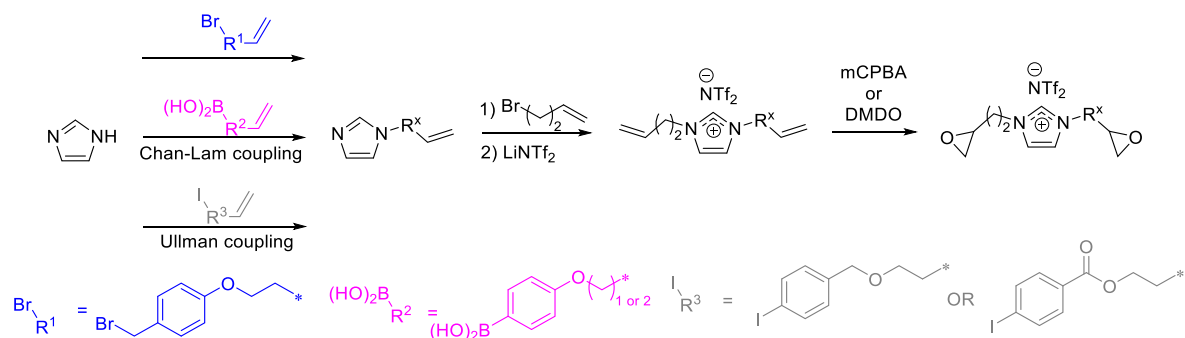




**Scheme II-15.** Synthesis of diepoxy triazolium-based IL monomer suggested by Drockenmuller and Duchet-Rumeau.<sup>118</sup>

To synthesize the epoxy-amino network, poly(propylene glycol) diamine (DP<sub>n</sub>=33) was used with the obtained diepoxy IL. The resulting networks exhibited good thermal stability with  $T_{10\text{wt}\% \text{ loss}} = 308^\circ\text{C}$  and  $T_g = -52^\circ\text{C}$ . The researchers found that the ionic conductivity of the network at  $30^\circ\text{C}$  reached a high value of  $2 \times 10^{-7} \text{ S cm}^{-1}$  and could be increased to  $10^{-6} \text{ S cm}^{-1}$  by adding 10 wt% of LiNTf<sub>2</sub>.

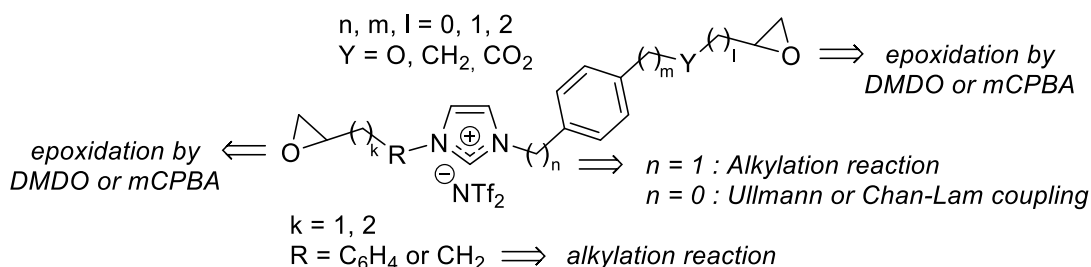
Livi and Baudoux made a notable contribution to the field of thermosets based on epoxidized ILs. They developed a robust and effective methodology for obtaining diepoxidized imidazolium salts. In their work, they first developed methods for obtaining various imidazolium salts with two vinylic functions. They used alkylation by alkyl halogenides, Chan-Lam coupling, and Ullman reaction to synthesize several alkenes (**Scheme II-16**). Then, the epoxidation reaction was optimized, and various methodologies were proposed using different reactive chemicals. The researchers found that dimethyldioxirane (DMDO) was a more efficient oxidizing agent than *m*CPBA. Using DMDO as the oxidizing agent allowed for high yield and fast epoxidation at room temperature. Additionally, only acetone is produced as a by-product, which can be easily removed through evaporation. The thermal properties of the resulting diepoxy ILs were studied, and it was found that the presence of ether or ester groups resulted in a slight decrease in degradation temperature, which is expected considering the additional degradation pathways. However, all of the salts that were studied exhibited excellent thermal stability (up to  $400^\circ\text{C}$ ).<sup>101</sup> The researchers noticed that the newly developed IL monomers produced networks with  $T_g$  values between  $-52$  and  $-30^\circ\text{C}$ .



**Scheme II-16.** Synthesis of diepoxy IL monomers suggested by Livi and Baudoux *et al.*<sup>101,119</sup>

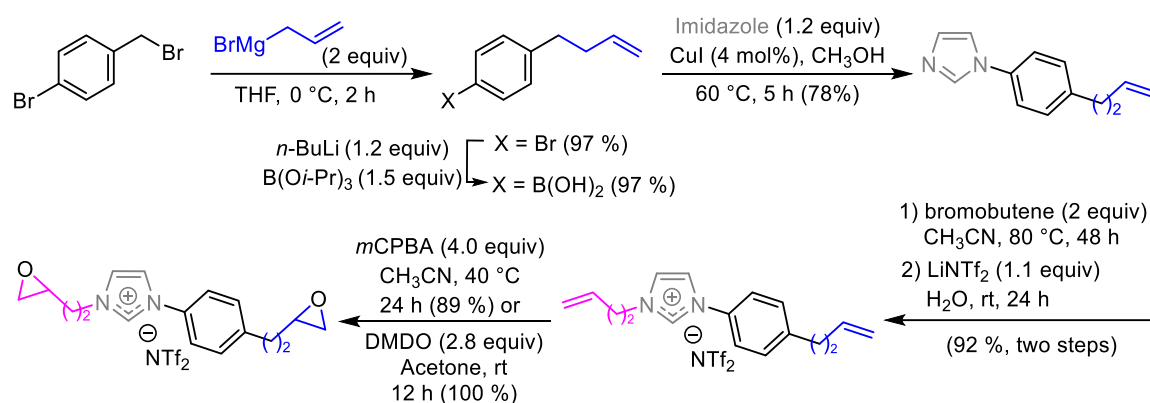
Livi and Baudoux *et al.* have then explored the reaction of the synthesized diepoxy IL with amines.<sup>120</sup> Through the use of model compounds, they demonstrated that the epoxy IL readily reacts with primary and secondary amines, while the reaction with tertiary amines is limited depending on the temperature conditions. No reaction between the hydroxy groups and the remaining epoxides was observed. This mechanism was applied to the reaction of diepoxy IL with polyetheramine (Jeffamine D230) to produce epoxy-amino networks. The researchers discovered that these networks have desirable properties, including high thermal stability ( $>300^\circ\text{C}$ ),  $T_g=55^\circ\text{C}$ , and an ionic conductivity of  $4 \times 10^{-4} \text{ S m}^{-1}$  at  $70^\circ\text{C}$ . Furthermore, these epoxy-amino materials demonstrated high efficacy against microorganisms, such as *Escherichia coli*, opening perspectives in the field of active surface coatings.<sup>121</sup>

More recently, our research group proposed various synthetic pathways for molecularly engineering epoxidized ILs and subsequently examined the polymer properties obtained. Several epoxidized-ILs were proposed bearing imidazolium and aromatic moieties. The Ullmann and Chan-Lam coupling reactions were used to introduce the aromatic rings into the monomer backbones. Additionally, the thermal stability and  $T_g$  were investigated as a function of the nature of  $n$ ,  $m$  or  $Y$  in the molecular backbone (**Fig. II-5**). The presence of aliphatic spacers ( $R$ ,  $k$  and  $l$ ) was also evaluated during the design of the novel monomers.



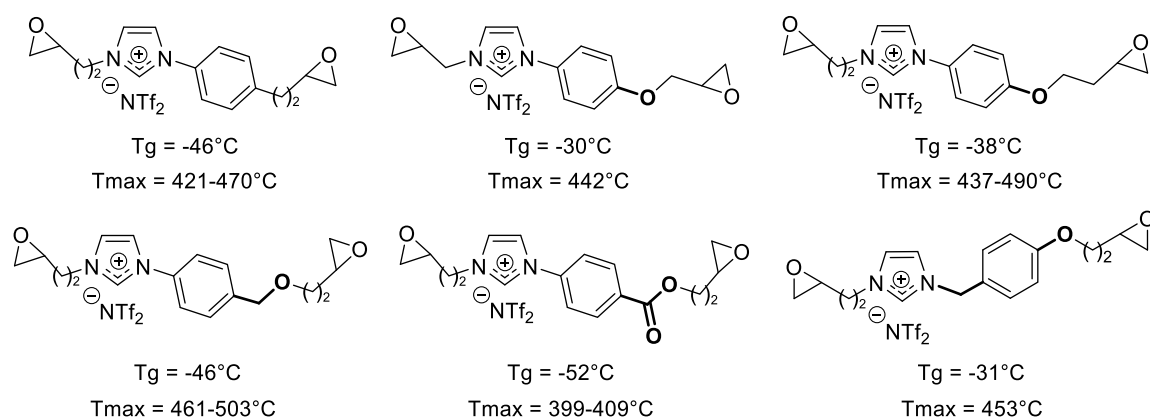
**Figure II-5.** Structure of the diepoxy aromatic imidazolium salts.<sup>101</sup>

This molecular design proposed a diepoxy imidazolium salt through a Cham-Lam coupling, according to the sequence below **Scheme II-17**. Using allylmagnesium bromide and 4-bromobenzyl bromide, the authors were able to synthesize aryl bromide with terminal alkene in a yield of 97%. Then, a carbon-nitrogen bond was created through copper-catalyzed arylation to form the aryl-imidazolium backbone. The resulting product was purified, and 4-bromo-1-butene was added to aryl-imidazole, yielding imidazolium bromide. The ionic exchange was carried out in water through an anionic metathesis using LiNTf<sub>2</sub>. The authors then oxidized the imidazolium-based substrate with an excess of *m*CPBA (4 equivalents) or DMDO (2.8 equivalents) to obtain the final epoxidized salt.



**Scheme II-17.** Synthesis of diepoxy aryl-imidazolium-based IL monomers.<sup>104</sup>

The thermal stabilities of the net epoxidized IL monomers were excellent, with a maximal degradation temperature ( $T_{\max}$ ) ranging from 390–400°C (**Fig. II-6**). The authors noted that a one-carbon aliphatic spacer between imidazolium and phenyl led to lower thermal stability. This confirmed the potential use of aryl-imidazolium combination for designing novel monomers.



**Figure II-6.** Some examples of diepoxy aryl-imidazolium salts.<sup>101,104</sup>

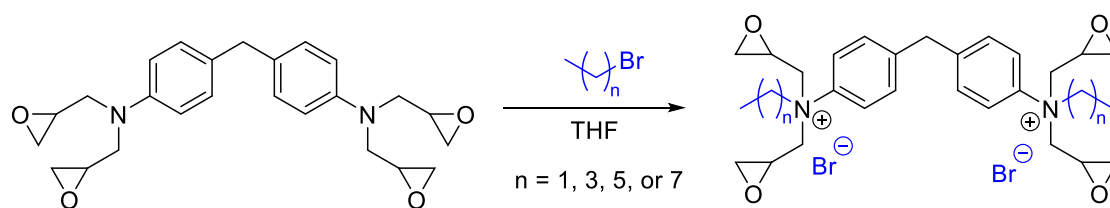
In 2020, a new IL monomer was synthesized by Radchenko & Chabane *et al.*, which had two imidazolium moieties and was used to prepare epoxy thermosets with isophorone diamine (IPD).<sup>126</sup> The authors demonstrated the formation of an inhomogeneous network characterized by the presence of two alpha transitions, which they attributed to the presence of unreacted secondary amines acting as chain extenders and displaying better molecular mobility. The resulting networks showed excellent thermal stabilities compared to conventional epoxy-amine networks (DGEBA-IPD), and had a Young's Modulus of 1.63 GPa and an elongation at break of 28%, instead of 2.6 GPa and 5%, respectively, for DGEBA-IPD networks. The authors explained this difference by the lower crosslinking density of the new networks. Additionally, the use of ILs as an epoxy prepolymer resulted in a hydrophobic network with contact angle values similar to those of a polytetrafluoroethylene matrix, which could lead to new and promising perspectives in the preparation of hydrophobic surface coatings for various applications, such as in the automotive, aerospace, or electronic fields.

Up to this stage, the methods presented for synthesizing diepoxy ILs have provided a variety of compounds with diverse functionalities. Some of these diepoxy ILs were used to prepare epoxy-amine networks that demonstrated favorable characteristics for applications such as solid electrolytes, gas separation membranes, or antibacterial coatings.

### 1.5. Epoxidized ILs With Multiple Epoxy Groups

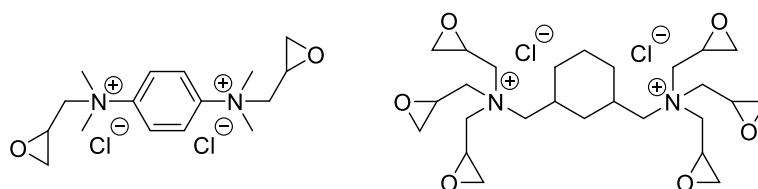
Monomers with more than two epoxy groups can be helpful to tailor the characteristics of epoxy-amine networks.<sup>122</sup> Although the synthesis of a tetra-epoxy ammonium salt was documented in 1963,<sup>75</sup> only one research article has reported the synthesis of an IL with more than two epoxides since then. To obtain tetra-functional epoxy IL monomers, Wynne *et al.* have used commercially available 4,4'-methylenebis(N,N-diglycidylaniline) in a one-step synthesis (**Scheme II-18**).<sup>123</sup>

The tetra-functional epoxy IL monomers synthesized were treated with di-amino polydimethylsiloxane to form networks that exhibit a remarkable capacity to eradicate as much as 99.9% of pathogenic bacteria from their surface. The glass transition temperatures ( $T_g$ ) of all the resulting poly(IL) networks were in the range of 66 – 85°C, whereas their storage modulus at 25°C varied from 150 to 230 MPa. According to the study, the networks containing quaternary ammonium moieties exhibited lower thermal stability, as indicated by their onset degradation temperatures ranging between 255 – 297°C. These temperatures were inferior to those observed for networks manufactured from the commercial monomer.



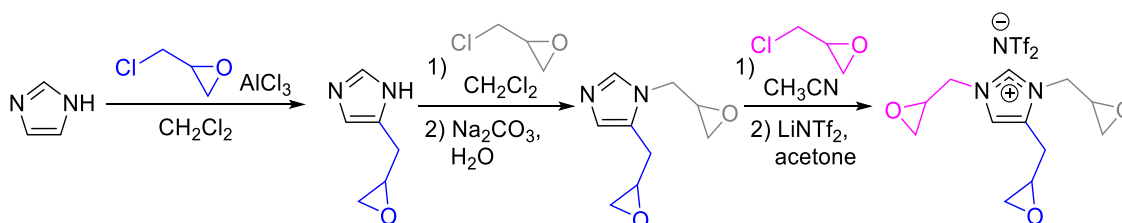
**Scheme II-18.** Synthesis of diepoxy IL monomers suggested by Wynne *et al.*<sup>123</sup>

Ammonium-based multi-epoxy salts can be found in other instances within patent literature.<sup>124</sup> Nishioka *et al.* detailed the synthesis of 24 distinct salts that contain epoxy-functionality ranging from 2 to 6, and **Fig. II-7** illustrates two examples. Nevertheless, despite the library of molecules that the authors proposed, the use of epichlorohydrin and the relatively limited thermal stability of quaternary ammonium salts hinder their potential for industrial application.



**Figure II-7.** Examples of the structures of the epoxy salts.<sup>124</sup>

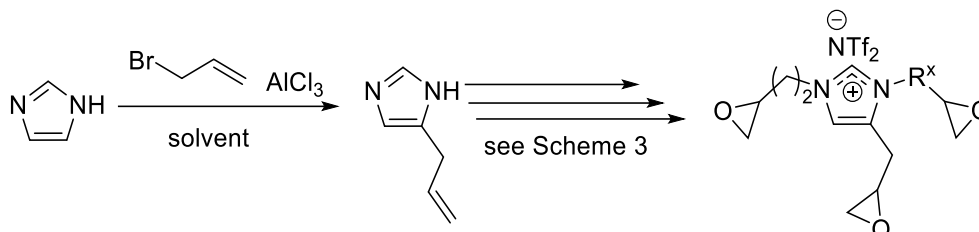
Despite its greater thermal stability compared to quaternary ammonium salts,<sup>120</sup> there is only one example of an imidazolium salt containing more than two epoxy groups reported in the literature.<sup>125</sup> The inventor proposed a synthetic route beginning by Friedel-Crafts alkylation of the imidazolium C-C bond with epichlorohydrin to introduce the first epoxy group (**Scheme II-19**). The second and third epoxy groups were introduced similarly to the previously described methodology through nucleophilic substitution reaction.<sup>86,113</sup> Unfortunately, the properties of the networks derived from the tri-epoxy imidazolium salt were not described probably due to the specificity and limitation of the patent.



**Scheme II-19.** Synthesis of triepoxy IL monomer from an epichlorohydrin-based route.<sup>125</sup>

Scrutinizing the literature, it seems clear the necessity of new and more sustainable methodologies to obtain multi-epoxidized IL monomers that are thermally stable and do not employ such toxic reagents as epichlorohydrin. The synthetic challenge is to develop

methodologies for the epoxidation reaction of complex substrates.<sup>101,104</sup> For example, the molecule presented in **Scheme II-20** could be synthesized from an allyl bromide via Friedel-Crafts reaction to obtain the C-substituted imidazole followed by two nucleophilic reaction and the epoxidation reaction proposed by Livi and Baudoux.<sup>101,119</sup>



**Scheme II-20.** A possible way to obtain triepoxy IL monomers.

This strategy of synthesizing epoxidized IL monomers, which is still in its early stages, presents exciting opportunities for designing novel epoxy monomers and thermosets with functional properties. This research area has demonstrated that it is possible to substitute DGEBA prepolymer for environmentally friendly monomers, offering a promising alternative to toxic and carcinogenic compounds like bisphenol A and epichlorohydrin. While these new monomers based on imidazolium or triazolium cores were initially produced for designing polymer gel electrolytes, they could also be used in combination with urea, anhydride, or amine hardeners to develop high-performance epoxy networks. The impact of architecture on the functional properties of these networks requires further investigation. Thus, developing new synthetic methods is crucial for designing innovative polymer materials and proposing sustainable solutions that meet the requirements of the circular economy, such as being durable, reusable, and recyclable.

Our research aims to manufacture multifunctional thermoset materials using an efficient design approach that involves creating molecular brick platforms that afford different features to polymers according to their designed structure. We also intend to implement the *design to degrade* concept to account for the end-of-life of these multifunctional materials and facilitate their reuse in a closed-loop supply chain.

## 2. Potential and Limitations of Recycling Thermosets and Composites

### 2.1. General Aspects & Environmental Regulations

Since the development of the first synthetic polymer, plastics have become an essential material in our lives, with applications ranging from consumer goods to medical and electronic devices.<sup>127</sup> The importance of plastics is ascribed to their outstanding properties, notably, their high strength, low density, chemical stability, low processing cost, and affordability.<sup>128</sup> However, the increasing demand for petroleum-based plastics is associated with

the pressing issue of air, water, and soil pollution.<sup>127</sup> The concept of circular economy popularized by the Ellen MacArthur Foundation advocates decreasing waste and pollution and the development of circular materials.<sup>129</sup> Although only 10% of all produced plastics are recycled worldwide, the recycling and reprocessing of thermoplastic materials can be relatively easily achieved from a technological point of view.<sup>130</sup>

Thermoset materials are classified among the most challenging materials to reprocess or recycle.<sup>131,132</sup> The defining feature of a thermoset is the presence of covalent inter-chain crosslinks that afford enhanced mechanical properties and resistance, avoiding chain sliding compared to thermoplastic analogues.<sup>131,132</sup> Consequently, these materials exhibit high thermal, chemical, and mechanical stability, becoming highly suitable for structural and protective applications.<sup>131</sup> However, a primary consequence of this chemical and thermal stability is difficult to reprocess and recycle.<sup>133,134</sup>

The main classes of thermosets are epoxies, polyurethane, polyester, phenolic and alkyds resins.<sup>131</sup> These thermosets are often employed as components in composites formulation to reinforce fibers, for instance, generating resistant lightweight materials.<sup>135</sup>

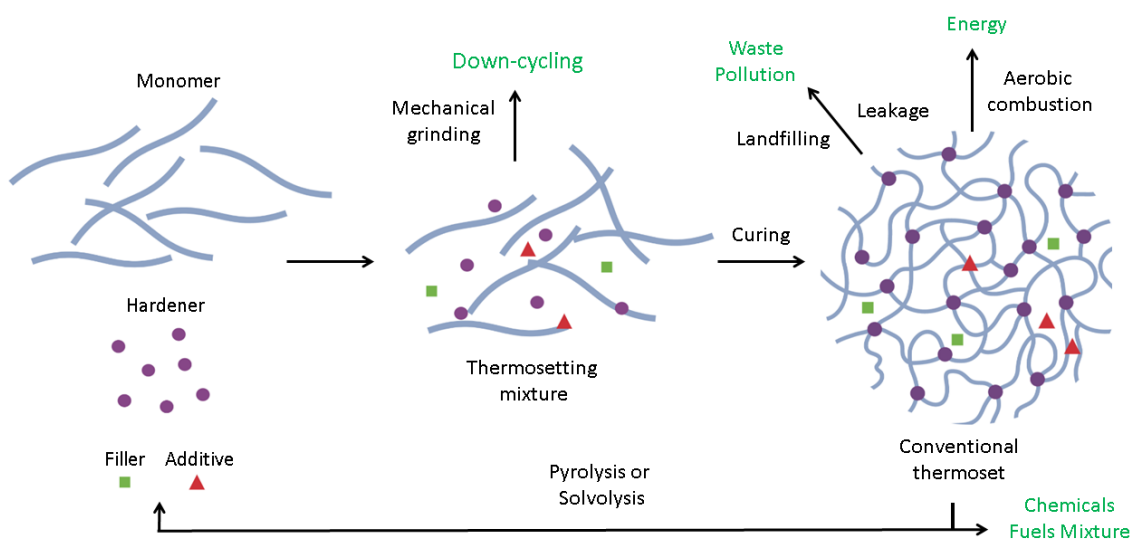
As environmental regulations are becoming more stringent, the importance of recycling is gaining widespread recognition.<sup>136</sup> In the coming years, many countries will pass laws to oversee the disposal of thermosets and carbon-fiber-reinforced polymers (CFRPs). The objective is to include such waste materials in the category of recyclable polymers.<sup>137</sup>

The landfill has almost disappeared in some countries, like Germany, Austria, Belgium, and Denmark, and composite materials can no longer be landfilled in Germany and Netherlands.<sup>138,139</sup> In France, since January 2022, composites containing more than 30% plastics cannot be deposited in landfills.<sup>138,140</sup> These statutes directly impact the waste management of retired wind turbine blades, typically composed of fiber glass, carbon fiber, and epoxy resins. The European Technology & Innovation Platform on Wind Energy predicts that the combined weight of decommissioned wind turbine blades will reach 66 ktons by 2025.<sup>138,141</sup>

## **2.2. Conventional Recycling Methodologies for Thermosets and Composites**

The development of thermoset and CFRP recycling methodologies has significantly accelerated in the past decades since European Union has devoted much effort to managing waste in landfills and producing eolic renewable energy from wind turbines built from thermosets.<sup>142</sup> Another driver is the recovery of carbon fibers and fillers from fiber-reinforced composites, considering that carbon-fiber are usually more valuable than the thermoset matrix.<sup>143–145</sup>

The European Union Waste Framework's guidelines suggest that the most effective recycling method is to reuse the materials in a similar or inferior performance application without any transformation step.<sup>139</sup> Although direct reuse is preferable, this alternative tends to be limited since the thermoset materials present non-adaptable fixed shapes. Therefore, direct reuse does not significantly contribute to solving the thermoset waste dilemma. Three main strategies have been industrially employed to address this question: mechanical, thermal, and chemical recycling processing.<sup>137</sup> A general scheme of conventional thermoset composite waste management and recycling strategies is represented in **Fig. II-8**.<sup>146</sup>



**Figure II-8.** Schematic overview of conventional thermoset composite waste processing and recycling routes.<sup>133,137,147,148</sup>

### 2.3. Mechanical Recycling

Mechanical recycling consists in reducing- and homogenization-size processing of solid waste materials and can be applied for thermoset or thermoplastic materials generating grains with the typical size of 50-100 mm.<sup>133,149</sup> This technique employs hammer mills or high-speed mills to crush the scrap flakes into thinner grains of several millimeters that can be thermally reprocessed for the thermoplastics.<sup>133</sup> In the case of CFRP, this technique is not considered the most adequate since it does not separate the carbon fiber from the thermoset matrices, providing at the end of the process a thin powder that can be employed as filler without the orientational properties of the initial fibers.<sup>137</sup>



According to Morin *et al.*, if a thermoset composite is filled with 50% of recovered CFs and combined with virgin CFs, its mechanical properties would not be significantly affected. However, if it is filled with more than 50% of recycled CFs, the mechanical properties are generally sensibly deteriorated.<sup>150</sup>

Palmer *et al.* managed this issue by developing a methodology in which they maintained the fibrous structures of the carbon fibers after the grinding process, which were effectively re-employed as reinforcing fillers in sheet molding compounds.<sup>151</sup> The elevated toughness of CFRP demands extremely resistant machinery and more frequent maintenance. Therefore, the mechanical recycling methodology has been mainly employed for simpler composites based on glass fibers instead of CFRP counterparts.<sup>137,152-154</sup>

## **2.4. Thermal Waste Management**

Thermal waste management can be divided into incineration and pyrolysis, corresponding to combustion in the presence or absence of oxygen, respectively.<sup>149,152,155</sup> The incineration results solely in energy recovery, whereas pyrolysis is often employed to recover and recycle the substrates of composites.<sup>149</sup> Indeed, pyrolysis involves the thermal decomposition of the polymeric matrix in a nearly oxygen-free environment, typically under an inert atmosphere of nitrogen or argon.<sup>156</sup>

The final properties of the recovered CFs rely on different parameters, namely, temperature, time, atmosphere composition, and nature of the thermoset matrices. Pickering *et al.* controlled the oxygen feeding during the combustion to selectively decompose the thermoset matrix and recover the carbon fibers from CFRP composites.<sup>152</sup>

Contrarily to the incineration process, pyrolysis imposes a limited decomposition degree meaning that the degradation products will partially preserve the chemical nature of the matrices.<sup>156</sup> The working range temperature is within 300-850 °C, and the yielding byproducts can be used as feedstock for future chemical processing.<sup>156</sup> The pyrolysis conditions enable the recovery and partial maintenance of the carbon-fiber properties when employed to recycle CFRPs.<sup>155,157</sup> The crystallinity, sizing, and surface composition modification are commonly observed during pyrolysis.<sup>133,152</sup> Additionally, the manufacture of virgin CFs typically involves an energy expenditure of 183-286 MJ kg<sup>-1</sup>, whereas pyrolysis requires 10 to 50% of that amount.<sup>158</sup>

The pyrolysis efficiency can be further enhanced in the presence of catalysts. Cipriotti and co-authors improved the recycling yield of waste electronic equipment waste by employing fly ash to catalyze the pyrolysis.<sup>159</sup> Though pyrolysis is considered as an economi-

cally and technologically scalable strategy, it is still questionable from a sustainability perspective. Thus, continuous research investigates the reduction of pollutant emissions, the selective decomposition and the better re-employment of thermal energy.<sup>133,134</sup>

## **2.5. Chemical Recycling**

Solvolysis, also known as chemical degradation, corresponds to the employment of a solvent to degrade, dissolve or depolymerize polymer networks, usually in the presence of a catalyst.<sup>160,161</sup> Like pyrolysis, it allows the recovery of reinforcing fibers or fillers from composites.<sup>156</sup> The advantage is that the degradation products derived from the thermoset's networks are often reused as molecular building blocks to build subsequent generations of materials.<sup>162</sup>

Solvolysis can be divided into three categories: hydrolysis, glycolysis and acid digestion.<sup>160,161</sup> The solvent choice and secondary conditions rely on the polymer reactivity and the targeted degradation reactions. More importantly, this strategy demonstrated suitability for various thermoset networks, including epoxy-amine,<sup>163</sup> epoxy-anhydride,<sup>164</sup> polyester,<sup>162</sup> and polyurethane.<sup>165</sup>

Recently, several researchers have investigated using supercritical fluids as solvents since they present advantageous features such as high mass transport coefficients, high diffusivities, and low viscosities that can be adjusted as a function of the pressure.<sup>166</sup>

Okajima and coworkers, for instance, used supercritical methanol at 270 °C and 8 MPa for 90 min to recover carbon fiber from epoxy-amine composites.<sup>167</sup> Other authors reported a recycling approach for anhydride-cured epoxy networks using alcohol and a catalyst to induce the degradation through a transesterification reaction.<sup>155,161,162</sup>

More recently, Dang *et al.* chemically dissolved conventional epoxy resins by employing a high concentrated nitric acid solution and an ultrasound microwave.<sup>168</sup> Such recycling methodologies devised for commercial-based polymers are inconvenient from an industrial point of view because they operate under elevated pressures and temperatures and require expensive catalysts or highly hazardous chemicals.<sup>155,161,162,169</sup>

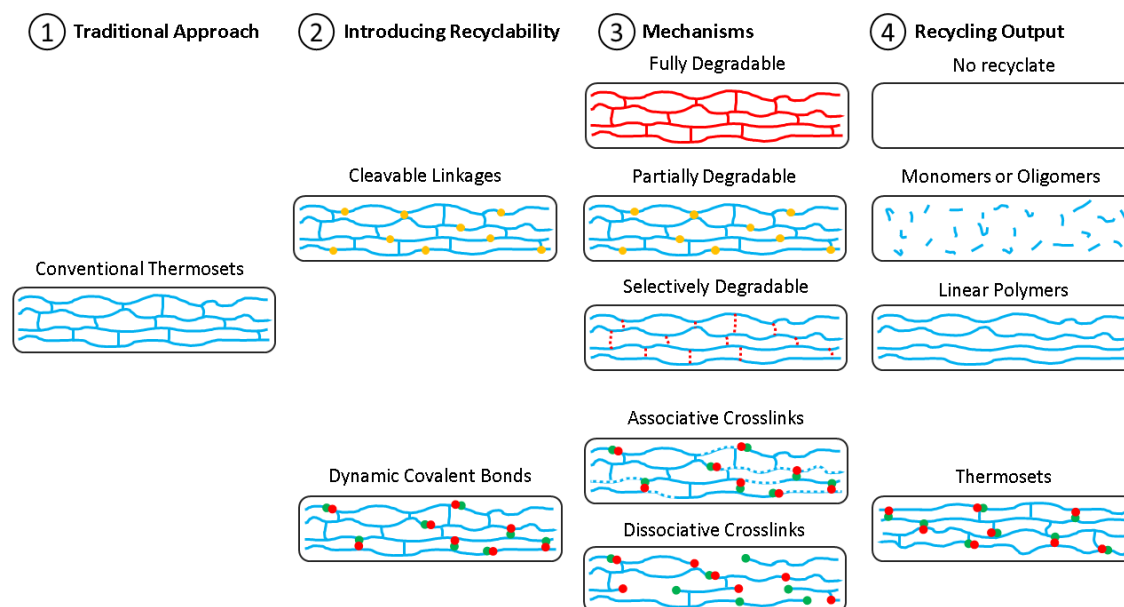
## **2.6. Designing Stimuli-Triggered Degradable Networks**

While conventional methodologies provide a partial solution to the challenge of thermoset recyclability, recycling both polymer substrates and additives is essential to achieve the circular economy objectives.<sup>170,171</sup> Alternatively, thermoset polymers can be designed in such a way that low energy-requiring external stimuli trigger degradation on demand while maintaining their outstanding performance.<sup>155,162</sup>

Incorporating stimuli-triggered cleavable linkages into the polymer has shown a promising approach outcome.<sup>133,146</sup> Examples of such linkages include esters,<sup>172</sup> ortho-esters,<sup>173</sup> sulfur,<sup>174</sup> carbonates,<sup>175</sup> acetal,<sup>176,177</sup> hemiacetal/hemiketal ester,<sup>176,178</sup> olefinic,<sup>179</sup> tertiary ether,<sup>180</sup> peroxide bonds,<sup>181</sup> vicinal tricarbonyl,<sup>182</sup> phosphorus-containing bonds,<sup>183</sup> and as well as groups involved in Diels-Alder mechanism.<sup>184</sup> These materials can exhibit dynamic reactive behavior triggered by various stimuli such as heating,<sup>185</sup> pH,<sup>176</sup> light,<sup>186</sup> or targeted reactions.<sup>155,187</sup>

Although they are often considered industrially irrelevant due to their poor mechanical properties and expensive chemistry, these new classes of thermosets are slowly gaining acceptance in the industrial sector,<sup>146</sup> and degradable and recyclable thermosets have become a viable option for the polymer market.<sup>188</sup>

Stimuli-triggered degradation is achieved by introducing labile bonds into the traditional crosslinked resin. The amount and position of these labile linkages within the polymer structure can lead to different degradation products.<sup>133,155</sup> **Fig. II-9** illustrates various mechanisms that can be employed to afford a more sustainable end-of-life for these thermoset materials. These include the complete breakdown of the polymer network into lower molecular weight organic substances, degradation of the polymer backbone resulting in monomers or oligomers, and degradation of crosslinking bonds, resulting in linear polymers.<sup>189–191</sup>

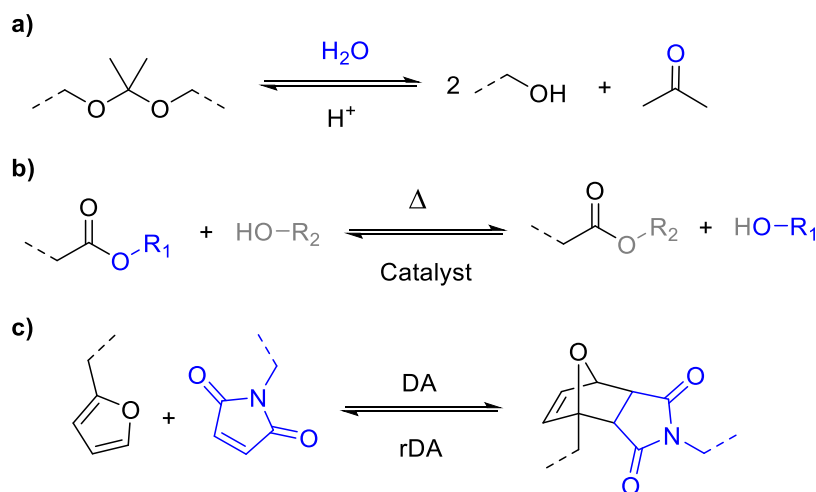


**Figure II-9.** Schematic overview of the existing concepts to develop recyclable thermoset polymers and different degradation pathways.<sup>133,141,155,192</sup>

While stimuli-triggered degradation can provide an eco-friendlier end-of-life solution for newly designed polymers, it frequently leads to permanent destruction of the polymer structure, making complete monomer regeneration challenging.<sup>155</sup> Consequently, the degraded products are generally repurposed for synthesizing new monomers or utilized in lower-performance applications through a downcycling approach.<sup>193,194</sup>

The concept is demonstrated in **Scheme II-21**, which shows that when acetal moieties are reversibly degraded in an acidic environment, it becomes possible, relying on the conditions, to employ this pathway to regenerate polymer precursors and eventually monomers by a straightforward methodology.<sup>176,177</sup> However, it is possible to recover structure-like monomers while maintaining the network properties by exploiting the reversibility of transesterification and Diels-Alder reactions.<sup>195,196</sup>

It is worth noting that these reactions take place via different mechanisms: transesterification proceeds through an associative mechanism where the exchange of involved groups occurs in an intermediate state, while Diels-Alder occurs through a dissociative mechanism where the dynamic bond dissociates before a new one is formed.<sup>184,192,197</sup>



**Scheme II-21.** Examples of molecular mechanisms describing the main concepts of recyclable thermosets; **a)** a degradable acetal linkage; **b)** an associative transesterification reaction; **c)** and a dissociative Diels-Alder reaction.<sup>155,176,184,196</sup>

## 2.7. Thermal Reworkable Networks

Polymers that exhibit a lowered degradation onset temperature ranging from 200°C up to 300°C are commonly referred to as thermally reworkable thermosets.<sup>175,185</sup> However, in this category of materials, the main challenge is to reduce the degradation temperature without compromising the material properties and their durability.<sup>198,199</sup>

Wong *et al.* presented an early instance of tuning the degradation temperature of epoxy-based thermosets by introducing thermal reworkable bonds.<sup>200,201</sup> The authors reported two sets of reworkable cycloaliphatic diepoxides, each containing thermally cleavable carbamate<sup>200</sup> or carbonate linkages.<sup>201</sup> The new monomers were cured with cyclic anhydride, which was similar to the process used for commercial cycloaliphatic epoxides.<sup>201</sup> Interestingly, the carbamate group present in the synthesized diepoxides self-catalyzed the curing reaction. The cured thermosets showed decomposition temperatures ranging from 200-300 °C, slightly lower than the commercial cycloaliphatic epoxide networks.

Liu *et al.* presented another example where they customized the degradation temperatures of various resins by incorporating phosphates and sulfite moieties into epoxy resins.<sup>183,202</sup> The authors demonstrated the ability to adjust the reworking temperature within 180-300 °C. They also observed that the carbon-oxygen bond in regular carbonates was more stable compared to its phosphodiester and thiodiester counterparts, which could be valuable information for developing new low temperature reworkable polymers.<sup>183,202</sup>

Acebo *et al.* modified epoxy thermosets by using poly(ethyleneimine)-poly(lactide) multiarm stars to adjust the reworkable temperature. They noted a minor reduction in the degradation temperature, which still remained high at about 400°C, raising concerns about the potential sustainability benefits of the proposed strategy.<sup>198</sup>

## **2.8. Cleavable Networks: Designing to Degrade**

Besides thermal activation, other stimuli have also been widely described to selectively break down polymers, such as the use of nucleophilic species,<sup>188,203,204</sup> acidic conditions,<sup>176,178</sup> or basic environments.<sup>187</sup> When exposed to strong acid solutions, thermosets bearing acid-sensitive linkages such as acetal,<sup>176,177</sup> ketal,<sup>205</sup> ester,<sup>172,180</sup> and Schiff base<sup>206</sup> exhibit high degradation activity.

An interesting method involves copolymerizing epoxy monomers and lactone precursors to produce thermosets that can degrade through the thermal pathway and alkaline hydrolysis of the resulting ester linkages in the networks.<sup>207,208</sup> Although alkaline hydrolysis occurs relatively slowly and results in only a 5% weight loss after two months of samples immersed in a basic solution, refluxing the samples at about 100°C can enhance the hydrolysis, leading to more than a 25% weight loss after only 24 hours.<sup>207,208</sup>

Tsujii *et al.* reported the effective and low-temperature cleavage of double bonds in epoxy-anhydride copolymers through ozonolysis.<sup>179</sup> The resulting thermosets exhibited high thermal stability up to 300 °C. They could be completely degraded via the ozonolysis pathway at temperatures ranging from -73 to 30 °C. The authors described that the reaction

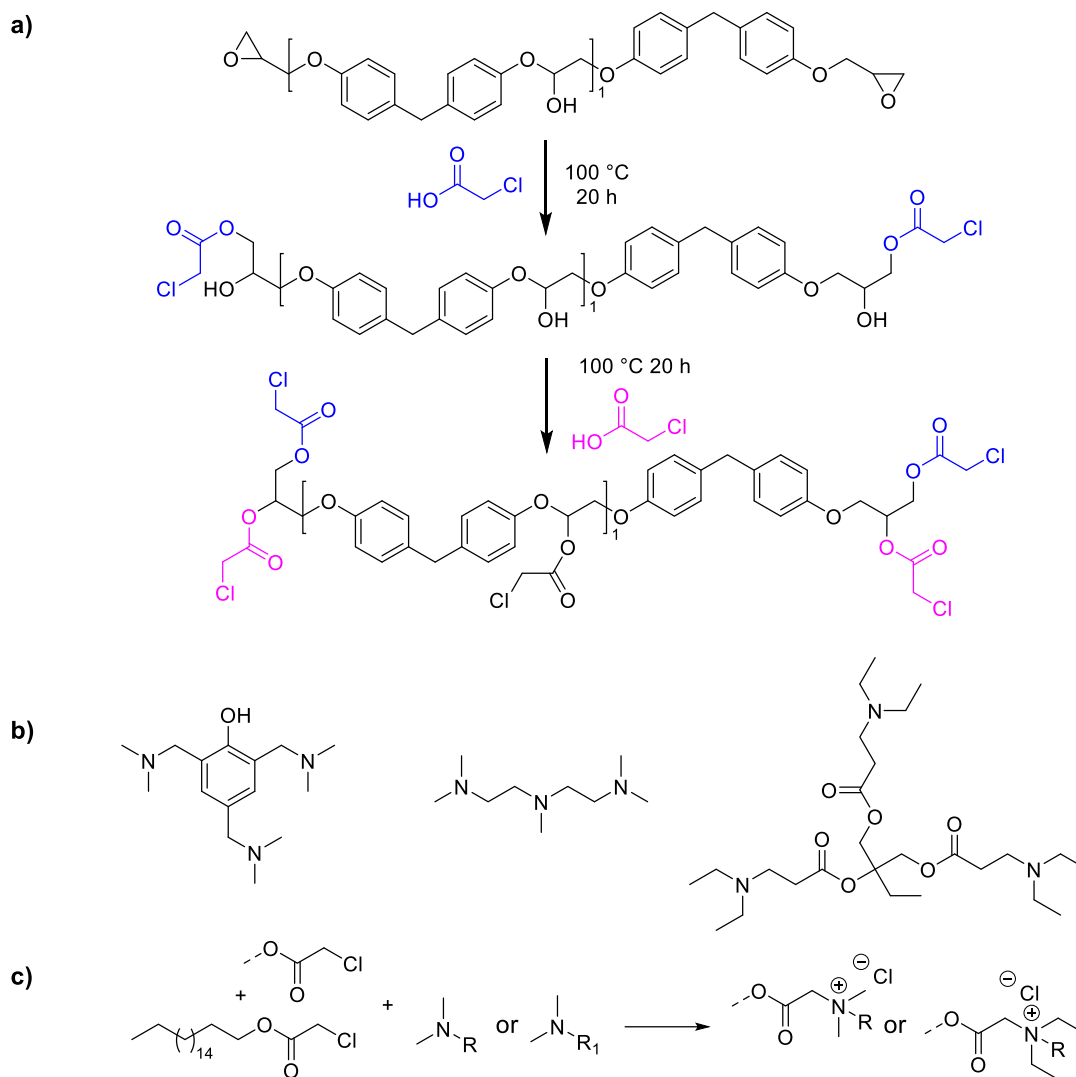
was more efficient at lower temperatures, which may be attributed to ozone gas's solubility and stability under these conditions. While this approach resulted in high yields of polymer degradation and did not require any supplementary separation processes, its applicability is diffculted by certain restrictions. These include the use of highly reactive ozone gas, which necessitates particular storage, and the requirement for cryogenic temperatures.<sup>179</sup>

In 2022, Patton *et al.* decided to use three novel dialkene acyclic ketal as comonomers to create crosslinked networks through radical-mediated thiol-ene photopolymerization.<sup>209</sup> All the thermoset materials revealed onset degradation temperature about 300 °C, negative glass transition temperatures between -10 to -30°C, and stress at break values ranging 1-2 MPa. The authors demonstrated that the degradation rate of these networks could be precisely tailored. They highlighted that acyclic dimethyl ketal-based networks degraded more rapidly, while networks containing acyclic cyclohexyl ketals took longer to degrade under the same conditions (pH 4.07, 30 °C).

Zhang *et al.* proposed an innovative bio-based approach to create degradable hyperbranched epoxy monomers from 2,5-furandicarboxylic acid (FDCA).<sup>210</sup> The resulting networks exhibited improved mechanical properties compared to the commonly used DGEBA polymers. Mainly in terms of tensile strength, flexural strength, storage modulus, and elongation. The researchers extensively analyzed the thermosets and composites using Raman imaging, AFM, SEM, DMA, dynamic light scattering, and positron annihilation lifetime spectroscopy. This deep investigation provided insights into the underlying mechanisms responsible for superior mechanical performances. They attributed the enhanced mechanical properties to the synergistic effects of crosslinking density, free volume, intermolecular cavity, hyperbranched topological structure, and toughening mechanisms. The researchers also proposed that integrating ester-derivative monomers into the thermosets and composites, can promote their degradation in a solution containing 2 mol L<sup>-1</sup> of phosphoric acid in ethylene glycol at 90 °C. As a result, this would enable the recovery of FDCA and fibers from the degraded mixture.<sup>210</sup>

In a different approach, Zhang and coworkers proposed a three-step process to prepare thermosets from DGEBA containing ammonium and ester cleavable groups in the networks (**Scheme II-22**).<sup>211</sup> Firstly, they reacted DGEBA with chloroacetic acid via an epoxy ring-opening reaction, followed by an esterification reaction, and finally, reacted the resulting precursor with tertiary amines to yield networks containing ammonium-chloride groups. The resulting thermosets exhibited outstanding mechanical properties, with a yield strength of 80 MPa. These materials demonstrated rapid degradation activity when exposed to mild alkali conditions similar to seawater conditions, attributable to the hydrolysis of the

ester groups introduced by the cetyl chloroacetate moiety. Additionally, the networks exhibited a bactericidal rate of 99.34% in one of the tests, which is likely due to the interaction between the cationic groups and the bacterial membranes. This research is yet another example of how we can engineer the molecular structure of the networks by introducing cationic groups and cleavable linkages to yield emerging properties in thermoset polymers.



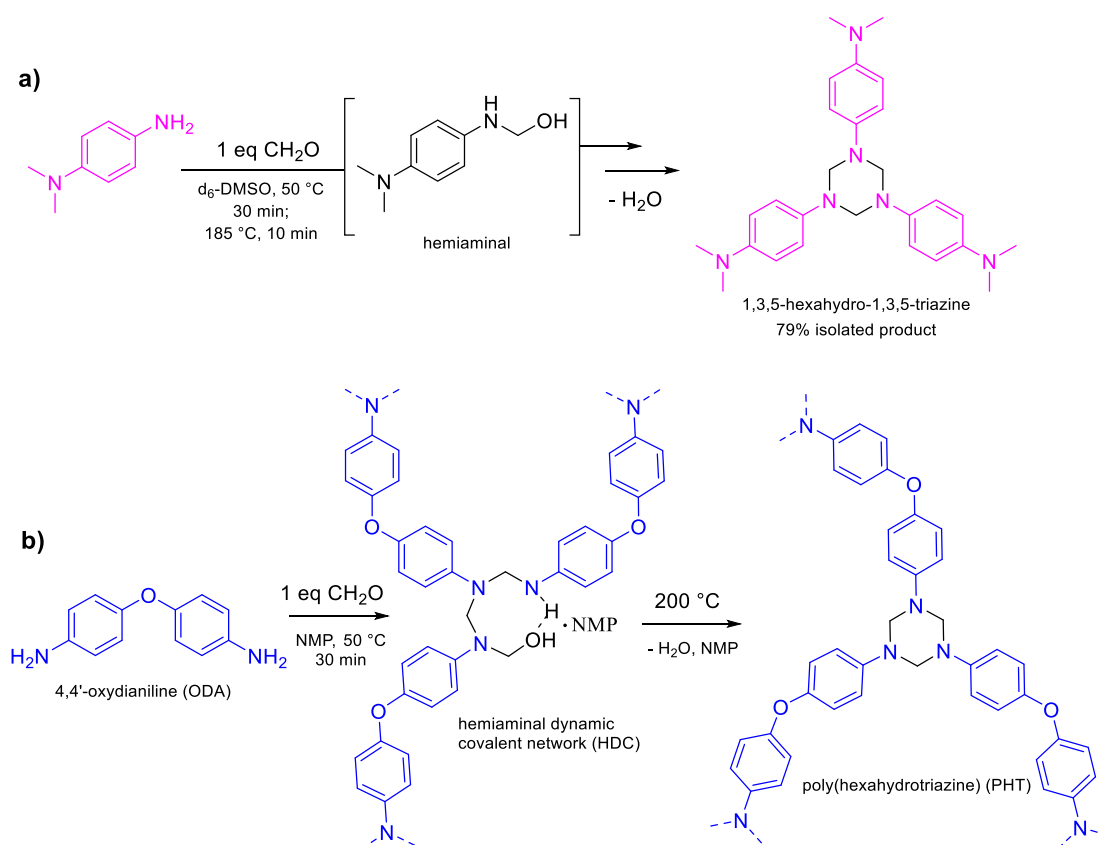
**Scheme II-22.** Synthetic routes of degradable and antibacterial thermosets crosslinked with betaine esters. In **a)** the synthetic route, involving a first ring-opening reaction by the nucleophilic addition of carboxyl group, **b)** the curing amines used, and **c)** the outline of the resulting networks bearing the ammonium-chloride moieties.<sup>211</sup>

## 2.9. Cleavable Networks: Design to Recycle

From the point of view of circular economy, it's better to selectively degrade polymers and recover their original monomers, molecular building blocks, thermoplastic chains, or

revalorize products at the end of their lifespans. This is more beneficial than just degrading thermosets to avoid them ending up in landfills.<sup>129,133,170</sup>

Garcia *et al.* recently reported promising findings in developing recyclable poly(hexahydrotriazine) (PHT) thermosets that can be degraded through acid digestion to recover the bisaniline monomers.<sup>212</sup> The PHT networks were synthesized via a one-pot, low-temperature polycondensation of paraformaldehyde and 4,4'-oxydianiline (ODA), which resulted in hemiaminal dynamic covalent networks (HDCNs) that undergo cyclization at high temperatures to yield poly(hexahydrotriazine)s (PHTs) (**Scheme II-23**).



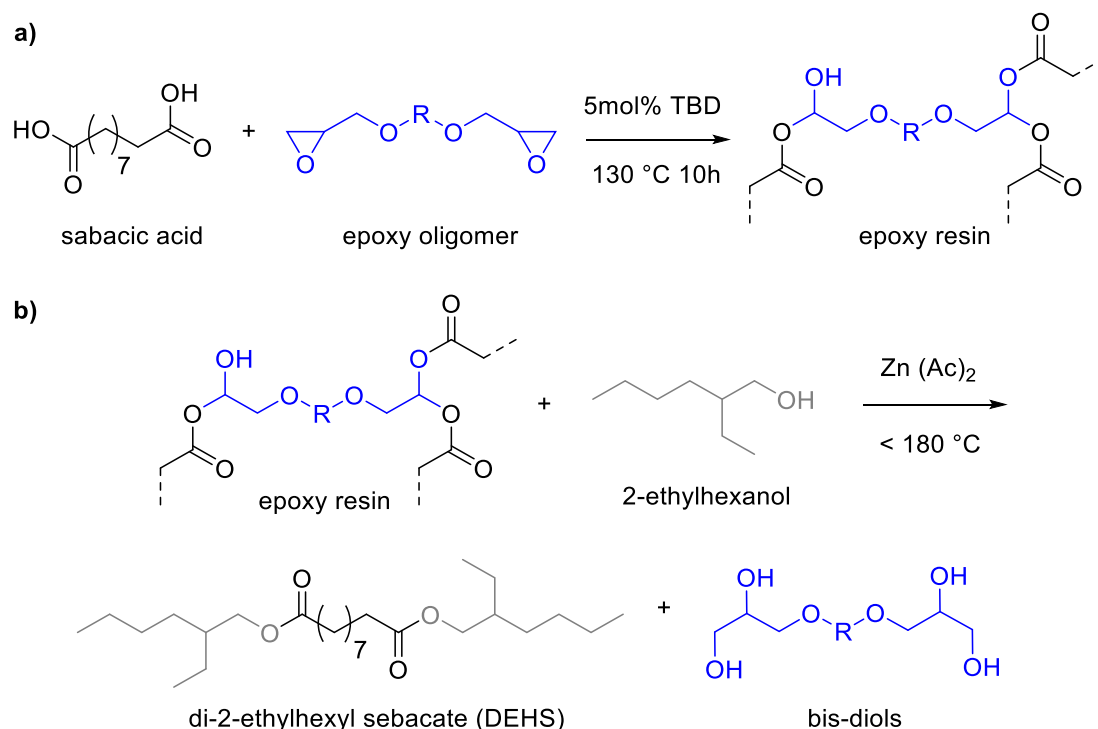
**Scheme II-23.** Overview of the chemistry employed to develop recyclable poly(hexahydrotriazine) (PHT). In **a)** the reaction between N,N-dimethyl-p-phenylene diamine and paraformaldehyde in a stoichiometric ratio. In **b)** the outline of the polycondensation of paraformaldehyde and 4,4'-oxydianiline to yield the recyclable thermoset.<sup>212</sup>

PHT and PHTs are classified as thermosets and exhibit remarkable mechanical properties, including high Young's moduli. Most notably, the digestion reaction of these materials under acidic conditions with a pH less than 2 enabled the recovery of the original bisaniline monomers.

Jerry Qi and his team outlined the manufacture of epoxy thermosets that can degrade over time and for repurposing the resulting degraded products.<sup>213</sup> They achieved this



by developing new types of epoxy networks based on different precursors, such as DGEBA copolymerized with a di-acid carboxylic and catalyzed by a strong base (**Scheme II-24**).

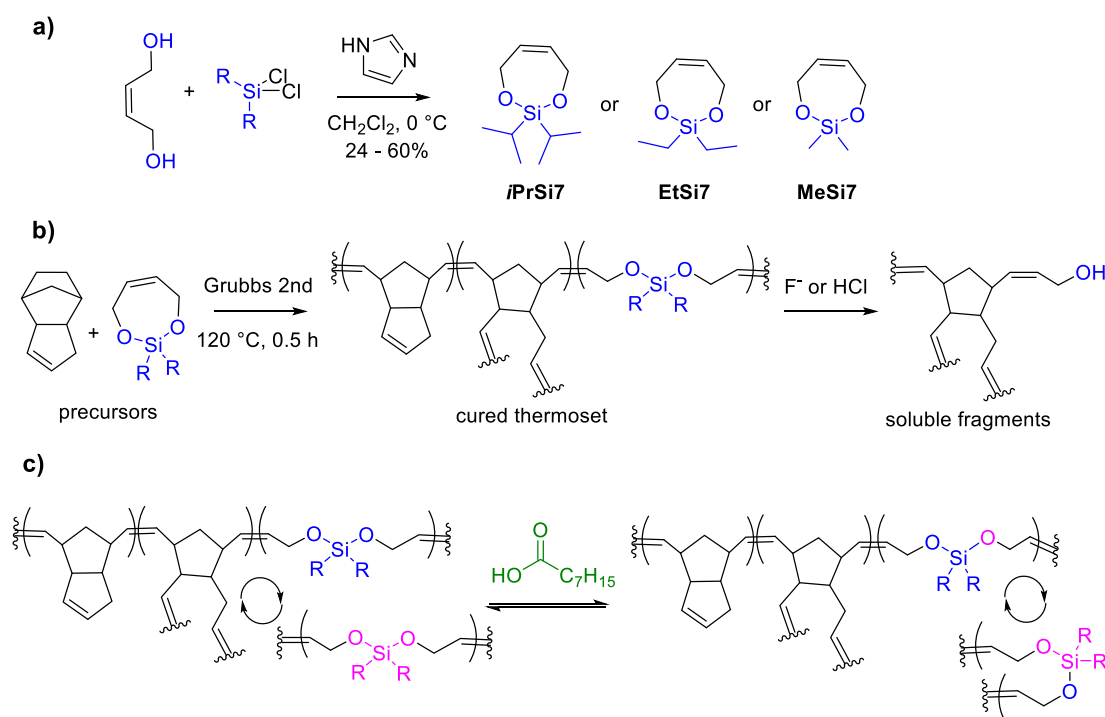


**Scheme II-24.** General overview of Jerry Qi group's proposal. In **a)** schematics showing the polymerization reaction between epoxy oligomer and sebacic acid catalyzed by TBD. In **b)** the outline of the solvolysis of the epoxy networks assisted by zinc acetate at elevated temperatures.<sup>213</sup>

The new networks had glass-transition temperatures ranging from -28 to 47 °C. The epoxy networks bearing carboxyl groups could be degraded using transesterification reaction in 2-ethyl-hexanol, catalyzed by a zinc acetylacetonate at temperatures below 170°C. The rate at which the thermoset dissolves augments with the increase in temperature and catalyst concentration. They also reported that they were able to recover bis-diols compounds derived from the initial epoxy backbone and dicarboxylic acid esters, which could be used to make high-value products, including lubricants, plasticizers, and fuel additives. They were able to harvest biolubricants from the thermoset waste in a feasible and cost-effective process that could be performed at mild temperatures and ordinary pressure. Additionally, the catalyst could be reclaimed and reused.<sup>213</sup>

Johnson's group has significantly contributed to researching and developing degradable, recyclable, and reprocessable thermosets. They initially reported the efficient copolymerization of bifunctional silyl ether (BSE)-based olefins with norbornene monomers

using ring-opening metathesis polymerization (ROMP) (**Scheme II-25a-b**).<sup>188</sup> By introducing a cleavable BSE-comonomer, they built degradable thermosets with tunable degradation rates relying on the percentage of BSE-comonomer.<sup>188</sup> Then, they investigated the installation of these cleavable bonds within the strands and between the strands, *i.e.*, as crosslinks of thermosets.<sup>203</sup> The location of the cleavable bonds was revealed as a design principle for achieving controlled thermoset degradation. Surprisingly, the thermosets produced by incorporating cleavable comonomers as crosslinks between the strands did not exhibit relevant degradation activity.



**Scheme II-25.** Schematics of the research conducted by Johnson's group towards developing novel degradable thermosets. In **a)** the structure of the degradable comonomers, **b)** the curing process followed by the degradation assisted by fluoride anions or acid solution and **c)** the development of reprocessable networks via rearrangement catalyzed by octanoic acid.

In a subsequent report, they explored the strategy developed in previous research to demonstrate the feasibility of building deconstructable and upcycling thermosets and composites.<sup>204</sup> Similarly to the previous approach, they synthesized poly(dicyclopentadiene) (pDCPD) thermosets by ROMP, and by introducing cleavable monomers, they tuned the degradability of the thermoset matrix, allowing the full recovery of carbon-fiber reinforcements.

The same authors recently developed a novel approach towards incorporating exchangeable bonds into commercial thermosets using bifunctional silyl ether-based comonomers (**Scheme II-25c**). They demonstrated the temperature- and time-dependent stress relaxation of pDCPD thermosets manufactured with BSE comonomers and enabled bulk remolding of pDCPD thermosets in the presence of octanoic acid. This work established acid-catalyzed BSE exchange as a versatile addition to the toolbox of dynamic covalent chemistry.

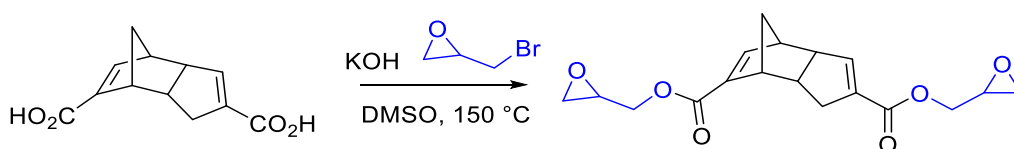
### 3. Cleavable Linkages in Thermosets: Opportunities and Applications

#### 3.1. Removable Adhesives

An adhesive is a substance that is applied to the surface of materials in order to bind them together and resist separation.<sup>214</sup> The materials being bound are referred to as adherends. However, at the end of the lifespan of these materials, recovering the adherends can be challenging.<sup>215,216</sup> Thus, there is a need to develop adhesives that are either degradable or reversible. A degradable thermoset adhesive would be particularly useful for recovering substrates and reusing adherends.<sup>217–219</sup>

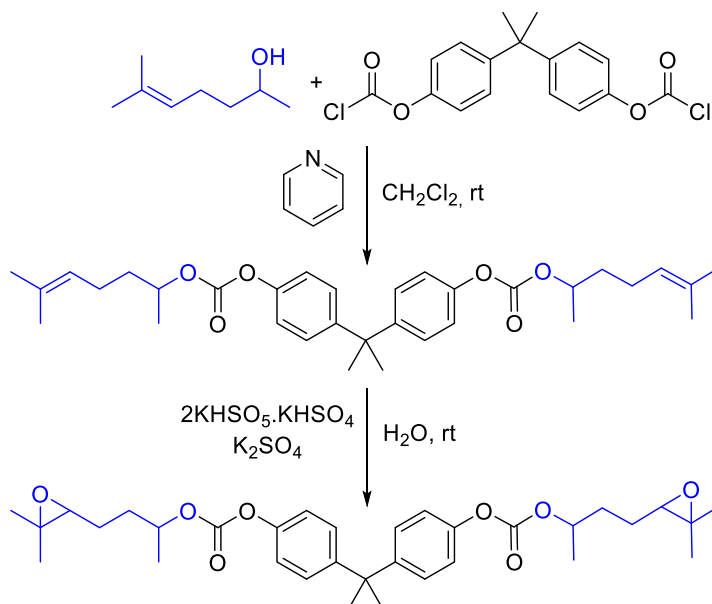
One of the most important applications of degradable adhesives is in the development of underfills.<sup>220</sup> These composite materials are typically made up of fillers or fibers that are reinforced with an epoxy polymer. Underfills are used in various industries, including automotive and electronics.<sup>199</sup> To develop underfills reinforced with degradable epoxy matrices; researchers have investigated different functional groups, such as ester bonds,<sup>175,201</sup> carbonate or carbamate linkages,<sup>201</sup> maleimides containing hemiacetal moieties,<sup>216</sup> and acetal linkages.<sup>221</sup>

Champagne and colleagues have created a thermal degradable underfill adhesive that is based on epoxy thermoset bearing thermal dynamic dicyclopentadiene (DCPD) moiety (**Scheme II-26**).<sup>222</sup> The synthesis of this monomer was simple and could be easily scaled up to industrial levels. The novel epoxy monomer was cured using imidazole as a curing agent and copolymerized with acrylic acid derivative monomers, revealing high  $T_g$  for all the newly designed networks. Introducing only 10% of DCPD-based monomer into the networks made the resulting materials degradable at temperatures above 160°C. This allowed the complete recovery of the electronic boards without causing any damage.



**Scheme II-26.** One-step synthetic route of a DCPD-based monomer from a diacid derivative.

Li and colleagues have designed a bifunctional-epoxy monomer that includes two carbonate groups (**Scheme II-27**).<sup>175</sup>



**Scheme II-27.** Synthesis of a Bisphenol A-based monomer containing carbonate groups.<sup>175</sup>

This monomer produced thermosets with  $T_g$  of around 90°C, and the resulting materials were fully degradable when exposed to 250 °C for 5 minutes. The authors could recover components of a printed circuit board using a dual-epoxy material containing 80% weight of silver flakes. When the material was exposed to high temperatures and then scraped with a wooden spatula and brushed manually, the small sites on the laminated board were easily cleaned.

The use of urea bonds<sup>223</sup> and DA adduct structures<sup>224</sup> to yield degradable thermosets was also reported for potential use in adhesives. By incorporating urea bonds and DA adduct structures into the polymer matrix, researchers have been able to create thermosets that are not only strong and durable but also able to degrade over time into non-toxic by-products.

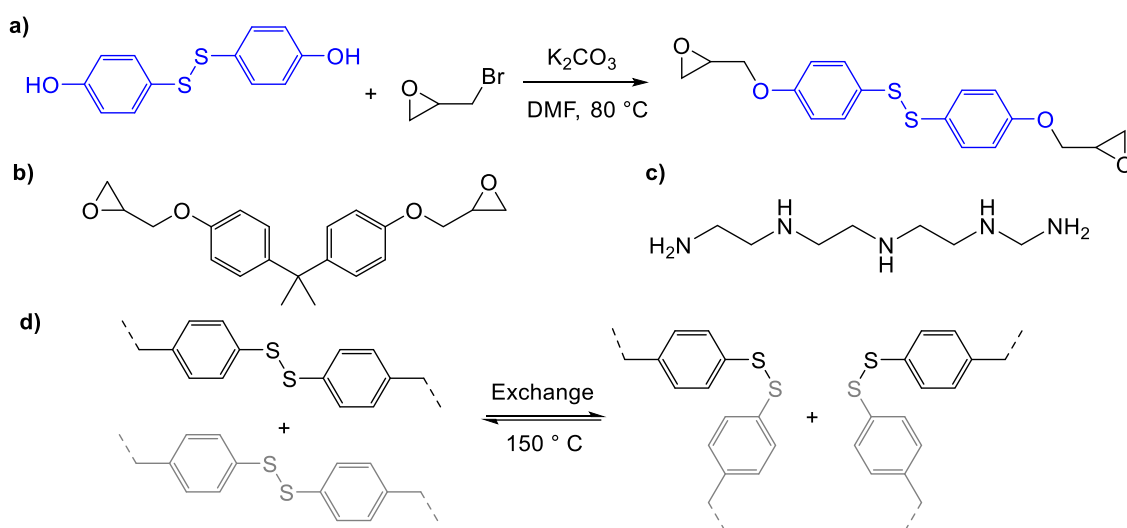
### 3.2. Electronic Packaging: Degrading Thermosets to Recycle Electronics

Thermosets are commonly used as electronic packaging materials because they provide environmental protection, mechanical stability, and thermal insulation to electronic

devices.<sup>225</sup> However, network crosslinks make repairing, disposing of, recycling, or reusing electronic components challenging.<sup>225,226</sup> To address this issue, degradable thermosets have been developed using phosphorus-containing structures,<sup>227</sup> disulfide bonds,<sup>228</sup> and other functionalities.

For instance, Liu *et al.* introduced phosphorus-containing epoxy resins that exhibit rapid thermal degradation at approximately 260 °C combined with outstanding fire resistance and mechanical properties, indicating their potential use as eco-friendly, reworkable electronic packaging resins that are free of halogens.<sup>227</sup>

In recent research, Chen and collaborators designed aromatic disulfide epoxy monomer to develop vitrimers for packaging electronic devices, namely LED and printed circuit boards (**Scheme II-28**).<sup>229</sup>



**Scheme II-28.** The reactions and precursors that underlie the creation of packaging made from vitrimers containing sulfur in Chen's work. In **a**) synthesis of the aromatic disulfide epoxy monomer; **b**) DGEBA monomer used to copolymerize with the synthetic monomer; **c**) curing amine and **d**) disulfide metathesis upon heating.

The epoxy networks presented  $T_g$  of about 115 °C and tensile strength of 71.9 MPa. Further, it revealed electrical resistivity comparable to the reference epoxy while low values for dielectric constant were observed. The LED light packed with the dynamic networks could be healed at 150 °C via disulfide metathesis and presented topology freezing transition at about 118 °C. The networks presented self-healing behavior and chemical degradability when exposed to dithiothreitol in dimethylformamide, which allowed the recovery and recycling of the electronic equipment.

### 3.3. Affording a More Sustainable End-Of-Life for Composites and Nanocomposites

Thermoset composites are commonly composed of thermoset polymer resins along with glass, carbon, or aramid fibers, resulting in materials with exceptional properties, particularly in terms of mechanical and thermal characteristics.<sup>134,162,230–232</sup> Waste management and recycling pose significant challenges due to the chemical nature of networks in these materials.<sup>133</sup>

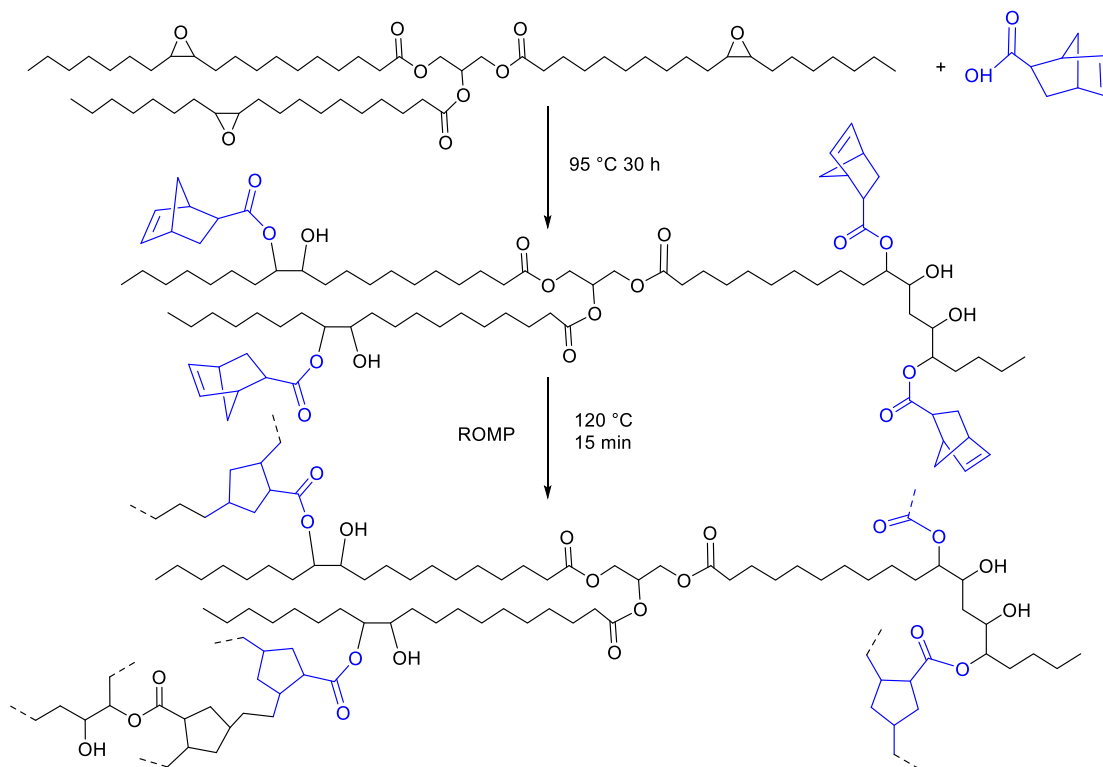
Yu *et al.* have shown that combining bisphenol A epoxy resin (DGEBA) and fatty acids is possible to produce degradable thermosets.<sup>233</sup> These networks' degradation is achieved through forming ester groups, which result from transesterification between carboxylic acid groups and hydroxyl groups that arise from the opened epoxy groups. The subsequent degradation is facilitated by transesterification in the presence of ethylene glycol, and the carbon fibers are recovered with a yield of approximately 100%.

Harris investigated a different approach, loading cellulose nanocrystals into epoxy networks to render the polymer phase degradable and recover the substrate of polymer nanocomposites.<sup>234</sup> The authors did not investigate the mechanism; however, their approach decreased thermal degradation temperature by 40 °C allowing the recovery of composite substrates in a moderate range temperature.

Qi and colleagues explored the nature of ester bonds to design novel epoxy-based vitrimers.<sup>235</sup> They employed carboxylic acids as a reactive additive, and by heating the samples, they induced the transesterification reaction, producing dynamic networks.<sup>164</sup> Later, the same authors developed anhydride-cured epoxy thermosets containing ester bonds cleaved through a transesterification reaction catalyzed by 1,5,7-triazabicyclo[4,4,0]dec-5-ene (TBD).<sup>236</sup> They extensively studied the kinetics of the degradation mechanism and proposed a kinetic model that shed light on the degradation of the anhydride-epoxy networks. Based on these findings, they designed degradable thermosets that could almost entirely degrade in ethylene glycol in 70 minutes at 170 °C under ambient pressure. By employing these thermosets, they demonstrated that they could manufacture CFRPs and recover the carbon-fibers (CFs) in their original state under mild conditions for 1.5 hours.

Yang and colleagues created eco-friendly thermosets and composites by using epoxidized oil (ESO) treated with norbornene moieties and flax fibers.<sup>237</sup> They used ring-opening metathesis (ROMP) to polymerize the prepolymers and achieved ESO-based thermosets displaying impressive thermal and mechanical properties (**Scheme II-29**). The thermoset matrix could completely break into oligomeric molecules when exposed to NaOH and KOH

aqueous solutions. This combination of prepolymer precursors and proposed solvolysis method allowed the recovery of the plant-based fibers.



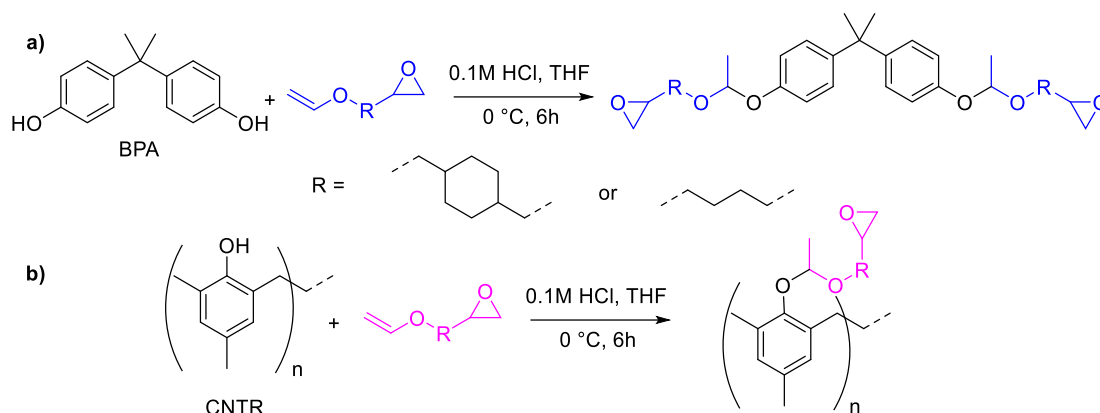
**Scheme II-29.** Synthesis of ESO-based thermoset from epoxidized soybean oil.<sup>237</sup>

Developing degradable thermosets without compromising their thermal and chemical stability is challenging. Acetal linkages have emerged as a promising alternative due to their stability in neutral and alkaline aqueous solutions.

In 1996, researchers at IBM reported the first successful synthesis of diepoxies containing an acetal moiety, which was used to build degradable epoxy thermosets.<sup>148,238,239</sup> Since then, several acetal epoxy thermosets and recyclable CFRPs have been developed by incorporating cleavable acetal linkages into curing agents and epoxy monomers. Acetal-based curing agents are currently widely reported for CFRP recycling, both in academia and industry. For instance, Connora Technologies (Hayward, CA, USA)<sup>185,240</sup> and Adesso Materials (Wuxi, China)<sup>177,241</sup> have developed amine hardeners that contain acetal linkages in their backbones. The resulting epoxy-amine networks exhibit excellent mechanical properties, with a tensile modulus and tensile strength ranging from 3-8 GPa and 61-70 MPa, respectively.

Hashimoto and colleagues also used the cleavable acetal linkage to create degradable epoxy networks and manufacture deconstructable CF composites.<sup>176,178,242</sup> They exploited the nucleophilic addition of a phenolic hydroxyl group in vinyl ether compounds to

form acetal linkages as the only product. Two different phenol derivatives were examined in this method: bisphenol A (BPA) and cresol novolak-type phenolic resin (CNTR) (**Scheme II-30**).

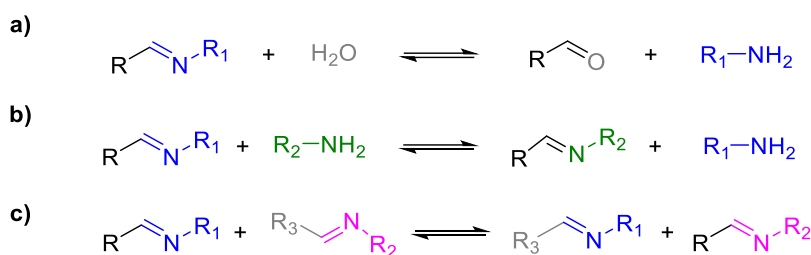


**Scheme II-30.** Novel acetal-based epoxy monomers synthesized from phenolic compounds: In **a)** Bisphenol A based monomers and **b)** cresol novolak-type phenolic resin (CNTR) precursors.

Multifunctional aliphatic amines were employed to cure all the newly developed monomers, resulting in networks with a  $T_g$  of up to 91°C and a degradation temperature for 5% weight loss ( $T_{d5\%}$ ) of up to 245°C. The CF composites obtained from the novel monomers were entirely degraded in a hydrochloric acid solution of 0.1 mol L<sup>-1</sup> at room temperature and ambient pressure for 24 h. The authors also demonstrated that the recovered CFs had only minor surface changes and nearly the same tensile strength as the virgin CFs. The researchers also designed networks based on DGEBA by increasing the percentage of cleavable acetal-based monomers to ensure heat resistance and toughness while maintaining their degradability. They showed that degradable networks could be achieved under the aforementioned conditions by increasing the proportion of newly designed acetal precursors to 20% in mass.<sup>176</sup>

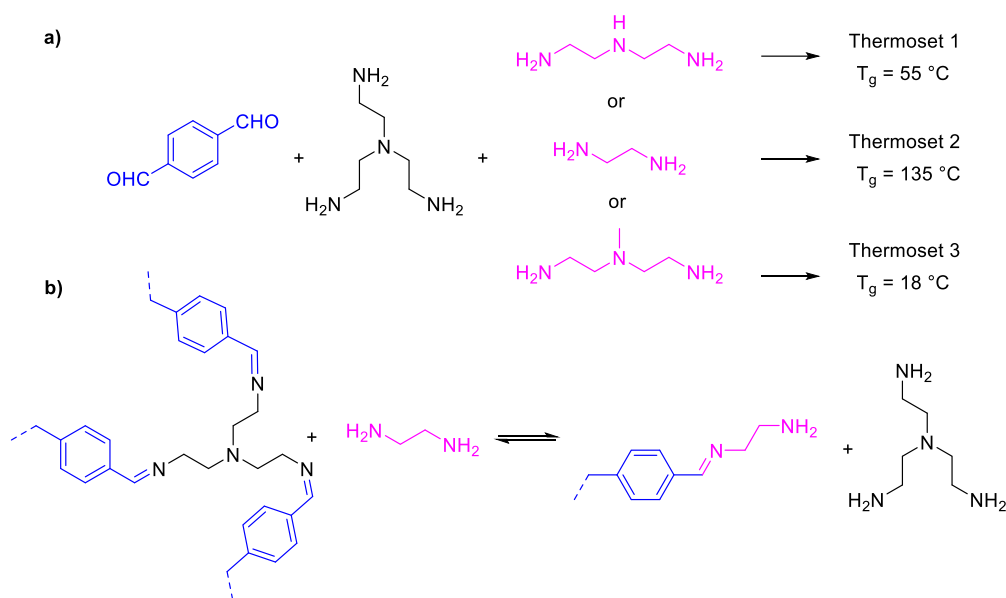
Another promising strategy consists of introducing imine groups into the epoxy networks.<sup>146,206</sup> Imines, also known as Schiff bases, are formed from the reaction between amines and aldehydes or ketones.<sup>243</sup> Interestingly, imines can be hydrolyzed (**Scheme II-31a**), generating the starting materials, or undergo exchange reactions such as transamination (**Scheme II-31b**) or imine metathesis (**Scheme II-31c**).





**Scheme II-31.** The dynamic nature of the imine chemistry. In **a)** the hydrolysis of a generic imine molecule; **b)** transamination reaction, and **c)** the imine metathesis.<sup>243</sup>

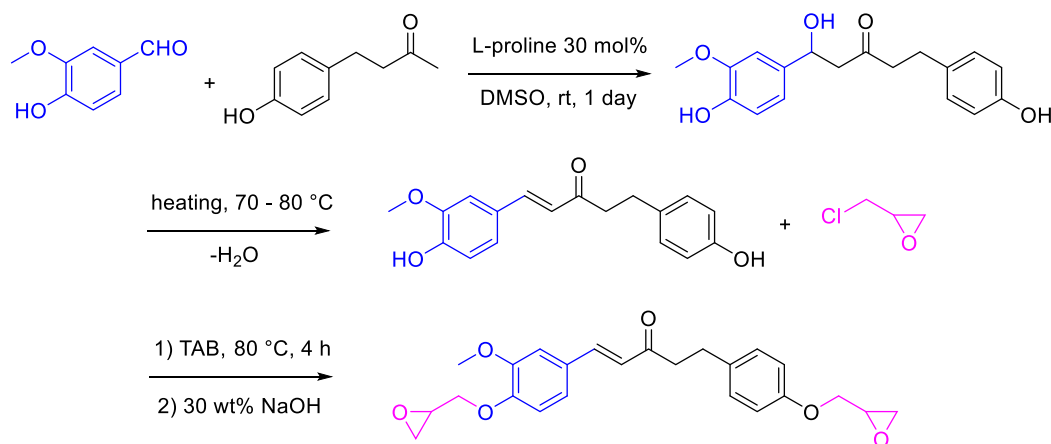
Zhang and colleagues have reported on malleable, mechanically resilient Schiff base thermosets applied to CFRPs, resulting in efficient closed-loop recycling.<sup>244</sup> The proposed synthetic route is simple and involves using an aldehyde and a triamine as precursor and crosslinker, respectively (**Scheme II-32a**). Additionally, a second diamine is employed to adjust the crosslink density, which leads to the fine-tuning of glass transition temperatures, tensile strength, and tensile modulus. The newly designed network was employed to develop CFRPs with tensile strength of 148-399 MPa and a tensile modulus of 12.2-15.5 GPa. The imines' dynamic nature yielded malleability composites, including flexible processing temperature, reparability, reshaping and weldability properties. The networks were degraded in mild conditions by immersing the samples in a diethylenetriamine solution (**Scheme II-32b**).



**Scheme II-32.** Synthesis of polyimine malleable thermosets. In **a)** the aldehyde precursor, the triamine precursor, and the three different diamine monomers that yield polymers with varying thermomechanical properties, and **b)** an example of transamination reaction related to the dynamic behaviour of the polyimine thermosets.<sup>244</sup>

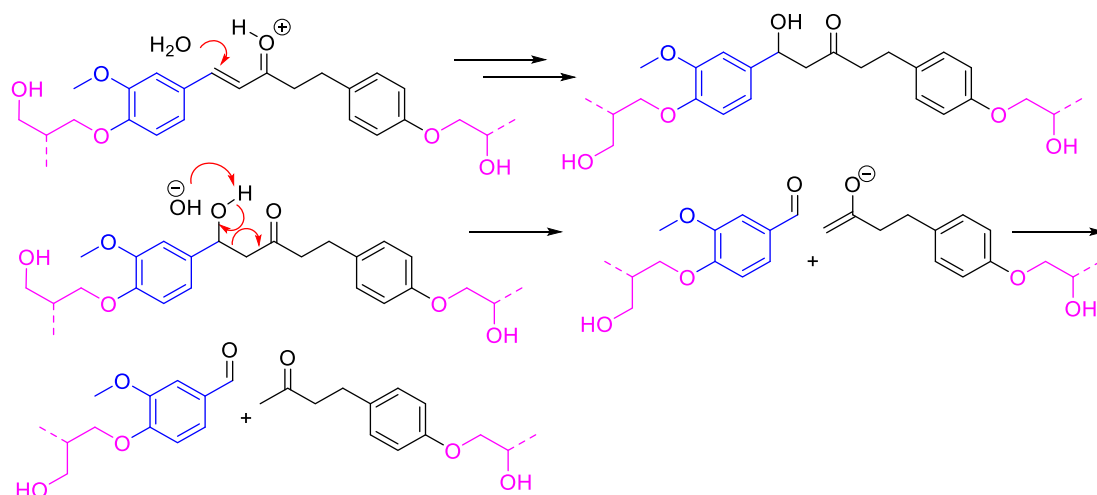
The degraded oligomers were easily reused by adding them to the starting material mixture in the correct proportions. This approach allowed the development of CF composites and subsequent recovery of the CFs, maintaining their surface chemical structure, mechanical properties, woven structure, and long dimensions. Due to the weldability of the Schiff base thermoset through transamination or metathesis (**Scheme II-31a-b**), the delaminated Schiff base CFRP could be conveniently repaired through heat pressing, and the flexural strength and modulus could recover 85-100%.

More recently, Goh *et al.* proposed an elegant strategy exploring the reversibility of aldol reaction to synthesize and then degrade epoxy thermosets and CFRPs.<sup>187</sup> The novel epoxy monomer was prepared from vanillin and raspberry ketone via an L-proline-catalyzed aldol condensation reaction (**Scheme II-33**).



**Scheme II-33.** The synthesis of bio-based epoxy monomer via aldol reaction followed by functionalization with epichlorohydrin.<sup>187</sup>

The novel epoxy bio-based monomer was cured with 4-aminophenyl sulfone (DDS) and exhibited excellent mechanical properties, including tensile strength and flexural strength of 58 MPa, and 183 MPa, respectively. Additionally, CFRP prepared from the synthesized monomer has shown excellent strength (957 MPa), Young's modulus (77 GPa), and interlaminar shear strength (49 MPa). Overall, the thermoset matrix and CFRP rapidly degraded through retro-aldo reaction by treating the samples with an HCl solution followed by NaOCl (**Scheme II-34**).



**Scheme II-34.** The thermosets are broken down through a selective degradation mechanism, driven by a retro-aldol reaction.<sup>187</sup>

In addition, CFRP prepared by using synthesized epoxy monomers exhibited excellent tensile strength (957 MPa), Young's modulus (77 GPa), and interlaminar shear strength (49 MPa). Interestingly, the CFRPs were rapidly degraded only under specific conditions. The reclaimed CFs retained 87% of their original tensile strength. These results suggest that novel bio-based monomers could be a viable alternative to DGEBA and BPA epoxy resins in producing CFRP.

Significant progress has been achieved in recycling thermosets and composites, particularly on CFRPs. The appropriate recycling method depends on the specific application, the original composition of composites, and other relevant considerations. However, it appears evident that developing new monomers capable of producing degradable networks is a promising approach. This is because such monomers enable the degradation of networks under mild conditions requiring low energy consumption and minimal equipment. As a result, the recovered CF, fillers and adherends exhibit excellent performance, similar to their original properties.

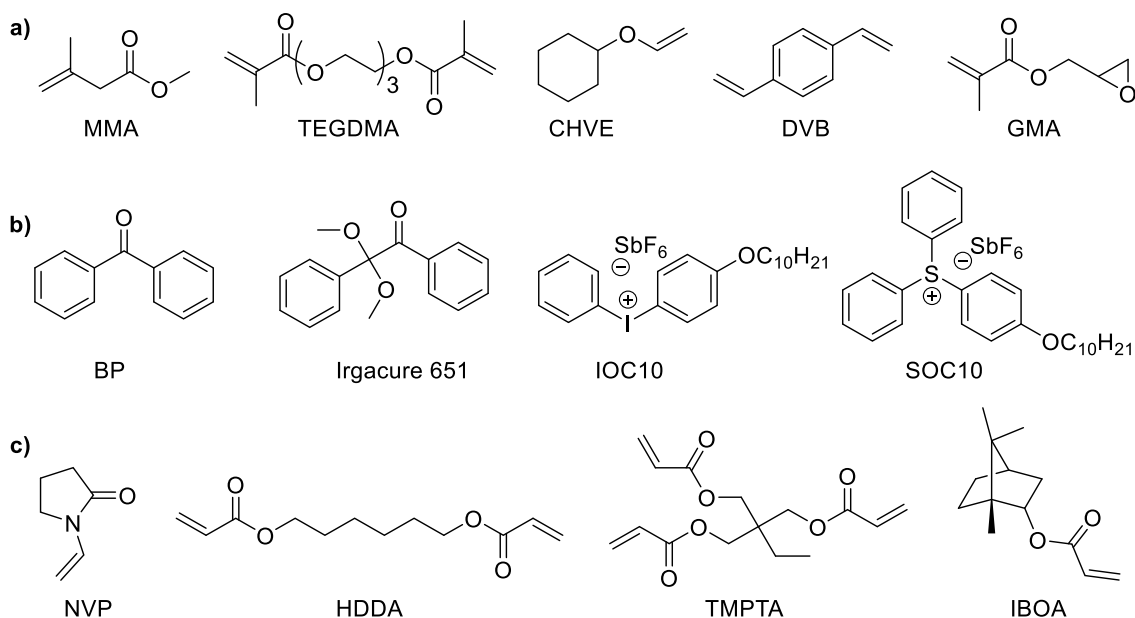
In addition, some future trends require consideration to continue advancing with degradable thermosets for CFRPs. First, cleavable bonds may lead to long-term instability due to oxidation or hydrolysis, necessitating focusing on the overall properties of CFRPs based on degradable thermosets. Introducing hydrophobic moieties into the monomer structures may be an adequate approach to manufacturing less water-sensitive materials. Second, using more suitable-cleavable bonds under mild conditions, such as ester, imine, hemiacetal/hemiketal linkages, and carbonate structures, could be employed to produce CFRPs. Third, for developing CFRPs for structural applications, obtaining thermoset matrices with higher  $T_g$  and enhanced mechanical properties is interesting. In fourth place, while

pursuing the recycling CFRPs, environmentally friendly reagents and recycling of reagents must also be considered to increase their industrial application potential and to conform to the green chemistry and circular economy principles.

#### 4. Exploring the Potential of Photopolymerization: An Overview of Techniques and Applications

Over the past two decades, there has been significant growth in radiation-curing technologies at academic and industrial levels, as evidenced by the rise in the design and synthesis of novel photopolymerizable monomers. This progress has been well-reported in several patents, textbooks and review articles.<sup>245–250</sup> These cutting-edge methods employ light irradiation to initiate photochemical reactions in organic materials, leading to the development of novel polymer materials directly applicable to various commercial sectors.<sup>251,252</sup>

A typical photopolymerizable formulation is composed of three major components (**Fig. II-10**).<sup>253,254</sup> The first component is a photoinitiator that absorbs light and generates the active species via a chemical reaction. The second element is a multifunctional reactive monomer or oligomer that undergoes crosslinking polymerization. The third component, the reactive diluents, is not always used, and its purpose is to adjust the viscosity of the formulation, facilitating the reaction's development as a co-solvent and comonomer.



**Figure II-10.** The main components of photopolymerizable formulations include **a)** photopolymerizable monomers, **b)** photoinitiators of type I or II, and **c)** reactive dilutants.<sup>254</sup>

The photoinduced polymerization begins with generating reactive species from a photoinitiator.<sup>255,256</sup> Photoinitiators can be classified as either type I or type II, depending

on their mechanism for initiating polymerization. Type I photoinitiators undergo homolytic cleavage upon excitation, generating radicals that can initiate the polymerization process. Type II photoinitiators require interaction with a second molecule upon irradiation to generate the initiating species. These reactive species engage in a chain-reaction mechanism to propagate the active center.<sup>253,255,257</sup> Then, the reactive species interact with monomers to drive the polymerization process forward.

The active centers can be radicals, cations, or, less often, anions. The key distinguishing factor between photopolymerization and conventional radical polymerization is that light produces the reactive initiator species.<sup>245,253,258,259</sup>

Research on UV-induced free radical polymerizations began early on due to the availability of existing free radical photoinitiators.<sup>251</sup> However, the cationic UV-curing process became popular in the late 1970s with the development of thermally stable cationic photoinitiators.<sup>260,261</sup>

The development of UV-curing methods is mainly driven by the economic and environmental benefits offered over traditional thermal curing processes.<sup>254,262</sup> These advantages include rapid cure, low energy consumption, room-temperature treatment, free-solvent formulations, and low material costs.<sup>263-265</sup>

One of the earliest breakthroughs was the development of UV-curing coatings for several substrates, including polymers,<sup>266</sup> metals,<sup>267</sup> wire,<sup>268</sup> pipes,<sup>251</sup> glass-reinforced fibers,<sup>269</sup> optical fibers.<sup>270</sup> Allowing their application in coatings,<sup>253</sup> adhesives,<sup>261</sup> dental materials,<sup>271</sup> printing inks,<sup>272</sup> and composites.<sup>273</sup>

More recently, the commercial development of various powerful lasers has opened up new possibilities for using laser-induced polymerization.<sup>274</sup> This technique shows promise in photoimaging,<sup>275</sup> microelectronics,<sup>276</sup> holographic image recording<sup>277</sup> and data storage.<sup>278</sup>

#### **4.1. Cationic Photo- & Thermal-Induced Polymerization**

Cationic photopolymerization has gained significant interest due to its advantages, as evidenced by numerous scientific publications and industrial applications.<sup>253</sup> One of the key benefits of cationic polymerization is the absence of air inhibition, which means that an inert atmosphere is not required during the curing process.<sup>253,279</sup> This property clearly distinguishes cationic polymerization from radical polymerization. After initiation, cationic polymerization is non-terminating and can continue even after removing the light source.<sup>253,254</sup> This process is called the dark reaction step, resulting in further monomer conversion without light exposure or thermal post-treatment. In contrast, several bimolecular

terminations can occur in light-induced free-radical reactions, and polymerization rapidly stops without light.<sup>260</sup>

In addition, the monomers and reactive oligomers that can be polymerized using cationic photopolymerization are typically associated with low human toxicity.<sup>253</sup> Moreover, cationic photopolymerization of epoxide monomers exhibits a lower volume shrinkage than corresponding radical-based systems, resulting in better adhesion, thermal and mechanical properties.<sup>279,280</sup> This makes them attractive alternatives to acrylate and methacrylate systems, commonly used in free-radical photopolymerizations.<sup>172,260</sup>

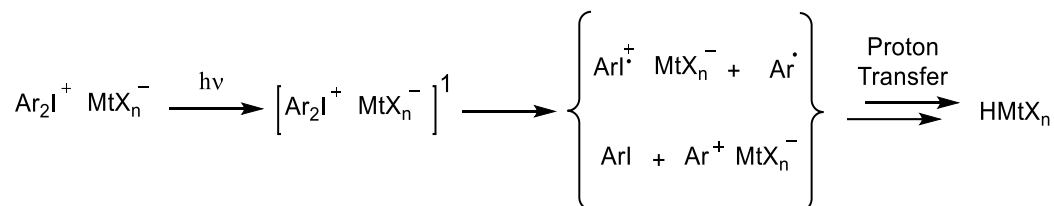
Onium salt photoinitiators are the most commonly photoinitiators used in cationic polymerization due to their excellent latency and remarkable thermal stability.<sup>253,281–283</sup> These salts are beneficial in the presence of highly reactive multifunctional monomers at ambient temperature.

Onium salt photoinitiators comprise an organic cation and an inorganic anion.<sup>245,284,285</sup> The aromatic organic cation absorbs light and plays an essential role in the photochemistry of the process since this fragment determines the thermal stability, UV absorption characteristics and quantum yield. The anion's nature will determine the strength of the acid formed by the photolysis of the initiator.<sup>286</sup> Consequently, the anions determine the reactivity and character of the polymerization propagation, directly impacting the kinetics and eventual termination of the polymerization reaction.

The process of initiating the polymerization reaction is quite complex when all the formed reactive species are considered. For iodonium salts, both homolytic and heterolytic cleavages of Ar-I bonds are induced by radiation (or thermal energy), yielding reactive cations, radical cations, and radicals (**Scheme II-35**).<sup>253,286</sup> Nevertheless, cationic polymerization does not directly involve these primary species. Instead, alternative chemical reactions occur between the primary reactive species and organic molecules that can provide a proton to these initial reactive species. This proton transfer generates strong Brønsted acids, the main ones responsible for initiating the cationic polymerization reaction.<sup>284</sup>

The mechanism was inferred by introducing monomers few seconds after photolyzing a diaryliodonium salt in an inert solvent. Despite the delayed addition of the monomers, the progression of reactive species led to creating Brønsted acids and consequently initiating the polymerization process.<sup>253,255</sup> In fact, the initially generated species are too reactive to remain active over the period and initiate polymerization. Rather than the unstable species, the initiation was credited to the formation *in situ* of more stable species, namely the Brønsted acid that originates from the anion of the onium salt. A similar mechanistic scheme

can also represent the photolysis of cationic photoinitiators derived from triaryl sulfonium salts.<sup>287</sup>



**Scheme II-35.** Simplified scheme for diaryliodonium salt photodecomposition.<sup>288</sup>

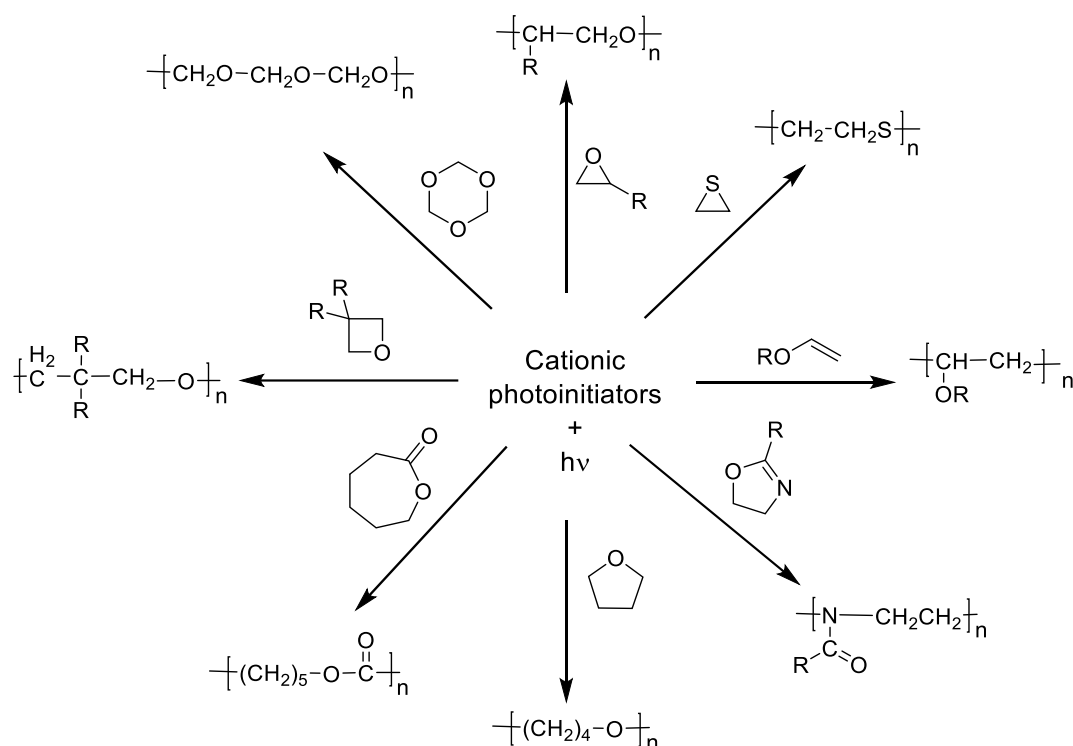
It should be emphasized that the iodonium or triaryl sulfonium salts can undergo degradation reactions via a photochemical or thermal pathway.<sup>253</sup> Likewise, when these salts are thermally degraded, they produce active species that continue to evolve until they form strong acids. This method was used in the development of new epoxy networks using cycloaliphatic epoxidized ILs, which will be discussed further in the following chapters.<sup>289</sup>

It is worth mentioning that the strength of the generated acids depends on the inorganic counterion. Typically, cationic polymerization photoinitiators bear  $\text{BF}_4^-$ ,  $\text{PF}_6^-$ ,  $\text{AsF}_6^-$ , and  $\text{SbF}_6^-$  to create superacids.<sup>287</sup> Diaryliodonium and triarylsulfonium salts are considered general photoinitiators due to their ability to initiate cationic polymerization in various monomers.

Their nucleophilicity and size determine the order of reactivity among the aforementioned anions and are as follows:  $\text{SbF}_6^- > \text{AsF}_6^- > \text{PF}_6^- > \text{BF}_4^-$ .<sup>287</sup> These two factors significantly impact the degree of association of the ion pair and, consequently, the propagating chain end.

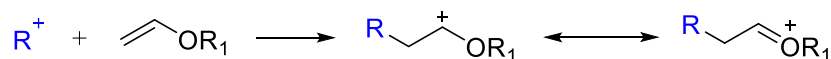
## 4.2. Cationically Photopolymerizable Monomers

The polymerization of unsaturated monomers, including vinyl ethers,<sup>258</sup> styrene,<sup>254</sup> N-vinylcarbazole,<sup>256</sup> cyclic ethers,<sup>283</sup> lactones,<sup>283</sup> and cyclic acetals,<sup>257</sup> as well as the ring-opening polymerizations of epoxy monomers,<sup>260</sup> have been carried out using photoinduced cationic polymerization. The broad range of monomers that can be polymerized via a cationic mechanism allows the synthesis of an extensive library of polymers (**Scheme II-36**).



**Scheme II-36.** The main functional groups employed to design photopolymerizable monomers via cationic polymerization.<sup>253</sup>

Vinyl ether monomers have become an attractive alternative to acrylates due to their insignificant toxicity, low vapor pressure, and high reactivity.<sup>282,290,291</sup> Further, vinyl ethers exhibit higher curing rates than epoxide monomers, with reactivity comparable to acrylates. The reactivity of vinyl ethers is due to the electron-rich nature of their carbon-carbon double bonds, which can be stabilized by the adjacent oxygen atom (**Scheme II-37**).

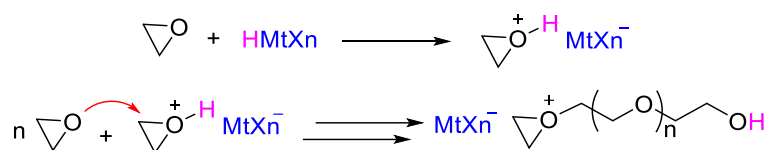


**Scheme II-37.** Resonance stabilization of the carbocation in vinyl ether.<sup>291</sup>

Moreover, the greater conversion rates of vinyl ether monomers relate to their relatively  $T_g$ , which minimizes the rate-retarding effects of matrix vitrification during the gelation process.<sup>260,282,292</sup> Conversely, under certain conditions, hydrolysis may compete with the polymerization of vinyl ether monomers.<sup>291</sup> This hydrolysis reaction, catalyzed by the same acid species that catalyzes the polymerization reactions, produces acetaldehyde and alcohol. In addition to this hydrolysis issue, vinyl ether monomers are not widely used in industrial UV-cure applications due to their high costs and relatively poor mechanical properties.



Epoxides are the most commercially significant class of cationically photocurable monomers, which undergo ring-opening polymerization through an oxiranium ion intermediate in the presence of a photogenerated acid (**Scheme II-38**).<sup>282</sup>



**Scheme II-38.** Mechanism of the cationic ring-opening polymerization of epoxide monomers.<sup>260</sup>

Crosslinking can easily occur when using difunctional epoxides as starting materials, resulting in a three-dimensional polymer network.<sup>293</sup> Unlike in radical-initiated polymerizations, the positively charged chain carriers do not interact with each other, so there are no termination reactions. This means the living polymerization continues to develop without UV exposure, leading to a dark cure effect.<sup>253</sup> However, termination can still occur through a chain transfer process that produces an inactive species or through a reaction of the propagating species with nucleophilic impurities, such as water or anions.<sup>282</sup>

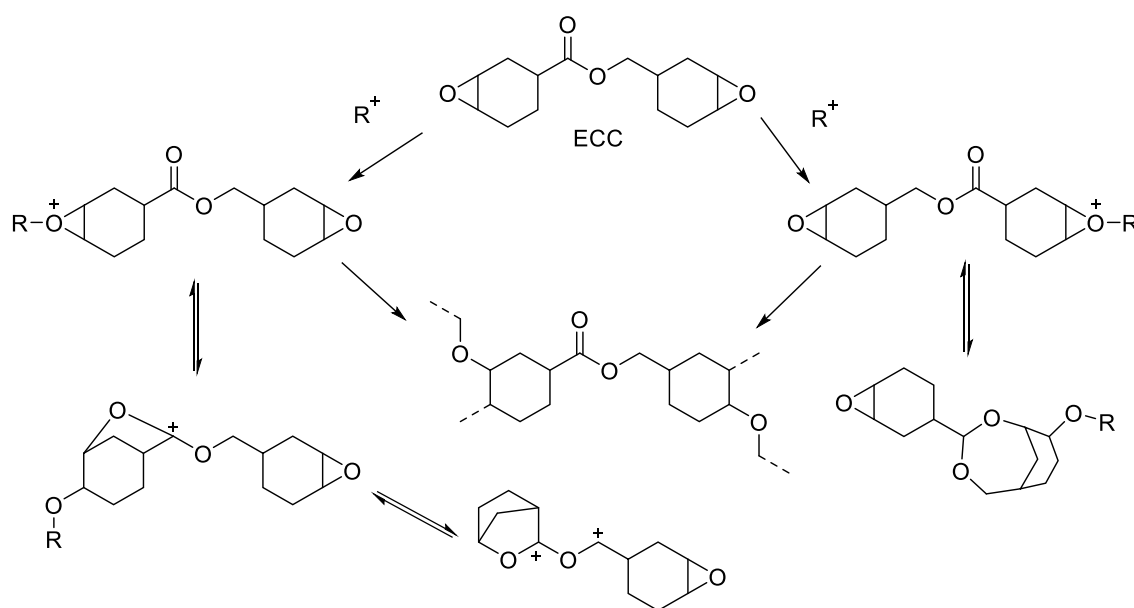
Cationic polymerization occurs rapidly until gelation, after which it slows down but continues as monomers diffuse to fixed propagating sites within the swollen gel.<sup>260,292</sup> However, when the  $T_g$  of the network approaches the temperature at which UV-curing is taking place, vitrification sets in, and polymerization virtually ceases. As a result, significant amounts of unreacted polymerizable epoxide groups remain trapped in the glassy UV-cured coatings.

Chain transfer agents, such as alcohols, can be used to delay the onset of gelation, which allows the overall polymerization rate to remain high and the overall apparent cure rate to be accelerated.<sup>294</sup> The structure of the alcohols used as chain transfer agents significantly affects the photoinitiated cationic polymerization of epoxides. Under high humidity conditions, the cationic UV-curing of vinyl ethers and some epoxide monomers is inhibited.<sup>295</sup> Interestingly, adding only a tiny amount of water to a formulation can enhance rates and conversion by chain transfer.<sup>294</sup> Contrarily, high humidity can lead to the localized concentration of water at a coating's surface, resulting in low molecular weight polymers due to excessive chain transfer. In the case of vinyl ether monomers, the presence of water during UV-cure can lead to their hydrolysis.<sup>291</sup>

Nevertheless, the polymerization rate for many types of difunctional epoxides is lower compared to acrylate monomers, probably due to a lower propagation rate con-

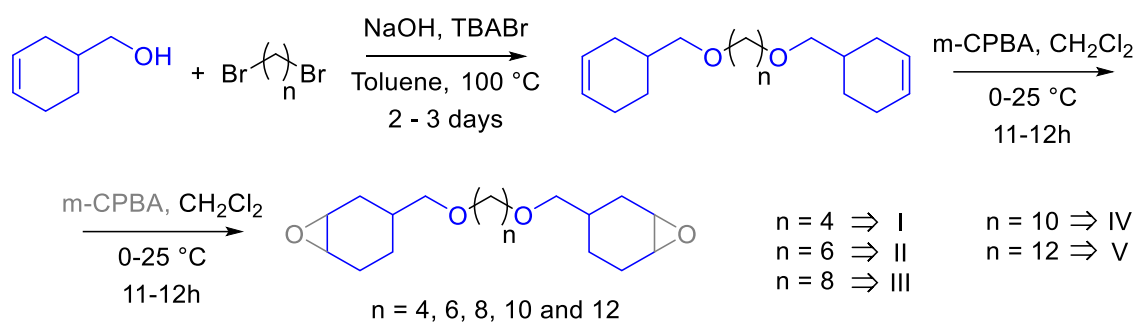
stant.<sup>262,265,296,297</sup> Only cycloaliphatic epoxides have reached substantial commercial significance due to their higher reactivity in cationic photopolymerization and their excellent adhesion, chemical resistance, and mechanical properties.<sup>245,260,294,296</sup> Cycloaliphatic epoxidized monomers exhibit higher reactivity due to the more significant ring strain.<sup>148</sup> When multifunctional epoxy monomers are UV-cured using photoinitiated cationic polymerization, the cure rate typically reaches a maximum and decreases rapidly.<sup>298</sup>

The monomers' chemical structures strongly impact the reactivity of epoxy precursors. For example, the most commonly used cycloaliphatic epoxy monomer denoted, 3,4-epoxycyclohexylmethyl-3,4-epoxycyclohexane carboxylate (ECC) displays lower reactivity than other cycloaliphatic monomers.<sup>296</sup> Indeed, the presence of ester groups influences the reactivity of epoxy monomers. Under the conditions of cationic photopolymerization, several side reactions can take place and hinder the propagation of polymerization (**Scheme II-39**).<sup>253</sup>



**Scheme II-39.** Mechanism of ring-opening polymerization including potential side reactions for ECC monomer by Crivello *et al.*<sup>253</sup>

The group led by James Crivello made a significant contribution to understanding the relationship between the chemical structure of monomers and their reactivity.<sup>246,279,296</sup> Initially, they observed that the presence of ester groups could yield parasite side reactions. In another study, they proposed synthesizing multiple monomer 1,4-Bis(3,4-Epoxy cyclohexylmethoxy)alkanes with varied chain lengths between the two cycloaliphatic epoxy groups (**Scheme II-40**).<sup>246</sup>



**Scheme II-40.** The synthetic route proposed for the syntheses of cycloaliphatic epoxy monomers with an aliphatic ether-based spacer.<sup>246</sup>

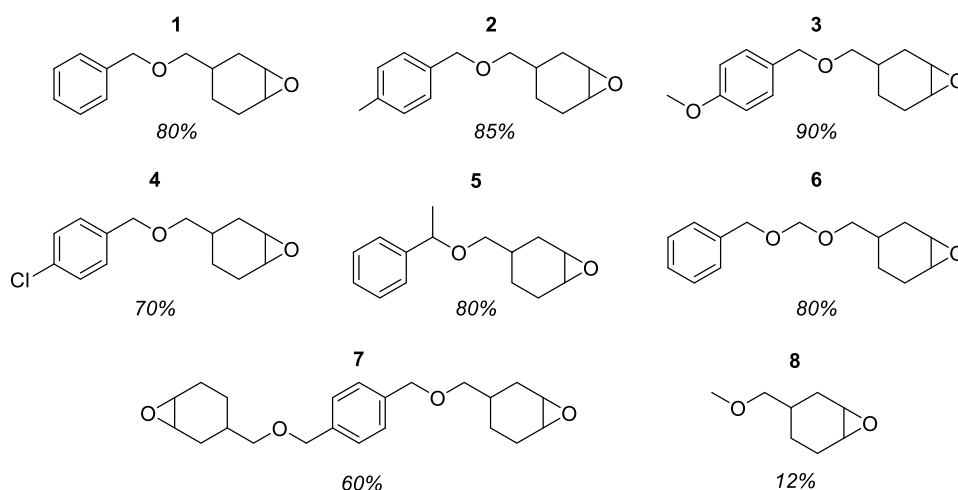
Interestingly, they found that the monomers lacking ester groups exhibited higher reactivity. Furthermore, they observed that increasing the carbon chain length reduced the reactivity of these photopolymerizable monomers. They argued that an increase of the distance between the photopolymerizable epoxy groups is not beneficial for the propagation of the polymerization reaction.

**Table II-1.** The conversion of epoxy groups using 0.5 mol% of photoinitiator after 800 seconds of UV-light exposure.

Compound	Epoxy Conversion (%)
ECC	30
I	50
II	75
III	18
IV	17
V	16

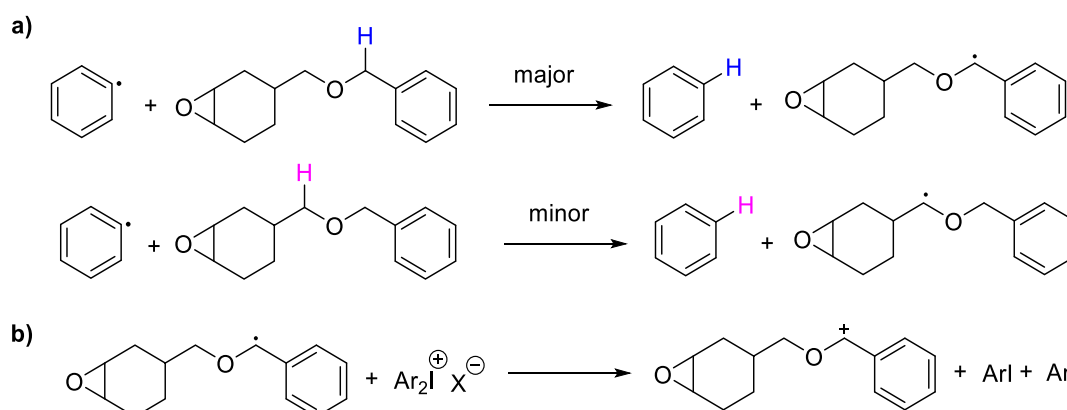
\*The photoinitiator employed in this study was 4-octyloxyphenyl]phenyliodonium hexafluoroantimonate (IOC).

Therefore, the authors synthesized a new series of epoxy monomers containing benzyl ether groups that can be photopolymerized through cationic ring-opening (**Fig. II-11**).<sup>279</sup> These monomers exhibited faster polymerization rates than their analogous without the benzyl ether moiety in their backbones.



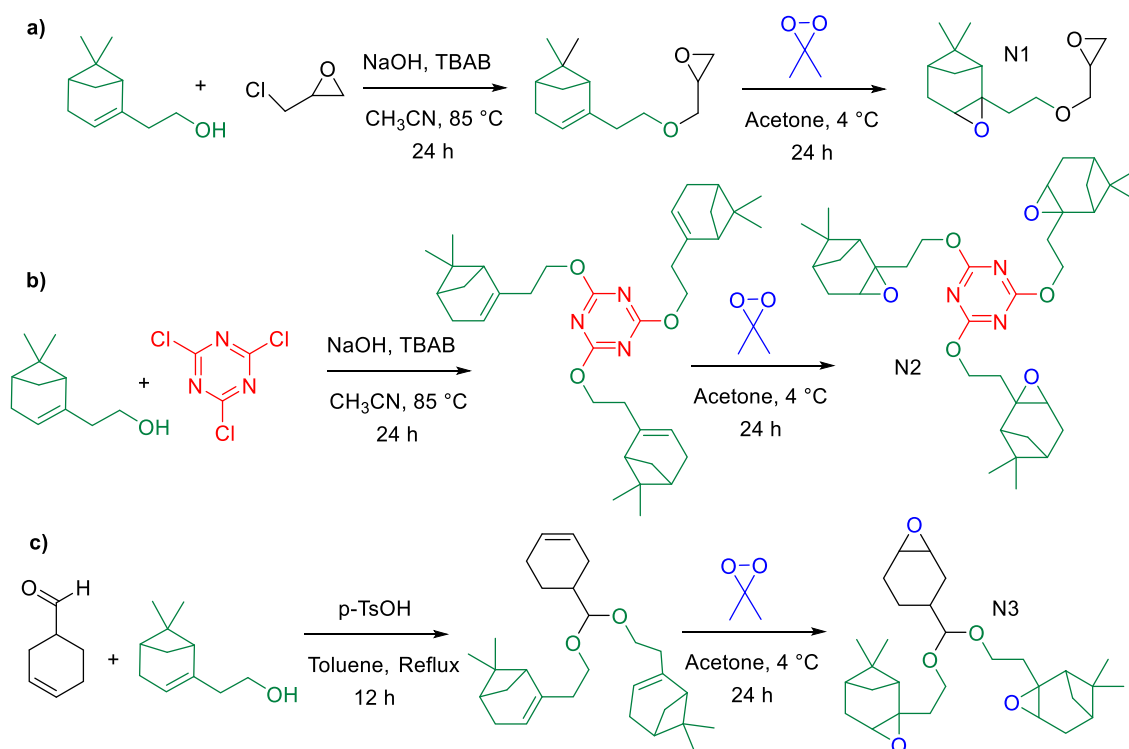
**Figure II-11.** The synthesized photopolymerizable cyclo aliphatic monomers containing moiety benzyl ether (**1-7**), and without the benzyl ether moiety (**8**). The percentage indicates the epoxy rate conversion after 100 seconds of UV irradiation in the presence of 1% of (4-n-decyloxyphenyl)phenyliodonium hexafluoroantimonate with light intensity  $52 \text{ J cm}^{-2} \text{ min}^{-1}$ .<sup>279</sup>

The authors proposed a mechanism in which a free-radical process occurs in conjunction with the classical cationic pathway. Under UV irradiation, aryl radicals are formed from an onium photoinitiator (**Scheme II-41**).<sup>279</sup> Subsequently, these aryl radicals abstract labile benzyl hydrogens to produce a relatively stable radical. The onium salt then oxidizes these benzyl radicals through a nonphotochemical process to form benzyl carbocations. This reactive carbocation can then initiate the cationic ring-opening polymerization pathway. The synergistic combination of the two mechanisms makes the benzyl ether-containing precursors a promising class of epoxy monomers for cationic polymerization.



**Scheme II-41.** The additional photopolymerization pathway coupled to the classical cationic mechanism. In **a)** the two most probable radicals that can be formed, followed by **b)** the oxidation of the radical by the iodonium salt to generate the reactive carbocation.<sup>279</sup>

More recently, Santos *et al.* proposed the synthesis of three novel biobased monomers (**Scheme II-42**).<sup>299</sup> They used *nopol* as a molecular platform, and via alkylation, nucleophilic aromatic substitution and acetalization, the bicyclic cycloalkene functionalities were incorporated. Then, the cycloalkene moieties were further epoxidized using dimethyl dioxirane (DMDO). The three epoxy monomers revealed high reactivity corroborated by the strained bicyclic structures. They observed an epoxy conversion of about 50% after less than 1 minute of irradiation in the presence of an iodonium salt. The  $T_g$  measured were 66, 60 and 12 °C for networks obtained from monomers N1, N2 and N3, respectively. Among the three starting materials, N2, an aromatic triazine epoxy monomer, demonstrated the highest thermal stability with an onset degradation temperature of 302 °C, as determined by TGA.



**Scheme II-42.** The synthetic routes for synthesized bio-based bicyclic cycloaliphatic epoxides. In **a)** N1, **b)** N2 and **c)** N3.

In summary, the use of cycloaliphatic epoxy monomers in cationic photopolymerization has shown promise, providing benefits compared to conventional free radical polymerization methods. Various researchers are currently synthesizing new monomers for advanced applications, with the chemical structures and starting materials relying on the research purpose. The reader will see later that incorporating IL moieties into the cycloaliphatic monomers is a potential approach to afford emerging properties to thermoset materials.

### 4.3. Ionic Liquids & Light: A Possible Wedding?

#### 4.3.1. Light Absorption and Photostability of ILs

Designing ILs that can eventually photopolymerize requires an understanding of the photochemical behaviour of the ILs and the effect of ILs on the photochemical reactions occurring in these media.<sup>300</sup> Indeed, the importance of the photophysical behaviour of ILs starts at the very beginning of the polymerization reaction with the absorption and generation of reactive species.<sup>301</sup>

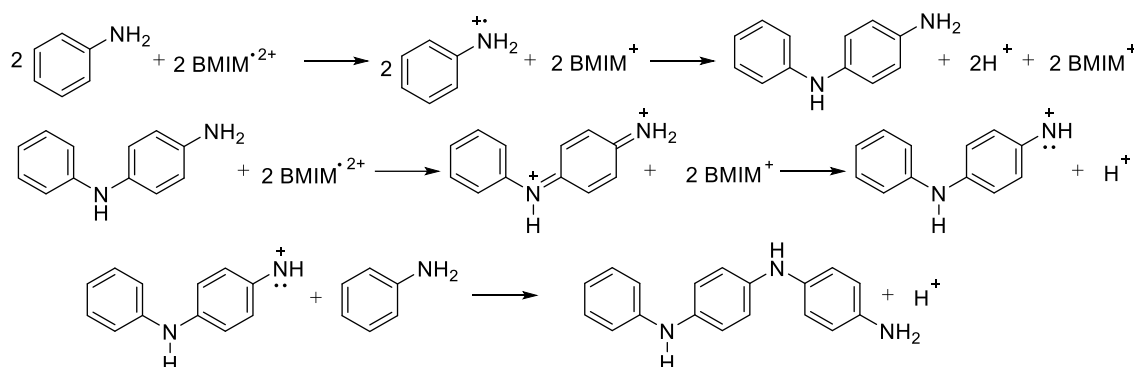
The primary point to verify is the light absorption by ILs. Most ILs do not absorb in low wavelengths of the UV region and are completely transparent in the visible region.<sup>302,303</sup> Aliphatic cation-based ILs tend to be colorless and have typical absorption spectra with very low extinction coefficients in the UV and visible regimes. Contrarily, the imidazolium ILs exhibit strong absorption between 200 and 300 nm due to the presence of the aromatic nature of the imidazolium and the consequent  $\pi-\pi^*$  transition.<sup>304</sup> The maximum absorption peak usually is at about 210 nm. Above 260 nm a shoulder is very often observed, passing into a long tail, well beyond 400 nm. Interestingly, the UV absorption spectra of ILs in vapor, liquid and aqueous phase have shown that the spectra are very similar, suggesting that the IL structure in vapor state is identical to the IL structures in solution.<sup>305</sup>

The literature on photochemical reactions involving ILs is very scarce, although a few examples exist.<sup>304,306</sup> Considering the chemical nature of the ILs, it is probable that due to their polar character, ILs will influence the photochemical reactions leading to the production of initiating radicals. Type II systems are expected to exhibit a noticeable impact, which involves stabilizing charged species and radicals followed by proton transfer.

For instance, the photoreduction of benzophenone (BP) by ILs was investigated.<sup>307</sup> The rate constants of hydrogen abstraction from ILs were sensibly lower than those observed in conventional solvents. This is probably because the activation energy for the hydrogen abstraction from imidazolium-based ILs is significantly higher than that observed in conventional solvents. The deprotonation of imidazolium ILs can yield a reduction in the stabilization of intermolecular interactions. Nevertheless, imidazolium ILs cannot be considered inert or spectators in photochemical reactions.

Measurements of reduction reaction induced by light in the presence of imidazolium-ILs also corroborate this reasoning. It was observed that methylene blue and anthraquinone could deprotonate the imidazolium probably via an electron transfer reaction.<sup>308</sup>

In this context, Yang *et al.* observed the polymerization of aniline using 1-Butyl-3-methylimidazolium hexafluorophosphate [bmim]PF<sub>6</sub> as the solvent (**Scheme II-43**).<sup>309</sup> According to the proposed mechanism, [bmim]<sup>+</sup> undergoes photoexcitation, forming [bmim]<sup>2+</sup> radical cations. These radical cations then oxidize aniline to its radical cations, which can combine through a head-to-tail coupling to produce dimers. The dimers are subsequently oxidized to form quinoid units, which can be deprotonated to generate nitrenium ions. These ions can then react with an aniline monomer to produce trimers. The reaction can continue, leading to the formation of oligomers and, ultimately, to polyaniline.



**Scheme II-43.** The potential mechanism of photoinduced polymerization of aniline in [bmim]PF<sub>6</sub>.<sup>309</sup>

The photostability of ILs plays a crucial role in their use as reaction media or photopolymerizable precursors.<sup>306,310,311</sup> However, a limited amount of scientific literature is available on this subject. To the best of our knowledge, only a few studies have explored the photostability of ILs based on imidazolium.

According to Gordon *et al.*, exposure of [bmim]PF<sub>6</sub> to wavelengths of 300 nm or above does not result in any alterations in the UV spectrum.<sup>310</sup> However, when subjected to 254 nm light, new bands emerge, and the sample takes on a colored appearance. The authors did not elucidate the chemical structures of the molecules formed.

Reynolds *et al.* observed no sign of chemical reactions when imidazolium ILs were irradiated for 24h using a medium-pressure Hg lamp at room temperature.<sup>311</sup> Pagni has described photoinduced electron transfer in RTILs. This report, among others, found that the conducting nature of ILs provided an excellent medium for generating and stabilization of radical ions.<sup>312</sup>

Recently, Takahashi and Katoh reported on the photodegradation of two ILs.<sup>313</sup> [bmim] NTf<sub>2</sub> and [bmim]I underwent complete degradation when exposed to 220 and 280 nm pulsed laser. The degradation of these compounds is believed to be one of the primary

channels of excited [bmim]<sup>+</sup>, but this action remains stable for only a few nanoseconds when bmimI is irradiated. The nature of the species produced after one-photon photolysis of various imidazolium ILs is not yet fully elucidated.

Although some studies have reported high stability of ILs under light exposure, reports suggest the opposite, particularly for ILs derived from imidazolium.<sup>314</sup> Hence, additional investigation is required to study the photostability of these ILs by examining various parameters such as wavelength, light power, and exposure time.

Indeed, during this doctorate research project, several pieces of evidence suggested that imidazolium-ILs become more reactive under visible-light exposure. Although there is insufficient evidence to confirm this, it is believed that light exposure facilitates the deprotonation of imidazolium-C2, which leads to the formation of a carbanion and, subsequently, an N-heterocyclic carbene. Carbenes can act as nucleophiles and electrophiles, thus making them capable of undergoing dimerization reactions. Notably, while synthesizing one of the IL monomers, the dimer of an imidazolium-IL was isolated, but this result has not yet been published.

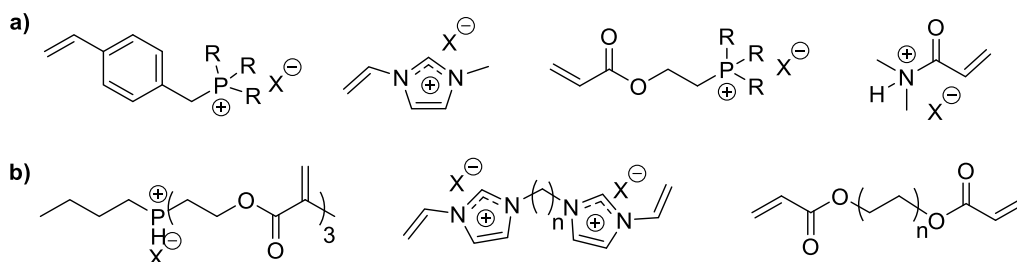
#### **4.3.2. The Potential of Photopolymerizable Ionic Liquids**

This section presents the synthesis and properties of photopolymerized ILs, focusing on strategies for monomer design, material fabrication, and their applications.

The tunable nature of ILs has led to the development of numerous photopolymerizable monomers.<sup>315–318</sup> **Fig. II-12** displays a selection of possibilities for photopolymerizable monomers and crosslinkers.<sup>316</sup> Importantly, the photoinitiators employed are the same as those previously presented earlier for conventional photopolymerization.

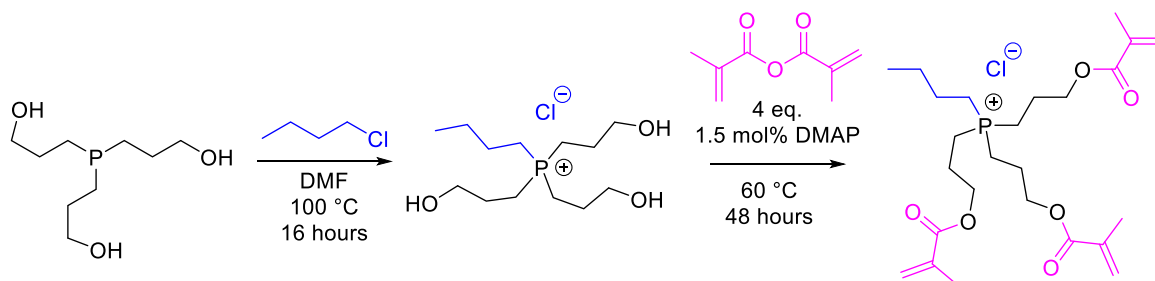
For the monomers, vinyl and (meth)acrylate derivatives are the most widely used, encompassing phosphonium,<sup>315</sup> imidazolium,<sup>319,320</sup> and ammonium<sup>321</sup> varieties. These monomers are typically copolymerized with crosslinkers to produce durable and insoluble materials. Neutral crosslinkers, such as TEGDMA and DVB (**Fig. II-10**), are frequently used, even if they reduce the network's ion content. Alternatively, several IL crosslinkers have been developed to maintain high-ion content while introducing crosslinks.<sup>316,322</sup>





**Figure II-12.** In developing polyelectrolytes using UV-curing processes, the employment of **a)** photopolymerizable ILs and **b)** reactive dilutants to adjust viscosity are essential factors.

Guterman's research group, now based at the Max Planck Institute, significantly contributed to designing novel photopolymerizable ILs. They, for instance, designed and synthesized a phosphonium-based IL for a specific coating application (**Scheme II-44**).<sup>315</sup>



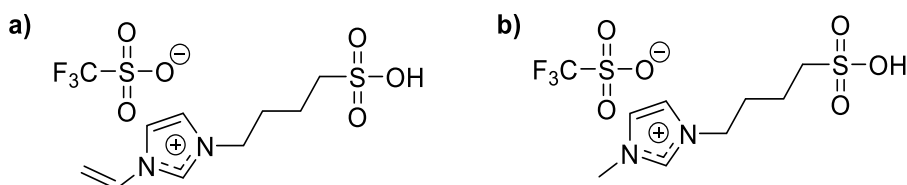
**Scheme II-44.** The synthetic route proposed by Guterman *et al.* to accomplish the synthesis of the phosphonium-based IL monomer.

This coating could be easily applied within minutes using a roll-to-roll process. They quantified the charges on the coating surface by conducting an anion exchange using nanocrystals of  $[\text{Au}_{25}\text{L}_{18}]^-$  ( $\text{L} = \text{SCH}_2\text{CH}_2\text{Ph}$ ). Interestingly, the nanocrystals remained intact, preserving their photophysical properties. The researchers have determined the loading of  $[\text{Au}_{25}\text{L}_{18}]^-$  and established the complete reversibility of loading and unloading of the intact nanocrystals in the polyelectrolyte surfaces.

Using a similar phosphonium-based IL, the same authors produced antibacterial films. They have shown that by introducing the phosphonium moiety by UV-curing procedure, the resulting films exhibited remarkable bactericidal activity and avoided bacterial growth.<sup>317</sup>

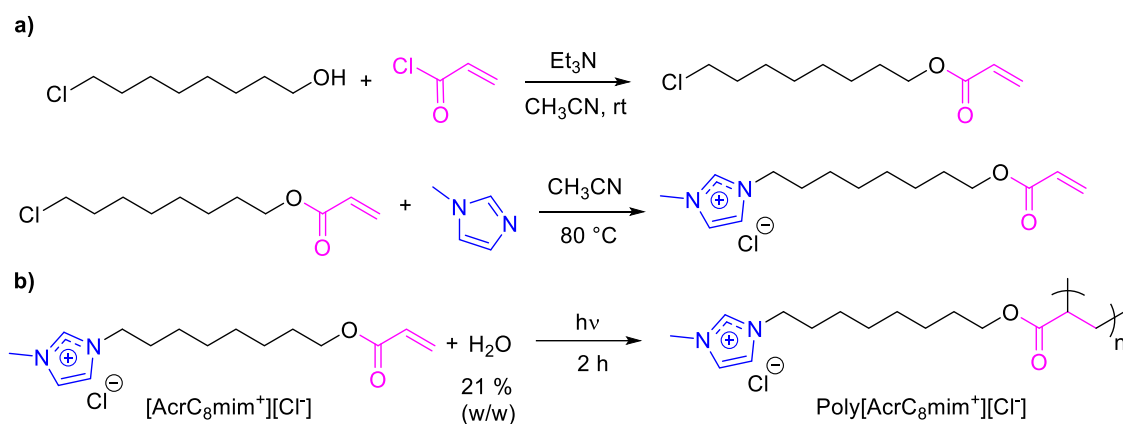
Remarkably, these poly(ILs) materials have applications beyond coatings. For example, they can be utilized to develop gel polymer electrolytes for proton exchange membrane fuel cells. Proton exchange membrane fuel cells are electrochemical devices that can convert chemical energy into electrical energy.

Aiming to develop fuel cell membranes, Mecerreyes *et al.* employed a photopolymerizable imidazolium-IL doped with a non-reactive and common IL (**Fig. II-13**).<sup>323</sup> The chemical affinity between these two materials resulted in stable, flexible, and transparent membranes. The researchers analyzed the effect of temperature and the quantity of non-polymerizable IL on ionic conductivity and fuel cell performance. The results of fuel cell tests and ionic conductivity experiments indicated that these IL-based membranes have great potential as proton exchange devices.



**Figure II-13.** The IL precursors employed by Mecerreyes *et al.* for developing membranes. In **a)** the photopolymerizable imidazolium-IL and **b)** an additive based on imidazolium-IL.<sup>323</sup>

More recently, few studies have been reporting the photopolymerization of IL monomers preserving the crystalline character of the monomers. In 2007, Firestone and colleagues designed and synthesized a photopolymerizable IL with methylimidazolium and acryloyl moieties tethered by an eight-carbon chain ([AcrC<sub>8</sub>mim<sup>+</sup>][Cl]) (**Scheme II-45**).<sup>324</sup>

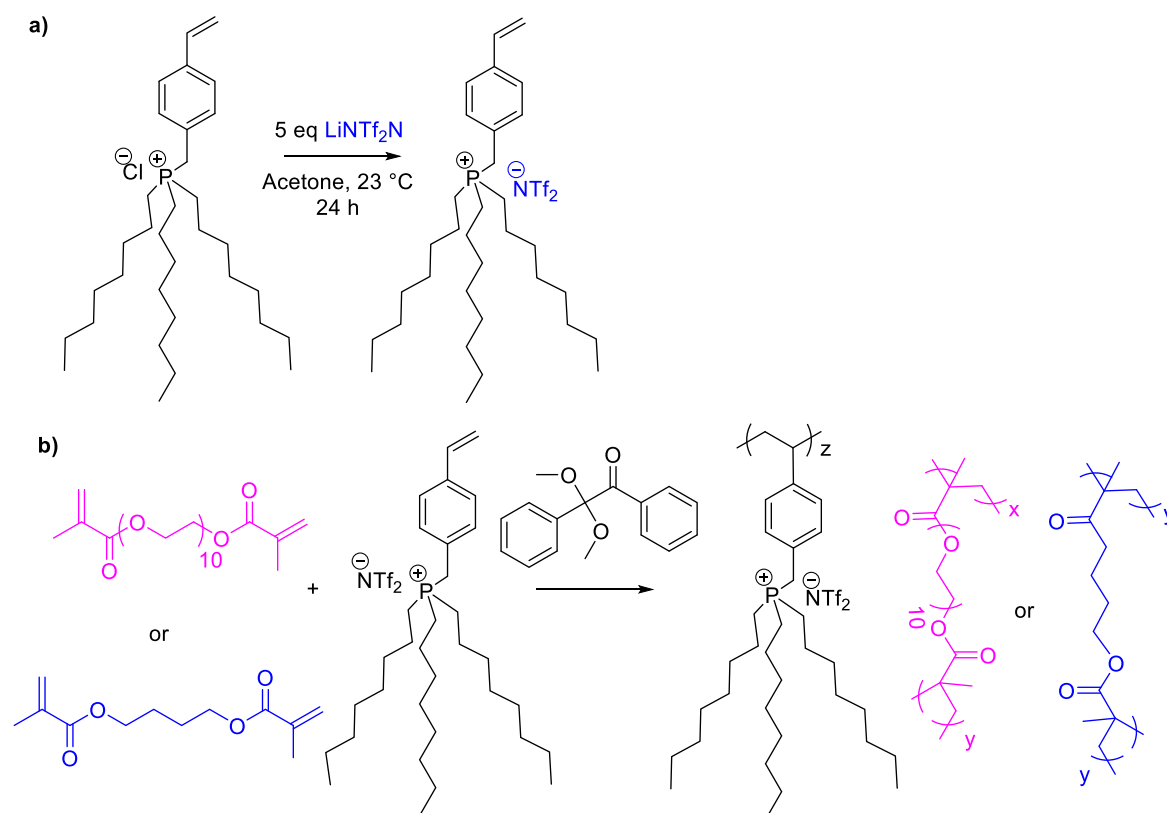


**Scheme II-45.** In **a)** the synthetic route proposed to obtain acrylate-based IL monomers and **b)** their further photopolymerization.

The new monomer was used to develop biomimetic liquid crystalline hydrogels. The authors observed that the IL monomers self-assemble in the presence of water and tend to polymerize when exposed to heating. Without an initiator, UV irradiation triggered photopolymerization, forming a hydrogel that could support itself.

The hydrogel possessed enhanced self-assembly properties compared to its precursor material. They also have shown by small-angle X-ray scattering (SAXS) that the hydrogels possessed an ordered lamellar bilayer liquid crystalline structure. The bilayers are similar to the structure of a cell wall in that they contain both hydrophobic and hydrophilic areas. The polymer underwent a reversible swelling of almost 200 times its original volume when it was exposed to water. This caused a change in its morphology from an ordered to a highly disordered lamellar structure while still maintaining its multi-bilayer ordering. The swelling was found to be most significant with water, but other solvents, such as ethanol, were also observed to induce swelling to a lesser extent.

Timothy Long and coworkers proposed the synthesis of a vinyl-derivative phosphonium IL as photopolymerizable monomer for micro stereolithography application.<sup>318</sup> This process has the advantage of requiring low UV light intensity and providing high digital resolution. Adjusting the phosphonium monomer concentration and diacrylate crosslinking comonomer (**Scheme II-47**), accurate 3D design and excellent polymer properties can be achieved. Thermal properties and solvent extraction confirmed the formation of a polymerized IL network, with gel fractions exceeding 95%.



**Scheme II-47.** In **a)** the ionic exchange performed to obtain the phosphonium IL precursor and **b)** its further polymerization.

The resulting crosslinked materials exhibited a unique combination of desirable properties, including high thermal stability, tunable glass transition temperature, optical clarity, and ion conductivity. These properties made them ideal for emerging electro-active membrane technologies since they also demonstrated promising ionic conductivity behavior.<sup>318</sup>

Ongoing research is being conducted to discover new photopolymerizable ILs using acrylate and dimethyl acrylate.<sup>325</sup> In recent work, Strehmel and colleagues synthesized novel methacrylates and dimethacrylates that contained ammonium moiety and various anions bis(trifluoromethylsulfonyl)imide (NTf<sub>2</sub>), tris(pentafluoroethyl)trifluorophosphate (FAP), triflate (TfI), and tri-fluoroacetate (TFA). They demonstrated that the type of anion influenced melting point and photopolymerization kinetics more than the cation counterparts. Photo-DSC experiments revealed significant differences in the reaction rate and final conversion depending on the polymerization techniques, namely, bulk or polymerization in solution. The chemical structure of the IL was found to be equally important. The results showed that NTf<sub>2</sub> or FAP are more preferable than TfI and TFAc for photoinitiated polymerization due to their faster reaction rates and higher final conversion. Interestingly, when an IL methacrylate with the same anion as the IL dimethacrylate was present during the photoinitiated polymerization of the latter, the final conversion increased. This could be due to a lower crosslink density of the network formed, resulting in higher mobility during the crosslinking process.

Up to this point, it has been noted that there is significant research on the design and synthesis of novel photopolymerizable ILs. By examining the existing scientific literature, it is remarkable that acrylates, methacrylates, and vinyl derivatives are the main functionalities used for this purpose. To date, there is no report of epoxidized ILs being photopolymerized by the cationic pathway, which prompted us to focus our research on achieving that.

## 5. Conclusion of Chapter II

In recent decades, ILs have gained significant importance in material science, offering a versatile platform for tailoring and inducing novel properties. Numerous studies have focused on synthesizing IL-based monomers and developing materials using various polymerization techniques. However, integrating these IL-based monomers and developing and characterizing these materials remain relatively underexplored in the existing literature. Additionally, several works have described the incorporation of cleavable groups into polymers to enhance sustainability. However, these approaches often rely on harsh and environmentally hazardous conditions. Furthermore, they face challenges obtaining materials with excellent properties and effectively valorizing the resulting degraded products. In the

realm of photopolymerization, the published literature has primarily focused on the free-radical polymerization of vinyl-derivative monomers, leaving the possibility for developing novel cationic photopolymerizable monomers. Taking inspiration from these advancements, our work strives to integrate computational chemistry, organic synthesis, material science, and green chemistry. We aim to create high-performance thermosets and composites that exhibit enhanced properties and a reduced environmental impact. Through this interdisciplinary approach, we aim to address the existing knowledge gaps in the literature, contribute to the progress of materials science, and lay the foundation for the development of more sustainable thermoset materials.

## 6. References

- (1) Marcus, Y. *Ionic Liquid Properties*; Springer International Publishing: Cham, **2016**. <https://doi.org/10.1007/978-3-319-30313-0>.
- (2) Siriwardana, A. I. Industrial Applications of Ionic Liquids. In *Electrochemistry in Ionic Liquids*; Springer International Publishing: Cham, **2015**; pp 563–603. [https://doi.org/10.1007/978-3-319-15132-8\\_20](https://doi.org/10.1007/978-3-319-15132-8_20).
- (3) MacFarlane, D. R.; Seddon, K. R. Ionic Liquids—Progress on the Fundamental Issues. *Australian Journal of Chemistry* **2007**, *60* (1), 3–17. <https://doi.org/10.1071/CH06478>.
- (4) Wilkes, J. S. A Short History of Ionic Liquids—from Molten Salts to Neoteric Solvents. *Green Chemistry* **2002**, *4* (2), 73–80. <https://doi.org/10.1039/b110838g>.
- (5) Wasserscheid, Peter; Welton, T. *Ionic Liquids in Synthesis*; Wasserscheid, P., Welton, T., Eds.; Wiley-VCH, Weinheim, Germany, **2007**. <https://doi.org/10.1002/9783527621194>.
- (6) Abbott, A. P.; Harris, R. C.; Ryder, K. S. Application of Hole Theory to Define Ionic Liquids by Their Transport Properties. *The Journal of Physical Chemistry B* **2007**, *111* (18), 4910–4913. <https://doi.org/10.1021/jp0671998>.
- (7) Vekariya, R. L. A Review of Ionic Liquids: Applications towards Catalytic Organic Transformations. *Journal of Molecular Liquids* **2017**, *227*, 44–60. <https://doi.org/10.1016/j.molliq.2016.11.123>.
- (8) Zhu, S.; Wu, Y.; Chen, Q.; Yu, Z.; Wang, C.; Jin, S.; Ding, Y.; Wu, G. Dissolution of Cellulose with Ionic Liquids and Its Application: A Mini-Review. *Green Chemistry* **2006**, *8* (4), 325–350. <https://doi.org/10.1039/b601395c>.

- (9) Ren, F.; Wang, J.; Xie, F.; Zan, K.; Wang, S.; Wang, S. Applications of Ionic Liquids in Starch Chemistry: A Review. *Green Chemistry* **2020**, *22* (7), 2162–2183. <https://doi.org/10.1039/C9GC03738A>.
- (10) Meksi, N.; Moussa, A. A Review of Progress in the Ecological Application of Ionic Liquids in Textile Processes. *Journal of Cleaner Production* **2017**, *161*, 105–126. <https://doi.org/10.1016/j.jclepro.2017.05.066>.
- (11) Ibrahim, M. H.; Hayyan, M.; Hashim, M. A.; Hayyan, A. The Role of Ionic Liquids in Desulfurization of Fuels: A Review. *Renewable and Sustainable Energy Reviews* **2017**, *76*, 1534–1549. <https://doi.org/10.1016/j.rser.2016.11.194>.
- (12) Plechkova, N. V.; Seddon, K. R. Applications of Ionic Liquids in the Chemical Industry. *Chem. Soc. Rev.* **2008**, *37* (1), 123–150. <https://doi.org/10.1039/B006677J>.
- (13) Lei, Z.; Chen, B.; Koo, Y. M.; Macfarlane, D. R. Introduction: Ionic Liquids. *Chemical Reviews* **2017**, *117* (10), 6633–6635. <https://doi.org/10.1021/acs.chemrev.7b00246>.
- (14) Goossens, K.; Lava, K.; Bielawski, C. W.; Binnemans, K. Ionic Liquid Crystals: Versatile Materials. *Chemical Reviews* **2016**, *116* (8), 4643–4807. <https://doi.org/10.1021/cr400334b>.
- (15) Graenacher, C. Cellulose Solution. US1943176A, December **1934**.
- (16) Holbrey, J. D.; Seddon, K. R. Ionic Liquids. *Clean Technologies and Environmental Policy* **1999**, *1* (4), 223–236. <https://doi.org/10.1007/s100980050036>.
- (17) Winterton, N. Solubilization of Polymers by Ionic Liquids. *Journal of Materials Chemistry* **2006**, *16* (44), 42–81. <https://doi.org/10.1039/b610143g>.
- (18) Zhang, J.; Wu, J.; Yu, J.; Zhang, X.; He, J.; Zhang, J. Application of Ionic Liquids for Dissolving Cellulose and Fabricating Cellulose-Based Materials: State of the Art and Future Trends. *Materials Chemistry Frontiers* **2017**, *1* (7), 1273–1290. <https://doi.org/10.1039/C6QM00348F>.
- (19) Liu, Y.-R.; Thomsen, K.; Nie, Y.; Zhang, S.-J.; Meyer, A. S. Predictive Screening of Ionic Liquids for Dissolving Cellulose and Experimental Verification. *Green Chemistry* **2016**, *18* (23), 6246–6254. <https://doi.org/10.1039/C6GC01827K>.
- (20) da Costa Lopes, A. M.; Bogel-Lukasik, R. Acidic Ionic Liquids as Sustainable Approach of Cellulose and Lignocellulosic Biomass Conversion without Additional Catalysts. *ChemSusChem* **2015**, *8* (6), 947–965. <https://doi.org/10.1002/cssc.201402950>.

- (21) Abbott, A. P.; Bell, T. J.; Handa, S.; Stoddart, B. O-Acetylation of Cellulose and Monosaccharides Using a Zinc Based Ionic Liquid. *Green Chemistry* **2005**, 7 (10), 70–95. <https://doi.org/10.1039/b511691k>.
- (22) Swatloski, R. P.; Spear, S. K.; Holbrey, J. D.; Rogers, R. D. Dissolution of Cellulose with Ionic Liquids. *Journal of the American Chemical Society* **2002**, 124 (18), 4974–4975. <https://doi.org/10.1021/ja025790m>.
- (23) Ohno, H.; Fukaya, Y. Task Specific Ionic Liquids for Cellulose Technology. *Chemistry Letters* **2009**, 38 (1), 2–7. <https://doi.org/10.1246/cl.2009.2>.
- (24) Wilkes, J. S.; Levisky, J. A.; Wilson, R. A.; Hussey, C. L. Dialkylimidazolium Chloroaluminate Melts: A New Class of Room-Temperature Ionic Liquids for Electrochemistry, Spectroscopy and Synthesis. *Inorganic Chemistry* **1982**, 21 (3), 1263–1264. <https://doi.org/10.1021/ic00133a078>.
- (25) Wilkes, J. S.; Zaworotko, M. J. Air and Water Stable 1-Ethyl-3-Methylimidazolium Based Ionic Liquids. *Journal of the Chemical Society, Chemical Communications* **1992**, No. 13, 965–1000. <https://doi.org/10.1039/c39920000965>.
- (26) Wilkes, J. S. The Past, Present and Future of Ionic Liquids as Battery Electrolytes. In *Green Industrial Applications of Ionic Liquids*; Springer Netherlands: Dordrecht, **2003**; pp 295–320. [https://doi.org/10.1007/978-94-010-0127-4\\_17](https://doi.org/10.1007/978-94-010-0127-4_17).
- (27) Armand, M.; Endres, F.; MacFarlane, D. R.; Ohno, H.; Scrosati, B. Ionic-Liquid Materials for the Electrochemical Challenges of the Future. In *Materials for Sustainable Energy*; Co-Published with Macmillan Publishers Ltd, UK, **2010**; pp 129–137. [https://doi.org/10.1142/9789814317665\\_0020](https://doi.org/10.1142/9789814317665_0020).
- (28) MacFarlane, D. R.; Forsyth, M.; Howlett, P. C.; Kar, M.; Passerini, S.; Pringle, J. M.; Ohno, H.; Watanabe, M.; Yan, F.; Zheng, W.; *et al.* Ionic Liquids and Their Solid-State Analogues as Materials for Energy Generation and Storage. *Nature Reviews Materials* **2016**, 1 (2), 15–55. <https://doi.org/10.1038/natrevmats.2015.5>.
- (29) Ishii, M.; Matsumiya, M.; Kawakami, S. Development of Recycling Process for Rare Earth Magnets by Electrodeposition Using Ionic Liquids Media. *ECS Transactions* **2013**, 50 (11), 549–560. <https://doi.org/10.1149/05011.0549ecst>.
- (30) Torimoto, T.; Tsuda, T.; Okazaki, K.; Kuwabata, S. New Frontiers in Materials Science Opened by Ionic Liquids. *Advanced Materials* **2010**, 22 (11), 1196–1221. <https://doi.org/10.1002/adma.200902184>.

- (31) Abbott, A. P.; McKenzie, K. J. Application of Ionic Liquids to the Electrodeposition of Metals. *Physical Chemistry Chemical Physics* **2006**, *8* (37), 42–65. <https://doi.org/10.1039/b607329h>.
- (32) Vygodskii, Y. S.; Lozinskaya, E. I.; Shaplov, A. S. Ionic Liquids as Novel Reaction Media for the Synthesis of Condensation Polymers. *Macromolecular Rapid Communications* **2002**, *23* (12), 676–680. [https://doi.org/10.1002/1521-3927\(20020801\)23:12<676::AID-MARC676>3.0.CO;2-2](https://doi.org/10.1002/1521-3927(20020801)23:12<676::AID-MARC676>3.0.CO;2-2).
- (33) Biedron, T.; Kubisa, P. Ionic Liquids as Reaction Media for Polymerization Processes: Atom Transfer Radical Polymerization (ATRP) of Acrylates in Ionic Liquids. *Polymer International* **2003**, *52* (10), 1584–1588. <https://doi.org/10.1002/pi.1343>.
- (34) Zhang, Q.; Zhu, S. Ionic Liquids: Versatile Media for Preparation of Vesicles from Polymerization-Induced Self-Assembly. *ACS Macro Letters* **2015**, *4* (7), 755–758. <https://doi.org/10.1021/acsmacrolett.5b00360>.
- (35) Wilpiszewska, K.; Spychaj, T. Ionic Liquids: Media for Starch Dissolution, Plasticization and Modification. *Carbohydrate Polymers* **2011**, *86* (2), 424–428. <https://doi.org/10.1016/j.carbpol.2011.06.001>.
- (36) Lu, J.; Yan, F.; Texter, J. Advanced Applications of Ionic Liquids in Polymer Science. *Progress in Polymer Science* **2009**, *34* (5), 431–448. <https://doi.org/10.1016/j.progpolymsci.2008.12.001>.
- (37) Vygodskii, Y. S.; Lozinskaya, E. I.; Shaplov, A. S.; Lyssenko, K. A.; Antipin, M. Y.; Urman, Y. G. Implementation of Ionic Liquids as Activating Media for Polycondensation Processes. *Polymer* **2004**, *45* (15), 5031–5045. <https://doi.org/10.1016/j.polymer.2004.05.025>.
- (38) Scott, M. P.; Brazel, C. S.; Benton, M. G.; Mays, J. W.; Holbrey, J. D.; Rogers, R. D. Application of Ionic Liquids as Plasticizers for Poly(Methyl Methacrylate). *Chemical Communications* **2002**, No. 13, 1370–1371. <https://doi.org/10.1039/b204316p>.
- (39) Scott, M. P.; Rahman, M.; Brazel, C. S. Application of Ionic Liquids as Low-Volatility Plasticizers for PMMA. *European Polymer Journal* **2003**, *39* (10), 1947–1953. [https://doi.org/10.1016/S0014-3057\(03\)00129-0](https://doi.org/10.1016/S0014-3057(03)00129-0).
- (40) Zdanowicz, M. Starch Treatment with Deep Eutectic Solvents, Ionic Liquids and Glycerol. A Comparative Study. *Carbohydrate Polymers* **2020**, *229*, 115–174. <https://doi.org/10.1016/j.carbpol.2019.115574>.



- (41) Zampino, D.; Mancuso, M.; Zacccone, R.; Ferreri, T.; Borzacchiello, A.; Zeppetelli, S.; Dattilo, S.; Ussia, M.; Ferreri, L.; Carbone, D. C.; *et al.* Thermo-Mechanical, Antimicrobial and Biocompatible Properties of PVC Blends Based on Imidazolium Ionic Liquids. *Materials Science and Engineering: C* **2021**, 122, 111–920. <https://doi.org/10.1016/j.msec.2021.111920>.
- (42) Rahman, M.; Brazel, C. S. Ionic Liquids: New Generation Stable Plasticizers for Poly(Vinyl Chloride). *Polymer Degradation and Stability* **2006**, 91 (12), 3371–3382. <https://doi.org/10.1016/j.polymdegradstab.2006.05.012>.
- (43) Lins, L. C.; Livi, S.; Duchet-Rumeau, J.; Gérard, J.-F. Phosphonium Ionic Liquids as New Compatibilizing Agents of Biopolymer Blends Composed of Poly(Butylene-Adipate-Co-Terephthalate)/Poly(Lactic Acid) (PBAT/PLA). *RSC Advances* **2015**, 5 (73), 59082–59092. <https://doi.org/10.1039/C5RA10241C>.
- (44) Yousfi, M.; Livi, S.; Duchet-Rumeau, J. Ionic Liquids: A New Way for the Compatibilization of Thermoplastic Blends. *Chemical Engineering Journal* **2014**, 255, 513–524. <https://doi.org/10.1016/j.cej.2014.06.080>.
- (45) Quitadamo, A.; Massardier, V.; Valente, M. Interactions between PLA, PE and Wood Flour: Effects of Compatibilizing Agents and Ionic Liquids. *Holzforschung* **2018**, 72 (8), 691–700. <https://doi.org/10.1515/hf-2017-0149>.
- (46) Lopes Pereira, E. C.; Farias da Silva, J. M.; Jesus, R. B.; Soares, B. G.; Livi, S. Bronsted Acidic Ionic Liquids: New Transesterification Agents for the Compatibilization of Polylactide/Ethylene-Co-Vinyl Acetate Blends. *European Polymer Journal* **2017**, 97, 104–111. <https://doi.org/10.1016/j.eurpolymj.2017.10.003>.
- (47) Yousfi, M.; Livi, S.; Dumas, A.; Crépin-Leblond, J.; Greenhill-Hooper, M.; Duchet-Rumeau, J. Ionic Compatibilization of Polypropylene/Polyamide 6 Blends Using an Ionic Liquids/Nanotalc Filler Combination: Morphology, Thermal and Mechanical Properties. *RSC Advances* **2015**, 5 (57), 46197–46205. <https://doi.org/10.1039/C5RA00816F>.
- (48) Livi, S.; Bugatti, V.; Marechal, M.; Soares, B. G.; Barra, G. M. O.; Duchet-Rumeau, J.; Gérard, J.-F. Ionic Liquids–Lignin Combination: An Innovative Way to Improve Mechanical Behaviour and Water Vapour Permeability of Eco-Designed Biodegradable Polymer Blends. *RSC Advances* **2015**, 5 (3), 1989–1998. <https://doi.org/10.1039/C4RA11919C>.

- (49) Kadokawa, J.; Kato, T.; Setoyama, M.; Yamamoto, K. Preparation of Galactomannan-Based Materials Compatibilized with Ionic Liquids. *Journal of Polymers and the Environment* **2013**, *21* (2), 512–519. <https://doi.org/10.1007/s10924-012-0495-5>.
- (50) Stolte, S.; Steudte, S.; Areitioaurtena, O.; Pagano, F.; Thöming, J.; Stepnowski, P.; Igartua, A. Ionic Liquids as Lubricants or Lubrication Additives: An Ecotoxicity and Biodegradability Assessment. *Chemosphere* **2012**, *89* (9), 1135–1141. <https://doi.org/10.1016/j.chemosphere.2012.05.102>.
- (51) Lépori, C. M. O.; Correa, N. M.; Silber, J. J.; Falcone, R. D.; López-López, M.; Moyá, M. L. Use of Ionic Liquids-like Surfactants for the Generation of Unilamellar Vesicles with Potential Applications in Biomedicine. *Langmuir* **2019**, *35* (41), 13332–13339. <https://doi.org/10.1021/acs.langmuir.9b01197>.
- (52) Z, M.; W, L.; S, Z.; Zhou, F. Functional Room-Temperature Ionic Liquids as Lubricants for an Aluminum-on-Steel System. *Chemistry Letters* **2007**, *33* (5), 524–525.
- (53) Jimenez, A.; Bermúdez, M. Ionic Liquids as Lubricants for Steel–Aluminum Contacts at Low and Elevated Temperatures. *Tribology Letters* **2007**, *26* (2), 53–60.
- (54) Sanes, J.; Carrión, F. J.; Bermúdez, M. D.; Martínez-Nicolás, G. Ionic Liquids as Lubricants of Polystyrene and Polyamide 6-Steel Contacts. Preparation and Properties of New Polymer-Ionic Liquid Dispersions. *Tribology Letters* **2006**, *21* (2), 121–133. <https://doi.org/10.1007/s11249-006-9028-5>.
- (55) Vashchuk, A.; Fainleib, A. M.; Starostenko, O.; Grande, D. Application of Ionic Liquids in Thermosetting Polymers: Epoxy and Cyanate Ester Resins. *Express Polymer Letters* **2018**, *12* (10), 898–917. <https://doi.org/10.3144/expresspolymlett.2018.77>.
- (56) Hameed, N.; Eyckens, D. J.; Long, B. M.; Salim, N. V.; Capricho, J. C.; Servinis, L.; De Souza, M.; Perus, M. D.; Varley, R. J.; Henderson, L. C. Rapid Cross-Linking of Epoxy Thermosets Induced by Solvate Ionic Liquids. *ACS Applied Polymer Materials* **2020**, *2* (7), 2651–2657. <https://doi.org/10.1021/acsapm.0c00257>.
- (57) Nguyen, T. K. L.; Livi, S.; Pruvost, S.; Soares, B. G.; Duchet-Rumeau, J. Ionic Liquids as Reactive Additives for the Preparation and Modification of Epoxy Networks. *Journal of Polymer Science Part A: Polymer Chemistry* **2014**, *8*, 252–285. <https://doi.org/10.1002/pola.27420>.
- (58) Kong, M.; Liu, C.; Tang, B.; Xu, W.; Huang, Y.; Li, G. Improved Mechanical and Thermal Properties of Trifunctional Epoxy Resins through Controlling Molecular Networks

by Ionic Liquids. *Industrial & Engineering Chemistry Research* **2019**, *58* (19), 8080–8089. <https://doi.org/10.1021/acs.iecr.9b00547>.

(59) Dzienia, A.; Tarnacka, M.; Koperwas, K.; Maksym, P.; Zięba, A.; Feder-Kubis, J.; Kamiński, K.; Paluch, M. Impact of Imidazolium-Based Ionic Liquids on the Curing Kinetics and Physicochemical Properties of Nascent Epoxy Resins. *Macromolecules* **2020**, *53* (15), 6341–6352. <https://doi.org/10.1021/acs.macromol.0c00783>.

(60) Vidil, T.; Tournilhac, F.; Musso, S.; Robisson, A.; Leibler, L. Control of Reactions and Network Structures of Epoxy Thermosets. *Progress in Polymer Science* **2016**, *62*, 126–179. <https://doi.org/10.1016/j.progpolymsci.2016.06.003>.

(61) *Applications of Ionic Liquids in Polymer Science and Technology*; Mecerreyes, D., Ed.; Springer Berlin Heidelberg: Berlin, Heidelberg, **2015**. <https://doi.org/10.1007/978-3-662-44903-5>.

(62) Binks, F. C.; Cavalli, G.; Henningsen, M.; Howlin, B. J.; Hamerton, I. Investigating the Mechanism through Which Ionic Liquids Initiate the Polymerisation of Epoxy Resins. *Polymer* **2018**, *139*, 163–176. <https://doi.org/10.1016/j.polymer.2018.01.087>.

(63) Rahmathullah, M. A. M.; Jeyarajasingam, A.; Merritt, B.; VanLandingham, M.; McKnight, S. H.; Palmese, G. R. Room Temperature Ionic Liquids as Thermally Latent Initiators for Polymerization of Epoxy Resins. *Macromolecules* **2009**, *42* (9), 3219–3221. <https://doi.org/10.1021/ma802669k>.

(64) Binks, F. C.; Cavalli, G.; Henningsen, M.; Howlin, B. J.; Hamerton, I. Examining the Effects of Storage on the Initiation Behaviour of Ionic Liquids towards the Cure of Epoxy Resins. *Reactive and Functional Polymers* **2018**, *133*, 9–20. <https://doi.org/10.1016/j.reactfunctpolym.2018.09.017>.

(65) Binks, F. C.; Cavalli, G.; Henningsen, M.; Howlin, B. J.; Hamerton, I. Examining the Nature of Network Formation during Epoxy Polymerisation Initiated with Ionic Liquids. *Polymer* **2018**, *150*, 318–325. <https://doi.org/10.1016/j.polymer.2018.07.046>.

(66) Ostrowska, S.; Markiewicz, B.; Wąsikowska, K.; Bączek, N.; Pernak, J.; Strzelec, K. Epoxy Resins Cured with Ionic Liquids as Novel Supports for Metal Complex Catalysts. *Comptes Rendus Chimie* **2013**, *16* (8), 752–760. <https://doi.org/10.1016/j.crci.2012.12.005>.

- (67) Kowalczyk, K.; Spychaj, T. Ionic Liquids as Convenient Latent Hardeners of Epoxy Resins. *Polimery* **2003**, *48* (11/12), 833–835. <https://doi.org/10.14314/polimery.2003.833>.
- (68) Maka, H.; Spychaj, T.; Pilawka, R. Epoxy Resin/Ionic Liquid Systems: The Influence of Imidazolium Cation Size and Anion Type on Reactivity and Thermomechanical Properties. *Industrial & Engineering Chemistry Research* **2012**, *51* (14), 5197–5206. <https://doi.org/10.1021/ie202321j>.
- (69) Mąka, H.; Spychaj, T.; Zenker, M. High Performance Epoxy Composites Cured with Ionic Liquids. *Journal of Industrial and Engineering Chemistry* **2015**, *31*, 192–198. <https://doi.org/10.1016/j.jiec.2015.06.023>.
- (70) Fonseca, E.; Demétrio da Silva, V.; Klitzke, J. S.; Schrekker, H. S.; Amico, S. C. Imidazolium Ionic Liquids as Fracture Toughening Agents in DGEBA-TETA Epoxy Resin. *Polymer Testing* **2020**, *87*, 106–156. <https://doi.org/10.1016/j.polymertesting.2020.106556>.
- (71) Mąka, H.; Spychaj, T.; Sikorski, W. Deep Eutectic Ionic Liquids as Epoxy Resin Curing Agents. *International Journal of Polymer Analysis and Characterization* **2014**, *19* (8), 682–692. <https://doi.org/10.1080/1023666X.2014.953835>.
- (72) Carvalho, A. P. A.; Santos, D. F.; Soares, B. G. Epoxy/Imidazolium-based Ionic Liquid Systems: The Effect of the Hardener on the Curing Behavior, Thermal Stability, and Microwave Absorbing Properties. *Journal of Applied Polymer Science* **2020**, *137* (5), 48–86. <https://doi.org/10.1002/app.48326>.
- (73) Mąka, H.; Spychaj, T. Epoxy Resin Crosslinked with Conventional and Deep Eutectic Ionic Liquids. *Polimery* **2012**, *57* (6), 456–462. <https://doi.org/10.14314/polimery.2012.456>.
- (74) McClure, J. D. Glycidyltrimethylammonium Chloride and Related Compounds. *The Journal of Organic Chemistry* **1970**, *35* (6), 2059–2061. <https://doi.org/10.1021/jo00831a093>.
- (75) Burness, D. M.; Bayer, H. O. Synthesis and Reactions of Quaternary Salts of Glycidyl Amines. *The Journal of Organic Chemistry* **1963**, *28* (9), 2283–2288. <https://doi.org/10.1021/jo01044a031>.
- (76) Prado, H. J.; Matulewicz, M. C. Cationization of Polysaccharides: A Path to Greener Derivatives with Many Industrial Applications. *European Polymer Journal* **2014**, *52*, 53–75. <https://doi.org/10.1016/j.eurpolymj.2013.12.011>.

- (77) Levy, N.; Garti, N.; Magdassi, S. Flocculation of Bentonite Suspensions with Cationic Guar. *Colloids and Surfaces A: Physicochemical and Engineering Aspects* **1995**, 97 (2), 91–99. [https://doi.org/10.1016/0927-7757\(94\)03072-8](https://doi.org/10.1016/0927-7757(94)03072-8).
- (78) Salimi, H.; Aryanasab, F.; Banazadeh, A. R.; Shabanian, M.; Seidi, F. Designing Syntheses of Cellulose and Starch Derivatives with Basic or Cationic N -Functions: Part I- Cellulose Derivatives. *Polymers for Advanced Technologies* **2016**, 27 (1), 5–32. <https://doi.org/10.1002/pat.3599>.
- (79) Chemelli, A.; Gomernik, F.; Thaler, F.; Huber, A.; Hirn, U.; Bauer, W.; Spirk, S. Cationic Starches in Paper-Based Applications—A Review on Analytical Methods. *Carbohydrate Polymers* **2020**, 235, 115964. <https://doi.org/10.1016/j.carbpol.2020.115964>.
- (80) Yang, Y.; Lu, Y.; Zeng, K.; Heinze, T.; Groth, T.; Zhang, K. Recent Progress on Cellulose-Based Ionic Compounds for Biomaterials. *Advanced Materials* **2021**, 33 (28), 2000717. <https://doi.org/10.1002/adma.202000717>.
- (81) Ciejk, J.; Wolski, K.; Nowakowska, M.; Pyrc, K.; Szczubiałka, K. Biopolymeric Nano/Microspheres for Selective and Reversible Adsorption of Coronaviruses. *Materials Science and Engineering: C* **2017**, 76, 735–742. <https://doi.org/10.1016/j.msec.2017.03.047>.
- (82) Zhao, Y.; Mai, Z.; Shen, P.; Ortega, E.; Shen, J.; Gao, C.; Van der Bruggen, B. Nanofiber Based Organic Solvent Anion Exchange Membranes for Selective Separation of Monovalent Anions. *ACS Applied Materials & Interfaces* **2020**, 12 (6), 7539–7547. <https://doi.org/10.1021/acsami.9b19962>.
- (83) Matsumoto, K.; Endo, T. Synthesis of Ion Conductive Networked Polymers Based on an Ionic Liquid Epoxide Having a Quaternary Ammonium Salt Structure. *Macromolecules* **2009**, 42 (13), 4580–4584. <https://doi.org/10.1021/ma900508q>.
- (84) Matsumoto, K.; Endo, T. Design and Synthesis of Ionic-Conductive Epoxy-Based Networked Polymers. *Reactive and Functional Polymers* **2013**, 73 (2), 278–282. <https://doi.org/10.1016/j.reactfunctpolym.2012.04.018>.
- (85) Liu, X.; Wu, D.; Liu, X.; Luo, X.; Liu, Y.; Zhao, Q.; Li, J.; Dong, D. Perfluorinated Comb-Shaped Cationic Polymer Containing Long-Range Ordered Main Chain for Anion Exchange Membrane. *Electrochimica Acta* **2020**, 336, 135757. <https://doi.org/10.1016/j.electacta.2020.135757>.

- (86) Dembereinyamba, D.; Yoon, S. J.; Lee, H. New Epoxide Molten Salts: Key Intermediates for Designing Novel Ionic Liquids. *Chemistry Letters* **2004**, 33 (5), 560–561. <https://doi.org/10.1246/cl.2004.560>.
- (87) Xie, Y.; Ding, K.; Liu, Z.; Li, J.; An, G.; Tao, R.; Sun, Z.; Yang, Z. The Immobilization of Glycidyl-Group-Containing Ionic Liquids and Its Application in CO<sub>2</sub> Cycloaddition Reactions. *Chemistry - A European Journal* **2010**, 16 (22), 6687–6692. <https://doi.org/10.1002/chem.201000020>.
- (88) Guo, Z.; Jiang, Q.; Shi, Y.; Li, J.; Yang, X.; Hou, W.; Zhou, Y.; Wang, J. Tethering Dual Hydroxyls into Mesoporous Poly(Ionic Liquid)s for Chemical Fixation of CO<sub>2</sub> at Ambient Conditions: A Combined Experimental and Theoretical Study. *ACS Catalysis* **2017**, 7 (10), 6770–6780. <https://doi.org/10.1021/acscatal.7b02399>.
- (89) Akbari, A.; Naderahmadian, A.; Eftekhari-Sis, B. Silver and Copper Nanoparticles Stabilized on Ionic Liquids-Functionalized Polyhedral Oligomeric Silsesquioxane (POSS): Highly Active and Recyclable Hybrid Catalysts. *Polyhedron* **2019**, 171, 228–236. <https://doi.org/10.1016/j.poly.2019.07.012>.
- (90) Xu, C.; Yuan, L.; Liang, G.; Gu, A. Building a Poly(Epoxy Propylimidazolium Ionic Liquid)/Graphene Hybrid through  $\pi$  Cation –  $\pi$  Interaction for Fabricating High-k Polymer Composites with Low Dielectric Loss and Percolation Threshold. *Journal of Materials Chemistry C* **2016**, 4 (15), 3175–3184. <https://doi.org/10.1039/C6TC00209A>.
- (91) Liu, X.; Chen, X.; Hu, Y.; Gong, T.; Li, H.; Zhang, Y. Ionic-Liquid-Functionalized Graphene Nanoribbons for Anion Exchange Membrane Fuel Cells. *Journal of The Electrochemical Society* **2017**, 164 (4), F433–F440. <https://doi.org/10.1149/2.0141706jes>.
- (92) Mahyari, M.; Shaabani, A.; Bide, Y. Gold Nanoparticles Supported on Supramolecular Ionic Liquid Grafted Graphene: A Bifunctional Catalyst for the Selective Aerobic Oxidation of Alcohols. *RSC Advances* **2013**, 3 (44), 22509. <https://doi.org/10.1039/c3ra44696d>.
- (93) Shojaei, S.; Ghasemi, Z.; Shahrissa, A. Cu(I)@Fe<sub>3</sub>O<sub>4</sub> Nanoparticles Supported on Imidazolium-based Ionic Liquid-grafted Cellulose: Green and Efficient Nanocatalyst for Multicomponent Synthesis of N-sulfonylamidines and N-sulfonylacrylamidines. *Applied Organometallic Chemistry* **2017**, 31 (11). <https://doi.org/10.1002/aoc.3788>.
- (94) Shojaei, S.; Ghasemi, Z.; Shahrissa, A. Three-Component Synthesis of N-Sulfonylformamidines in the Presence of Magnetic Cellulose Supported N-Heterocyclic

Carbene-Copper Complex, as an Efficient Heterogeneous Nanocatalyst. *Tetrahedron Letters* **2017**, 58 (42), 3957–3965. <https://doi.org/10.1016/j.tetlet.2017.08.075>.

(95) Lou, Z.; Xing, S.; Xiao, X.; Shan, W.; Xiong, Y.; Fan, Y. Selective Adsorption of Re(VII) by Chitosan Modified with Imidazolium-Based Ionic Liquid. *Hydrometallurgy* **2018**, 179, 141–148. <https://doi.org/10.1016/j.hydromet.2018.05.025>.

(96) Rahimi, M.; Shafiei-Irannejad, V.; D. Safa, K.; Salehi, R. Multi-Branched Ionic Liquid-Chitosan as a Smart and Biocompatible Nano-Vehicle for Combination Chemotherapy with Stealth and Targeted Properties. *Carbohydrate Polymers* **2018**, 196, 299–312. <https://doi.org/10.1016/j.carbpol.2018.05.059>.

(97) Lobregas, M. O. S.; Camacho, D. H. Gel Polymer Electrolyte System Based on Starch Grafted with Ionic Liquid: Synthesis, Characterization and Its Application in Dye-Sensitized Solar Cell. *Electrochimica Acta* **2019**, 298, 219–228. <https://doi.org/10.1016/j.electacta.2018.12.090>.

(98) Zhang, H.; Wang, D.; Wang, F.; Jin, X.; Yang, T.; Cai, Z.; Zhang, J. Corrosion Inhibition of Mild Steel in Hydrochloric Acid Solution by Quaternary Ammonium Salt Derivatives of Corn Stalk Polysaccharide (QAPS). *Desalination* **2015**, 372, 57–66. <https://doi.org/10.1016/j.desal.2015.06.021>.

(99) Fellingner, T.-P.; Thomas, A.; Yuan, J.; Antonietti, M. 25th Anniversary Article: “Cooking Carbon with Salt”: Carbon Materials and Carbonaceous Frameworks from Ionic Liquids and Poly(Ionic Liquid)S. *Advanced Materials* **2013**, 25 (41), 5838–5855. <https://doi.org/10.1002/adma.201301975>.

(100) Liao, C.; Liu, R.; Hou, X.; Sun, X.; Dai, S. Easy Synthesis of Poly(Ionic Liquid) for Use as a Porous Carbon Precursor. *New Carbon Materials* **2014**, 29 (1), 78–80. [https://doi.org/10.1016/S1872-5805\(14\)60127-X](https://doi.org/10.1016/S1872-5805(14)60127-X).

(101) Chardin, C.; Rouden, J.; Livi, S.; Baudoux, J. Dimethyldioxirane (DMDO) as a Valuable Oxidant for the Synthesis of Polyfunctional Aromatic Imidazolium Monomers Bearing Epoxides. *Green Chem.* **2017**, 19 (21), 5054–5059. <https://doi.org/10.1039/C7GC02372C>.

(102) Wang, X.; Zhou, Y.; Chen, G.; Li, J.; Long, Z.; Wang, J. Morphology-Controlled Preparation of Heteropolyanion-Derived Mesoporous Solid Base. *ACS Sustainable Chemistry & Engineering* **2014**, 2 (7), 1918–1927. <https://doi.org/10.1021/sc500259v>.

- (103) Tsuda, T.; Iwasaki, K.; Kumagai, K.; Kuwabata, S. Epoxy-Containing Ionic Liquids with Tunable Functionality. *Molecules* **2019**, *24* (14), 2591. <https://doi.org/10.3390/molecules24142591>.
- (104) Nein, Y. I.; Polyakova, A. Y.; Morzherin, Y. Y.; Savel'eva, E. A.; Rozin, Y. A.; Bakulev, V. A. Synthesis of 1-Substituted 3-Alkyl-1,2,3-Triazol-3-ium-5-Olates. *Russian Journal of Organic Chemistry* **2004**, *40* (6), 879–883. <https://doi.org/10.1023/B:RUJO.0000044553.95915.78>.
- (105) Meinel, R. S.; Almeida, A. das C.; Stroppa, P. H. F.; Glanzmann, N.; Coimbra, E. S.; da Silva, A. D. Novel Functionalized 1,2,3-Triazole Derivatives Exhibit Antileishmanial Activity, Increase in Total and Mitochondrial-ROS and Depolarization of Mitochondrial Membrane Potential of Leishmania Amazonensis. *Chemico-Biological Interactions* **2020**, *315*, 108850. <https://doi.org/10.1016/j.cbi.2019.108850>.
- (106) Vasanthakumar, A.; Bahadur, I.; Redhi, G. G.; Gengan, R. M.; Anand, K. Synthesis, Characterization and Thermophysical Properties of Ionic Liquid N-Methyl-N-(2',3'-Epoxypropyl)-2-Oxopyrrolidinium Chloride and Its Binary Mixtures with Water or Ethanol at Different Temperatures. *Journal of Molecular Liquids* **2016**, *219*, 685–693. <https://doi.org/10.1016/j.molliq.2016.03.080>.
- (107) Vasanthakumar, A.; Bahadur, I.; Redhi, G.; Gengan, R. M. Synthesis and Characterization of 2',3'-Epoxy Propyl-N-Methyl-2-Oxopyrrolidinium Salicylate Ionic Liquid and Study of Its Interaction with Water or Methanol. *RSC Advances* **2016**, *6* (66), 61566–61575. <https://doi.org/10.1039/C6RA11327C>.
- (108) Vasantha Kumar, A.; Redhi, G. G.; Gengan, R. M. Influence of Epoxy Group in 2-Pyrrolidonium Ionic Liquid Interactions and Thermo-Physical Properties with Ethanoic or Propanoic Acid at Various Temperatures. *ACS Sustainable Chemistry & Engineering* **2016**, *4* (9), 4951–4964. <https://doi.org/10.1021/acssuschemeng.6b01262>.
- (109) Arumugam, V.; Redhi, G. G.; Gengan, R. M. Synthesis, Characterization and Thermophysical Properties of Novel 2', 3'-N-Epoxypropyl- N -Methyl-2-Oxopyrrolidinium Acetate Ionic Liquid and Their Binary Mixtures with Water or Methanol. *Journal of Molecular Liquids* **2017**, *242*, 1215–1227. <https://doi.org/10.1016/j.molliq.2017.07.099>.
- (110) Arumugam, V.; Moodley, K. G.; Ogundele, O. P.; Redhi, G. G.; Moodley, A.; Gao, Y. Physicochemical and Thermodynamic Properties of Pyrrolidinium-Based Ionic Liquids and Their Binary Mixtures with Carboxylic Acids. *Journal of Molecular Liquids* **2020**, *310*, 113183. <https://doi.org/10.1016/j.molliq.2020.113183>.



- (111) Arumugam, V.; Kabane, B.; Moodley, K. G.; Gao, Y.; Redhi, G. G. Activity Coefficients at Infinite Dilution of Organic Solutes, Using Novel N-(2', 3'-Epoxypropyl)-N-Methyl-2-Oxopyrrolidinium Chloride Ionic Liquid by GLC. *Fluid Phase Equilibria* **2020**, *505*, 112362. <https://doi.org/10.1016/j.fluid.2019.112362>.
- (112) Vytr̃as, K.; Kalous, J.; Symerský, J. Determination of Some Ampholytic and Cationic Surfactants by Potentiometric Titrations Based on Ion-Pair Formation. *Analytica Chimica Acta* **1985**, *177*, 219–223. [https://doi.org/10.1016/S0003-2670\(00\)82955-4](https://doi.org/10.1016/S0003-2670(00)82955-4).
- (113) Aslanov, A. F.; Korotkikh, N. I.; Shvaika, O. P. Synthesis of 1,3-Diglycidylimidazolium Salts. *Chemistry of Heterocyclic Compounds* **1996**, *32* (8), 914–917. <https://doi.org/10.1007/BF01176966>.
- (114) McDanel, W. M.; Cowan, M. G.; Carlisle, T. K.; Swanson, A. K.; Noble, R. D.; Gin, D. L. Cross-Linked Ionic Resins and Gels from Epoxide-Functionalized Imidazolium Ionic Liquid Monomers. *Polymer* **2014**, *55* (16), 3305–3313. <https://doi.org/10.1016/j.polymer.2014.04.039>.
- (115) McDanel, W. M.; Cowan, M. G.; Chisholm, N. O.; Gin, D. L.; Noble, R. D. Fixed-Site-Carrier Facilitated Transport of Carbon Dioxide through Ionic-Liquid-Based Epoxy-Amine Ion Gel Membranes. *Journal of Membrane Science* **2015**, *492*, 303–311. <https://doi.org/10.1016/j.memsci.2015.05.034>.
- (116) Friess, K.; Lanč, M.; Pilnáček, K.; Fíla, V.; Vopička, O.; Sedláková, Z.; Cowan, M. G.; McDanel, W. M.; Noble, R. D.; Gin, D. L.; *et al.* CO<sub>2</sub>/CH<sub>4</sub> Separation Performance of Ionic-Liquid-Based Epoxy-Amine Ion Gel Membranes under Mixed Feed Conditions Relevant to Biogas Processing. *Journal of Membrane Science* **2017**, *528*, 64–71. <https://doi.org/10.1016/j.memsci.2017.01.016>.
- (117) McDanel, W. M.; Cowan, M. G.; Barton, J. A.; Gin, D. L.; Noble, R. D. Effect of Monomer Structure on Curing Behavior, CO<sub>2</sub> Solubility, and Gas Permeability of Ionic Liquid-Based Epoxy-Amine Resins and Ion-Gels. *Industrial & Engineering Chemistry Research* **2015**, *54* (16), 4396–4406. <https://doi.org/10.1021/ie5035122>.
- (118) Ly Nguyen, T. K.; Obadia, M. M.; Serghei, A.; Livi, S.; Duchet-Rumeau, J.; Drockenmuller, E. 1,2,3-Triazolium-Based Epoxy-Amine Networks: Ion-Conducting Polymer Electrolytes. *Macromolecular Rapid Communications* **2016**, *37* (14), 1168–1174. <https://doi.org/10.1002/marc.201600018>.

- (119) Chardin, C.; Rouden, J.; Livi, S.; Baudoux, J. 3-[2-(Oxiran-2-yl)Ethyl]-1-{4-[(2-Oxiran-2-yl)Ethoxy]Benzyl}imidazolium Bis(Trifluoromethane)Sulfonimide. *Molbank* **2018**, 2018 (1), 9–74. <https://doi.org/10.3390/M974>.
- (120) Livi, S.; Chardin, C.; Lins, L. C.; Halawani, N.; Pruvost, S.; Duchet-Rumeau, J.; Gérard, J.-F. F.; Baudoux, J. From Ionic Liquid Epoxy Monomer to Tunable Epoxy–Amine Network: Reaction Mechanism and Final Properties. *ACS Sustainable Chemistry & Engineering* **2019**, 7 (3), 3602–3613. <https://doi.org/10.1021/acssuschemeng.8b06271>.
- (121) Livi, S.; Lins, L. C.; Capeletti, L. B.; Chardin, C.; Halawani, N.; Baudoux, J.; Cardoso, M. B. Antibacterial Surface Based on New Epoxy-Amine Networks from Ionic Liquid Monomers. *European Polymer Journal* **2019**, 116, 56–64. <https://doi.org/10.1016/j.eurpolymj.2019.04.008>.
- (122) Yin, J.; Zhang, C.; Yu, Y.; Hao, T.; Wang, H.; Ding, X.; Meng, J. Tuning the Microstructure of Crosslinked Poly(Ionic Liquid) Membranes and Gels via a Multicomponent Reaction for Improved CO<sub>2</sub> Capture Performance. *Journal of Membrane Science* **2020**, 593, 117405. <https://doi.org/10.1016/j.memsci.2019.117405>.
- (123) Pant, R. R.; Buckley, J. L.; Fulmer, P. A.; Wynne, J. H.; McCluskey, D. M.; Phillips, J. P. Hybrid Siloxane Epoxy Coatings Containing Quaternary Ammonium Moieties. *Journal of Applied Polymer Science* **2008**, 110 (5), 3080–3086. <https://doi.org/10.1002/app.28670>.
- (124) Nishioka, S.; Yamada, S.; Yamauchi, K.; Kikuchi, Y. Electroconductive Member for Electrophotography and Quaternary Ammonium Salts, **2019**.
- (125) Masaki Yamada; Sosuke Yamaguchi; Hideya Arimura; Kazuhiro Yamauchi; Satoru Nishioka. Electrophotographic Member, Process Cartridge, and Electrophotographic Apparatus, **2018**.
- (126) Ochi, M.; Okazaki, M.; Shimbo, M. Mechanical Relaxation Mechanism of Epoxide Resins Cured with Aliphatic Diamines. *Journal of Polymer Science: Polymer Physics Edition* **1982**, 20 (4), 689–699. <https://doi.org/10.1002/pol.1982.180200411>.
- (127) Geyer, R. A Brief History of Plastics. In *Mare Plasticum - The Plastic Sea*; Springer International Publishing: Cham, **2020**; pp 31–47. [https://doi.org/10.1007/978-3-030-38945-1\\_2](https://doi.org/10.1007/978-3-030-38945-1_2).
- (128) Rahman, M.; Brazel, C. S. The Plasticizer Market: An Assessment of Traditional Plasticizers and Research Trends to Meet New Challenges. *Progress in Polymer Science (Oxford)* **2004**, 29 (12), 1223–1248. <https://doi.org/10.1016/j.progpolymsci.2004.10.001>.

- (129) Dumée, L. Circular Economy and Sustainability. In *Circular Economy and Sustainability*; Elsevier, **2022**; pp 359–372. <https://doi.org/10.1016/C2019-0-04146-5>.
- (130) Siddique, R.; Khatib, J.; Kaur, I. Use of Recycled Plastic in Concrete: A Review. *Waste Management* **2008**, *28* (10), 1835–1852. <https://doi.org/10.1016/j.wasman.2007.09.011>.
- (131) Mullins, M. J.; Liu, D.; Sue, H.-J. Mechanical Properties of Thermosets. In *Thermosets*; Elsevier, **2018**; pp 35–68. <https://doi.org/10.1016/B978-0-08-101021-1.00002-2>.
- (132) Ratna, D. Thermal Properties of Thermosets. In *Thermosets*; Elsevier, **2012**; pp 62–91. <https://doi.org/10.1533/9780857097637.1.62>.
- (133) Post, W.; Susa, A.; Blaauw, R.; Molenveld, K.; Knoop, R. J. I. A Review on the Potential and Limitations of Recyclable Thermosets for Structural Applications. *Polymer Reviews* **2020**, *60* (2), 359–388. <https://doi.org/10.1080/15583724.2019.1673406>.
- (134) Pickering, S. J. Recycling Technologies for Thermoset Composite Materials—Current Status. *Composites Part A: Applied Science and Manufacturing* **2006**, *37* (8), 1206–1215. <https://doi.org/10.1016/j.compositesa.2005.05.030>.
- (135) Qiao, Y.; Fring, L. D.; Pallaka, M. R.; Simmons, K. L. A Review of the Fabrication Methods and Mechanical Behavior of Continuous Thermoplastic Polymer Fiber–Thermoplastic Polymer Matrix Composites. *Polymer Composites* **2022**, No. October, 1–40. <https://doi.org/10.1002/pc.27139>.
- (136) Babu, B. R.; Parande, A. K.; Basha, C. A. Electrical and Electronic Waste: A Global Environmental Problem. *Waste Management and Research* **2007**, *25* (4), 307–318. <https://doi.org/10.1177/0734242X07076941>.
- (137) Pakdel, E.; Kashi, S.; Varley, R.; Wang, X. Recent Progress in Recycling Carbon Fibre Reinforced Composites and Dry Carbon Fibre Wastes. *Resources, Conservation and Recycling* **2021**, *166* (November 2020), 105340. <https://doi.org/10.1016/j.resconrec.2020.105340>.
- (138) Beauson, J.; Laurent, A.; Rudolph, D. P.; Pagh Jensen, J. The Complex End-of-Life of Wind Turbine Blades: A Review of the European Context. *Renewable and Sustainable Energy Reviews* **2022**, *155*, 111847. <https://doi.org/10.1016/j.rser.2021.111847>.
- (139) European Union. Municipal Waste Treatment in the EU in **2018** <https://eswet.eu/documents/municipal-waste-treatment-in-the-eu-in-2018/> (accessed Mar 1, 2023).

(140) La loi anti-gaspillage pour une économie circulaire <https://www.ecologie.gouv.fr/loi-anti-gaspillage-economie-circulaire> (accessed Mar 1, 2023).

(141) Energy, E. T. & I. P. on W. An overview of composite recycling in the wind energy industry <https://etipwind.eu/files/reports/ETIPWind-How-wind-is-going-circular-blade-recycling.pdf>.

(142) Khalid, M. Y.; Arif, Z. U.; Ahmed, W.; Arshad, H. Recent Trends in Recycling and Reusing Techniques of Different Plastic Polymers and Their Composite Materials. *Sustainable Materials and Technologies* **2022**, *31*, e00382. <https://doi.org/10.1016/j.susmat.2021.e00382>.

(143) Pérez, R. L.; Ayala, C. E.; Opiri, M. M.; Ezzir, A.; Li, G.; Warner, I. M. Recycling Thermoset Epoxy Resin Using Alkyl-Methyl-Imidazolium Ionic Liquids as Green Solvents. *ACS Applied Polymer Materials* **2021**, *3* (11), 5588–5595. <https://doi.org/10.1021/acsapm.1c00896>.

(144) Wang, B.; Ma, S.; Xu, X.; Li, Q.; Yu, T.; Wang, S.; Yan, S.; Liu, Y.; Zhu, J. High-Performance, Biobased, Degradable Polyurethane Thermoset and Its Application in Readily Recyclable Carbon Fiber Composites. *ACS Sustainable Chemistry and Engineering* **2020**, *8* (30), 11162–11170. <https://doi.org/10.1021/acssuschemeng.0c02330>.

(145) Meyer, L. O.; Schulte, K.; Grove-Nielsen, E. CFRP-Recycling Following a Pyrolysis Route: Process Optimization and Potentials. *Journal of Composite Materials* **2009**, *43* (9), 1121–1132. <https://doi.org/10.1177/0021998308097737>.

(146) Ma, S.; Webster, D. C. Degradable Thermosets Based on Labile Bonds or Linkages: A Review. *Progress in Polymer Science* **2018**, *76*, 65–110. <https://doi.org/10.1016/j.progpolymsci.2017.07.008>.

(147) Khosravi, E.; Musa, O. M. Thermally Degradable Thermosetting Materials. *European Polymer Journal* **2011**, *47* (4), 465–473. <https://doi.org/10.1016/j.eurpolymj.2010.09.023>.

(148) Buchwalter, S. L.; Kosbar, L. L. Cleavable Epoxy Resins: Design for Disassembly of a Thermoset. *Journal of Polymer Science, Part A: Polymer Chemistry* **1996**, *34* (2), 249–260. [https://doi.org/10.1002/\(SICI\)1099-0518\(19960130\)34:2<249::AID-POLA11>3.0.CO;2-Q](https://doi.org/10.1002/(SICI)1099-0518(19960130)34:2<249::AID-POLA11>3.0.CO;2-Q).

(149) Xue, X.; Liu, S.-Y. Y.; Zhang, Z.-Y. Y.; Wang, Q.-Z. Z.; Xiao, C.-Z. Z. A Technology Review of Recycling Methods for Fiber-Reinforced Thermosets. *Journal of Reinforced*

*Plastics and Composites* **2022**, *41* (11–12), 459–480.  
<https://doi.org/10.1177/07316844211055208>.

(150) Morin, C.; Loppinet-Serani, A.; Cansell, F.; Aymonier, C. Near- and Supercritical Solvolysis of Carbon Fibre Reinforced Polymers (CFRPs) for Recycling Carbon Fibers as a Valuable Resource: State of the Art. *The Journal of Supercritical Fluids* **2012**, *66*, 232–240. <https://doi.org/10.1016/j.supflu.2012.02.001>.

(151) Palmer, J.; Ghita, O. R.; Savage, L.; Evans, K. E. Successful Closed-Loop Recycling of Thermoset Composites. *Composites Part A: Applied Science and Manufacturing* **2009**, *40* (4), 490–498. <https://doi.org/10.1016/j.compositesa.2009.02.002>.

(152) Pickering, S. J. Recycling Technologies for Thermoset Composite Materials- Current Status. *Composites Part A: Applied Science and Manufacturing* **2006**, *37* (8), 1206–1215. <https://doi.org/10.1016/j.compositesa.2005.05.030>.

(153) Durante, M.; Boccarusso, L.; De Fazio, D.; Formisano, A.; Langella, A. Investigation on the Mechanical Recycling of Carbon Fiber-Reinforced Polymers by Peripheral Down-Milling. *Polymers* **2023**, *15* (4), 854. <https://doi.org/10.3390/polym15040854>.

(154) Khalid, M. Y.; Arif, Z. U.; Hossain, M.; Umer, R. Recycling of Wind Turbine Blades through Modern Recycling Technologies: A Road to Zero Waste. *Renewable Energy Focus* **2023**, *44*, 373–389. <https://doi.org/10.1016/j.ref.2023.02.001>.

(155) Fortman, D. J.; Brutman, J. P.; De Hoe, G. X.; Snyder, R. L.; Dichtel, W. R.; Hillmyer, M. A. Approaches to Sustainable and Continually Recyclable Cross-Linked Polymers. *ACS Sustainable Chemistry and Engineering* **2018**, *6* (9), 11145–11159. <https://doi.org/10.1021/acssuschemeng.8b02355>.

(156) Lopez-Urionabarrenechea, A.; Gastelu, N.; Acha, E.; Caballero, B. M.; de Marco, I. Production of Hydrogen-Rich Gases in the Recycling Process of Residual Carbon Fiber Reinforced Polymers by Pyrolysis. *Waste Management* **2021**, *128*, 73–82. <https://doi.org/10.1016/j.wasman.2021.04.044>.

(157) Lopez-Urionabarrenechea, A.; Gastelu, N.; Acha, E.; Caballero, B. M.; Orue, A.; Jiménez-Suárez, A.; Prolongo, S. G.; de Marco, I. Reclamation of Carbon Fibers and Added-Value Gases in a Pyrolysis-Based Composites Recycling Process. *Journal of Cleaner Production* **2020**, *273*, 123173. <https://doi.org/10.1016/j.jclepro.2020.123173>.

(158) Utekar, S.; V K, S.; More, N.; Rao, A. Comprehensive Study of Recycling of Thermosetting Polymer Composites – Driving Force, Challenges and Methods. *Composites*

Part B: Engineering 2021, 207 (5), 108596.  
<https://doi.org/10.1016/j.compositesb.2020.108596>.

(159) Benedetti, M.; Cafiero, L.; De Angelis, D.; Dell'Era, A.; Pasquali, M.; Stendardo, S.; Tuffi, R.; Cipriotti, S. V. Pyrolysis of WEEE Plastics Using Catalysts Produced from Fly Ash of Coal Gasification. *Frontiers of Environmental Science & Engineering* **2017**, 11 (5), 11. <https://doi.org/10.1007/s11783-017-0998-3>.

(160) Yang, P.; Zhou, Q.; Yuan, X.-X.; van Kasteren, J. M. N.; Wang, Y.-Z. Highly Efficient Solvolysis of Epoxy Resin Using Poly(Ethylene Glycol)/NaOH Systems. *Polymer Degradation and Stability* **2012**, 97 (7), 1101–1106. <https://doi.org/10.1016/j.polymdegradstab.2012.04.007>.

(161) Xanthos, M.; Patel, S. H. Solvolysis. In *Frontiers in the Science and Technology of Polymer Recycling*; Springer Netherlands: Dordrecht, **1998**; pp 425–436. [https://doi.org/10.1007/978-94-017-1626-0\\_20](https://doi.org/10.1007/978-94-017-1626-0_20).

(162) Shen, M.; Cao, H.; Robertson, M. L. Hydrolysis and Solvolysis as Benign Routes for the End-of-Life Management of Thermoset Polymer Waste. *Annual Review of Chemical and Biomolecular Engineering* **2020**, 11 (1), 183–201. <https://doi.org/10.1146/annurev-chembioeng-120919-012253>.

(163) Zhou, Q.; Zhu, X.; Zhang, W.; Song, N.; Ni, L. Recyclable High Performance Epoxy Composites Based on Double Dynamic Carbon-Nitrogen and Disulfide Bonds. *ACS Applied Polymer Materials* **2020**, 2 (5), 1865–1873. <https://doi.org/10.1021/acsapm.0c00105>.

(164) Kuang, X.; Shi, Q.; Zhou, Y.; Zhao, Z.; Wang, T.; Qi, H. J. Dissolution of Epoxy Thermosets: Via Mild Alcoholysis: The Mechanism and Kinetics Study. *RSC Advances* **2018**, 8 (3), 1493–1502. <https://doi.org/10.1039/c7ra12787a>.

(165) Wang, M.; Liu, H.-Y.; Ke, N.-W.; Wu, G.; Chen, S.-C.; Wang, Y.-Z. Toward Regulating Biodegradation in Stages of Polyurethane Copolymers with Bicontinuous Microphase Separation. *Journal of Materials Chemistry B* **2023**, 11 (14), 3164–3175. <https://doi.org/10.1039/D3TB00011G>.

(166) Keskin, S.; Kayrak-Talay, D.; Akman, U.; Hortaçsu, Ö. A Review of Ionic Liquids towards Supercritical Fluid Applications. *The Journal of Supercritical Fluids* **2007**, 43 (1), 150–180. <https://doi.org/10.1016/j.supflu.2007.05.013>.

- (167) Okajima, I.; Hiramatsu, M.; Shimamura, Y.; Awaya, T.; Sako, T. Chemical Recycling of Carbon Fiber Reinforced Plastic Using Supercritical Methanol. *Journal of Supercritical Fluids* **2014**, *91*, 68–76. <https://doi.org/10.1016/j.supflu.2014.04.011>.
- (168) Dang, W.; Kubouchi, M.; Yamamoto, S.; Sembokuya, H.; Tsuda, K. An Approach to Chemical Recycling of Epoxy Resin Cured with Amine Using Nitric Acid. *Polymer* **2002**, *43* (10), 2953–2958. [https://doi.org/10.1016/S0032-3861\(02\)00100-3](https://doi.org/10.1016/S0032-3861(02)00100-3).
- (169) Henry, L.; Schneller, A.; Doerfler, J.; Mueller, W. M.; Aymonier, C.; Horn, S. Semi-Continuous Flow Recycling Method for Carbon Fibre Reinforced Thermoset Polymers by near- and Supercritical Solvolysis. *Polymer Degradation and Stability* **2016**, *133*, 264–274. <https://doi.org/10.1016/j.polymdegradstab.2016.09.002>.
- (170) Naqvi, S. R.; Prabhakara, H. M.; Bramer, E. A.; Dierkes, W.; Akkerman, R.; Brem, G. A Critical Review on Recycling of End-of-Life Carbon Fibre/Glass Fibre Reinforced Composites Waste Using Pyrolysis towards a Circular Economy. *Resources, Conservation and Recycling* **2018**, *136*, 118–129. <https://doi.org/10.1016/j.resconrec.2018.04.013>.
- (171) Mativenga, P. T.; Sultan, A. A. M.; Agwa-Ejon, J.; Mbohwa, C. Composites in a Circular Economy: A Study of United Kingdom and South Africa. *Procedia CIRP* **2017**, *61*, 691–696. <https://doi.org/10.1016/j.procir.2016.11.270>.
- (172) Shirai, M.; Mitsukura, K.; Okamura, H. Chain Propagation in UV Curing of Di(Meth)Acrylates. *Chemistry of Materials* **2008**, *20* (5), 1971–1976. <https://doi.org/10.1021/cm702965e>.
- (173) Heller, J.; Barr, J.; Ng, S. Y.; Abdellauoi, K. S.; Gurny, R. Poly(Ortho Esters): Synthesis, Characterization, Properties and Uses. *Advanced Drug Delivery Reviews* **2002**, *54* (7), 1015–1039. [https://doi.org/10.1016/S0169-409X\(02\)00055-8](https://doi.org/10.1016/S0169-409X(02)00055-8).
- (174) Johnson, L. M.; Ledet, E.; Huffman, N. D.; Swarner, S. L.; Shepherd, S. D.; Durham, P. G.; Rothrock, G. D. Controlled Degradation of Disulfide-Based Epoxy Thermosets for Extreme Environments. *Polymer* **2015**, *64*, 84–92. <https://doi.org/10.1016/j.polymer.2015.03.020>.
- (175) Li, H.; Wong, C. P. P. A Reworkable Epoxy Resin for Isotropically Conductive Adhesive. *IEEE Transactions on Advanced Packaging* **2004**, *27* (1), 165–172. <https://doi.org/10.1109/TADVP.2004.824939>.
- (176) Hashimoto, T.; Meiji, H.; Urushisaki, M.; Sakaguchi, T.; Kawabe, K.; Tsuchida, C.; Kondo, K. Degradable and Chemically Recyclable Epoxy Resins Containing Acetal Linkages: Synthesis, Properties, and Application for Carbon Fiber-Reinforced Plastics.

*Journal of Polymer Science Part A: Polymer Chemistry* **2012**, *50* (17), 3674–3681.  
<https://doi.org/10.1002/pola.26160>.

(177) B. Liang; Qin, B.; X. Li. Amine Curing Agents Containing Acetal Linkages, **2013**.

(178) Kakichi, Y.; Yamaguchi, A.; Hashimoto, T.; Urushisaki, M.; Sakaguchi, T.; Kawabe, K.; Kondo, K.; Iyo, H. Development of Recyclable Carbon Fiber-Reinforced Plastics (CFRPs) with Controlled Degradability and Stability Using Acetal Linkage-Containing Epoxy Resins. *Polymer Journal* **2017**, *49* (12), 851–859. <https://doi.org/10.1038/pj.2017.68>.

(179) Tsujii, A.; Namba, M.; Okamura, H.; Matsumoto, A. Radical Alternating Copolymerization of Twisted 1,3-Butadienes with Maleic Anhydride as a New Approach for Degradable Thermosetting Resin. *Macromolecules* **2014**, *47* (19), 6619–6626. <https://doi.org/10.1021/ma501555n>.

(180) Okamura, H.; Yamauchi, E.; Shirai, M. Photo-Cross-Linking and de-Cross-Linking of Modified Polystyrenes Having Degradable Linkages. *Reactive and Functional Polymers* **2011**, *71* (4), 480–488. <https://doi.org/10.1016/j.reactfunctpolym.2011.01.008>.

(181) Mukundan, T.; Kishore, K. Synthesis, Characterization and Reactivity of Polymeric Peroxides. *Progress in Polymer Science* **1990**, *15* (3), 475–505. [https://doi.org/10.1016/0079-6700\(90\)90004-K](https://doi.org/10.1016/0079-6700(90)90004-K).

(182) Yuki, T.; Yonekawa, M.; Matsumoto, K.; Tomita, I.; Endo, T. Construction of Reversible Crosslinking–Decrosslinking System Consisting of a Polymer Bearing Vicinal Tricarbonyl Structure and Poly(Ethylene Glycol). *Polymer Bulletin* **2016**, *73* (2), 345–356. <https://doi.org/10.1007/s00289-015-1490-5>.

(183) Zhao, H.; Duan, H.; Zhang, J.; Chen, L.; Wan, C.; Zhang, C.; Liu, C.; Ma, H. An Itaconic Acid-Based Phosphorus-Containing Oligomer Endowing Epoxy Resins with Good Flame Retardancy and Toughness. *Macromolecular Materials and Engineering* **2023**, *308* (4). <https://doi.org/10.1002/mame.202200550>.

(184) Wojtecki, R. J.; Meador, M. A.; Rowan, S. J. Using the Dynamic Bond to Access Macroscopically Responsive Structurally Dynamic Polymers. *Nature Materials* **2011**, *10* (1), 14–27. <https://doi.org/10.1038/nmat2891>.

(185) Pastine, J.; Liang, B.; Qin, B. Agents for Reworkable Epoxy Resins, 2011.

(186) Maes, S.; Scholiers, V.; Du Prez, F. E. Photo-Crosslinking and Reductive Decrosslinking of Polymethacrylate-Based Copolymers Containing 1,2-Dithiolane Rings.



*Macromolecular Chemistry and Physics* **2023**, *224* (1), 2100445.  
<https://doi.org/10.1002/macp.202100445>.

(187) Hong, Y.; Jeong, J.; Oh, D.; Kim, M.; Lee, M. W.; Goh, M. On-Demand and Fast Recyclable Bio-Epoxy. *Journal of Industrial and Engineering Chemistry* **2023**, *117*, 490–499.  
<https://doi.org/10.1016/j.jiec.2022.10.036>.

(188) Shieh, P.; Zhang, W.; Husted, K. E. L.; Kristufek, S. L.; Xiong, B.; Lundberg, D. J.; Lem, J.; Veyssset, D.; Sun, Y.; Nelson, K. A.; *et al.* Cleavable Comonomers Enable Degradable, Recyclable Thermoset Plastics. *Nature* **2020**, *583* (7817), 542–547.  
<https://doi.org/10.1038/s41586-020-2495-2>.

(189) Kazemi, M.; Faisal Kabir, S.; Fini, E. H. State of the Art in Recycling Waste Thermoplastics and Thermosets and Their Applications in Construction. *Resources, Conservation and Recycling* **2021**, *174*, 105776.  
<https://doi.org/10.1016/j.resconrec.2021.105776>.

(190) Guo, Y.; Chen, S.; Sun, L.; Yang, L.; Zhang, L.; Lou, J.; You, Z. Degradable and Fully Recyclable Dynamic Thermoset Elastomer for 3D-Printed Wearable Electronics. *Advanced Functional Materials* **2021**, *31* (9), 1–7.  
<https://doi.org/10.1002/adfm.202009799>.

(191) Miller, K. A.; Morado, E. G.; Samanta, S. R.; Walker, B. A.; Nelson, A. Z.; Sen, S.; Tran, D. T.; Whitaker, D. J.; Ewoldt, R. H.; Braun, P. V.; *et al.* Acid-Triggered, Acid-Generating, and Self-Amplifying Degradable Polymers. *Journal of the American Chemical Society* **2019**, *141* (7), 2838–2842. <https://doi.org/10.1021/jacs.8b07705>.

(192) Xinbo, W.; Longnan, H. Degradable Epoxy Resins. *Progress in Chemistry* **2009**, *21* (12), 2704–2711.

(193) Chen, H.; Qin, R.; Chow, C. L.; Lau, D. Recycling Thermoset Plastic Waste for Manufacturing Green Cement Mortar. *Cement and Concrete Composites* **2023**, *137*, 104922.  
<https://doi.org/10.1016/j.cemconcomp.2022.104922>.

(194) Perli, G.; Wylie, L.; Demir, B.; Gerard, J. F.; Pádua, A. A. H.; Gomes, M. C.; Duchet-Rumeau, J.; Baudoux, J.; Livi, S. From the Design of Novel Tri- and Tetra-Epoxidized Ionic Liquid Monomers to the End-of-Life of Multifunctional Degradable Epoxy Thermosets. *ACS Sustainable Chemistry and Engineering* **2022**, *10* (47), 15450–15466.  
<https://doi.org/10.1021/acssuschemeng.2c04499>.

- (195) Kumar, A.; Connal, L. A. Biobased Transesterification Vitrimers. *Macromolecular Rapid Communications* **2023**, *44* (7). <https://doi.org/10.1002/marc.202200892>.
- (196) Cuminet, F.; Caillol, S.; Dantras, É.; Leclerc, É.; Lemouzy, S.; Totée, C.; Guille, O.; Ladmiral, V. Synthesis of a Transesterification Vitrimer Activated by Fluorine from an  $\alpha,\alpha$ -Difluoro Carboxylic Acid and a Diepoxy. *European Polymer Journal* **2023**, *182*, 111718. <https://doi.org/10.1016/j.eurpolymj.2022.111718>.
- (197) Elling, B. R.; Dichtel, W. R. Reprocessable Cross-Linked Polymer Networks: Are Associative Exchange Mechanisms Desirable? *ACS Central Science* **2020**, *6* (9), 1488–1496. <https://doi.org/10.1021/acscentsci.0c00567>.
- (198) Acebo, C.; Fernández-Francos, X.; Ferrando, F.; Serra, À.; Ramis, X. New Epoxy Thermosets Modified with Multiarm Star Poly(Lactide) with Poly(Ethyleneimine) as Core of Different Molecular Weight. *European Polymer Journal* **2013**, *49* (8), 2316–2326. <https://doi.org/10.1016/j.eurpolymj.2013.05.015>.
- (199) Yang, S.; Chen, J.-S.; Körner, H.; Breiner, T.; Ober, C. K.; Poliks, M. D. Reworkable Epoxies: Thermosets with Thermally Cleavable Groups for Controlled Network Breakdown. *Chemistry of Materials* **1998**, *10* (6), 1475–1482. <https://doi.org/10.1021/cm970667t>.
- (200) Wang, L.; Wong, C. P. Syntheses and Characterizations of Thermally Reworkable Epoxy Resins. Part I. *Journal of Polymer Science Part A: Polymer Chemistry* **1999**, *37* (15), 2991–3001. [https://doi.org/10.1002/\(SICI\)1099-0518\(19990801\)37:15<2991::AID-POLA32>3.0.CO;2-V](https://doi.org/10.1002/(SICI)1099-0518(19990801)37:15<2991::AID-POLA32>3.0.CO;2-V).
- (201) Li, H.; Wang, L.; Jacob, K.; Wong, C. P. Syntheses and Characterizations of Thermally Reworkable Epoxy Resins II. *Journal of Polymer Science, Part A: Polymer Chemistry* **2000**, *38* (11), 3771–3782. <https://doi.org/10.1002/pola.10258>.
- (202) Liu, W.; Wang, Z.; Chen, Z.; Zhao, L. Thermo-Initiated Cationic Polymerization of Phosphorus-Containing Cycloaliphatic Epoxides with Tunable Degradable Temperature. *Polymer Degradation and Stability* **2012**, *97* (5), 810–815. <https://doi.org/10.1016/j.polymdegradstab.2012.01.028>.
- (203) Husted, K. E. L.; Brown, C. M.; Shieh, P.; Kevlishvili, I.; Kristufek, S. L.; Zafar, H.; Accardo, J. V.; Cooper, J. C.; Klausen, R. S.; Kulik, H. J.; *et al.* Remolding and Deconstruction of Industrial Thermosets via Carboxylic Acid-Catalyzed Bifunctional Silyl Ether Exchange.

*Journal of the American Chemical Society* **2023**, *145* (3), 1916–1923.  
<https://doi.org/10.1021/jacs.2c11858>.

(204) Lloyd, E. M.; Cooper, J. C.; Shieh, P.; Ivanoff, D. G.; Parikh, N. A.; Mejia, E. B.; Husted, K. E. L.; Costa, L. C.; Sottos, N. R.; Johnson, J. A.; *et al.* Efficient Manufacture, Deconstruction, and Upcycling of High-Performance Thermosets and Composites. *ACS Applied Engineering Materials* **2023**, *1* (1), 477–485.  
<https://doi.org/10.1021/acsaenm.2c00115>.

(205) Alameda, B. M.; Palmer, T. C.; Sisemore, J. D.; Pierini, N. G.; Patton, D. L. Hydrolytically Degradable Poly( $\beta$ -Thioether Ester Ketal) Thermosets: Via Radical-Mediated Thiol-Ene Photopolymerization. *Polymer Chemistry* **2019**, *10* (41), 5635–5644.  
<https://doi.org/10.1039/c9py01082c>.

(206) Jiang, Y.; Wang, S.; Dong, W.; Kaneko, T.; Chen, M.; Shi, D. High-Strength, Degradable and Recyclable Epoxy Resin Based on Imine Bonds for Its Carbon-Fiber-Reinforced Composites. *Materials* **2023**, *16* (4), 1604.  
<https://doi.org/10.3390/ma16041604>.

(207) Sangermano, M.; Tonin, M.; Yagci, Y. Degradable Epoxy Coatings by Photoinitiated Cationic Copolymerization of Bisepoxide with  $\epsilon$ -Caprolactone. *European Polymer Journal* **2010**, *46* (2), 254–259. <https://doi.org/10.1016/j.eurpolymj.2009.10.023>.

(208) Giménez, R.; Fernández-Francos, X.; Salla, J. M.; Serra, A.; Mantecón, A.; Ramis, X. New Degradable Thermosets Obtained by Cationic Copolymerization of DGEBA with an  $s(\gamma$ -Butyrolactone). *Polymer* **2005**, *46* (24), 10637–10647.  
<https://doi.org/10.1016/j.polymer.2005.09.026>.

(209) Alameda, B. M.; Murphy, J. S.; Barea-López, B. L.; Knox, K. D.; Sisemore, J. D.; Patton, D. L. Hydrolyzable Poly( $\beta$ -thioether Ester Ketal) Thermosets via Acyclic Ketal Monomers. *Macromolecular Rapid Communications* **2022**, *43* (24), 2200028.  
<https://doi.org/10.1002/marc.202200028>.

(210) Chen, X.; Chen, S.; Xu, Z.; Zhang, J.; Miao, M.; Zhang, D. Degradable and Recyclable Bio-Based Thermoset Epoxy Resins. *Green Chemistry* **2020**, *22* (13), 4187–4198.  
<https://doi.org/10.1039/D0GC01250E>.

(211) Han, J.; Chen, Q.; Feng, Y.; Shen, Y.; Wu, D.; Zhong, M.; Zhang, Q.; Zhao, Z.; Zhai, Y.; Bockstaller, M. R. Seawater-Degradable and Antibacterial Epoxy Thermosets Employing Betaine Ester Linkages. *ACS Applied Polymer Materials* **2023**.  
<https://doi.org/10.1021/acsapm.2c02239>.

- (212) García, J. M.; Jones, G. O.; Virwani, K.; McCloskey, B. D.; Boday, D. J.; ter Huurne, G. M.; Horn, H. W.; Coady, D. J.; Bintaleb, A. M.; Alabdulrahman, A. M. S.; *et al.* Recyclable, Strong Thermosets and Organogels via Paraformaldehyde Condensation with Diamines. *Science* **2014**, *344* (6185), 732–735. <https://doi.org/10.1126/science.1251484>.
- (213) Kuang, X.; Guo, E.; Chen, K.; Qi, H. J. Extraction of Biolubricant via Chemical Recycling of Thermosetting Polymers. *ACS Sustainable Chemistry and Engineering* **2019**, *7* (7), 6880–6888. <https://doi.org/10.1021/acssuschemeng.8b06409>.
- (214) Wake, W. C. Theories of Adhesion and Uses of Adhesives: A Review. *Polymer* **1978**, *19* (3), 291–308. [https://doi.org/10.1016/0032-3861\(78\)90223-9](https://doi.org/10.1016/0032-3861(78)90223-9).
- (215) Kang, J. S.; Myles, A. J.; Harris, K. D. Thermally-Degradable Thermoset Adhesive Based on a Cellulose Nanocrystals/Epoxy Nanocomposite. *ACS Applied Polymer Materials* **2020**, *2* (11), 4626–4631. <https://doi.org/10.1021/acsapm.0c00698>.
- (216) Zhang, X.; Chen, G. G.; Collins, A.; Jacobson, S.; Morganelli, P.; Dar, Y. L.; Musa, O. M. Thermally Degradable Maleimides for Reworkable Adhesives. *Journal of Polymer Science Part A: Polymer Chemistry* **2009**, *47* (4), 1073–1084. <https://doi.org/10.1002/pola.23217>.
- (217) Oguri, T.; Kawahara, A.; Kihara, N. Epoxy Resin Bearing Diacylhydrazine Moiety as a Degradable Adhesive for Traceless Oxidative Removal. *Polymer* **2016**, *99*, 83–89. <https://doi.org/10.1016/j.polymer.2016.06.066>.
- (218) Luo, K.; Xie, T.; Rzayev, J. Synthesis of Thermally Degradable Epoxy Adhesives. *Journal of Polymer Science Part A: Polymer Chemistry* **2013**, *51* (23), 4992–4997. <https://doi.org/10.1002/pola.26926>.
- (219) Yang, H.; Li, C.; Tang, J.; Suo, Z. Strong and Degradable Adhesion of Hydrogels. *ACS Applied Bio Materials* **2019**, *2* (5), 1781–1786. <https://doi.org/10.1021/acsabm.9b00103>.
- (220) Luo, S.; Wong, C. P. Adhesion between an Underfill and the Passivation Layer in Flip-Chip Packaging. *Journal of Adhesion Science and Technology* **2004**, *18* (2), 275–285. <https://doi.org/10.1163/156856104772759467>.
- (221) Moreno, A.; Morsali, M.; Sipponen, M. H. Catalyst-Free Synthesis of Lignin Vitrimers with Tunable Mechanical Properties: Circular Polymers and Recoverable Adhesives. *ACS Applied Materials & Interfaces* **2021**, *13* (48), 57952–57961. <https://doi.org/10.1021/acsami.1c17412>.

(222) M. Sridhar, L.; M. Champagne, T. High-Performance Reworkable Underfill Adhesives Based on Dicyclopentadiene Epoxy Thermoset. In *Next Generation Fiber-Reinforced Composites - New Insights*; IntechOpen, 2023; pp 11–23. <https://doi.org/10.5772/intechopen.107334>.

(223) Bhagat, V.; Becker, M. L. Degradable Adhesives for Surgery and Tissue Engineering. *Biomacromolecules* **2017**, *18* (10), 3009–3039. <https://doi.org/10.1021/acs.biomac.7b00969>.

(224) M. Sridhar, L.; M. Champagne, T. High-Performance Reworkable Underfill Adhesives Based on Dicyclopentadiene Epoxy Thermoset. In *Next Generation Fiber-Reinforced Composites - New Insights*; IntechOpen, 2023; pp 11–23. <https://doi.org/10.5772/intechopen.107334>.

(225) Wen, Y.; Chen, C.; Ye, Y.; Xue, Z.; Liu, H.; Zhou, X.; Zhang, Y.; Li, D.; Xie, X.; Mai, Y. Advances on Thermally Conductive Epoxy-Based Composites as Electronic Packaging Underfill Materials—A Review. *Advanced Materials* **2022**, *34* (52), 2201023. <https://doi.org/10.1002/adma.202201023>.

(226) Torpanyacharn, O.; Sukpuang, P.; Petchsuk, A.; Opaprakasit, P.; Opaprakasit, M. Curable Precursors Derived from Chemical Recycling of Poly(Ethylene Terephthalate) and Polylactic Acid and Physical Properties of Their Thermosetting (Co)Polyesters. *Polymer Bulletin* **2018**, *75* (1), 395–414. <https://doi.org/10.1007/s00289-017-2039-6>.

(227) Liu, W.; Wang, Z.; Xiong, L.; Zhao, L. Phosphorus-Containing Liquid Cycloaliphatic Epoxy Resins for Reworkable Environment-Friendly Electronic Packaging Materials. *Polymer* **2010**, *51* (21), 4776–4783. <https://doi.org/10.1016/j.polymer.2010.08.039>.

(228) Zhao, L.; Liu, Y.; Wang, Z.; Li, J.; Liu, W.; Chen, Z. Synthesis and Degradable Property of Novel Sulfite-Containing Cycloaliphatic Epoxy Resins. *Polymer Degradation and Stability* **2013**, *98* (11), 2125–2130. <https://doi.org/10.1016/j.polymdegradstab.2013.09.007>.

(229) Zhang, H.; Zhou, L.; Zhang, F.; Yang, Q.; Chen, M.; Chen, Z.; Zhang, Y.; Xiao, P.; Yu, S.; Song, L.; *et al.* Aromatic Disulfide Epoxy Vitrimer Packaged Electronic Devices: Nondestructive Healing and Recycling. *Polymer* **2022**, *255*, 125163. <https://doi.org/10.1016/j.polymer.2022.125163>.

- (230) Asmatulu, E.; Twomey, J.; Overcash, M. Recycling of Fiber-Reinforced Composites and Direct Structural Composite Recycling Concept. *Journal of Composite Materials* **2014**, *48* (5), 593–608. <https://doi.org/10.1177/0021998313476325>.
- (231) Krauklis, A. E.; Karl, C. W.; Gagani, A. I.; Jørgensen, J. K. Composite Material Recycling Technology—State-of-the-Art and Sustainable Development for the 2020s. *Journal of Composites Science* **2021**, *5* (1), 28. <https://doi.org/10.3390/jcs5010028>.
- (232) Piñero-Hernanz, R.; Dodds, C.; Hyde, J.; García-Serna, J.; Poliakoff, M.; Lester, E.; Cocero, M. J.; Kingman, S.; Pickering, S.; Wong, K. H. Chemical Recycling of Carbon Fibre Reinforced Composites in Nearcritical and Supercritical Water. *Composites Part A: Applied Science and Manufacturing* **2008**, *39* (3), 454–461. <https://doi.org/10.1016/j.compositesa.2008.01.001>.
- (233) Yu, K.; Shi, Q.; Dunn, M. L.; Wang, T.; Qi, H. J. Carbon Fiber Reinforced Thermoset Composite with Near 100% Recyclability. *Advanced Functional Materials* **2016**, *26* (33), 6098–6106. <https://doi.org/10.1002/adfm.201602056>.
- (234) Kang, J.-S.; Myles, A. J.; Harris, K. D. Thermally-Degradable Thermoset Adhesive Based on a Cellulose Nanocrystals/Epoxy Nanocomposite. *ACS Applied Polymer Materials* **2020**, *2* (11), 4626–4631. <https://doi.org/10.1021/acsapm.0c00698>.
- (235) Yu, K.; Shi, Q.; Dunn, M. L.; Wang, T.; Qi, H. J. Carbon Fiber Reinforced Thermoset Composite with Near 100% Recyclability. *Advanced Functional Materials* **2016**, *26* (33), 6098–6106. <https://doi.org/10.1002/adfm.201602056>.
- (236) Kuang, X.; Zhou, Y.; Shi, Q.; Wang, T.; Qi, H. J. Recycling of Epoxy Thermoset and Composites via Good Solvent Assisted and Small Molecules Participated Exchange Reactions. *ACS Sustainable Chemistry and Engineering* **2018**, *6* (7), 9189–9197. <https://doi.org/10.1021/acssuschemeng.8b01538>.
- (237) Li, W.; Zhan, Q.; Yang, P. Facile Approach for the Synthesis of Performance-Advantaged Degradable Bio-Based Thermoset via Ring-Opening Metathesis Polymerization from Epoxidized Soybean Oil. *ACS Sustainable Chemistry & Engineering* **2023**, *11* (3), 1200–1206. <https://doi.org/10.1021/acssuschemeng.2c06787>.
- (238) Afzali-Ardakani, A.; S. L. Buchwalter; Gelorme, J. D.; Kosbar, L. L.; Newman, B. H.; Pompeo, F. L. Cleavable Diepoxide for Removable Epoxy Compositions, 1996.
- (239) Buchwalter, S.; Kuczynski, J.; Stephanie, J. Cleavable Diepoxide for Removable Epoxy Compositions, **1999**.

- (240) Malik, J.; Clarson, S. J. A Thermally Reworkable UV Curable Acrylic Adhesive Prototype. *International Journal of Adhesion and Adhesives* **2002**, 22 (4), 283–289. [https://doi.org/10.1016/S0143-7496\(02\)00005-2](https://doi.org/10.1016/S0143-7496(02)00005-2).
- (241) Liang, B.; Qin, B.; Pastine, S. J.; Li, X. Amine Hardeners for Deconstructable Thermosets and Composites, 2013.
- (242) Deng, J.; Dai, Z.; Deng, L. Synthesis of Crosslinked PEG/IL Blend Membrane via One-pot Thiol–Ene/Epoxy Chemistry. *Journal of Polymer Science* **2020**, 58 (18), 2575–2585. <https://doi.org/10.1002/pol.20190195>.
- (243) Belowich, M. E.; Stoddart, J. F. Dynamic Imine Chemistry. *Chemical Society Reviews* **2012**, 41 (6), 2003. <https://doi.org/10.1039/c2cs15305j>.
- (244) Taynton, P.; Ni, H.; Zhu, C.; Yu, K.; Loob, S.; Jin, Y.; Qi, H. J.; Zhang, W. Repairable Woven Carbon Fiber Composites with Full Recyclability Enabled by Malleable Polyimine Networks. *Advanced Materials* **2016**, 28 (15), 2904–2909. <https://doi.org/10.1002/adma.201505245>.
- (245) Crivello, J. V.; Lee, J. L. The Synthesis, Characterization, and Photoinitiated Cationic Polymerization of Silicon-containing Epoxy Resins. *Journal of Polymer Science Part A: Polymer Chemistry* **1990**, 28 (3), 479–503. <https://doi.org/10.1002/pola.1990.080280303>.
- (246) Crivello, J. V.; Varlemann, U. The Synthesis and Study of the Photoinitiated Cationic Polymerization of Novel Cycloaliphatic Epoxides. *Journal of Polymer Science Part A: Polymer Chemistry* **1995**, 33 (14), 2463–2471. <https://doi.org/10.1002/pola.1995.080331420>.
- (247) Zhang, J.; Xiao, P.; Dietlin, C.; Campolo, D.; Dumur, F.; Gigmes, D.; Morlet-Savary, F.; Fouassier, J. P.; Lalevée, J. Cationic Photoinitiators for Near UV and Visible LEDs: A Particular Insight into One-Component Systems. *Macromolecular Chemistry and Physics* **2016**, 217 (11), 1214–1227. <https://doi.org/10.1002/macp.201500546>.
- (248) Kowalczyk, K.; Kowalczyk, A. Influence of Cationic Photoinitiator Type on Properties of Coating Materials Based on Cycloaliphatic and Glycidyl Epoxy Resins. *Progress in Organic Coatings* **2017**, 112 (June), 1–8. <https://doi.org/10.1016/j.porgcoat.2017.06.024>.
- (249) Maréchal, D.; Allonas, X.; Lecomère, M.; Criqui, A. Novel Dual-Cure Initiating System for Cationic Polymerization of Epoxides. *Macromolecular Chemistry and Physics* **2016**, 217 (10), 1169–1173. <https://doi.org/10.1002/macp.201500523>.

(250) Li, W.; Bakhtiary Noodeh, M.; Delpouve, N.; Saiter, J. M.; Tan, L.; Negahban, M. Printing Continuously Graded Interpenetrating Polymer Networks of Acrylate/Epoxy by Manipulating Cationic Network Formation during Stereolithography. *Express Polymer Letters* **2016**, *10* (12), 1003–1015. <https://doi.org/10.3144/expresspolymlett.2016.93>.

(251) Kaur, M.; Srivastava, A. K. PHOTOPOLYMERIZATION: A REVIEW. *Journal of Macromolecular Science, Part C: Polymer Reviews* **2002**, *42* (4), 481–512. <https://doi.org/10.1081/MC-120015988>.

(252) Zhang, F.; Zhu, L.; Li, Z.; Wang, S.; Shi, J.; Tang, W.; Li, N.; Yang, J. The Recent Development of Vat Photopolymerization: A Review. *Additive Manufacturing* **2021**, *48*, 102423. <https://doi.org/10.1016/j.addma.2021.102423>.

(253) Sangermano, M.; Razza, N.; Crivello, J. V. Cationic UV-Curing: Technology and Applications. *Macromolecular Materials and Engineering* **2014**, *299* (7), 775–793. <https://doi.org/10.1002/mame.201300349>.

(254) Sangermano, M.; Roppolo, I.; Chiappone, A. New Horizons in Cationic Photopolymerization. *Polymers* **2018**, *10* (2), 136–144. <https://doi.org/10.3390/polym10020136>.

(255) Villotte, S.; Gigmes, D.; Dumur, F.; Lalevée, J. Design of Iodonium Salts for UV or Near-UV LEDs for Photoacid Generator and Polymerization Purposes. *Molecules* **2020**, *25* (1), 22–25. <https://doi.org/10.3390/molecules25010149>.

(256) Mokbel, H.; Anderson, D.; Plenderleith, R.; Dietlin, C.; Morlet-Savary, F.; Dumur, F.; Gigmes, D.; Fouassier, J. P.; Lalevée, J. Simultaneous Initiation of Radical and Cationic Polymerization Reactions Using the “G1” Copper Complex as Photoredox Catalyst: Applications of Free Radical/Cationic Hybrid Photopolymerization in the Composites and 3D Printing Fields. *Progress in Organic Coatings* **2019**, *132* (February), 50–61. <https://doi.org/10.1016/j.porgcoat.2019.02.044>.

(257) Xiao, P.; Lalevée, J.; Allonas, X.; Fouassier, J. P.; Ley, C.; El-Roz, M.; Shi, S. Q.; Nie, J. Photoinitiation Mechanism of Free Radical Photopolymerization in the Presence of Cyclic Acetals and Related Compounds. *Journal of Polymer Science Part A: Polymer Chemistry* **2010**, *48* (24), 5758–5766. <https://doi.org/10.1002/pola.24383>.

(258) Topa, M.; Hola, E.; Galek, M.; Petko, F.; Pilch, M.; Popielarz, R.; Morlet-Savary, F.; Graff, B.; Lalevée, J.; Ortyl, J. One-Component Cationic Photoinitiators Based on Coumarin Scaffold Iodonium Salts as Highly Sensitive Photoacid Generators for 3D Printing IPN



Photopolymers under Visible LED Sources. *Polymer Chemistry* **2020**, 11 (32), 5261–5278. <https://doi.org/10.1039/d0py00677g>.

(259) Crivello, J. V. The Discovery and Development of Onium Salt Cationic Photoinitiators. *Journal of Polymer Science Part A: Polymer Chemistry* **1999**, 37 (23), 4241–4254. [https://doi.org/10.1002/\(SICI\)1099-0518\(19991201\)37:23<4241::AID-POLA1>3.0.CO;2-R](https://doi.org/10.1002/(SICI)1099-0518(19991201)37:23<4241::AID-POLA1>3.0.CO;2-R).

(260) Stanford, J. L.; Ryan, A. J.; Yang, Y. Photoinitiated Cationic Polymerization of Epoxides. *Polymer International* **2001**, 50 (9), 986–997. <https://doi.org/10.1002/pi.730>.

(261) Corcione, C. E.; Greco, A.; Maffezzoli, A. Photopolymerization Kinetics of an Epoxy-Based Resin for Stereolithography. *Journal of Applied Polymer Science* **2004**, 92 (6), 3484–3491. <https://doi.org/10.1002/app.20347>.

(262) Decker, C. Kinetic Study and New Applications of UV Radiation Curing. *Macromolecular Rapid Communications* **2002**, 23 (18), 1067–1093. <https://doi.org/10.1002/marc.200290014>.

(263) Decker, C.; Keller, L.; Zahouily, K.; Benfarhi, S. Synthesis of Nanocomposite Polymers by UV-Radiation Curing. *Polymer* **2005**, 46 (17), 6640–6648. <https://doi.org/10.1016/j.polymer.2005.05.018>.

(264) Decker, C. The Use of UV Irradiation in Polymerization. *Polymer International* **1998**, 45 (2), 133–141. [https://doi.org/10.1002/\(SICI\)1097-0126\(199802\)45:2<133::AID-PI969>3.0.CO;2-F](https://doi.org/10.1002/(SICI)1097-0126(199802)45:2<133::AID-PI969>3.0.CO;2-F).

(265) Decker, C. Decker - Kinetic Study of Light-Induced Polymerization by Real-Time UV and IR Spectroscopy - 1992.Pdf.

(266) Ganguly, S.; Kanovsky, N.; Das, P.; Gedanken, A.; Margel, S. Photopolymerized Thin Coating of Polypyrrole/Graphene Nanofiber/Iron Oxide onto Nonpolar Plastic for Flexible Electromagnetic Radiation Shielding, Strain Sensing, and Non-Contact Heating Applications. *Advanced Materials Interfaces* **2021**, 8 (23), 2101255. <https://doi.org/10.1002/admi.202101255>.

(267) Li, B.; Yang, H.; He, J.; Yu, S.; Xiao, R.; Luo, H.; Wen, Y.; Peng, S.; Liao, X.; Yang, D. Photopolymerization of Coating Materials for Protection against Carbon Steel Corrosion. *Materials* **2023**, 16 (5), 2015. <https://doi.org/10.3390/ma16052015>.

(268) FEIT, E. D. Photopolymerization of Urethane-Modified Methacrylates for Insulating Magnet Wire; **1973**; pp 269–278. <https://doi.org/10.1021/ba-1973-0129.ch018>.

(269) Fouassier, J. .; Allonas, X.; Burget, D. Photopolymerization Reactions under Visible Lights: Principle, Mechanisms and Examples of Applications. *Progress in Organic Coatings* **2003**, 47 (1), 16–36. [https://doi.org/10.1016/S0300-9440\(03\)00011-0](https://doi.org/10.1016/S0300-9440(03)00011-0).

(270) Bachelot, R.; Ecoffet, C.; Deloeil, D.; Royer, P.; Loughnot, D.-J. Integration of Micrometer-Sized Polymer Elements at the End of Optical Fibers by Free-Radical Photopolymerization. *Applied Optics* **2001**, 40 (32), 5860. <https://doi.org/10.1364/AO.40.005860>.

(271) STANSBURY, J. W. Curing Dental Resins and Composites by Photopolymerization. *Journal of Esthetic and Restorative Dentistry* **2000**, 12 (6), 300–308. <https://doi.org/10.1111/j.1708-8240.2000.tb00239.x>.

(272) Ligon, S. C.; Liska, R.; Stampfl, J.; Gurr, M.; Mülhaupt, R. Polymers for 3D Printing and Customized Additive Manufacturing. *Chemical Reviews* **2017**, 117 (15), 10212–10290. <https://doi.org/10.1021/acs.chemrev.7b00074>.

(273) Garra, P.; Dietlin, C.; Morlet-Savary, F.; Dumur, F.; Gigmès, D.; Fouassier, J.-P.; Lalevée, J. Photopolymerization Processes of Thick Films and in Shadow Areas: A Review for the Access to Composites. *Polymer Chemistry* **2017**, 8 (46), 7088–7101. <https://doi.org/10.1039/C7PY01778B>.

(274) Slusher, R. E. Laser Technology. *Reviews of Modern Physics* **1999**, 71 (2), S471–S479. <https://doi.org/10.1103/RevModPhys.71.S471>.

(275) Allen, N. S. *Photopolymerisation and Photoimaging Science and Technology*; Allen, N. S., Ed.; Springer Netherlands: Dordrecht, 1989. <https://doi.org/10.1007/978-94-009-1127-7>.

(276) Baikerikar, K. .; Scranton, A. . Photopolymerizable Liquid Encapsulants for Microelectronic Devices. *Polymer* **2001**, 42 (2), 431–441. [https://doi.org/10.1016/S0032-3861\(00\)00388-8](https://doi.org/10.1016/S0032-3861(00)00388-8).

(277) Lawrence, J. R.; O'Neill, F. T.; Sheridan, J. T. Photopolymer Holographic Recording Material. *Optik* **2001**, 112 (10), 449–463. <https://doi.org/10.1078/0030-4026-00091>.

(278) Guo, J.; Gleeson, M. R.; Sheridan, J. T. A Review of the Optimisation of Photopolymer Materials for Holographic Data Storage. *Physics Research International* **2012**, 2012, 1–16. <https://doi.org/10.1155/2012/803439>.

(279) Crivello, J. V.; Ortiz, R. A. Synthesis of Epoxy Monomers That Undergo Synergistic Photopolymerization by a Radical-Induced Cationic Mechanism. *Journal of*

*Polymer Science Part A: Polymer Chemistry* **2001**, *39* (20), 3578–3592.  
<https://doi.org/10.1002/pola.10015>.

(280) Xie, M.; Wang, Z. Synthesis and Properties of a Novel Cycloaliphatic Epoxide. *Macromolecular Rapid Communications* **2001**, *22* (8), 620–623.  
[https://doi.org/10.1002/1521-3927\(20010501\)22:8<620::AID-MARC620>3.0.CO;2-J](https://doi.org/10.1002/1521-3927(20010501)22:8<620::AID-MARC620>3.0.CO;2-J).

(281) Shi, S.; Croutxé-Barghorn, C.; Allonas, X. Photoinitiating Systems for Cationic Photopolymerization: Ongoing Push toward Long Wavelengths and Low Light Intensities. *Progress in Polymer Science* **2017**, *65*, 1–41.  
<https://doi.org/10.1016/j.progpolymsci.2016.09.007>.

(282) Sangermano, M. Advances in Cationic Photopolymerization. *Pure and Applied Chemistry* **2012**, *84* (10), 2089–2101. <https://doi.org/10.1351/PAC-CON-12-04-11>.

(283) Crivello, J. V.; Lam, J. H. W. New Photoinitiators for Cationic Polymerization. *J Polym Sci Polym Symp* **1977**, *10* (56), 383–395.

(284) Klikovits, N.; Knaack, P.; Bomze, D.; Krossing, I.; Liska, R. Novel Photoacid Generators for Cationic Photopolymerization. *Polymer Chemistry* **2017**, *8* (30), 4414–4421.  
<https://doi.org/10.1039/C7PY00855D>.

(285) Crivello, J. V.; Ma, J.; Jiang, F. Synthesis and Photoactivity of Novel 5-Arylthianthrenium Salt Cationic Photoinitiators. *Journal of Polymer Science Part A: Polymer Chemistry* **2002**, *40* (20), 3465–3480. <https://doi.org/10.1002/pola.10425>.

(286) Crivello, J. V.; Lam, J. H. W. Dye-Sensitized Photoinitiated Cationic Polymerization. *Journal of Polymer Science: Polymer Chemistry Edition* **1978**, *16* (10), 2441–2451. <https://doi.org/10.1002/pol.1978.170161004>.

(287) Crivello, J. V.; Kong, S. Synthesis and Characterization of Second-Generation Dialkylphenacylsulfonium Salt Photoinitiators. *Macromolecules* **2000**, *33* (3), 825–832.  
<https://doi.org/10.1021/ma991661n>.

(288) Ortyl, J.; Popielarz, R. New Photoinitiators for Cationic Polymerization. *Polimery/Polymers* **2012**, *57* (7–8), 510–517.  
<https://doi.org/10.14314/polimery.2012.510>.

(289) Perli, G.; Demir, B.; Pruvost, S.; Duchet-Rumeau, J.; Baudoux, J.; Livi, S. From the Design of Multifunctional Degradable Epoxy Thermosets to Their End of Life. *ACS Sustainable Chemistry & Engineering* **2022**, *10* (33), 11004–11015.  
<https://doi.org/10.1021/acssuschemeng.2c03326>.

(290) Cho, J. D.; Hong, J. W. UV-Initiated Free Radical and Cationic Photopolymerizations of Acrylate/Epoxy and Acrylate/Vinyl Ether Hybrid Systems with and without Photosensitizer. *Journal of Applied Polymer Science* **2004**, 93 (3), 1473–1483. <https://doi.org/10.1002/app.20597>.

(291) Sangermano, M.; Malucelli, G.; Morel, F.; Decker, C.; Priola, A. Cationic Photopolymerization of Vinyl Ether Systems: Influence of the Presence of Hydrogen Donor Additives. *European Polymer Journal* **1999**, 35 (4), 639–645. [https://doi.org/10.1016/S0014-3057\(98\)00168-2](https://doi.org/10.1016/S0014-3057(98)00168-2).

(292) Golaz, B.; Michaud, V.; Letierrier, Y.; Mnson, J. A. E. UV Intensity, Temperature and Dark-Curing Effects in Cationic Photo-Polymerization of a Cycloaliphatic Epoxy Resin. *Polymer* **2012**, 53 (10), 2038–2048. <https://doi.org/10.1016/j.polymer.2012.03.025>.

(293) Scherzer, T.; Buchmeiser, M. R. Photoinitiated Cationic Polymerization of Cycloaliphatic Epoxide/Vinyl Ether Systems Studied by near-Infrared Reflection Spectroscopy. *Macromolecular Chemistry and Physics* **2007**, 208 (9), 946–954. <https://doi.org/10.1002/macp.200600649>.

(294) Dillman, B.; Jessop, J. L. P. Chain Transfer Agents in Cationic Photopolymerization of a Bis-Cycloaliphatic Epoxide Monomer: Kinetic and Physical Property Effects. *Journal of Polymer Science Part A: Polymer Chemistry* **2013**, 51 (9), 2058–2067. <https://doi.org/10.1002/pola.26595>.

(295) Tehfe, M.; Louradour, F.; Lalevée, J.; Fouassier, J.-P. Photopolymerization Reactions: On the Way to a Green and Sustainable Chemistry. *Applied Sciences* **2013**, 3 (2), 490–514. <https://doi.org/10.3390/app3020490>.

(296) Crivello, J. V. The Synthesis and Cationic Polymerization of Novel Epoxide Monomers. *Polymer Engineering & Science* **1992**, 32 (20), 1462–1465. <https://doi.org/10.1002/pen.760322003>.

(297) Chen, Y.; Li, G.; Zhang, H.; Wang, T. Visible Light Curing of Bisphenol-A Epoxides and Acrylates Photoinitiated by ( $\eta$  6-Benzophenone)( $\eta$  5-Cyclopentadienyl) Iron Hexafluorophosphate. *Journal of Polymer Research* **2011**, 18 (6), 1425–1429. <https://doi.org/10.1007/s10965-010-9547-5>.

(298) Cho, J. D.; Hong, J. W. Photo-Curing Kinetics for the UV-Initiated Cationic Polymerization of a Cycloaliphatic Diepoxy System Photosensitized by Thioxanthone. *European Polymer Journal* **2005**, 41 (2), 367–374. <https://doi.org/10.1016/j.eurpolymj.2004.10.006>.

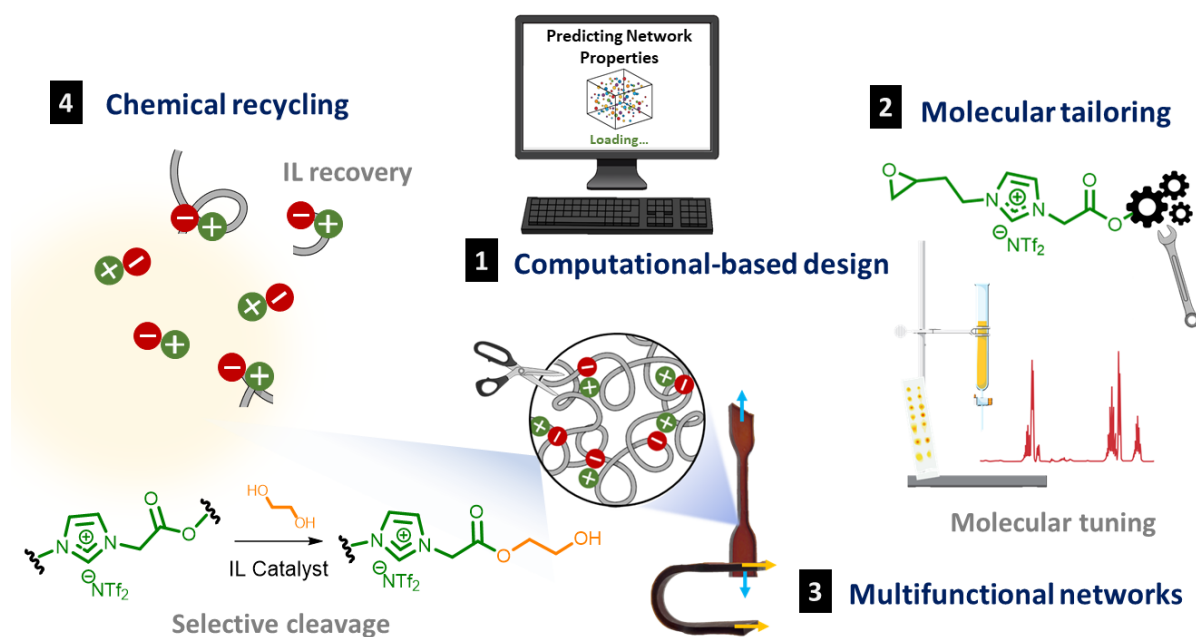
- (299) Acosta Ortiz, R.; García Valdez, A. E.; Hernández Cruz, D.; Nestoso Jiménez, G.; Hernández Jiménez, A. I.; Téllez Padilla, J. G.; Guerrero Santos, R. Highly Reactive Novel Biobased Cycloaliphatic Epoxy Resins Derived from Nopol and a Study of Their Cationic Photopolymerization. *Journal of Polymer Research* **2020**, *27* (6), 144. <https://doi.org/10.1007/s10965-020-02106-4>.
- (300) Andrzejewska, E. Photoinitiated Polymerization in Ionic Liquids and Its Application. *Polymer International* **2017**, *66* (3), 366–381. <https://doi.org/10.1002/pi.5255>.
- (301) Zhong, R.; Cao, C. G. Synthesis and Photo-Initiating Properties of a Quaternary Ammonium Salts Photoinitiator with Ionic Liquids Structure. *Advanced Materials Research* **2012**, *557–559*, 798–801. <https://doi.org/10.4028/www.scientific.net/AMR.557-559.798>.
- (302) Falcone, R. D.; Correa, N. M.; Silber, J. J. On the Formation of New Reverse Micelles: A Comparative Study of Benzene/Surfactants/Ionic Liquids Systems Using UV–Visible Absorption Spectroscopy and Dynamic Light Scattering. *Langmuir* **2009**, *25* (18), 10426–10429. <https://doi.org/10.1021/la901498e>.
- (303) Paul, A.; Mandal, P. K.; Samanta, A. On the Optical Properties of the Imidazolium Ionic Liquids. *The Journal of Physical Chemistry B* **2005**, *109* (18), 9148–9153. <https://doi.org/10.1021/jp0503967>.
- (304) Nese, C.; Unterreiner, A.-N. Photochemical Processes in Ionic Liquids on Ultrafast Timescales. *Physical Chemistry Chemical Physics* **2010**, *12* (8), 1698. <https://doi.org/10.1039/b916799b>.
- (305) Wang, C.; Luo, H.; Luo, X.; Li, H.; Dai, S. Equimolar CO<sub>2</sub> Capture by Imidazolium-Based Ionic Liquids and Superbase Systems. *Green Chemistry* **2010**, *12* (11), 2019. <https://doi.org/10.1039/c0gc00070a>.
- (306) Takahashi, K.; Wishart, J. Radiation Chemistry and Photochemistry of Ionic Liquids. In *Charged Particle and Photon Interactions with Matter*; CRC Press, 2010; pp 265–287. <https://doi.org/10.1201/b10389-12>.
- (307) Muldon, M.; McLean, A.; Charles, G.; Dunkin, I. Hydrogen Abstraction from Ionic Liquids by Benzophenone Triplet Excited States Electronic Supplementary Information (ESI) Available: Transient Spectra of 3Bp\* and KR in [Omim][Tf<sub>2</sub>N]. Purification of Starting Materials for Ionic Liquids. Arrhenius Plots Obt. *Chem. Commun.* **2001**, *22*, 210–229. <https://doi.org/https://doi.org/10.1039/b107730a>.

- (308) Izawa, H.; Wakizono, S.; Kadokawa, J. Fluorescence Resonance-Energy-Transfer in Systems of Rhodamine 6G with Ionic Liquid Showing Emissions by Excitation at Wide Wavelength Areas. *Chemical Communications* **2010**, 46 (34), 6359. <https://doi.org/10.1039/c0cc01066a>.
- (309) Zhou, Z.; He, D.; Guo, Y.; Cui, Z.; Zeng, L.; Li, G.; Yang, R. Photo-Induced Polymerization in Ionic Liquid Medium: 1. Preparation of Polyaniline Nanoparticles. *Polymer Bulletin* **2009**, 62 (5), 573–580. <https://doi.org/10.1007/s00289-009-0038-y>.
- (310) Gordon, C. M. Photochemistry in Ionic Liquids. In *Green Industrial Applications of Ionic Liquids*; Springer Netherlands: Dordrecht, 2003; pp 365–383. [https://doi.org/10.1007/978-94-010-0127-4\\_21](https://doi.org/10.1007/978-94-010-0127-4_21).
- (311) Reynolds, J. L.; Erdner, K. R.; Jones, P. B. Photoreduction of Benzophenones by Amines in Room-Temperature Ionic Liquids. *Organic Letters* **2002**, 4 (6), 917–919. <https://doi.org/10.1021/ol017290o>.
- (312) Lee, C.; Winston, T.; Unni, A.; Pagni, R. M.; Mamantov, G. Photoinduced Electron Transfer Chemistry of 9-Methylanthracene. Substrate as Both Electron Donor and Acceptor in the Presence of the 1-Ethyl-3-Methylimidazolium Ion. *Journal of the American Chemical Society* **1996**, 118 (21), 4919–4924. <https://doi.org/10.1021/ja953337n>.
- (313) Katoh, R.; Takahashi, K. Photo-Degradation of Imidazolium Ionic Liquids. *Radiation Physics and Chemistry* **2009**, 78 (12), 1126–1128. <https://doi.org/10.1016/j.radphyschem.2009.07.002>.
- (314) Siedlecka, E. M.; Czerwicka, M.; Neumann, J.; Stepnowski, P.; Fernandez, J. ; Thming, J. Ionic Liquids: Methods of Degradation and Recovery. In *Ionic Liquids: Theory, Properties, New Approaches*; InTech, 2011. <https://doi.org/10.5772/15463>.
- (315) Guterman, R.; Hesari, M.; Ragogna, P. J.; Workentin, M. S. Anion-Exchange Reactions on a Robust Phosphonium Photopolymer for the Controlled Deposition of Ionic Gold Nanoclusters. *Langmuir* **2013**, 29 (21), 6460–6466. <https://doi.org/10.1021/la400516v>.
- (316) Guterman, R.; Smith, C. A. Photopolymerization of Ionic Liquids – A Mutually Beneficial Approach for Materials Fabrication. *Israel Journal of Chemistry* **2019**, 59 (9), 803–812. <https://doi.org/10.1002/ijch.201800123>.
- (317) Cuthbert, T. J.; Guterman, R.; Ragogna, P. J.; Gillies, E. R. Contact Active Antibacterial Phosphonium Coatings Cured with UV Light. *Journal of Materials Chemistry B* **2015**, 3 (8), 1474–1478. <https://doi.org/10.1039/C4TB01857E>.

- (318) Schultz, A. R.; Lambert, P. M.; Chartrain, N. A.; Ruohoniemi, D. M.; Zhang, Z.; Jangu, C.; Zhang, M.; Williams, C. B.; Long, T. E. 3D Printing Phosphonium Ionic Liquid Networks with Mask Projection Microstereolithography. *ACS Macro Letters* **2014**, 3 (11), 1205–1209. <https://doi.org/10.1021/mz5006316>.
- (319) Guterman, R.; Smith, C. A. Photopolymerization of Ionic Liquids – A Mutually Beneficial Approach for Materials Fabrication. *Israel Journal of Chemistry* **2019**, 59 (9), 803–812. <https://doi.org/10.1002/ijch.201800123>.
- (320) Whitley, J. W.; Jeffrey Horne, W.; Shannon, M. S.; Andrews, M. A.; Terrell, K. L.; Hayward, S. S.; Yue, S.; Mittenthal, M. S.; O'Harra, K. E.; Bara, J. E. Systematic Investigation of the Photopolymerization of Imidazolium-Based Ionic Liquid Styrene and Vinyl Monomers. *Journal of Polymer Science Part A: Polymer Chemistry* **2018**, 56 (20), 2364–2375. <https://doi.org/10.1002/pola.29211>.
- (321) Xu, S. Q.; Fendler, J. H. Photopolymerization of Two-Component Monolayers: Mixtures of Bis[2-(n-Hexadecanoyloxy)Ethyl]Methyl(4-Vinylbenzyl) Ammonium Chloride and Dioctadecyldimethylammonium Bromide. *Macromolecules* **1989**, 22 (7), 2962–2968. <https://doi.org/10.1021/ma00197a015>.
- (322) Schultz, A. R.; Lambert, P. M.; Chartrain, N. A.; Ruohoniemi, D. M.; Zhang, Z.; Jangu, C.; Zhang, M.; Williams, C. B.; Long, T. E. 3D Printing Phosphonium Ionic Liquid Networks with Mask Projection Microstereolithography. *ACS Macro Letters* **2014**, 3 (11), 1205–1209. <https://doi.org/10.1021/mz5006316>.
- (323) Mecerreyes, D. Polymeric Ionic Liquids: Broadening the Properties and Applications of Polyelectrolytes. *Progress in Polymer Science* **2011**, 36 (12), 1629–1648. <https://doi.org/10.1016/j.progpolymsci.2011.05.007>.
- (324) Batra, D.; Hay, Firestone, M. A. Formation of a Biomimetic, Liquid-Crystalline Hydrogel by Self-Assembly and Polymerization of an Ionic Liquid. *Chemistry of Materials* **2007**, 19 (18), 4423–4431. <https://doi.org/10.1021/cm062992z>.
- (325) Strehmel, V.; Kaestner, P. I.; Strehmel, B. Synthesis and Photoinitiated Polymerization of New Ionic Liquid Methacrylates. *Journal of Polymer Science* **2023**, 61 (3), 234–250. <https://doi.org/10.1002/pol.20220361>.

# 03

## From the Design of Novel Tri- and Tetra-Epoxydized Ionic Liquid Monomers to the End-of-Life of Multifunctional Degradable Epoxy Thermosets





## **1. De la conception de nouveaux monomères liquides ioniques tri- et tétra-époxydés à la fin de vie des thermodurcissables époxy multifonctionnels dégradables**

### **1.1. Résumé**

Récemment, la conception et le développement de thermodurcissables époxy multifonctionnels ont motivé la recherche sur de nouveaux monomères époxy dégradables. Dans cette étude, des monomères d'imidazolium tri- et tétra-époxydés ont été conçus avec des groupes ester clivables et synthétisés à l'échelle du multigramme (jusqu'à 100 g), produisant des liquides ioniques à température ambiante (LIs). Ces monomères ont été utilisés comme éléments constitutifs moléculaires et durcis avec trois amines primaires de réactivités différentes ; conduisant à l'obtention de six architectures distinctes de réseaux. Dans l'ensemble, les réseaux époxy-amine obtenus présentent une haute stabilité thermique ( $> 350\text{ }^{\circ}\text{C}$ ), d'excellentes propriétés mécaniques combinées à un comportement de mémoire de forme, des températures de transition vitreuse ( $T_g$ ) allant de  $55$  à  $120\text{ }^{\circ}\text{C}$  et une dégradabilité complète dans des conditions douces. De plus, des simulations en dynamique moléculaire ont été effectuées dans le but d'étudier les interactions moléculaires lors de la polymérisation, basée sur la réaction de polyaddition, puis pour prédire les propriétés thermomécaniques et mécaniques des réseaux. Ainsi, ce travail lie la chimie computationnelle, la synthèse organique et la science des matériaux pour développer des réseaux performants et plus respectueux de l'environnement dans le but de répondre aux exigences de l'économie circulaire.

**Mots-clés :** Polymères thermodurcissables, Conception moléculaire, Simulations dynamiques moléculaires, Conception pour la dégradation

## **2. From the Design of Novel Tri- and Tetra-Epoxidized Ionic Liquid Monomers to the End-of-Life of Multifunctional Degradable Epoxy Thermosets**

### **2.1. Abstract**

The design and development of multifunctional epoxy thermosets have recently stimulated continuous research on new degradable epoxy monomers. Herein, tri- and tetra-epoxidized imidazolium monomers were rationally designed with cleavable ester groups and synthesized on a multigram scale (up to 100g) yielding room-temperature ionic liquids (ILs). These monomers were used as molecular building blocks and cured with three primary amine hardeners having different reactivities, leading to six different network architectures. Overall, the resulting epoxy-amine networks exhibit high thermal stability ( $>350^{\circ}\text{C}$ ), excellent mechanical properties combined with a shape memory behavior, glass transition temperatures ( $T_g$ ) from  $55$  to  $120^{\circ}\text{C}$  and complete degradability under mild conditions. In addition, non-polarizable, all-atom molecular dynamics (MD) simulations were applied in order to investigate the molecular interactions during the polyaddition reaction-based polymerization and then to predict the thermomechanical and mechanical properties of the resulting networks. Thus, this work employs computational chemistry, organic synthesis, and material science to develop high-performance as well as environmentally friendly networks to meet the requirements of the circular economy.

**Keywords:** Thermoset Polymers, Molecular Designing, Molecular Dynamic Simulations, Design for Degradation

### 3. Introduction

Designing multifunctional and sustainable polymer materials that can be reusable and recyclable is needed urgently to meet the requirements of the circular economy.<sup>1-3</sup> Notably, the circular economy does not reduce itself to recycling useless products but also stimulates maximum usage of each material during its lifecycle.<sup>2,4,5</sup> Therefore, rationally designing degradable thermosetting polymer that can be re-used or re-incorporated in other materials at its end-of-life reduces thermoset waste to the minimum since these degraded materials are maintained in the economy wherever possible.<sup>3,6,7</sup>

Rational molecular design is an attractive strategy to create and introduce molecular brick subunits into networks facilitating the appearance of aimed functions.<sup>2,8-10</sup> This molecular design approach is also essential to ensure that these materials have sustainable end-of-life, corroborating the concept *design to degrade*.<sup>11-14</sup> Their controlled degradation produces oligomers or monomers that can be used to build new multifunctional networks re-feeding a sustainable circle.<sup>15-17</sup>

Epoxy-amine polyaddition reaction is commonly used to create versatile and tunable thermosets with easy-to-source and tailor prepolymers.<sup>18-21</sup> Moreover, the ability to customize both the epoxy prepolymer and the amine hardener used allows the creation of adaptable networks for specific applications.<sup>19,21</sup> Due to their excellent thermal and mechanical properties, durability, and flexible nature, there have been several applications for these networks in industrial settings ranging from adhesives, coatings, electronics, automotive, and aerospace to 3D printing applications.<sup>22-24</sup> Currently, bisphenol A diglycidyl ether (DGEBA) is the most commonly used epoxy prepolymer industrially for thermosetting polymers.<sup>25,26</sup> However, DGEBA precursors and derivatives are reported as estrogen and androgen receptor antagonists and thus represent a risk for humans and the environment.<sup>27</sup>

Despite the outstanding features of the conventional thermosetting epoxy resins, there are two essential aspects that have been largely neglected: recyclability and sustainable treatment of waste.<sup>15,28,29</sup> Unlike thermoplastics, thermosetting polymers are highly crosslinked networks, which, while providing them exceptional physical and chemical strength makes them particularly difficult to recycle.<sup>17,30,31</sup> Consequently, a significant quantity of non-recyclable epoxy waste is accumulated in landfills.<sup>32,33</sup> To manage this, pyrolysis and mechanical degradation are commonly employed in industry.<sup>34</sup> Although these strategies are potentially scalable, they are extremely energy-consuming as well as causing air and soil pollution.<sup>34</sup>

To address this issue, extensive research has been undertaken employing supercritical solvents, catalysts, and acids or bases to degrade these thermosetting networks.<sup>29,35,36</sup> Okajima and coworkers used supercritical methanol at 270 °C under elevated pressures to recover carbon fiber from epoxy composites.<sup>36</sup> Other authors reported a recycling approach for anhydride-cured epoxy networks by using alcohol with the presence of a catalyst inducing a transesterification reaction.<sup>37–39</sup> After soaking and swelling networks in the presence of a transesterification catalyst, the epoxy network can be decomposed after many hours at higher temperatures (> 150 °C) and re-polymerized, extruded, injection molded or compression molded through vitrimerization process. Qi and co-authors explored the potential for 1,5,7-triazabicyclo[4,4,0]dec-5-ene (TBD) as an organic base and ethylene glycol (EG) to depolymerize anhydride-epoxy materials at ambient pressure and elevated temperatures (around 180 °C) leading to diester and tetra-alcohol by-products.<sup>33</sup> More recently, Liu *et al.* chemically dissolved conventional epoxy resins by using a highly concentrated nitric acid solution and an ultrasound-microwave.<sup>29</sup> Such recycling methodologies are inconvenient from an industrial point of view because they operate under elevated pressures or temperatures and require the use of expensive catalysts or highly hazardous chemicals.<sup>15,16,32,40</sup>

For the first time, this study proposes the design of molecularly engineered tri- and tetra-epoxidized imidazolium IL monomers with esters as cleavable linkages to create multifunctional degradable networks. Prior to now, very few studies were dedicated to the development of efficient synthetic routes for epoxy imidazolium monomers and to the best of our knowledge, no works reported this approach.<sup>41,42</sup> Gin *et al.* used an epichlorohydrin-based route to synthesize diepoxidized imidazolium monomers as precursors of epoxy-amine membranes for gas separation applications.<sup>43</sup> While in contrast, other authors utilized epoxy monomers based on quaternary ammonium or triazolium cations to build low  $T_g$  solid electrolytes with increased ionic conductivity.<sup>44–46</sup> In 2017, our research group presented an efficient synthetic route without using epichlorohydrin and bisphenol A derivatives to synthesize mono- and di-epoxidized ILs.<sup>47</sup> From this versatile methodology, we designed different epoxy-amine coatings based on diepoxidized IL monomers.<sup>48</sup> These networks exhibited hydrophobic behavior, antibacterial properties, and mechanical performances similar to DGEBA-based materials.<sup>48</sup>

Previous theoretical studies have suggested that the key role in the polymerization of the epoxy-amine networks was the ability of strong hydrogen bonding to occur between the amine group and the oxygen in the epoxy group.<sup>49</sup> This interaction was hypothesized to be the trigger for the autocatalytic opening of the epoxy group to allow amine addition to the carbon, thus causing the polymerization to take place.<sup>50</sup> Whereas this is the predominant

mechanism at room temperature, it should be noted that this is not the only possible reaction at higher temperatures favoring noncatalytic reactions due to the higher kinetic energy present.<sup>51</sup> In this study, we investigated the effect of the chemical nature of IL epoxy monomers on the thermodynamics of the amine addition with the potential increase of interaction between the epoxy monomer and the amine. For these reasons, we have selected three amine hardeners with 3 different reactivities, namely Jeffamine D230 (D230), 4,4-diaminodicyclohexylmethane (PACM) and sulfanilamide (SAA). Thus, non-polarizable MD simulation was used to investigate the molecular interactions between amine groups and these novel tri- and tetra-epoxidized IL monomers. In addition, all-atom MD simulations were performed to predict the thermomechanical and mechanical properties of the resulting networks and the results were compared with our experimental data.

This study combines MD simulations, organic synthesis, and material science to develop multifunctional degradable shape-memory epoxy networks. Based on a computational-assisted approach, we tuned the degradability, thermal stability, and mechanical properties, providing high-performance environmentally friendly epoxy networks.

## 4. Experimental section

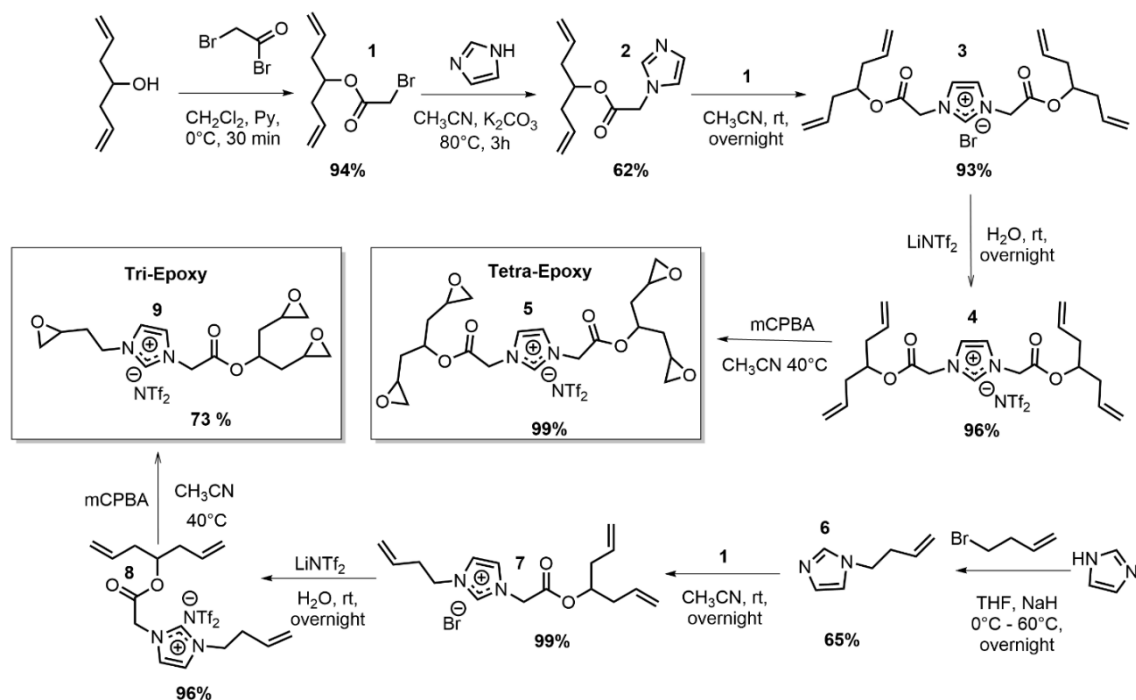
### 4.1. Materials

All reagents were purchased from Sigma Aldrich, and were used without further purification. All solvents including anhydrous solvents were purchased from Carlos Erba and used as received. Tetrahydrofuran and dichloromethane in anhydrous grade were obtained in sealed flasks and used under nitrogen atmosphere.

### 4.2. Synthesis of tri- and tetra-epoxidized IL monomers

The tetra-epoxidized IL and tri-epoxidized IL monomers were synthesized on a multigram scale (up to 100g) in five and four steps, respectively (**see Scheme III-1**). To accomplish the synthesis of the tetra-epoxidized IL monomer, compound **1** was synthesized at a 94% yield by slowly dropping bromoacetyl bromide (1.3 eq., 115 mmol, 10 mL) into a mixture of 3-cyclohexene-1-methanol (11.6 mL, 89 mmol) and pyridine (1.5 eq., 11 mL, 134 mmol) under an inert atmosphere at 0 °C for 2 h. In the presence of potassium carbonate (2 eq., 0.25 g, 1.8 mmol), imidazole (1.2 eq., 0.07 g, 1.0 mmol) and **1** (0.2 g, 0.86 mmol) were stirred in acetonitrile (4 mL) overnight at 80 °C, resulting in a 62% yield of **2**. Compound **2** was purified by column chromatography, employing a gradient of ethyl acetate in n-hexane, from 0 to 50% (v/v). Subsequently, compound **2** (0.1 g, 0.45 mmol) was dissolved in acetonitrile (1 mL) and **1** (1.2 eq., 0.127 g, 0.55 mmol) was added dropwise. The reactional

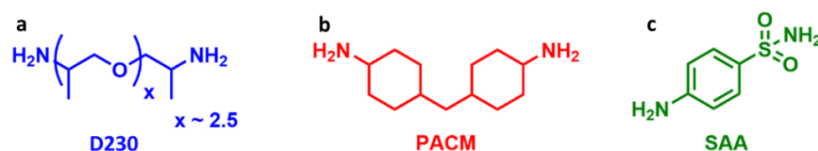
mixture was stirred overnight at room temperature and subsequently precipitated into diethyl ether. The ion exchange was carried out by solubilizing compound **3** (0.19 g, 0.68 mmol) in water (4 mL) at 80 °C and adding an aqueous solution of bis(trifluoromethane)sulfonimide lithium salt (2 eq., 0.395 g, 1.36 mmol). The reactional mixture was left to stir at room temperature for 12 h. From the aqueous phase, product **4** was extracted five times with 35 mL of dichloromethane yielding **4** in 96%. Product **5** was synthesized by the classical Prilezhaev reaction with *m*CPBA (6 eq., 0.525 g, 2.3 mmol), in acetonitrile at 40 °C for 72 h. The crude material was solubilized in a small quantity of dichloromethane and precipitated into a mixture of diethyl ether and petroleum ether (50:50) (v/v). Tetra-epoxidized IL monomer was obtained as a transparent, colorless, and viscous oil, with purity confirmed by <sup>1</sup>H, <sup>13</sup>C, <sup>19</sup>F and 2D NMR techniques, IR, and HRMS (ESI<sup>+</sup>) which showed its corresponding ion peak 437.19188 for calcd. C<sub>21</sub>H<sub>29</sub>N<sub>2</sub>O<sub>4</sub> [M]<sup>+</sup>: 437.19184. To synthesize the tri-epoxidized IL monomer a straightforward methodology was also employed. Compound **6** was synthesized through a nucleophilic substitution in tetrahydrofuran (100 mL) using 4-bromo-1-butene (1.2 eq., 6.35 mL, 62.5 mmol), sodium hydride dispersion at 60% in mineral oil (2 eq., 4.17 g, 104 mmol) and imidazole (3.54 g, 52 mmol) under an inert atmosphere. This reaction was quenched with methanol at 0 °C and it was purified by column chromatography using a gradient of methanol in chloroform from 0 to 4%. Then, previously synthesized ester **1** (1 eq., 0.2 g, 0.86 mmol) was added dropwise to **6** (0.1 g, 0.86 mmol) in acetonitrile yielding product **7** at a yield of 99%. Afterwards, the anion exchange was carried out solubilizing **7** (0.24 g, 0.68 mmol) in water (13 mL) at 80 °C and by adding a solution of bis(trifluoromethane)sulfonimide lithium salt (2 eq., 0.395 g, 1.36 mmol) to result in a yellowish viscous oil. Finally, compound **8** (0.3 g, 0.56 mmol) was epoxidized by *m*CPBA (6 eq., 0.76 g, 3.3 mmol) at 40 °C in acetonitrile (40 mL) to give molecule **9**. Tri-epoxidized IL monomer was obtained as transparent and colorless oil, and the efficiency of the synthesis was confirmed by <sup>1</sup>H, <sup>13</sup>C, <sup>19</sup>F and 2D NMR techniques, IR, and HRMS (ESI<sup>+</sup>) that revealed its corresponding ion molecular peak 323.1600 for calcd. C<sub>16</sub>H<sub>23</sub>N<sub>2</sub>O<sub>5</sub> [M]<sup>+</sup>: 323.1601.



**Scheme III-1.** Synthetic route used to obtain the IL monomers.

### 4.3. Epoxy Network Preparation

The IL monomers were polymerized with selected nitrogen nucleophiles *i.e.* an aliphatic, cyclic or aromatic primary amine. These amines are Jeffamine-D230 (D230), 4,4-Diaminodicyclohexylmethane (PACM), and 4-Aminobenzenesulfonamide (SAA), shown in **Fig. III-1** and are known to have varied reactivities due to their diverse steric hindrance and electronic effects.



**Figure III-1.** Chemical structures of the three hardeners **a)** D230, **b)** PACM, and **c)** SAA.

The corresponding hardeners were mixed homogeneously with the tri- and tetra-epoxidized IL monomers **5** or **9** in a stoichiometric ratio, *i.e.*, epoxy to amino hydrogen equal to 1 in order to prepare the epoxy-amine networks. D230 and SAA were thoroughly mixed with both monomers in a single-step process. PACM was heated to 40 °C for 30 minutes to ensure complete melting and was subsequently mixed with the monomers. Following this, the epoxy-amine mixtures were poured into silicone molds, and the corresponding curing protocol was used according to **Table III-1**.

**Table III-1.** Curing protocols determined for the curing of the epoxy-amine networks.

		D230	PACM	SAA
or  5	Triepoxy 9	6h 80 °C	4h 80 °C	
		6h 160 °C	4h 160 °C	24h 175 °C
	Tetraepoxy	2h 180 °C	2h 180 °C	

#### 4.4. Characterization methods

*Nuclear Magnetic Resonance (NMR) Techniques.*  $^1\text{H}$ ,  $^{13}\text{C}$ ,  $^{19}\text{F}$  and two-dimensional NMR spectra were recorded on a Bruker Avance III 400 MHz spectrometer. The chemical shifts are expressed in ppm relative to internal tetramethylsilane for  $^1\text{H}$  and  $^{13}\text{C}$  nuclei, and coupling constants are indicated in Hz. The abbreviations for signal coupling are assigned as follows singlet (*s*), doublet (*d*), doublet of doublets (*dd*), triplets (*t*), quartets (*q*), quintet (*qt*), multiplet (*m*), and broad signal (*b*). Additional two-dimensional NMR experiments (COSY, HSQC, HMBC) were employed to accurately assign the signals to the different protons and carbon atoms.

*High Resolution Mass Spectra (HRMS).* High-resolution mass spectra were acquired using a Micromass-Waters Q-TOF Ultima Global mass spectrometer through the Electrospray Ionization (ESI) technique. The samples were prepared in methanol or acetonitrile and injected directly into the mass spectrometer. Before each analysis, the spectrometer was externally calibrated with phosphoric acid in the range of 98 to 1300 m/z.

*Fourier Transform Infrared Spectroscopy (FT-IR).* The FT-IR spectra were recorded using a Nicolet Magna 550 spectrometer under the attenuated total reflection (ATR) mode. The spectra were acquired over 32 scans with a spectral resolution of 4  $\text{cm}^{-1}$  from 4000 to 500  $\text{cm}^{-1}$  at room temperature.

*Thermogravimetric Analyses (TGA).* The thermal stability of IL monomers and the resulting networks were investigated through TGA using a Q500 Thermogravimetric Analyzer (TA Instruments). The samples were heated from 30 °C to 800 °C at a rate of 10 °C  $\text{min}^{-1}$  under a nitrogen atmosphere. The thermograms are expressed in terms of the percentage of remaining mass as a function of temperature, allowing the determination of onset ( $T_D^0$ ) and maximum ( $T_D^{\text{MAX}}$ ) degradation temperature.

*Differential Scanning Calorimetry (DSC).* The IL monomers in the presence of the hardeners, as well as alone, in addition to the resulting networks were analyzed by DSC. This analysis was carried out using a Q10 Calorimeter (TA Instruments) employing the dynamic mode with a heating rate of 10 °C  $\text{min}^{-1}$  from -70 °C to 250 °C under nitrogen flow.



The DSC technique was employed to determine the glass transition temperatures ( $T_g$ ) of the six resulting networks.

*Dynamic Mechanical Analysis (DMA).* The thermo-mechanical properties of the epoxy-amine materials were investigated by DMA. An ARES G2 Rheometer (TA Instruments) equipped with a torsional fixture module was initially employed to determine the linear viscoelastic region of each material. Then, rectangular-shaped samples with dimensions of  $30 \times 4 \times 1.5 \text{ mm}^3$  were analyzed with a heating rate of  $3 \text{ }^\circ\text{C min}^{-1}$  from  $-100$  up to  $250 \text{ }^\circ\text{C}$  at the frequency of  $0.5 \text{ Hz}$ . Storage Modulus  $G'$  was acquired and expressed in a logarithm scale to emphasize the molecular transitions. The loss factors  $\tan \delta$  were measured for the same interval and reported on a linear scale.

*Transmission Electron Microscopy (TEM).* The morphology of the networks was assessed using a Phillips CM 120 microscope operated at  $120 \text{ kV}$ . The samples were prepared by slashing ultrathin sections using an ultramicrotome equipped with a diamond knife. The samples were obtained as thin layers using an ultramicrotome equipped with a diamond knife. The ultrathin polymer layers were set on the TEM grids (Carbon Film-Copper, 300 mesh, EMS) and analyzed. The sample morphologies were investigated at micro- and nano-scales. The images were acquired using the Olympus imaging system equipped with a Categra G2 camera  $2048 \times 2048$  pixels, 14 bits). The images were processed, and the scale bars were included on the iTEM software.

*Surface Energy Test.* The contact angle and surface energies of the resulting epoxy-amine networks were measured through the sessile drop technique using a Digidrop-GBX Goniometer. Water and diiodomethane were used as liquid probes, and the dispersive and non-dispersive components of the surface energy were determined by using Owens-Wendt's theory.<sup>52</sup>

*Shape Memory (SM).* The samples were placed in the oven at their corresponding deformation temperatures ( $T_{df}$ ) for 45 minutes. Once the thermal equilibrium was reached, the samples were bent using a U-shaped mold. Then, the samples were cooled down to room temperature, retaining the U-shape by an external force for 5 minutes. Subsequently, the external force was removed, and the fixed bending angles were measured ( $\theta_f$ ). The samples were re-heated up to  $100^\circ\text{C}$ , the initial shapes were gradually recovered, and at the end of this cycle, the recovered angles were registered ( $\theta_r$ ). The SM parameters were measured by determining shape fixity ( $R_f$ ) and shape recovery ratio ( $R_r$ ) through equations 1 and 2, respectively.

$$R_f = \frac{180 - \theta_f}{180} \cdot 100\% \quad (1)$$

$$R_r = \frac{\theta_r}{180} \cdot 100\% \quad (2)$$

*Chemical Degradation Methodology.* A chemical recycling methodology was developed by employing trihexyltetradecylphosphonium cation and bis(2,4,4-trimethylpentyl)phosphinate anion (IL104) as catalyst and ethylene glycol (EG) as solvent. Rectangular samples (15 x 4 x 1.5 mm<sup>3</sup>, 100 mg) were placed into closed glass vials. A hot plate magnetic stirrer coupled to a module Labortechnik Variomag 40ST was employed to heat the systems to 200 °C for 4.5 hours. Six different IL104:EG ratios were evaluated (100:0, 20:80, 10:90, 5:95, 1:99 and 0:100 in wt%). In constant intervals, the evolution of the degradation process was visually monitored. At the end of the process, the degradation activities were determined for the different conditions, and the degradation products were systematically characterized by NMR spectroscopy and HRMS.

At the end of the recycling procedure (4.5 h), the residual mass was weighed, and the degradation activity was determined using Equation 3, where  $m_i$  and  $m_f$  are the initial and final mass, respectively. All the experiments were carried out in triplicate.

$$R_f = \frac{m_i - m_f}{m_i} \cdot 100\% \quad (3)$$

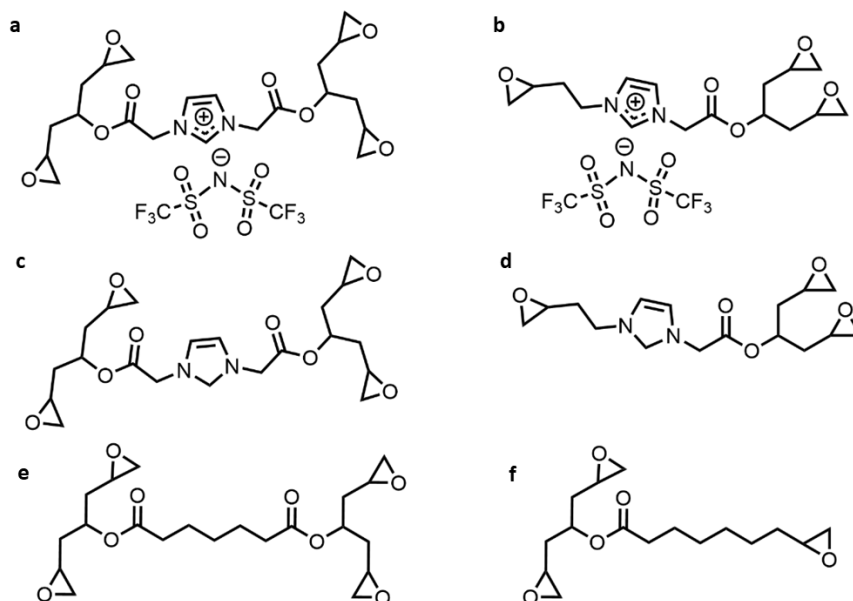
## 4.5. Simulation Methods

### *Investigation of Molecular Interactions*

*Non-polarizable Molecular Dynamics (MD)* was applied using the LAMMPS software package to give a large-scale picture of the interactions between amine groups and epoxy groups.<sup>53</sup> The systems were constructed using the 3 amines studied experimentally, D230, PACM and SAA, with tri- and tetra-epoxidized cations, and bis(trifluoromethane)sulfonimide (NTf<sub>2</sub>) anions. In addition to the tri- and tetra-epoxidized imidazolium cations, an uncharged version with imidazole was also studied, as well as imidazolium substituted with a butyl chain. The set of epoxy molecules being studied is shown in Chart 1. For the imidazolium group on the epoxy monomer and for NTf<sub>2</sub>, parameters from the CL&P forcefield were used.<sup>54</sup> In the ester, epoxy, non-charged epoxy imidazolium and alkyl chain components of the epoxy monomer, as well as the D230, PACM and SAA, parameters were obtained using QM calculations to determine the partial atomic charges as well as the bond lengths and angles with non-bonding Lennard-Jones parameters taken from the OPLS-AA forcefield.<sup>55</sup> Charges were found using the Charges from Electrostatic Potentials using a Grid-based (CHELPG) method, and equilibrium angles and bond lengths were found through optimizations using the B97-D3 functional with Dunning's cc-pVDZ basis set, as had been used for the IL parameters in the CL&P model. In the case of D230, a length of  $x = 1$  was applied to reduce computational costs of repeated ether groups not participating in interactions of interest.<sup>56-58</sup> Systems were run using 300 of each epoxy imidazolium, NTf<sub>2</sub> and the amine to simulate the experimental conditions. An equilibration run of 2 ns in NpT was carried out to attain an equilibrium system state, then used as initial configuration for a 10 ns production run which was used for analysis.

The probability of interaction can provide insight to the likelihood of amine groups and epoxy groups to be in a position for polymerization to occur. Radial distribution functions (RDFs) were used to determine the probability of the amine to be present at a given distance from an epoxy group. The distance was measured from the center of mass of the epoxy group to the nitrogen of the amine. RDFs were also taken for the spatial correlations between the amine group and the NTf<sub>2</sub> anion to determine the interaction between these two components and ascertain if this was significantly reducing the probability of the amine interacting with the epoxy groups. In this instance the oxygen was used as the reference atoms in NTf<sub>2</sub>, with the nitrogen of the amine again used for the amine. The integral of each of these RDFs up to the first minima, defined as the end of the first solvation shell was used to determine the coordination number of each chosen site. In addition to RDF analysis, spatial distribution functions (SDFs) were also calculated to determine the region of the epoxy

with which the amine is interacting, with angular resolution. These diagrams were used to understand how this may differ for each amine studied, with the lone epoxy group on one side of the tri-epoxidized imidazolium and the diepoxy groups on the same side of the imidazolium ring in the tri- and tetra-epoxidized imidazolium cations, respectively. RDFs and SDFs were calculated using the TRAVIS<sup>59</sup> software package with the hydrogen bond acceptor (the epoxy or the NTf<sub>2</sub> anion) as the reference component and the hydrogen bond donor (the amine group) as the observed component.



**Chart III-1.** Epoxy molecules studied using MD simulations with D230, PACM and SAA, with **a)** and **b)** being the charged imidazolium NTf<sub>2</sub> epoxy, **c)** and **d)** being the uncharged imidazole epoxy and **e)** and **f)** being the alkyl chain substituted epoxy molecules. **a), b)** and **c)** are tetra-epoxidized molecules and **b), d)** and **f)** are tri-epoxidized molecules.

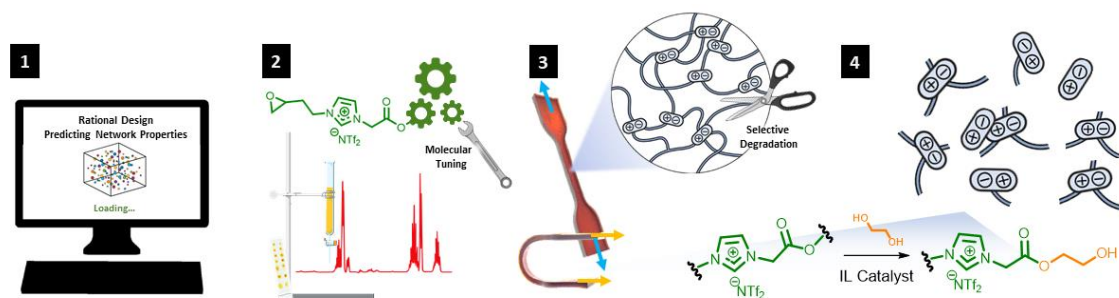
#### *Predicting the Network Properties*

All-atom molecular dynamics (MD) simulations were performed using the DREIDING force field.<sup>60</sup> The initial structures were generated using the AVOGADRO software program.<sup>61</sup> The number of ions/monomers for each system was reported in **Table III-S1**. The ions/monomers were randomly placed in a cubic simulation cell with periodic boundary conditions (PBCs) using the PACKMOL software program.<sup>62</sup> The initial cubic samples were generated at low density (200 Å in each principal direction) to avoid atomic overlaps during the packing the ions/molecules. The simulation procedure reported in the literature was followed to polymerize the liquid precursor mixtures and predict the thermo-mechanical properties of the resulting polymers.<sup>63</sup> More information about the simulation methodology has been provided in the supporting information.

## 5. Results and Discussion

### 5.1. Design and Synthesis of Degradable Multifunctional Networks

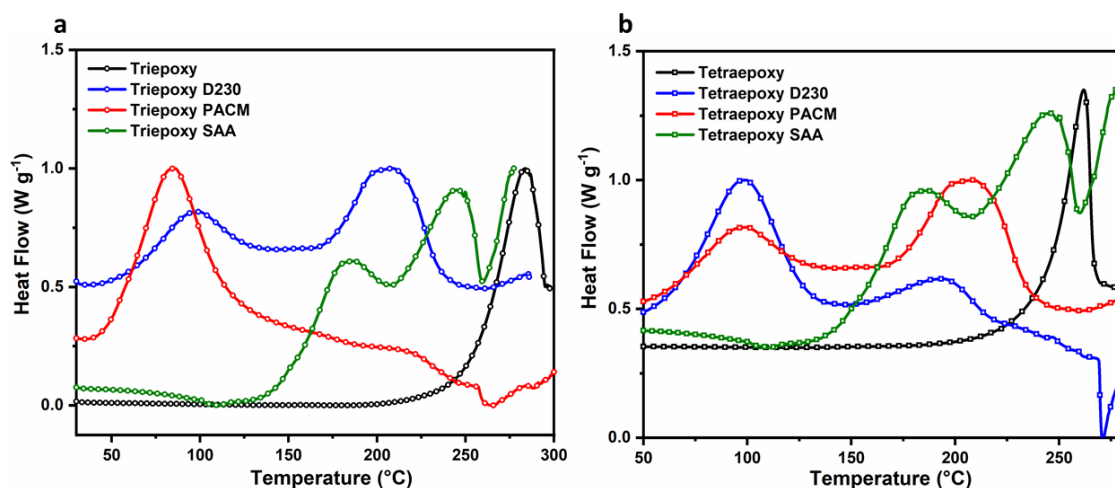
The six networks developed and characterized in this work meet the properties of epoxy thermosetting materials<sup>64,65</sup> with high chemical and thermal stability simultaneously. These features are mainly provided through the crosslinks present in the networks. These properties are also closely linked to the challenge of recycling these materials.<sup>8,16,64</sup> Indeed, tri- and tetra-epoxidized monomers **5** and **9** were designed not only to tailor high-performance thermosets but also to be degradable or reprocessable. This rational design is aligned with the principles of Green Chemistry: specifically, the 4<sup>th</sup> principle of 'Designing Safer Chemicals' and the 10<sup>th</sup> principle of 'Designing for Degradation'.<sup>2,11</sup> To achieve these goals, the IL monomers bear ester bonds that were strategically installed to tune the degradability under mild conditions regenerating imidazolium-type ILs (**Fig. III-2**).



**Figure III-2.** General scheme. **(1)** Understanding structure-property relationships and mechanical property predictions. **(2)** Molecular tailoring and organic synthesis. **(3)** Development of new multifunctional materials and their characterization. **(4)** Chemical recycling and proposed mechanism of degradation.

### 5.2. Polymerization of the Epoxy-Amine Systems: Investigation of Molecular Interactions and Reactivity Study (DSC)

Non-polarizable Molecular Dynamics (MD) was applied to have a large-scale picture of the intermolecular interactions between the amine hardeners and the IL monomers and compared to the differential scanning calorimetry (DSC) results to further understand the chemical reactivities of these systems (**Fig. III-3**). Moreover, the extent of interaction between the epoxy groups with other epoxy groups from neighboring monomers was also performed. This analysis is essential because the presence of two exothermic peaks (**see Fig. III-3**) can be ascribed to a bimodal behavior corresponding to two different reaction mechanisms or a two-step mechanism.<sup>41,66,67</sup>



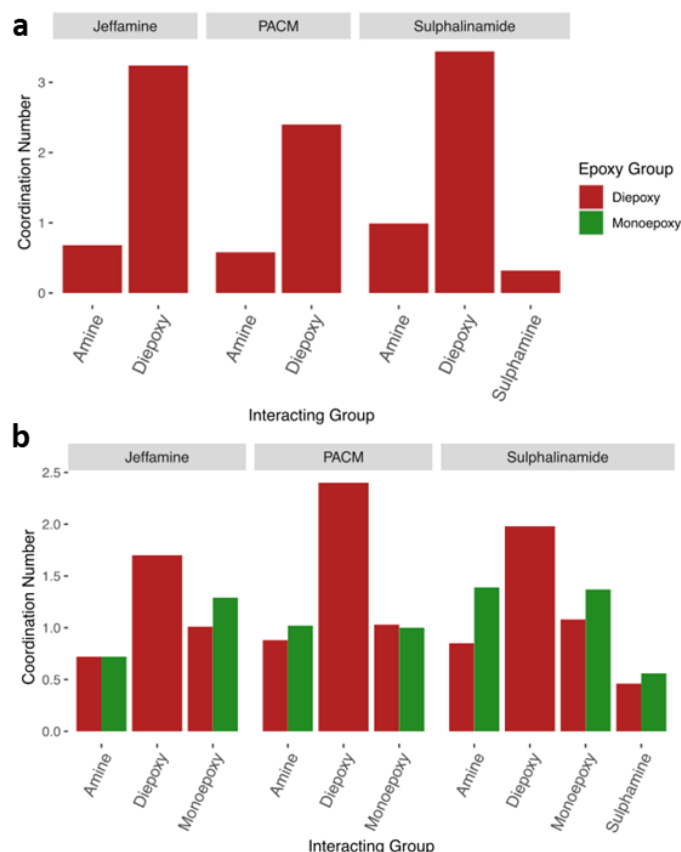
**Figure III-3.** DSC thermograms of the corresponding reactional mixture for **a)** triepoxy and **b)** tetraepoxy. The curves corresponding to the exothermic peak of polymerization (exo up).

These simulations and the radial distribution functions (RDFs) indicate that there are notable spatial correlations between the amine groups of the three possible amines and the epoxy groups of the tri- and tetra-epoxidized cations, as well as, to an even greater extent, with other epoxy groups, which together account for a majority of the epoxy groups interactions. The strength of the interaction was shown by the coordination number of the 2 types of examined groups, with a higher coordination number indicating a higher probability of these groups interacting. In the case of the D230 amine, in its interactions with the tetra-epoxidized ionic liquid (IL) monomer, wherein there is a diepoxy ester group on both sides of the imidazolium cation, the coordination number of the first interaction was found to be 0.68, whilst it was slightly larger for both the diepoxy and monoepoxy sides of the tri-epoxidized imidazolium, wherein its coordination number was found to be 0.72. This slight variation implies a stronger interaction between the individual epoxy groups of the tri-epoxidized than the tetra-epoxidized imidazolium cation due to a reduced total number of epoxy groups concentrating the interaction to those present. These results are confirmed by the reactivity study performed by DSC, showing two exothermic peaks around 80-85 °C and 180-200 °C in both cases. However, the DSC curves also show a slight but enhanced reactivity for the tri-epoxidized IL monomer.

In the case of PACM, the increased steric bulk emphasized the stronger association between the amine group and the tri-epoxidized imidazolium group compared to its tetra-epoxidized cation counterpart. This is seen in the coordination number of 0.88 in the diepoxy group of tri-epoxidized IL cation in comparison to 0.58 for the tetra-epoxidized cation, as shown in **Fig. III-4**. The monoepoxy group of the tri-epoxidized imidazolium salt was found to be even more highly coordinating than the diepoxy, with a coordination number of

1.02, further indicating the preference of PACM to interact with non-sterically hindered epoxy groups. Overall, it is evident that the steric hindrance of the epoxy environment plays a more significant role in PACM than in D230, where the coordination number remained relatively similar between the tri- and tetra-epoxidized cations. These observations are further confirmed by the results that show a single exothermic peak for the tri-epoxidized IL-PACM system compared to the presence of two exothermic peaks for the tetra-epoxidized IL-PACM mixture.

However, both systems containing PACM and D230 amines, epoxy groups are shown to prefer local environments with other epoxy groups instead of with amines. This is shown by the coordination number of epoxy groups in the tetra-epoxidized IL monomer being 3.24 and 2.40 for D230 and PACM, respectively. High epoxy-epoxy interactions are also shown in the diepoxy and monoepoxy groups of the tri-epoxidized IL monomer, although to a lesser extent, with, for example, the largest coordination number of the monoepoxy groups in the tri-epoxidized IL monomer and D230 system being with itself at 1.29. This indicated that although there is notable interaction between the amine and the epoxy, epoxy groups prefer similar groups, likely therefore creating strong epoxy-epoxy domains linking these cations together.



**Figure III-4.** Coordination number of tetra-epoxidized imidazolium **a)** and tri-epoxidized imidazolium **b)** epoxy groups with themselves and amines to determine strengths of inter-molecular interactions.

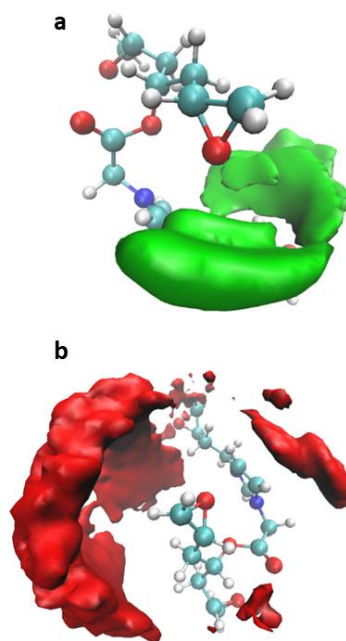
These results agree with the DSC curves that show a bimodal behavior.<sup>68,69</sup> Indeed, a competition reaction can occur between the primary and secondary amine-epoxy addition. Also, a homopolymerization pathway can take place at higher temperatures.<sup>41,48,68</sup>

In the case of the SAA amine, an increase in maximum coordination number between the epoxy groups and the amine groups was shown in comparison to other amine hardeners. It was also possible to provide further analysis due to the amine groups' asymmetry. Between the two different amine groups, the amine bonded to the phenyl-derived ring was found to have a higher coordination number compared to the amine attached to the sulfonamide group, with the epoxy groups present in the tetra-epoxidized IL monomer. This was shown through a coordination number of 0.99 for the SAA amine with the epoxy group in the tetra-epoxidized IL cation, compared to a coordination number of 0.32 for the sulfonamide amine. As with PACM and D230, the tri-epoxidized IL monomer was found to have a higher coordination number than the tetra-epoxidized IL monomer, with the monoepoxy group on this cation having the highest coordination number with amines of any of the



epoxy groups analyzed corroborating the DSC results. The monoepoxy group was found to have a coordination number of 1.39 with the phenyl amine group of the SAA and 0.56 with the sulfonamide amine group, with all phenyl epoxy-amine coordination numbers being notably higher than any amine-epoxy interactions in PACM or D230 systems. The significant difference in coordination numbers between the two amine groups indicates that, while in PACM and D230 the two amines present are equally likely to interact with the epoxy group due to their symmetry, the SAA has a clear directionality to which amine is more likely to undergo polymerization.

To understand the directionality of the interactions inferred through the coordination numbers previously shown, spatial distribution functions (SDFs) were utilized. As shown in **Fig. III-5**, the range of interactions between the epoxy group and the amine group of D230, as well as its epoxy groups for neighboring tri-epoxidized IL cations are broadly distributed.



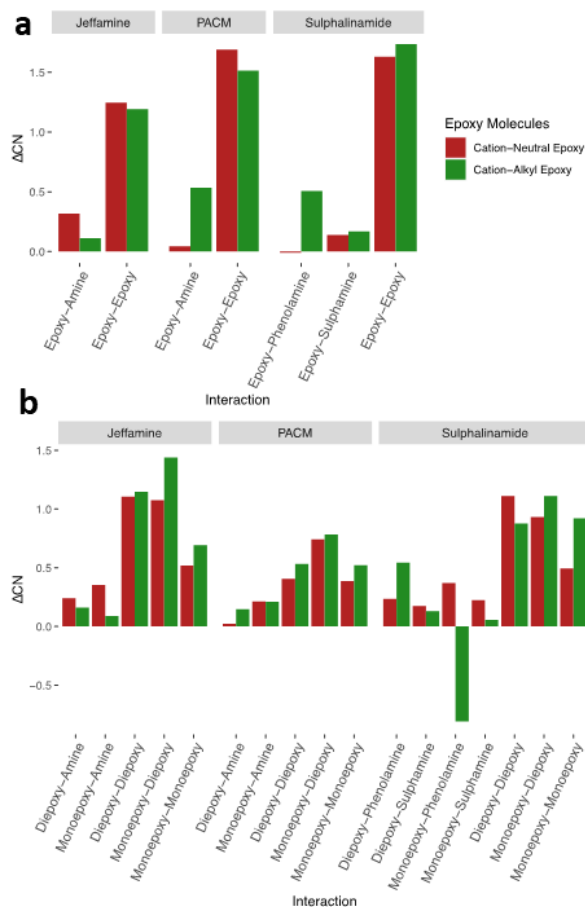
**Figure III-5.** Spatial distribution functions (SDFs) for epoxy groups in tri-epoxidized imidazolium D230 systems with amine groups of D230 (top) and other epoxy groups of tri-epoxidized imidazolium (bottom). Isovalues used were 10, and the center of mass of the epoxy ring as the reference point and the nitrogen of the amine (top) and center of mass of intermolecular epoxy groups (bottom) being the observed points.

Interactions between amine groups and epoxy groups are shown to be very close-ranged, with the average distance between the nitrogen of D230 and the center of mass of the epoxy group of the diepoxy group on tri-epoxidized IL monomer being 3.68 Å.

The epoxy-amine interaction is also shown to be highly directional, with a majority of density of the amine being adjacent to the oxygen of the epoxy, showing this interaction is due to hydrogen bonding between the hydrogen bond donating amine and the receiving epoxy oxygen. In contrast, the epoxy-epoxy interaction was found to be relatively long-ranged, with the average interaction distance being 4.72 Å between two adjacent epoxy groups (from the diepoxy) in the tri-epoxidized IL monomer/ D230 system. The directionality of the epoxy-epoxy interaction is seen to be evenly distributed around the oxygens and the carbons, focused largely on the side facing away from the epoxy group on the same molecule. A notable gap above the oxygen of the epoxy is also seen, with this being the region in which the amine-epoxy contacts are located. This indicates that instead of it being a strong electrostatic interaction as is seen in amine-epoxy, the interaction between 2 epoxy groups on neighboring tri-epoxidized IL molecules is in the form of dispersion interactions, which would allow for domains of epoxy groups to form. Although in both PACM and D230, there is a distinct preference for epoxy-epoxy interactions, as shown by the coordination number analysis, there is a heavily directional interaction between the amine and the epoxy groups due to hydrogen bonding which likely allows for polymerization reactions to occur. Although epoxy-epoxy interactions are preferred from a molecular point of view, DSCs show that the polymerization kinetics of the epoxy-amine reaction is favored by temperature during the curing process. In fact, the homopolymerization reaction of tri- and tetra-epoxidized monomers occurs only at higher temperatures (260 and 290 °C), as shown by DSC curves.

To determine the effect of the ionic component as well as of the imidazolium ring on the epoxy interactions, the imidazolium ring was substituted with uncharged imidazole as well as with an alkyl chain and simulated in the same conditions as the original systems. RDF results from these systems indicated that, as expected, the coordination number increased without a charged component in almost all instances, due to the NTf<sub>2</sub> anion being taken away allowing for other interactions to increase (**Fig. III-6**). Significantly, the epoxy-epoxy interactions are seen to account for a majority of the increase in epoxy interactions, with the epoxy-amine interactions only increasing slightly when the charge is removed. This is seen in particular in the PACM tetra-epoxidized system, wherein the difference in coordination number between the systems with imidazolium cation and with the neutral imidazolium is 0.04 for epoxy-amine interactions and 1.69 for epoxy-epoxy interactions, as shown in **Fig. III-5**. This result also translates to the tri-epoxidized monomer systems, whereas for the PACM system the diepoxy-amine and the monoepoxy-amine interactions increased by only 0.02 and 0.21, respectively, whilst the diepoxy-diepoxy, diepoxy-monoepoxy and the monoepoxy-monoepoxy increased by 0.41, 0.74 and 0.39, respectively. This trend was also

observed in the D230 and SAA amine systems, with a higher coordination number found for epoxy-epoxy interactions and only a slight increase in epoxy-amine interactions.



**Figure III-6.** Differences between coordination numbers ( $\Delta CN$ ) of the uncharged imidazole epoxy and the alkyl-chain epoxy with the charged cation imidazolium epoxy in the tri-epoxidized monomer **a)** and the tetra-epoxidized monomer **b)**, with all epoxy monomers shown in **Chart 1**.

When comparing the epoxy imidazolium cations with the neutral alkyl imidazolium monomers, similar trends are observed to those of the imidazolium cation comparisons to neutral imidazole, with a majority of the increase in coordination number being attributed to epoxy-epoxy interactions. The exception to this is the SAA systems, wherein epoxy-epoxy interactions decrease in the alkyl chain epoxy monomer in comparison to the imidazolium cation epoxy monomer. To compensate for the epoxy-epoxy decrease, epoxy-amine interactions increase: the epoxy-epoxy coordination number decrease by 0.57 in the tetra-epoxidized monomer, while the epoxy-phenyl amine and epoxy-sulfonamide amine coordination numbers increase by 0.66 and 0.27 respectively.

The likely reason for this is the smaller size and highly ionic nature of SAA, enhancing its ability to interact with amines when the imidazolium ring is not present, to increase

steric hindrance and provide an addition site for ionic interactions. The comparison of IL systems to those wherein the IL backbone is removed indicate that, for the PACM and D230 containing systems, the NTf<sub>2</sub> anion and imidazolium cations portions of the system do not significantly reduce the epoxy-amine interactions necessary for polymerization to occur, instead only reducing the epoxy-epoxy interactions. In contrast, the SAA systems saw a slight decrease in epoxy-amine interactions in comparison to the (non-imidazole containing) alkyl epoxy monomer. This however was found to be due to the decrease of steric bulk and overall removal of the imidazole ring instead of the removal of the charge. Therefore, the anion and cation charge present in these monomer mixtures do not adversely affect the epoxy-amine interactions and thus are unlikely to decrease reactivity.

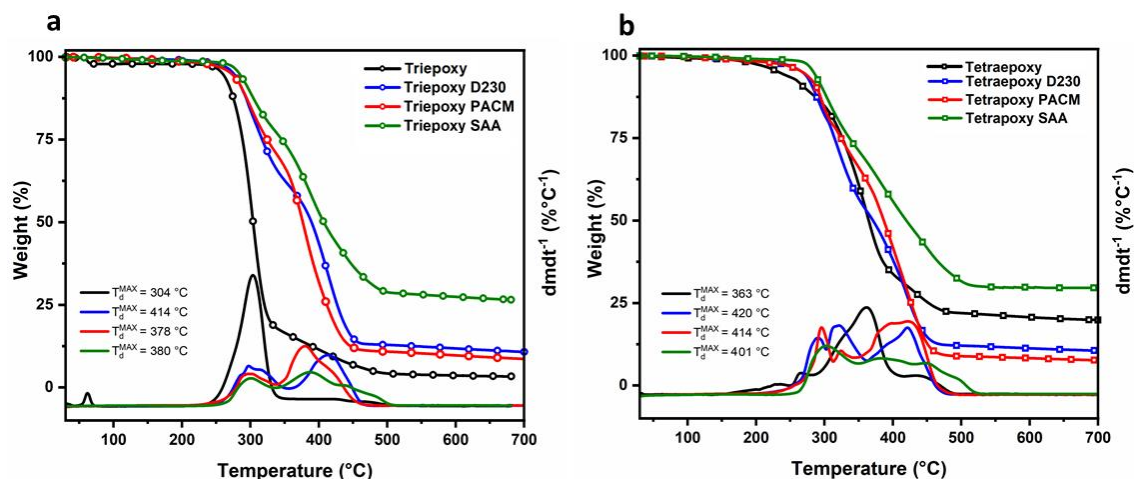
### 5.3. Network Tailoring and Thermal Stability

The synthetic IL monomers are colorless oils and behave as Newtonian liquids at room temperature, which facilitates their homogenization with amine hardeners, *i.e.* D230, PACM and SAA, without using solvents (**Fig. III-S18**). More importantly, both tri- and tetra-epoxidized IL monomers have shown excellent thermal stability investigated in both static and isothermal modes. Only 2 and 5% mass losses at 200 °C were obtained after two hours for tetra- and tri-epoxidized ILs, respectively (**Fig. III-S19**). The higher thermal stability of the tetra-epoxy monomer was also confirmed by the  $T_D^{MAX}$  being 59 °C higher than tri-epoxy  $T_D^{MAX}$  (**Fig. III-7**).

These results are unexpected due to ester groups typically being more reactive than alkyl chains. However, as MD results revealed, an energetically favorable intramolecular hydrogen bond has the potential to form in the tri-epoxidized imidazolium cation. This finding has been further investigated by quantum mechanics (QM) and will be the study topic of a future work. Briefly, the monoepoxy group can interact through a hydrogen bond with the hydrogen at position C-2 of the imidazolium cation, activating this C-H bond. This interaction turns the H even more acidic, and its deprotonation generates an imidazole-2-ylidene carbene that can initiate a degradation reaction pathway. This particular hydrogen bond is less likely for the tetra-epoxidized imidazolium cation due to the increased bulkiness of this molecule.

This hypothesis is corroborated by the fact that after the polymerization with the amine hardeners, the six epoxy-amine networks have identical  $T_D^0$  and  $T_D^{MAX}$ . Overall the resulting networks exhibited excellent thermal stability, with the first weight loss starting only above 250 °C, independent of the monomer-hardener combination. It is also possible to observe that the degradation pathways take place at two different temperatures, which

could suggest two main degradation mechanisms corresponding to the competition between the amine-epoxy addition reaction and the homopolymerization reaction. Remarkably, the six systems presented thermal stabilities comparable to DGEBA-based networks and confirmed previous works investigating the thermal stability of polyionic networks.<sup>41,42,47</sup>

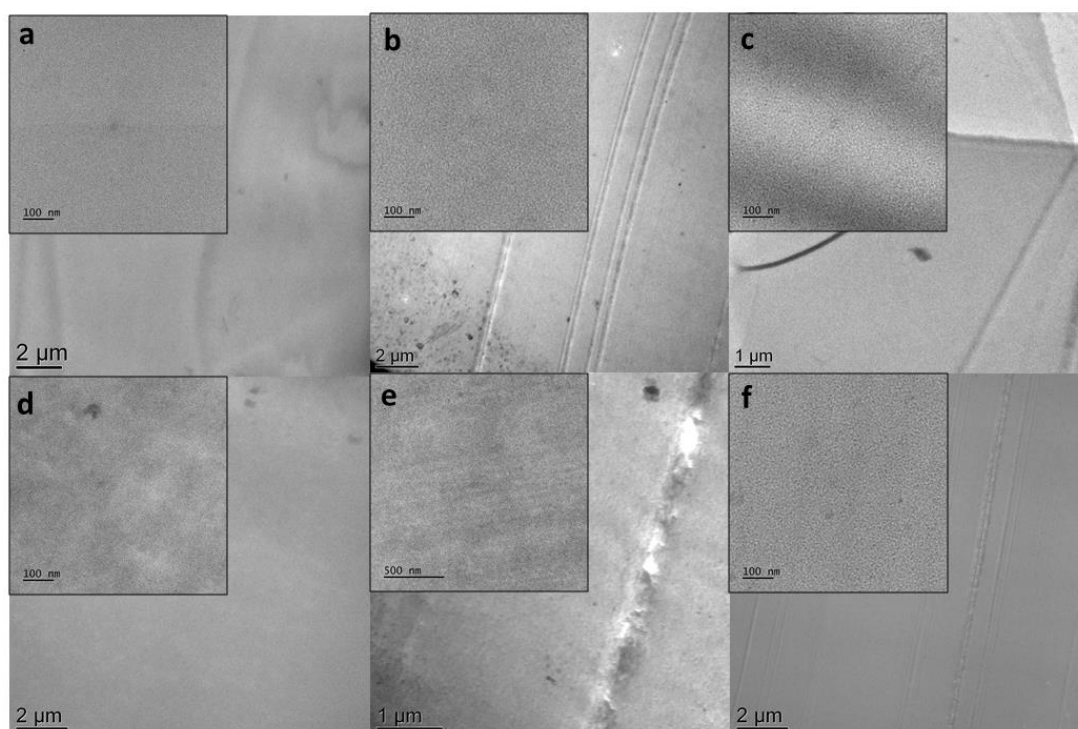


**Figure III-7.** TGA thermograms of neat epoxy monomers and the corresponding epoxy-amine networks based on **a)** tri-epoxidized and **b)** tetra-epoxidized monomers (heating rate: 10 °C min<sup>-1</sup> under nitrogen gas).

#### 5.4. Investigation of the Network Morphology

The design of epoxy-monomer bearing ionic groups has the potential of eliciting properties that would only be obtained using heterogeneous composite formulations. Previously, the interaction simulations revealed more favorable thermodynamic interactions between the epoxy groups of the monomers than between the monomers and amine hardeners. Indeed, sparse homogeneity and phase separation are typical drawbacks, and overcoming these issues is essential in developing high-performance networks.<sup>66,70</sup>

Herein, transmission electron microscopy (TEM) was employed to investigate the morphologies of networks (**Fig. III-8**). Overall, no phase separation was observed for any of the six systems. However, in the PACM-based samples, darker spots were detected, presumably due to the higher reactivity between PACM and both monomers. In fact, PACM reacted with tri- and tetra-epoxidized IL monomers during the mixing process at room temperature. The beginning of the crosslinking reactions was shown to release thermal energy locally and further catalyze the formation of non-uniform networks. It is worth noticing that when PACM is employed as a curing agent the exothermic peaks appear at lower temperatures corroborating this hypothesis.



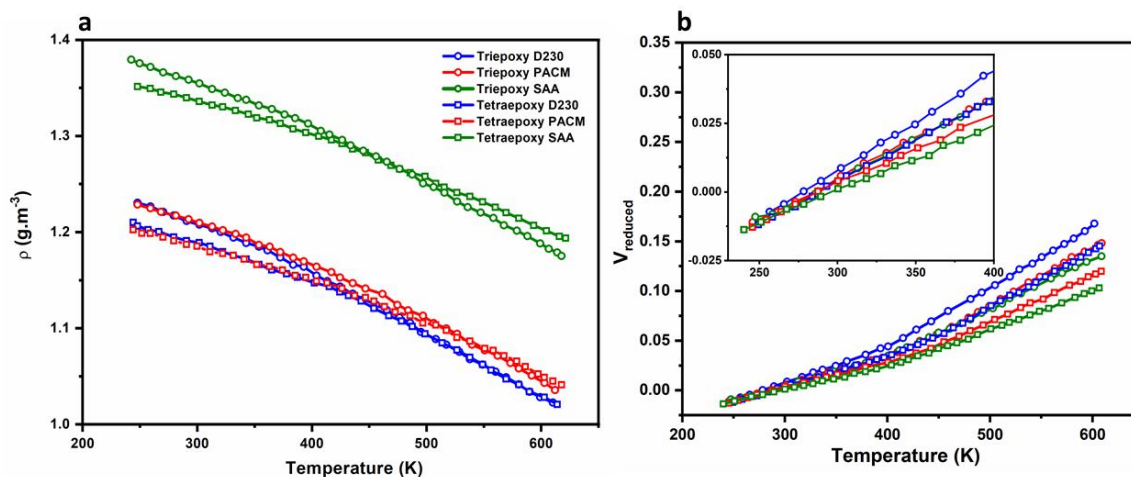
**Figure III-8.** TEM images for **a)** tri-D230, **b)** tri-PACM, **c)** tri-SAA, **d)** tetra-D230, **e)** tetra-PACM and **f)** tetra-SAA. The square sections magnify specific regions and highlight the nanometric structural morphology of the networks.

Our previous studies revealed similar cluster formation when an epoxidized IL monomer and a cyclo-aliphatic amine were used. In this work, an amine analogous to PACM was employed, and an identical aggregation pattern was observed by TEM.<sup>41</sup> More importantly, the TEM investigation at the nanoscale confirmed the high homogeneity of the six resulting networks (**see highlighted squares in Fig. III-8**).

### 5.5. Theoretical and Experimental Investigation of Networks' Preliminary Physicochemical Properties.

The mechanical strength and impact performance are fundamentally related to molecular packing in polymers.<sup>66</sup> Consequently, densities should be predicted precisely and employed as a first criterion to validate the model.<sup>71</sup> For these reasons, the density of the cured networks was experimentally and theoretically determined by using the water displacement method and calculated by NPT simulations, respectively. The cell densities can provide insights into polymers' packing modes and structures. Consequently, densities should be predicted precisely and employed as a first criterion to validate the model.<sup>71</sup> Herein, the densities and reduced volumes were investigated as a function of temperature (**Fig. III-9a and III-9b**). As indicated in **Table III-2**, the experimental densities of the different networks were found to be very close to the simulation results. The slight differences

may be due to the degree of cross-linking (DOC) of the modeled networks estimated to 80%. Indeed, depending on the selected DOC, the equilibrium density will change. However, the average predicted equilibrium density of the cured networks is in satisfactory agreement with the measured one.



**Figure III-9.** Variation of **a)** density and **b)** reduced volume as function of temperature. Theoretical values predicted by simulation.

Following this, the  $T_g$  of the corresponding networks were predicted by MD simulations from the density and reduced volumes (**Table III-2**). In the case of networks prepared from tri-epoxidized IL monomers, the  $T_g$  were determined to be 88 °C and 111 °C for D230 and PACM amine hardeners, respectively.

The hardeners, including aromatic moieties, can impart higher molecular packing compared to the linear and cyclo-aliphatic amines. This decrease of volume at the molecular level is due to stronger non-covalent interactions, namely  $\pi$ - $\pi$  stacking. While, for the tetra-epoxidized IL, the incorporation of an extra epoxide function was shown to lead to an increased  $T_g$  to be 104 and 122 °C for the corresponding networks. These results are consistent with the chemical structure of the IL monomers, in particular with the symmetry of the monomer architecture. The difference observed for the glass transitions obtained by the experimental and the theoretical approach can be explained by the fact that the computational routine developed in this work only takes into consideration the reactions between the epoxy-IL monomers and the amine hardeners.

**Table III-2.** Theoretical and experimental densities and  $T_g$ .

		Theoretical Prediction		Experimental Data	
		Density ( $\text{g}\cdot\text{cm}^{-3}$ ) <sup>1</sup>	$T_g$ ( $^{\circ}\text{C}$ )	Density ( $\text{g}\cdot\text{cm}^{-3}$ ) <sup>1</sup>	$T_g$ ( $^{\circ}\text{C}$ ) <sup>2</sup>
Tri	D230	1.197	$88.7 \pm 15.6$	1.250	56
	PACM	1.201	$110.6 \pm 13.9$	1.231	73
	SAA	1.332	$92.8 \pm 9.4$	1.338	111
Tetra	D230	1.181	$122.1 \pm 7.5$	1.231	68
	PACM	1.177	$115.4 \pm 6.6$	1.213	117
	SAA	1.316	$103.8 \pm 8.4$	1.322	85

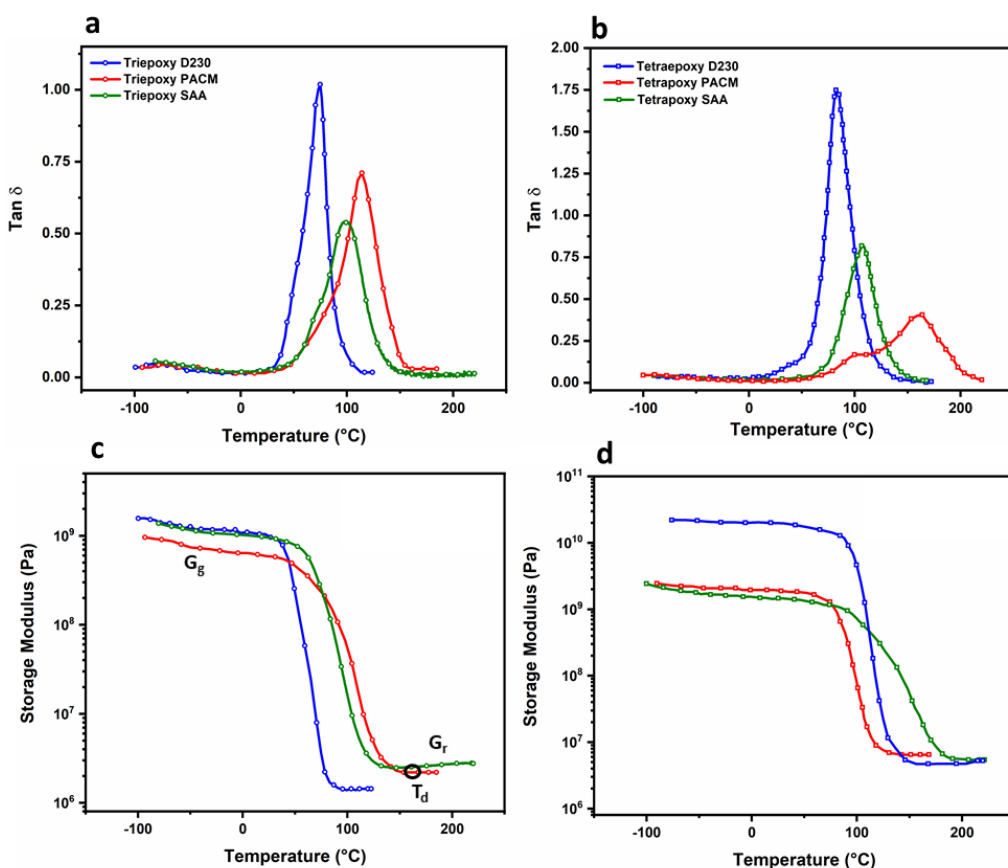
<sup>1</sup> The densities were estimated at 300K. <sup>2</sup>The glass-transitions temperatures were determined by differential scanning calorimetry; heating rate of  $10^{\circ}\text{C min}^{-1}$  from  $-70^{\circ}\text{C}$  to  $250^{\circ}\text{C}$  under nitrogen flow.

The non-polarizable MD data suggested a stronger interaction between the epoxy moieties of neighboring monomers which could be associated with a higher local concentration of monomers corroborating the homopolymerization observed by DSC. Notably, the higher reactivity of PACM towards the IL monomers overcomes the homopolymerization pathway, and consequently the resulting networks present  $T_g$  coherent to the values predicted by MD simulations.

## 5.6. Thermo-Mechanical Properties of the Networks and Shape Memory Behavior

The thermo-mechanical properties of the six resulting networks were also investigated by dynamic mechanical analysis (DMA). All the networks exhibited storage modulus  $G'$  in the order of magnitude of GPa and MPa for the glassy and rubbery plateaus, respectively. On average, the networks tailored from the tetra-epoxidized IL monomer presented higher  $G'$  values than those based on tri-epoxidized IL monomer (**Fig. III-10**). Importantly, the incorporation of imidazolium IL in the monomer backbone allowed the ratio  $G_g:G_r$  tuning. This is a striking due to the ratio being strongly correlated to SM performance. Our previous report on designing hybrid networks showed that the integration of an IL-monomer into a classical epoxy network can increase the  $G_g:G_r$  ratio from 31 to 351, improving the SM performance as a function of IL monomer proportion.<sup>72</sup>





**Figure III-10.** Loss factor,  $\tan \delta$  for networks based on **a)** tri- and **b)** tetra-epoxidized IL monomers, and storage modulus,  $G'$  for networks based on **c)** tri- and **d)** tetra-epoxidized IL monomers. Data determined by DMA at 1 Hz.

The onset alpha transition temperatures ( $T_{\alpha 0}$ ) and deformation temperatures ( $T_d$ ) were found from the  $G'$  curves. The  $T_{\alpha 0}$ s values were determined using the beginning of  $G'$  curves drop while  $T_d$ s values were obtained from the temperature at which  $G'$  becomes constant. The determination of  $T_d$  was necessary for this research to set up the SM experiment (**Fig. III-10**).

The alpha transition temperatures ( $T_{\alpha}$ ) were determined from the  $\tan \delta$  plots. Corroborating the MD simulations, the higher  $T_{\alpha}$  were found for the tetra-epoxy based networks. The chemical nature of the hardeners played a key role in the maximum amplitude and area under the  $\tan \delta$  curves. The  $\tan \delta$  curve profiles indicate the total energy that the materials absorb. In recent work by our group, it was noticed that the introduction of IL-monomers into a classical epoxy-network significantly increased the amplitude of  $\tan \delta_{\max}$ .<sup>72</sup> Herein, the employment of D230 yielded greater amplitudes of  $\tan \delta_{\max}$ , which is associated with greater molecular mobility, meaning that the material can better absorb and dissipate energy. Remarkably, the six networks studied presented mechanical behavior comparable to DGEBA-based polymers (**see Fig. III-10**), and the DMA study provided crucial principles

for the molecular designing of polymer aiming to tailor mechanical properties (**Table III-3**).

**Table III-3.** Relevant thermomechanical parameters obtained from DMA.

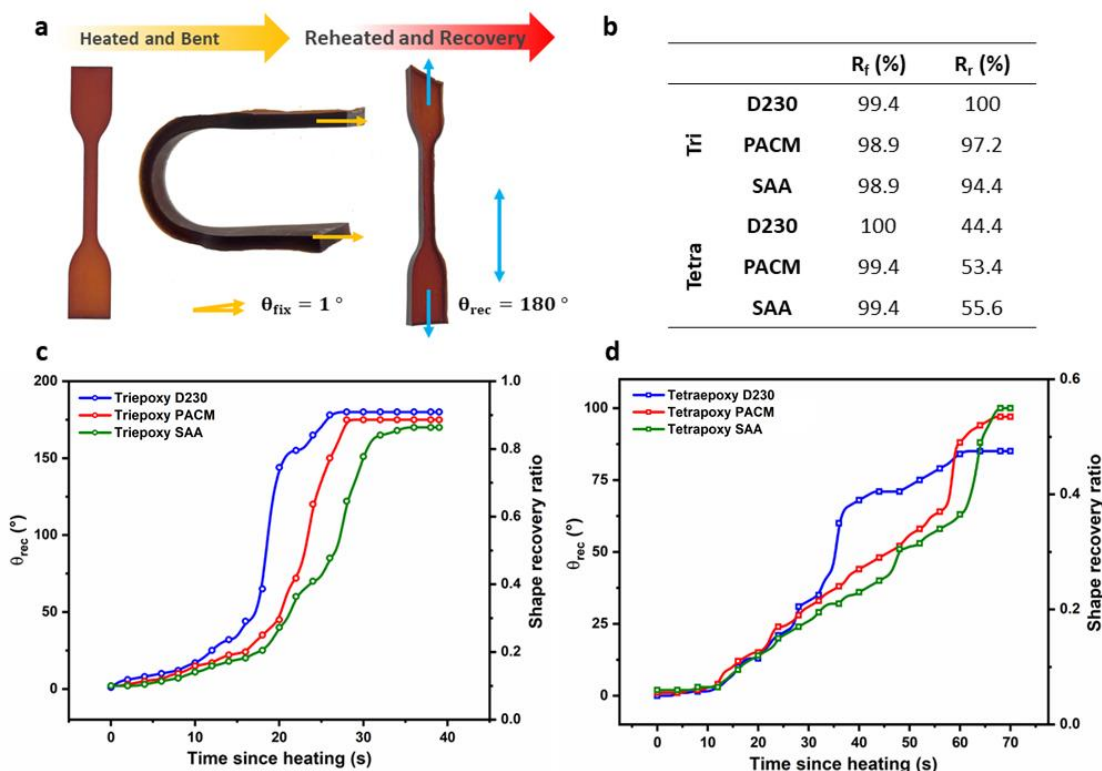
		$T_{\alpha 0}$ (°C)	$T_{\alpha}$ (°C)	$T_{df}$ (°C)	$G_g$ (GPa)	$G_r$ (MPa)	Ratio $G_g:G_r$
<b>Tri</b>	<b>D230</b>	28	73	76	1.2	1.6	750
	<b>PACM</b>	50	115	130	0.7	2.1	785
	<b>SAA</b>	53	98	112	1.1	2.6	269
<b>Tetra</b>	<b>D230</b>	38	75	80	20	4.5	242
	<b>PACM</b>	53	157	118	2	8	250
	<b>SAA</b>	59	100	179	1.7	7.5	142

In order to design shape-memory networks, several parameters can be tailored, including curing extent, monomer-hardener ratio, number of phases, and the nature of monomers and hardeners.<sup>30,41,73</sup> Although the curing degree allows the development of SM networks, the change of the materials' properties is often observed.<sup>74</sup> Similarly, adjusting the monomer-hardener ratio or developing co-networks may negatively impact their thermal and mechanical properties.<sup>74</sup> In the current work, the IL monomers were designed with three and four epoxy functionalities and an imidazolium moiety. By this approach, the cross-linking degree and the polymer chain mobility were tailored, affording SM behavior to the networks in water at 100 °C.

The SM performance of the resulting networks was evaluated by the shape fixity ( $R_f$ ) and shape recovery ratio ( $R_r$ ).<sup>74</sup>  $R_f$  defines the ability of materials to keep a temporary shape after removing the application of an external force.<sup>74</sup> Its value is expressed in equation 1, corresponding to 100% when the materials completely keep the shape induced by the external force.<sup>74</sup>  $R_r$  measures the recovery ratio when the polymer is re-heated to the deformation temperature and anomalously,  $R_r$  is 1 when the polymer fully recovers its initial shape (**Fig. III-11a and III-11b**).

Scrutinizing the experimental results, it is possible to observe that the SM performances in water at 100 °C expressed by  $R_f$  and  $R_r$  rely on the hardener and monomer structures. Regarding the hardener nature, the SM behavior seems to be associated with their molecular flexibility. The SM performances were shown to improve from the aliphatic to the aromatic amine. This behavior trend can be predicted by the coefficient of volumetric thermal expansion (CVTE) that evaluates the flexibility of the polymers in terms of the response to heating. Indeed, the evolution of the reduced volume as a function of temperature presented in **Fig. III-11** coherently describes the trend in SM performance.

The shape recovery was also investigated through a dynamical analysis evaluating the evolution of the recovered shape as a function of time (**Fig. III-11c and III-11d, and videos on Appendix I**). The networks based on tri-epoxidized IL monomer exhibited a sigmoidal profile with a greater recovery rate at about 20 s. Interestingly, the networks built from tetra-epoxidized IL exhibited a smoother linear recovery tendency.



**Figure III-11.** Characterization of shape-memory behavior in water at 100 °C. **a)** Fold-deploy experiment illustrating SM behavior of tri-epoxidized IL-D230 network. **b)** Fixity and recovery angles. Evolution of recovery angle as function of time for networks based on **c)** tri- and **d)** tetra-epoxy.

## 5.7. IL-based Green Methodology and Degradation Studies

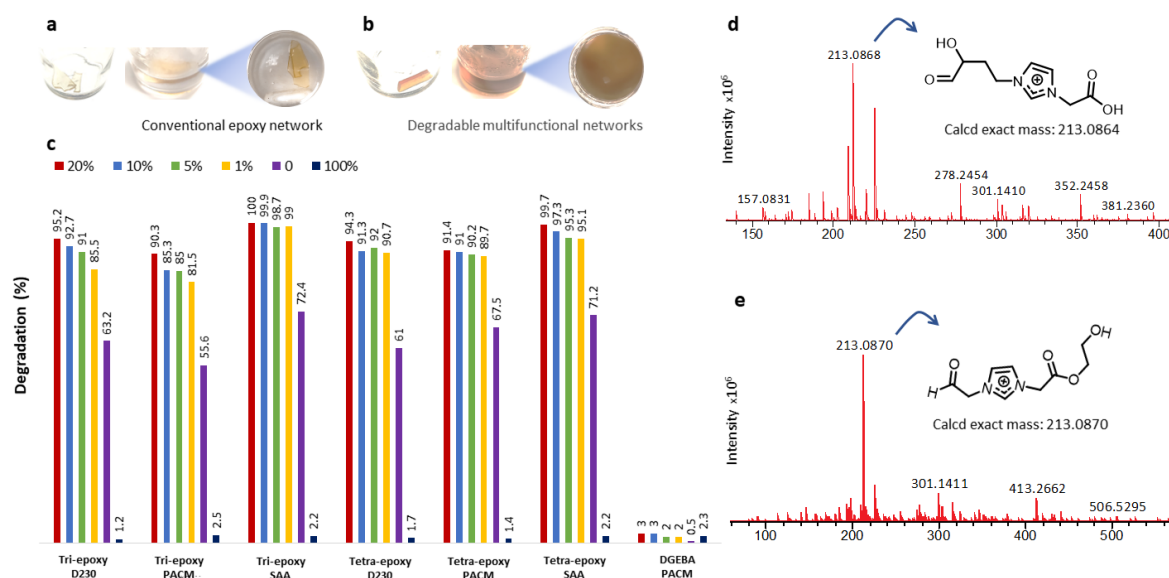
Recycling thermosetting materials is a substantial challenge due to the high chemical- and thermal-stabilities intrinsic to polymers containing crosslinking.<sup>15,64</sup> Compared to most existing epoxy prepolymers, tri- and tetra-epoxidized IL monomers were systematically designed with cleavable ester bonds to be depolymerized under mild conditions<sup>12,17</sup> addressing the principle *design to degrade*. Polymer degradation or depolymerization is often carried out under strong acid or basic conditions, inducing laborious and costly post-treatments of residues.<sup>29,40</sup> Recent works have investigated more mild strategies to recycle or chemically dissolve thermosetting materials.<sup>33,75</sup> Kuang *et al.* investigated several catalysts to degrade anhydride-epoxy thermosets in the presence of alcohols.<sup>33</sup> Further, Warner

*et al.* used ethylene glycol (EG) and imidazolium IL mixtures to chemically dissolve commercial epoxy resins and disassemble carbon fiber reinforced epoxy composites.<sup>75</sup>

This current research focuses on developing networks that can be degraded by a straightforward and economically viable method. Herein, an electrophilic phosphonium IL was employed to catalyze a solvent-assisted transesterification mediated by EG. First, the crosslinked networks had their dimensions and weight measured to evaluate the evolution of degradation. Then, the samples were placed into vial flasks in different proportions of IL:EG. The chemical dissolution phenomena manifested by **(1)** an initial solution color change, evolving to **(2)** the sample swelling and **(3)** the increase of viscosity of the solutions. Initially, the gain mass due to the swelling phenomenon was monitored to further understand the kinetics of solvent penetration into the crosslinked matrices. However, in practice, the swelling and dissolution phenomena occur almost concomitantly, hindering the accurate of monitoring the mass increase as a function of time.

Following from this, the chemical dissolution was investigated in six different conditions with, a conventional network corresponding to the DGEBA cured with PACM used as control. From this, the resulting networks based on tri- and tetra-epoxidized IL monomers elicited high chemical dissolution (90-100%), whereas the DGEBA-based specimens did not undergo notable degradation under the same conditions (0.5-3%) (**Fig. III-12a-b**). This behavior is dependent on the molecular structure of DGEBA and PACM, which do not contain cleavable groups. Moreover, DGEBA thermosets did not swell, meaning that EG and IL molecules cannot penetrate the covalently cross-linked matrices. This primarily swelling phenomenon is crucial due to it creating free space between the chains, increasing the surface contact area and further allowing the degradation reactions.

Moreover, the CVTE determination was found to be a valuable tool in inferring the polymer swelling behavior and consequently potential degradability of thermosets. The CVTE predictions at 200 °C allow for the estimation of the space creation in the networks which are able to host the solvent and catalyst molecules. Consequently, this contact at the molecular level with the cleavable ester groups favors the degradation reactions.



**Figure III-12.** Study of network degradability under mild conditions. **a)** DGEBA-PACM sample shows that conventional epoxy networks do not degrade under any of the employed conditions. **b)** degraded solutions for networks based on tri-epoxidized IL and D230 illustrating the full degradability of the designed networks. **c)** degradation conversion under five different conditions. Structure elucidation of the degradation products for networks tailored from **d)** tri- and **e)** tetra-epoxidized IL monomers with D230 as amine hardener. The additional MS spectra for the other four degraded networks are presented in the supporting information.

The degradation activity increased with the IL proportion, which corroborates its role as a transesterification catalyst by activating the ester carbonyls.<sup>76</sup> Conversely, the chemical dissolution in neat IL proved to be unfavorable (**Fig. III-12c**). The thermoset degradation results from the compromise between the solvent (and catalyst) diffusion into the networks and the rate of the transesterification reactions. The employment of the highly viscous phosphonium IL deters the first step, and the absence of nucleophilic groups, like hydroxyl, does not allow the trans-esterification reaction to proceed. Integrating these observations, the use of neat EG showed degradation activity over 50% but still less than other conditions for which the IL was used. The significant degradation activity in the presence of neat EG suggests that the imidazolium fragments may self-catalyze the network degradation, which could be referred to as a chain-shattering degradation. Moreover, the increased degradation activities for the SAA-based networks reveal that the structure-degradation properties also rely on the hardeners. The incorporation of the hydrolysable sulfonamide group into the networks yields additional degradation pathways allowing the full degradation of these networks.

Moreover, over 4.5 h, the degradation degree using 1 and 20 wt.% of IL104 in EG showed comparable values, which makes this procedure more economically viable and a suitable alternative to replace pyrolysis and mechanical degradation industrially.<sup>28,77</sup>

To further investigate the degradation mechanisms and elucidate the structures of the degradation products, <sup>1</sup>H NMR, and HRMS were performed. At the end of 4.5 h, the resulting reactional mixtures were dried under vacuum at 150 °C in order to remove the EG solvent. Then, several deuterated solvents were investigated for their ability to solubilize the degradation products; including ACN-d<sub>3</sub>, CDCl<sub>3</sub>, DMF-d<sub>7</sub>, DMSO-d<sub>6</sub>, and MeOD-d<sub>4</sub>. DMSO-d<sub>6</sub> and MeOD-d<sub>4</sub> proved to be the most effective.

Comparing the <sup>1</sup>H NMR spectra of degradation products with their corresponding precursors (*i.e.* tri- or tetra-epoxy monomers), allowed for hydrogen peaks assignment, in particular for those resulting from imidazolium derivatives (**Fig. I-S30**). This NMR characterization is a preliminary confirmation that the imidazolium-ILs are regenerated which is further supported by the HRMS analysis. More important than confirming the regeneration of the imidazolium-ILs is the structural identification of the degradation products. The degradation of networks tailored from tri- and tetra-epoxidized IL monomers with D230, yielded precursors with mass-to-charge ratios of 213.0868 and 213.0870, respectively. The determination of their exact mass coupled with the NMR analysis allowed to determine the chemical structures of the degradation products (**Fig. III-12d and III-12e**). Similarly, the structural identification was carried out for the degradation products derived from networks built with PACM, and SAA (**Fig. I-S33-S36**). When the tri-epoxidized IL monomer was employed as a molecular building-block, the same degradation product was generated for the networks designed with PACM and SAA. Interestingly, the same degradation product was observed for the three networks tailored from the tetra-epoxidized IL monomer (**Fig. I-S32, I-S34 and I-S36**). The investigation of the chemical structures of the degradation products further confirms the selective mechanism by cleaving at the ester bonds regenerating two IL-derivatives. These results confirm that incorporation of ester groups to be a promising molecular design approach that yields faster degradation under mild conditions and maintains excellent chemical and physical properties. The degradation products can then be isolated by precipitation and potentially used for developing vitrimers, to tune mechanical properties of polymers or different applications, including gas capture,<sup>78</sup> lubricants,<sup>79</sup> dispersing,<sup>80</sup> and compatibilizing agents.<sup>81</sup> We are currently investigating the vitrimerization and re-insertion of these IL derivatives into thermosets and analyzing their mechanical performances to continue developing sustainable polymer technologies to extend

the lifecycle of these polymer materials as a means of addressing the compelling needs of the circular economy.

## 6. Conclusion of Chapter III

Herein, we rationally designed a series of next-generation epoxy monomers through two computationally-assisted methodologies followed by synthesis. The epoxidized ILs were synthesized bearing three and four epoxy groups, and three amines were employed as hardeners, leading to six multifunctional poly(IL) networks. Systematically installing cleavable ester bonds and an imidazolium backbone core, the physicochemical and degradable properties of the networks were tailored. The resulting networks demonstrated increased thermal stability ( $> 300\text{ }^{\circ}\text{C}$ ), high homogeneity, shape-memory behavior, and mechanical properties comparable to DGEBA resins, making them promising candidates to replace Bisphenol A-derived polymers. More importantly, the novel materials demonstrated high degradation activity under mild conditions. The network degradation was shown to be over 50% in neat ethylene glycol suggesting a self-catalysis mechanism in which the imidazolium fragments participate in chain shattering. Practically complete degradation of networks is achieved when an electrophilic phosphonium IL is employed as a catalyst. It is noted that few additional studies could further enrich this current research, such as fully understanding the mechanism of the final degradation products and re-employing the regenerated IL-derivatives to create second-generation materials; both investigations will be topics for future studies. Indeed, our findings lay the foundation for rationally designing multifunctional degradable epoxy networks based on ILs, enabling the future advancement of high-performance materials to meet the expectations of a circular economy.

## Supporting Information

The general methodology for characterization and purification, the detailed procedure for the synthesis of the tri- and tetra- epoxidized ionic liquid and its intermediates, the NMR spectra, the molecular dynamics simulations outputs, and the mass spectra of the degradation products.

## 7. References

- (1) Hoornweg, D.; Bhada-Tata, P.; Kennedy, C. Environment: Waste Production Must Peak This Century. *Nature* **2013**, *502* (7473), 615–617. <https://doi.org/10.1038/502615a>.
- (2) Sobkowicz, M. J. Polymer Design for the Circular Economy. *Science* (80-. ). **2021**, *374* (6567), 540–540. <https://doi.org/10.1126/science.abm2306>.

- (3) Sardon, H.; Li, Z.-C. Introduction to Plastics in a Circular Economy. *Polym. Chem.* **2020**, *11* (30), 4828–4829. <https://doi.org/10.1039/D0PY90117B>.
- (4) Stavropoulos, P.; Spetsieris, A.; Papacharalampopoulos, A. A Circular Economy Based Decision Support System for the Assembly/Disassembly of Multi-Material Components. *Procedia CIRP* **2019**, *85*, 49–54. <https://doi.org/10.1016/j.procir.2019.09.033>.
- (5) Dumée, L. Circular Economy and Sustainability. In *Circular Economy and Sustainability*; Elsevier, 2022; pp 359–372. <https://doi.org/10.1016/C2019-0-04146-5>.
- (6) Babbitt, C. W.; Althaf, S.; Cruz Rios, F.; Bilec, M. M.; Graedel, T. E. The Role of Design in Circular Economy Solutions for Critical Materials. *One Earth* **2021**, *4* (3), 353–362. <https://doi.org/10.1016/j.oneear.2021.02.014>.
- (7) Bachmann, J.; Yi, X.; Tserpes, K.; Sguazzo, C.; Barbu, L. G.; Tse, B.; Soutis, C.; Ramón, E.; Linuesa, H.; Bechtel, S. Towards a Circular Economy in the Aviation Sector Using Eco-Composites for Interior and Secondary Structures. Results and Recommendations from the EU/China Project ECO-COMPASS. *Aerospace* **2021**, *8* (5), 131. <https://doi.org/10.3390/aerospace8050131>.
- (8) Zheng, N.; Xu, Y.; Zhao, Q.; Xie, T. Dynamic Covalent Polymer Networks: A Molecular Platform for Designing Functions beyond Chemical Recycling and Self-Healing. *Chem. Rev.* **2021**, *121* (3), 1716–1745. <https://doi.org/10.1021/acs.chemrev.0c00938>.
- (9) Xu, C.; Puente-Santiago, A. R.; Rodríguez-Padrón, D.; Muñoz-Batista, M. J.; Ahsan, M. A.; Noveron, J. C.; Luque, R. Nature-Inspired Hierarchical Materials for Sensing and Energy Storage Applications. *Chem. Soc. Rev.* **2021**, *50* (8), 4856–4871. <https://doi.org/10.1039/C8CS00652K>.
- (10) Gong, M.; Wan, P. Bioinspired Stiff yet Tough Healable Nanocomposites: From Molecular Design to Structural Processing. *Matter* **2021**, *4* (7), 2108–2111. <https://doi.org/10.1016/j.matt.2021.06.013>.
- (11) Anastas, P. T.; Warner, J. C. Green Chemistry: Theory and Practice. In *Green Chemistry: Theory and Practice*; Oxford University Press, 2000, 1998; pp 30–35.
- (12) Hatti-Kaul, R.; Nilsson, L. J.; Zhang, B.; Rehnberg, N.; Lundmark, S. Designing Biobased Recyclable Polymers for Plastics. *Trends Biotechnol.* **2020**, *38* (1), 50–67. <https://doi.org/10.1016/j.tibtech.2019.04.011>.



- (13) Hu, H.; Tian, Y.; Wang, J.; Zhang, R.; Zhu, J. Enhanced Degradation and Gas Barrier of PBAT through Composition Design of Aliphatic Units. *Polym. Degrad. Stab.* **2022**, *195*, 109795. <https://doi.org/10.1016/j.polymdegradstab.2021.109795>.
- (14) Kim, S.; Lee, Y.; Kim, C.; Choi, S. Analysis of Mechanical Property Degradation of Outdoor Weather-Exposed Polymers. *Polymers (Basel)*. **2022**, *14* (2), 357. <https://doi.org/10.3390/polym14020357>.
- (15) Ma, S.; Webster, D. C. Degradable Thermosets Based on Labile Bonds or Linkages: A Review. *Prog. Polym. Sci.* **2018**, *76*, 65–110. <https://doi.org/10.1016/j.progpolymsci.2017.07.008>.
- (16) Hamad, K.; Kaseem, M.; Deri, F. Recycling of Waste from Polymer Materials: An Overview of the Recent Works. *Polym. Degrad. Stab.* **2013**, *98* (12), 2801–2812. <https://doi.org/10.1016/j.polymdegradstab.2013.09.025>.
- (17) Pickering, S. J. Recycling Technologies for Thermoset Composite Materials-Current Status. *Compos. Part A Appl. Sci. Manuf.* **2006**, *37* (8), 1206–1215. <https://doi.org/10.1016/j.compositesa.2005.05.030>.
- (18) Silva, A. A.; Livi, S.; Netto, D. B.; Soares, B. G.; Duchet, J.; Gérard, J. F. New Epoxy Systems Based on Ionic Liquid. *Polymer (Guildf)*. **2013**, *54* (8), 2123–2129. <https://doi.org/10.1016/j.polymer.2013.02.021>.
- (19) Matsumoto, K.; Endo, T. Design and Synthesis of Ionic-Conductive Epoxy-Based Networked Polymers. *React. Funct. Polym.* **2013**, *73* (2), 278–282. <https://doi.org/10.1016/j.reactfunctpolym.2012.04.018>.
- (20) Tian, F.; Wang, X. L.; Yang, Y.; An, W.; Zhao, X.; Xu, S.; Wang, Y. Z. Energy-Efficient Conversion of Amine-Cured Epoxy Resins into Functional Chemicals Based on Swelling-Induced Nanopores. *ACS Sustain. Chem. Eng.* **2020**, *8* (5), 2226–2235. <https://doi.org/10.1021/acssuschemeng.9b06013>.
- (21) Garcia, F. G.; Soares, B. G.; Pita, V. J. R. R.; Sánchez, R.; Rieumont, J.; Rangel, A. Mechanical Properties of Epoxy Networks Based on DGEBA and Aliphatic Amines. *J Appl Polym Sci* **2007**, *106*, 2047–2055. <https://doi.org/10.1002/app.24895>.
- (22) Kwon, S. J.; Kim, T.; Jung, B. M.; Lee, S. B.; Choi, U. H. Multifunctional Epoxy-Based Solid Polymer Electrolytes for Solid-State Supercapacitors. *ACS Appl. Mater. Interfaces* **2018**, *10* (41), 35108–35117. <https://doi.org/10.1021/acsami.8b11016>.

- (23) Ligon, S. C.; Liska, R.; Stampfl, J.; Gurr, M.; Mülhaupt, R. Polymers for 3D Printing and Customized Additive Manufacturing. *Chem. Rev.* **2017**, *117* (15), 10212–10290. <https://doi.org/10.1021/acs.chemrev.7b00074>.
- (24) Mohd Yusoff, N. H.; Irene Teo, L.-R.; Phang, S. J.; Wong, V.-L.; Cheah, K. H.; Lim, S.-S. Recent Advances in Polymer-Based 3D Printing for Wastewater Treatment Application: An Overview. *Chem. Eng. J.* **2022**, *429*, 132–311. <https://doi.org/10.1016/j.cej.2021.132311>.
- (25) Achilias, D. S.; Karabela, M. M.; Varkopoulou, E. A.; Sideridou, I. D. Cure Kinetics Study of Two Epoxy Systems with Fourier Transform Infrared Spectroscopy (FTIR) and Differential Scanning Calorimetry (DSC). *J. Macromol. Sci. Part A* **2012**, *49* (8), 630–638. <https://doi.org/10.1080/10601325.2012.696995>.
- (26) Zabihi, O. Modeling of Phenomenological Mechanisms during Thermal Formation and Degradation of an Epoxy-Based Nanocomposite. *Thermochim. Acta* **2012**, *543*, 239–245. <https://doi.org/10.1016/j.tca.2012.05.032>.
- (27) Zago, E.; Dubreucq, E.; Lecomte, J.; Villeneuve, P.; Fine, F.; Fulcrand, H.; Aouf, C. Synthesis of Bio-Based Epoxy Monomers from Natural Allyl- and Vinyl Phenols and the Estimation of Their Affinity to the Estrogen Receptor  $\alpha$  by Molecular Docking. *New J. Chem.* **2016**, *40* (9), 7701–7710. <https://doi.org/10.1039/C6NJ00782A>.
- (28) Hamad, K.; Kaseem, M.; Deri, F. Recycling of Waste from Polymer Materials: An Overview of the Recent Works. *Polym. Degrad. Stab.* **2013**, *98* (12), 2801–2812. <https://doi.org/10.1016/j.polymdegradstab.2013.09.025>.
- (29) Dang, W.; Kubouchi, M.; Yamamoto, S.; Sembokuya, H.; Tsuda, K. An Approach to Chemical Recycling of Epoxy Resin Cured with Amine Using Nitric Acid. *Polymer (Guildf)*. **2002**, *43* (10), 2953–2958. [https://doi.org/10.1016/S0032-3861\(02\)00100-3](https://doi.org/10.1016/S0032-3861(02)00100-3).
- (30) Di Mauro, C.; Malburet, S.; Graillot, A.; Mija, A. Recyclable, Repairable, and Reshapable (3R) Thermoset Materials with Shape Memory Properties from Bio-Based Epoxidized Vegetable Oils. *ACS Appl. Bio Mater.* **2020**, *3* (11), 8094–8104. <https://doi.org/10.1021/acsabm.0c01199>.
- (31) Utekar, S.; V K, S.; More, N.; Rao, A. Comprehensive Study of Recycling of Thermosetting Polymer Composites – Driving Force, Challenges and Methods. *Compos. Part B Eng.* **2021**, *207* (5), 108596. <https://doi.org/10.1016/j.compositesb.2020.108596>.

- (32) Babu, B. R.; Parande, A. K.; Basha, C. A. Electrical and Electronic Waste: A Global Environmental Problem. *Waste Manag. Res.* **2007**, *25* (4), 307–318. <https://doi.org/10.1177/0734242X07076941>.
- (33) Kuang, X.; Shi, Q.; Zhou, Y.; Zhao, Z.; Wang, T.; Qi, H. J. Dissolution of Epoxy Thermosets: Via Mild Alcoholysis: The Mechanism and Kinetics Study. *RSC Adv.* **2018**, *8* (3), 1493–1502. <https://doi.org/10.1039/c7ra12787a>.
- (34) McEwen, W. E.; DeMassa, J. W. Acid Generation in the Thermal Decomposition of Diaryliodonium Salts. *Heteroat. Chem.* **1996**, *7* (5), 349–354. [https://doi.org/10.1002/\(SICI\)1098-1071\(199610\)7:5<349::AID-HC10>3.0.CO;2-Q](https://doi.org/10.1002/(SICI)1098-1071(199610)7:5<349::AID-HC10>3.0.CO;2-Q).
- (35) Kuang, X.; Zhou, Y.; Shi, Q.; Wang, T.; Qi, H. J. Recycling of Epoxy Thermoset and Composites via Good Solvent Assisted and Small Molecules Participated Exchange Reactions. *ACS Sustain. Chem. Eng.* **2018**, *6* (7), 9189–9197. <https://doi.org/10.1021/acssuschemeng.8b01538>.
- (36) Okajima, I.; Hiramatsu, M.; Shimamura, Y.; Awaya, T.; Sako, T. Chemical Recycling of Carbon Fiber Reinforced Plastic Using Supercritical Methanol. *J. Supercrit. Fluids* **2014**, *91*, 68–76. <https://doi.org/10.1016/j.supflu.2014.04.011>.
- (37) Shi, X.; Luo, C.; Lu, H.; Yu, K. Primary Recycling of Anhydride-Cured Engineering Epoxy Using Alcohol Solvent. *Polym. Eng. Sci.* **2019**, *59* (s2), E111–E119. <https://doi.org/10.1002/pen.24997>.
- (38) Yue, L.; Amirkhosravi, M.; Gong, X.; Gray, T. G.; Manas-Zloczower, I. Recycling Epoxy by Vitrimization: Influence of an Initial Thermoset Chemical Structure. *ACS Sustain. Chem. Eng.* **2020**, *8* (33), 12706–12712. <https://doi.org/10.1021/acssuschemeng.0c04815>.
- (39) Yue, L.; Guo, H.; Kennedy, A.; Patel, A.; Gong, X.; Ju, T.; Gray, T.; Manas-Zloczower, I. Vitrimization: Converting Thermoset Polymers into Vitrimers. *ACS Macro Lett.* **2020**, *9* (6), 836–842. <https://doi.org/10.1021/acsmacrolett.0c00299>.
- (40) Yang, R.; Xu, G.; Dong, B.; Hou, H.; Wang, Q. A “Polymer to Polymer” Chemical Recycling of PLA Plastics by the “DE–RE Polymerization” Strategy. *Macromolecules* **2022**, *55* (5), 1726–1735. <https://doi.org/10.1021/acs.macromol.1c02085>.
- (41) Radchenko, A. V.; Chabane, H.; Demir, B.; Searles, D. J.; Duchet-Rumeau, J.; Gérard, J. F.; Baudoux, J.; Livi, S. New Epoxy Thermosets Derived from a Bisimidazolium Ionic Liquid Monomer: An Experimental and Modeling Investigation. *ACS Sustain. Chem. Eng.* **2020**, *8* (32), 12208–12221. <https://doi.org/10.1021/acssuschemeng.0c03832>.

- (42) Radchenko, A. V.; Duchet-Rumeau, J.; Gérard, J. F.; Baudoux, J.; Livi, S. Cycloaliphatic Epoxidized Ionic Liquids as New Versatile Monomers for the Development of Shape Memory PIL Networks by 3D Printing. *Polym. Chem.* **2020**, *11* (34), 5475–5483. <https://doi.org/10.1039/d0py00704h>.
- (43) McDanel, W. M.; Cowan, M. G.; Carlisle, T. K.; Swanson, A. K.; Noble, R. D.; Gin, D. L. Cross-Linked Ionic Resins and Gels from Epoxide-Functionalized Imidazolium Ionic Liquid Monomers. *Polymer (Guildf)*. **2014**, *55* (16), 3305–3313. <https://doi.org/10.1016/j.polymer.2014.04.039>.
- (44) Matsumoto, K.; Endo, T. Synthesis of Ion Conductive Networked Polymers Based on an Ionic Liquid Epoxide Having a Quaternary Ammonium Salt Structure. *Macromolecules* **2009**, *42* (13), 4580–4584. <https://doi.org/10.1021/ma900508q>.
- (45) Burness, D. M.; Bayer, H. O. Synthesis and Reactions of Quaternary Salts of Glycidyl Amines. *J. Org. Chem.* **1963**, *28* (9), 2283–2288. <https://doi.org/10.1021/jo01044a031>.
- (46) Ly Nguyen, T. K.; Obadia, M. M.; Serghei, A.; Livi, S.; Duchet-Rumeau, J.; Drockenmuller, E. 1,2,3-Triazolium-Based Epoxy-Amine Networks: Ion-Conducting Polymer Electrolytes. *Macromol. Rapid Commun.* **2016**, *37* (14), 1168–1174. <https://doi.org/10.1002/marc.201600018>.
- (47) Chardin, C.; Rouden, J.; Livi, S.; Baudoux, J. Dimethyldioxirane (DMDO) as a Valuable Oxidant for the Synthesis of Polyfunctional Aromatic Imidazolium Monomers Bearing Epoxides. *Green Chem.* **2017**, *19* (21), 5054–5059. <https://doi.org/10.1039/c7gc02372c>.
- (48) Livi, S.; Lins, L. C.; Capeletti, L. B.; Chardin, C.; Halawani, N.; Baudoux, J.; Cardoso, M. B. Antibacterial Surface Based on New Epoxy-Amine Networks from Ionic Liquid Monomers. *Eur. Polym. J.* **2019**, *116*, 56–64. <https://doi.org/10.1016/j.eurpolymj.2019.04.008>.
- (49) Ehlers, J.-E.; Rondan, N. G.; Huynh, L. K.; Pham, H.; Marks, M.; Truong, T. N. Theoretical Study on Mechanisms of the Epoxy-Amine Curing Reaction. *Macromolecules* **2007**, *40* (12), 4370–4377. <https://doi.org/10.1021/ma070423m>.
- (50) Mezzenga, R.; Boogh, L.; Månson, J.-A. E.; Pettersson, B. Effects of the Branching Architecture on the Reactivity of Epoxy-Amine Groups. *Macromolecules* **2000**, *33* (12), 4373–4379. <https://doi.org/10.1021/ma991906w>.

- (51) Riccardi, C. C.; Adabbo, H. E.; Williams, R. J. J. Curing Reaction of Epoxy Resins with Diamines. *J. Appl. Polym. Sci.* **1984**, *29* (8), 2481–2492. <https://doi.org/10.1002/app.1984.070290805>.
- (52) D.K. Owens, R. C. W. Estimation of the Surface Free Energy of Polymers. *J. Appl. Polym. Sci.* **1969**, *13*, 1741–1747.
- (53) Thompson, A. P.; Aktulga, H. M.; Berger, R.; Bolintineanu, D. S.; Brown, W. M.; Crozier, P. S.; in 't Veld, P. J.; Kohlmeyer, A.; Moore, S. G.; Nguyen, T. D.; Shan, R.; Stevens, M. J.; Tranchida, J.; Trott, C.; Plimpton, S. J. LAMMPS - a Flexible Simulation Tool for Particle-Based Materials Modeling at the Atomic, Meso, and Continuum Scales. *Comput. Phys. Commun.* **2022**, *271*, 108171. <https://doi.org/10.1016/j.cpc.2021.108171>.
- (54) Canongia Lopes, J. N.; Pádua, A. A. H. CL&P: A Generic and Systematic Force Field for Ionic Liquids Modeling. *Theor. Chem. Acc.* **2012**, *131* (3), 1129. <https://doi.org/10.1007/s00214-012-1129-7>.
- (55) Jorgensen, W. L.; Maxwell, D. S.; Tirado-Rives, J. Development and Testing of the OPLS All-Atom Force Field on Conformational Energetics and Properties of Organic Liquids. *J. Am. Chem. Soc.* **1996**, *118* (45), 11225–11236. <https://doi.org/10.1021/ja9621760>.
- (56) Becke, A. D. Density-Functional Thermochemistry. V. Systematic Optimization of Exchange-Correlation Functionals. *J. Chem. Phys.* **1997**, *107* (20), 8554–8560. <https://doi.org/10.1063/1.475007>.
- (57) Grimme, S.; Ehrlich, S.; Goerigk, L. Effect of the Damping Function in Dispersion Corrected Density Functional Theory. *J. Comput. Chem.* **2011**, *32* (7), 1456–1465. <https://doi.org/10.1002/jcc.21759>.
- (58) Dunning, T. H. Gaussian Basis Sets for Use in Correlated Molecular Calculations. I. The Atoms Boron through Neon and Hydrogen. *J. Chem. Phys.* **1989**, *90* (2), 1007–1023. <https://doi.org/10.1063/1.456153>.
- (59) Brehm, M.; Thomas, M.; Gehrke, S.; Kirchner, B. TRAVIS—A Free Analyzer for Trajectories from Molecular Simulation. *J. Chem. Phys.* **2020**, *152* (16), 164105. <https://doi.org/10.1063/5.0005078>.
- (60) Mayo, S. L.; Olafson, B. D.; Goddard, W. A. DREIDING: A Generic Force Field for Molecular Simulations. *J. Phys. Chem.* **1990**, *94* (26), 8897–8909. <https://doi.org/10.1021/j100389a010>.

- (61) Hanwell, M. D.; Curtis, D. E.; Lonie, D. C.; Vandermeersch, T.; Zurek, E.; Hutchison, G. R. Avogadro: An Advanced Semantic Chemical Editor, Visualization, and Analysis Platform. *J. Cheminform.* **2012**, *4* (8), 1–17. <https://doi.org/10.1186/1758-2946-4-17>.
- (62) Martinez, L.; Andrade, R.; Birgin, E. G.; Martínez, J. M. PACKMOL: A Package for Building Initial Configurations for Molecular Dynamics Simulations. *J. Comput. Chem.* **2009**, *30* (13), 2157–2164. <https://doi.org/10.1002/JCC.21224>.
- (63) Demir, B.; Perli, G.; Chan, K.-Y.; Duchet-Rumeau, J.; Livi, S. Molecular-Level Investigation of Cycloaliphatic Epoxidised Ionic Liquids as a New Generation of Monomers for Versatile Poly(Ionic Liquids). *Polymers (Basel)*. **2021**, *13* (9), 1–15. <https://doi.org/10.3390/polym13091512>.
- (64) Kazemi, M.; Faisal Kabir, S.; Fini, E. H. State of the Art in Recycling Waste Thermoplastics and Thermosets and Their Applications in Construction. *Resour. Conserv. Recycl.* **2021**, *174*, 105776. <https://doi.org/10.1016/j.resconrec.2021.105776>.
- (65) Xue, X.; Liu, S.-Y.; Zhang, Z.-Y.; Wang, Q.-Z.; Xiao, C.-Z. A Technology Review of Recycling Methods for Fiber-Reinforced Thermosets. *J. Reinf. Plast. Compos.* **2021**, *19*, 552–610. <https://doi.org/10.1177/07316844211055208>.
- (66) Demir, B.; Walsh, T. R. A Robust and Reproducible Procedure for Cross-Linking Thermoset Polymers Using Molecular Simulation. *Soft Matter* **2016**, *12* (8), 2453–2464. <https://doi.org/10.1039/c5sm02788h>.
- (67) Maka, H.; Spychaj, T.; Pilawka, R. Epoxy Resin/Ionic Liquid Systems: The Influence of Imidazolium Cation Size and Anion Type on Reactivity and Thermomechanical Properties. *Ind. Eng. Chem. Res.* **2012**, *51* (14), 5197–5206. <https://doi.org/10.1021/ie202321j>.
- (68) Livi, S.; Chardin, C.; Lins, L. C.; Halawani, N.; Pruvost, S.; Duchet-Rumeau, J.; Gérard, J. F.; Baudoux, J. From Ionic Liquid Epoxy Monomer to Tunable Epoxy-Amine Network: Reaction Mechanism and Final Properties. *ACS Sustain. Chem. Eng.* **2019**, *7* (3), 3602–3613. <https://doi.org/10.1021/acssuschemeng.8b06271>.
- (69) Nguyen, T. K. L.; Livi, S.; Soares, B. G.; Pruvost, S.; Duchet-Rumeau, J.; Gérard, J.-F. Ionic Liquids: A New Route for the Design of Epoxy Networks. *ACS Sustain. Chem. Eng.* **2016**, *4* (2), 481–490. <https://doi.org/10.1021/acssuschemeng.5b00953>.

- (70) Soares, B. G.; Silva, A. A.; Livi, S.; Duchet-Rumeau, J.; Gerard, J. F. New Epoxy/Jeffamine Networks Modified with Ionic Liquids. *J. Appl. Polym. Sci.* **2014**, *131* (3), 1–6. <https://doi.org/10.1002/app.39834>.
- (71) Demir, B.; Chan, K. Y.; J. Searles, D.; Searles, D. J. Structural Electrolytes Based on Epoxy Resins and Ionic Liquids: A Molecular-Level Investigation. *Macromolecules* **2020**, *53* (18), 7635–7649. <https://doi.org/10.1021/acs.macromol.0c00824>.
- (72) Perli, G.; Pessoa, A. C. S. N.; Balbino, T. A.; de la Torre, L. G. Ionic Strength for Tailoring the Synthesis of Monomodal Stealth Cationic Liposomes in Microfluidic Devices. *Colloids and Surfaces B: Biointerfaces*. 2019, pp 233–241. <https://doi.org/10.1016/j.colsurfb.2019.03.056>.
- (73) Wu, X.; Yang, X.; Zhang, Y.; Huang, W. A New Shape Memory Epoxy Resin with Excellent Comprehensive Properties. *J. Mater. Sci.* **2016**, *51* (6), 3231–3240. <https://doi.org/10.1007/s10853-015-9634-4>.
- (74) Sun, L.; Wang, T. X.; Chen, H. M.; Salvekar, A. V.; Naveen, B. S.; Xu, Q.; Weng, Y.; Guo, X.; Chen, Y.; Huang, W. M. A Brief Review of the Shape Memory Phenomena in Polymers and Their Typical Sensor Applications. *Polymers*. 2019. <https://doi.org/10.3390/polym11061049>.
- (75) Pérez, R. L.; Ayala, C. E.; Opiri, M. M.; Ezzir, A.; Li, G.; Warner, I. M. Recycling Thermoset Epoxy Resin Using Alkyl-Methyl-Imidazolium Ionic Liquids as Green Solvents. *ACS Appl. Polym. Mater.* **2021**, *3* (11), 5588–5595. <https://doi.org/10.1021/acsapm.1c00896>.
- (76) Macarie, L.; Simulescu, V.; Ilia, G. Phosphonium-Based Ionic Liquids Used as Reagents or Catalysts. *ChemistrySelect* **2019**, *4* (32), 9285–9299. <https://doi.org/10.1002/slct.201901712>.
- (77) Meyer, L. O.; Schulte, K.; Grove-Nielsen, E. CFRP-Recycling Following a Pyrolysis Route: Process Optimization and Potentials. *J. Compos. Mater.* **2009**, *43* (9), 1121–1132. <https://doi.org/10.1177/0021998308097737>.
- (78) Ramdin, M.; De Loos, T. W.; Vlugt, T. J. H. State-of-the-Art of CO<sub>2</sub> Capture with Ionic Liquids. *Ind. Eng. Chem. Res.* **2012**, *51* (24), 8149–8177. <https://doi.org/10.1021/ie3003705>.
- (79) Somers, A. E.; Howlett, P. C.; MacFarlane, D. R.; Forsyth, M. A Review of Ionic Liquid Lubricants. *Lubricants* **2013**, *1* (1), 3–21. <https://doi.org/10.3390/lubricants1010003>.

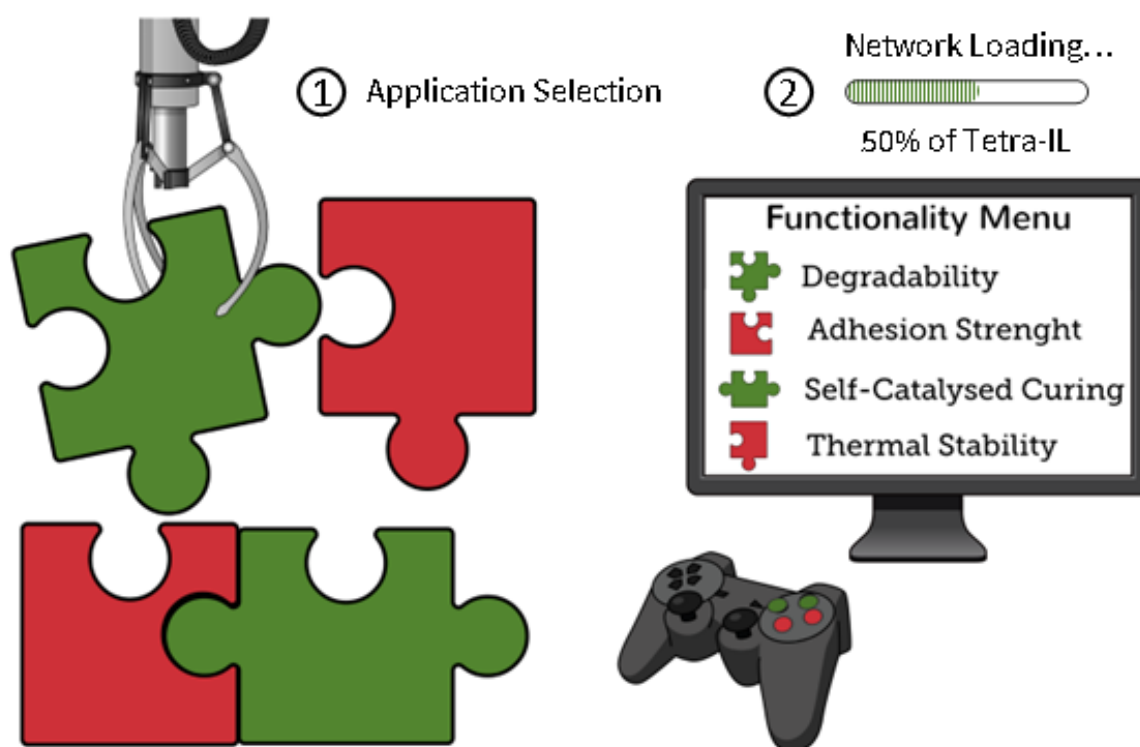
(80) Caldas, C. M.; Soares, B. G.; Indrusiak, T.; Barra, G. M. O. Ionic Liquids as Dispersing Agents of Graphene Nanoplatelets in Poly(Methyl Methacrylate) Composites with Microwave Absorbing Properties. *J. Appl. Polym. Sci.* **2021**, *138* (6), 1–18. <https://doi.org/10.1002/app.49814>.

(81) Livi, S.; Duchet-Rumeau, J.; Pham, T. N.; Gérard, J. F. A Comparative Study on Different Ionic Liquids Used as Surfactants: Effect on Thermal and Mechanical Properties of High-Density Polyethylene Nanocomposites. *J. Colloid Interface Sci.* **2010**, *349* (1), 424–433. <https://doi.org/10.1016/j.jcis.2009.09.036>.



# 04

## Design for Disassembly of Composites and Thermoset by Using Cleavable Ionic Liquid Monomers as Molecular Building Blocks



# **1. Conception pour le démontage des composites et des thermodurcissables en utilisant des monomères liquides ioniques clivables comme éléments constitutifs moléculaires**

## **1.1. Résumé**

Avec la forte demande des industries aéronautique et automobile et l'augmentation du nombre de pales de turbines d'éoliennes, l'obtention de polymères et de composites plus durables est une nécessité. En effet, pour s'inscrire dans une économie circulaire, les polymères qui renforcent les fibres, et les fibres elles-mêmes doivent pouvoir être recyclables et réutilisables. Dans cette étude, nous avons conçu et synthétisé un monomère liquide ionique d'imidazolium tétraépoxydé (Tetra-IL) contenant des groupes ester clivables. Ce monomère a été incorporé dans des réseaux époxy-amine conventionnels pour ajuster les propriétés physiques et améliorer la fin de vie des réseaux. L'introduction de seulement 10 % de comonomères à base d'IL a réduit de 85 % le temps de gélification. Ce résultat est prometteur et ouvre des perspectives d'utilisation de ce type de monomère dans le domaine des revêtements à cuisson rapide. Tous les réseaux conçus dans ce travail présentaient une haute stabilité thermique ( $>350$  °C), des  $T_g$  élevées comprises entre 180 et 230 °C combinées à un comportement hydrophobe. L'augmentation de la quantité de monomère IL dans les réseaux a amélioré l'homogénéité des thermodurcissables et la mouillabilité des résines époxy avec les fibres de carbone (CF). Plus important encore, l'utilisation du Tetra-IL a permis le développement de réseaux dégradables dans des conditions douces en un laps de temps court (4,5 heures), tout en permettant la récupération des CF. Les tests préliminaires d'adhérence ont montré que le Tetra-IL induisait une augmentation de la ductilité des réseaux. Le comportement dégradable a permis de récupérer les adhérents dans leurs états d'origine à la fin de la durée de vie des composites. En résumé, cette étude a mis en évidence le fort potentiel des comonomères à base d'IL comme brique moléculaire dans des thermodurcissables époxy conventionnels. Cette stratégie est prometteuse pour ajuster les propriétés physiques et améliorer la durabilité et la dégradabilité des polymères thermodurcissables et des composites haute performance.

**Mots-clés :** Thermodurcissables, Dégradables, Ingénierie Moléculaire, Composites Durables, Monomères Liquides Ioniques.

## **2. Design for Disassembly of Composites and Thermoset by Using Cleavable Ionic Liquid Monomers as Molecular Building Blocks**

### **2.1. Abstract**

Aircraft, automotive industries and the increasing numbers of wind turbine blade lead to a huge amount of carbon fiber reinforced polymers requiring to be recycled and/or reused in a closed loop supply chain or circularity of materials. Herein, we have designed and synthesized a tetra-epoxidized imidazolium ionic liquid (Tetra-IL) monomer containing ester-cleavable groups. This monomer was incorporated as a molecular brick platform into conventional epoxy-amine networks in order to tailor the physical properties as well as the end-of-life of the resulting networks. Thus, the introduction of only 10% of IL-based comonomers significantly reduced the gel time by 85% opening perspectives in the field of fast-cure epoxy resins. Overall, all the networks designed in this work presented high thermal stability ( $> 350\text{ }^{\circ}\text{C}$ ), higher  $T_g$  included between  $180$  to  $230\text{ }^{\circ}\text{C}$  combined with hydrophobic behavior. Increasing the amount of IL monomer in the networks improved the homogeneity of thermosets and wettability of the epoxy resins with the carbon fibers (CF). Most importantly, the use of Tetra-IL led to the development of degradable networks under mild conditions within a brief timeframe (4.5 hours) and allowing to recover the carbon fibers. The preliminary adhesion tests showed that Tetra-IL induced an increase of the ductility of the networks characterized by an improvement of the strain at break. Moreover, this degradable behavior enabled the adherend's recovery to the original state at the end of the composites' lifespans. In summary, this study highlighted the great potential of IL-based comonomers as molecular brick into conventional epoxy thermosets as a promising strategy to tailor the physical properties versus sustainability/degradability for the development of high-performance thermosets and composites.

**Keywords:** Degradable Thermosets, Molecular Engineering, Sustainable Composites, Ionic Liquid Monomers.

### 3. Introduction

Carbon fiber reinforced polymers (CFRPs) are a class of composites where the solid phase, carbon fibers (CFs), are dispersed in a polymer matrix, which acts as the continuous phase.<sup>1-3</sup> Relying on the polymer resin, the CF properties, and how they are combined in the composite architecture can result in several desirable properties such as suitable rigidity, high strength, lightweight, high thermal stability, and chemical resistance.<sup>1,3</sup> As a result, these materials have become widely adopted in various high-end industries, such as sports equipment, medical devices, construction and infrastructure, automobiles, and aerospace.<sup>3,4</sup>

Over the past decade, the demand for CFRPs has experienced substantial growth, with global consumption reaching 123,710 tons valued at approximately US\$18,800 million in 2022. This trend is expected to continue, with a projected compound annual growth rate of 12% during the forecast period of 2023-2032.<sup>5</sup> This growing demand for CFRPs stresses the urgency of recycling carbon fibers to reduce the amount of discarded materials that have been typically incinerated or landfilled.<sup>6,7</sup> Although these methods are cost-effective and can be easily scaled in an industrial setting, they do not align with the principles of a circular economy because no materials are recovered at the end of their lifespans.<sup>8,9</sup>

As environmental regulations are becoming more stringent, the importance of recycling and upcycling is gaining widespread recognition. In the coming years, many countries will pass laws to oversee the disposal of CFRP waste and include it in the category of recyclable materials.<sup>6</sup> The landfill has almost disappeared in some countries, like Germany, Austria, Belgium, and Denmark, and composite materials can no longer be landfilled in Germany and Netherlands.<sup>10,11</sup> In France, since January 2022, composites containing more than 30% plastics cannot be deposited in landfills.<sup>10,12</sup> These statutes directly impact the waste management of retired wind turbine blades, typically composed of fiber glass, carbon fiber, and epoxy resins. The European Technology & Innovation Platform on Wind Energy predicts that the combined weight of decommissioned wind turbine blades will reach 66 ktons by 2025.<sup>10,13</sup>

Considering the context, the interest in efficient and low-cost recycling methods to produce valuable products and recover CF and adherends, *i.e.*, composite substrates, has significantly augmented.<sup>6</sup> However, the recycling of CFRP continues to pose a challenge as most polymer matrices utilized are crosslinked thermosets.<sup>3,14</sup> While these crosslinks provide exceptional mechanical and thermal properties, they also make it extremely difficult to reclaim the carbon fibers without fully degrading the polymer matrix, hindering the ease of processing.<sup>15-17</sup>

Currently, the most common CF recycling methods are mechanical grinding, pyrolysis, and solvolysis.<sup>6,18,19</sup> The mechanical process consists in grinding the scrap composite material and reducing it into a thin powder.<sup>18,20</sup> This particulate product is high in resin content, making it suitable only for use as fillers or energy sources, presenting thus low added value.<sup>18</sup> The pyrolytic methods comprise ordinary pyrolysis, fluidized bed reactors, and microwave-assisted techniques.<sup>21</sup> The pyrolytic processes involve heating the composite materials to elevated temperatures under aerobic or vapor conditions to degrade the thermoset resins to recover the carbon fibers or fillers.<sup>22,23</sup> Although the pyrolysis processes are relatively easily implemented, they are highly energy-demanding and can affect the mechanical properties of CFs.<sup>24</sup> This is due to the high temperatures and severe conditions that cause oxidation reactions on the surface of the fibers, resulting in the production of carbon oxides that negatively impact their mechanical strength.<sup>25</sup>

Solvolytic processing can be categorized into high- and low-temperature methods.<sup>6,19</sup> The high-temperature and high-pressure methods, which mainly employ supercritical technology, are associated with high energy consumption and require complex industrial infrastructure.<sup>26</sup> The low-temperature ( $T < 200\text{ }^{\circ}\text{C}$ ) solvolytic method generally involves the use of concentrated acid or basic solutions at boiling or refluxing temperatures.<sup>19</sup> These extreme conditions pose potential hazards to health and safety, particularly when carried out on a large scale in industries.<sup>27</sup>

Developing degradable thermosets and adhesives as a basis for readily recycle CFRPs seems to be the crucial aspect of solving the recycling issues of CFRPs.<sup>28,29</sup> This is because designing new thermosets that retain their properties but can degrade under milder conditions helps to maintain the integrity of the reclaimed CFs and adherends, and allows, in some cases, re-valorize the recovered resin-derivatives.<sup>14,27,30</sup> These recently developed thermosets present a certain amount of cleavable bonds in the crosslinked networks that can be selectively cleaved under specific conditions.<sup>31,32</sup>

Furthermore, using adhesives for joining composite parts can result in lighter and more cost-effective material assemblies.<sup>33,34</sup> The multiphase composites can be built from a combination of different materials, namely, metals,<sup>35</sup> plastics,<sup>36</sup> glass<sup>37</sup> and carbon fibers<sup>38</sup> using welding,<sup>39</sup> hot melt bonding,<sup>40</sup> or thermoset adhesives.<sup>41</sup> One of the most significant challenges associated with using thermoset adhesives is their lack of recyclability and the difficulty of recovering adherends.<sup>33,38,39</sup> Therefore, developing recyclable or degradable adhesives has stimulated continuous research in academia and industry.<sup>42</sup>

In our recent research, we have reported the design and synthesis of next-generation epoxy monomers bearing ionic liquid (IL) moieties and cleavable groups to build multifunctional and degradable thermosets.<sup>32</sup> In this contribution, we discuss the use of an epoxidized IL monomer as a strategic molecular building block to selectively trigger the network degradability and facilitate the recovery of carbon fibers through transesterification-assisted solvolysis under gentle conditions and in a short time.

## 4. Materials and Characterization Methods

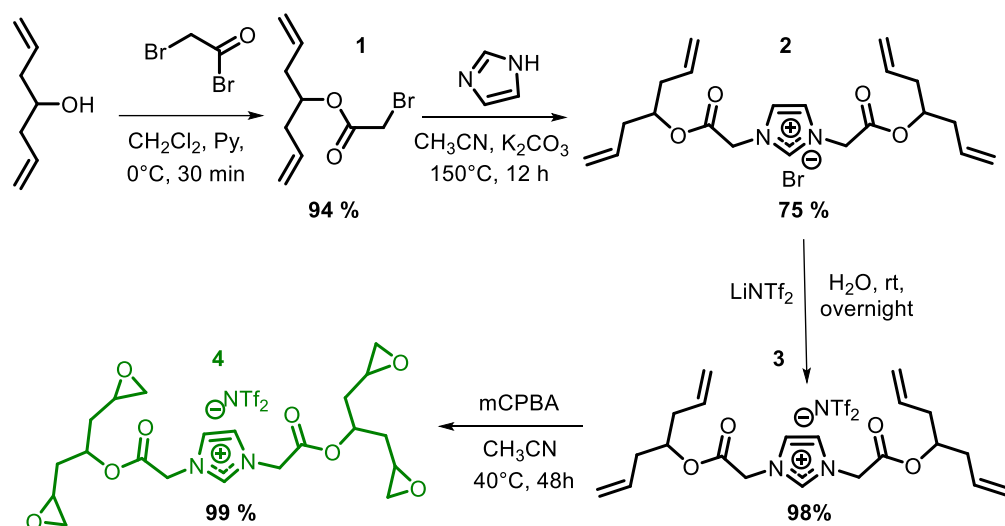
### 4.1. Materials.

Sigma Aldrich supplied all the reagents were employed as received, including the monomer 4,4'-Methylenebis(N,N - diglycidylaniline) with epoxide equivalent weight (EEW) of 105.63 g.mol<sup>-1</sup> and the hardener 3-(Aminomethyl)-3,5,5-trimethylcyclohexan-1-amine with an amine hydrogen equivalent weight (AHEW) of 42.58 g.mol<sup>-1</sup>, both hereafter referred to Tetra-N and IPDA, respectively. The solvents, including those anhydrous, were acquired from Carlos Erba and used in their original state. Tetrahydrofuran and dichloromethane in their anhydrous form were purchased in sealed flasks and were employed under Argon atmosphere. The non-sized high resistance carbon-fibers were obtained from Mitsubishi chemical carbon fibers and composites (Irvine, USA) under the commercial name Grafil® 34-700.

### 4.2. Synthesis of Tetra-Epoxidized IL Monomer (Tetra-IL)

Tetra-epoxidized IL was synthesized at multigram scale (up to 200 grams) through an optimized-modified methodology.<sup>32</sup> The new synthetic route requires only four reaction steps and does not involve column chromatography purification (**see Scheme IV-1**). In fact, the intermediate compounds are purified through either liquid-liquid extraction or precipitation methods to facilitate large-scale synthesis. To design the tetra-epoxidized IL monomer, compound **1** was firstly prepared with a yield of 94%. This synthesis was achieved by slowly adding bromoacetyl bromide (1.3 eq., 115 mmol, 10 mL) to a mixture of 3-cyclohexene-1-methanol (11.6 mL, 89 mmol) and pyridine (1.5 eq., 11 mL, 134 mmol) under an inert atmosphere at 0 °C for 2 h. Next, compound **1** (21 g, 93.45 mmol) was combined with imidazole (1.2 eq., 7.35 g, 105 mmol) and potassium carbonate (2 eq., 26.25 g, 189 mmol) in acetonitrile (420 mL). The reaction mixture was stirred at 150 °C for 12 h, then concentrated under reduced pressure, and precipitated in diethyl ether. Diethyl ether was removed, and the product was re-dissolved in dichloromethane and reprecipitated in diethyl ether. The diethyl ether supernatant was removed, and the product was re-solubilized in dichloromethane and then precipitated once more in diethyl ether, yielding compound **2** as

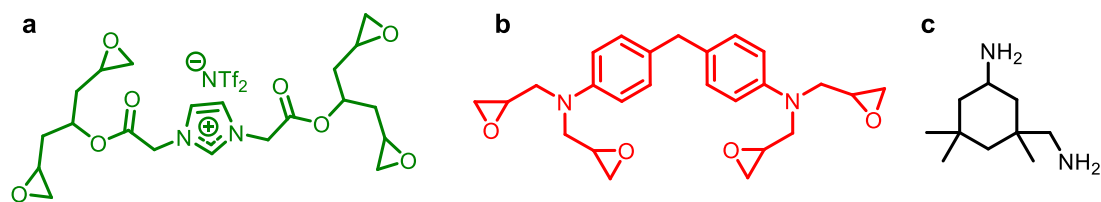
a brownish solid in a yield of 80%. Product **2** (9.5 g, 34 mmol) was thoroughly dried for 24 h and completely solubilized in 200 mL of deionized water at 80 °C. Then, a saturated solution of bis(trifluoromethane) sulfonimide lithium salt (2 eq., 0.395 g, 1.36 mmol) was combined with the solution of product **2**, and left to stir at room temperature overnight. After the ionic exchange reaction was completed, the resulting product was precipitated and recovered by extracting the aqueous solution using dichloromethane, yielding compound **3** (96%). Tetra-IL was obtained by epoxidizing compound **3** (30 g, 41.84 mmol) with *m*CPBA (6 eq., 0.525 g, 2.3 mmol) in acetonitrile at 40 °C for 72 h. The crude material was dissolved in a small amount of dichloromethane and then precipitated into a mixture of diethyl ether and petroleum ether (50:50)(v/v). The resulting product was obtained as a transparent, colorless, and viscous oil at room temperature. The product purity was confirmed by NMR techniques (see Fig. III-S1-S5) and HRMS (ESI+), which detected a molecular ion peak of 437.19188, corresponding to the calculated molecular weight of  $C_{21}H_{29}N_2O_4$   $[M]^+$ : 437.19184. For additional information, please check the supporting information material.



**Scheme IV-1.** Synthetic route used to obtain the Tetra-IL monomer.

#### 4.3. Design and Curing of the Thermoset Networks.

The epoxy prepolymers, namely Tetra-N, Tetra IL and the IPDA were homogenously mixed in a stoichiometric ratio, *i.e.*, epoxy to amino hydrogen in a 1:1 ratio (see structures in Fig. IV-1). Then, the epoxy-amine mixtures were poured into silicone molds, and cured under optimized conditions: 2h at 80 °C, and 5h at 160 °C. Five epoxy networks were created: Tetra-N, Tetra-N Tetra-IL10, Tetra-N Tetra-IL20, Tetra-N Tetra-IL50, and Tetra-IL. These blends were built by adjusting the proportion of Tetra-IL and Tetra-N epoxy monomers, without using solvents. The mole fraction of Tetra-IL was increased gradually from 0, 10, 20, 50, to 100% to produce the aforementioned networks.



**Figure IV-1.** The chemical structures of the networks' components. **a)** Tetra-epoxidized ionic liquid (Tetra-IL), **b)** 4,4'-Methylenebis(N,N-diglycidylaniline) (Tetra-N), and **c)** 3-(Aminomethyl)-3,5,5-trimethylcyclohexan-1-amine (IPDA).

#### 4.4. Composite Manufacture

The CF rovings were stretched by connecting their ends on a metallic support. The epoxy-amine blends were homogeneously mixed and applied on the CF rovings using a brush. The resin was perfectly distributed saturating the fibers without creating drips or runs, and precured at 80 °C for 1 h. After applying a second layer of resin, the CFs were cured in an oven at 80°C for 2 hours followed by an additional 5 hours at 160°C.

#### 4.5. Characterization Methods

*Nuclear Magnetic Resonance (NMR) Analyses* were carried out using a Bruker Avance III 400 MHz spectrometer to record the  $^1\text{H}$ ,  $^{13}\text{C}$ ,  $^{19}\text{F}$  and two-dimensional NMR spectra. Chemical shifts for  $^1\text{H}$  and  $^{13}\text{C}$  nuclei were expressed in ppm and calculated regarding internal tetramethylsilane reference, while coupling constants were measured in Hz. The abbreviations for signal coupling were designated as singlet (*s*), doublet (*d*), doublet of doublets (*dd*), triplets (*t*), quartets (*q*), quintet (*qt*), multiplet (*m*), and broad signal (*b*).

*High Resolution Mass Spectra (HRMS)* were performed using the electrospray ionization (ESI) technique with a Micromass-Waters Q-TOF Ultima Global mass spectrometer. The samples were prepared in methanol or acetonitrile and immediately introduced to the mass spectrometer. Before each analysis, calibration was performed on the mass spectrometer using phosphoric acid with a range of 98 to 1300 *m/z*.

*Fourier Transform Infrared Spectroscopy (FT-IR)* was carried out using a Nicolet Magna 550 spectrometer in attenuated total reflection (ATR) mode to acquire FT-IR spectra. The spectra were obtained at room temperature over the range of 4000 to 500  $\text{cm}^{-1}$ , with a resolution of 4  $\text{cm}^{-1}$ , and via 32 scans.

*Differential Scanning Calorimetry (DSC)* was carried out using a Q10 Calorimeter (TA Instruments) with a heating rate of 10 °C  $\text{min}^{-1}$  under nitrogen flow, the IL monomers were analyzed in the presence of the hardeners, as well as the resulting networks. This analysis



was performed in the dynamic mode from -70 °C to 250 °C to determine the polymerization temperature and the glass transition temperatures ( $T_g$ ) of the five resulting networks.

*Chemiorheology Assays* were conducted on an ARES G2 Rheometer (TA Instruments) to identify the gel point of the curing system and track the evolution of the curing process, thereby providing additional information on the kinetics of gelation. The gelation time was identified based on the point at which  $G'$  and  $G''$  crossed over each other. The epoxy monomers and hardeners were blended at room temperature in a disposable 40 mm parallel-plate cup geometry (**see Fig. IV-S6**) immediately before the beginning of the experiment. Tetra-IL, Tetra-N and IPDA were combined in adequate proportion, as previously stated in the section *Design and Curing of the Thermoset Networks*. Isothermal time sweep tests were carried out at 50°C. A strain of 5% and a frequency of 1 rad/s were used for all measurements.

*Thermogravimetric Analyses (TGA)* were conducted on a Q500 Thermogravimetric Analyzer (TA Instruments) under nitrogen atmosphere. The samples were heated at a rate of 10 °C min<sup>-1</sup>, from 30 °C to 800 °C. The results were displayed as a percentage of remaining mass as function of temperature, which enabled the identification of T5% and T50% corresponding to degradation temperatures of 5 and 50wt%, respectively.

*Dynamic Mechanical Analyses (DMA)* were conducted on an ARES G2 Rheometer (TA Instruments) equipped with a torsional fixture module. Then, rectangular-shaped samples measuring 30 x 4 x 1.5 mm<sup>3</sup> were analyzed using a heating rate of 3 °C min<sup>-1</sup>, from -100 up to 250 °C, at a frequency of 0.5 Hz. The storage modulus  $G'$  was obtained and represented on a logarithmic scale to highlight the molecular transitions. The loss factors  $\tan \delta$  were also measured for the same range and reported on a linear scale.

*Scanning Electron Microscopy (SEM) Analyses* were carried out on a Tescan Vega 3 scanning electron microscope (TESCAN Ltd.) operating at an accelerating voltage of 10 kV, and a working distance of about 10 mm. The samples were fixed with carbon-tape and then sputter-coated with a 5 nm layer of gold using Bal-Tec SCD 005 under the operating parameters of 30 mA and 90 s. The images were processed, and the scale bars were added on ImageJ software. The surface networks, matrix-carbon fiber interfaces, and reclaimed carbon fibers were evaluated for their respective morphologies.

*Optical Contact Angle Measurement.* The optical contact angles with water were measured through the sessile drop technique using an OCA 25 Goniometer at 25 °C. The images were captured using a high-performance camera using a 6.5-fold zoom lens.

*Solvolysis Methodology and CF recovery.* The transesterification-assisted methodology was developed using 1-(4-sulfobutyl)-3-methylimidazolium hydrogen sulfate (acid IL) and ethylene glycol (EG), as the catalyst and reactive solvent, respectively. To carry out the experiment on the thermoset networks, rectangular samples measuring 15 x 4 x 1.5 mm<sup>3</sup> and weighing 100 mg were placed into closed glass vials (**Fig. IV-6b**). The vials were then heated to 190 °C for 4.5 hours using a hot plate magnetic stirrer coupled to a module Labor-technik Variomag 40ST. Four different proportions of IL were tested in ethylene glycol, 1, 3, 5 and 10 in wt.%. During the process, the degradation progress was observed visually at regular intervals. After the procedure, the degradation activities were evaluated for the different conditions, and the degradation products were systematically analyzed using HRMS. The remaining mass was weighed, and the degradation activity was calculated using Equation 1, where  $m_i$  and  $m_f$  represent the initial and final masses, respectively. All experiments were performed in triplicate.

$$R_f = \frac{m_i - m_f}{m_i} \cdot 100\% \quad (1)$$

Similarly, the thermoset portion of the composites underwent degradation for five hours at 190 °C utilizing a blend of 5% IL in EG. After the polymer matrices had undergone degradation, the carbon fibers were rinsed with acetone and subsequently dried overnight at 80 °C in a vacuum oven.

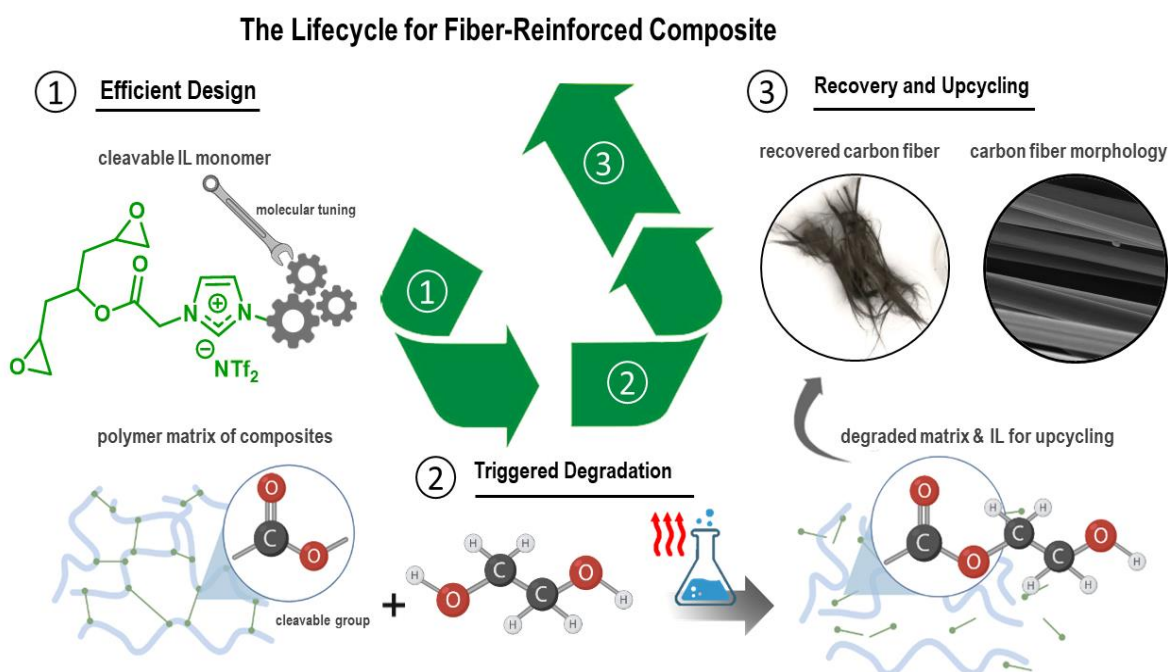
*Lap Shear Test.* The different epoxy amine formulations containing varying amounts of Tetra-IL (0, 10, 20, 50, and 100%) were used to bond two aluminum specimens, each measuring 16x25x100 mm. The samples were polished, cleaned with acetone, dried and placed in a machined mould, as shown in **Fig. IV-S7**. A layer of resin measuring 0.1x25x13 mm and weighing 100 mg was applied and cured according to the curing protocol outlined in the *Design and Curing of the Thermoset Networks* section. The specimens were then subjected to a tensile test using an Instron machine with an extensometer at room temperature and a cross-head speed of 1 mm/min. After the test, the aluminium plaques were separated and immersed in a beaker containing ethanolamine, which was heated to 150 °C for 1 hour.

## 5. Results and Discussion

### 5.1. Design of Degradable Epoxy Networks and Fiber-Reinforced Epoxy Composites

The epoxy thermosets and composites tailored in this work present the main advantages of these crosslinked materials, such as excellent mechanical properties and high

thermal and chemical stabilities.<sup>15,43,44</sup> Although these crosslinks afford remarkable features, they turn these materials unrecyclable.<sup>18,45–47</sup> To address this issue, an IL comonomer bearing cleavable ester groups was strategically installed into the networks affording the programable deconstruction of composites and adhesives (**Fig. IV-2**).



**Figure IV-2.** Route for efficient design, processing, disassembly and recycling thermosets and composites. **1)** Molecular design and synthesis of epoxidized IL monomer bearing a cleavable ester group. **2)** Selective triggered degradation of the thermoset matrix through transesterification reaction. **3)** Recovering of carbon fibers or composite components and potential valorization of degraded IL derivatives.

## 5.2. Reactivity Study and Thermomechanical Property Investigation

To evaluate the curing process of epoxy-amine systems containing Tetra-IL, DSC and chemio-rheology were performed (**Fig. IV-3a-b**)<sup>48–50</sup> The evolution of the viscosity of different Tetra-N/Tetra-IL networks was studied under dynamic and isothermal conditions while the gel time was calculated from the crossover between G' and G'' curves<sup>51</sup> Due to the high reactivity and rapidly increase of viscosity, the measurements were conducted at 50°C rather than 80°C, which correspond to the first temperature ramp of the curing protocol (**see Table IV-1**).

**Table IV-1.** Gel time observed for the different epoxy systems.<sup>x</sup>

	Tetra-N	Tetra-N Tetra-IL10	Tetra-N Tetra-IL20	Tetra-N Tetra-IL50	Tetra-IL
<b>Gel Time (min)</b>	140	42	26	26	25

<sup>x</sup> Experiment carried out under 50°C, strain of 5% and a frequency of 1 rad/s.

Using Tetra-IL as molecular brick platform led to a significant reduction of the gel time, from 140 min to 25 minutes. It can be clearly seen that quantities of 10 and 20% are sufficient to significantly reduce the gel time of epoxy systems. Thus, Tetra-IL plays a dual role in the formation of the epoxy-amine network, *i.e.* as a catalyst and as comonomer of the epoxy-amine polymerization. According to the literature, several authors including Livi *et al.*, Maka *et al.* have highlighted that imidazolium and phosphonium ILs (*no epoxidized*) combined with nucleophilic counter anions could be used as hardeners triggering and accelerating the polymerization in epoxy systems.<sup>52,53</sup>

This study shows for the first time that employing an epoxidized IL monomer can lead to a catalytic effect of the epoxy-amine reaction. The curing behavior of the epoxy systems was also investigated by DSC (**Fig. IV-3b**) where the exothermic peak temperatures indicated the ability of the Tetra-IL to induce and participate in the polymerization of the epoxy-amine networks. Given the aforementioned literature,<sup>53–58</sup> and the chemical nature of Tetra-IL, we proposed that the activation of the epoxy groups occurs through a dipole ion coordinating interaction or a hydrogen bond with the imidazolium moiety (**Fig. IV-3b**).

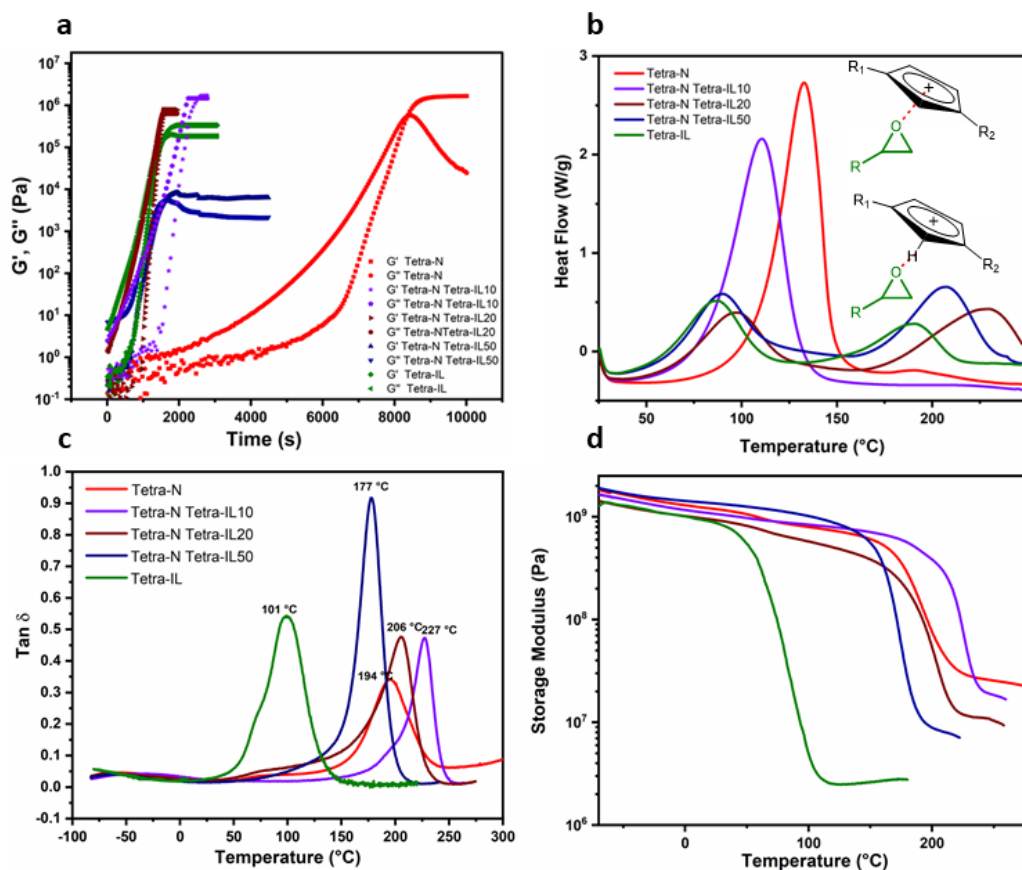
In fact, the incorporation of 10 and 20% of Tetra-IL into epoxy-amine network reduced the exothermic peak temperatures from 135 °C to 110°C and 100 °C, respectively. For Tetra-N Tetra-IL10 network, only one single exothermic peak was observed compared to Tetra-N containing 20, 50% of Tetra-IL having two exothermic peak temperatures at 80 °C and 180-200°C. These results can be explained by the bimodal character *i.e.*, a two-step mechanism as previously suggested by our previous works on the design of epoxy thermosets derived from different imidazolium IL monomers.<sup>59,60</sup>

The  $\alpha$ -relaxation temperatures ( $T_\alpha$ ) were determined by dynamical mechanical analysis (DMA) and summarized in **Table IV-2**.

**Table IV-2.** Main relaxation temperature ( $T_\alpha$ ) related to the glass transition temperature ( $T_g$ ).

<b>Network</b>	<b><math>T_\alpha</math> (°C)</b>
<b>Tetra-N</b>	190
<b>Tetra-N Tetra-IL10</b>	227
<b>Tetra-N Tetra-IL20</b>	206
<b>Tetra-N Tetra-IL50</b>	177
<b>Tetra-IL</b>	101

In all cases, the addition of Tetra-IL also affected the  $\alpha$ -relaxation temperatures, showing an interesting tendency. For only 10% of Tetra-IL, a significant increase of the  $T_\alpha$  was observed from 190 °C to 230 °C which can be explained by the catalytic effect of this amount inducing the crosslinking of the network from 110°C instead of 130°C. As the percentage of IL comonomer increases to 20 and 50%, a reduction of the  $T_\alpha$  was observed to 206 and 180 °C, respectively. These results can be firstly explained by the increase in the proportion of Tetra-IL knowing that the epoxy network prepared from 100% of Tetra-IL has only a  $T_\alpha$  of 100°C. Secondly, as previously discussed, we have demonstrated a two-step mechanism of the epoxy-amine reaction for 20 and 50% of Tetra-IL compared to Tetra-N and Tetra-N Tetra-IL10.



**Figure IV-3.** Examination of the kinetics of the curing reaction and the thermomechanical properties. **a)** Determination of the gel time at 50 °C. **b)** DSC thermograms of the corresponding epoxy-amine mixture, highlighting the exothermic peaks of polymerization (exo up). **c)** Tan  $\delta$  highlighting the alpha transition temperatures and **d)** Storage modulus for the five yielding thermosets.

As the gel time is significantly reduced at 25 min, all of the amine functions do not have time to be completely consumed during the first curing step (80 °C) requiring thus the second curing step at elevated temperature (160 °C).

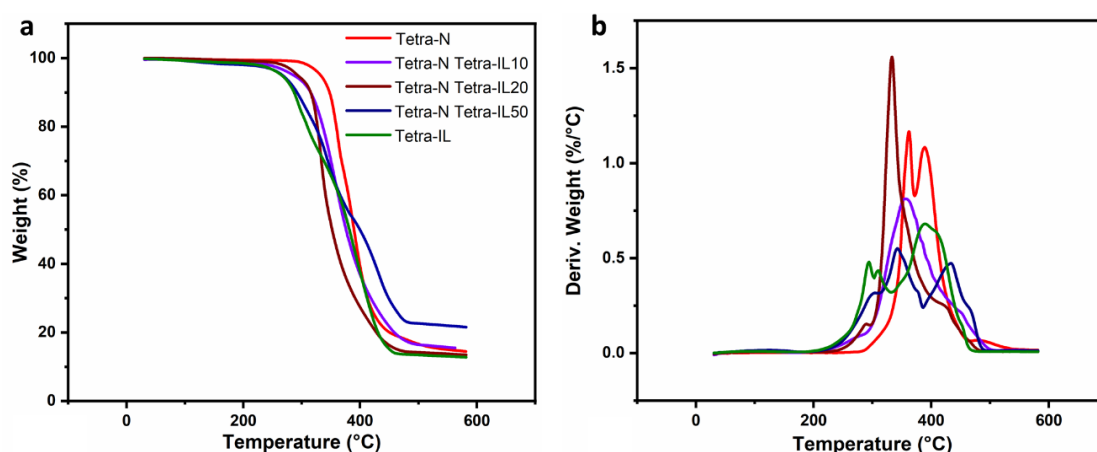
Importantly, tailoring  $T_\alpha$  can be beneficial for creating ductile materials for well-suited composite development.<sup>61,62</sup> In addition, a noticeable decrease in the storage modulus at the rubbery plateau was obtained. This result is associated with the shape memory behavior, making it highly beneficial for designing materials with shape memory and shape fixity, as we have shown in our recent research.<sup>31,32,59</sup> In summary, the use of Tetra-IL as molecular brick platform into epoxy networks opens future perspectives in the field of aircraft or automotive applications requiring high  $T_g$  formulations.

Thermogravimetric analysis (TGA) was performed to determine the impact of the Tetra-IL comonomers on the thermal stability of the epoxy-amine networks. The evolution of the weight loss in a function of the temperature is summarized in **Table IV-3** and **Fig. IV-4**.

**Table IV-3.** Temperatures corresponding to 5 and 50% of mass loss.

	T <sub>5%</sub> (°C)	T <sub>50%</sub> (°C)
<b>Tetra-N</b>	332	385
<b>Tetra-N Tetra-IL10</b>	286	369
<b>Tetra-N Tetra-IL20</b>	292	345
<b>Tetra-N Tetra-IL50</b>	266	380
<b>Tetra-IL</b>	265	373

The resulting networks exhibited excellent thermal stabilities (> 350°C). Nevertheless, some differences can be observed during the incorporation of IL-based monomer, *i.e.* Tetra-IL. In fact, two degradation temperatures at 265 and 400 °C are evidenced for the epoxy-amine network using only Tetra-IL as epoxy prepolymers which can be explained by the presence of the ester bonds well-known to be more sensitive to the temperature. On the contrary, Tetra-N presents only one degradation temperature around 380 °C. Thus, the combination of the two monomers, *i.e.* Tetra-N and Tetra-IL allows to reduce this phenomenon leading to a delay of the decomposition temperatures for the networks containing 10, 20 and 50% of Tetra-IL. Finally, the thermal stability of the epoxy networks is similar to the DGEBA-derivative materials.<sup>63,64</sup>

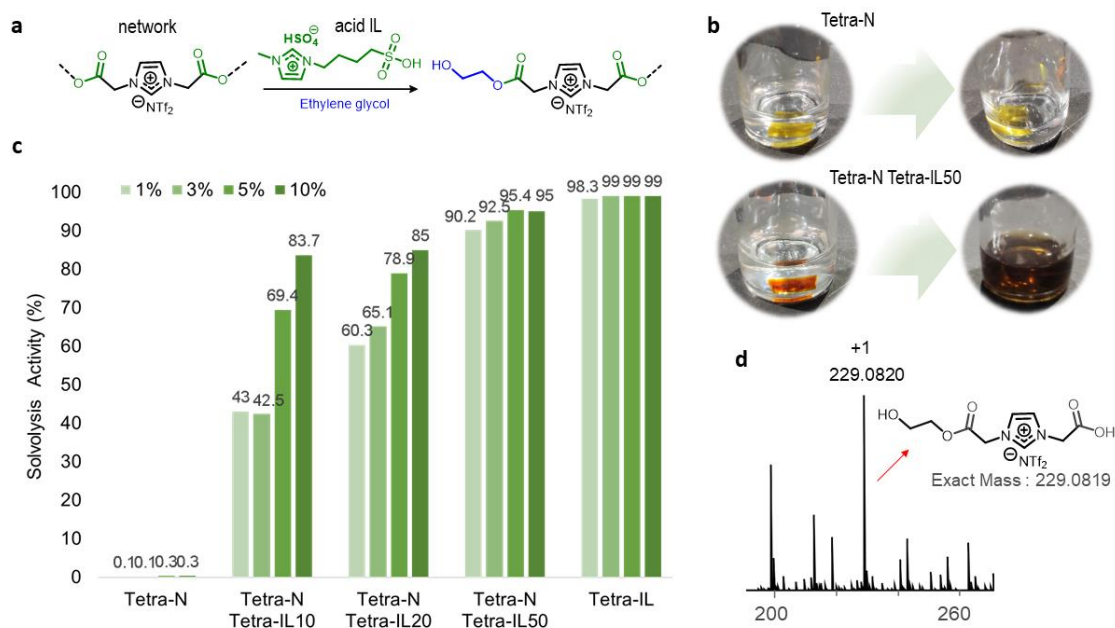


**Figure IV-4.** Study of thermal stability of resulting networks. **a)** thermogravimetric analysis thermograms and **b)** derivative weight loss (heating rate: 10 °C min<sup>-1</sup> under nitrogen gas).

### 5.3. Transesterification-Assisted Solvolysis

Several studies have outlined methods for breaking down thermosetting materials using harsh conditions such as strong acids, bases, and high energy. However, these methods tend to be costly and require extensive follow-up treatment, making them unlikely to be used on an industrial scale.<sup>17,19,26,47</sup> Kuang and coworkers investigated various organic catalysts for breaking down thermosets made of epoxy-anhydride in the presence of different alcohols.<sup>65</sup> Additionally, Warner and his team used a combination of ethylene glycol and imidazolium ILs to degrade and up-recycle commercial epoxy resins.<sup>66</sup>

In this study, we proposed the introduction of Tetra-IL as a cleavable building block for tailoring the degradation of thermoset networks. To accomplish this goal, we designed a solvent-assisted transesterification reaction using ethylene glycol and an acid IL as the solvent and catalyst, respectively (**Fig. IV-5a**). Our outcomes demonstrate the feasibility of this approach for recycling carbon fiber-reinforced epoxy and developing degradable epoxy adhesives.



**Figure IV-5.** Sustainable and effective solvolysis methodology to degrade thermosets using mild conditions. **a)** Networks degradation takes place through a transesterification reaction. **b)** The networks exclusively based on the commercial products (top) did not reveal significant degradability compared to the samples built from Tetra-IL (down). **c)** The solvolysis activity does not rely only on the Tetra-IL percentage but also on the amount of acid IL used. **d)** The degradation process occurs in a targeted manner.



The process of solvolysis involves three stages: a change in the color of the solution, swelling of the samples, and gradual dissolution of the specimens. When the networks were constructed solely from the commercial monomer Tetra-N, no color change or significant degradation was observed, even when the concentration of acid IL was increased up to 10% **(see Fig. IV-5b and IV-S8)** This is because the commercial epoxy monomer does not contain any cleavable bond that can be targeted and broken under mild conditions. In contrast, the other systems confirmed the catalytic role of the acid IL, as increasing its concentration greatly increased the amount of degraded material **(Fig. IV-5c)**. Additionally, the highest level of degradation was observed when the concentration of Tetra-IL in the network was highest.

The introduction of 10% Tetra-IL comonomer in the network with 10% of acid IL lead to a degradation activity of 83.7%. Notably, when 50% Tetra-IL was installed into the networks, it resulted in 95% degradation of the thermosets while maintaining excellent thermal and mechanical properties, such as a  $T_{5\%}$  superior to 250 °C and a  $T_{\alpha}$  of 177 °C.

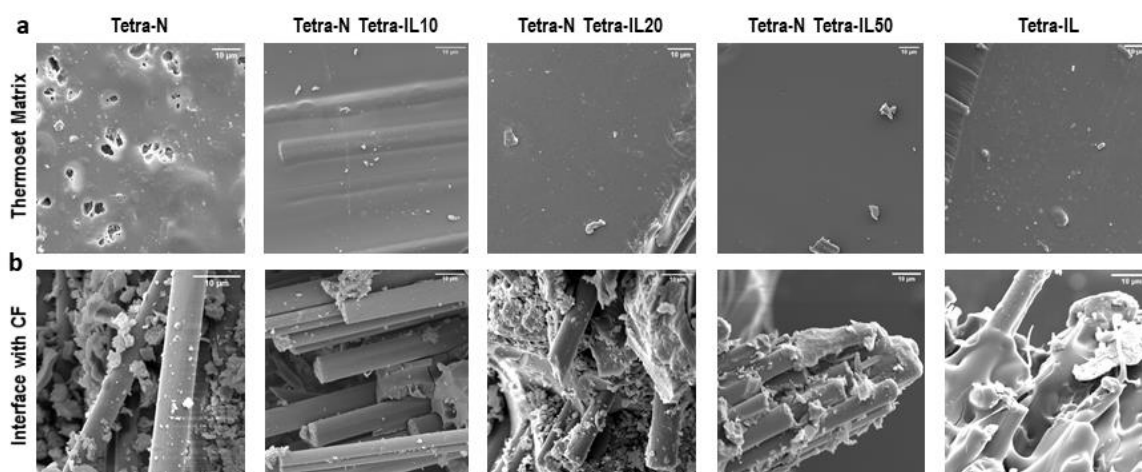
To further understand the degradation mechanism and improve the design of degradable thermosets, we attempted to analyze the structures of the degradation products. While determining the exact structures of these compounds is difficult due to the complexity of the degraded solutions, the selectivity of the degradation pathway can be confirmed by the products formed by the solvent-assisted transesterification reaction. For example, the main degradation product obtained from Tetra-N Tetra-IL50 had a mass-to-charge ratio of 290.820, corresponding to the cation derived from the cleavage of ester bonds, as shown in **Fig. IV-5d**.

#### **5.4. Composite Manufacture, Surface Properties, Morphological Structure, and CF Compatibility**

The study of the surface morphology of the composites revealed that the network homogeneity and carbon-fiber wettability enhanced with the introduction of IL comonomer. The IL comonomer appears to play a dual role of sizing and catalyst of the epoxy-amine polymerization by decreasing the gel time. Thus, the presence of the IL moiety impacts the intermolecular interactions between the epoxy-amine matrix and the CFs leading to an improvement of the adhesion. Secondly, its catalyst effect improves the polymerization process leading to more homogenous polymer structures, as observed in **Fig. IV-6a**.

The surface tension of untreated carbon fibers is not similar to that of epoxy resin. Carbon fibers typically have a surface tension of around 30-40 mN/m, while epoxy resins

usually have a surface tension in the range of 50-60 mN/m.<sup>67,68</sup> As a result, achieving sufficient wetting of the carbon fibers by epoxy materials can be difficult. The ion-pair formation constant measures the binding energy between the ions in ILs, and their magnitudes relate to the constant of the adsorption of ILs. It is well established that the pair imidazolium-NTf<sub>2</sub> presents a high ion-pair association, leading to more elevated adsorption of ILs onto the CF structures.<sup>67</sup> Additionally, the intermolecular interactions between the IL-moiety and the CF surface are further enhanced by the  $\pi - \pi$  stacking interactions between the imidazolium ring system and the CF surface, as well as the non-polar NTf<sub>2</sub> ion.<sup>69-72</sup> **Fig. IV-6b** demonstrates the correlation between the percentage of IL comonomer and the improvement of the wettability on carbon fiber. As the percentage of IL comonomer increases, the wettability of the carbon fiber also enhances.



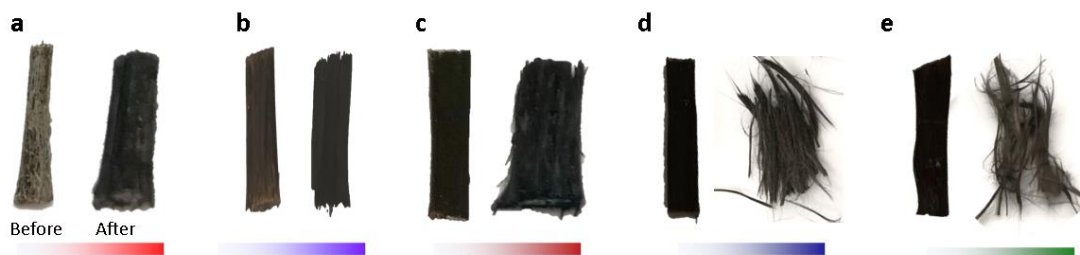
**Figure IV-6.** Morphology investigation through high-resolution scanning electron microscopy. The influence of the IL monomer percentage on **a)** the morphological structures of the polymer matrix and **b)** on the carbon fiber wettability by the thermoset resins. The white scale bars correspond to 10  $\mu\text{m}$ .

This study also examined the water contact angles revealing an interesting behavior (see Fig. IV-S9). The addition of 10% and 20% of Tetra-IL had a negligible effect on the hydrophobicity. However, when the percentage of Tetra-IL in the networks reached 50%, a strong hydrophobic behavior was obtained with water angle of 123 °C. This result can be explained by the presence of hydrophobic NTf<sub>2</sub> counterion. However, for 100% of Tetra-IL, a significant decrease of the water contact angle was obtained which can be explained by the rising of the polar ester groups.

## 5.5. Composite Deconstruction

Recent studies have investigated the decomposition of composites made of CFs/epoxy resin under milder temperatures and conditions.<sup>2,6</sup> Jiang and colleagues examined the degradation and repurposing of carbon fiber composites that use DGEBA and 4,4'-diaminodiphenylmethane networks with  $T_g$  of about 80 °C. This investigation was conducted using a 2.6 mol of  $H_3PO_4$  in tetrahydrofuran.<sup>73</sup> Other authors such as Xu *et al.* have investigated the disassembly of the epoxy-amine matrix in the presence of hydrogen peroxide and dimethylformamide mixtures. By optimizing the ratio of DMF to  $H_2O_2$ , they achieved an efficiency of 99% when temperatures were above 90 °C.<sup>28</sup>

Herein, fiber-reinforced epoxy composites were prepared and their disassembly were studied in order to confirm the sustainability of our strategy. Thus, we have demonstrated that the integration of Tetra-IL comonomer into the network led to a significant disassembly of the composites at the following optimized conditions: 190°C for 4.5 hours by using 10% of acid IL catalyst (see Fig. IV-7).

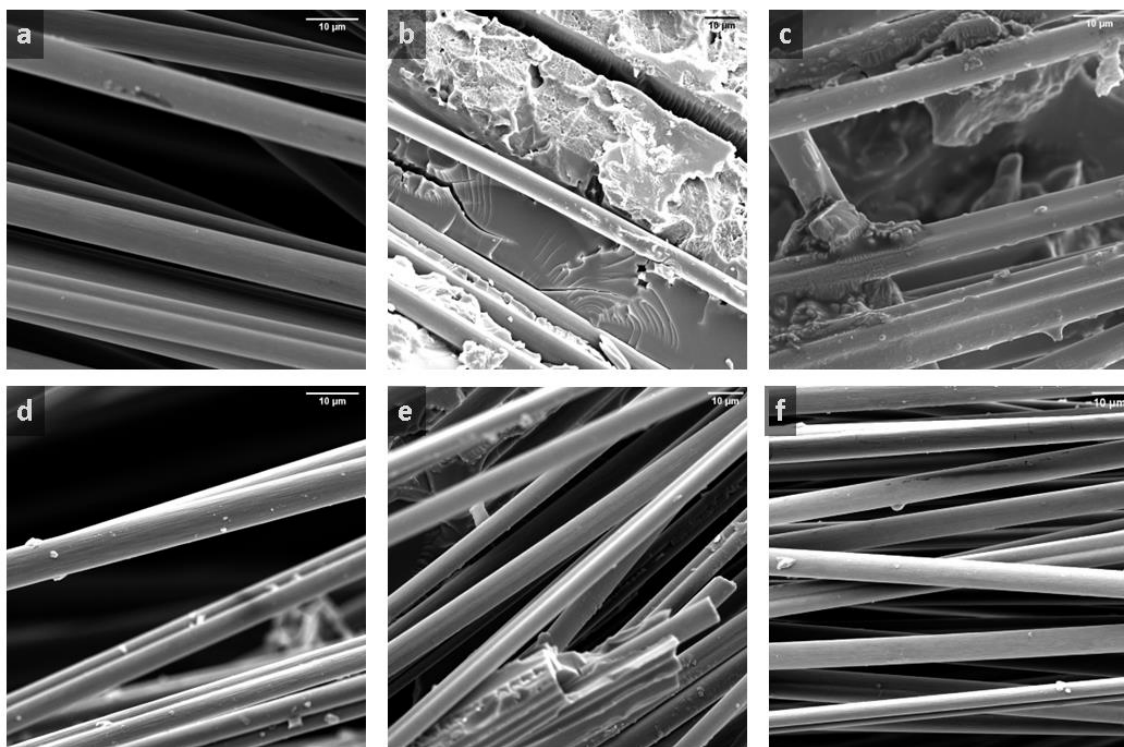


**Figure IV-7.** Composite samples before and after the solvolysis treatment employing 10% of acid IL in ethylene glycol, for 4.5 hours at 190 °C. Samples built from **a)** 0, **b)** 10, **c)** 20, **d)** 50 and 100% mole of Tetra-IL.

Remarkably, increasing the proportion of Tetra-IL comonomer in the composite, yields a more significant degradation of the thermoset component, ensuring the full recovery of the CFs. Our previous experiments have provided evidence to support these results, indicating that using 20% of Tetra-IL can lead to the degradation of 85% of the thermoset matrix. This is also demonstrated by the comparison of composites before and after thermoset solvolysis in **Fig. IV-7**.

To further validate the efficiency of this approach, SEM analyses was performed to observe the potential residual amount of epoxy resin on the carbon fibers surfaces (**Fig. IV-8**). The SEM micrographs highlighted that the presence of Tetra-IL have a significant impact on the dissolution of the epoxy networks. For 20% of Tetra-IL, only a small residual amount

of epoxy-amine resin is observed on the surface of the CFs. By using 50% of Tetra-IL comonomer under the same solvolysis conditions, clean and resin-free carbon fiber surface were obtained. In contrast to previous findings, these outcomes show promise as the recovery of the CFs was achieved without using volatile and toxic organic solvents, high temperatures and long periods of time.



**Figure IV-8.** Morphology investigation through high-resolution scanning electron microscopy of recycled carbon fibers. In **a)** the raw carbon-fibers used as comparative control, and the networks built from **b)** 0, **c)** 10, **d)** 20, **e)** 50 and **f)** 100% of tetra-IL. The white scale bars correspond to 10  $\mu\text{m}$ .

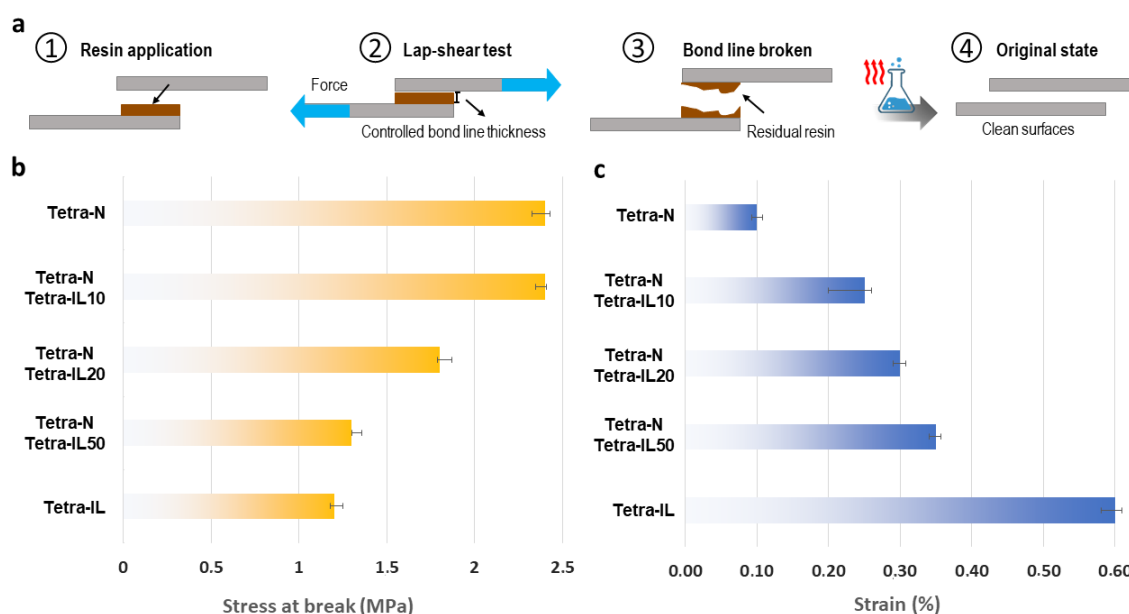
This novel approach presents promising possibilities for advancing degradable networks with high  $T_g$  (180-230°C) for use in structural composite applications. Few parameters can be further optimized, like temperature, time conditions, and choice of ILs bearing Brønsted or Lewis acid sites, which are established as catalysts for transesterification reactions.<sup>65,74</sup>

The significance of this statement lies in the fact that, although further experimentation is required to fully characterize the mechanical properties of CFs, the use of mild conditions ensures the absence of undesirable reactions preventing the deterioration of CFs. Thus, this study serves as a basis for future research that aims to expand upon the knowledge on efficient recycling of CFs.

## 5.6. Degradable Epoxy Thermoset Adhesives

The investigation into the development of degradable epoxy adhesives was prompted by the tailored thermoset properties that can be afforded relying on Tetra-IL monomer percentage. These properties include improved interfacial compatibility, faster gel time, tailored hydrophobicity, and the ability to trigger network degradation under mild conditions. Incorporating cleavable ester bonds into thermoset networks can address the significant challenge of creating permanent degradable adhesives. Additionally, the extent of intermolecular interactions is directly proportional to the adhesion capability, which can be significantly enhanced by the presence of imidazolium-moiety, providing H-bonds,  $\pi - \pi$  stacking, and ionic bonds.<sup>75</sup>

With regard to these aspects, an adhesion test was conceived, as shown in **Fig. IV-9a**. The lap shear test (ASTM) was selected to evaluate the capability of the resins to withstand stresses applied in a plane, which is one of the most common stresses that a bonded joint can face during service, particularly for adhesives intended for structural bonding.<sup>34,76</sup>



**Figure IV-9.** Removable epoxy thermosetting adhesives. In **a**) a general outline describing the sample preparation, the lap-shear testing, and the degradation of the residual epoxy adhesive. **b**) stress at break measured in MPa and **c**) the displacement measured in %.

The specimens' stress at break observed in this study falls within the range of 1 to 5 MPa obtained for conventional epoxy-amine adhesives (**Fig. IV-9b**). However, our results showed a significant decrease in bond strength with an increase in the percentage of IL comonomer in the network. Upon examining our results and previous reports on adhesives,

it appears that the reduction in adhesive performance stems from the decrease in the crosslink density. Although Tetra-IL presents four epoxy groups similar to Tetra-N, the IL-based monomer is comparatively longer, which directly affects the crosslink density and, as a result, the adhesion properties. On the other hand, this monomer offers more ductile epoxy thermosets, which can be advantageous for applications requiring a certain degree of flexibility. This tendency is demonstrated in **Fig. IV-9c**, where we can observe an increase in the strain at the break in function of the amount of Tetra-IL.

Ethanolamine was chosen as the agent for degrading the epoxy adhesives on the aluminum plates, based on previous research indicating that ester groups readily undergo amidation with small amine compounds.<sup>77-79</sup> Thus, it was found that the incorporation of only 10% of the Tetra-IL was sufficient to achieve full degradability of the epoxy-amine networks (**Fig. IV-S10**). This means that subjecting the IL-based thermosets to a temperature of 190 °C for 2 hours resulted in their complete elimination from the aluminum substrates.

Overall, it is evident that further optimization and experimental exploration are necessary to establish and define IL-based monomers as adhesive thermoset precursors. However, it is worth mentioning that this is the first time an epoxidized IL has been utilized for this particular application. Despite the need for further optimization, IL-based comonomers can be advantageous for fine-tuning ionic and electric conductivity and the coefficient of thermal expansion in adhesives, which are parameters already investigated in our previous work.<sup>31</sup>

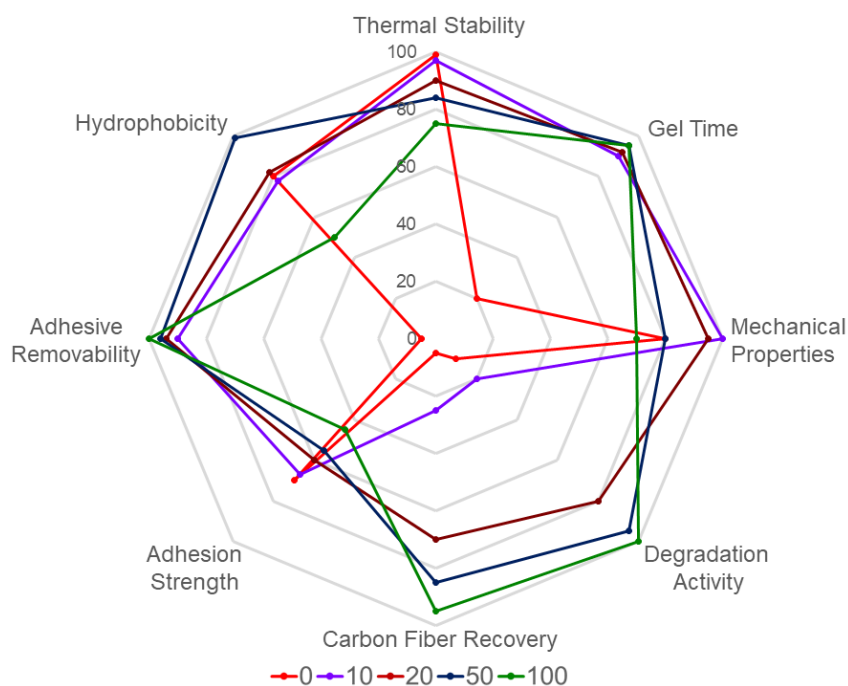
Notably, employing ethanolamine as a solvent in the absence of catalysts may be a promising method to recover carbon fibers instead of using ethylene glycol/acid IL mixtures. The degraded imidazolium derivatives can catalyze the degradation of networks through self-catalysis. This is because the imidazolium derivatives can interact with the carbonyl groups, activating them for nucleophilic attack and facilitating the network degradation.<sup>32</sup>

### **5.7. Using Tetra-IL to Tailor Physical Properties of Epoxy-Amine Networks.**

It is widely recognized that the optimal characteristics of materials are contingent upon the envisioned application. To ensure that the material possesses the desired properties for a targeted application, a better understanding of the polymer architecture-morphology-physical properties relationships is required. This enables the material to be designed to meet the specific application's requirements. The use of Tetra-IL as a building block was designed for two primary purposes:

1. To tailor various polymer characteristics and gain insights into designing thermosets and composites based on IL monomers;
2. To enable the selective degradation pathway of the polymer matrices under mild conditions and to recover the CFs and the composite substrates.

**Fig. IV-10** demonstrates how Tetra-IL content significantly impacts several aspects, including thermal stability, mechanical properties, gel time, and recycling possibilities.



**Figure IV-10.** Set of material properties individually normalized for each characteristic. Five different compositions were investigated in this study with 0, 10, 20, 50 and 100% of Tetra-IL.

Given the synthetic route of Tetra-IL and its desirable properties, particularly regarding the end-of-life of the composites, it appears more reasonable to consider using 10 to 20% of Tetra-IL for the development of high-performance thermosets for structural applications such as aerospace, and automotive. This approach offers a promising strategy for facilitating the transition towards a circular society, where materials and resources are kept in use for as long as possible.

## 6. Conclusion of Chapter IV

In this work, we designed and synthesized a tetra-epoxidized IL bearing an imidazolium-NTf<sub>2</sub> moiety and cleavable ester bonds at a multigram scale (up to 100 g). The synthetic methodology was optimized to ensure it is straightforward and does not involve hazardous chemicals like epichlorohydrin and bisphenol A derivatives. Consequently, the synthesis can be potentially transferred to an industrial scale. Here, Tetra-IL was employed as

a cleavable building block, and we have demonstrated that the incorporation of only 10% into the epoxy network was sufficient to tailor the gel time, thermal stability, hydrophobicity, mechanical performances, and degradability. The thermoset networks produced exhibit great mechanical performances and excellent thermal stabilities ( $> 350^{\circ}\text{C}$ ), which are similar to conventional DGEBA-based materials. One other advantage of using Tetra-IL resulted in improved carbon fiber surface wettability with the epoxy matrix and enhanced homogeneity of the morphological network, potentially facilitating the development of defect-free materials. In addition, the thermosets turned nearly completely degradable with an increase in Tetra-IL proportion to 10%, while 50% percent was found to be the most effective for CF recovery. Although further experiments are required for adhesive properties, preliminary results indicated that using Tetra-IL led to a good compromise between stiffness and strain at rate providing ductility to networks. Moreover, it enabled the adhesives to be degradable under mild conditions and in a short period, thus allowing for the recovery of adherends. It is worth mentioning that there are a few aspects for additional exploration that could enhance the scope of this research. These include using regenerated IL derivatives and recovered CFs to develop second-generation epoxy networks, which will be pursued in future studies. Ultimately, our findings pave the way for the efficient design of degradable epoxy thermosets utilizing ILs, thereby facilitating the development of high-performance thermosets and composites in line with the circular economy's expectations.

## 7. References

- (1) Peijs, T.; Kirschbaum, R.; Lemstra, P. J. Chapter 5: A Critical Review of Carbon Fiber and Related Products from an Industrial Perspective. *Advanced Industrial and Engineering Polymer Research* **2022**, *5* (2), 90–106. <https://doi.org/10.1016/j.aiepr.2022.03.008>.
- (2) Wang, B.; Ma, S.; Yan, S.; Zhu, J. Readily Recyclable Carbon Fiber Reinforced Composites Based on Degradable Thermosets: A Review. *Green Chemistry* **2019**, *21* (21), 5781–5796. <https://doi.org/10.1039/C9GC01760G>.
- (3) Navarro, C. A.; Giffin, C. R.; Zhang, B.; Yu, Z.; Nutt, S. R.; Williams, T. J. A Structural Chemistry Look at Composites Recycling. *Materials Horizons* **2020**, *7* (10), 2479–2486. <https://doi.org/10.1039/D0MH01085E>.
- (4) Zhang, J.; Lin, G.; Vaidya, U.; Wang, H. Past, Present and Future Prospective of Global Carbon Fibre Composite Developments and Applications. *Composites Part B: Engineering* **2023**, *250*, 110463. <https://doi.org/10.1016/j.compositesb.2022.110463>.



- (5) Holmes, M. Global Carbon Fibre Market Remains on Upward Trend. *Reinforced Plastics* **2014**, *58* (6), 38–45. [https://doi.org/10.1016/S0034-3617\(14\)70251-6](https://doi.org/10.1016/S0034-3617(14)70251-6).
- (6) Pakdel, E.; Kashi, S.; Varley, R.; Wang, X. Recent Progress in Recycling Carbon Fibre Reinforced Composites and Dry Carbon Fibre Wastes. *Resources, Conservation and Recycling* **2021**, *166* (November 2020), 105340. <https://doi.org/10.1016/j.resconrec.2020.105340>.
- (7) Ma, X.; Xu, H.; Xu, Z.; Jiang, Y.; Chen, S.; Cheng, J.; Zhang, J.; Miao, M.; Zhang, D. Closed-Loop Recycling of Both Resin and Fiber from High-Performance Thermoset Epoxy/Carbon Fiber Composites. *ACS Macro Letters* **2021**, *10* (9), 1113–1118. <https://doi.org/10.1021/acsmacrolett.1c00437>.
- (8) Sardon, H.; Li, Z.-C. Introduction to Plastics in a Circular Economy. *Polymer Chemistry* **2020**, *11* (30), 4828–4829. <https://doi.org/10.1039/D0PY90117B>.
- (9) Sobkowicz, M. J. Polymer Design for the Circular Economy. *Science* **2021**, *374* (6567), 540–540. <https://doi.org/10.1126/science.abm2306>.
- (10) Beauson, J.; Laurent, A.; Rudolph, D. P.; Pagh Jensen, J. The Complex End-of-Life of Wind Turbine Blades: A Review of the European Context. *Renewable and Sustainable Energy Reviews* **2022**, *155*, 111847. <https://doi.org/10.1016/j.rser.2021.111847>.
- (11) European Union. Municipal Waste Treatment in the EU in 2018 <https://eswet.eu/documents/municipal-waste-treatment-in-the-eu-in-2018/> (accessed Mar 1, 2023).
- (12) La loi anti-gaspillage pour une économie circulaire <https://www.ecologie.gouv.fr/loi-anti-gaspillage-economie-circulaire> (accessed Mar 1, 2023).
- (13) Energy, E. T. & I. P. on W. An overview of composite recycling in the wind energy industry <https://etipwind.eu/files/reports/ETIPWind-How-wind-is-going-circular-blade-recycling.pdf>.
- (14) Yuan, Y.; Sun, Y.; Yan, S.; Zhao, J.; Liu, S.; Zhang, M.; Zheng, X.; Jia, L. Multiply Fully Recyclable Carbon Fibre Reinforced Heat-Resistant Covalent Thermosetting Advanced Composites. *Nature Communications* **2017**, *8* (1), 14657. <https://doi.org/10.1038/ncomms14657>.
- (15) Rebizant, V.; Venet, A.-S.; Tournilhac, F.; Girard-Reydet, E.; Navarro, C.; Pascault, J.-P.; Leibler, L. Chemistry and Mechanical Properties of Epoxy-Based Thermosets

- Reinforced by Reactive and Nonreactive SBMX Block Copolymers. *Macromolecules* **2004**, 37 (21), 8017–8027. <https://doi.org/10.1021/ma0490754>.
- (16) Ma, S.; Webster, D. C. Degradable Thermosets Based on Labile Bonds or Linkages: A Review. *Progress in Polymer Science* **2018**, 76, 65–110. <https://doi.org/10.1016/j.progpolymsci.2017.07.008>.
- (17) Chen, J.; Ober, C. K.; Poliks, M. D.; Zhang, Y.; Wiesner, U.; Cohen, C. Controlled Degradation of Epoxy Networks: Analysis of Crosslink Density and Glass Transition Temperature Changes in Thermally Reworkable Thermosets. *Polymer* **2004**, 45 (6), 1939–1950. <https://doi.org/10.1016/j.polymer.2004.01.011>.
- (18) Palmer, J.; Ghita, O. R.; Savage, L.; Evans, K. E. Successful Closed-Loop Recycling of Thermoset Composites. *Composites Part A: Applied Science and Manufacturing* **2009**, 40 (4), 490–498. <https://doi.org/10.1016/j.compositesa.2009.02.002>.
- (19) Fortman, D. J.; Brutman, J. P.; De Hoe, G. X.; Snyder, R. L.; Dichtel, W. R.; Hillmyer, M. A. Approaches to Sustainable and Continually Recyclable Cross-Linked Polymers. *ACS Sustainable Chemistry and Engineering* **2018**, 6 (9), 11145–11159. <https://doi.org/10.1021/acssuschemeng.8b02355>.
- (20) Pickering, S. J. Recycling Technologies for Thermoset Composite Materials-Current Status. *Composites Part A: Applied Science and Manufacturing* **2006**, 37 (8), 1206–1215. <https://doi.org/10.1016/j.compositesa.2005.05.030>.
- (21) Torres, A. Recycling by Pyrolysis of Thermoset Composites: Characteristics of the Liquid and Gaseous Fuels Obtained. *Fuel* **2000**, 79 (8), 897–902. [https://doi.org/10.1016/S0016-2361\(99\)00220-3](https://doi.org/10.1016/S0016-2361(99)00220-3).
- (22) Xue, X.; Liu, S.-Y. Y.; Zhang, Z.-Y. Y.; Wang, Q.-Z. Z.; Xiao, C.-Z. Z. A Technology Review of Recycling Methods for Fiber-Reinforced Thermosets. *Journal of Reinforced Plastics and Composites* **2022**, 41 (11–12), 459–480. <https://doi.org/10.1177/07316844211055208>.
- (23) Meyer, L. O.; Schulte, K.; Grove-Nielsen, E. CFRP-Recycling Following a Pyrolysis Route: Process Optimization and Potentials. *Journal of Composite Materials* **2009**, 43 (9), 1121–1132. <https://doi.org/10.1177/0021998308097737>.
- (24) Liu, Y.; Wang, B.; Ma, S.; Yu, T.; Xu, X.; Li, Q.; Wang, S.; Han, Y.; Yu, Z.; Zhu, J. Catalyst-Free Malleable, Degradable, Bio-Based Epoxy Thermosets and Its Application in Recyclable Carbon Fiber Composites. *Composites Part B: Engineering* **2021**, 211 (1219), 108654. <https://doi.org/10.1016/j.compositesb.2021.108654>.

- (25) Lopez-Urionabarrenechea, A.; Gastelu, N.; Acha, E.; Caballero, B. M.; Orue, A.; Jiménez-Suárez, A.; Prolongo, S. G.; de Marco, I. Reclamation of Carbon Fibers and Added-Value Gases in a Pyrolysis-Based Composites Recycling Process. *Journal of Cleaner Production* **2020**, 273, 123173. <https://doi.org/10.1016/j.jclepro.2020.123173>.
- (26) Shen, M.; Cao, H.; Robertson, M. L. Hydrolysis and Solvolysis as Benign Routes for the End-of-Life Management of Thermoset Polymer Waste. *Annual Review of Chemical and Biomolecular Engineering* **2020**, 11 (1), 183–201. <https://doi.org/10.1146/annurev-chembioeng-120919-012253>.
- (27) Wang, B.; Wang, Y.; Du, S.; Zhu, J.; Ma, S. Upcycling of Thermosetting Polymers into High-Value Materials. *Materials Horizons* **2023**, 10 (1), 41–51. <https://doi.org/10.1039/D2MH01128J>.
- (28) Xu, N.; Kim, S.; Liu, Y.; Adraro, Y. A.; Li, Z.; Hu, J.; Liu, L.; Hu, Z.; Huang, Y. Facile Preparation of Rapidly Recyclable Tough Thermosetting Composites via Cross-Linking Structure Regulation. *Polymer* **2020**, 189 (September 2019), 122163. <https://doi.org/10.1016/j.polymer.2020.122163>.
- (29) Feng, H.; Jin, D.; Wang, S.; Hu, J.; Dai, J.; Yan, S.; Liu, X. Design of Controllable Degradable Epoxy Resin: High Performance and Feasible Upcycling. *Polymers for Advanced Technologies* **2022**, 33 (5), 1665–1676. <https://doi.org/10.1002/pat.5629>.
- (30) Wang, S.; Xing, X.; Zhang, X.; Wang, X.; Jing, X. Room-Temperature Fully Recyclable Carbon Fibre Reinforced Phenolic Composites through Dynamic Covalent Boronic Ester Bonds. *Journal of Materials Chemistry A* **2018**, 6 (23), 10868–10878. <https://doi.org/10.1039/C8TA01801D>.
- (31) Perli, G.; Demir, B.; Pruvost, S.; Duchet-Rumeau, J.; Baudoux, J.; Livi, S. From the Design of Multifunctional Degradable Epoxy Thermosets to Their End of Life. *ACS Sustainable Chemistry & Engineering* **2022**, 10 (33), 11004–11015. <https://doi.org/10.1021/acssuschemeng.2c03326>.
- (32) Perli, G.; Wylie, L.; Demir, B.; Gerard, J.; P, A. H.; Gomes, M. C.; Duchet-rumeau, J.; Livi, S. From the Design of Novel Tri- and Tetra-Epoxidized Ionic Liquid Monomers to the End-of-Life of Multifunctional Degradable Epoxy Thermosets. **2022**. <https://doi.org/10.1021/acssuschemeng.2c04499>.
- (33) Jeevi, G.; Nayak, S. K.; Abdul Kader, M. Review on Adhesive Joints and Their Application in Hybrid Composite Structures. *Journal of Adhesion Science and*

- Technology* **2019**, *33* (14), 1497–1520.  
<https://doi.org/10.1080/01694243.2018.1543528>.
- (34) Sanghvi, M. R.; Tambare, O. H.; More, A. P. Performance of Various Fillers in Adhesives Applications: A Review. *Polymer Bulletin* **2022**, *79* (12), 10491–10553.  
<https://doi.org/10.1007/s00289-021-04022-z>.
- (35) Nasreen, A.; Shaker, K.; Nawab, Y. Effect of Surface Treatments on Metal–Composite Adhesive Bonding for High-Performance Structures: An Overview. *Composite Interfaces* **2021**, *28* (12), 1221–1256.  
<https://doi.org/10.1080/09276440.2020.1870192>.
- (36) Stokes, V. K. Joining Methods for Plastics and Plastic Composites: An Overview. *Polymer Engineering and Science* **1989**, *29* (19), 1310–1324.  
<https://doi.org/10.1002/pen.760291903>.
- (37) Goss, B. Bonding Glass and Other Substrates with UV Curing Adhesives. *International Journal of Adhesion and Adhesives* **2002**, *22* (5), 405–408.  
[https://doi.org/10.1016/S0143-7496\(02\)00022-2](https://doi.org/10.1016/S0143-7496(02)00022-2).
- (38) Li, J.; Luo, R.; Bi, Y.; Xiang, Q.; Lin, C.; Zhang, Y.; An, N. The Preparation and Performance of Short Carbon Fiber Reinforced Adhesive for Bonding Carbon/Carbon Composites. *Carbon* **2008**, *46* (14), 1957–1965.  
<https://doi.org/10.1016/j.carbon.2008.08.011>.
- (39) Yousefpour, A.; Hojjati, M.; Immarigeon, J.-P. Fusion Bonding/Welding of Thermoplastic Composites. *Journal of Thermoplastic Composite Materials* **2004**, *17* (4), 303–341. <https://doi.org/10.1177/0892705704045187>.
- (40) Karakaya, N.; Papila, M.; Özkoç, G. Effects of Hot Melt Adhesives on the Interfacial Properties of Overmolded Hybrid Structures of Polyamide-6 on Continuous Carbon Fiber/Epoxy Composites. *Composites Part A: Applied Science and Manufacturing* **2020**, *139*, 106106. <https://doi.org/10.1016/j.compositesa.2020.106106>.
- (41) An, X.; Ding, Y.; Xu, Y.; Zhu, J.; Wei, C.; Pan, X. Epoxy Resin with Exchangeable Diselenide Crosslinks to Obtain Reprocessable, Repairable and Recyclable Fiber-Reinforced Thermoset Composites. *Reactive and Functional Polymers* **2022**, *172*, 105189. <https://doi.org/10.1016/j.reactfunctpolym.2022.105189>.
- (42) Bayat, S.; Moini Jazani, O.; Molla-Abbasi, P.; Jouyandeh, M.; Saeb, M. R. Thin Films of Epoxy Adhesives Containing Recycled Polymers and Graphene Oxide Nanoflakes for

- Metal/Polymer Composite Interface. *Progress in Organic Coatings* **2019**, *136*, 105201. <https://doi.org/10.1016/j.porgcoat.2019.06.047>.
- (43) Pascault, Jean-Pierre; Williams, R. Epoxy Polymers: New Materials and Innovations. In *Epoxy Polymers: New Materials and Innovations*; Wiley-VCH, Weinheim, Germany, 2009; pp 25–73.
- (44) Post, W.; Susa, A.; Blaauw, R.; Molenveld, K.; Knoop, R. J. I. A Review on the Potential and Limitations of Recyclable Thermosets for Structural Applications. *Polymer Reviews* **2020**, *60* (2), 359–388. <https://doi.org/10.1080/15583724.2019.1673406>.
- (45) Yang, X.; Ke, Y.; Chen, Q.; Shen, L.; Xue, J.; Quirino, R. L.; Yan, Z.; Luo, Y.; Zhang, C. Efficient Transformation of Renewable Vanillin into Reprocessable, Acid-Degradable and Flame Retardant Polyimide Vitrimers. *Journal of Cleaner Production* **2022**, *333* (June 2021), 130043. <https://doi.org/10.1016/j.jclepro.2021.130043>.
- (46) Khosravi, E.; Musa, O. M. Thermally Degradable Thermosetting Materials. *European Polymer Journal* **2011**, *47* (4), 465–473. <https://doi.org/10.1016/j.eurpolymj.2010.09.023>.
- (47) Chen, X.; Chen, S.; Xu, Z.; Zhang, J.; Miao, M.; Zhang, D. Degradable and Recyclable Bio-Based Thermoset Epoxy Resins. *Green Chemistry* **2020**, *22* (13), 4187–4198. <https://doi.org/10.1039/D0GC01250E>.
- (48) Halley, P. J.; Mackay, M. E. Chemorheology of Thermosets: An Overview. *Polymer Engineering & Science* **1996**, *36* (5), 593–609. <https://doi.org/10.1002/pen.10447>.
- (49) Dkier, M.; Yousfi, M.; Lamnawar, K.; Maazouz, A. Chemo-Rheological Studies and Monitoring of High-Tg Reactive Polyphthalamides towards a Fast Innovative RTM Processing of Fiber-Reinforced Thermoplastic Composites. *European Polymer Journal* **2019**, *120*, 109227. <https://doi.org/10.1016/j.eurpolymj.2019.109227>.
- (50) El Omari, Y.; Yousfi, M.; Duchet-Rumeau, J.; Maazouz, A. Interfacial Rheology for Probing the In-Situ Chemical Reaction at Interfaces of Molten Polymer Systems. *Materials Today Communications* **2023**, *35*, 105640. <https://doi.org/10.1016/j.mtcomm.2023.105640>.
- (51) Gillham, J. K.; Benci, J. A.; Noshay, A. Isothermal Transitions of a Thermosetting System. *Journal of Applied Polymer Science* **1974**, *18* (4), 951–961. <https://doi.org/10.1002/app.1974.070180401>.
- (52) Nguyen, T. K. L.; Livi, S.; Pruvost, S.; Soares, B. G.; Duchet-Rumeau, J. Ionic Liquids as Reactive Additives for the Preparation and Modification of Epoxy Networks. *Journal*

- of Polymer Science Part A: Polymer Chemistry* **2014**, *8*, 252–285.  
<https://doi.org/10.1002/pola.27420>.
- (53) Mąka, H.; Sychaj, T.; Zenker, M. High Performance Epoxy Composites Cured with Ionic Liquids. *Journal of Industrial and Engineering Chemistry* **2015**, *31*, 192–198.  
<https://doi.org/10.1016/j.jiec.2015.06.023>.
- (54) Mąka, H.; Sychaj, T.; Pilawka, R. Epoxy Resin/Ionic Liquid Systems: The Influence of Imidazolium Cation Size and Anion Type on Reactivity and Thermomechanical Properties. *Industrial & Engineering Chemistry Research* **2012**, *51* (14), 5197–5206.  
<https://doi.org/10.1021/ie202321j>.
- (55) Silva, A. A.; Livi, S.; Netto, D. B.; Soares, B. G.; Duchet, J.; Gérard, J.-F. F. New Epoxy Systems Based on Ionic Liquid. *Polymer* **2013**, *54* (8), 2123–2129.  
<https://doi.org/10.1016/j.polymer.2013.02.021>.
- (56) Livi, S.; Silva, A. A.; Thimont, Y.; Nguyen, T. K. L.; Soares, B. G.; Gérard, J.-F.; Duchet-Rumeau, J. Nanostructured Thermosets from Ionic Liquid Building Block–Epoxy Prepolymer Mixtures. *RSC Adv.* **2014**, *4* (53), 28099–28106.  
<https://doi.org/10.1039/C4RA03643C>.
- (57) Leclère, M.; Bernard, L.; Livi, S.; Bardet, M.; Guillermo, A.; Picard, L.; Duchet-Rumeau, J. Gelled Electrolyte Containing Phosphonium Ionic Liquids for Lithium-Ion Batteries. *Nanomaterials* **2018**, *8* (6), 435–500. <https://doi.org/10.3390/nano8060435>.
- (58) Nguyen, T. K. L.; Livi, S.; Soares, B. G.; Pruvost, S.; Duchet-Rumeau, J.; Gérard, J.-F. F. Ionic Liquids: A New Route for the Design of Epoxy Networks. *ACS Sustainable Chemistry & Engineering* **2016**, *4* (2), 481–490.  
<https://doi.org/10.1021/acssuschemeng.5b00953>.
- (59) Radchenko, A. V.; Chabane, H.; Demir, B.; Searles, D. J.; Duchet-Rumeau, J.; Gérard, J.-F. F.; Baudoux, J.; Livi, S. New Epoxy Thermosets Derived from a Bisimidazolium Ionic Liquid Monomer: An Experimental and Modeling Investigation. *ACS Sustainable Chemistry and Engineering* **2020**, *8* (32), 12208–12221.  
<https://doi.org/10.1021/acssuschemeng.0c03832>.
- (60) Livi, S.; Baudoux, J.; Gérard, J.; Duchet-Rumeau, J. Ionic Liquids: A Versatile Platform for the Design of a Multifunctional Epoxy Networks 2.0 Generation. *Progress in Polymer Science* **2022**, *132*, 101581.  
<https://doi.org/10.1016/j.progpolymsci.2022.101581>.

- (61) Garcia, F. G.; Soares, B. G.; Pita, V. J. R. R.; Sánchez, R.; Rieumont, J.; Rangel, A. Mechanical Properties of Epoxy Networks Based on DGEBA and Aliphatic Amines. *Journal of Applied Polymer Science* **2007**, *106* (3), 2047–2055. <https://doi.org/10.1002/app.24895>.
- (62) Urbaczewski-Espuche, E.; Galy, J.; Gerard, J.-F.; Pascault, J.-P.; Sautereau, H. Influence of Chain Flexibility and Crosslink Density on Mechanical Properties of Epoxy/Amine Networks. *Polymer Engineering and Science* **1991**, *31* (22), 1572–1580. <https://doi.org/10.1002/pen.760312204>.
- (63) Wanghofer, F.; Wolfberger, A.; Wolfahrt, M.; Schlögl, S. Cross-Linking and Evaluation of the Thermo-Mechanical Behavior of Epoxy Based Poly(Ionic Liquid) Thermosets. *Polymers* **2021**, *13* (22), 3914. <https://doi.org/10.3390/polym13223914>.
- (64) El Gouri, M.; El Bachiri, A.; Hegazi, S. E.; Rafik, M.; El Harfi, A. Thermal Degradation of a Reactive Flame Retardant Based on Cyclotriphosphazene and Its Blend with DGEBA Epoxy Resin. *Polymer Degradation and Stability* **2009**, *94* (11), 2101–2106. <https://doi.org/10.1016/j.polymdegradstab.2009.08.009>.
- (65) Kuang, X.; Shi, Q.; Zhou, Y.; Zhao, Z.; Wang, T.; Qi, H. J. Dissolution of Epoxy Thermosets: Via Mild Alcoholysis: The Mechanism and Kinetics Study. *RSC Advances* **2018**, *8* (3), 1493–1502. <https://doi.org/10.1039/c7ra12787a>.
- (66) Pérez, R. L.; Ayala, C. E.; Opiri, M. M.; Ezzir, A.; Li, G.; Warner, I. M. Recycling Thermoset Epoxy Resin Using Alkyl-Methyl-Imidazolium Ionic Liquids as Green Solvents. *ACS Applied Polymer Materials* **2021**, *3* (11), 5588–5595. <https://doi.org/10.1021/acsapm.1c00896>.
- (67) Ghafoor, B.; Schrekker, H. S.; Morais, J.; Campos, S. Surface Modification of Carbon Fiber with Imidazolium Ionic Liquids. *Composite Interfaces* **2022**, *29* (8), 915–928. <https://doi.org/10.1080/09276440.2022.2029310>.
- (68) Voronina, S. Y.; Shalygina, T. A.; Voronchikhin, V. D.; Vlasov, A. Y.; Ovchinnikov, A. N.; Grotskaya, N. N. Data for Determining the Surface Properties of Carbon Fiber in Contact Interaction with Polymeric Binders. *Data in Brief* **2021**, *35*, 106847. <https://doi.org/10.1016/j.dib.2021.106847>.
- (69) França, J. M. P.; Nieto de Castro, C. A.; Pádua, A. A. H. Molecular Interactions and Thermal Transport in Ionic Liquids with Carbon Nanomaterials. *Physical Chemistry Chemical Physics* **2017**, *19* (26), 17075–17087. <https://doi.org/10.1039/C7CP01952A>.

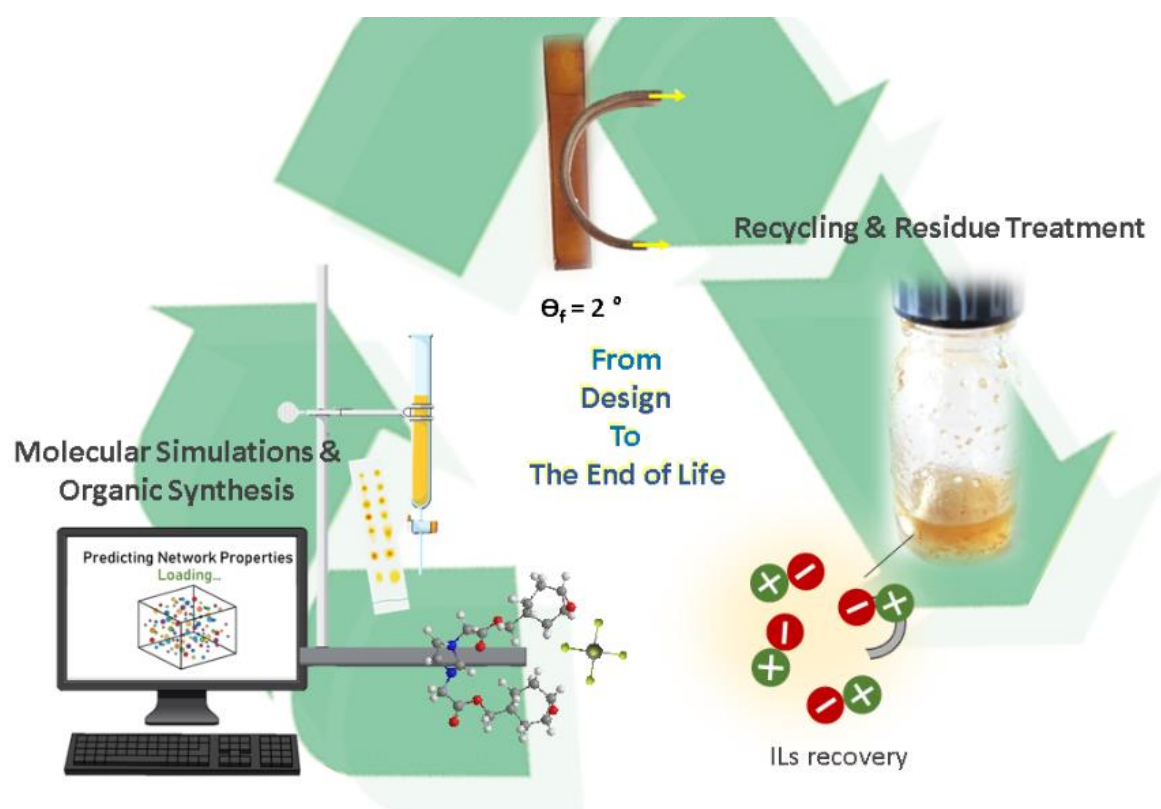
- (70) Yang, Y.-K.; He, C.-E.; Peng, R.-G.; Baji, A.; Du, X.-S.; Huang, Y.-L.; Xie, X.-L.; Mai, Y.-W. Non-Covalently Modified Graphene Sheets by Imidazolium Ionic Liquids for Multifunctional Polymer Nanocomposites. *Journal of Materials Chemistry* **2012**, 22 (12), 5666. <https://doi.org/10.1039/c2jm16006d>.
- (71) Eyckens, D. J.; Servinis, L.; Scheffler, C.; Wölfel, E.; Demir, B.; Walsh, T. R.; Henderson, L. C. Synergistic Interfacial Effects of Ionic Liquids as Sizing Agents and Surface Modified Carbon Fibers. *Journal of Materials Chemistry A* **2018**, 6 (10), 4504–4514. <https://doi.org/10.1039/C7TA10516A>.
- (72) Pensado, A. S.; Malberg, F.; Gomes, M. F. C.; Pádua, A. A. H.; Fernández, J.; Kirchner, B. Interactions and Structure of Ionic Liquids on Graphene and Carbon Nanotubes Surfaces. *RSC Adv.* **2014**, 4 (35), 18017–18024. <https://doi.org/10.1039/C4RA02059F>.
- (73) Jiang, Y.; Wang, S.; Dong, W.; Kaneko, T.; Chen, M.; Shi, D. High-Strength, Degradable and Recyclable Epoxy Resin Based on Imine Bonds for Its Carbon-Fiber-Reinforced Composites. *Materials* **2023**, 16 (4), 1604. <https://doi.org/10.3390/ma16041604>.
- (74) Lopes Pereira, E. C.; Farias da Silva, J. M.; Jesus, R. B.; Soares, B. G.; Livi, S. Bronsted Acidic Ionic Liquids: New Transesterification Agents for the Compatibilization of Polylactide/Ethylene-Co-Vinyl Acetate Blends. *European Polymer Journal* **2017**, 97, 104–111. <https://doi.org/10.1016/j.eurpolymj.2017.10.003>.
- (75) Zhang, J.; Wang, W.; Zhang, Y.; Wei, Q.; Han, F.; Dong, S.; Liu, D.; Zhang, S. Small-Molecule Ionic Liquid-Based Adhesive with Strong Room-Temperature Adhesion Promoted by Electrostatic Interaction. *Nature Communications* **2022**, 13 (1), 5214. <https://doi.org/10.1038/s41467-022-32997-4>.
- (76) Prolongo, S. G.; Del Rosario, G.; Ureña, A. Comparative Study on the Adhesive Properties of Different Epoxy Resins. *International Journal of Adhesion and Adhesives* **2006**, 26 (3), 125–132. <https://doi.org/10.1016/j.ijadhadh.2005.02.004>.
- (77) Song, F.; Li, Z.; Jia, P.; Zhang, M.; Bo, C.; Feng, G.; Hu, L.; Zhou, Y. Tunable “Soft and Stiff”, Self-Healing, Recyclable, Thermadapt Shape Memory Biomass Polymers Based on Multiple Hydrogen Bonds and Dynamic Imine Bonds. *Journal of Materials Chemistry A* **2019**, 7 (21), 13400–13410. <https://doi.org/10.1039/C9TA03872H>.
- (78) Xu, S.; Lamm, M. E.; Rahman, M. A.; Zhang, X.; Zhu, T.; Zhao, Z.; Tang, C. Renewable Atom-Efficient Polyesters and Thermosetting Resins Derived from High Oleic



- Soybean Oil. *Green Chemistry* **2018**, 20 (5), 1106–1112.  
<https://doi.org/10.1039/c7gc03774k>.
- (79) Yuan, L.; Wang, Z.; Trenor, N. M.; Tang, C. Amidation of Triglycerides by Amino Alcohols and Their Impact on Plant Oil-Derived Polymers. *Polymer Chemistry* **2016**, 7 (16), 2790–2798. <https://doi.org/10.1039/C6PY00048G>.

# 05

## Activated Cycloaliphatic Epoxidized Ionic Liquids as New Versatile Monomers for the Construction of Multifunctional Degradable Thermosets



## **1. Liquides ioniques époxydés cycloaliphatiques activés comme nouveaux monomères pour le développement de thermodurcissables multifonctionnels dégradables**

### **1.1. Résumé**

Le développement de thermodurcissables époxy multifonctionnels, qui répondent aux exigences du développement durable en créant de nouvelles architectures macromoléculaires, est un vrai défi. Un liquide ionique bis-imidazolium cycloaliphatique époxydé à température ambiante (CEIL) a été synthétisé avec succès à l'échelle du multigramme. Ce monomère a été utilisé comme brique moléculaire pour former différents réseaux. En s'appuyant sur plusieurs simulations informatiques, trois réseaux époxy ont été développés par polymérisation cationique en utilisant le CEIL et l'Epoxycyclohexylméthyl-3',4'-époxycyclohexane carboxylate (ECC) en présence d'un amorceur thermoacide. Les réseaux à base de CEIL ont présenté des stabilités thermiques plus élevées ( $> 450^{\circ}\text{C}$ ), de bonnes performances mécaniques et un comportement de mémoire de forme. L'incorporation de cette brique moléculaire ionique dans l'architecture des réseaux, à 50% ou 100%, a permis d'obtenir une dégradabilité complète des polymères thermodurcissables dans des conditions douces et de répondre au concept *design to degrade*.

**Mots-clés :** conception moléculaire, monomère liquide ionique, simulations dynamiques moléculaires, comportement de mémoire de forme et conception pour la dégradation.

## 2. Activated Cycloaliphatic Epoxidized Ionic Liquids as New Versatile Monomers for the Construction of Multifunctional Degradable Thermosets

### 2.1. Abstract

Creating new macromolecular architectures for multifunctional epoxy thermosets that satisfy sustainable development demands poses a significant challenge. Herein, a bis-imidazolium cycloaliphatic epoxidized ionic liquid (CEIL) was successfully synthesized at a multi-gram scale and used as a molecular brick platform to build various thermosets. Thus, three epoxy networks were developed by cationic polymerization using CEIL and 3,4-Epoxy-cyclohexylmethyl-3',4'-epoxycyclohexane carboxylate (ECC) in the presence of a thermoacid initiator. The CEIL-based networks presented higher thermal stabilities ( $> 450^{\circ}\text{C}$ ), and great mechanical performances combined with a promising shape memory behavior. Most importantly, incorporating CEIL monomer into the networks (50 or 100%) addresses the concept *design to degrade* inducing degradability under mild conditions (up to 99.4% of p-CEIL dissolution in 4.5 h).

**Keywords:** Molecular Designing, Ionic Liquid Monomer, Molecular Dynamic Simulations, Shape Memory Behavior, Design for Degradation

### 3. Introduction

Designing smart and multifunctional-dedicated epoxy thermosets that meet the requirements of the circular economy, *i.e.* to be durable, reusable, and recyclable, is an urgent need.<sup>1-4</sup> Scientists must thus propose through a '*Functional Materials by Design*' approach the development of molecular brick platforms to integrate the polymer matrices and afford the networks the target functions.<sup>4-9</sup>

Simultaneously, the end-of-life of these thermoset materials should be considered through the concept of *design to degrade*.<sup>10-12</sup> The controlled degradation or depolymerization of these networks yields oligomers or monomers that can be potentially used to be re-polymerized or re-incorporated into thermosetting matrices.<sup>1,4,13-15</sup>

Due to their outstanding properties, such as excellent insulation, tunable mechanical performances, and high chemical and thermal resistance, thermoset epoxy resins (TERs) are widely used and represent one of the most important thermosetting polymers.<sup>16,17</sup> Among the commercially available TERs, diglycidyl ether bisphenol A (DGEBA) is the most commonly used for automotive, aircraft, coating and electronic applications.<sup>18-20</sup> Despite its advantages, one of the starting precursors of DGEBA, namely bisphenol A is reported as an estrogen and androgen receptor antagonist and represents a risk for humans and the environment.<sup>21-25</sup>

In this context, cycloaliphatic epoxy resins emerge as an attractive alternative to DGEBA-derived polymers, exhibiting several advantages such as UV resistance,<sup>22</sup> higher hydrophobicity,<sup>25</sup> and electrical resistivity.<sup>26</sup> Moreover, cycloaliphatic epoxies are usually more reactive than DGEBA monomers due to their higher ring strain and nucleophilicity,<sup>28</sup> which enables the development of epoxy networks without employing hardeners.<sup>29,30</sup> The polymerization of cycloaliphatic epoxies can occur by thermal- or UV-initiation, allowing their application through non-conventional processing methods, specifically 3D and 4D printing technologies.<sup>31-33</sup>

Unlike thermoplastics, thermosetting polymers present high crosslinking degrees, providing exceptional physical and chemical resistance and making them particularly hard to recycle through conventional methodologies.<sup>12,34</sup>

The significant amount of epoxy material waste that is landfilled or pyrolyzed stresses the need to develop recyclable or degradable epoxy thermosets.<sup>35-37</sup> To address the challenge of recycling thermosetting materials, considerable research has been undertaken, including developing re-processable crosslinked polymers<sup>38-44</sup> and using depolymerizing and degradation methods.<sup>13,45,46</sup>

Chalker and co-authors have been developing dynamic and reprocessable polymers based on the chemistry of inverse vulcanization that explores the reversible nature of S-S bonds. In recent work, they elucidated the mechanism involved in the S-S bond exchange, revealing that the S-S metathesis can take place rapidly at room temperature in the presence of nucleophiles.<sup>44</sup> Alike, Hasell *et al.* built a range of crosslinked sulfur polymers with increased tensile elongation and toughness. Interestingly, the resulting crosslinked sulfur polymers revealed selective solubility in polar solvents, which can be fully re-crosslinked after evaporating the solvent due to the high sulfur contents in the polymer networks. Although the authors improved the mechanical properties, efficient thermal recycling features typical of inverse vulcanized materials were preserved.<sup>42</sup>

Okajima and coworkers, pursuing to depolymerize carbon fiber epoxy composites, have employed supercritical acetone at 350 °C under 14 MPa.<sup>45</sup> In another study, Qi and co-authors proposed a method to depolymerize anhydride-epoxy networks employing an organic catalyst. They achieved 95% of chemical dissolution at 170 °C under ambient pressure and claimed the use of the decomposed epoxy oligomers to build new TERs.<sup>47</sup> Further, Liu *et al.* fully dissolved TERs employing a nitric acid solution associated with ultrasound-microwave. These authors applied the degradation products to dip coat a melamine foam that exhibited excellent water/oil separation performance.<sup>13</sup> Such recycling methodologies present several drawbacks like operating under elevated pressures,<sup>45</sup> the need for expensive catalysts,<sup>14,47</sup> and the use of highly hazardous chemical products.<sup>46,48</sup>

The molecular design of cycloaliphatic epoxidized ionic liquids (ILs) is a potential answer to create new and degradable multifunctional-dedicated TERs. The numerous cation-anion combinations<sup>49</sup> and the unique properties of ILs,<sup>50</sup> such as high thermal stability,<sup>51</sup> recyclability,<sup>49</sup> tailored viscosity,<sup>52</sup> and high ionic conductivity,<sup>53,54</sup> make them promising precursors for the development of a library of new generation TERs.

Thus far, very few studies have exploited this opportunity.<sup>55–60</sup> Gin *et al.* have developed an epichlorohydrin-based route to synthesize diepoxidized imidazolium monomers that were polymerized with amine hardeners to result in membranes for gas separation.<sup>55</sup> Employing a similar route, an epoxidized IL was synthesized and incorporated into carbon fiber composites to tune cryogenic tanks' hydrogen permeability and mechanical properties.<sup>58</sup> Other authors have also exploited epoxidized ILs based on ammonium or triazolium to build low  $T_g$  materials with enhanced ionic conductivity.<sup>61,62</sup> More recently, our group reported for the first time a more sustainable strategy to synthesize ILs bearing oxirane moieties without using highly toxic reagents like epichlorohydrin or bisphenol A deriva-

tives.<sup>51</sup> In successive work, we designed different epoxy-amine coatings based on diepoxidized IL monomers. These films exhibited hydrophobic and antibacterial behavior and thermomechanical properties comparable to DGEBA-based materials.<sup>63</sup> These first works were mainly dedicated to developing synthetic procedures to obtain different IL monomers, including few contributions in which the networks were built and characterized. Herein, we endeavor to continue evolving this research, now employing a computational-assisted approach to develop a novel cycloaliphatic epoxidized IL monomer that, when polymerized, results in multifunctional networks that degrade under mild conditions to regenerate ILs.

Overall, developing next-generation TERs with adaptative properties, excellent thermal stability, outstanding mechanical performance, and full degradability under mild conditions is a compelling circular economy demand.<sup>11,64,65</sup> It is worth noting that the circular economy does not limit itself to recycling materials but encourages maximum use of each material during its lifecycle. Therefore, rationally designing polymers that, once degraded, generate ILs that can be re-incorporated into the materials conveys reducing thermoset waste to a minimum since these materials are kept in the economy wherever possible. These novel materials will hopefully, in the future, interrupt the conventional, linear economy model, which is established on a take-make-consume-throw-away pattern.

## **4. Materials and Methods**

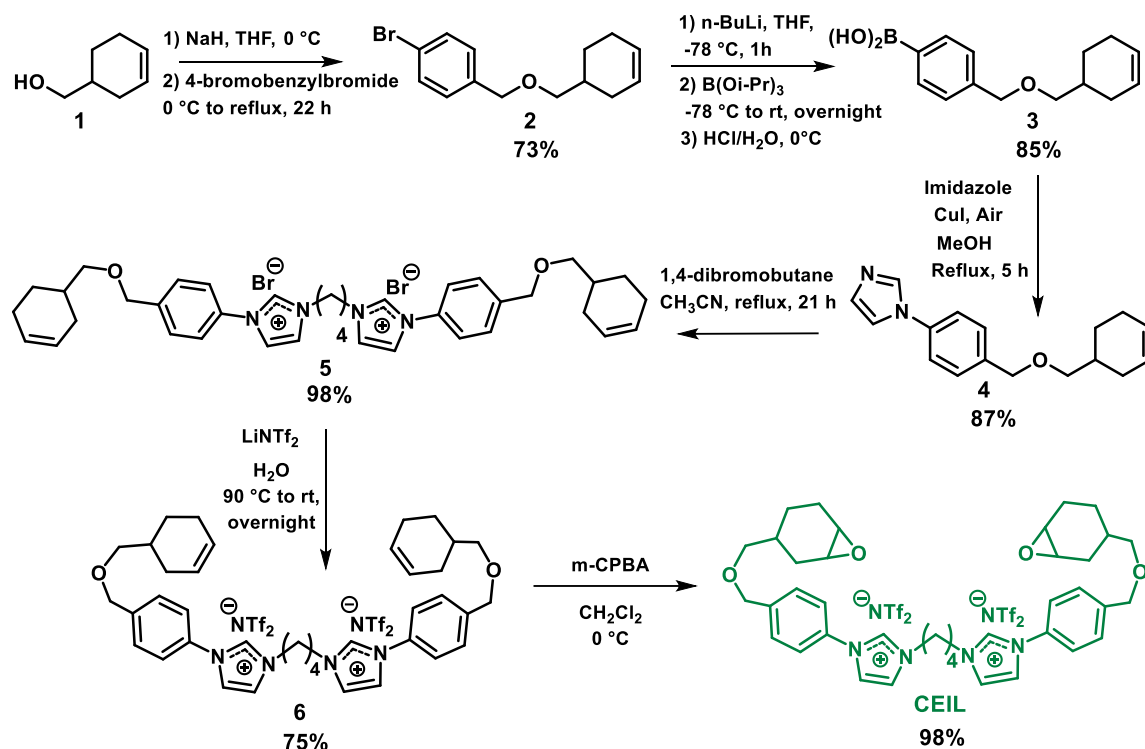
### **4.1. Materials**

All chemical reagents, including 3,4-Epoxy cyclohexylmethyl-3',4'-epoxycyclohexane carboxylate (ECC) were purchased from Sigma Aldrich, and used without further purification. All the solvents, including anhydrous ones were purchased from Carlos Erba and used as received. The thermal initiator, diaryliodonium hexafluoroantimonate, denoted Sylanto-7MS (S7MS) was kindly provided by Synthos S.A.

### **4.2. Synthesis of Cycloaliphatic Epoxidized Ionic Liquid (CEIL)**

The cycloaliphatic epoxidized IL-based monomer was synthesized in a six-step route, according to a methodology developed by our research group. The synthetic route starts with a cycloaliphatic alcohol **1** reacting with *p*-bromobenzyl bromide, by a conventional nucleophilic substitution. Then, the bromide intermediate **2** was converted to a boronic acid derivative **3** that reacted by a Chan-Lam coupling with imidazole to yield **4**. Compound **4** was reacted with 1,4-dibromo butane to originate a bis-imidazolium bromide salt **5**. Aiming to increase the hydrophobic character and the thermal stability behavior of the IL-based monomer, an anionic metathesis step with LiNTf<sub>2</sub> was carried out to provide **6**. Finally, the alkenes' oxidation was performed in the presence of *m*CPBA (2.2 eq.) at 0 °C to

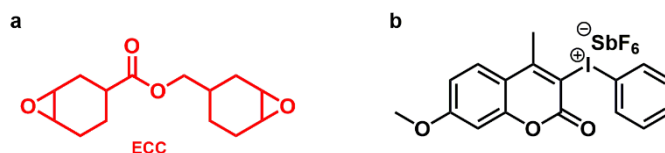
obtain a room temperature **CEIL (Scheme V-1)**. All synthesis details are provided in **Appendix III**.



**Scheme V-1.** Synthetic route of Cycloaliphatic Epoxidized Ionic Liquid monomer (CEIL)

#### 4.3. Epoxy Network Preparation

To prepare epoxy networks at different weight ratios (100:0, 50:50, 0:100), two cycloaliphatic epoxy monomers were employed, namely, CEIL and ECC (**Scheme V-1** and **Fig. V-1a**). The epoxy monomers were combined in the corresponding percentage and completely homogenized with the thermal initiator in the proportion of 2% by weight at room temperature (**Fig. V-1b**). Then, the blends were placed into the silicon template and cured according to the protocol, 6 h at 80 °C, and 6 h at 170 °C with a post-curing of 2h at 180 °C.



**Figure V-1.** Structures of **a)** 3,4-Epoxycyclohexylmethyl-3',4'-epoxycyclohexane carboxylate (ECC) and **b)** Sylanto 7MS (S7MS).



#### 4.4. Characterization Methods

*Thermogravimetric Analyses (TGA)* of the resulting networks were performed on a Q500 thermogravimetric analyzer (TA instruments). The samples were heated from 30 to 800 °C at 10 °C min<sup>-1</sup> under nitrogen flow.

*Differential Scanning Calorimetry measurements (DSC)* of cycloaliphatic epoxy uncured blends (3-5 mg) and fully-cured networks were performed on a Q10 (TA instruments) from -70 to 250 °C under nitrogen flow. The samples were sealed in hermetic aluminium pans and kept for 3 min at 250 °C to erase the thermal history before being heated or cooled at 10 °C min<sup>-1</sup> under a nitrogen flow of 50 mL min<sup>-1</sup>.

*Transmission Electron Microscopy (TEM)* was performed at the Technical Center of Microstructures (University of Lyon) using a Phillips CM 120 microscope operating at 80 kV to characterize the dispersion of thermoplastic phases in the epoxy networks. 60 nm thick ultrathin sections of samples were obtained using an ultramicrotome equipped with a diamond knife and were then set on copper grids.

*Dynamic Mechanical Analysis (DMA)* was performed on rectangular samples with dimensions 15 mm and 5 mm and a thickness of 1 mm using an ARES-G2 rheometer with torsional fixture (TA Instruments). The material response was measured with a heating rate of 3 °C min<sup>-1</sup>. Storage modulus  $G'$  and Loss Modulus  $G''$  were measured for temperature ramps from -100 °C up to 250 °C. All tests were performed within the linear viscoelastic region of each material at a frequency of 1 Hz.

*Shape-memory behavior* of the epoxy networks was investigated by the fold-deploy experiment. The samples were placed in the oven at their corresponding deformation temperatures ( $T_{df} = T_{\alpha} + 30$  K) for 30 minutes. Once the specimens were equilibrated at their  $T_{df}$  and bent using an U-shaped template (**Fig. V-S13**). Then, the samples were cooled down to room temperature, keeping the U-shape by an external force for 5 minutes. The force was then removed, and the fixed bending angles were measured ( $\theta_f$ ). When the samples were re-heated up to their  $T_{df}$ , the initial shapes were gradually recovered, and at the end of this cycle, the recovered angles were registered ( $\theta_r$ ). Next, the shape memory properties were quantified by determining Shape Fixity ( $R_f$ ) and Shape Memory Recovery ( $R_r$ ) using Equations 1 and 2, respectively.

$$R_f = \frac{180 - \theta_f}{180} \cdot 100\% \quad (1)$$

$$R_r = \frac{\theta_r}{180} \cdot 100\% \quad (2)$$

*Tensile tests* were carried out using an MTS 2/M at  $24 \pm 1$  °C at a crosshead speed of  $1 \text{ mm min}^{-1}$  in a controlled humidity room. The ASTM D695 standard test was employed, and Young's moduli were obtained from the slope of the stress-strain curve in the linear domain (response inferior to 0.05). The strains at break and toughness were also determined from the maximum stress value and the area under the stress-strain curve, respectively. The experimental values were compared to the theoretical results.

#### 4.5. Chemical Recycling Methodology

The same chemical recycling methodology was applied to the three different TERs. Rectangular samples ( $15 \times 4 \times 1.5 \text{ mm}^3$ , 100 mg) were weighed and placed into glass vials containing a mixture of phosphonium IL (IL104) and ethylene glycol (EG) (4 mL). A hot plate magnetic stirrer coupled to a module Labortechnik Variomag 40ST was employed to heat the systems to 200 °C under stirring for 4.5 h. Four different IL104:EG ratios were evaluated (100:0, 20:80, 5:95 and 0:100 in wt%). Every hour the flasks were removed from the oil bath for a few seconds to observe the evolution of the degradation process. At the end of the recycling procedure (4.5 h), the residual mass was weighted, and the degradation activity was determined using Equation 3, where  $m_i$  and  $m_f$  are the initial and final mass, respectively. All the experiments were carried out in triplicate.

$$R_f = \frac{m_i - m_f}{m_i} \cdot 100\% \quad (3)$$

#### 4.6. Simulation Methods

All-atom molecular dynamics (MD) simulations were performed using the DREIDING force field.<sup>66</sup> The initial structures were generated using the AVOGADRO software.<sup>67</sup> The number of ions/monomers for each system was reported in **Table V-S1**. The ions/monomers were randomly placed in a cubic simulation cell with periodic boundary conditions (PBCs) using the PACKMOL software.<sup>68</sup> The initial cubic samples were generated at low density (200 Å in each principal direction) to avoid atomic overlaps while packing the ions/molecules. The simulation procedure reported in the literature was followed to polymerize the liquid precursor mixtures and predict the thermo-mechanical properties of the resulting polymers. More information about the simulation methodology has been provided in the Supporting Information.

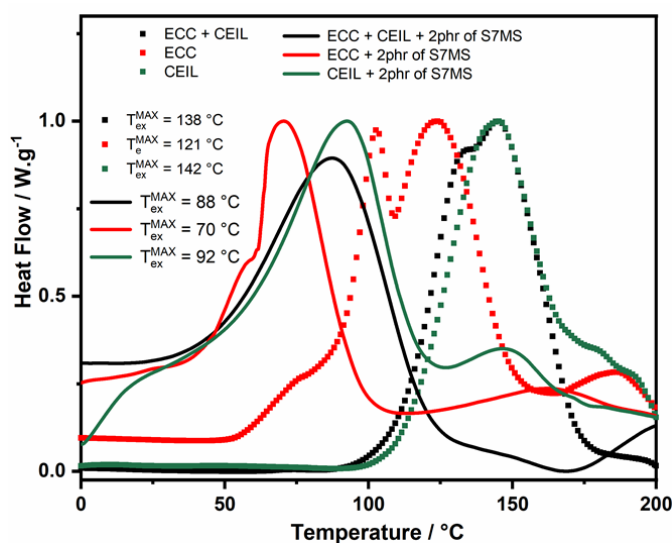
### 5. Results and Discussion

#### 5.1. Development of Networks and Preliminary Thermal Characterizations

It is well established that epoxy thermosetting materials present high chemical and solvent resistance.<sup>16</sup> For these reasons, their end-of-life is a major issue due to the crosslinks

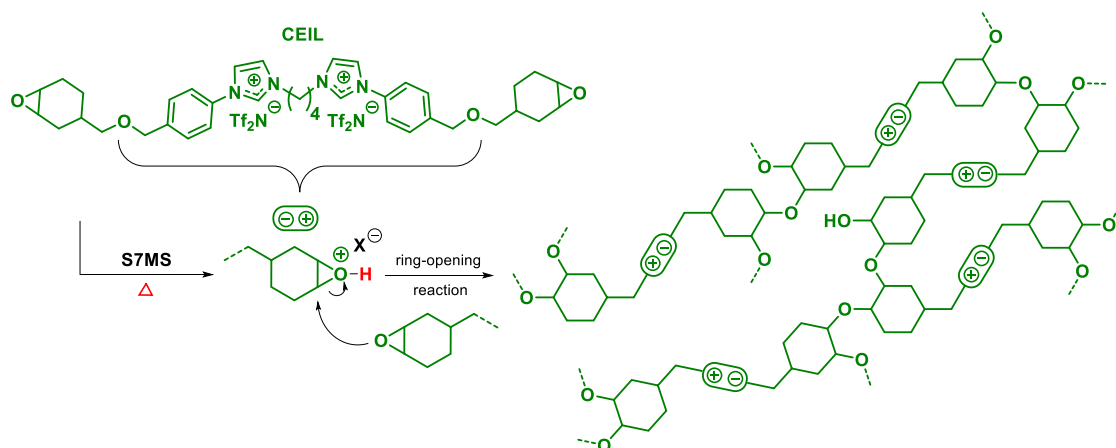
of the thermoset matrices that hinder their reprocessability by traditional methodologies.<sup>20</sup> Hence, rationally designing degradable networks and developing suitable recycling methods become crucial to address the circular economy's needs.

The polymerization of the epoxy-prepolymers was initially investigated by differential scanning calorimetry (DSC) in the presence of S7MS. This experiment corroborates that the thermal activation of the initiator allows the catalysis of the epoxy curing reaction since the polymerization temperature decreased by at least 50 °C when the initiator was employed in 2 wt.% (**Fig. V-2**).



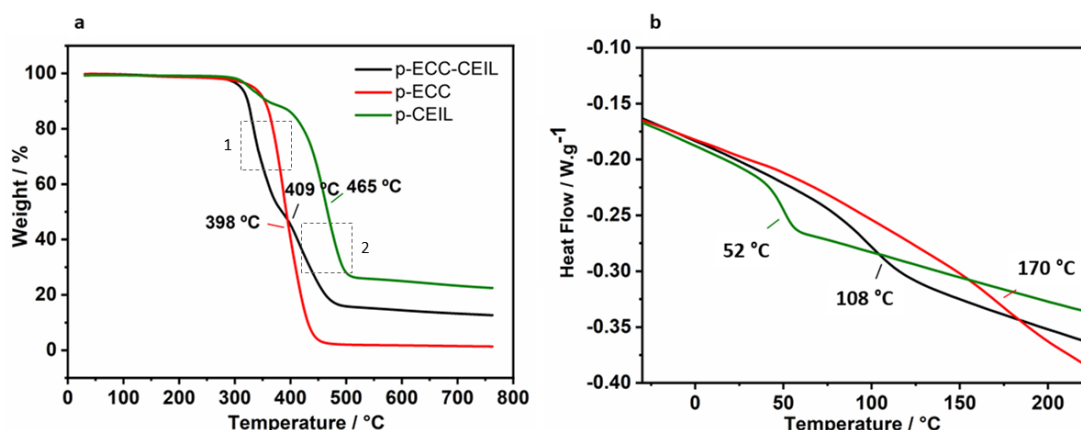
**Figure V-2.** DSC of the corresponding reactional mixture in the absence (dotted line) and presence (solid line) of photoinitiator Sylanto 7MS. The curves correspond to the exothermic peak of polymerization (exo up).

The curing process occurs through a cationic ring-opening pathway mediated by a thermal initiator. Briefly, S7MS thermally degrades, generating a proton that activates the cycloaliphatic epoxy moieties. These activated species suffer a nucleophilic attack from another epoxy monomer further developing the networks. (**Scheme V-2**) This preliminary finding enables the development of more straightforward curing protocols by using initiators to trigger and accelerate the polymerization reaction and to provide homogenous networks.



**Scheme V-2.** Mechanism of cationic polymerization of CEIL triggered by the initiator, S7MS.

The incorporation of ILs in the polymer matrix significantly increases the thermal stability of the developed materials. Polymer degradation is a multi-variable phenomenon,<sup>69,70</sup> and under nitrogen atmosphere, the more likely mechanism for the thermal decomposition is the random scission of covalent bonds.<sup>69</sup> The thermal energy absorption promotes the increase of bond vibrations, and when the molecular vibration reaches its elastic limit by absorbing thermal energy, the bonds break, resulting in decomposition.<sup>69</sup> The incorporation of IL-moieties in the polymer chain allows the release of thermal energy through an extended mechanism decay because the combination of the cations and anions freedom modes are also potential pathways for energy decay.<sup>18,51,71</sup> This reasoning is evident in **Fig. V-3a**, since p-CEIL exhibited thermal stability significantly higher than the non-ionic network (p-ECC). Furthermore, integrating CEIL into the bi-component network (p-ECC-CEIL) increased the thermal stability by several degrees compared to p-ECC. Thus, the employment of two monomers resulted in two mass loss steps; **(1)** a first region due to the degradation of ECC, and **(2)** a second mass loss at higher temperatures ascribed to the presence of CEIL (**Fig. V-3a**).



**Figure V-3.** In **a)** TGA highlighting the temperature of 50% weight loss and **b)** DSC thermograms for the networks p-ECC-CEIL, p-ECC, and p-CEIL (heating rate: 10 °C min<sup>-1</sup> under nitrogen gas). Networks prepared by adding 2 wt% of S7MS.

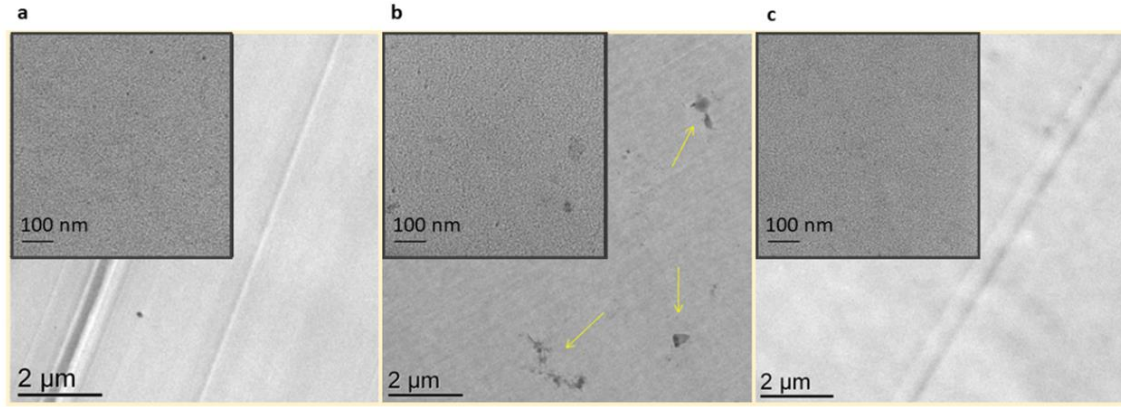
The embodying of CEIL into the networks also affected the  $T_g$  ranges, significantly lowering their values (**Fig. V-3b**). The CEIL monomer possesses a longer aliphatic chain which ensures greater positional and rotational mobility, increasing the flexibility of p-ECC-CEIL and p-CEIL networks. To this end, the coefficient of volumetric thermal expansion (CVTE) is a convenient metric for evaluating the polymers' flexibility regarding heating response. MD simulation results revealed that the p-ECC system obtained the lowest CVTE, both above and below the  $T_g$  (**Table V-S2**). Adding CEIL in the polymer system by 50 wt% (p-ECC-CEIL) increased the CVTEs by 70 and 50% below and above the  $T_g$ , respectively. The pure CEIL polymer showed the maximum CVTEs, which were 110 and 127% higher than those obtained for the p-ECC-CEIL below and above the  $T_g$ , respectively.

Similar to the previous TGA results, the DSC thermogram further confirmed the high homogeneity of the p-ECC-CEIL networks expected. The bi-component network (p-ECC-CEIL) exhibited  $T_g$  of 108 °C very close to 111 °C which corresponds to the average of the  $T_g$  of p-CEIL (52 °C) and p-ECC (170 °C).

## 5.2. Morphological Investigation of Networks

Transmission electron microscopy (TEM) and molecular dynamics (MD) simulation were employed to explore the network morphology. The TEM images revealed no phase separation for any of the developed networks. However, in p-ECC specimens, small clusters presumably originated from the initiator aggregation were observed (**Fig. V-4**). S7MS is sparingly soluble in ECC prepolymer. By considering it, it seems natural the phenomenon of thermos-initiator aggregation. Given the low vapor pressure and unique solvent properties

of ILs,<sup>49,72</sup> using an IL-derived monomer appears suitable for creating bi-component networks and solving the solubility issue. Additionally, ILs exhibit remarkable thermal properties such as high heat capacity and thermal conductivity, resulting in great heat transfer properties. Introducing CEIL might enhance the mixtures' thermal energy conduction, further assisting homogenous curing.<sup>73–76</sup>



**Figure V-4.** TEM images for **a)** p-ECC-CEIL, **b)** p-ECC, and **c)** p-CEIL. The square sections magnify specific regions to highlight the nanometric structural pattern of the networks. Networks prepared by adding 2 wt% of S7MS.

This reasoning is corroborated by **Fig. V-4a and V-4c**, in which we can see that no phase separation or nano-aggregation phenomena were observed when CEIL was employed to build the new homogenous TERs. These results are in total coherence with the theoretical investigation that did not predict any complete phase separation, as evidenced in the snapshots reported in **Fig. V-S14**.

### 5.3. Thermomechanical and Shape Memory Behavior of the Epoxy Networks

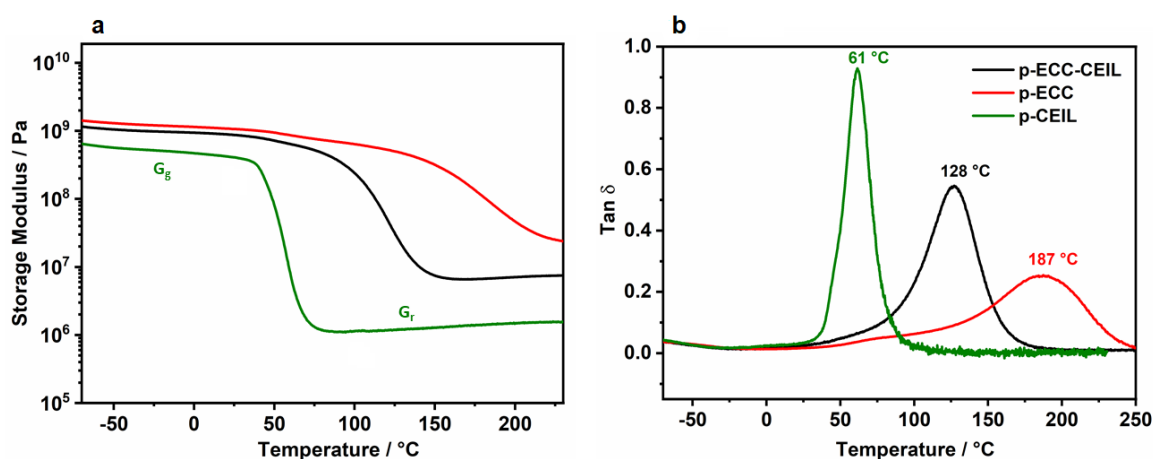
The thermo-mechanical properties of the TERs were obtained by dynamic mechanical analysis (DMA). The  $\alpha$ -relaxation temperatures ( $T_\alpha$ ) were found by determining the maximum values of  $\tan \delta$ . In addition, the epoxy networks' crosslinking densities, denoted as,  $\nu_e$  (mol m<sup>-3</sup>), were estimated using the elasticity theory (**Equation V-4**), where  $R$  is the ideal gas constant ( $R = 8.314 \text{ J K}^{-1} \text{ mol}^{-1}$ ),  $T_{df} = T_\alpha + 50 \text{ K}$ , and  $G_r$  corresponds to the storage modulus in the rubbery state (**Table V-1**).<sup>77,78</sup>

$$\nu_e = \frac{G_r}{3RT_d} \quad (4)$$

**Table V-1.** Transition temperatures and crosslinking density.

	$T_{\alpha}$ (°C)	$v_e$ (mol.m <sup>-3</sup> )
<b>p-ECC-CEIL</b>	130	0.58
<b>p-ECC</b>	185	1.85
<b>p-CEIL</b>	62	0.12

The incorporation of CEIL monomer led to a significant reduction of the crosslinking density from 1.93 to 0.60 mol m<sup>-3</sup>. The CEIL monomer presents a longer aliphatic chain resulting in networks with crosslinks more widely spaced compared to p-ECC. This reasoning is also corroborated by the lower  $T_{\alpha}$  and CVTEs values for TERs based on CEIL. The simulation results indicate that the average distance between the reactive atomic sites of CEIL did not change when the CEIL composition decreased from 100 to 50 wt.%, which was around 22.7 Å. This means that the addition of ECC to the polymer system did not affect the intrinsic flexibility of CEIL. The change in the  $T_{\alpha}$  can then be attributed to the decreased proportion of CEIL in the polymer matrix.



**Figure V-5.** In **a)** Storage modulus ( $G'$ ), and **b)** loss factor ( $\tan \delta$ ) as a function of temperature at 1 Hz and heating rate of 3 °C min<sup>-1</sup>. Networks prepared by adding 2 wt% of S7MS.

Equally important, the storage modulus for the glassy ( $G_g$ ) and rubbery ( $G_r$ ) states were also determined, being these parameters crucial for the development of SM polymers (**Figure V-5**).<sup>79</sup> Tailoring the  $G_g$ :  $G_r$  ratio allows the design of high-efficiency SM materials since the recovery behavior is enhanced with the  $G_g$ :  $G_r$  ratio increase.<sup>79</sup> Remarkably, the CEIL-based polymers presented higher values of  $G_g$ :  $G_r$  conferring to these materials more suitable SM properties (**Table V-2**). The three epoxy networks possess comparable magnitudes of  $G_g$ . Nonetheless, the increment of CEIL content progressively decreased the storage modulus at the rubbery state ( $G_r$ ). This structure-property relationship can be explained by

the fact that  $G_g$  strongly depends on the molecular density of the materials, which is roughly the same for the three systems (**Table V-S2**).

**Table V-2.** Storage modulus measured by torsional fixture at room temperature.

	$G_g$ / MPa	$G_r$ / MPa	Ratio $G_g:G_r$
<b>p-ECC-CEIL</b>	861.4	6.5	132.5
<b>p-ECC</b>	722.2	23.5	30.7
<b>p-CEIL</b>	421.5	1.2	351.25

Further, the SM behavior of obtained materials was evaluated and quantified by the shape fixity ( $R_f$ ) and shape recovery ratios ( $R_r$ ).  $R_f$  describes the ability of a polymer to keep a temporary shape after applying an external force. Its value is 100% when the material fully keeps the shape induced by the external stimulus.<sup>79,80</sup> As regards  $R_r$ , this parameter weights the percentage of recovery when the polymer is heated up to the  $T_r$ .  $R_r$  corresponds to 100% when the material can entirely recover its initial shape.<sup>79,80</sup>

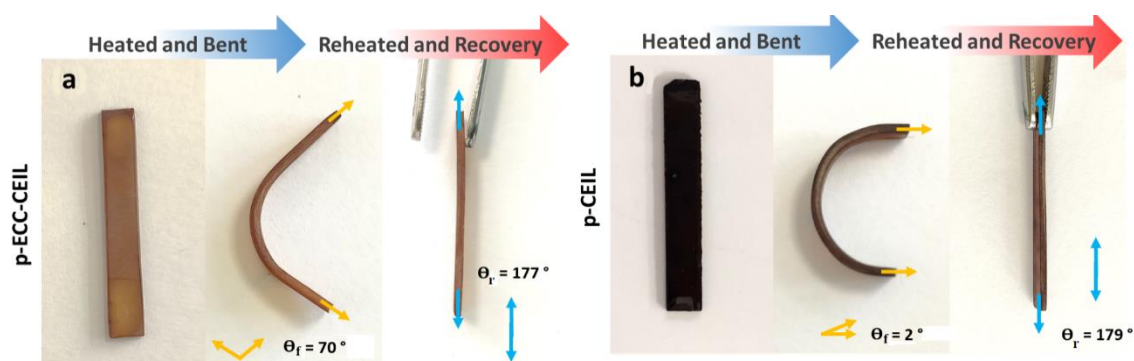
Several parameters can be adjusted, including curing extent, monomer-hardener ratio, and blend formulations to afford shape memory behaviour to thermosets.<sup>15,79–81</sup> Recently, we demonstrated that exploring the synergistic use of polyetherimide (PEI) and a commercial phosphonium IL is a suitable approach to induce shape memory behavior in DGEBA-based materials.<sup>82</sup> The ternary hybrid materials presented shape-memory performance dependent on the PEI content that impacts the intrinsic entropy of materials, minimizing the internal stresses during the macroscopic deformations.

In this current contribution, we investigated the possibility of introducing shape memory behavior to epoxy thermosets by molecularly designing a novel CEIL. The  $R_f$  and  $R_r$  were determined only for p-ECC-CEIL and p-CEIL TERs since SM behavior could not be demonstrated for p-ECC. Like other purely epoxy-based networks, p-ECC presents a high crosslinking density and elevated brittleness.<sup>27</sup> During the heating and bending cycles, several p-ECC specimens were broken, probably due to its highly crosslinked structure (**Table V-1**), resulting in high constraints on the polymer chains.<sup>16,83</sup> Thus, even heating up to temperatures higher than its  $T_{df}$  was not enough to create the chain mobility necessary to bend the p-ECC samples. Notably, the incorporation of CEIL was suitable not only to tailor  $T_g$ , mechanical modulus, and Young modulus but also to introduce shape memory response into the new networks. By preparing a bi-component network, the crosslinking density was adjusted, generating higher molecular mobility confirmed by DMA and MD simulation.

The fold-deploy experiment is summarized in **Fig. V-6**, evidencing the corresponding fixed ( $\theta_f$ ) and recovered angles ( $\theta_r$ ). Notwithstanding, p-ECC-CEIL presented SM behavior and the performance of p-CEIL was comparatively better in terms of  $R_f$ . While p-CEIL



conferred an  $R_f$  of 99%, the p-ECC-CEIL led to  $R_f$  of 61%. Regarding the recovery response, both networks revealed results comparable, with recovery ratios ( $R_r$ ) of approximately 99%.



**Figure V-6.** Fold-deploy experiment for **a)** p-ECC-CEIL and **b)** p-CEIL. Networks prepared by adding 2 wt% of S7MS.

All the epoxy materials presented Young's Moduli comparable to DGEBA TERs.<sup>84,85</sup> The increment of CEIL lowered the tensile stiffness but was compensated by a significant increase in ductility and toughness properties. Increasing toughness is desirable since this property ponders strength and ductility.<sup>86,87</sup> Considering the elevated brittleness of epoxy material,<sup>87,88</sup> we proved that by introducing CEIL, we can tune the toughness building network more capable of absorbing energy and plastically deforming without fracturing (**Table V-3**). This behavior probably derives from the lower crosslinking densities of CEIL-based networks and the presence of the IL moieties.

**Table V-3.** Young Modulus, strains at the break and toughness for the three networks prepared by adding 2 wt. % of S7MS.

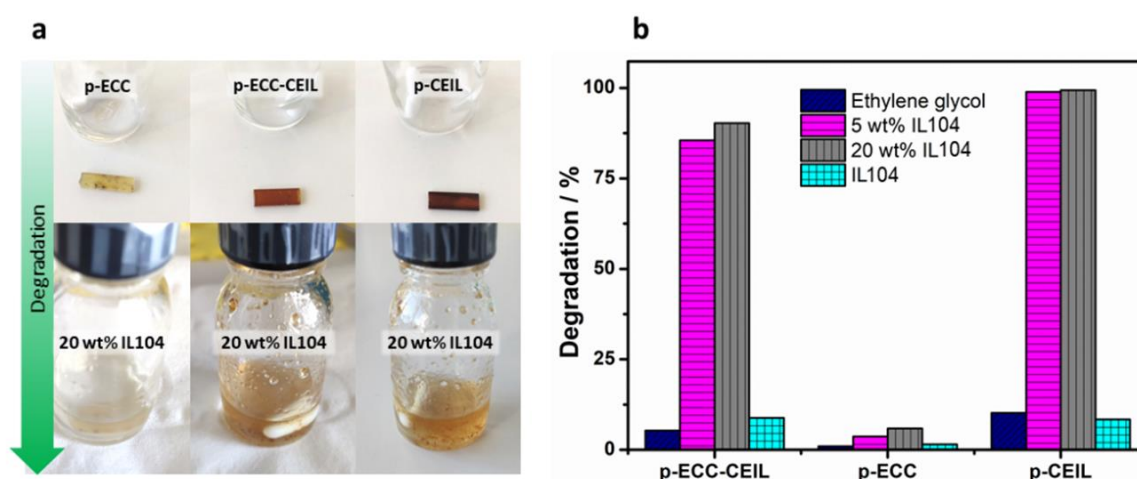
	Young Modulus GPa	Strain at Break %	Toughness $U_T$ $\text{kJm}^{-3}$
<b>p-ECC-CEIL</b>	$2.84 \pm 0.05$	$0.98 \pm 0.02$	$61.8 \pm 0.2$
<b>p-ECC</b>	$3.71 \pm 0.06$	$0.58 \pm 0.01$	$40.8 \pm 0.1$
<b>p-CEIL</b>	$0.28 \pm 0.03$	$7.37 \pm 0.09$	$277.2 \pm 0.1$

#### 5.4. Sustainable Treatment and Chemical Recycling

In order to transition to a circular economy, a molecular ionic brick (CEIL) was strategically incorporated into the network structure. This brick possesses potential cleavable C-N and ether bonds, enabling the materials to degrade under mild conditions. As a result, IL molecules are regenerated, allowing them to either undergo re-curing with polymer resins or be utilized again for various IL applications. In practice, IL recovery reduces thermoset waste to a minimum, since when these networks reach their end of life, they are maintained within the economy into a new material or for another application.<sup>64,65</sup> These can be productively reused repeatedly, thereby creating further value.<sup>3,11,64,65</sup>

Considering their tailored viscosity, excellent thermal stability, potential reactivity and recyclability, several works have investigated ILs as solvents or catalysts to degrade polymer materials.<sup>89–92</sup> Aiming to assist the degradation of the resulting networks, an electrophilic phosphonium IL (IL104) was employed as a more environmentally friendly catalyst alternative (**Fig. V-S16**).

Initially, the samples were measured, weighed, and placed into the vial flasks in determined proportions of IL104:EG (100:0, 20:80, 5:95 and 0:100 in wt%). The degradation phenomenon was visually monitored and followed by an initial color change of solutions evolving to the sample swelling. Subsequently, the physicochemical degradation manifested through the apparent increase of the solution viscosity yielding homogenous oils (**Fig. V-7a**).



**Figure V-7.** In **a**) the polymerized networks and their aspect after the degradation process and **b**) the percentage of degradation for the three networks in four different conditions. Networks prepared by adding 2 wt% of S7MS.

These degraded solutions were filtered, washed and dried to provide the non-degraded residual mass, that were measured to further determine the degradation activity according to Equation 3. The solvolysis of the three networks was investigated in four different media, and p-ECC did not reveal any relevant degradation degree in none of the conditions. The different mechanisms involved in the degradation pathways were investigated for a better understanding. According to our observation, the samples are swollen by the solvent creating free space and increasing the contact surface area inside the polymer networks. Then, the degradation reactions start to take place.

The theoretical investigation predicted low values of CVTE for the p-ECC at temperatures below and above the  $T_g$ . This analysis suggests negligible polymer expansion and flexibility in this range of temperature. Since the primary step does not befall, the degradation

phenomenon does not go further for p-ECC specimens. Remarkably, the incorporation of 50% in wt. of CEIL enhanced the polymer degradability by at least 80% in the presence of 5 and 20 wt% of IL104 in EG. Under the same conditions, the fully CEIL-based networks demonstrated degradation rates close to 100% (**Fig. V-7b**).

This result is in agreement with the increase of the CVTE values and ties in with the presence of cleavable bonds in the CEIL structure. The degradation activity in neat EG was minor, which corroborates the role of the IL104 as a catalyst, while the chemical dissolution in neat IL104 seems similarly unfavorable. Indeed, thermoset dissolution derives from the compromise between solvent (and catalyst) diffusion into polymers and the rate of degradation reactions. Employing the highly viscous IL104 definitely does not favor the first stage. Interestingly, the TER degradations in 5 wt% of IL104 in EG provided comparable values to the medium containing 20 wt.% of IL104. The possibility of employing catalytic amounts of IL104 makes this procedure more economically viable and a potential method to replace landfilling and pyrolysis in industries.<sup>70,93</sup>

To further understand the degradation mechanism and the structures of the resulting products, <sup>1</sup>H NMR and HRMS experiments were performed (**Fig. V-S17a**). The solutions resulting from the degradation reactions were dried under vacuum at 150 °C to eliminate excess EG. Then, different deuterated solvents were investigated to solubilize the samples, including CDCl<sub>3</sub>, DMSO-d<sub>6</sub>, DMF-d<sub>7</sub>, ACN-d<sub>3</sub>, and MeOD-d<sub>4</sub>, which proved to be the most appropriate.

The degradation of p-ECC did not yield a homogenous solution, and its <sup>1</sup>H NMR spectrum did not show any elucidating information. Otherwise, the <sup>1</sup>H NMR analysis of the solutions derived from p-ECC-CEIL and p-CEIL indicates that the cycloaliphatic moieties of CEIL remain intact during the degradation process. The imidazolium and the aromatic segments were preserved, although the peaks corresponding to these moieties present low intensity and multiple chemical shifts. The inferior peak amplitudes arise from the low concentration of matter and elevated acidity of the hydrogen on position C-2 of the imidazolium ring. The HRMS investigation further supports the <sup>1</sup>H NMR results, evidencing the presence of multi-species single positively charged (**Fig. V-S17b**). More important than confirming the maintenance of the imidazolium segments is the possibility of predicting the molecular formula by accurately determining the exact mass. By this analysis, it was possible to provide the molecular structure of the ion with the mass-to-charge ratio of 313.2267 and approximately predict the molecular structure of secondary ions.

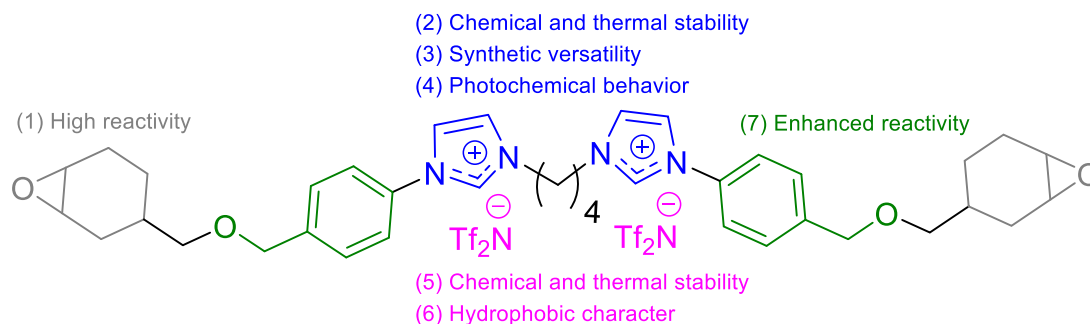
The most striking result from this experiment is that we engineered next-generation TERs, and their degradation under mild conditions recovered IL species that can be easily extracted from the degraded solutions. These degradation derivative ILs can be potentially used for different applications,<sup>94</sup> including gas capture,<sup>95</sup> lubricants,<sup>96</sup> dispersing,<sup>97</sup> and compatibilizing agents.<sup>98</sup> In future works, we aim to reintroduce these IL products into the TERs or re-polymerize them and investigate their mechanical properties to continue developing sustainable polymer technologies.

## 6. Conclusion of Chapter V and Perspectives

A cycloaliphatic epoxidized IL (CEIL) monomer was successfully synthesized through an optimized and scalable route. Then, three different networks were developed in the presence of an initiator through cationic polymerization. The networks containing 50 and 100 % of CEIL presented glass transition temperatures from 65 °C to 130 °C, increased thermal stability, similar mechanical properties to commercial epoxy resins, and outstanding shape memory behavior. Remarkably, introducing CEIL molecular bricks afforded high degradability to the multifunctional networks under mild conditions. Finally, the degradation products were characterized, which allows their reemployment into the networks to develop high-performance, environmentally friendly polymers for the continuous progress of a circular economy.

It is worth noting that the present study has started with the primary objective of synthesizing cationically photopolymerizable ILs to develop ionic 3D printing inks. In pursuit of this objective, an extensive review of the scientific literature was conducted to identify the most relevant information for designing the best candidate molecules (**Fig. V-8**). It is worth noting that no prior studies have been found that report the cationic photopolymerization of ILs.

Based on our previous research on epoxy-based materials, and the enhanced reactivity of cycloaliphatic epoxides, we identified these groups as the ideal polymerizing moiety (**Fig. V-8**). Subsequently, considering the exceptional stability of imidazolium-based ILs, their synthetic versatility, and their ability to absorb UV light, we selected imidazolium as the most suitable cation. Bistriflimide (NTf<sub>2</sub>) was chosen for the counterion due to its hydrophobic nature and significant thermal stability. Also, we incorporated the benzyl ether moiety further to enhance the system's reactivity towards cationic photopolymerization. This design decision was supported by previous research conducted by Crivello and co-authors (**as presented in Scheme II-41**).<sup>279</sup> Furthermore, incorporating aromatic fragments, as observed in DGEBA or analogous precursors, has been demonstrated to improve mechanical properties.



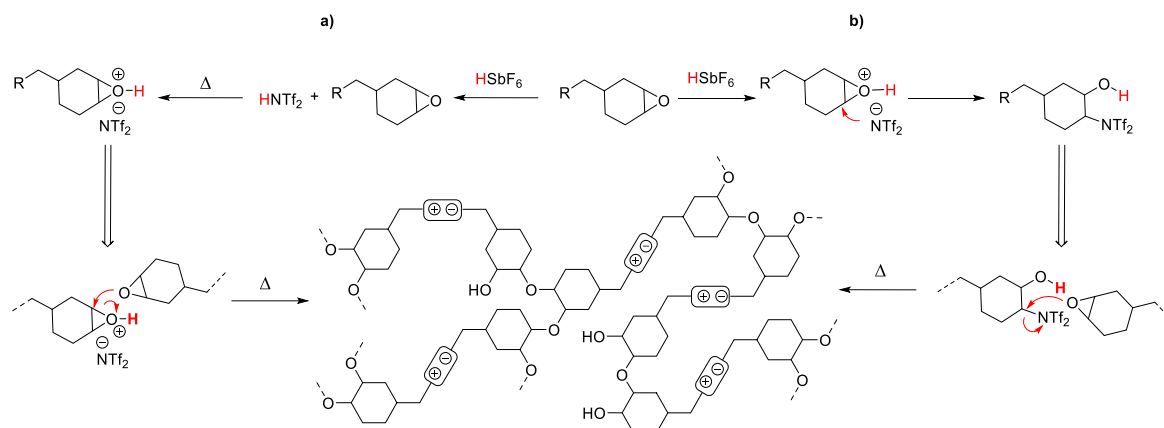
**Figure V-8.** The cycloaliphatic epoxidized IL was systematically designed by molecularly installing the most beneficial groups for each molecule part.

Upon examining the cationic photopolymerization of CEIL under UV light (2 phr of S7MS, 10 cycles of 0.1 s, 365 nm, 554 mJ cm<sup>-2</sup>), we observed that the system underwent gelation with an epoxy conversion rate inferior to 20%. Various parameters were investigated as potential optimization factors, including light wavelength, lamp power, exposure time, photoinitiator concentration, sample thickness, reactive dilutants, and distance between the UV lamp and the samples. Despite our efforts to optimize the process, we could not significantly increase the conversion yield.

Our initial observations indicated that the heat generated by the UV lamp was triggering the cationic polymerization. Therefore, we decided to utilize the iodonium salt (as depicted in **Figure V-1**) to mediate the thermal cationic photopolymerization of CEIL. The resulting networks exhibited promising properties, as demonstrated before in this chapter.

After considering all possible scenarios, we formulated a hypothesis that the presence of the NTF<sub>2</sub> counter ion was terminating the cationic photopolymerization pathway. Specifically, we postulated that NTF<sub>2</sub> was trapping the proton initially generated by the photoinitiator (**Scheme V-3a**). As the photoacid was used in a small proportion, the anion NTF<sub>2</sub> was present in excess relative to the proton formed. Consequently, the NTF<sub>2</sub> anion would quench the reaction at room temperature. However, heating the system allows the proton to be ionized again and used to protonate the epoxy group, thus enabling the polymerization pathway. This hypothesis is consistent with the pK<sub>a</sub> values of the acids involved in the process.

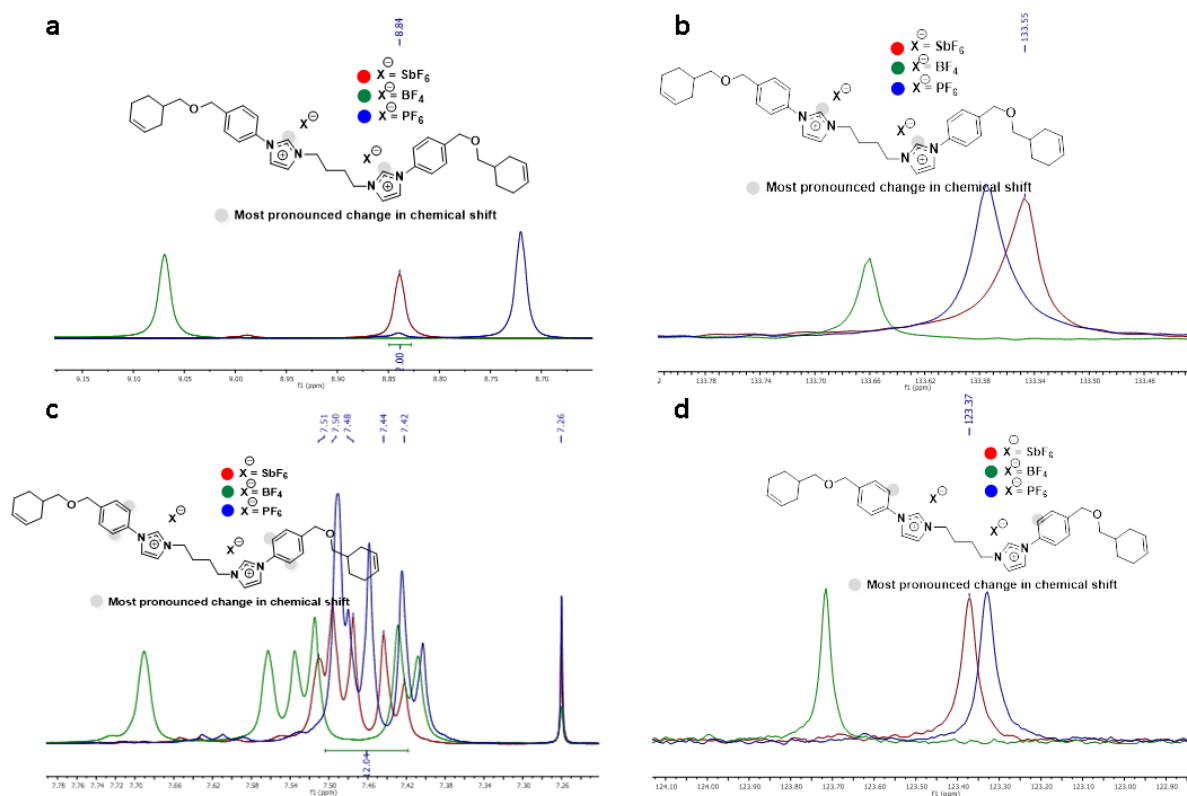
Another possibility we considered was that the activated epoxy group could be attacked by the NTF<sub>2</sub> anion, thereby initially terminating the polymerization reaction (**Scheme V-3b**). However, by heating the system, the NTF<sub>2</sub> anion could act as a leaving group, allowing the substrate to react via a substitution reaction.



**Scheme V-3.** A hypothetical mechanism is proposed to account for the termination of photopolymerization. It is suggested that in scenario **a)**, the proton produced is captured by the counterion NTf<sub>2</sub>, while in the scenario; **b)** the anion NTf<sub>2</sub> participates in the epoxy ring-opening reaction.

Several photoinitiators utilized in cationic photopolymerization are organic salts, frequently containing counterions such as SbF<sub>6</sub><sup>-</sup>, PF<sub>6</sub><sup>-</sup>, and BF<sub>4</sub><sup>-</sup>. The efficiency of these photoinitiators relies on their anions' reactivity, which increases according to the sequence: BF<sub>4</sub><sup>-</sup> < PF<sub>6</sub><sup>-</sup> < AsF<sub>6</sub><sup>-</sup> < SbF<sub>6</sub><sup>-</sup>.<sup>287</sup> To improve the reactivity of CEIL family monomers, NTf<sub>2</sub> was replaced by SbF<sub>6</sub><sup>-</sup>, PF<sub>6</sub><sup>-</sup>, and BF<sub>4</sub><sup>-</sup>.

After synthesizing the cationic substrate (CEIL), our focus shifted to optimizing the ionic exchange process for various anions. Since we hypothesized that the anion inhibited the cationic polymerization, we comprehensively characterized the ionic-exchange reactions using NMR spectroscopy and HRMS (**Fig. V-9**).



**Figure V-9.** The comprehensive investigation of the ionic exchange reaction by NMR spectroscopy. **a)** and **b)** highlight the change in the chemical environment of the imidazolium-ring by  $^1\text{H}$  and  $^{13}\text{C}$  NMR spectroscopy. In **c)** and **d)**, similarly it is observed the main chemical shift for the aromatic moiety. Please see the complete analyses in **Appendix III**.

It is important to note that this characterization is often neglected. However, in our case, even minor inorganic impurities significantly impact the propagation of the polymerization. Therefore, the ionic exchange step is critical to synthesizing photopolymerizable IL monomers. The detailed methodologies for the ionic exchange reactions are described in the **Appendix III**.

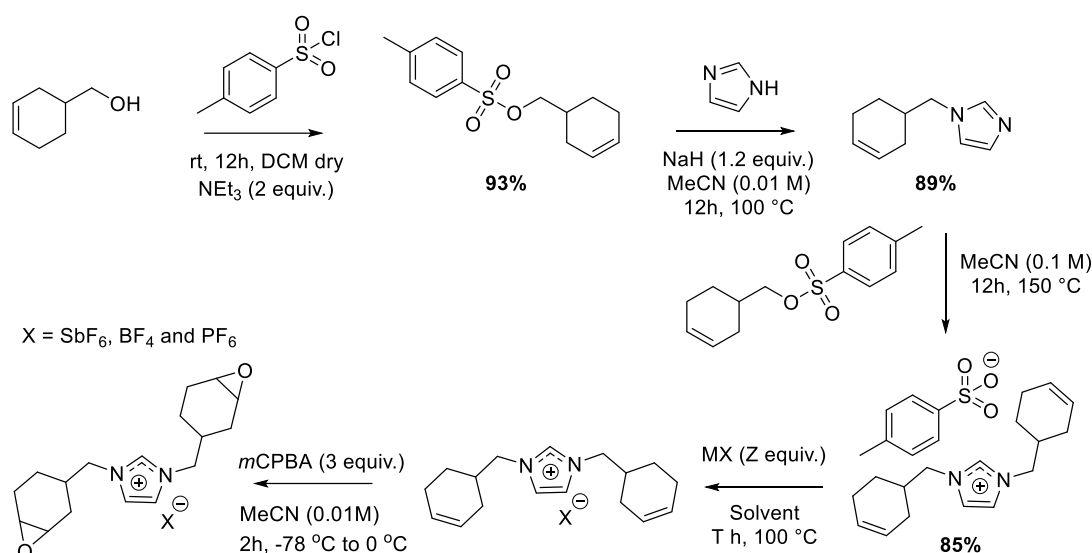
Subsequently, the epoxidation reactions were optimized, adapting a methodology previously developed by our group, using *m*CPBA in acetonitrile. The products were all purified by precipitation in diethyl ether, yielding colorless room-temperature ILs. The three novel cycloaliphatic epoxidized ILs bearing  $\text{SbF}_6^-$ ,  $\text{BF}_4^-$  and  $\text{PF}_6^-$  as counterions have shown excellent chemical stability when stored at  $-4^\circ\text{C}$  and protected from light exposure. However, they turned active and photopolymerized at room temperature, under Argon atmosphere, and visible-light exposure over 12 h.

While this information helps develop cationically photopolymerizable ILs due to their increased activity, their uncontrolled photopolymerization in mild conditions and



short timeframes presents a challenge. As a result, we are currently resynthesizing these monomers and attempting to control their self-homopolymerization to create 3D printing resins.

Alongside synthesizing the CEIL family of monomers, we opted to explore another imidazolium-backbone substrate that also contains anions frequently used in cationic photopolymerization processes, namely  $\text{SbF}_6$ ,  $\text{BF}_4$  and  $\text{PF}_6$  (**Scheme V-4**).



**Scheme V-4.** Synthetic route designed to synthesize a cationic photopolymerizable IL monomer. The selection of tosylate as the anion was based on its lower nucleophilicity compared to halide ions and its detectability using  $^1\text{H}$  NMR.

We aimed to identify the most straightforward cationic substrate with an imidazolium group and two cycloaliphatic epoxy groups. As we gained experience with the epoxidation reaction, we realized that avoiding residual nucleophilic anions in the medium would be advantageous even with optimized ionic exchange reactions. For instance, in the synthesis of CEIL, the ionic exchange involves replacing bromide with bis(trifluoromethane)sulfonylimide, and the remaining bromide may trigger the degradation of the IL epoxy monomers. Additionally, detecting the residual bromide species through routine spectroscopy techniques, like infrared or NMR, can be extremely challenging. To circumvent these issues, we designed a synthetic route using tosylate as a counterion to prevent a nucleophilic attack of the epoxy rings and further confirm the effectiveness of the ionic exchange by  $^1\text{H}$  NMR.

Similarly to the synthesis of CEIL analogous, the ionic exchange reaction was optimized, and the results are presented below.

**Table V-4.** Ionic exchange reaction to introduce antimony pentafluoride

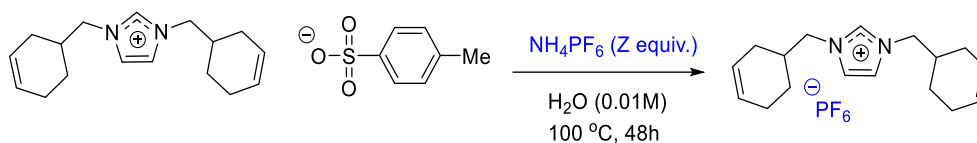
$\text{NaSbF}_6$  (X equiv.)  
 Acetone:DCE  
 (0.01M; ratio 1:1)  
 100 °C, 24h

Entry	Z (equiv.)	T (°C)	Yield (%) <sup>[a]</sup>
1	4	80	58
2	6	80	83
3	4	100	84
<b>4</b>	<b>6</b>	<b>100</b>	<b>87</b>

**Table V-5.** Ionic exchange reaction to introduce tetrafluoroborate

$\text{LiBF}_4$  (Z equiv.)  
 $\text{H}_2\text{O}$  (0.01M)  
 100 °C, 48h

Entry	Z (equiv.)	T (°C)	Yield (%) <sup>[a]</sup>
1	2	100	<35
2	5	100	49
<b>3</b>	<b>10</b>	<b>100</b>	<b>88</b>

**Table V-6.** Ionic exchange reaction to introduce hexafluorophosphate

Entry	Z (equiv.)	T (°C)	Yield (%) <sup>[a]</sup>
1	2	100	40
2	5	100	85
<b>3</b>	<b>10</b>	<b>100</b>	<b>88</b>

**[a]** Estimated based on the  $^1\text{H}$  NMR crude employing 1,3,5-trimethoxybenzene as internal reference.

We were able to make significant progress with the ionic exchange allowing the increase of the IL library available for different applications. Despite having prior experience with the epoxidation reaction, we still faced some challenges regarding this step. In this last work, we observed the formation of the epoxidized IL monomers followed by their degradation or polymerization *in situ*. The best outcomes were achieved under very strict conditions, including anhydrous solvent, an inert atmosphere and maintaining the reaction between  $-78\text{ }^{\circ}\text{C}$  to  $0\text{ }^{\circ}\text{C}$ . At the current moment of this research, we are working to isolate the final products, and we are also considering the polymerization of the cycloalkenes using ring-opening metathesis polymerization (ROMP).

In conclusion, although we did not achieve the goal of developing an ionic 3D printing resin, we overcame various challenges regarding the synthesis of cycloaliphatic epoxidized ILs. Certainly, we made some contributions to the rationalization and development of synthetic methodologies that can pave the way for future works on the topic.

### Supporting Information

The general methodology for characterization and purification, the detailed procedure for the synthesis of the cycloaliphatic epoxidized ionic liquid and its intermediates, the NMR spectra, the molecular dynamics simulations outputs, and the mass spectra of the degradation products.

## 7. References

- (1) Babbitt, C. W.; Althaf, S.; Cruz Rios, F.; Bilec, M. M.; Graedel, T. E. The Role of Design in Circular Economy Solutions for Critical Materials. *One Earth* **2021**, 4 (3), 353–362. <https://doi.org/10.1016/j.oneear.2021.02.014>.

- (2) Morel, J.-C.; Charef, R.; Hamard, E.; Fabbri, A.; Beckett, C.; Bui, Q.-B. Earth as Construction Material in the Circular Economy Context: Practitioner Perspectives on Barriers to Overcome. *Philos. Trans. R. Soc. B Biol. Sci.* **2021**, *376* (1834), 20200182. <https://doi.org/10.1098/rstb.2020.0182>.
- (3) Bachmann, J.; Yi, X.; Tserpes, K.; Sguazzo, C.; Barbu, L. G.; Tse, B.; Soutis, C.; Ramón, E.; Linuesa, H.; Bechtel, S. Towards a Circular Economy in the Aviation Sector Using Eco-Composites for Interior and Secondary Structures. Results and Recommendations from the EU/China Project ECO-COMPASS. *Aerospace* **2021**, *8* (5), 131. <https://doi.org/10.3390/aerospace8050131>.
- (4) Zhang, B.; De Alwis Watuthanthrige, N.; Wanasinghe, S. V.; Averick, S.; Konkolewicz, D. Complementary Dynamic Chemistries for Multifunctional Polymeric Materials. *Adv. Funct. Mater.* **2022**, *32* (8), 2108431. <https://doi.org/10.1002/adfm.202108431>.
- (5) Xi, G.; Xiao, M.; Wang, S.; Han, D.; Li, Y.; Meng, Y. Polymer-Based Solid Electrolytes: Material Selection, Design, and Application. *Adv. Funct. Mater.* **2021**, *31* (9), 2007598. <https://doi.org/10.1002/adfm.202007598>.
- (6) Liu, C.; Zhang, Y.; An, Q. Functional Material Systems Based on Soft Cages. *Chem. – An Asian J.* **2021**, *16* (10), 1198–1215. <https://doi.org/10.1002/asia.202100178>.
- (7) Zhang, X.; Lin, H.; Shang, H.; Xu, J.; Zhu, J.; Huang, W. Recent Advances in Functional Fiber Electronics. *SusMat* **2021**, *1* (1), 105–126. <https://doi.org/10.1002/sus2.1>.
- (8) Zheng, N.; Xu, Y.; Zhao, Q.; Xie, T. Dynamic Covalent Polymer Networks: A Molecular Platform for Designing Functions beyond Chemical Recycling and Self-Healing. *Chem. Rev.* **2021**, *121* (3), 1716–1745. <https://doi.org/10.1021/acs.chemrev.0c00938>.
- (9) Guo, X.; Han, L.; Hou, X. Insights into the Device Structure, Processing and Material Design for an Organic Thin-Film Transistor towards Functional Circuit Integration. *Mater. Chem. Front.* **2021**, *5* (18), 6760–6778. <https://doi.org/10.1039/D1QM00334H>.
- (10) Chiong, J. A.; Zheng, Y.; Zhang, S.; Ma, G.; Wu, Y.; Ngaruka, G.; Lin, Y.; Gu, X.; Bao, Z. Impact of Molecular Design on Degradation Lifetimes of Degradable Imine-Based Semiconducting Polymers. *J. Am. Chem. Soc.* **2022**, *144* (8), 3717–3726. <https://doi.org/10.1021/jacs.1c12845>.
- (11) Sobkowicz, M. J. Polymer Design for the Circular Economy. *Science (80-. )*. **2021**, *374* (6567), 540–540. <https://doi.org/10.1126/science.abm2306>.

- (12) Ma, S.; Webster, D. C. Degradable Thermosets Based on Labile Bonds or Linkages: A Review. *Prog. Polym. Sci.* **2018**, *76*, 65–110. <https://doi.org/10.1016/j.progpolymsci.2017.07.008>.
- (13) Liu, X.; Tian, F.; Zhao, X.; Du, R.; Xu, S.; Wang, Y. Z. Recycling Waste Epoxy Resin as Hydrophobic Coating of Melamine Foam for High-Efficiency Oil Absorption. *Appl. Surf. Sci.* **2020**, *529* (May), 147–151. <https://doi.org/10.1016/j.apsusc.2020.147151>.
- (14) Pickering, S. J. Recycling Technologies for Thermoset Composite Materials-Current Status. *Compos. Part A Appl. Sci. Manuf.* **2006**, *37* (8), 1206–1215. <https://doi.org/10.1016/j.compositesa.2005.05.030>.
- (15) Di Mauro, C.; Malburet, S.; Graillot, A.; Mija, A. Recyclable, Repairable, and Reshapable (3R) Thermoset Materials with Shape Memory Properties from Bio-Based Epoxidized Vegetable Oils. *ACS Appl. Bio Mater.* **2020**, *3* (11), 8094–8104. <https://doi.org/10.1021/acsabm.0c01199>.
- (16) Auvergne, R.; Caillol, S.; David, G.; Boutevin, B.; Pascault, J.-P. Biobased Thermosetting Epoxy: Present and Future. *Chem. Rev.* **2014**, *114* (2), 1082–1115. <https://doi.org/10.1021/cr3001274>.
- (17) Wanghofer, F.; Wolfberger, A.; Wolfahrt, M.; Schlögl, S. Cross-Linking and Evaluation of the Thermo-Mechanical Behavior of Epoxy Based Poly(Ionic Liquid) Thermosets. *Polymers (Basel)*. **2021**, *13* (22), 3914. <https://doi.org/10.3390/polym13223914>.
- (18) Silva, A. A.; Livi, S.; Netto, D. B.; Soares, B. G.; Duchet, J.; Gérard, J. F. New Epoxy Systems Based on Ionic Liquid. *Polymer (Guildf)*. **2013**, *54* (8), 2123–2129. <https://doi.org/10.1016/j.polymer.2013.02.021>.
- (19) Jilani, W.; Mzabi, N.; Fourati, N.; Zerrouki, C.; Gallot-Lavallée, O.; Zerrouki, R.; Guermazi, H. A Comparative Study of Structural and Dielectric Properties of Diglycidyl Ether of Bisphenol A (DGEBA) Cured with Aromatic or Aliphatic Hardeners. *J. Mater. Sci.* **2016**, *51* (17), 7874–7886. <https://doi.org/10.1007/s10853-016-0043-0>.
- (20) Pascault, Jean-Pierre; Williams, R. Epoxy Polymers: New Materials and Innovations. In *Epoxy Polymers: New Materials and Innovations*; Wiley-VCH, Weinheim, Germany, 2009; pp 25–73.

- (21) Jin, F. L.; Li, X.; Park, S. J. Synthesis and Application of Epoxy Resins: A Review. *Journal of Industrial and Engineering Chemistry*. 2015, pp 1–11. <https://doi.org/10.1016/j.jiec.2015.03.026>.
- (22) Tao, Z.; Yang, S.; Chen, J.; Fan, L. Synthesis and Characterization of Imide Ring and Siloxane-Containing Cycloaliphatic Epoxy Resins. *Eur. Polym. J.* **2007**, 43 (4), 1470–1479. <https://doi.org/10.1016/j.eurpolymj.2007.01.039>.
- (23) Isarn, I.; Gamardella, F.; Massagués, L.; Fernández-Francos, X.; Serra, À.; Ferrando, F. New Epoxy Composite Thermosets with Enhanced Thermal Conductivity and High Tg Obtained by Cationic Homopolymerization. *Polym. Compos.* **2018**, 39 (5), 1760–1769. <https://doi.org/10.1002/pc.24774>.
- (24) Roppolo, I.; Shahzad, N.; Sacco, A.; Tresso, E.; Sangermano, M. Multifunctional NIR-Reflective and Self-Cleaning UV-Cured Coating for Solar Cell Applications Based on Cycloaliphatic Epoxy Resin. *Prog. Org. Coatings* **2014**, 77 (2), 458–462. <https://doi.org/10.1016/j.porgcoat.2013.11.009>.
- (25) Chakraborty, R.; Soucek, M. D. Synthesis of Telechelic Methacrylic Siloxanes with Cycloaliphatic Substituents Groups for UV-Curable Applications. *Eur. Polym. J.* **2008**, 44 (10), 3326–3334. <https://doi.org/10.1016/j.eurpolymj.2008.07.051>.
- (26) Wang, Z.; Xie, M.; Zhao, Y.; Yu, Y.; Fang, S. Synthesis and Properties of Novel Liquid Ester-Free Reworkable Cycloaliphatic Diepoxides for Electronic Packaging Application. *Polymer (Guildf)*. **2003**, 44 (4), 923–929. [https://doi.org/10.1016/S0032-3861\(02\)00873-X](https://doi.org/10.1016/S0032-3861(02)00873-X).
- (27) Crivello, J. V. The Synthesis and Cationic Polymerization of Novel Epoxide Monomers. *Polym. Eng. Sci.* **1992**, 32 (20), 1462–1465. <https://doi.org/10.1002/pen.760322003>.
- (28) Sasaki, H. Curing Properties of Cycloaliphatic Epoxy Derivatives. *Prog. Org. Coatings* **2007**, 58 (2–3), 227–230. <https://doi.org/10.1016/j.porgcoat.2006.09.030>.
- (29) Stanford, J. L.; Ryan, A. J.; Yang, Y. Photoinitiated Cationic Polymerization of Epoxides. *Polym. Int.* **2001**, 50 (9), 986–997. <https://doi.org/10.1002/pi.730>.
- (30) Cho, J. D.; Kim, H. K.; Kim, Y. S.; Hong, J. W. Dual Curing of Cationic UV-Curable Clear and Pigmented Coating Systems Photosensitized by Thioxanthone and Anthracene. *Polym. Test.* **2003**, 22 (6), 633–645. [https://doi.org/10.1016/S0142-9418\(02\)00169-1](https://doi.org/10.1016/S0142-9418(02)00169-1).

- (31) Cho, J. D.; Hong, J. W. UV-Initiated Free Radical and Cationic Photopolymerizations of Acrylate/Epoxy and Acrylate/Vinyl Ether Hybrid Systems with and without Photosensitizer. *J. Appl. Polym. Sci.* **2004**, *93* (3), 1473–1483. <https://doi.org/10.1002/app.20597>.
- (32) Scherzer, T.; Buchmeiser, M. R. Photoinitiated Cationic Polymerization of Cycloaliphatic Epoxy/Vinyl Ether Systems Studied by near-Infrared Reflection Spectroscopy. *Macromol. Chem. Phys.* **2007**, *208* (9), 946–954. <https://doi.org/10.1002/macp.200600649>.
- (33) Cho, J. D.; Hong, J. W. Photo-Curing Kinetics for the UV-Initiated Cationic Polymerization of a Cycloaliphatic Diepoxide System Photosensitized by Thioxanthone. *Eur. Polym. J.* **2005**, *41* (2), 367–374. <https://doi.org/10.1016/j.eurpolymj.2004.10.006>.
- (34) Tian, F.; Wang, X. L.; Yang, Y.; An, W.; Zhao, X.; Xu, S.; Wang, Y. Z. Energy-Efficient Conversion of Amine-Cured Epoxy Resins into Functional Chemicals Based on Swelling-Induced Nanopores. *ACS Sustain. Chem. Eng.* **2020**, *8* (5), 2226–2235. <https://doi.org/10.1021/acssuschemeng.9b06013>.
- (35) Babu, B. R.; Parande, A. K.; Basha, C. A. Electrical and Electronic Waste: A Global Environmental Problem. *Waste Manag. Res.* **2007**, *25* (4), 307–318. <https://doi.org/10.1177/0734242X07076941>.
- (36) Xue, X.; Liu, S.-Y.; Zhang, Z.-Y.; Wang, Q.-Z.; Xiao, C.-Z. A Technology Review of Recycling Methods for Fiber-Reinforced Thermosets. *J. Reinf. Plast. Compos.* **2021**, *19*, 552–610. <https://doi.org/10.1177/07316844211055208>.
- (37) Buchwalter, S. L.; Kosbar, L. L. Cleavable Epoxy Resins: Design for Disassembly of a Thermoset. *J. Polym. Sci. Part A Polym. Chem.* **1996**, *34* (2), 249–260. [https://doi.org/10.1002/\(SICI\)1099-0518\(19960130\)34:2<249::AID-POLA11>3.0.CO;2-Q](https://doi.org/10.1002/(SICI)1099-0518(19960130)34:2<249::AID-POLA11>3.0.CO;2-Q).
- (38) Elling, B. R.; Dichtel, W. R. Reprocessable Crosslinked Polymer Networks: Are Associative Exchange Mechanisms Desirable? *ACS Cent. Sci.* **2020**, *6* (9), 1488–1496. <https://doi.org/10.1021/acscentsci.0c00567>.
- (39) Fortman, D. J.; Brutman, J. P.; De Hoe, G. X.; Snyder, R. L.; Dichtel, W. R.; Hillmyer, M. A. Approaches to Sustainable and Continually Recyclable Crosslinked Polymers. *ACS Sustain. Chem. Eng.* **2018**, *6* (9), 11145–11159. <https://doi.org/10.1021/acssuschemeng.8b02355>.

- (40) Griebel, J. J.; Nguyen, N. A.; Namnabat, S.; Anderson, L. E.; Glass, R. S.; Norwood, R. A.; Mackay, M. E.; Char, K.; Pyun, J. Dynamic Covalent Polymers via Inverse Vulcanization of Elemental Sulfur for Healable Infrared Optical Materials. *ACS Macro Lett.* **2015**, *4* (9), 862–866. <https://doi.org/10.1021/acsmacrolett.5b00502>.
- (41) Tonkin, S. J.; Gibson, C. T.; Campbell, J. A.; Lewis, D. A.; Karton, A.; Hasell, T.; Chalker, J. M. Chemically Induced Repair, Adhesion, and Recycling of Polymers Made by Inverse Vulcanization. *Chem. Sci.* **2020**, *11* (21), 5537–5546. <https://doi.org/10.1039/d0sc00855a>.
- (42) Yan, P.; Zhao, W.; Tonkin, S. J.; Chalker, J. M.; Schiller, T. L.; Hasell, T. Stretchable and Durable Inverse Vulcanized Polymers with Chemical and Thermal Recycling. *Chem. Mater.* **2022**, *34* (3), 1167–1178. <https://doi.org/10.1021/acs.chemmater.1c03662>.
- (43) Stojcevski, F.; Stanfield, M. K.; Hayne, D. J.; Mann, M.; Lundquist, N. A.; Chalker, J. M.; Henderson, L. C. Inverse Vulcanisation of Canola Oil as a Route to Recyclable Chopped Carbon Fibre Composites. *Sustain. Mater. Technol.* **2022**, *32* (January), e00400. <https://doi.org/10.1016/j.susmat.2022.e00400>.
- (44) Tonkin, S. J.; Gibson, C. T.; Campbell, J. A.; Lewis, D. A.; Karton, A.; Hasell, T.; Chalker, J. M. Chemically Induced Repair, Adhesion, and Recycling of Polymers Made by Inverse Vulcanization. *Chem. Sci.* **2020**, *11* (21), 5537–5546. <https://doi.org/10.1039/D0SC00855A>.
- (45) Okajima, I.; Hiramatsu, M.; Shimamura, Y.; Awaya, T.; Sako, T. Chemical Recycling of Carbon Fiber Reinforced Plastic Using Supercritical Methanol. *J. Supercrit. Fluids* **2014**, *91*, 68–76. <https://doi.org/10.1016/j.supflu.2014.04.011>.
- (46) Kuang, X.; Shi, Q.; Zhou, Y.; Zhao, Z.; Wang, T.; Qi, H. J. Dissolution of Epoxy Thermosets: Via Mild Alcoholysis: The Mechanism and Kinetics Study. *RSC Adv.* **2018**, *8* (3), 1493–1502. <https://doi.org/10.1039/c7ra12787a>.
- (47) Kuang, X.; Zhou, Y.; Shi, Q.; Wang, T.; Qi, H. J. Recycling of Epoxy Thermoset and Composites via Good Solvent Assisted and Small Molecules Participated Exchange Reactions. *ACS Sustain. Chem. Eng.* **2018**, *6* (7), 9189–9197. <https://doi.org/10.1021/acssuschemeng.8b01538>.
- (48) Dang, W.; Kubouchi, M.; Yamamoto, S.; Sembokuya, H.; Tsuda, K. An Approach to Chemical Recycling of Epoxy Resin Cured with Amine Using Nitric Acid. *Polymer (Guildf)*. **2002**, *43* (10), 2953–2958. [https://doi.org/10.1016/S0032-3861\(02\)00100-3](https://doi.org/10.1016/S0032-3861(02)00100-3).



- (49) Singh, S. K.; Savoy, A. W. Ionic Liquids Synthesis and Applications: An Overview. *J. Mol. Liq.* **2020**, 297 (8), 112–150. <https://doi.org/10.1016/j.molliq.2019.112038>.
- (50) Lei, Z.; Chen, B.; Koo, Y. M.; Macfarlane, D. R. Introduction: Ionic Liquids. *Chem. Rev.* **2017**, 117 (10), 6633–6635. <https://doi.org/10.1021/acs.chemrev.7b00246>.
- (51) Chardin, C.; Rouden, J.; Livi, S.; Baudoux, J. Dimethyldioxirane (DMDO) as a Valuable Oxidant for the Synthesis of Polyfunctional Aromatic Imidazolium Monomers Bearing Epoxides. *Green Chem.* **2017**, 19 (21), 5054–5059. <https://doi.org/10.1039/c7gc02372c>.
- (52) Paduszyński, K.; Domańska, U. Viscosity of Ionic Liquids: An Extensive Database and a New Group Contribution Model Based on a Feed-Forward Artificial Neural Network. *J. Chem. Inf. Model.* **2014**, 54 (5), 1311–1324. <https://doi.org/10.1021/ci500206u>.
- (53) Kim, H.; Char, K. Dielectric Changes during the Curing of Epoxy Resin Based on the Diglycidyl Ether of Bisphenol A (DGEBA) with Diamine. *Bull. Korean Chem. Soc.* **1999**, 20 (11), 1329–1334.
- (54) Koh, J. K.; Koh, J. H.; Ahn, S. H.; Kim, J. H.; Kang, Y. S. Solid-State Dye-Sensitized Solar Cells Employing One-Pot Synthesized Supramolecular Electrolytes with Multiple Hydrogen Bonding. *Electrochim. Acta* **2010**, 55 (7), 2567–2574. <https://doi.org/10.1016/j.electacta.2009.12.035>.
- (55) McDanel, W. M.; Cowan, M. G.; Carlisle, T. K.; Swanson, A. K.; Noble, R. D.; Gin, D. L. Crosslinked Ionic Resins and Gels from Epoxide-Functionalized Imidazolium Ionic Liquid Monomers. *Polymer (Guildf)*. **2014**, 55 (16), 3305–3313. <https://doi.org/10.1016/j.polymer.2014.04.039>.
- (56) Radchenko, A. V.; Chabane, H.; Demir, B.; Searles, D. J.; Duchet-Rumeau, J.; Gérard, J. F.; Baudoux, J.; Livi, S. New Epoxy Thermosets Derived from a Bisimidazolium Ionic Liquid Monomer: An Experimental and Modeling Investigation. *ACS Sustain. Chem. Eng.* **2020**, 8 (32), 12208–12221. <https://doi.org/10.1021/acssuschemeng.0c03832>.
- (57) Livi, S.; Chardin, C.; Lins, L. C.; Halawani, N.; Pruvost, S.; Duchet-Rumeau, J.; Gérard, J. F.; Baudoux, J. From Ionic Liquid Epoxy Monomer to Tunable Epoxy-Amine Network: Reaction Mechanism and Final Properties. *ACS Sustain. Chem. Eng.* **2019**, 7 (3), 3602–3613. <https://doi.org/10.1021/acssuschemeng.8b06271>.

- (58) Grugel, R. N.; Hastings, W. C.; Rabenberg, E.; Kaukler, W. F.; Henry, C. Evaluation of Carbon Fiber Composites Fabricated Using Ionic Liquid Based Epoxies for Cryogenic Fluid Applications. *Results Phys.* **2016**, *6*, 1188–1189. <https://doi.org/10.1016/j.rinp.2016.11.011>.
- (59) Chardin, C.; Durand, A.; Jarsalé, K.; Rouden, J.; Livi, S.; Baudoux, J. Sulfonimides versus Ketosulfonamides as Epoxidized Imidazolium Counterions: Towards a New Generation of Ionic Liquid Monomers. *New J. Chem.* **2021**, *45* (6), 2953–2957. <https://doi.org/10.1039/D0NJ05126H>.
- (60) Matsumoto, K.; Endo, T. Synthesis of Networked Polymers by Copolymerization of Monoepoxy-Substituted Lithium Sulfonylimide and Diepoxy-Substituted Poly(Ethylene Glycol), and Their Properties. *J. Polym. Sci. Part A Polym. Chem.* **2011**, *49* (8), 1874–1880. <https://doi.org/10.1002/pola.24614>.
- (61) Ly Nguyen, T. K.; Obadia, M. M.; Serghei, A.; Livi, S.; Duchet-Rumeau, J.; Drockenmuller, E. 1,2,3-Triazolium-Based Epoxy-Amine Networks: Ion-Conducting Polymer Electrolytes. *Macromol. Rapid Commun.* **2016**, *37* (14), 1168–1174. <https://doi.org/10.1002/marc.201600018>.
- (62) Matsumoto, K.; Endo, T. Synthesis of Ion Conductive Networked Polymers Based on an Ionic Liquid Epoxide Having a Quaternary Ammonium Salt Structure. *Macromolecules* **2009**, *42* (13), 4580–4584. <https://doi.org/10.1021/ma900508q>.
- (63) Livi, S.; Lins, L. C.; Capeletti, L. B.; Chardin, C.; Halawani, N.; Baudoux, J.; Cardoso, M. B. Antibacterial Surface Based on New Epoxy-Amine Networks from Ionic Liquid Monomers. *Eur. Polym. J.* **2019**, *116*, 56–64. <https://doi.org/10.1016/j.eurpolymj.2019.04.008>.
- (64) Stavropoulos, P.; Spetsieris, A.; Papacharalampopoulos, A. A Circular Economy Based Decision Support System for the Assembly/Disassembly of Multi-Material Components. *Procedia CIRP* **2019**, *85*, 49–54. <https://doi.org/10.1016/j.procir.2019.09.033>.
- (65) Dumée, L. Circular Economy and Sustainability. In *Circular Economy and Sustainability*; Elsevier, 2022; pp 359–372. <https://doi.org/10.1016/C2019-0-04146-5>.
- (66) Mayo, S. L.; Olafson, B. D.; Goddard, W. A. DREIDING: A Generic Force Field for Molecular Simulations. *J. Phys. Chem.* **1990**, *94* (26), 8897–8909. <https://doi.org/10.1021/j100389a010>.

- (67) Hanwell, M. D.; Curtis, D. E.; Lonie, D. C.; Vandermeersch, T.; Zurek, E.; Hutchison, G. R. Avogadro: An Advanced Semantic Chemical Editor, Visualization, and Analysis Platform. *J. Cheminform.* **2012**, *4* (8), 1–17. <https://doi.org/10.1186/1758-2946-4-17>.
- (68) Martinez, L.; Andrade, R.; Birgin, E. G.; Martínez, J. M. PACKMOL: A Package for Building Initial Configurations for Molecular Dynamics Simulations. *J. Comput. Chem.* **2009**, *30* (13), 2157–2164. <https://doi.org/10.1002/JCC.21224>.
- (69) Madorsky, S. L.; Straus, S. Thermal Degradation of Polymers at High Temperatures. *J. Res. Natl. Bur. Stand. Sect. A Phys. Chem.* **1959**, *63A* (3), 261. <https://doi.org/10.6028/jres.063a.020>.
- (70) Meyer, L. O.; Schulte, K.; Grove-Nielsen, E. CFRP-Recycling Following a Pyrolysis Route: Process Optimization and Potentials. *J. Compos. Mater.* **2009**, *43* (9), 1121–1132. <https://doi.org/10.1177/0021998308097737>.
- (71) Zhang, Z.; Reddy, R. G. Thermal Stability of Ionic Liquids. In *Ionic Liquids*; De Gruyter, 2019; pp 1–16. <https://doi.org/10.1515/9783110583632-001>.
- (72) Yang, Z.; Pan, W. Ionic Liquids: Green Solvents for Nonaqueous Biocatalysis. *Enzyme Microb. Technol.* **2005**, *37* (1), 19–28. <https://doi.org/10.1016/j.enzmictec.2005.02.014>.
- (73) Mousavi, S. P.; Atashrouz, S.; Rezaei, F.; Peyvastegan, M.-E.; Hemmati-Sarapardeh, A.; Mohaddespour, A. Modeling Thermal Conductivity of Ionic Liquids: A Comparison between Chemical Structure and Thermodynamic Properties-Based Models. *J. Mol. Liq.* **2021**, *322*, 114911. <https://doi.org/10.1016/j.molliq.2020.114911>.
- (74) França, J. M. P.; Lourenço, M. J. V.; Murshed, S. M. S.; Pádua, A. A. H.; Nieto de Castro, C. A. Thermal Conductivity of Ionic Liquids and Ionanofluids and Their Feasibility as Heat Transfer Fluids. *Ind. Eng. Chem. Res.* **2018**, *57* (18), 6516–6529. <https://doi.org/10.1021/acs.iecr.7b04770>.
- (75) Yebra, F.; Troncoso, J.; Romaní, L. Thermal Conductivity of Ionic Liquids under Pressure. *Fluid Phase Equilib.* **2020**, *515*, 112573. <https://doi.org/10.1016/j.fluid.2020.112573>.
- (76) Paredes, X.; Lourenço, M. J.; Castro, C. N. de; Wakeham, W. Thermal Conductivity of Ionic Liquids and Ionanofluids. Can Molecular Theory Help? *Fluids* **2021**, *6* (3), 116. <https://doi.org/10.3390/fluids6030116>.

- (77) Nguyen, T. K. L.; Livi, S.; Pruvost, S.; Soares, B. G.; Duchet-Rumeau, J. Ionic Liquids as Reactive Additives for the Preparation and Modification of Epoxy Networks. *J. Polym. Sci. Part A Polym. Chem.* **2014**, *8*, 252–285. <https://doi.org/10.1002/pola.27420>.
- (78) Nguyen, T. K. L.; Livi, S.; Soares, B. G.; Pruvost, S.; Duchet-Rumeau, J.; Gérard, J.-F. Ionic Liquids: A New Route for the Design of Epoxy Networks. *ACS Sustain. Chem. Eng.* **2016**, *4* (2), 481–490. <https://doi.org/10.1021/acssuschemeng.5b00953>.
- (79) Karger-Kocsis, J.; Kéki, S. Recent Advances in Shape Memory Epoxy Resins and Composites. In *Multifunctionality of Polymer Composites*; Elsevier, 2015; pp 822–841. <https://doi.org/10.1016/B978-0-323-26434-1.00027-1>.
- (80) Wu, X.; Yang, X.; Zhang, Y.; Huang, W. A New Shape Memory Epoxy Resin with Excellent Comprehensive Properties. *J. Mater. Sci.* **2016**, *51* (6), 3231–3240. <https://doi.org/10.1007/s10853-015-9634-4>.
- (81) Sun, L.; Wang, T. X.; Chen, H. M.; Salvekar, A. V.; Naveen, B. S.; Xu, Q.; Weng, Y.; Guo, X.; Chen, Y.; Huang, W. M. A Brief Review of the Shape Memory Phenomena in Polymers and Their Typical Sensor Applications. *Polymers*. 2019. <https://doi.org/10.3390/polym11061049>.
- (82) Halawani, N.; Donato, R.; Benes, H.; Brus, J.; Kobera, L.; Pruvost, S.; Duchet-Rumeau, J.; Gérard, J.-F.; Livi, S. Thermoset-Thermoplastic-Ionic Liquid Ternary Hybrids as Novel Functional Polymer Materials. *Polymer (Guildf)*. **2021**, *218*, 123–137. <https://doi.org/10.1016/j.polymer.2021.123507>.
- (83) Urbaczewski-Espuche, E.; Galy, J.; Gerard, J.-F.; Pascault, J.-P.; Sautereau, H. Influence of Chain Flexibility and Crosslink Density on Mechanical Properties of Epoxy/Amine Networks. *Polym. Eng. Sci.* **1991**, *31* (22), 1572–1580. <https://doi.org/10.1002/pen.760312204>.
- (84) Garcia, F. G.; Soares, B. G.; Pita, V. J. R. R.; Sánchez, R.; Rieumont, J.; Rangel, A. Mechanical Properties of Epoxy Networks Based on DGEBA and Aliphatic Amines. *J Appl Polym Sci* **2007**, *106*, 2047–2055. <https://doi.org/10.1002/app.24895>.
- (85) Qi, B.; Zhang, Q. X.; Bannister, M.; Mai, Y. W. Investigation of the Mechanical Properties of DGEBA-Based Epoxy Resin with Nanoclay Additives. *Compos. Struct.* **2006**, *75* (1–4), 514–519. <https://doi.org/10.1016/J.COMPSTRUCT.2006.04.032>.
- (86) Liu, S.; Zhang, H.; Zhang, Z.; Zhang, T.; Sprenger, S. Tailoring the Mechanical Performance of Epoxy Resin by Various Nanoparticles. *Polym. Polym. Compos.* **2008**, *16* (8), 527–533. <https://doi.org/10.1177/096739110801600806>.

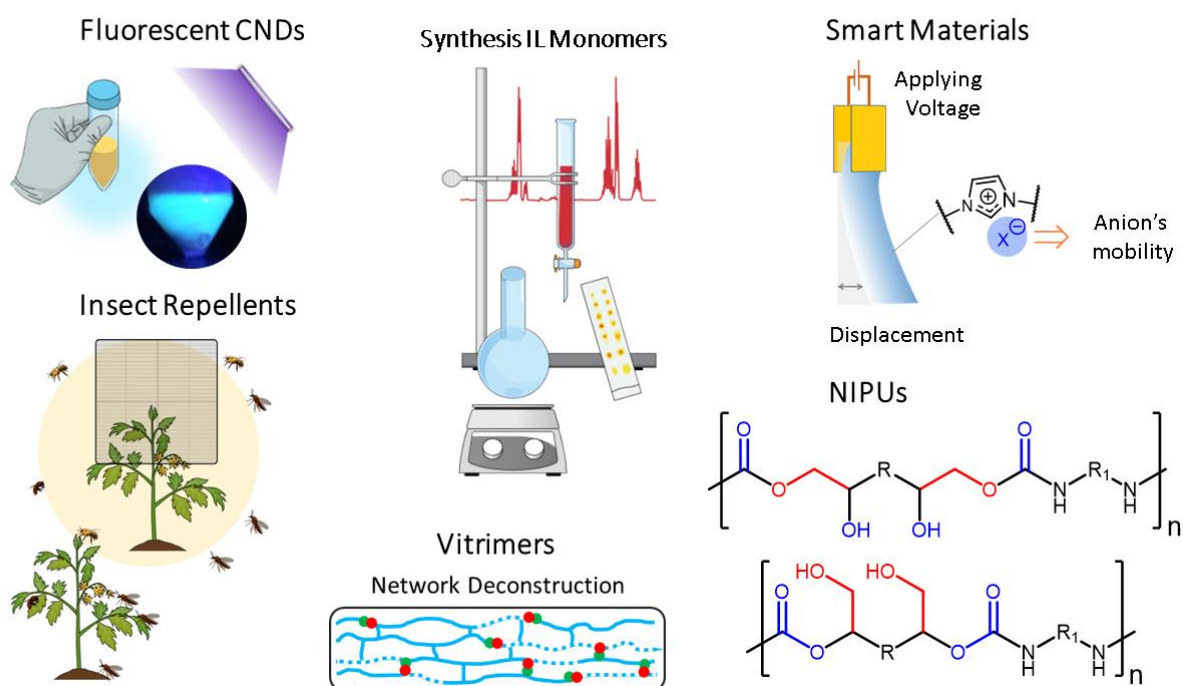
- (87) Balguri, P. K.; Samuel, D. G. H.; Thumu, U. A Review on Mechanical Properties of Epoxy Nanocomposites. *Mater. Today Proc.* **2021**, *44*, 346–355. <https://doi.org/10.1016/j.matpr.2020.09.742>.
- (88) Ponyrko, S.; Donato, R. K.; Matějka, L. Tailored High Performance Shape Memory Epoxy–Silica Nanocomposites. Structure Design. *Polym. Chem.* **2016**, *7* (3), 560–572. <https://doi.org/10.1039/C5PY01450F>.
- (89) Pandit, A.; Khare, L.; Ganatra, P.; Jain, R.; Dandekar, P. Intriguing Role of Novel Ionic Liquids in Stochastic Degradation of Chitosan. *Carbohydr. Polym.* **2021**, *260*, 117828. <https://doi.org/10.1016/j.carbpol.2021.117828>.
- (90) Mahmood, H.; Moniruzzaman, M.; Yusup, S.; Welton, T. Ionic Liquids Assisted Processing of Renewable Resources for the Fabrication of Biodegradable Composite Materials. *Green Chem.* **2017**, *19* (9), 2051–2075. <https://doi.org/10.1039/C7GC00318H>.
- (91) Wang, H.; Li, Z.; Liu, Y.; Zhang, X.; Zhang, S. Degradation of Poly(Ethylene Terephthalate) Using Ionic Liquids. *Green Chem.* **2009**, *11* (10), 1568. <https://doi.org/10.1039/b906831g>.
- (92) Park, K. I.; Xanthos, M. A Study on the Degradation of Polylactic Acid in the Presence of Phosphonium Ionic Liquids. *Polym. Degrad. Stab.* **2009**, *94* (5), 834–844. <https://doi.org/10.1016/j.polymdegradstab.2009.01.030>.
- (93) Anastas, P. T.; Warner, J. C. Green Chemistry: Theory and Practice. In *Green Chemistry: Theory and Practice*; Oxford University Press, 2000, 1998; pp 30–35.
- (94) Hamad, K.; Kaseem, M.; Deri, F. Recycling of Waste from Polymer Materials: An Overview of the Recent Works. *Polym. Degrad. Stab.* **2013**, *98* (12), 2801–2812. <https://doi.org/10.1016/j.polymdegradstab.2013.09.025>.
- (95) Ramdin, M.; De Loos, T. W.; Vlught, T. J. H. State-of-the-Art of CO<sub>2</sub> Capture with Ionic Liquids. *Ind. Eng. Chem. Res.* **2012**, *51* (24), 8149–8177. <https://doi.org/10.1021/ie3003705>.
- (96) Somers, A. E.; Howlett, P. C.; MacFarlane, D. R.; Forsyth, M. A Review of Ionic Liquid Lubricants. *Lubricants* **2013**, *1* (1), 3–21. <https://doi.org/10.3390/lubricants1010003>.
- (97) Caldas, C. M.; Soares, B. G.; Indrusiak, T.; Barra, G. M. O. Ionic Liquids as Dispersing Agents of Graphene Nanoplatelets in Poly(Methyl Methacrylate) Composites with

Microwave Absorbing Properties. *J. Appl. Polym. Sci.* **2021**, *138* (6), 1–18.  
<https://doi.org/10.1002/app.49814>.

- (98) Livi, S.; Duchet-Rumeau, J.; Pham, T. N.; Gérard, J. F. A Comparative Study on Different Ionic Liquids Used as Surfactants: Effect on Thermal and Mechanical Properties of High-Density Polyethylene Nanocomposites. *J. Colloid Interface Sci.* **2010**, *349* (1), 424–433. <https://doi.org/10.1016/j.jcis.2009.09.036>.

# 06

## Conclusion and Perspectives



## Conclusion and Perspectives

In this doctoral research, we aimed to develop a library of second-generation epoxy monomers to build multifunctional and high-performance thermosets and composites with a more sustainable and eco-friendlier end-of-life. A computational methodology facilitated the monomer's design, saving significant energy, time, and effort. We referred to this approach as *efficient design*, which has demonstrated advantages for molecular engineering building blocks with IL moieties and cleavable groups. Each study employed different curing agents, and the resulting networks demonstrated improved thermal stability, excellent mechanical properties and tailored degradability. The resulting networks were subjected to selective chemical solvolysis, which enabled the recovery of IL specimens. These IL compounds can be reintroduced into thermosets or directly re-employed in lower-quality applications to prolong their lifespans.

Our first study tailors the thermosets' mechanical, physicochemical and degradable properties by molecular engineering monomers bearing ester groups, an imidazolium backbone and multiple adjacent epoxy groups. The resulting epoxy-amine networks have shown high homogeneity, shape-memory behavior, and mechanical properties comparable to DGEBA thermosets.

The second study uses a tetra-epoxidized IL as a cleavable building block, to develop more sustainable composites. Introducing this co-monomer improves the carbon fiber surface wettability with the epoxy matrices and enhances the morphological network's homogeneity. More importantly, the cleavable co-monomer, tetra-epoxy, allowed the degradation of the thermoset matrices, ensuring the full recovery of the CFs in their virgin state.

The third study presented the synthesis of several cycloaliphatic epoxidized ILs. One of the monomers, CEIL, was employed as a comonomer to build networks with excellent thermal stability and mechanical properties. Further, the last part of this work showed promising advancements in synthesizing reactive monomers for cationic photoinduced polymerizations.

The three studies illustrate the potential of ILs as monomers in creating degradable epoxy thermosets under mild conditions. These findings provide a foundation for developing high-performance, environmentally friendly thermosets and composites in line with the circular economy's expectations.

Currently, additional characterizations of the networks and composites developed in this work have been done:



*Mechanical tests:* The preliminary tensile tests demonstrated that the introduction of IL moieties had a notable effect on the ductility of thermoset materials. This is particularly promising since epoxy thermosets tend to be rigid and brittle, and the modify this characteristic is significant. Determining the energy required to fracture the samples through a fracture test is vital as we intend to create thermosets for structural applications. Additionally, it would be advantageous to investigate whether using ILs can enhance the material's resistance to fatigue. With the addition of ILs, additional channels for energy dissipation are introduced, which could improve their mechanical resilience. Completing this mechanical characterization is essential to envision future aircraft, automobile, and ship manufacturing applications.

*Liquid and gas permeation testing:* Liquid gas permeation testing can provide valuable information about the ability of these polymers to store and transport gases. The thermosets based on the novel monomers can also be used to selectively develop membranes to separate gas. Further, water barrier testing can inform the development of new materials with improved moisture resistance and help optimize the processing conditions to achieve the desired water barrier properties.

*Anti-icing testing:* Evaluating a material's anti-icing properties involves measuring its ability to delay or prevent ice formation on its surface when exposed to freezing conditions. A promising approach to reduce ice formation and adhesion involves using coatings made from synthetic IL monomers that create a hydrophobic surface, repelling water. Developing IL-based networks with improved anti-icing properties could significantly affect various industries. For instance, in aerospace, ice formation on aircraft surfaces can lead to undesired situations, and in infrastructure and transportation, ice formation can result in damage and safety hazards.

*Further optimization of the solvolysis methodology:* The existing method developed during this doctorate research has enabled the complete degradation of the networks. However, further optimization would be beneficial to control the reaction kinetics and facilitate the formation of a single product.

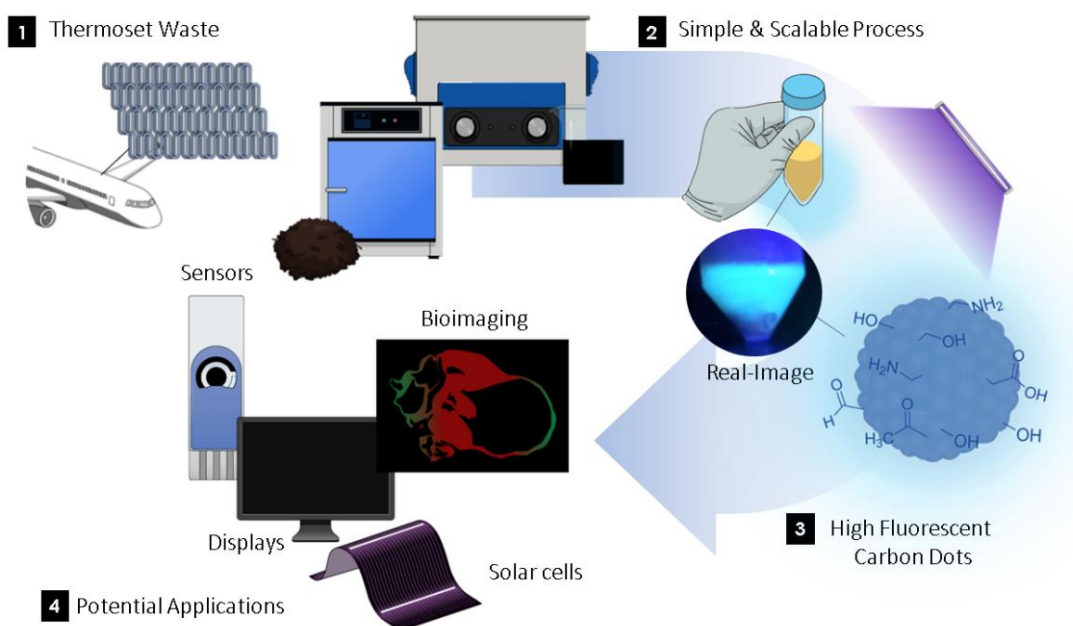
*Single fiber pull-out test:* Even though we have used SEM to gather information about the compatibility between CFs and the epoxy matrix, the interfacial properties of this system are not fully understood. Single-fiber pull-out testing is necessary to determine the bonding strength between the two phases, which is crucial for stress transfer from the matrix to the reinforcing fibers and for identifying any defects at the interface.

*Tensile test of single fibers:* In order to verify that the original properties of the reclaimed CFs were preserved, we conducted single-fiber tensile strength tests before and after the recycling methodologies. The test results were consistent with the microscopy images that had shown no damage to the carbon fibers.

It is worth noting that we have several ongoing projects that employ IL-based monomers to develop smart and sustainable polymer technologies. Among these projects, we can mention:

### **1. From Thermoset Waste to High Blue-Light Fluorescent Carbon Dots: A Up-recycling Plot Twist**

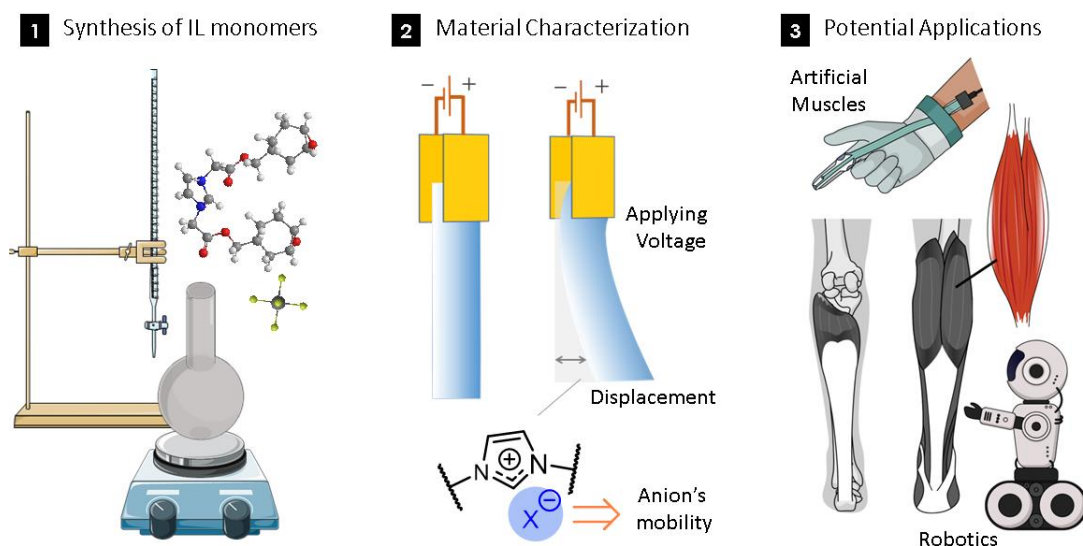
Our doctoral research aimed to build novel materials and promote a more sustainable end-of-life for them. Through our experiments, we discovered a promising pathway for achieving this goal: synthesizing high-fluorescence carbon nanodots (CNDs) from discarded thermosets based on tri- and tetra-epoxies (**Fig. VI-1**). CNDs are promising materials due to their intrinsic fluorescence, electron-transfer properties, and low toxicity. In this work, we developed a sustainable, cheap, scalable methodology to obtain high fluorescent CNDs. The thermoset materials based on tri- and tetra-epoxies were subjected to a thermal treatment, followed by nanosizing in a ultrasound bath. The resulting colloidal dispersion was filtered resulting in a production of highly fluorescent CNDs. The CNDs have shown an unexpectedly strong blue-light fluorescence in the aqueous and solid phases. Therefore, this study presents an uprecycling approach for producing fluorescent materials from thermoset residue. These CNDs have the potential to replace costly and toxic rare-earth and heavy-metal materials, which are commonly used in displays, solar cells, bioimaging, and sensing.



**Figure VI-1.** The general outline of the high blue-light fluorescent CNDs synthesis from thermoset waste. In **(1)** and **(2)**, the thermoset waste and the thermal treatment followed by nanofragmentation using an ultrasound bath. **(3)** Displays the fluorescent investigation, and **(4)** the future potential applications.

## 2. Smart Material Actuators Based on Epoxidized IL Monomers

An example worth mentioning is the project that was jointly developed with the research team led by Gildas Coativy (LGEF, INSA Lyon, France). This project aimed to develop actuators and understand the mechanism of displacement induced by an external electrical field (**Fig. VI-2**). To the best of our knowledge, there are no published reports on using epoxidized ILs for developing thermosets with a stimulus-response to electrical fields. This study cured the novel epoxidized ILs with amines to produce low  $T_g$  materials. The response of these materials under the influence of an electrical field was examined. The findings are quite promising as they indicate a reversible shape memory effect mediated by the external electrical field and originated by the anion's displacement.

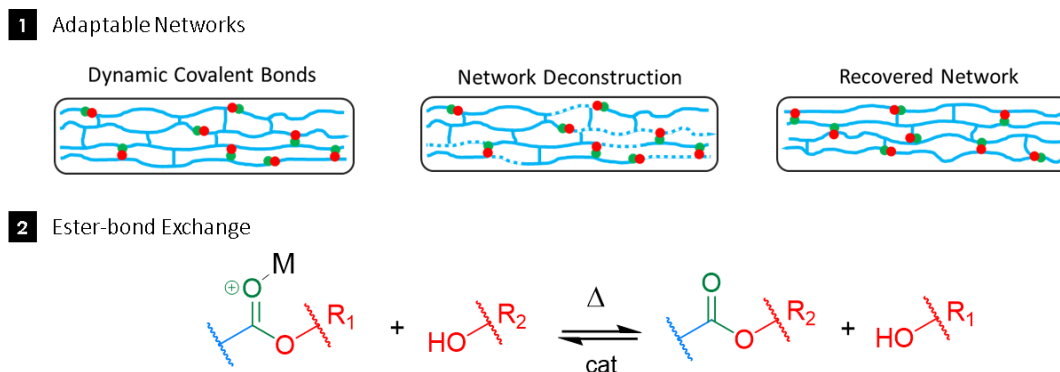


**Figure VI-2.** General overview of actuator's development. In **(1)** the design and synthesis of ILs bearing different anions with different mobilities, **(2)** material characterization and comprehension of the actuating mechanism. Finally, **(3)** the investigation of potential applications.

### 3. Design and Development of High Performance and Multifunctional Vitri-mer Materials using Epoxidized Ionic Liquids and Metallic Ionic Curing Agents

In another collaboration, Dr. Ruan Henriques from the research group of Professor Bluma Soares Brazil (LMPCC, Federal University of Rio de Janeiro, Brazil) employed the monomers synthesized during this doctoral research to build multifunctional vitrimers (**Fig. VI-3**). This study presents the epoxidized imidazolium ILs, anhydride (MTHPA), and metallic iron phosphonium IL, as a platform for developing vitrimer systems. The study examined the precursors' curing behaviour and the resulting polymer's features, including thermal, mechanical, reprocessing, and shape memory properties. Results indicate that the anhydride and phosphonium IL work synergistically to cure the epoxidized IL monomers. The newly formed networks exhibited thermomechanical properties ( $T_{df}$  and  $T_{\alpha}$ ) that were similar to those of commercially available thermosets. The system containing tetra-epoxy showed superior properties, as it could achieve a higher crosslink density. All materials demonstrated recyclability and reprocessability, allowing for the dynamic exchange of ester bonds within the crosslinked networks. Recycling was accomplished through thermomechanical and chemical reprocessing, using hot pressing and ethylene glycol dissolution. The recycled materials retained their original mechanical properties. The new epoxy system also displayed a shape memory and self-healing effects, fully recovering its shape at the programming temperature. By emphasizing the sustainability of vitrimers, this study's findings

highlight the use of epoxidized imidazolium-ILs, anhydride, and iron-based ILs as a molecular platform for developing multifunctional vitrimers. This approach enables the design of materials with remarkable properties while promoting the circular economy and reducing waste.

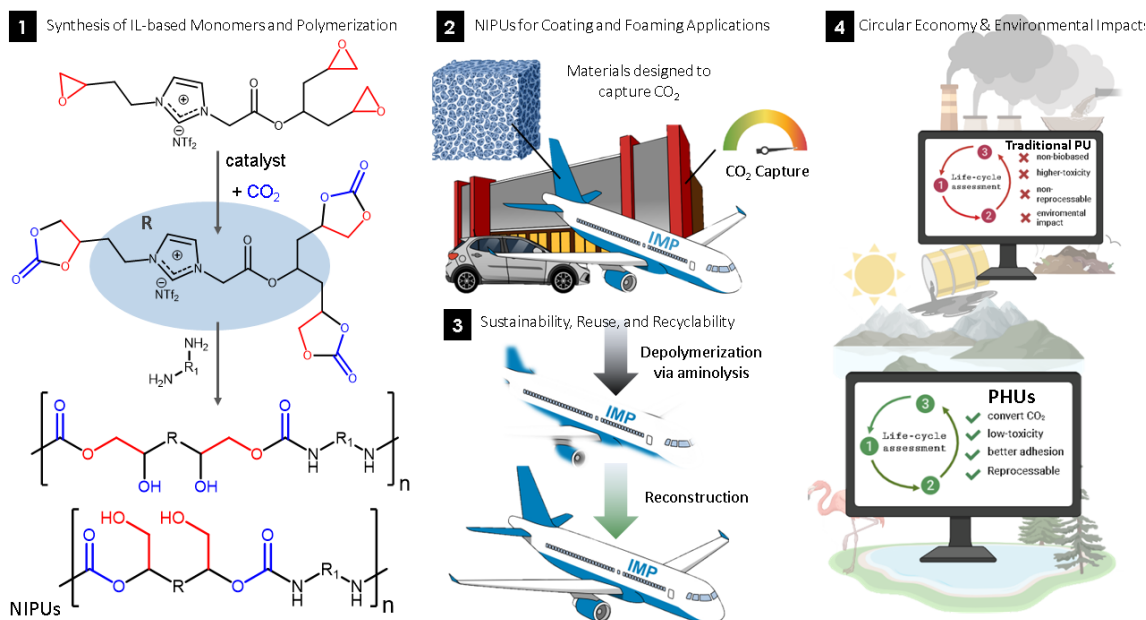


**Figure VI-3.** Development of vitrimer systems based on IL monomers and a metallic IL curing agent. **(1)** Exhibits the steps of the development of network development, and **(2)** the mechanism of transesterification that yield the dynamic behavior of the networks.

#### 4. High-performance CO<sub>2</sub> Capture Exploring the Synergistic Effects of Epoxidized Ionic Liquids and Their Conversion to Sustainable Polyurethanes

We also investigated at our laboratory the potential of using tri- and tetra-epoxy monomers as a molecular platform for synthesising Non-Isocyanate PolyUrethanes (NIPUs). NIPUs are polyurethane synthesized without using isocyanates, which are known to be harmful to human health and the environment. Instead, NIPUs are made by reacting amines with cyclic carbonates or carbamates derived from CO<sub>2</sub>, making them more sustainable and environmentally friendly. The importance of NIPUs lies in their potential to replace traditional polyurethanes, which are widely used in industry but have negative environmental and health impacts. NIPUs offer a greener alternative with comparable or superior properties to conventional polyurethanes. Additionally, NIPUs can be designed using waste CO<sub>2</sub> as a feedstock, reducing greenhouse CO<sub>2</sub> from its incorporation into the plastic matrices. This study explored epoxidized-ILs to solubilize and further activate and react with CO<sub>2</sub> demonstrating high CO<sub>2</sub> capture capability (**Fig. VI-4**). Under the optimal supercritical conditions, the epoxidized ILs were converted to cyclo carbonate in high yields without solvents and with a small amount of IL catalyst. These cyclocarbonate precursors were then polymerized with various types of amines (aliphatic, cycloaliphatic, and aromatic) to yield NIPUs. Using epoxidized ILs as CO<sub>2</sub>-capturing agents provides a more environmentally friendly approach than traditional methods, as they do not require harsh chemicals or solvents. Overall, this study demonstrates the potential of epoxidized ILs for use in sustainable

CO<sub>2</sub> capturing and utilization and the development of NIPUs with desirable properties. These findings have implications for the design and synthesis of high-performance materials with potential for sustainable applications.



**Figure VI-4.** The general workflow on the development of NIPUs from IL monomers. In **(1)**, the cyclo-carbonate derivative synthesis is followed by the curing process with amines. **(2)** the development of CO<sub>2</sub>-capturing coatings **(3)** and their chemical recycling. Finally, in **(4)**, the measurement of environmental impacts.

In the past three years, synthetic IL monomers have been envisioned for various applications, such as developing gas separation membranes, fuel cells, solid electrolytes, porous materials, electronic packaging, adhesives, and dielectric and insulating materials. We have attempted to explore some of these possibilities. Nevertheless, it seems clear that time was a limiting factor since we endeavored to design and synthesize new monomers, develop and characterize materials, and ensure their sustainability at the end of life. So, we look forward to exploring the potential applications of these novel monomers, networks, and composites in future research conducted in our laboratory.

Regardless, it may be worthwhile to revisit the second sub-question of the Introduction: What is the real value of this doctoral research to the fields of Polymer and Material Science?

While some progress has been made in developing thermosets based on IL monomers, it remains uncertain what the true contribution of this research will be. Only with time and the further development of novel materials and related research will provide a

clearer view of its significance. Thus, it is crucial to continue exploring and pushing the boundaries to unlock new discoveries and develop materials that can potentially impact real life in the coming decades, with a little bit of luck.

# **Appendix I - From the Design of Novel Tri- and Tetra-epoxidized Ionic Liquid Monomers to the End-of-Life of Multifunctional Degradable Epoxy Thermosets**



# From the Design of Novel Tri- and Tetra-epoxidized Ionic Liquid Monomers to the End-of-Life of Multifunctional Degradable Epoxy Thermosets

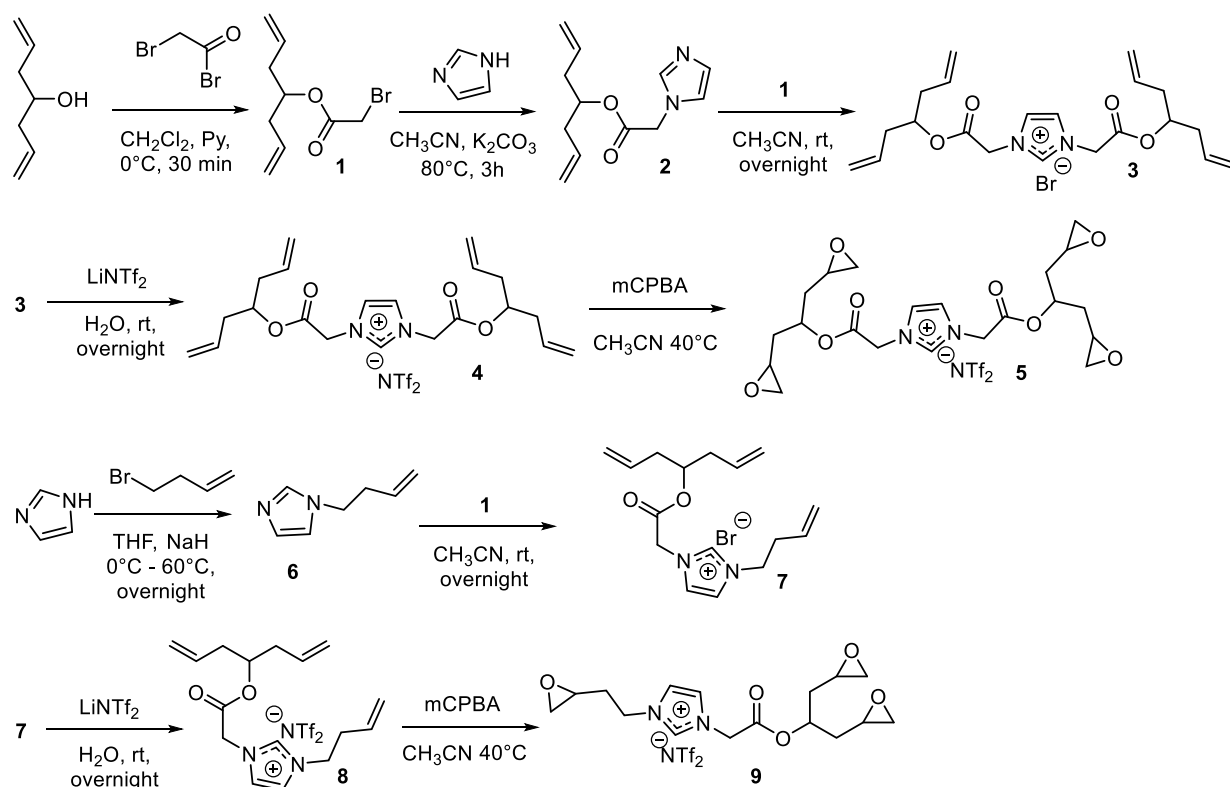
## General Methodology

### Characterization and Purification Methods

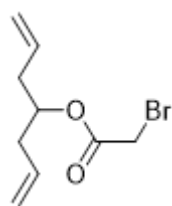
$^1\text{H}$  and  $^{13}\text{C}$  spectra were recorded on a Bruker Avance III spectrometer operating at 400 MHz or 500 MHz. Spectra were obtained using solutions of *ca.* 10 mg in appropriate deuterated solvents. The chemical shifts ( $\delta$ ) are expressed in ppm relative to internal tetramethylsilane for  $^1\text{H}$  and  $^{13}\text{C}$  nuclei. The coupling constants were automatically obtained by TopSpin® and expressed in Hz. Abbreviations for signal coupling are indicated as: s = singlet; d=doublet; dd=doublet of doublets; t=triplet; q=quartet; quin=quintet; m=multiplet; br=broad signal. To accurately determine the molecular structure of the monomer CEIL and its intermediates additional 2D NMR experiments (COSY, HSQC, HMBC) were performed.

High Resolution Mass Spectra HRMS was carried out on by a Micromass-Waters Q-TOF Ultima Global by the technique of Electrospray Ionization (ESI).

Thin Layer Chromatography (TLC) was run using different eluent mixtures on pre-coated aluminum plates of silica gel 60 F-254 (Merck).



### Hepta-1,6-dien-4-yl 2-bromoacetate (1)



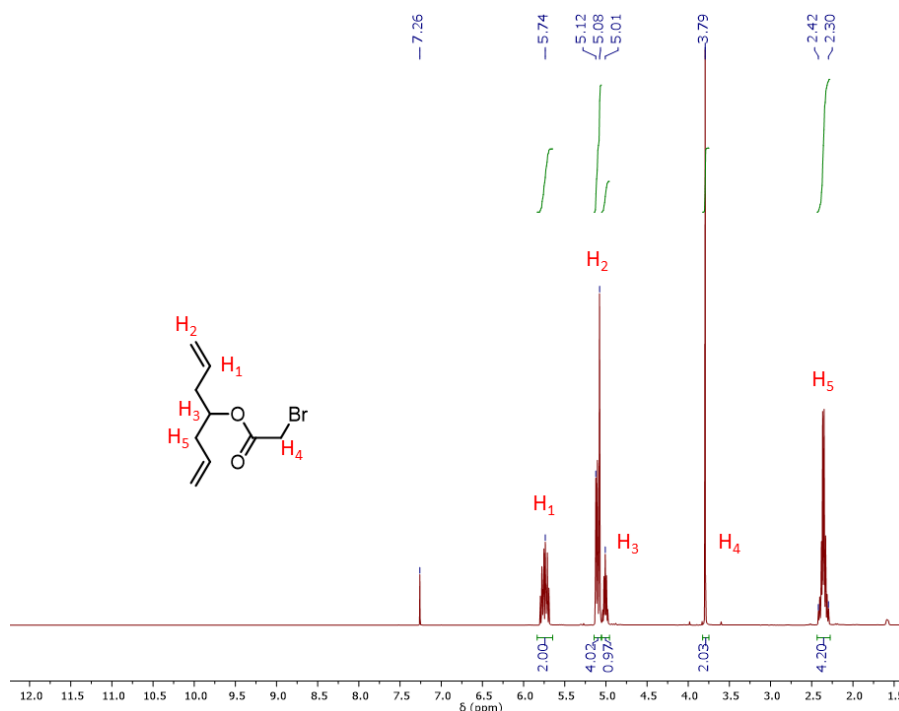
Hepta-1,6-dien-4-ol (11.6 mL, 89 mmol) and pyridine (11 mL, 134 mmol) were dissolved in 400 mL of anhydrous  $\text{CH}_2\text{Cl}_2$  under Ar atmosphere. The solution was cooled down to  $0^\circ\text{C}$  and 10 mL (115 mmol) of 2-bromoacetyl bromide were added dropwise during 20 min. The mixture was stirred for 30 min and then 200 mL of  $\text{NH}_4\text{Cl}$  saturated solution in water were introduced. The product was extracted 2 times by  $\text{CH}_2\text{Cl}_2$ , organic extracts were washed 2 times by HCl 1 M and 1 time by brine solution, dried over  $\text{MgSO}_4$  and filtered. The solvent was removed under reduced pressure and the crude product was purified by column chromatography (*n*-hexane:Ethyl acetate, 164 g  $\text{SiO}_2$ ). Yield: 19.5 g, 94%.

$^1\text{H}$  NMR (400 MHz, Chloroform-*d*)  $\delta$ : 5.74 (ddt,  $J = 17.2, 10.3, 7.1$  Hz, 2H), 5.22 – 5.05 (m, 4H), 5.01 (d,  $J = 6.5$  Hz, 1H), 3.79 (s, 2H), 2.57 – 2.16 (m, 4H).

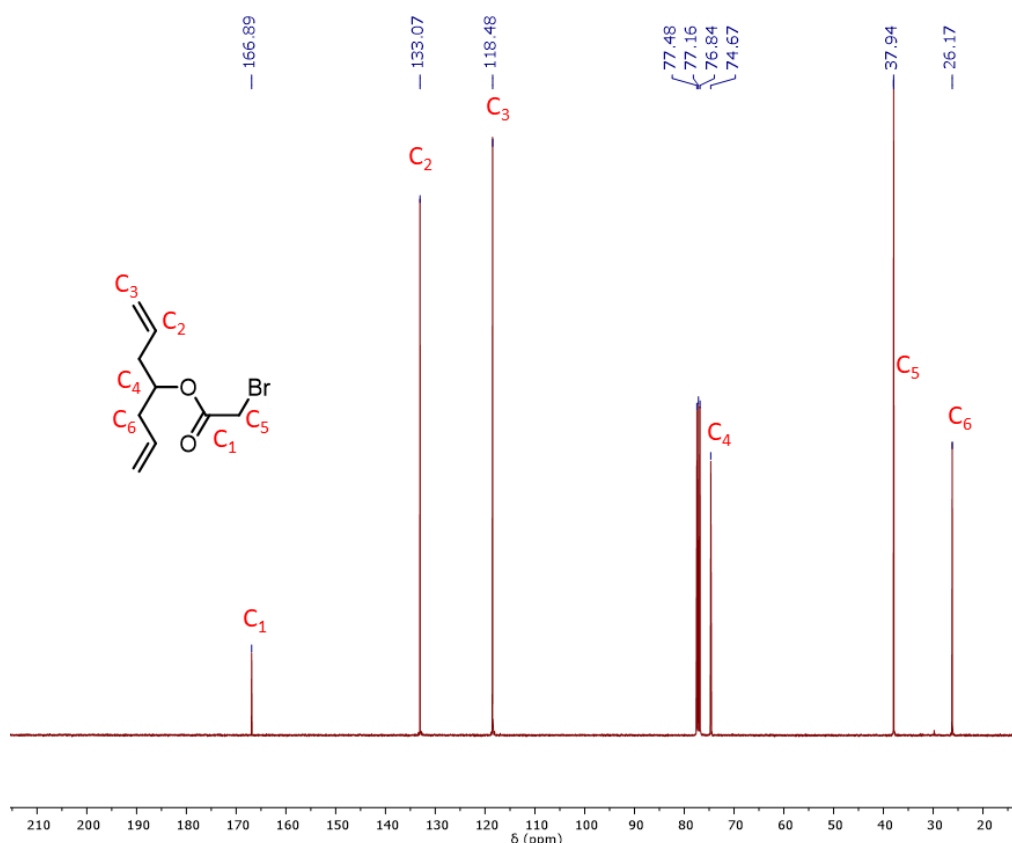
$^{13}\text{C}$  NMR (101 MHz, Chloroform-*d*)  $\delta$ : 166.9, 133.1, 118.5, 74.7, 37.9, 26.2.

IR (neat)  $\text{cm}^{-1}$ : 3079, 2980, 1733, 1275, 1166, 1107, 993, 977, 917.

HRMS  $m/z$  (ESI): calcd. for  $\text{C}_9\text{H}_{13}\text{O}_2\text{BrNa}$   $[\text{M}+\text{Na}]^+$ : 254.9991, found: 254.9989.

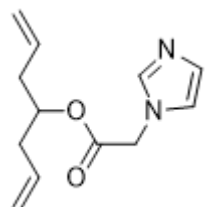


**Figure III-S1.**  $^1\text{H}$  NMR spectrum of Hepta-1,6-dien-4-yl 2-bromoacetate (1) (400 MHz,  $\text{CDCl}_3$ ,  $25^\circ\text{C}$ ).



**Figure III-S2.**  $^{13}\text{C}$  NMR spectrum of Hepta-1,6-dien-4-yl 2-bromoacetate (**1**) (400 MHz,  $\text{CDCl}_3$ , 25  $^\circ\text{C}$ ).

#### Hepta-1,6-dien-4-yl 2-(1H-imidazol-1-yl)acetate (**2**)



Imidazole (0.07 g, 1.0 mmol) and **1** (0.2 g, 0.86 mmol) were dissolved in 4 mL of  $\text{CH}_3\text{CN}$ . Then, 0.25 g of potassium carbonate were added to the solution and the mixture was stirred for 3 hours at 80  $^\circ\text{C}$ . Then the mixture was cooled down until room temperature, diluted with 30 mL of  $\text{CH}_2\text{Cl}_2$ , washed twice by water and one by brine solution, dried over

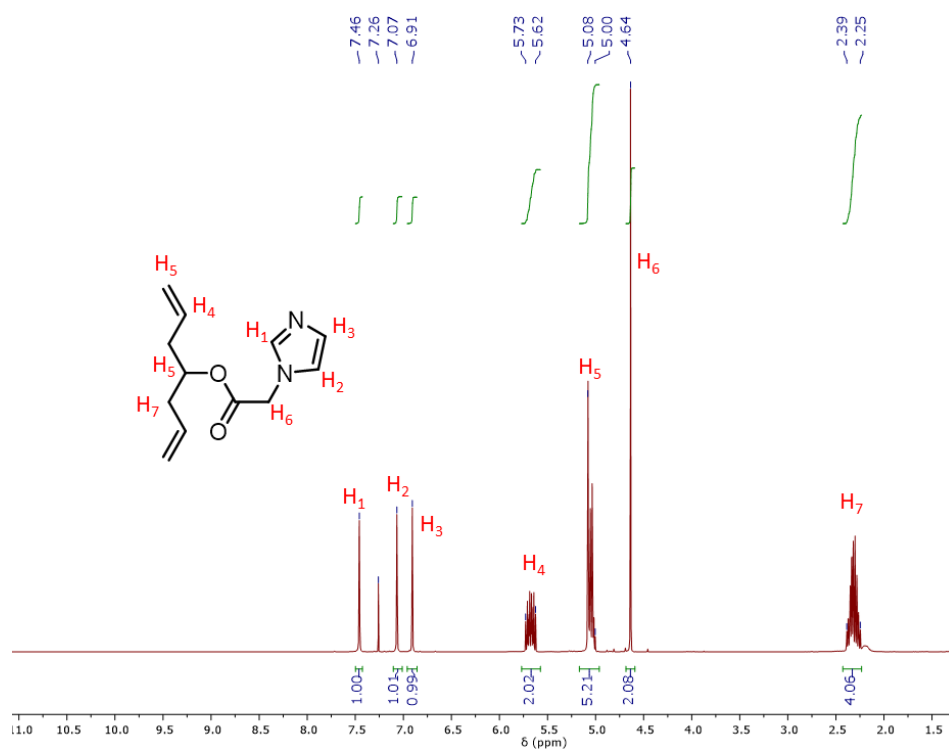
$\text{MgSO}_4$  and filtered. The solvent was removed under reduced pressure, and the crude product was purified by column chromatography (Ethyl acetate, 6 g  $\text{SiO}_2$ ). Yield: 0.12 g, 62%.

**$^1\text{H}$  NMR (400 MHz, Chloroform-*d*)  $\delta$ :** 7.46 (s, 1H), 7.07 (s, 1H), 6.91 (s, 1H), 5.74 – 5.59 (m, 2H), 5.10 – 4.98 (m, 5H), 4.64 (s, 2H), 2.40 – 2.20 (m, 4H).

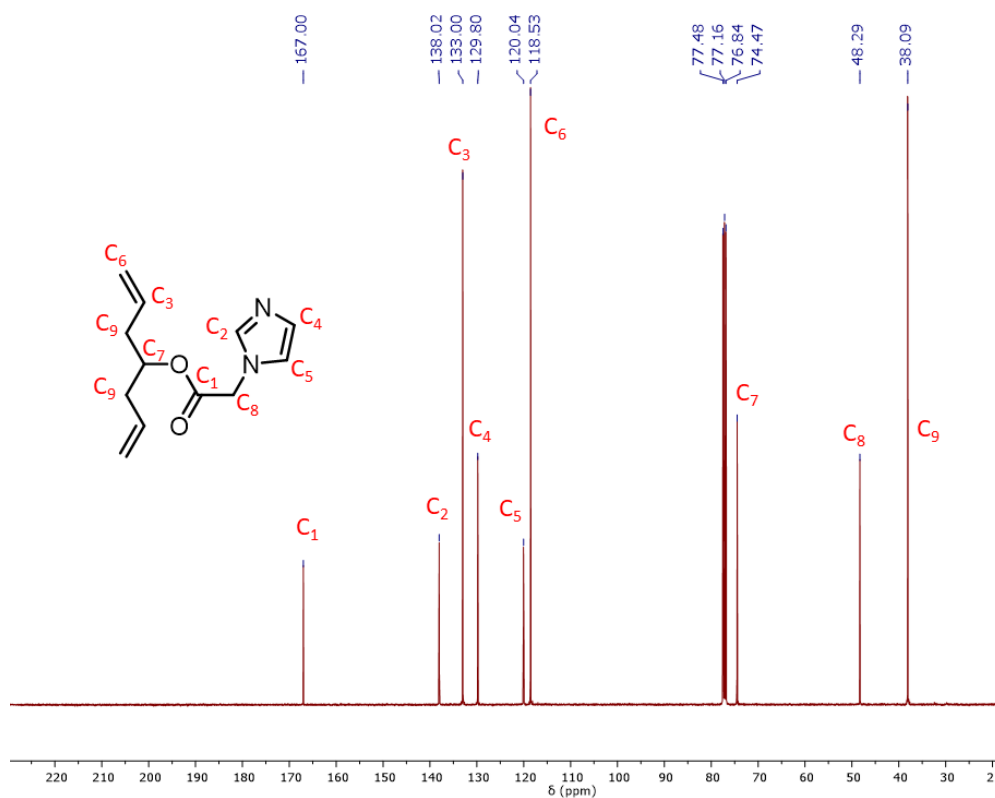
**$^{13}\text{C}$  NMR (101 MHz, Chloroform-*d*)  $\delta$ :** 167.0, 138.0, 133.0, 129.8, 120.0, 118.5, 74.5, 48.3, 38.1.

**IR (neat)  $\text{cm}^{-1}$ :** 3078, 2979, 1743, 1642, 1507, 1208, 1077, 994, 916, 734.

**HRMS  $m/z$  (ESI):** calcd. for  $\text{C}_{12}\text{H}_{17}\text{N}_2\text{O}_2$   $[\text{M}+\text{H}]^+$ : 221.1285, found: 221.1283.

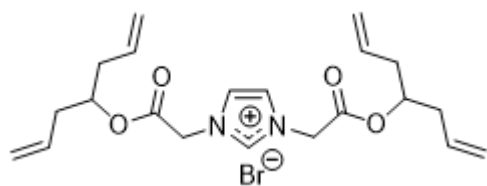


**Figure III-S3.** <sup>1</sup>H NMR spectrum of Hepta-1,6-dien-4-yl 2-(1H-imidazol-1-yl)acetate (2) (400 MHz, CDCl<sub>3</sub>, 25 °C).



**Figure III-S4.** <sup>13</sup>C NMR spectrum of Hepta-1,6-dien-4-yl 2-(1H-imidazol-1-yl)acetate (2) (400 MHz, CDCl<sub>3</sub>, 25 °C).

**1,3-bis(2-(hepta-1,6-dien-4-yloxy)-2-oxoethyl)-1H-3l4-imidazol-1-ium bromide (3)**



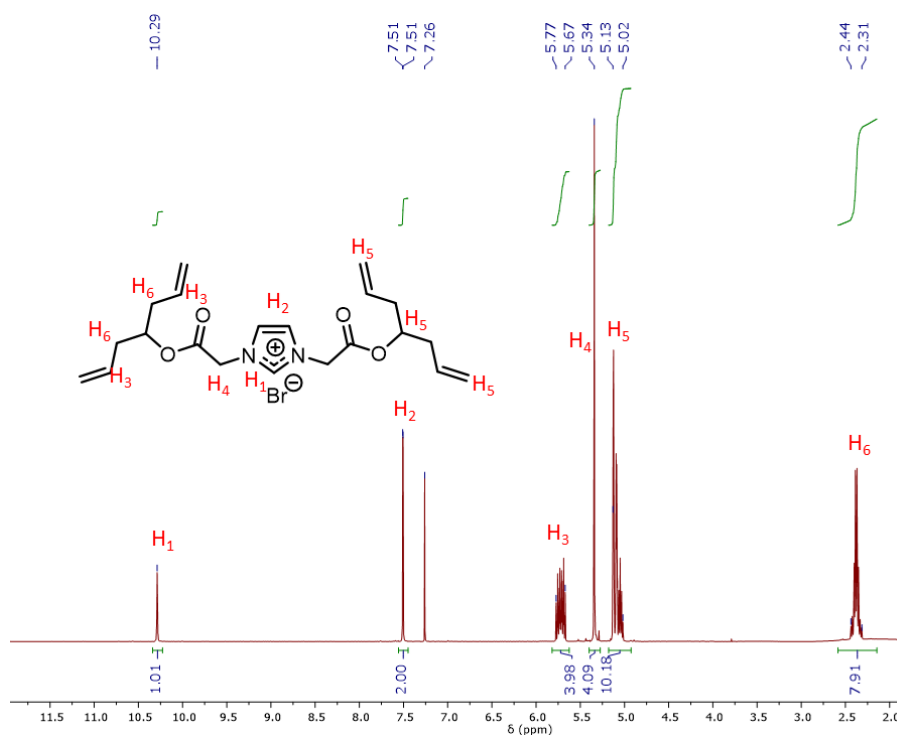
Subsequently, compound **2** (0.1 g, 0.45 mmol) was dissolved in 1 mL of CH<sub>3</sub>CN and **1** (0.127 g, 0.55 mmol) was added. The mixture was stirred overnight at room temperature and precipitated in 100 mL of Et<sub>2</sub>O; the product was washed twice with Et<sub>2</sub>O and dried under vacuum. Yield: 0.2 g, 93%.

**<sup>1</sup>H NMR (400 MHz, Chloroform-*d*) δ:** 10.29 (s, 1H), 7.51 (d, *J* = 1.6 Hz, 2H), 5.78 – 5.65 (m, 4H), 5.34 (s, 4H), 5.16 – 5.00 (m, 10H), 2.44 – 2.31 (m, 8H).

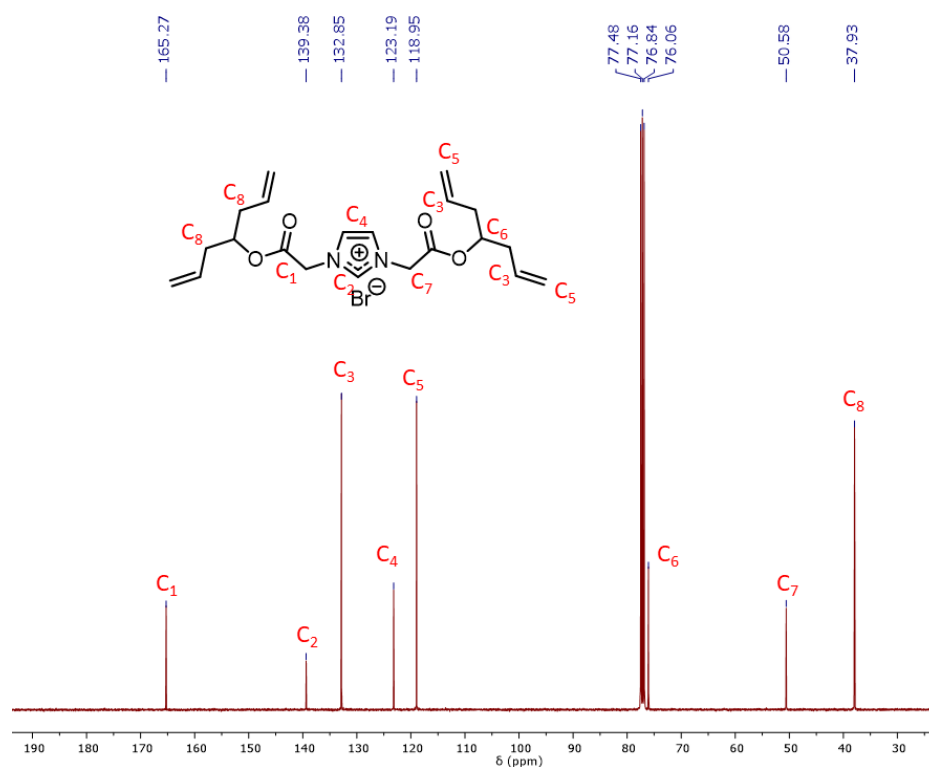
**<sup>13</sup>C NMR (101 MHz, Chloroform-*d*) δ:** 165.3, 139.4, 132.8, 123.2, 118.9, 76.1, 50.6, 37.9.

**IR (neat) cm<sup>-1</sup>:** 3082, 2977, 2920, 1750, 1377, 1205, 1180, 971, 926.

**HRMS *m/z* (ESI):** calcd. for C<sub>21</sub>H<sub>29</sub>N<sub>2</sub>O<sub>4</sub> [M]<sup>+</sup>: 373.212184, found: 373.212153.

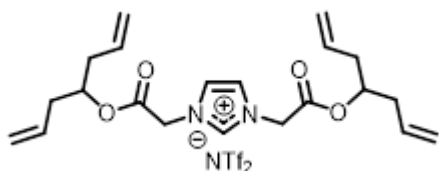


**Figure III-S5.** <sup>1</sup>H NMR spectrum of 1,3-bis(2-(hepta-1,6-dien-4-yloxy)-2-oxoethyl)-1H-3l4-imidazol-1-ium bromide (**3**) (400 MHz, CDCl<sub>3</sub>, 25 °C).



**Figure III-S6.**  $^{13}\text{C}$  NMR spectrum of 1,3-bis(2-(hepta-1,6-dien-4-yloxy)-2-oxoethyl)-1H-3,4-imidazol-1-ium bromide (**3**) (400 MHz,  $\text{CDCl}_3$ , 25  $^\circ\text{C}$ ).

**1,3-bis(2-(hepta-1,6-dien-4-yloxy)-2-oxoethyl)-1H-3,4-imidazol-1-ium bistrifluoromethanesulfonimide (**4**)**



The compound **3** (0.19 g, 0.68 mmol) was dissolved in 4 mL of  $\text{H}_2\text{O}$  at 80 $^\circ\text{C}$ , the solution of  $\text{LiNTf}_2$  (0.15 g, 0.5 mmol) in 4 mL of  $\text{H}_2\text{O}$  was added, and the mixture was left overnight at room temperature. The mixture

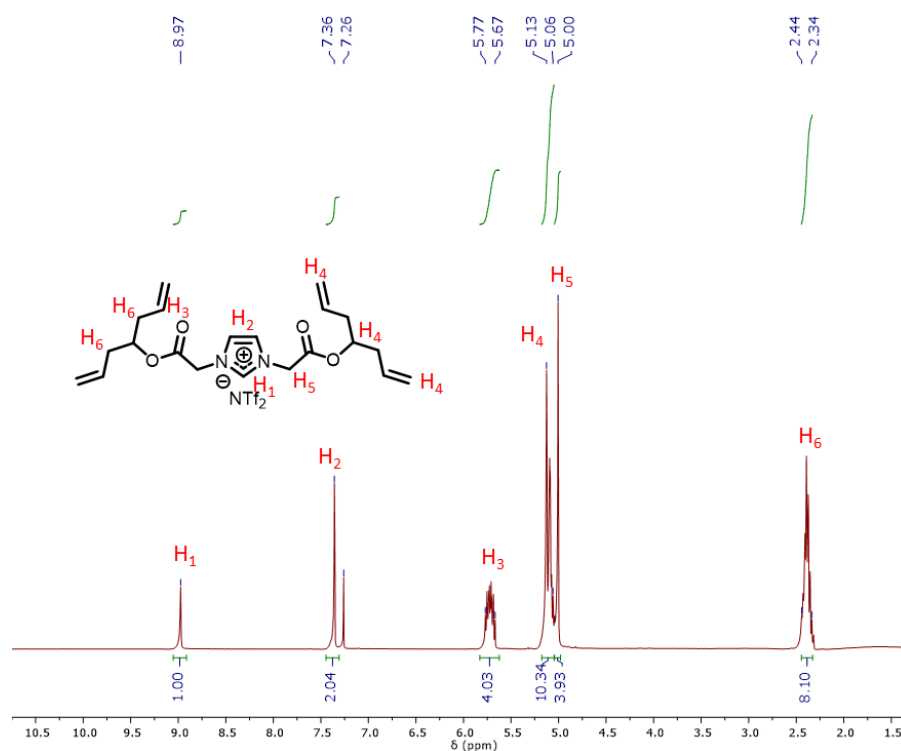
was extracted three times by  $\text{CH}_2\text{Cl}_2$  (3x10mL). Organic extracts were combined and washed twice with water, dried over  $\text{MgSO}_4$  and filtered. The solvent was removed under reduced pressure ( $m = 0.25$  g, 96%).

**$^1\text{H}$  NMR (400 MHz, Chloroform- $d$ )  $\delta$ :** 9.00 (s, 1H), 7.38 (s, 2H), 5.74 (ddt,  $J = 19.4, 9.5, 7.1$  Hz, 4H), 5.21 – 5.06 (m, 10H), 5.03 (s, 4H), 2.49 – 2.33 (m, 8H).

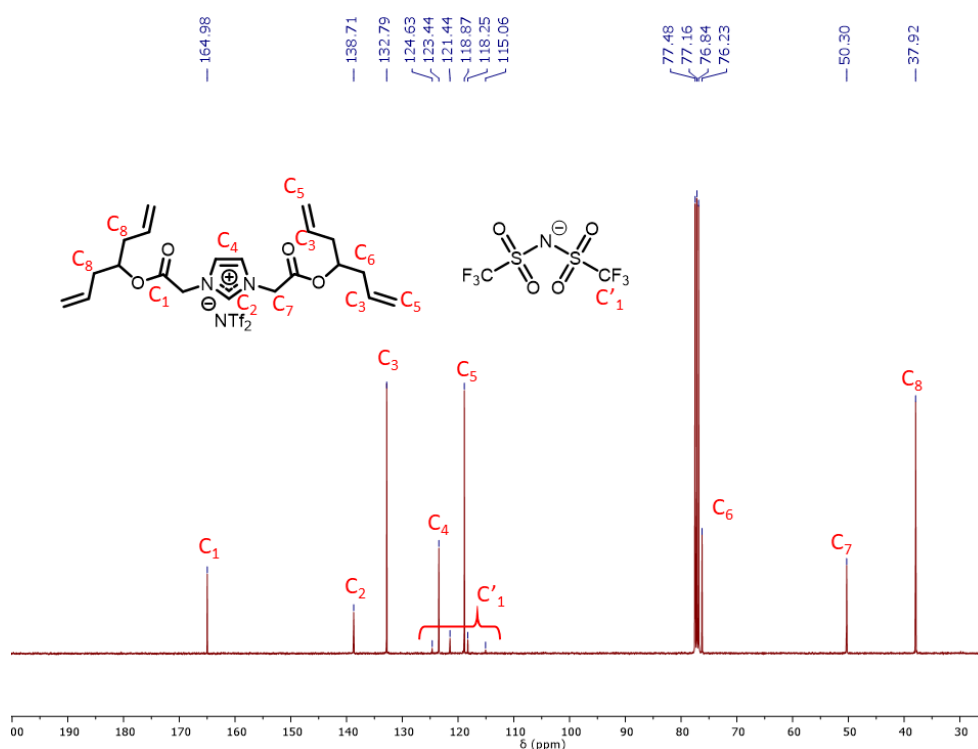
**$^{13}\text{C}$  NMR (101 MHz, Chloroform- $d$ )  $\delta$ :** 164.8, 138.6, 132.6, 123.3, 119.7 (q,  $J = 321.0$  Hz), 118.7, 76.1, 50.2, 37.8.

**IR (neat)  $\text{cm}^{-1}$ :** 3085, 1743, 1643, 1570, 1435, 1348, 1205, 1134, 1054, 993, 919, 870, 788, 739.

**HRMS  $m/z$  (ESI):** calcd. for  $\text{C}_{21}\text{H}_{29}\text{N}_2\text{O}_4$   $[\text{M}]^+$ : 373.21221, found: 373.212184.

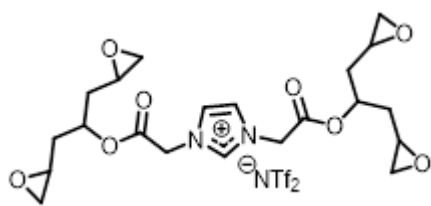


**Figure III-S7.**  $^1\text{H}$  NMR spectrum of 1,3-bis(2-(hepta-1,6-dien-4-yloxy)-2-oxoethyl)-1H-3l4-imidazol-1-ium bistrifluoromethanesulfonimide (4) (400 MHz,  $\text{CDCl}_3$ , 25  $^\circ\text{C}$ ).



**Figure III-S8.**  $^{13}\text{C}$  NMR spectrum of 1,3-bis(2-(hepta-1,6-dien-4-yloxy)-2-oxoethyl)-1H-3l4-imidazol-1-ium bistrifluoromethanesulfonimide (4) (400 MHz,  $\text{CDCl}_3$ , 25  $^\circ\text{C}$ ).

**bis(1,3-di(oxiran-2-yl)propan-2-yl) 2,2'-(1H-3l4-imidazole-1,3-diyl)diacetate bistrifluoromethanesulfonimide (5)**



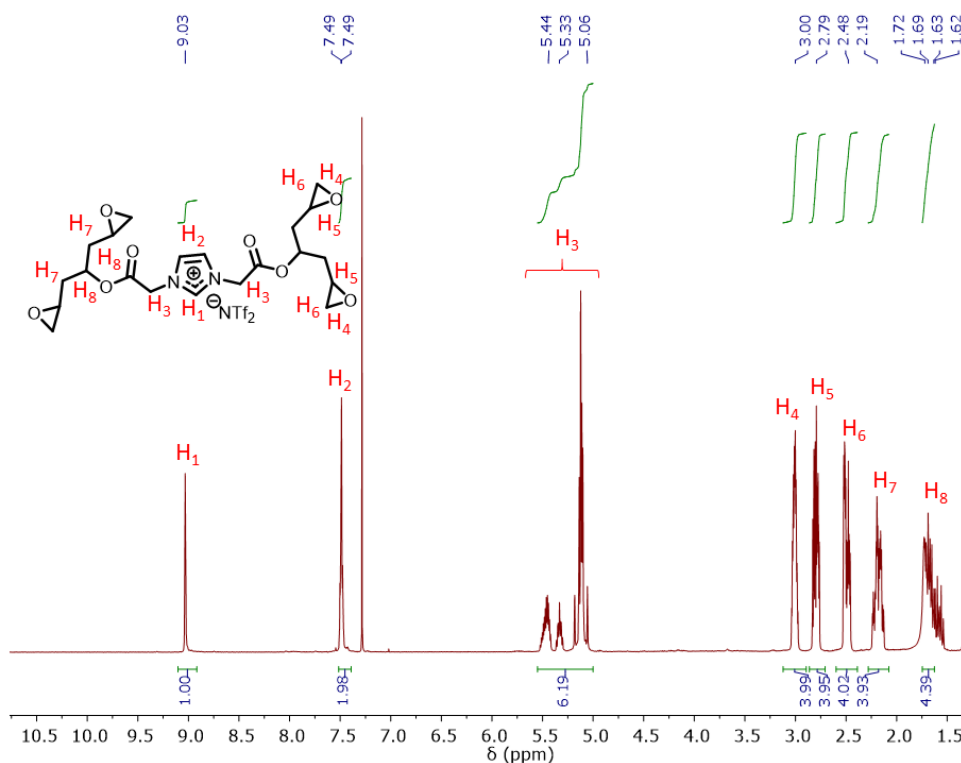
Subsequently, 0.525 g (2.3 mmol) of *m*CPBA were added to the solution of compound **8** (0.25 g, 0.38 mmol) in CH<sub>3</sub>CN (10.2 mL). The mixture was stirred for 72 at 40 °C, filtered through a glass filter and concentrated under reduced pressure. The residue was washed four times with Et<sub>2</sub>O and dried under vacuum (m = 0.1937 g, 99%).

**<sup>1</sup>H NMR (400 MHz, Chloroform-*d*)**  $\delta$ : 9.0 (s, 1H), 7.5 (s, 2H), 5.5 – 5.3 (m, 2H), 5.2 – 5.0 (m, 4H), 3.1 – 2.9 (m, 4H), 2.8 – 2.7 (m, 4H), 2.5 – 2.4 (m, 4H), 2.2 – 2.1 (m, 4H), 1.7 – 1.5 (m, 4H).

**<sup>13</sup>C NMR (101 MHz, Chloroform-*d*)**  $\delta$ : 165.4, 138.6, 123.6, 121.3, 73.5, 73.3, 50.4, 50.4, 50.2, 49.3, 49.1, 48.5, 48.5, 46.9, 46.7, 46.1, 46.1, 37.6, 37.0, 36.6.

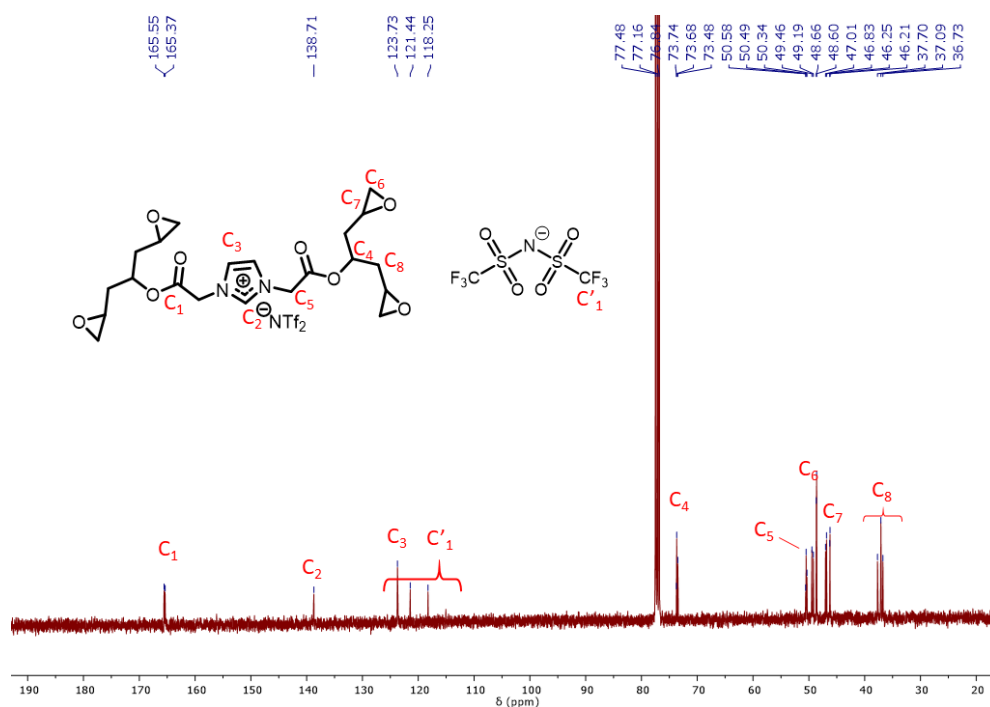
**IR (neat) cm<sup>-1</sup>**: 1748, 1570, 1347, 1205, 1132, 1053, 914, 845, 788, 739.

**HRMS *m/z* (ESI)**: calcd. for C<sub>21</sub>H<sub>29</sub>N<sub>2</sub>O<sub>4</sub> [M]<sup>+</sup>: 437.19184, found: 437.19188.



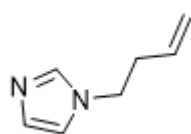
**Figure III-S9.** <sup>1</sup>H NMR spectrum of bis(1,3-di(oxiran-2-yl)propan-2-yl) 2,2'-(1H-3l4-imidazole-1,3-diyl)diacetate bistrifluoromethanesulfonimide (**5**) (400 MHz, CDCl<sub>3</sub>, 25 °C).





**Figure III-S10.**  $^{13}\text{C}$  NMR spectrum of bis(1,3-di(oxiran-2-yl)propan-2-yl) 2,2'-(1H-3l4-imidazole-1,3-diyl)diacetate bistrifluoromethanesulfonimide (5) (400 MHz,  $\text{CDCl}_3$ , 25  $^\circ\text{C}$ ).

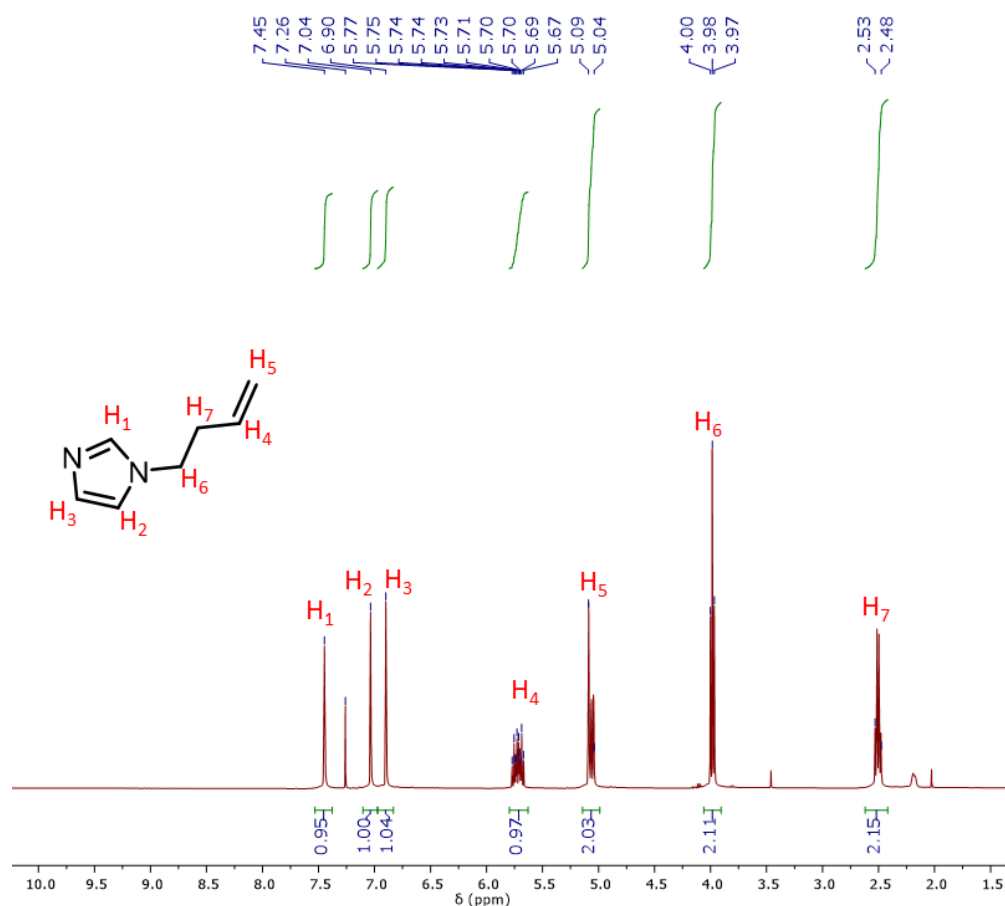
#### 1-(but-3-en-1-yl)-1H-imidazole (6)



Imidazole (3.54 g, 52 mmol) was slowly added to the mixture of NaH (4.17 g (60% in mineral oil), 104 mmol) and THF (100 mL) at 0 $^\circ\text{C}$ . The mixture was stirred for 1 h at room temperature, and then 4-bromobutene (6.35 mL, 62.5 mmol) was added dropwise at 0 $^\circ\text{C}$ . The reaction was left overnight at 60  $^\circ\text{C}$ . The mixture was cooled down to 0 $^\circ\text{C}$ , and 30 mL of  $\text{H}_2\text{O}$  were added slowly. The mixture was concentrated under reduced pressure, extracted twice by  $\text{CH}_2\text{Cl}_2$ ; organic extracts were washed twice by water, dried with  $\text{MgSO}_4$  and filtered. The solvent was removed under reduced pressure and the crude product was purified by column chromatography (Ethyl acetate, 35 g  $\text{SiO}_2$ ). Yield: 3.1 g, 60%.

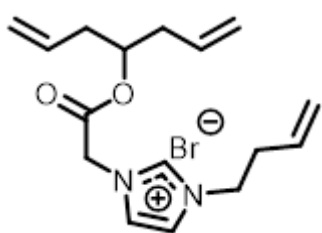
*Org. Lett.* 2002, 4, 24, 4345–4348 <https://doi.org/10.1021/ol0270024>

**$^1\text{H}$  NMR (400 MHz, Chloroform-*d*)  $\delta$ :** 7.45 (s, 1H), 7.04 (s, 1H), 6.90 (s, 1H), 5.72 (ddt,  $J$  = 16.4, 10.8, 6.8 Hz, 1H), 5.14 – 4.92 (m, 2H), 3.98 (t,  $J$  = 7.1 Hz, 2H), 2.59 – 2.39 (m, 2H).



**Figure III-S11.**  $^1\text{H}$  NMR spectrum of 1-(but-3-en-1-yl)-1H-imidazole (**6**) (400 MHz,  $\text{CDCl}_3$ , 25  $^\circ\text{C}$ ).

**1-(but-3-en-1-yl)-3-(2-(di-allylmethoxy)-2-oxoethyl)-1H-imidazol-3-ium bromide (**7**)**



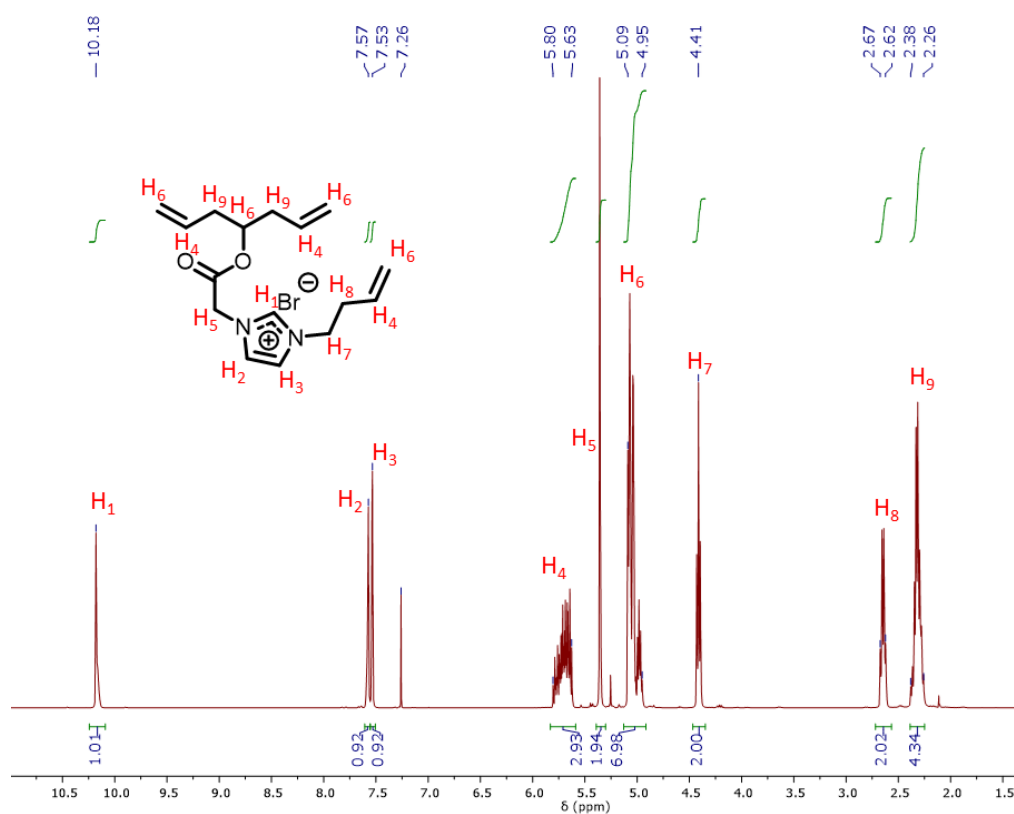
The compound **6** (0.1 g, 0.86 mmol) was dissolved in 2 mL of  $\text{CH}_3\text{CN}$  and **1** (0.2 g, 0.86 mmol) was added. The mixture was stirred overnight at room temperature and precipitated in 100 mL of  $\text{Et}_2\text{O}$ ; the product was washed twice with  $\text{Et}_2\text{O}$  and dried under vacuum. Yield: 0.3 g, 99%.

**$^1\text{H}$  NMR (400 MHz, Chloroform- $d$ )  $\delta$ :** 10.34 – 10.00 (m, 1H), 7.59 – 7.56 (m, 1H), 7.55 – 7.52 (m, 1H), 5.88 – 5.57 (m, 3H), 5.36 (s, 2H), 5.13 – 4.91 (m, 7H), 4.41 (t,  $J$  = 6.9 Hz, 2H), 2.71 – 2.57 (m, 2H), 2.41 – 2.22 (m, 4H).

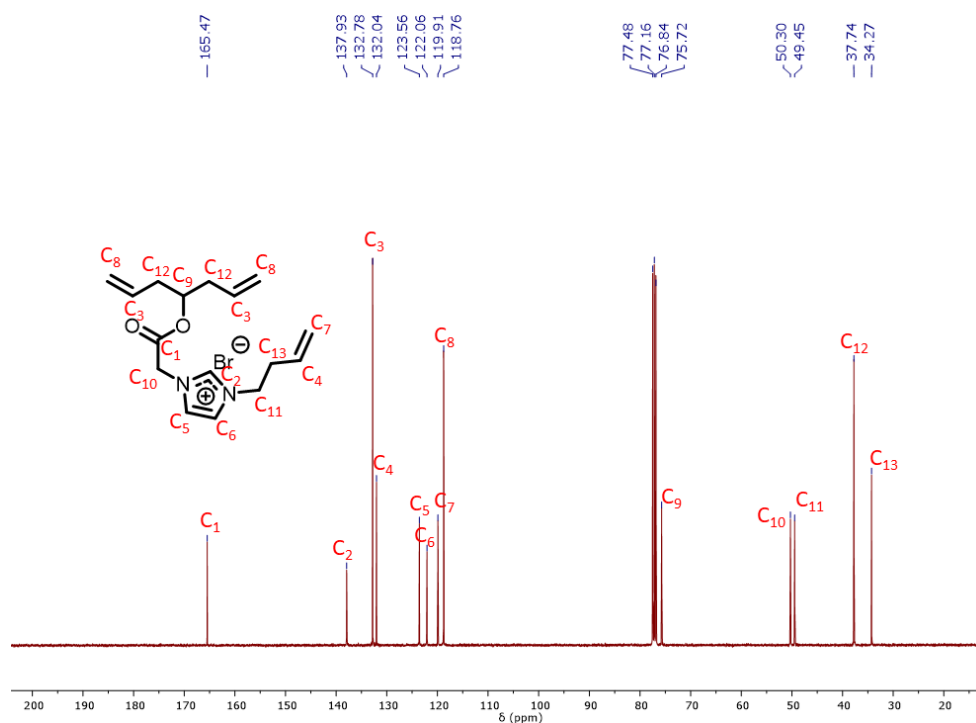
**$^{13}\text{C}$  NMR (101 MHz, Chloroform- $d$ )  $\delta$ :** 165.5, 137.9, 132.8, 132.0, 123.6, 122.1, 119.9, 118.8, 75.7, 50.3, 49.5, 37.7, 34.3.

**IR (neat)  $\text{cm}^{-1}$ :** 3075, 2978, 1743, 1564, 1221, 1167, 994, 917

**HRMS  $m/z$  (ESI):** calcd. for  $\text{C}_{16}\text{H}_{23}\text{N}_2\text{O}_2$   $[\text{M}]^+$ : 275.1754, found: 275.1754.

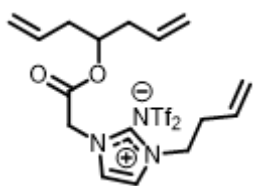


**Figure III-S12.** <sup>1</sup>H NMR spectrum of 1-(but-3-en-1-yl)-3-(2-(di-allylmethoxy)-2-oxoethyl)-1H-imidazol-3-ium bromide (7) (400 MHz, CDCl<sub>3</sub>, 25 °C).



**Figure III-S13.** <sup>13</sup>C NMR spectrum of 1-(but-3-en-1-yl)-3-(2-(di-allylmethoxy)-2-oxoethyl)-1H-imidazol-3-ium bromide (7) (400 MHz, CDCl<sub>3</sub>, 25 °C).

**1-(but-3-en-1-yl)-3-(2-(di-allylmethoxy)-2-oxoethyl)-1H-imidazol-3-ium bistrifluoromethanesulfonimide (8)**



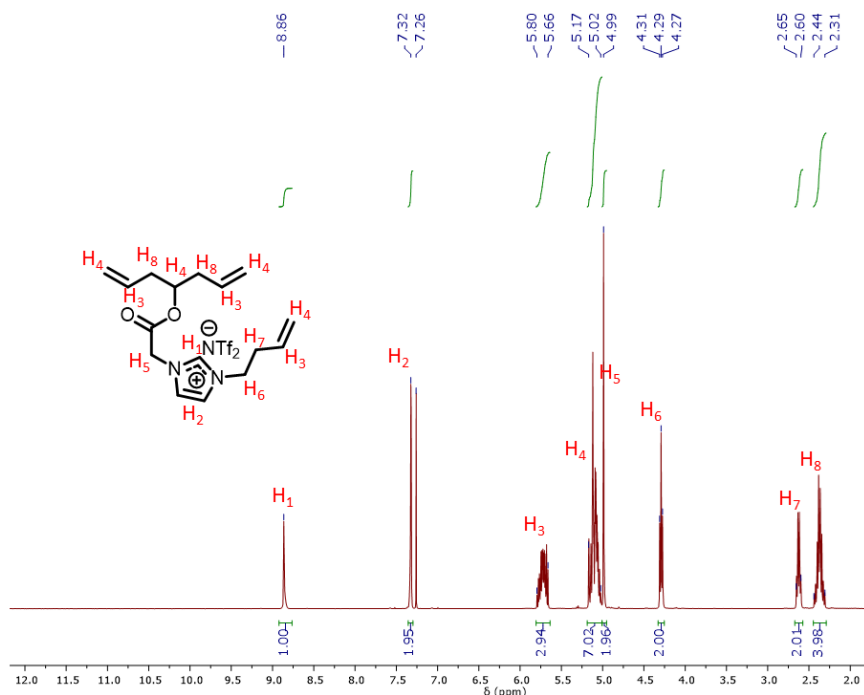
Then, compound **7** (0.24 g, 0.68 mmol) was dissolved in 13 mL of H<sub>2</sub>O at room temperature, the LiNTf<sub>2</sub> (0.24 g, 0.82 mmol) was added, and the mixture was left overnight at room temperature. The mixture was extracted three times by CH<sub>2</sub>Cl<sub>2</sub>. Organic extracts were combined and washed twice with water, dried over MgSO<sub>4</sub> and filtered. The solvent was removed under reduced pressure. Yield: 0.36 g, 96%.

**<sup>1</sup>H NMR (400 MHz, Chloroform-*d*)**  $\delta$ : 8.94 – 8.78 (m, 1H), 7.39 – 7.29 (m, 2H), 5.85 – 5.62 (m, 3H), 5.18 – 5.01 (m, 7H), 4.99 (s, 2H), 4.29 (t, *J* = 6.8 Hz, 2H), 2.71 – 2.54 (m, 2H), 2.51 – 2.27 (m, 4H).

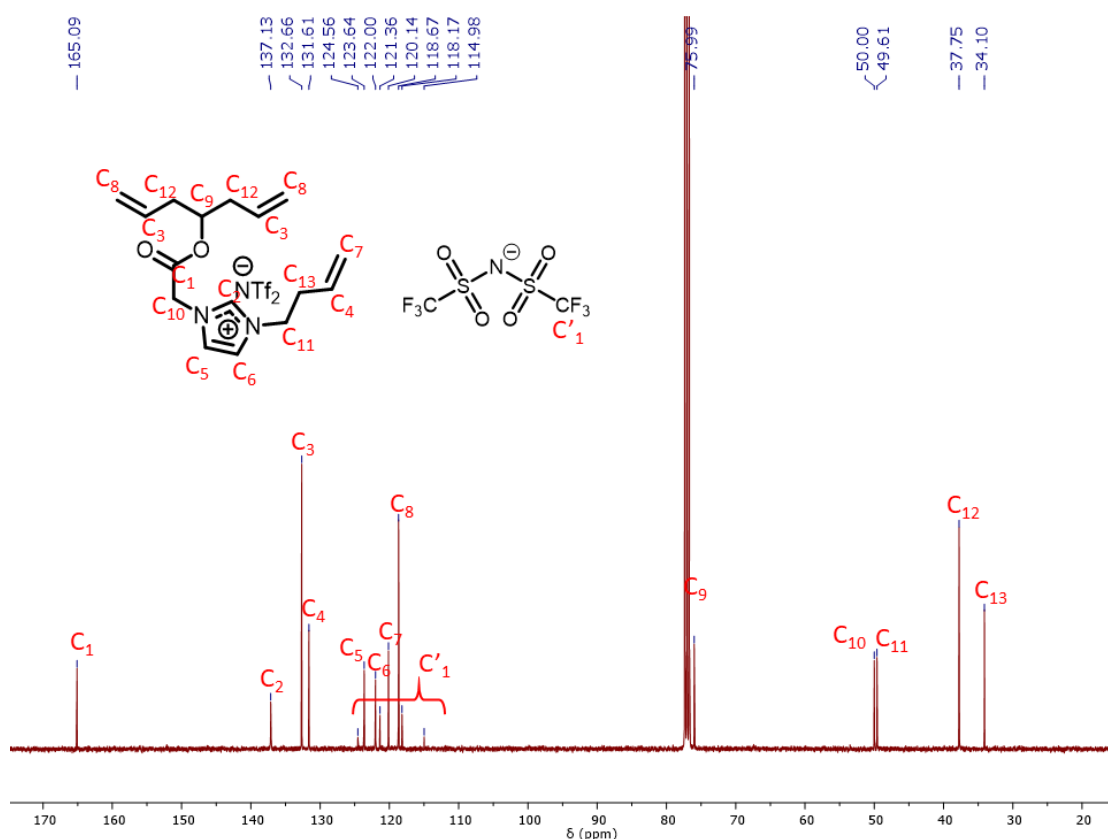
**<sup>13</sup>C NMR (101 MHz, Chloroform-*d*)**  $\delta$ : 165.1, 137.1, 132.7, 131.6, 123.6, 122.0, 120.1, 119.8 (q, *J* = 321.2 Hz), 118.7, 76.0, 50.0, 49.6, 37.8, 34.1.

**IR (neat) cm<sup>-1</sup>**: 3153, 3089, 1749, 1567, 1347, 1182, 1133, 1053

**HRMS *m/z* (ESI)**: calcd. for C<sub>16</sub>H<sub>23</sub>N<sub>2</sub>O<sub>2</sub> [M]<sup>+</sup>: 275.1754, found: 275.1755

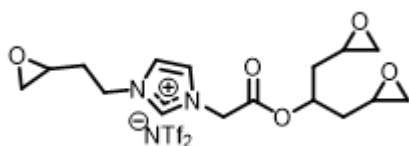


**Figure III-S14.** <sup>1</sup>H NMR spectrum of 1-(but-3-en-1-yl)-3-(2-(di-allylmethoxy)-2-oxoethyl)-1H-imidazol-3-ium bistrifluoromethanesulfonimide (**8**) (400 MHz, CDCl<sub>3</sub>, 25 °C).



**Figure III-S15.**  $^{13}\text{C}$  NMR spectrum of 1-(but-3-en-1-yl)-3-(2-(di-allylmethoxy)-2-oxoethyl)-1H-imidazol-3-ium bistrifluoromethanesulfonimide (8) (400 MHz,  $\text{CDCl}_3$ , 25 °C).

**1-(2-((1,3-di(oxiran-2-yl)propan-2-yl)oxy)-2-oxoethyl)-3-(2-(oxiran-2-yl)ethyl)-1H-3l4-imidazol-1-ium bistrifluoromethanesulfonimide (9)**



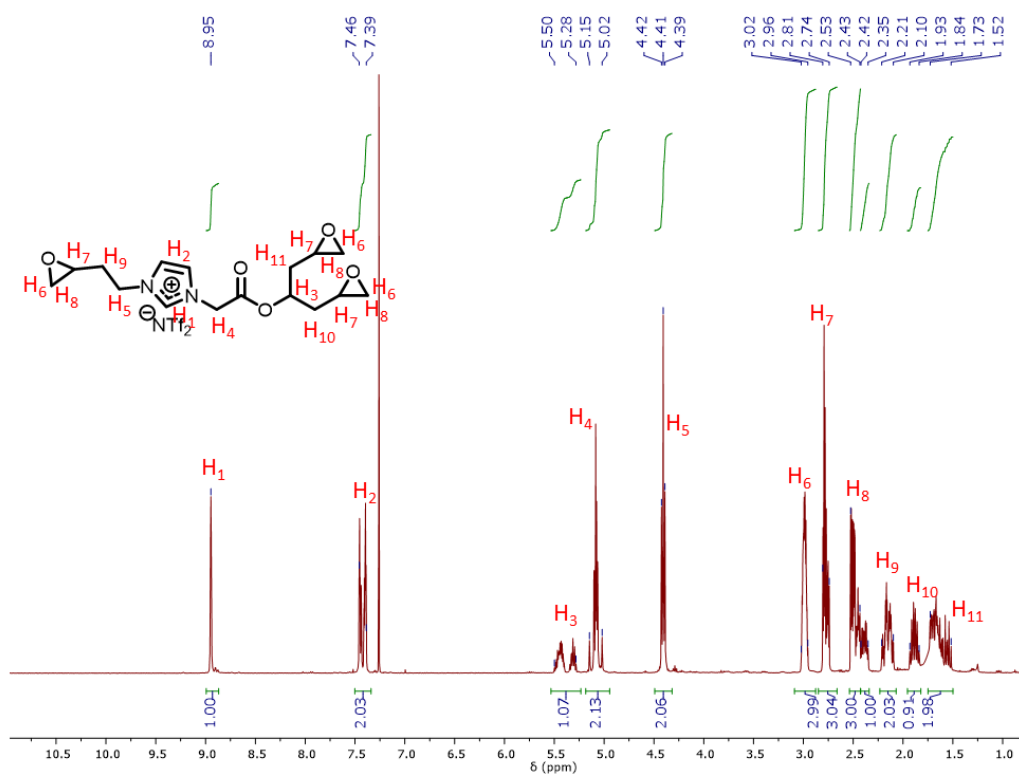
The compound 7 (0.3 g, 0.56 mmol) was dissolved in 15 mL of  $\text{CH}_3\text{CN}$  and mixed with 0.76 g (3.3 mmol) of *m*CPBA. The mixture was stirred 40 °C for 69 h. Then the solvent was evaporated under reduced pressure, and the residue was washed three times with  $\text{Et}_2\text{O}$ ; the solvent was removed by decantation, and the product was dried in a vacuum (0.25 g, 73%).

**$^1\text{H}$  NMR (400 MHz, Chloroform-*d*)  $\delta$ :** 8.95 (s, 1H), 7.50 – 7.38 (m, 2H), 5.52 – 5.27 (m, 1H), 5.16 – 5.00 (m, 2H), 4.41 (t,  $J$  = 6.8 Hz, 2H), 3.04 – 2.94 (m, 3H), 2.82 – 2.73 (m, 3H), 2.58 – 2.43 (m, 3H), 2.43 – 2.33 (m, 1H), 2.23 – 2.08 (m, 2H), 1.95 – 1.83 (m, 1H), 1.75 – 1.51 (m, 2H).

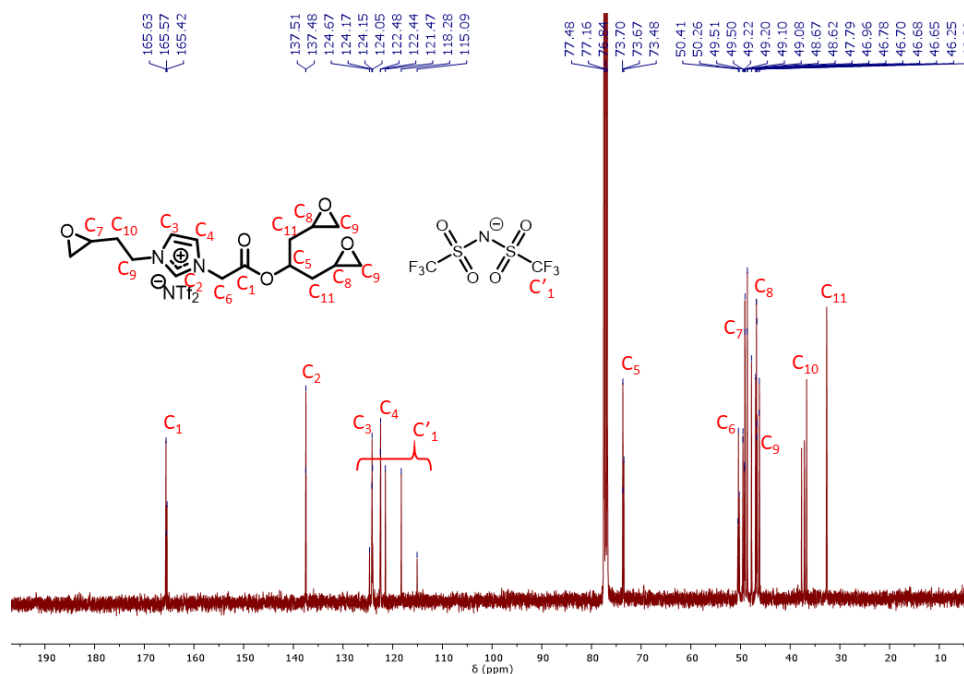
**$^{13}\text{C}$  NMR (101 MHz, Chloroform-*d*) mixture of stereoisomers  $\delta$ :** 165.6, 165.6, 165.4, 137.5, 137.5, 124.2, 124.1, 122.5, 122.4, 119.9 (q,  $J$  = 321.1 Hz), 73.7, 73.7, 73.5, 50.5, 50.4, 50.3, 49.5, 49.2, 49.2, 49.1, 49.1, 48.7, 48.6, 47.8, 47.0, 46.8, 46.7, 46.7, 46.2, 46.2, 37.7, 37.1, 37.1, 36.7, 32.7.

**IR (neat)  $\text{cm}^{-1}$ :** 3154, 3002, 2926, 1750, 1347, 1180, 1132, 1052, 841.

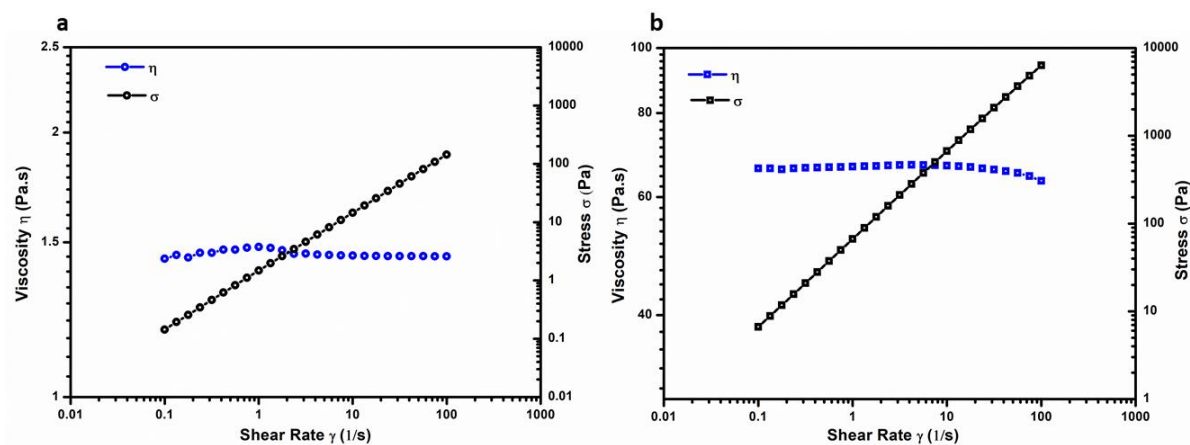
**HRMS  $m/z$  (ESI):** calcd. for  $\text{C}_{16}\text{H}_{23}\text{N}_2\text{O}_5$   $[\text{M}]^+$ : 323.1601, found: 323.1600.



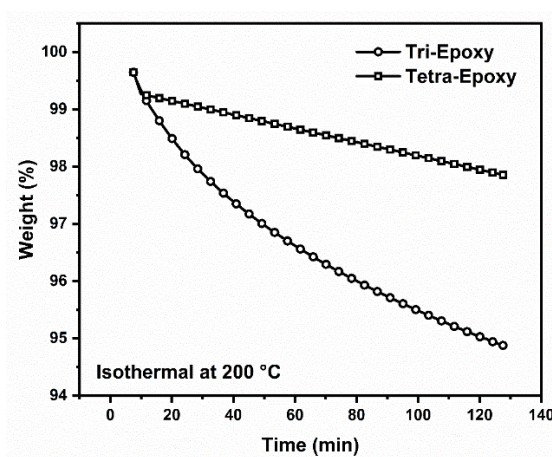
**Figure III-S16.**  $^1\text{H}$  NMR spectrum of 1-(2-((1,3-di(oxiran-2-yl)propan-2-yl)oxy)-2-oxoethyl)-3-(2-(oxiran-2-yl)ethyl)-1H-3H-imidazol-1-ium bistrifluoromethanesulfonimide (9) (400 MHz,  $\text{CDCl}_3$ , 25  $^\circ\text{C}$ ).



**Figure III-S17.**  $^{13}\text{C}$  NMR spectrum of 1-(2-((1,3-di(oxiran-2-yl)propan-2-yl)oxy)-2-oxoethyl)-3-(2-(oxiran-2-yl)ethyl)-1H-3H-imidazol-1-ium bistrifluoromethanesulfonimide (9) (400 MHz,  $\text{CDCl}_3$ , 25  $^\circ\text{C}$ ).



**Figure III-S18.** Rheological behavior of **a)** tri- and **b)** tetra-epoxidized ILs.



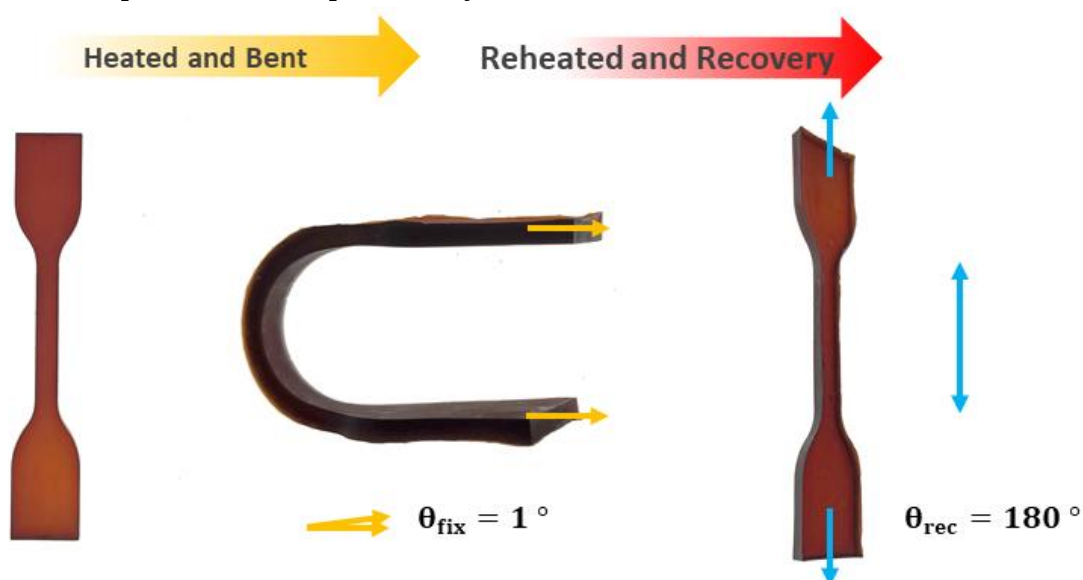
**Figure III-S19.** Thermogravimetric analysis for tri- and tetra-epoxidized ILs. Isothermal at 200 °C for 120 min.



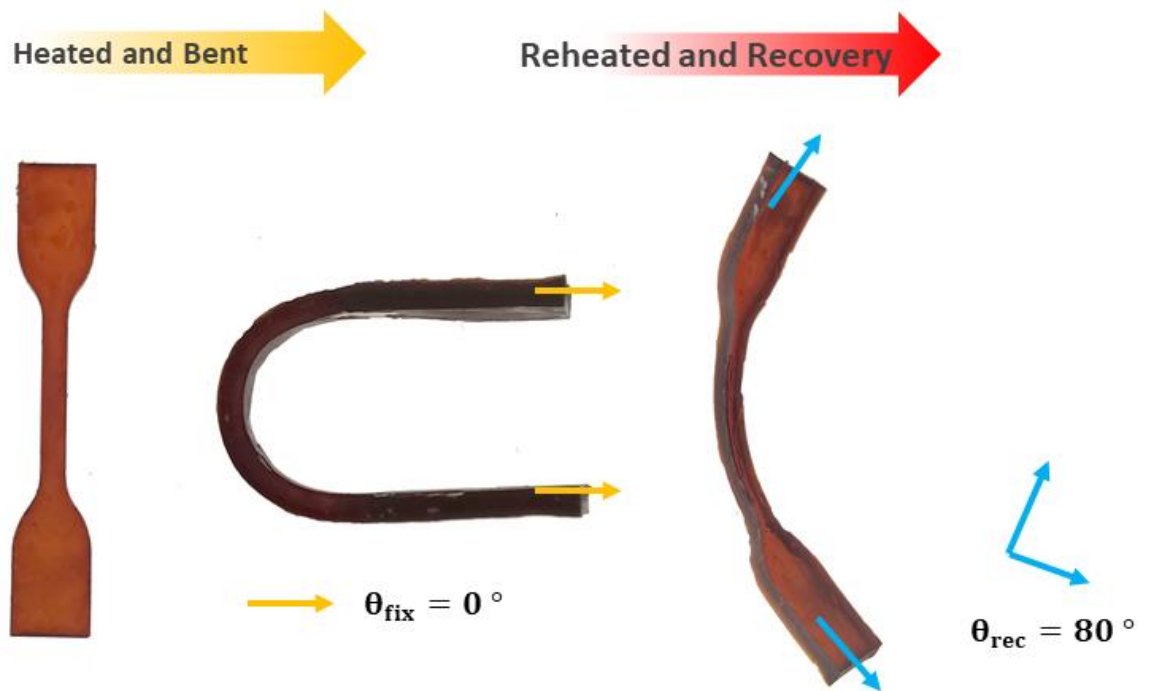
**Table III-S1** - Density (at 300 K) and glass transition temperature ( $T_g$ ) for the polymerised samples.

	Density (300 K)	$T_g$ / °C	Std dev for $T_g$ / °C
Tri - D230	1.197	88.7	15.6
Tri - PACM	1.201	110.6	13.9
Tri - SAA	1.332	92.8	9.4
Tetra - D230	1.181	122.1	7.5
Tetra - PACM	1.177	115.4	6.6
Tetra - SAA	1.316	103.8	8.4

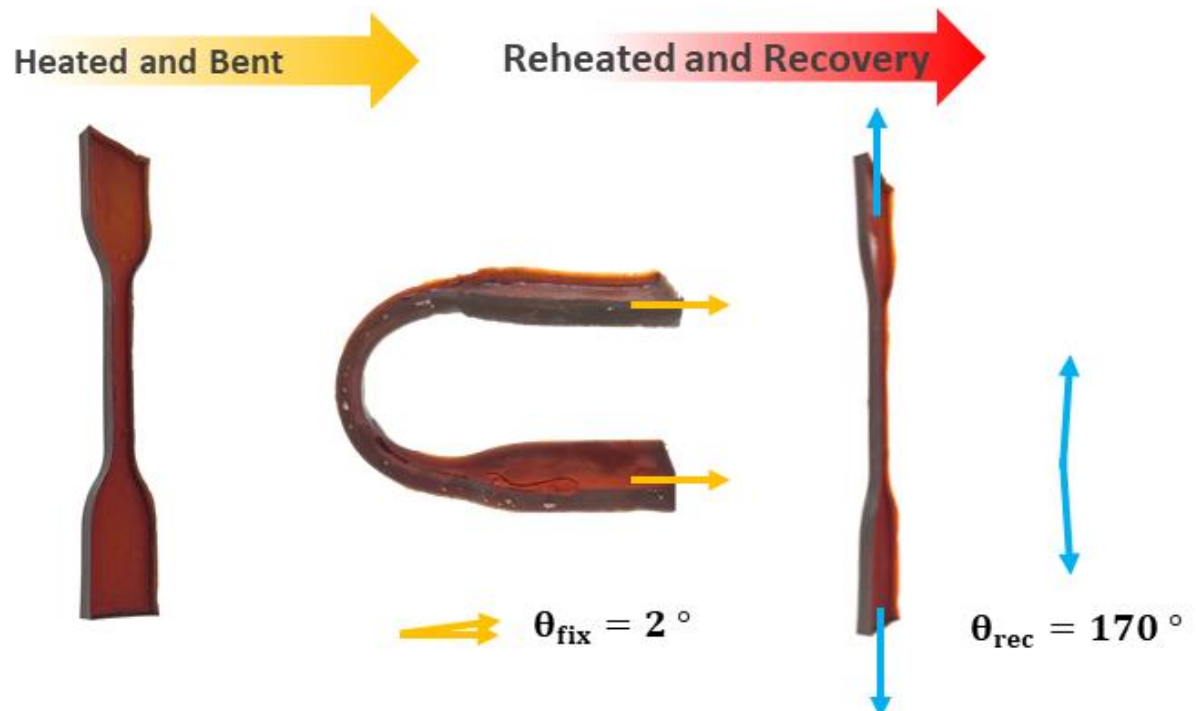
### Mechanical Properties and Shape Memory



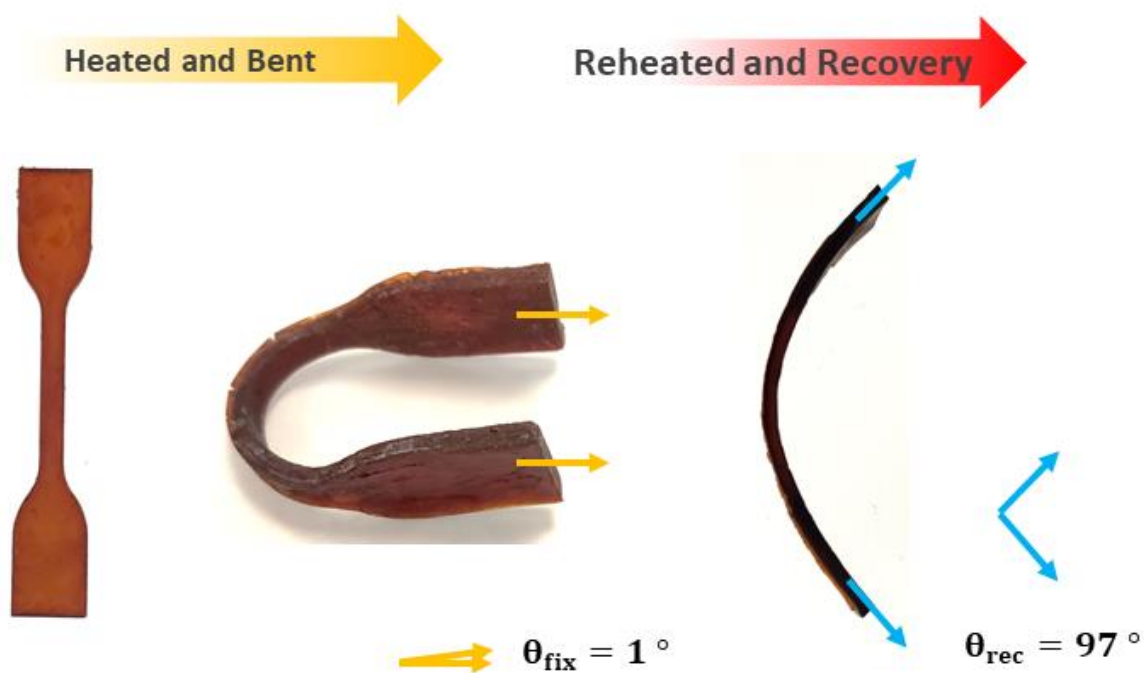
**Figure III-S20.** Shape memory behavior of triepoxy-D230. Initial shape (left), deformed sample (in the middle) and shape recovery after heating to 100 °C in a boiling water bath.



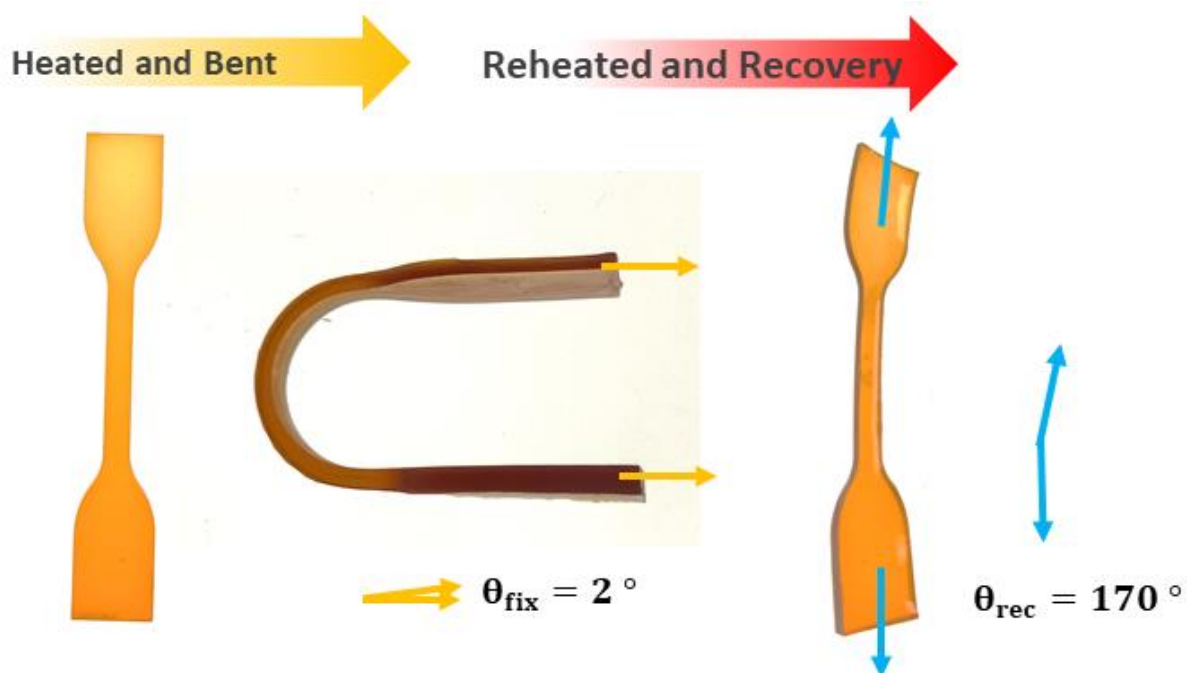
**Figure III-S21.** Shape memory behavior of tetrapoxy-D230. Initial shape (left), deformed sample (in the middle) and shape recovery after heating to 100 °C in a boiling water bath



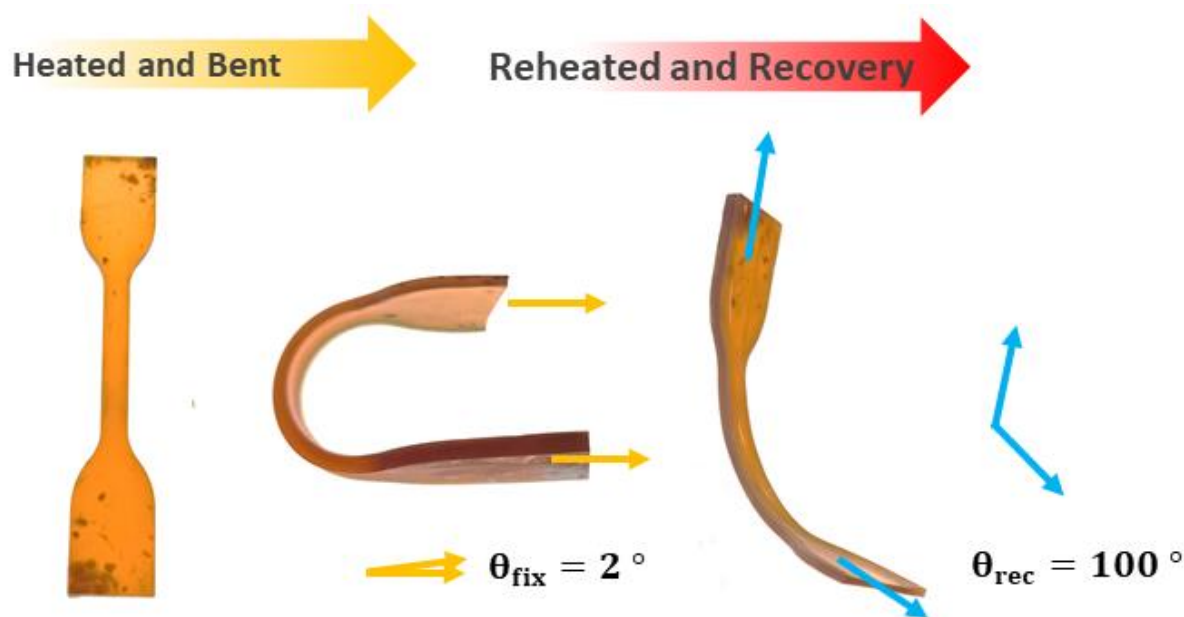
**Figure III-S22.** Shape memory behavior of triepoxy-PACM. Initial shape (left), deformed sample (in the middle) and shape recovery after heating to 100 °C in a boiling water bath.



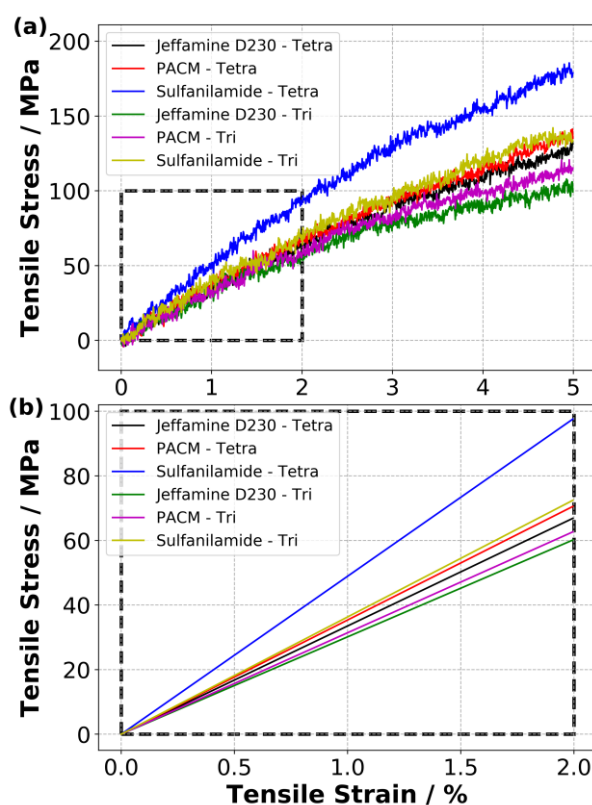
**Figure III-S23.** Shape memory behavior of tetra-PACM. Initial shape (left), deformed sample (in the middle) and shape recovery after heating to 100 °C in a boiling water bath.



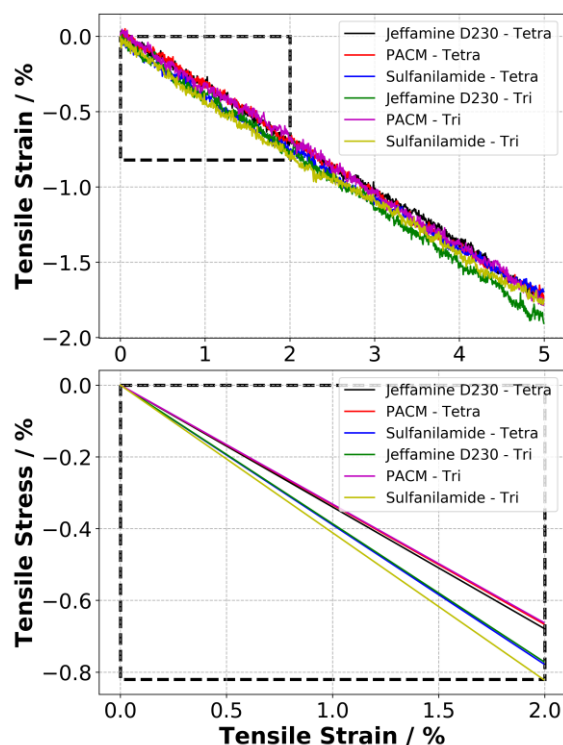
**Figure III-S24.** Shape memory behavior of triepoxy-SAA. Initial shape (left), deformed sample (in the middle) and shape recovery after heating to 100 °C in a boiling water bath.



**Figure III-S25.** Shape memory behavior of tetraepoxy-SAA. Initial shape (left), deformed sample (in the middle) and shape recovery after heating to 100 °C in a boiling water bath.



**Figure III-S26 - a)** Tensile stress-strain curves calculated at 300 K for each polymer system with a DOC of 80%. **b)** The lines fitted to the 2% of strain data to predict Young's moduli.



**Figure III-S27. a)** Tensile strain-tensile strain curves calculated at 300 K for each polymer system with a DOC of 80%. **b)** The lines fitted to the 2% of strain data to predict the Poisson's ratio.

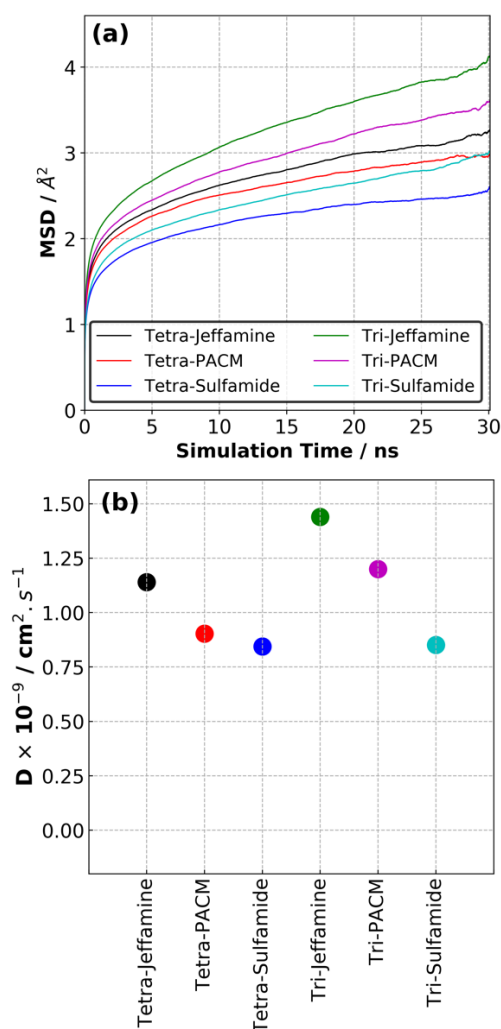
**Table III-S2.** Predicted Young's modulus at 300 K for the polymerized samples.

	Young's Modulus / GPa	Poisson's Ratio
<b>Tetra – D230</b>	3.35	0.34
<b>Tetra – PACM</b>	3.53	0.33
<b>Tetra – SAA</b>	4.89	0.39
<b>Tri – D230</b>	3.01	0.39
<b>Tri – PACM</b>	3.14	0.33
<b>Tri – SAA</b>	3.63	0.41

## Mobility of Ions

The mean square displacement (MSD) of anions ( $\text{NTf}_2$ ) were calculated at 300 K in each system. MSD curves are averaged over three independent runs. Our results show that the mobility of anions is faster in the polymer systems cured with Jeffamine, irrespective of the type of monomer (*i.e.* tetra- or tri-functional epoxy monomer). The slowest mobility of anions is observed in the samples cured with Sulfonamide, again the type of monomer did not change this order.

It notes that the diffusion coefficients of anions reported in **Figure III-S28a** are not accurate as the MSD curves did not arrive at a diffusive regime yet. However, they can be used as a general trend in these polymers.



**Figure III-S28. a)** Mean square displacement and **b)** diffusion coefficient of anions in each polyçer system at 300K.

**Table III-S3.** Young Modulus obtained theoretically and experimentally

		Theoretical	Experimental
		Young Modulus (GPa)	Young Modulus (GPa)
Tri	D230	3.01	1.05
	PACM	3.14	5.64
	SAA	3.63	2.66
Tetra	D230	3.35	0.91
	PACM	3.53	2.68
	SAA	4.89	1.40

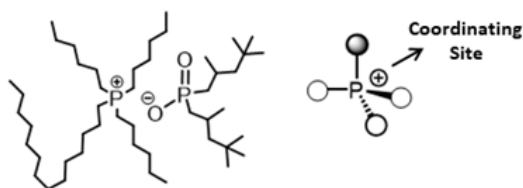
### Investigation of Surface Network Wettability

Aiming to investigate the surface energy of the networks, water and diiodomethane were employed as probe liquids and deposited on the sample surfaces by the sessile drop method. The average contact angles with water and diiodomethane were determined. Afterward, the dispersive and non-dispersive surface energies were calculated by using the Owens-Wendt equation. As expected, the use of IL monomers has no influence on the average water contact angle as well as the total surface energy (**Table III-S4**). In fact, the six networks presented surface wettability behaviors similar to DGEBA-derivative materials. Although the matrices are composed of polar groups the presence of fluorinated anion ( $\text{NTf}_2^-$ ) counterbalances the wettability affording an intermediate hydrophobic character. Among the amines, SAA is the one that most introduced hydrophobic nature into the networks, while D230 and PACM afforded similar surface wettability. These results seems to be promising because recently, Ollivier-Lamarque *et al.* have demonstrated that for epoxy-amine and epoxy-IL networks having similar surface energies, a lower water diffusion coefficient (2-3 times) was determined for epoxy-IL systems combined with no decrease of the glass transition temperature.<sup>69</sup>

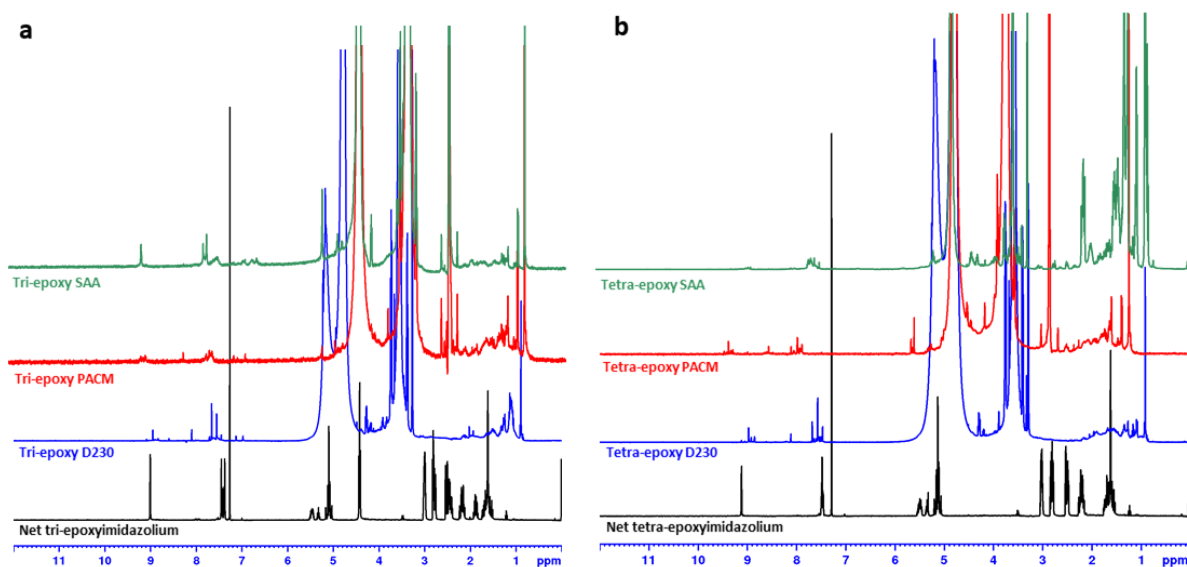
**Table III-S4.** Contact angles and surface energies

		Wa- ter (°)	CH <sub>2</sub> I <sub>2</sub> (°)	Disp. Surface Energy (mJ.m <sup>-2</sup> )	Polar Surface Energy (mJ.m <sup>-2</sup> )	Total Surface Energy (mJ.m <sup>-2</sup> )
<b>Tri</b>	<b>D230</b>	75 ± 1	43 ± 2	32.7	6.8	39.5
	<b>PAC</b>	66 ± 3	40 ± 1	32.3	11.7	44.0
	<b>SAA</b>	73 ± 1	63 ± 4	22.5	5.5	28.0
<b>Tetra</b>	<b>D230</b>	73 ± 1	45 ± 2	31.4	8.2	39.6
	<b>PAC</b>	69 ± 2	45 ± 3	30.3	10.7	41.0
	<b>SAA</b>	84 ± 1	41 ± 1	35.1	4.0	39.1

**Electrophilic Phosphonium IL**

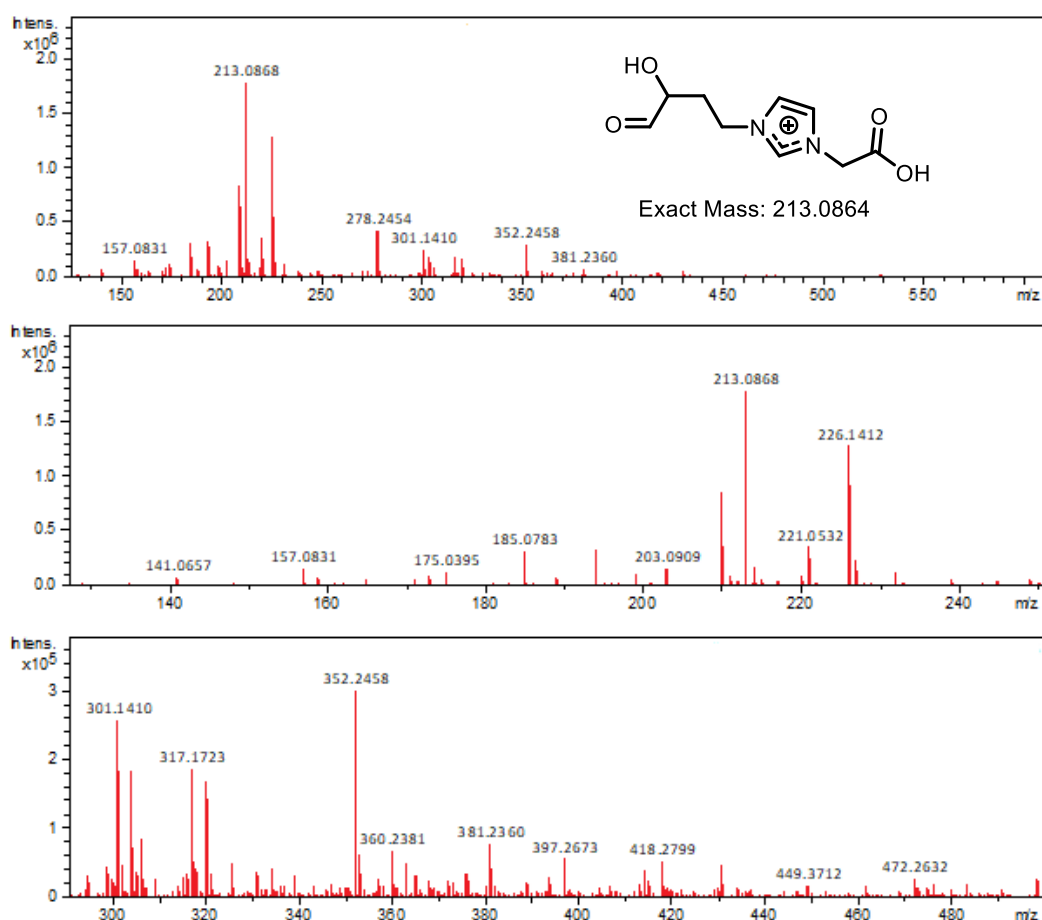


**Figure III-S29.** Phosphonium IL structure.



**Figure III-S30.** NMR spectra for the degraded solutions derived from the network based on **a)** tri-epoxidized IL and **b)** tetra-epoxidized IL.

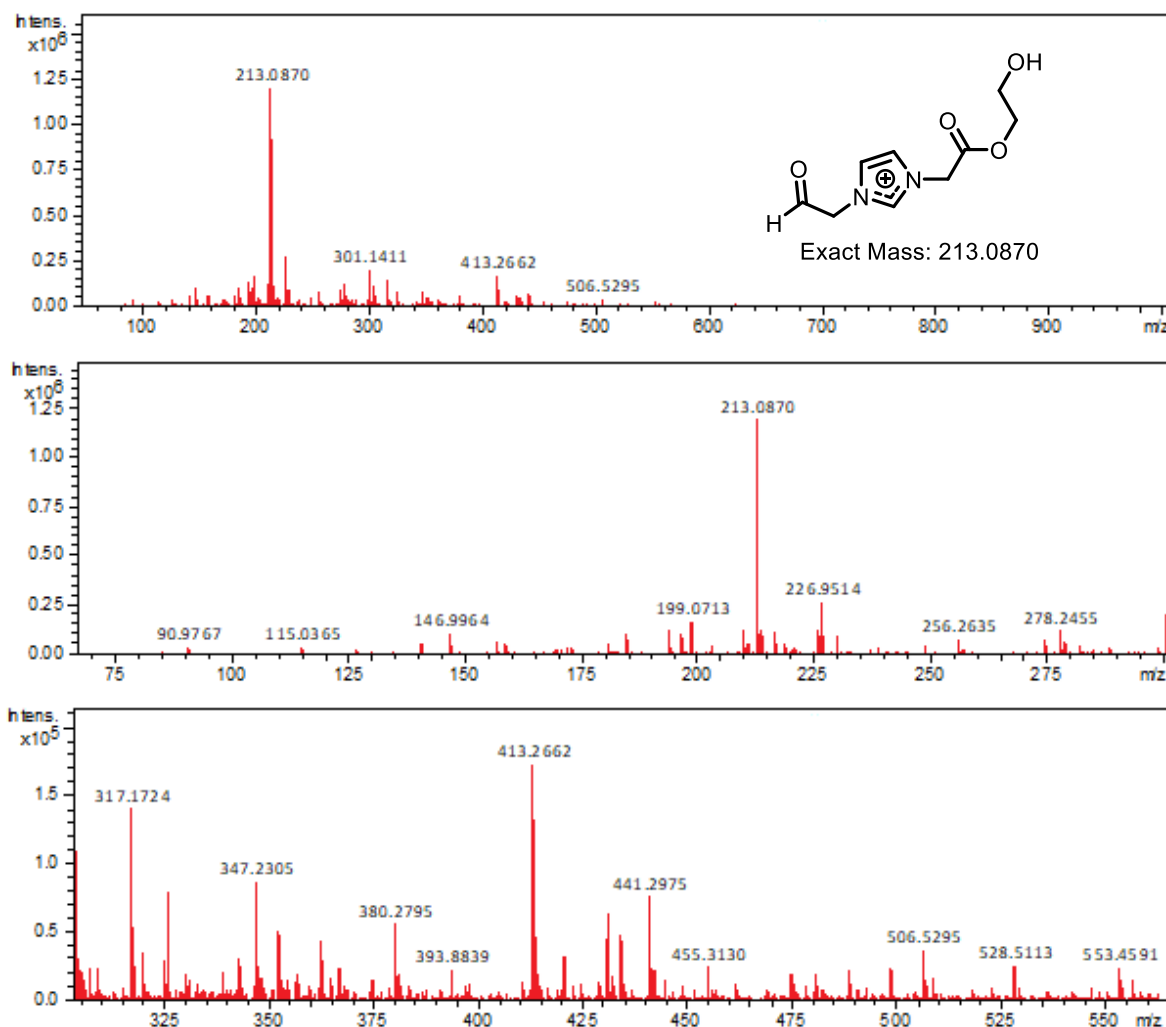




**Figure III-S31.** ESI(+)-QTOF mass spectrum of degradation products for the network based on tri-epoxidized IL and D230.

**Table III-S5.** Molecular ions obtained from ESI(+)-QTOF spectrometry of the degradation products for the network based on tri-epoxidized IL and D230

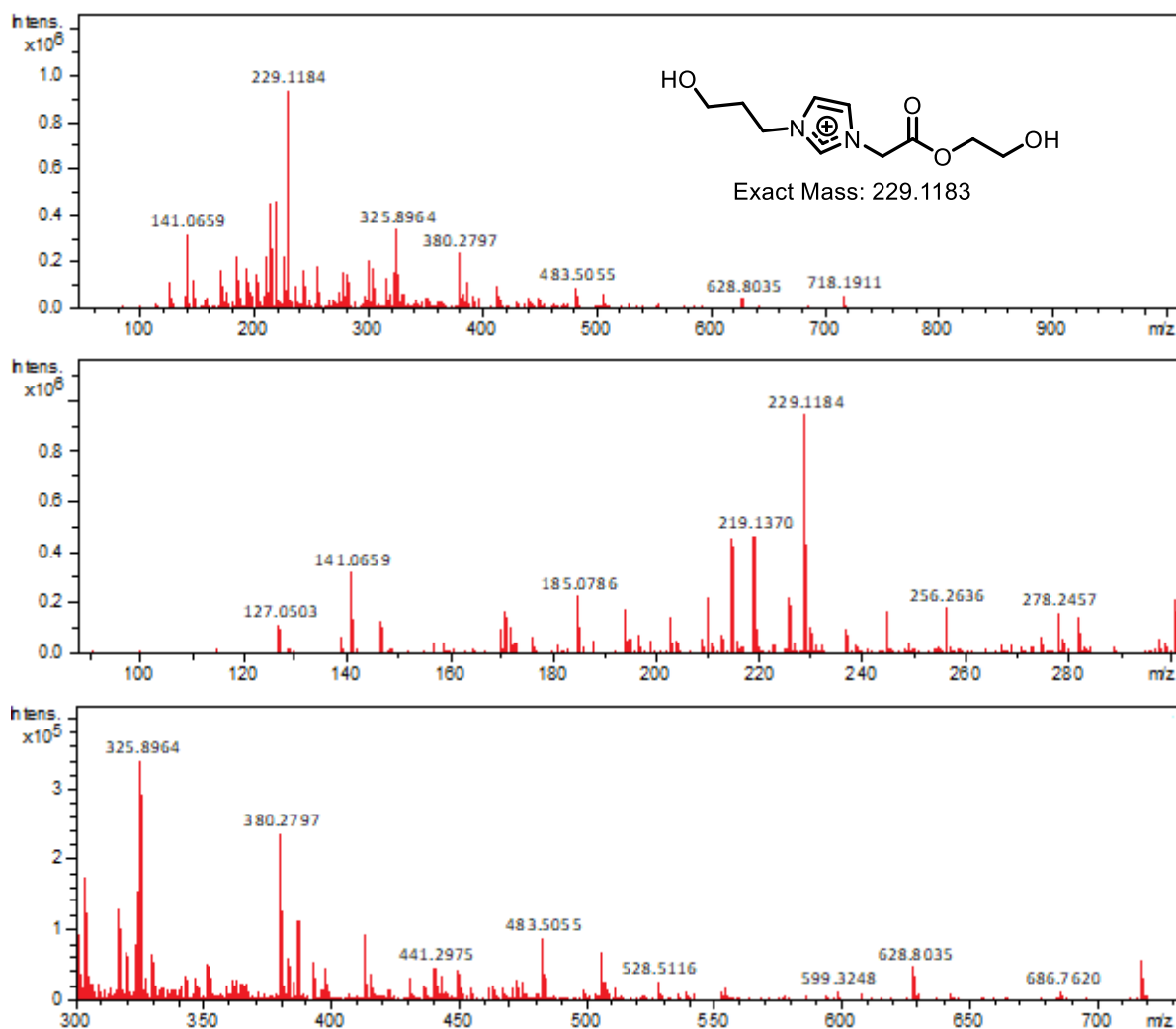
Meas. m/z	Ion Formula	m/z	err [ppm]	z
213.0868	C <sub>9</sub> H <sub>13</sub> N <sub>2</sub> O <sub>4</sub>	213.087	0.7	1+
	C <sub>10</sub> H <sub>9</sub> N <sub>6</sub>	213.0883	7	1+
278.2454	C <sub>13</sub> H <sub>32</sub> N <sub>3</sub> O <sub>3</sub>	278.2438	-5.7	1+
352.2458	C <sub>16</sub> H <sub>30</sub> N <sub>7</sub> O <sub>2</sub>	352.2455	-0.7	1+
	C <sub>15</sub> H <sub>34</sub> N <sub>3</sub> O <sub>6</sub>	352.2442	-4.5	1+
	C <sub>16</sub> H <sub>30</sub> N <sub>7</sub> O <sub>2</sub>	352.2455	-0.7	1+
	C <sub>15</sub> H <sub>34</sub> N <sub>3</sub> O <sub>6</sub>	352.2442	-4.5	1+



**Figure III-S32.** ESI(+)-QTOF mass spectrum of degradation products for the network based on tetra-epoxidized IL and D230.

**Table III-S6.** Molecular ions obtained from ESI(+)-QTOF spectrometry of the degradation products for the network based on tetra-epoxidized IL and D230

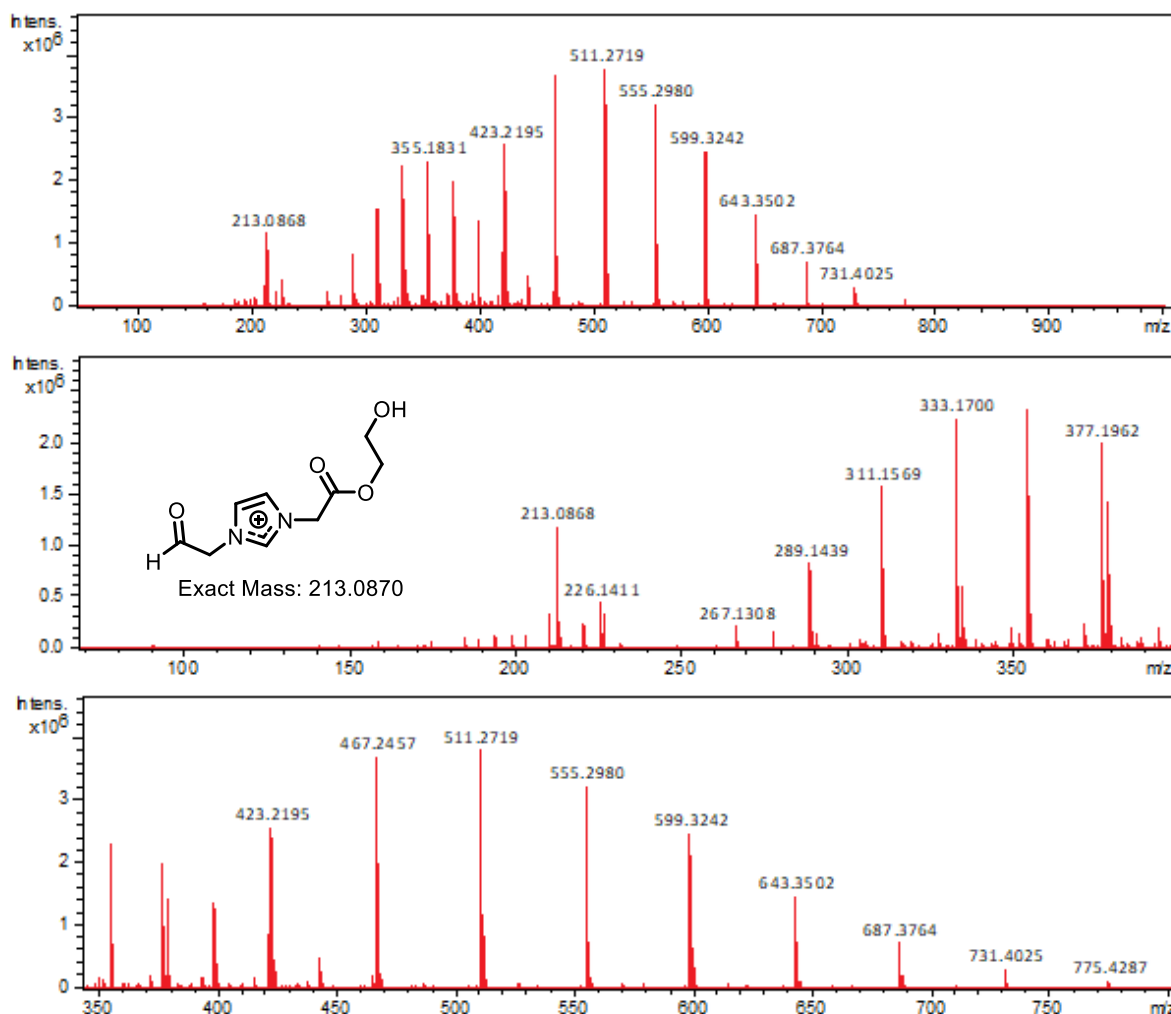
Meas. m/z	Ion Formula	m/z	err [ppm]	z
213.087	C <sub>9</sub> H <sub>13</sub> N <sub>2</sub> O <sub>4</sub>	213.087	0.2	1+
	C <sub>9</sub> H <sub>13</sub> N <sub>2</sub> O <sub>4</sub>	213.087	0.2	1+
301.1411	C <sub>14</sub> H <sub>17</sub> N <sub>6</sub> O <sub>2</sub>	301.1408	-1	1+
	C <sub>14</sub> H <sub>17</sub> N <sub>6</sub> O <sub>2</sub>	301.1408	-1	1+
413.2662	C <sub>22</sub> H <sub>33</sub> N <sub>6</sub> O <sub>2</sub>	413.266	-0.7	1+
	C <sub>21</sub> H <sub>37</sub> N <sub>2</sub> O <sub>6</sub>	413.2646	-3.9	1+
	C <sub>22</sub> H <sub>33</sub> N <sub>6</sub> O <sub>2</sub>	413.266	-0.7	1+
	C <sub>21</sub> H <sub>37</sub> N <sub>2</sub> O <sub>6</sub>	413.2646	-3.9	1+



**Figure III-S33.** ESI(+)-QTOF mass spectrum of degradation products for the network based on tri-epoxidized IL and PACM.

**Table III-S7.** Molecular ions obtained from ESI(+)-QTOF spectrometry of the degradation products for the network based on tri-epoxidized and PACM.

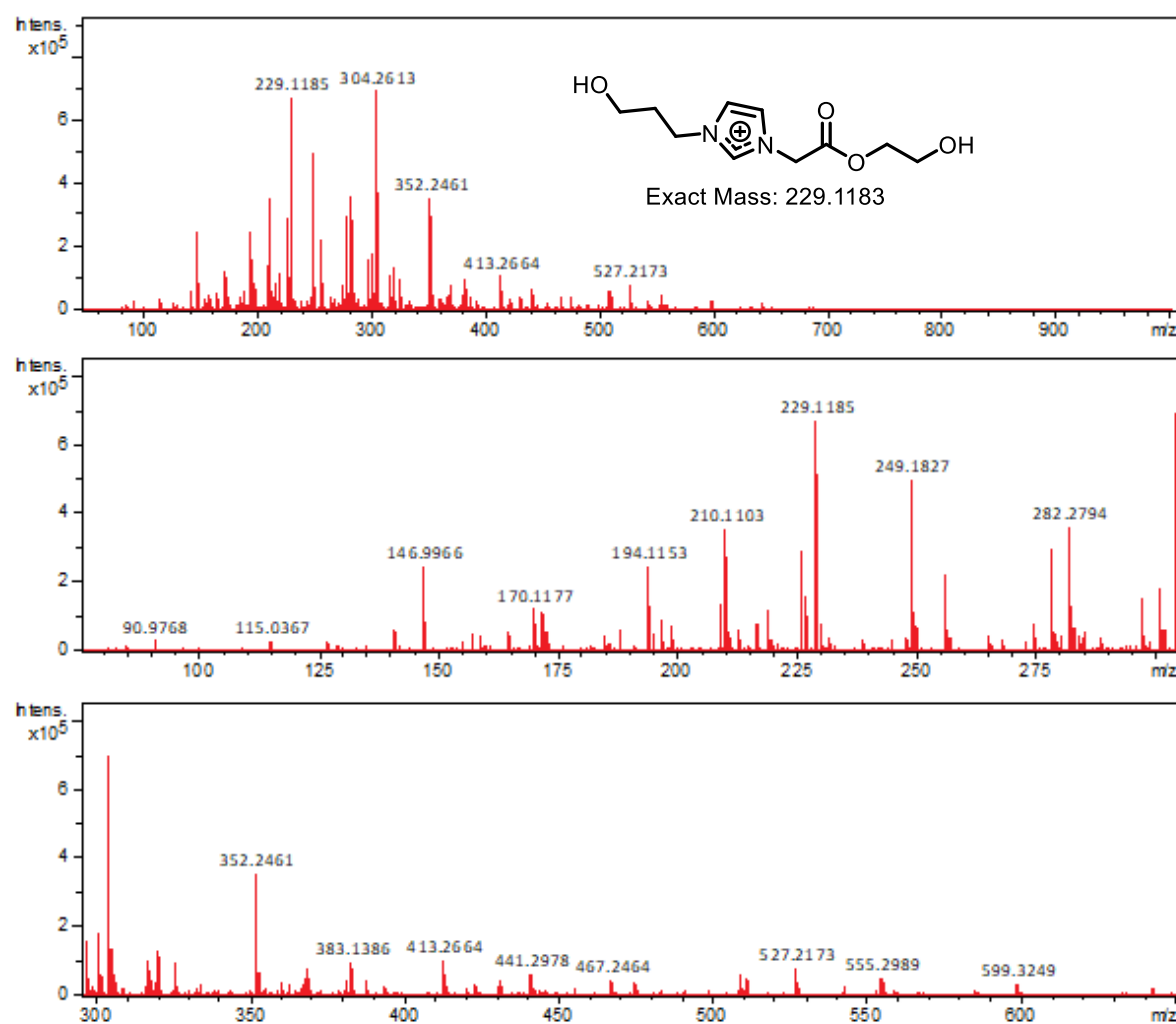
Meas. m/z	Ion For-	m/z	err [ppm]	z
141.0659	C <sub>6</sub> H <sub>9</sub> N <sub>2</sub> O <sub>2</sub>	141.0659	-0.5	1+
	C <sub>6</sub> H <sub>9</sub> N <sub>2</sub> O <sub>2</sub>	141.0659	-0.5	1+
185.0786	C <sub>5</sub> H <sub>9</sub> N <sub>6</sub> O <sub>2</sub>	185.0781	-2.4	1+
	C <sub>5</sub> H <sub>9</sub> N <sub>6</sub> O <sub>2</sub>	185.0781	-2.4	1+
380.2797	C <sub>22</sub> H <sub>38</sub> NO <sub>4</sub>	380.2795	-0.3	1+
	C <sub>23</sub> H <sub>34</sub> N <sub>5</sub>	380.2809	3.2	1+
	C <sub>22</sub> H <sub>38</sub> NO <sub>4</sub>	380.2795	-0.3	1+
	C <sub>23</sub> H <sub>34</sub> N <sub>5</sub>	380.2809	3.2	1+



**Figure III-S34.** ESI(+)-QTOF mass spectrum of degradation products for the network based on tetra-epoxidized IL and PACM.

**Table III-S8.** Molecular ions obtained from ESI(+)-QTOF spectrometry of the degradation products for the network based on tetra-epoxidized IL and PACM.

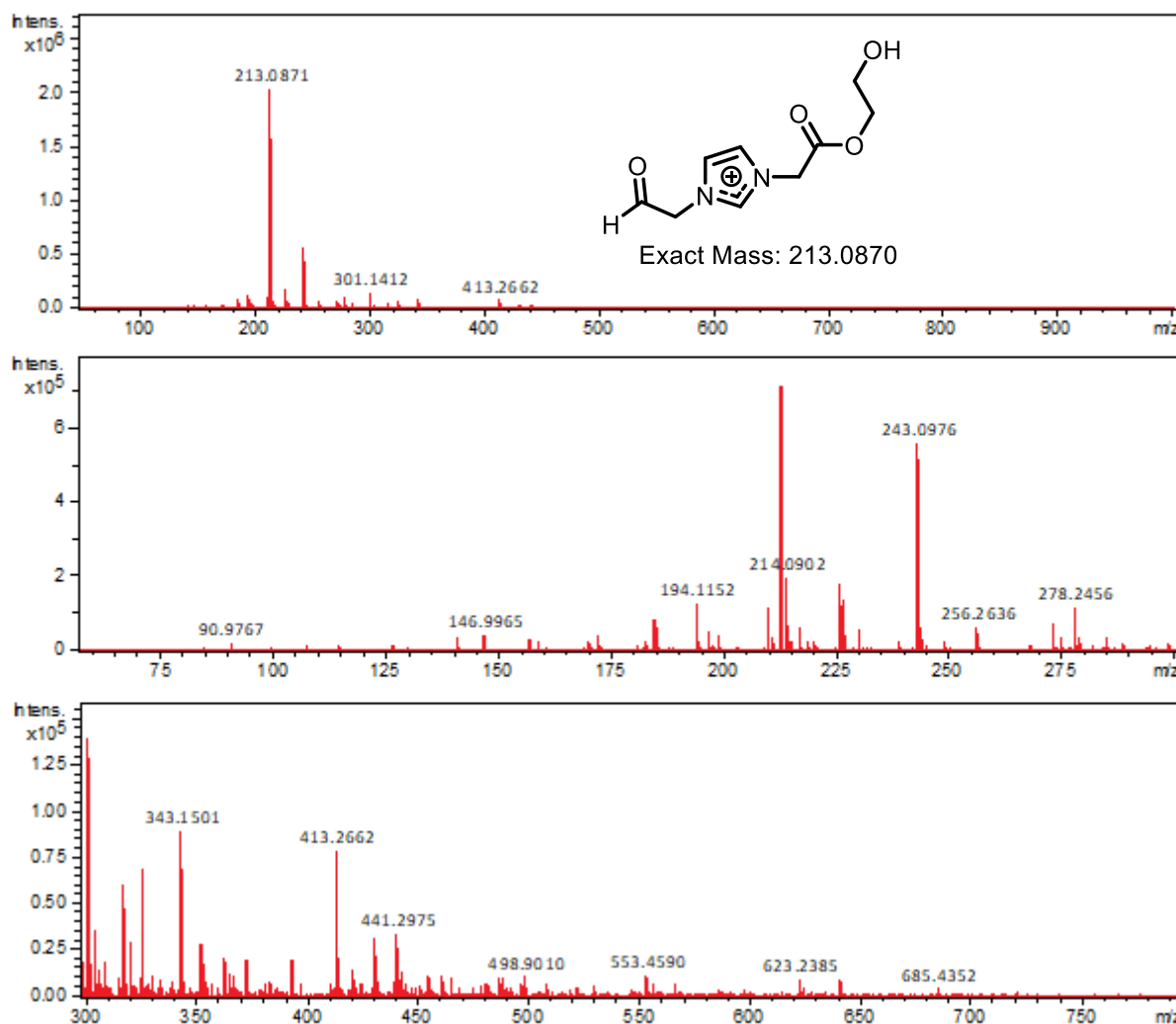
Meas. m/z	Ion Formula	m/z	err [ppm]	z
213.0868	C <sub>9</sub> H <sub>13</sub> N <sub>2</sub> O <sub>4</sub>	213.087	1.1	1+
	C <sub>10</sub> H <sub>9</sub> N <sub>6</sub>	213.0883	7.3	1+
289.1439	C <sub>17</sub> H <sub>21</sub> O <sub>4</sub>	289.1434	-1.6	1+
	C <sub>18</sub> H <sub>17</sub> N <sub>4</sub>	289.1448	3	1+
377.1962	C <sub>21</sub> H <sub>29</sub> O <sub>6</sub>	377.1959	-1	1+
	C <sub>22</sub> H <sub>25</sub> N <sub>4</sub> O <sub>2</sub>	377.1972	2.6	1+
	C <sub>22</sub> H <sub>25</sub> N <sub>4</sub> O <sub>2</sub>	377.1972	2.6	1+



**Figure III-S35.** ESI(+)-QTOF mass spectrum of degradation products for the network based on tri-epoxidized IL and SAA.

**Table III-S9.** Molecular ions obtained from ESI(+)-QTOF spectrometry of the degradation products for the network based on tri-epoxidized IL and SAA

Meas. m/z	Ion Formula	m/z	err [ppm]	z
229.1185	C <sub>10</sub> H <sub>17</sub> N <sub>2</sub> O <sub>4</sub>	229.1183	-1.1	1+
	C <sub>11</sub> H <sub>13</sub> N <sub>6</sub>	229.1196	4.7	1+
	C <sub>10</sub> H <sub>17</sub> N <sub>2</sub> O <sub>4</sub>	229.1183	-1.1	1+
	C <sub>11</sub> H <sub>13</sub> N <sub>6</sub>	229.1196	4.7	1+
249.1827	C <sub>12</sub> H <sub>21</sub> N <sub>6</sub>	249.1822	-2.1	1+
	C <sub>11</sub> H <sub>25</sub> N <sub>2</sub> O <sub>4</sub>	249.1809	-7.5	1+
	C <sub>12</sub> H <sub>21</sub> N <sub>6</sub>	249.1822	-2.1	1+
	C <sub>11</sub> H <sub>25</sub> N <sub>2</sub> O <sub>4</sub>	249.1809	-7.5	1+
304.2613	C <sub>15</sub> H <sub>34</sub> N <sub>3</sub> O <sub>3</sub>	304.2595	-6.1	1+
	C <sub>15</sub> H <sub>34</sub> N <sub>3</sub> O <sub>3</sub>	304.2595	-6.1	1+
352.2461	C <sub>16</sub> H <sub>30</sub> N <sub>7</sub> O <sub>2</sub>	352.2455	-1.5	1+
	C <sub>16</sub> H <sub>30</sub> N <sub>7</sub> O <sub>2</sub>	352.2455	-1.5	1+
	C <sub>15</sub> H <sub>34</sub> N <sub>3</sub> O <sub>6</sub>	352.2442	-5.3	1+



**Figure III-S36.** ESI(+)-QTOF mass spectrum of degradation products for the network based on tetra-epoxidized IL and SAA.

**Table III-S10.** Molecular ions obtained from ESI(+)-QTOF spectrometry of the degradation products for the network based on tetra-epoxidized IL and SAA.

Meas. m/z	Ion Formula	m/z	err [ppm]	z
213.0871	C <sub>9</sub> H <sub>13</sub> N <sub>2</sub> O <sub>4</sub>	213.087	-0.3	1+
	C <sub>9</sub> H <sub>13</sub> N <sub>2</sub> O <sub>4</sub>	213.087	-0.3	1+
243.0976	C <sub>10</sub> H <sub>15</sub> N <sub>2</sub> O <sub>5</sub>	243.0975	-0.4	1+
	C <sub>10</sub> H <sub>15</sub> N <sub>2</sub> O <sub>5</sub>	243.0975	-0.4	1+
413.2662	C <sub>22</sub> H <sub>33</sub> N <sub>6</sub> O <sub>2</sub>	413.266	-0.6	1+
	C <sub>21</sub> H <sub>37</sub> N <sub>2</sub> O <sub>6</sub>	413.2646	-3.9	1+
	C <sub>22</sub> H <sub>33</sub> N <sub>6</sub> O <sub>2</sub>	413.266	-0.6	1+
	C <sub>21</sub> H <sub>37</sub> N <sub>2</sub> O <sub>6</sub>	413.2646	-3.9	1+

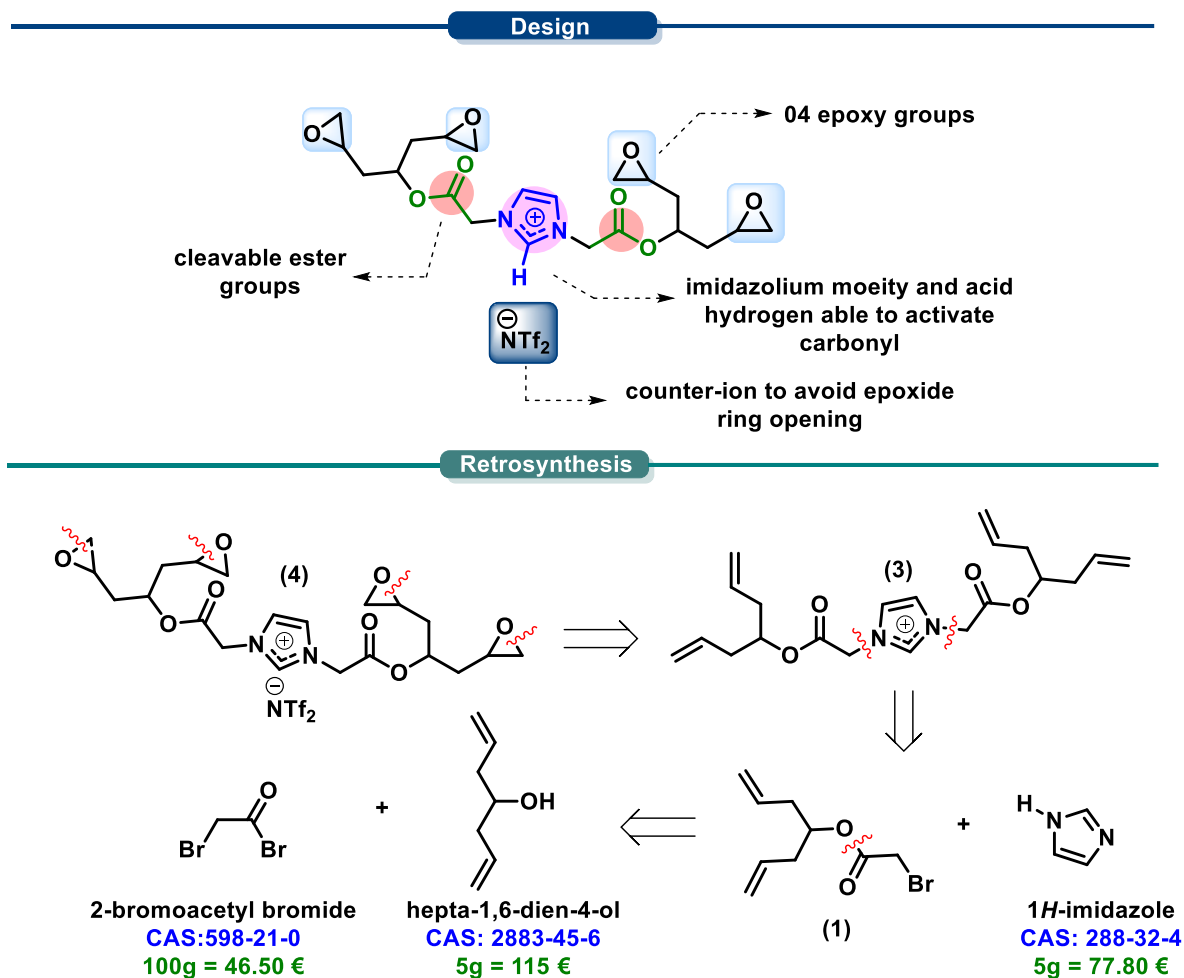
## **Appendix II - Design for Disassembly of Composites and Thermosets by Using Cleavable Ionic Liquid Monomers as Molecular Building Blocks**



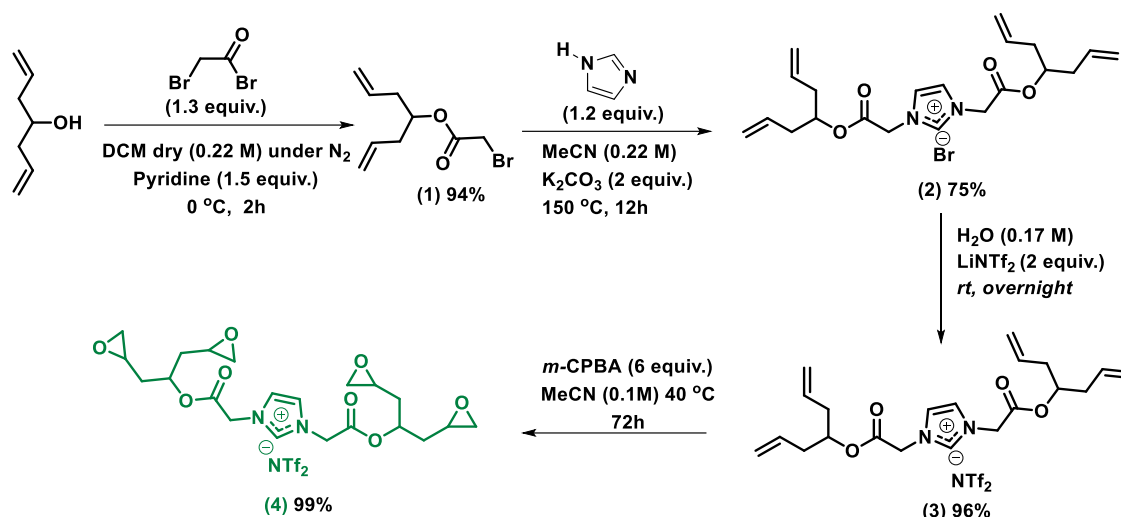
## General Methodology

### Characterization and Purification Methods

The  $^1\text{H}$  and  $^{13}\text{C}$  spectra of a solution of around 10 mg of a substance in a deuterated solvent were recorded using a Bruker Avance III spectrometer at either 400 MHz or 500 MHz. The chemical shifts for  $^1\text{H}$  and  $^{13}\text{C}$  nuclei were expressed in ppm relative to internal tetramethylsilane and coupling constants were determined using TopSpin© and given in Hz. Signal coupling is represented by s = singlet, d=doublet, dd=doublet of doublets, t=triplet, q=quartet, quin=quintet, m=multiplet, br=broad signal. To determine the molecular structure of the substance, additional 2D NMR experiments such as COSY, HSQC, and HMBC were also performed. High Resolution Mass Spectra HRMS was carried out on by a Micro-mass-Waters Q-TOF Ultima Global by the Electrospray Ionization (ESI) technique.

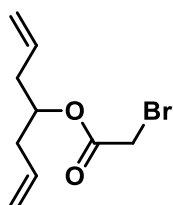


**Scheme IV-S1. a) Rational planning and b) Retrosynthetic analysis of the planned compound 4.**



**Scheme IV-S2.** Synthetic route employed to obtain the Tetra-IL epoxide monomer.<sup>1</sup>

### Compound 1



Hepta-1,6-dien-4-ol and pyridine were dissolved in 400 mL of anhydrous  $\text{CH}_2\text{Cl}_2$  under an argon atmosphere, cooled to  $0^\circ\text{C}$ , and 2-bromoacetyl bromide was added dropwise over a period of 20 minutes. The mixture was stirred for 30 minutes, then  $\text{NH}_4\text{Cl}$  saturated solution in water was added.

The product was extracted twice with  $\text{CH}_2\text{Cl}_2$ , washed with  $\text{HCl}$  1 M twice and brine solution once, dried using  $\text{MgSO}_4$  and filtered. The solvent was then removed under reduced pressure and the crude product was purified using column chromatography with n-hexane:Ethyl acetate and 164 g  $\text{SiO}_2$ . The yield of the product was 94% (19.5 g).

**$^1\text{H}$  NMR (400 MHz, Chloroform-*d*)  $\delta$ :** 5.74 (ddt,  $J = 17.2, 10.3, 7.1$  Hz, 2H), 5.22 – 5.05 (m, 4H), 5.01 (d,  $J = 6.5$  Hz, 1H), 3.79 (s, 2H), 2.57 – 2.16 (m, 4H).

**$^{13}\text{C}$  NMR (101 MHz, Chloroform-*d*)  $\delta$ :** 166.9, 133.1, 118.5, 74.7, 37.9, 26.2.

**IR (neat)  $\text{cm}^{-1}$ :** 3079, 2980, 1733, 1275, 1166, 1107, 993, 977, 917.

**HRMS  $m/z$  (ESI):** calcd. for  $\text{C}_9\text{H}_{13}\text{O}_2\text{BrNa}$   $[\text{M}+\text{Na}]^+$ : 254.9991, found: 254.9989.

<sup>1</sup> For more details of the synthetic route, see: Perli, G.; Wylie, L.; Demir, B. *et al.* *ACS Sustainable Chem. Eng.* **2022**, *10*, 15450-15466. [\[link\]](#)



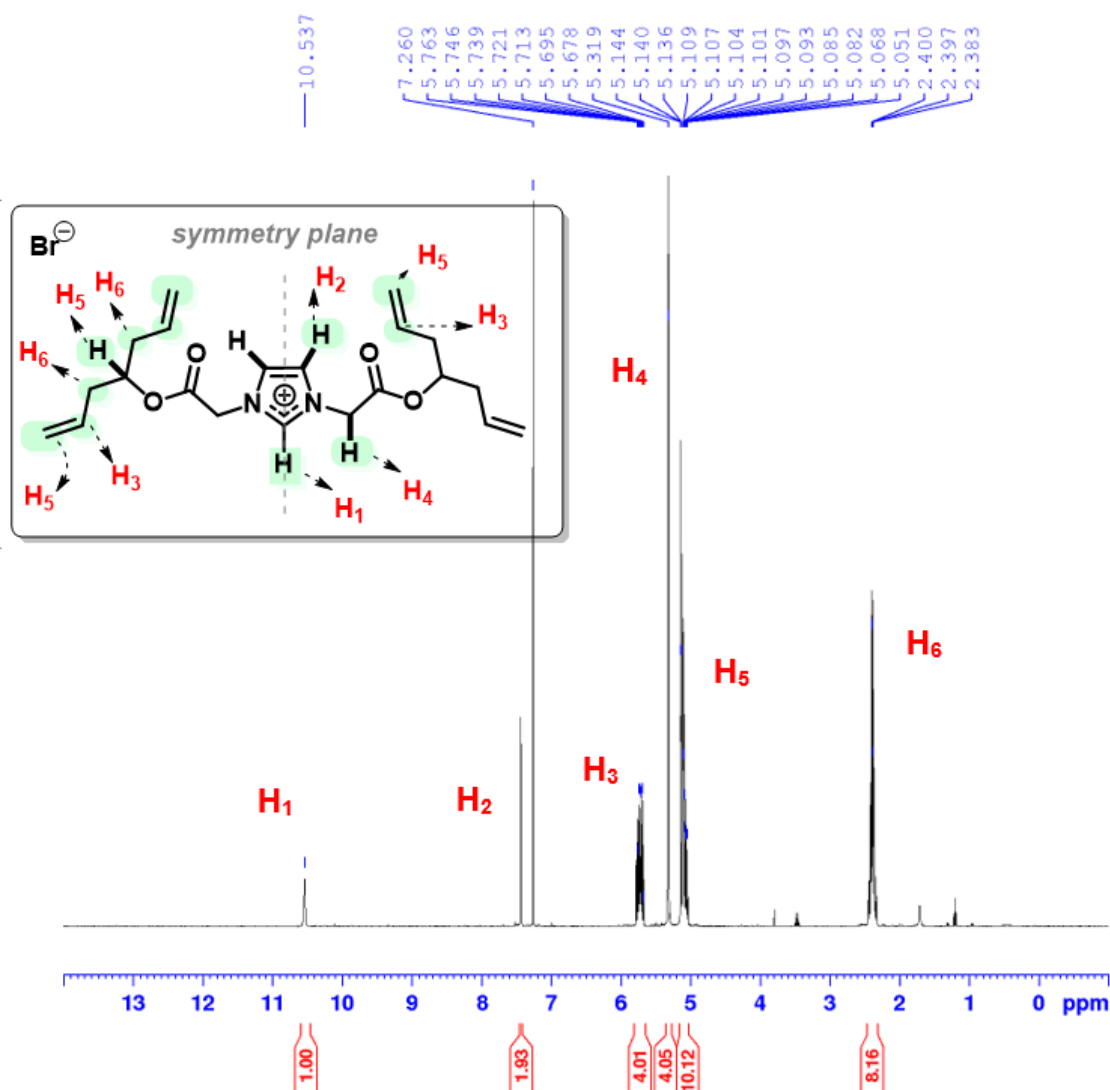
solid and it was obtained with 80% of the yield. Important to mention that bromide derivative impurities can be observed and it will be probably responsible for the brownish aspect of the sample.

**$^1\text{H}$  NMR (400 MHz, Chloroform-*d*)  $\delta$ :** 10.29 (s, 1H), 7.51 (d,  $J$  = 1.6 Hz, 2H), 5.78 – 5.65 (m, 4H), 5.34 (s, 4H), 5.16 – 5.00 (m, 10H), 2.44 – 2.31 (m, 8H) ppm.

**$^{13}\text{C}$  NMR (101 MHz, Chloroform-*d*)  $\delta$ :** 165.3, 139.4, 132.8, 123.2, 118.9, 76.1, 50.6, 37.9 ppm.

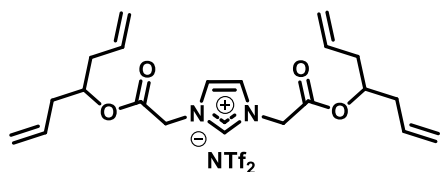
**IR (neat)  $\text{cm}^{-1}$ :** 3082, 2977, 2920, 1750, 1377, 1205, 1180, 971, 926.

**HRMS  $m/z$  (ESI):** calcd. for  $\text{C}_{21}\text{H}_{29}\text{N}_2\text{O}_4$   $[\text{M}]^+$ : 373.212184, found: 373.212153.



**Figure IV-S2.**  $^1\text{H}$  NMR spectrum of compound 2 (400 MHz,  $\text{CDCl}_3$ , 25 °C).

### Compound 3



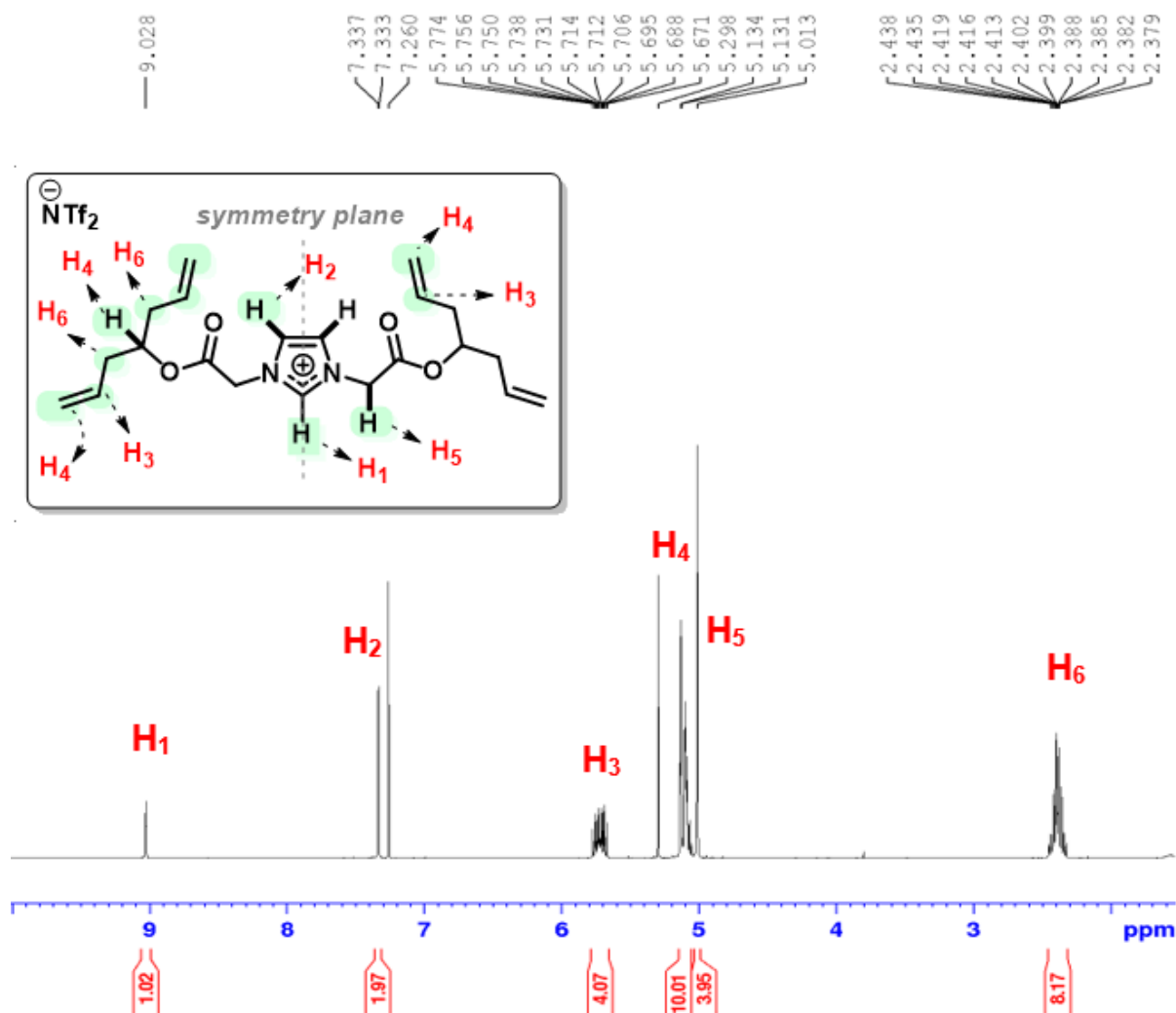
Compound 2 (0.19 g, 0.68 mmol) was dissolved in 4 mL of H<sub>2</sub>O at 80°C, the LiNTf<sub>2</sub> solution (0.15 g, 0.5 mmol) in 4 mL of H<sub>2</sub>O was added, and the mixture was left to stir overnight at room temperature. The mixture was extracted three times using CH<sub>2</sub>Cl<sub>2</sub> (3x10 mL). The organic extracted phases were combined and washed twice with water, dried using MgSO<sub>4</sub> and filtered. The solvent was then removed under reduced pressure. The yield was 0.25 g, 96%.

**<sup>1</sup>H NMR (400 MHz, Chloroform-*d*)**  $\delta$ : 9.00 (s, 1H), 7.38 (s, 2H), 5.74 (ddt, *J* = 19.4, 9.5, 7.1 Hz, 4H), 5.21 – 5.06 (m, 10H), 5.03 (s, 4H), 2.49 – 2.33 (m, 8H) ppm.

**<sup>13</sup>C NMR (101 MHz, Chloroform-*d*)**  $\delta$ : 164.8, 138.6, 132.6, 123.3, 119.7 (q, *J* = 321.0 Hz), 118.7, 76.1, 50.2, 37.8 ppm.

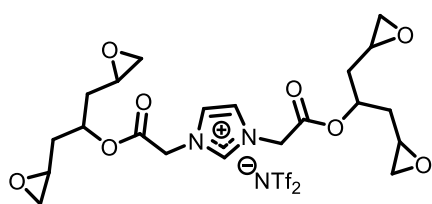
**IR (neat) cm<sup>-1</sup>**: 3085, 1743, 1643, 1570, 1435, 1348, 1205, 1134, 1054, 993, 919, 870, 788, 739.

**HRMS *m/z* (ESI)**: calcd. for C<sub>21</sub>H<sub>29</sub>N<sub>2</sub>O<sub>4</sub> [M]<sup>+</sup>: 373.21221, found: 373.212184.



**Figure IV-S3.**  $^1\text{H}$  NMR spectrum of compound 3 (400 MHz,  $\text{CDCl}_3$ , 25  $^\circ\text{C}$ ).

#### Compound 4



Next *m*CPBA (0.525 g, 2.3 mmol) was added to the solution of compound 3 (0.25 g, 0.38 mmol) in  $\text{CH}_3\text{CN}$  (10.2 mL). The reaction was stirred for 72 hours at 40 $^\circ\text{C}$  and monitored by  $^1\text{H}$  NMR. The reaction was worked up by filtering the *m*CPBA excess and concen-

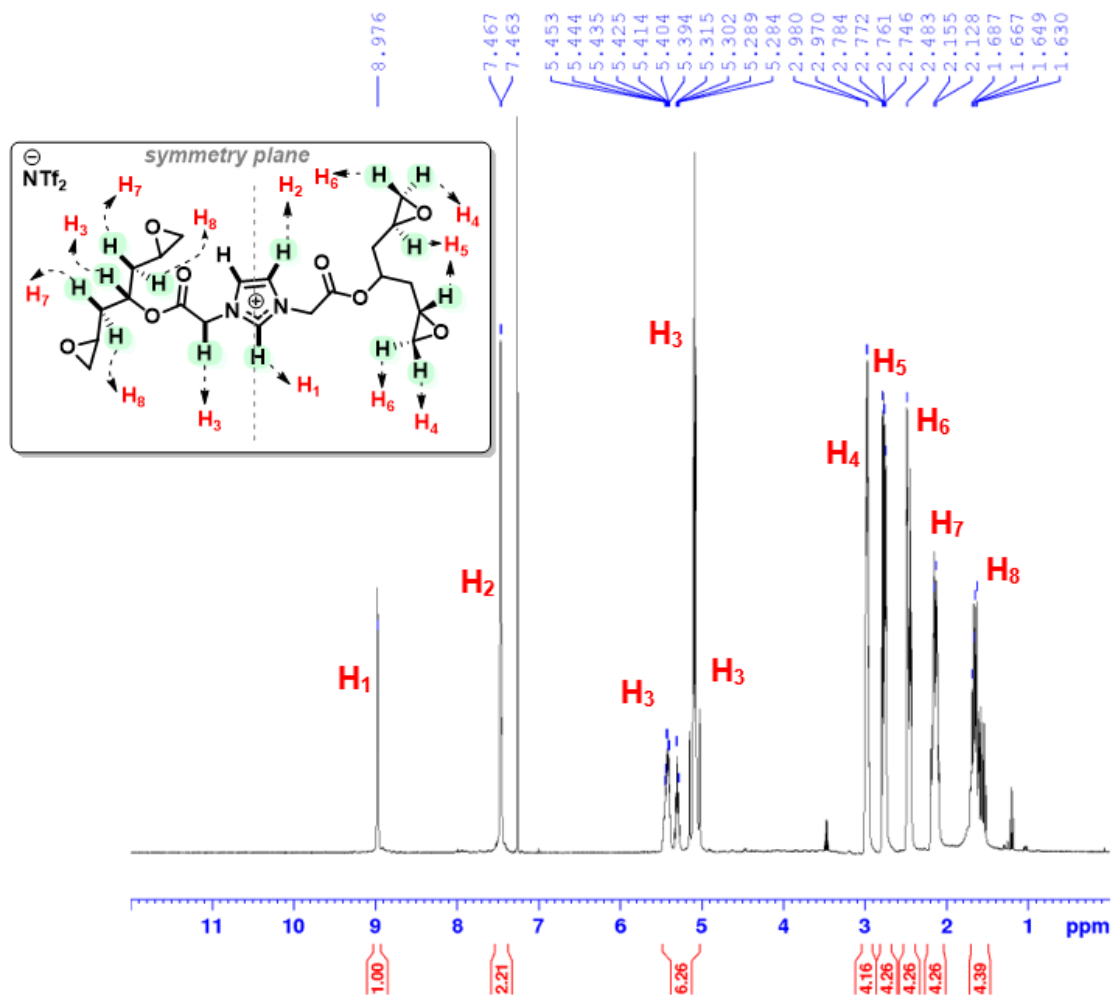
trating under reduced pressure. The product was then washed until not observing visually and by  $^1\text{H}$  NMR the presence of *m*CPBA residue. The product was finally dried yielding a colorless oil (XX g, 99%).

**$^1\text{H}$  NMR (400 MHz, Chloroform-*d*)  $\delta$ :** 9.0 (s, 1H), 7.5 (s, 2H), 5.5 – 5.3 (m, 2H), 5.2 – 5.0 (m, 4H), 3.1 – 2.9 (m, 4H), 2.8 – 2.7 (m, 4H), 2.5 – 2.4 (m, 4H), 2.2 – 2.1 (m, 4H), 1.7 – 1.5 (m, 4H) ppm.

$^{13}\text{C}$  NMR (101 MHz, Chloroform-*d*)  $\delta$ : 165.4, 138.6, 123.6, 121.3, 73.5, 73.3, 50.4, 50.4, 50.2, 49.3, 49.1, 48.5, 48.5, 46.9, 46.7, 46.1, 46.1, 37.6, 37.0, 36.6 ppm.

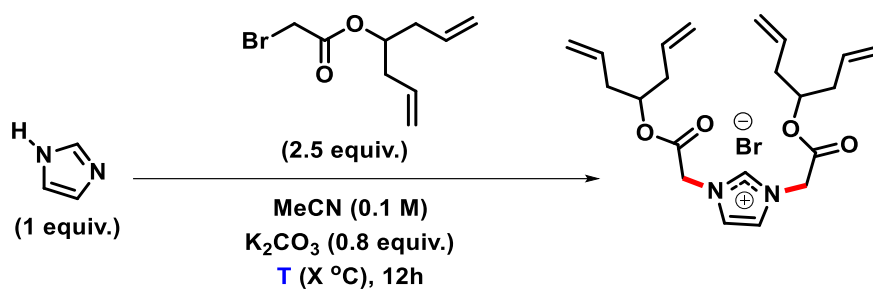
IR (neat)  $\text{cm}^{-1}$ : 1748, 1570, 1347, 1205, 1132, 1053, 914, 845, 788, 739.

HRMS  $m/z$  (ESI): calcd. for  $\text{C}_{21}\text{H}_{29}\text{N}_2\text{O}_4$   $[\text{M}]^+$ : 437.19184, found: 437.19188.



**Figure IV-S4.**  $^1\text{H}$  NMR spectrum of compound **4** (400 MHz,  $\text{CDCl}_3$ , 25  $^\circ\text{C}$ ).

**Table IV-S1.** Optimization of reaction conditions for tetra-IL synthesis.<sup>2</sup>

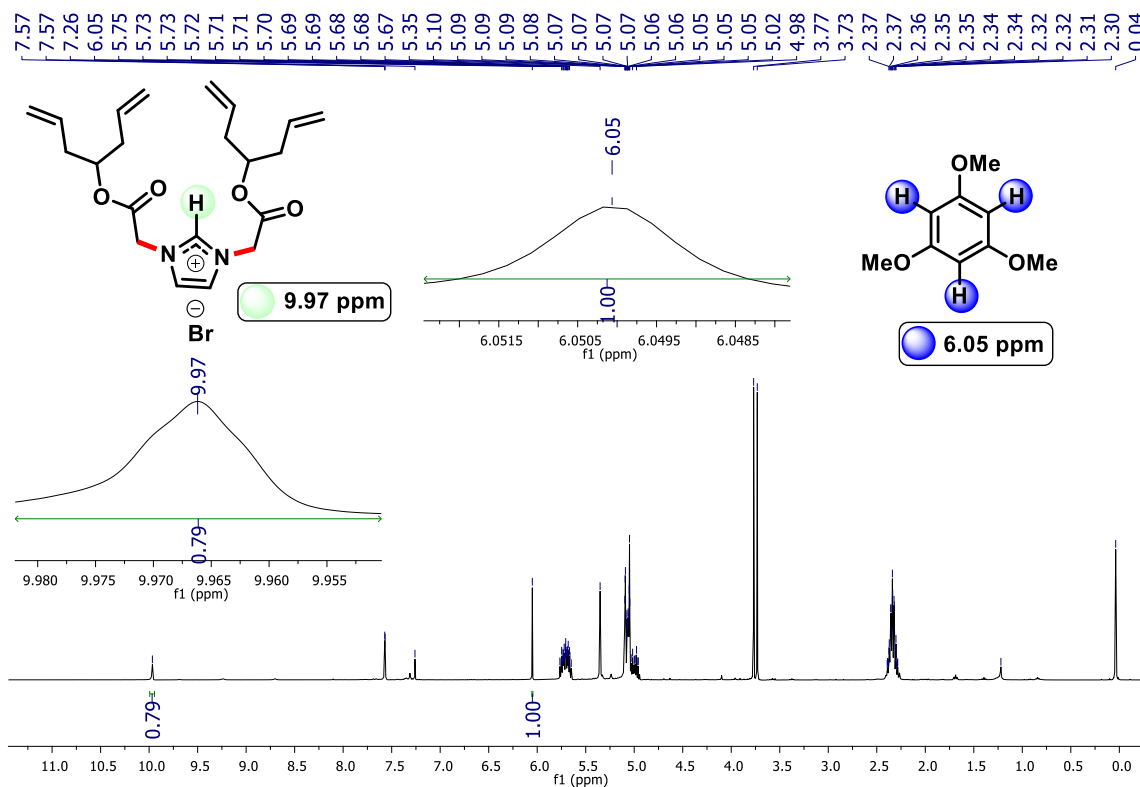


Entry	T (°C)	Yield (%) <sup>[a]</sup>
1	85	47
2	100	57
3	120	70 <sup>[c]</sup>
4	150	75 <sup>[b]</sup>

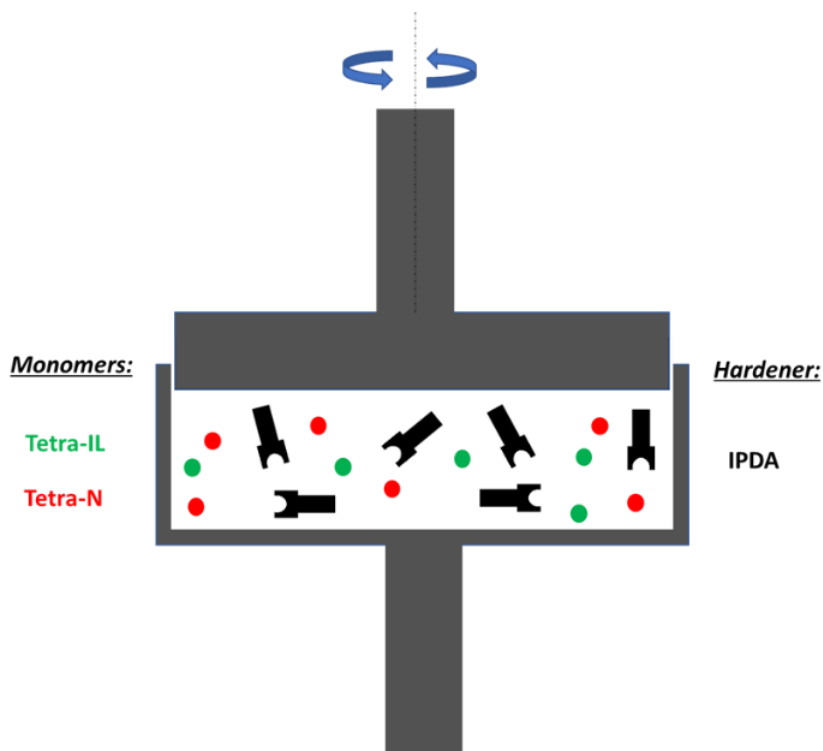
**[a]** Estimated based on the <sup>1</sup>H NMR crude employing 1,3,5-trimethoxybenzene as internal reference. **[b]** degradation starts to take place. **[c]** Product was isolated with precipitation in dimethyl ether and washing with hexane and AcOEt.

<sup>2</sup> For the reaction of pyrrole-like nitrogen alkylation and pyridine-like nitrogen quaternization in just one step, see: Zhang, Y.; *et al. Chem. Commun.* **2020**, 56, 3309-3312. [\[link\]](#)

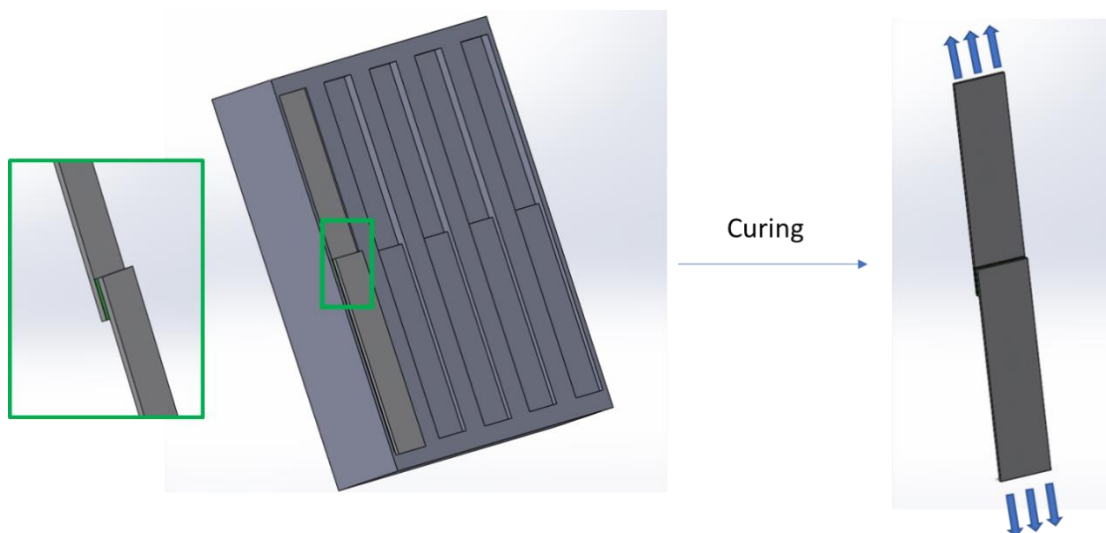




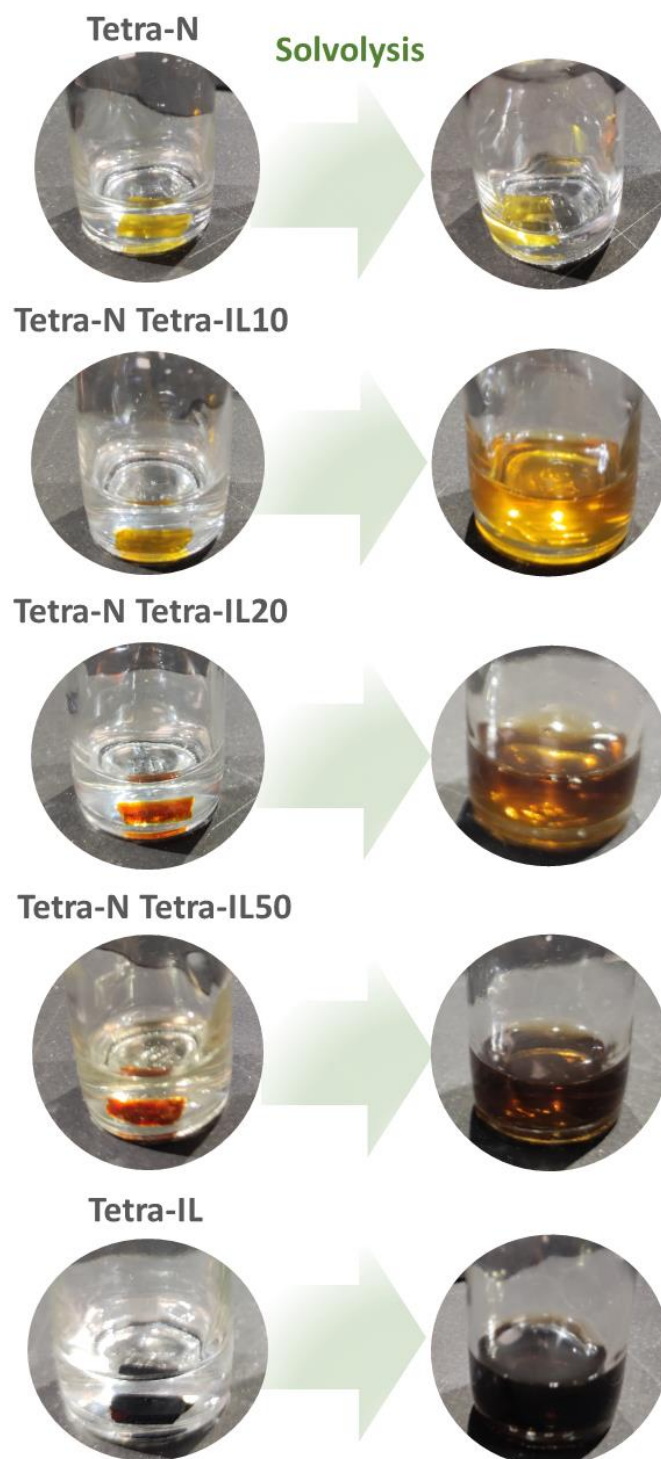
**Figure IV-S5.** NMR spectrum employed to quantify the yield of the reaction using TMB as an internal standard (400 MHz, CDCl<sub>3</sub>, 25 °C).



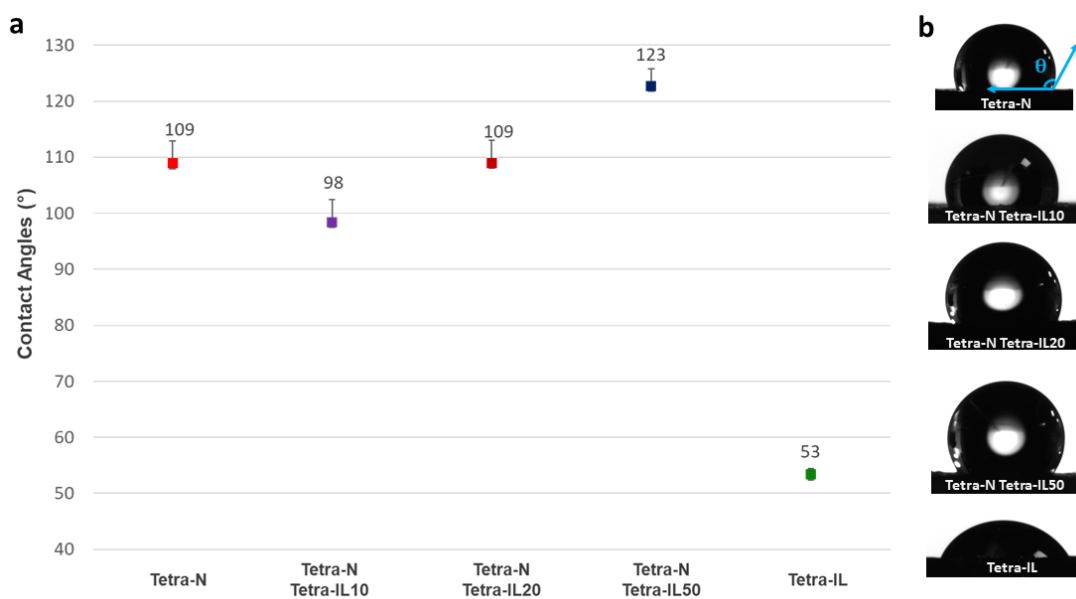
**Figure IV- S6.** Parallel-plate cup geometry employed in the rheological assay.



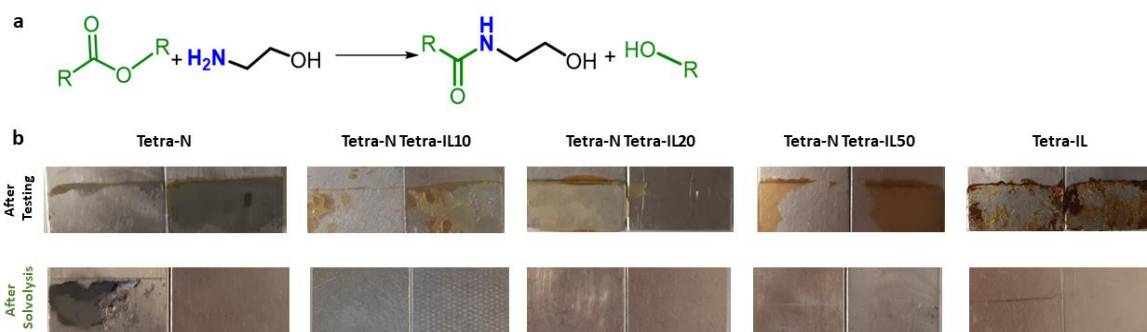
**Figure IV-S7.** Mold employed to cure the adhesives and the tensile testing.



**Figure IV-S8.** The thermoset networks before and after the solvolysis performed in ethylene glycol and in the presence of 10% of the acid catalyst.



**Figure IV-S9.** Contact angles with water for the five different networks. **a)** the average of the contact angles with water and **b)** the image of water droplets deposited on the network surfaces.



**Figure IV-S10.** Proposed mechanism for the thermoset network depolymerization and the specimens after the tensile testing and after the solvolysis.

# **Appendix III - Activated Cycloaliphatic Epoxidized Ionic Liquids as New Versatile Monomers for the Construction of Multifunctional Degradable Thermosets**

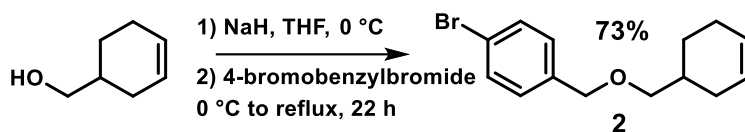
## General Methodology

### Characterization and Purification Methods

$^1\text{H}$  and  $^{13}\text{C}$  spectra were recorded on a Bruker Avance III spectrometer operating at 400 MHz or 500 MHz. Spectra were obtained using solutions of *ca.* 10 mg in an appropriate deuterated solvents. The chemical shifts ( $\delta$ ) are expressed in ppm relative to internal tetramethylsilane for  $^1\text{H}$  and  $^{13}\text{C}$  nuclei. The coupling constants were automatically obtained by TopSpin© and expressed in Hz. Abbreviations for signal coupling are indicated as: s = singlet; d=doublet; dd=doublet of doublets; t=triplet; q=quartet; quin=quintet; m=multiplet; br=broad signal. To accurately determine the molecular structure of the monomer CEIL and its intermediates additional 2D NMR experiments (COSY, HSQC, HMBC) were performed.

High Resolution Mass Spectra HRMS was carried out on by a Micromass-Waters Q-TOF Ultima Global by the technique of Electrospray Ionization (ESI).

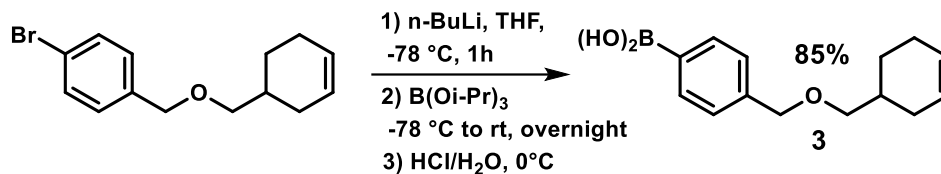
Thin Layer Chromatography (TLC) was run using different eluent mixtures on pre-coated aluminum plates of silica gel 60 F-254 (Merck).



#### 4-Bromobenzyl (cyclohex-3-en-1-ylmethyl) ether (**2**).

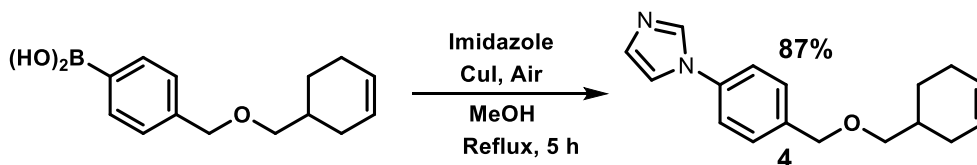
Under Argon atmosphere, cyclohex-3-en-1-ylmethanol (12.5 mL, 0.11 mol) was added dropwise to a stirred suspension of NaH (5.6 g (60 % in mineral oil), 0.14 mol) in anhydrous THF (200 mL) at 0 °C. After the addition, the mixture was left to stir for 30 min at 0 °C. Then, more 200 mL of anhydrous THF was added followed by the addition of 4-bromobenzylbromide (26.75 g, 0.12 mol). The reactional mixture was stirred for 30 min at 27 °C. Finally, the reactional mixture was heated for 22 h under reflux and Argon atmosphere. The reaction was cooled to 0 °C and it was quenched by adding 50 g of ice cubes. The reactional mixture was stirred for 1 h to ensure the complete quenching. The reaction was filtered using paper filter and extracted five times with dichloromethane and dd-water. The organic layer was dried over MgSO<sub>4</sub> and concentrated in vacuo. The product was further purified by column chromatography using silica gel and hexane: ethyl acetate (solvent mixture gradient from 100:0 until 95:5) as eluent. Compound **2** was obtained as a colorless and transparent oil with 73% of yield.  **$^1\text{H}$  NMR (500 MHz, Chloroform-*d*)**  $\delta$ : 7.45 (d, *J* = 8.3 Hz, 2H), 7.22 (d, *J* = 8.5 Hz, 2H), 5.76–5.61 (m, 2H), 4.47 (s, 2H), 3.41–3.30 (m, 2H), 2.17–2.09 (m, 1H), 2.09–2.03 (m, 2H), 1.99–1.90 (m, 1H), 1.88–1.80 (m, 1H), 1.80–1.70 (m, 1H), 1.34–1.21 (m, 1H).

**<sup>13</sup>C NMR (126 MHz, Chloroform-d) δ:** 138.8, 132.5, 129.3, 127.2, 126.7, 122.3, 74.5, 73.3, 33.5, 27.6, 24.9, 25.6.



#### 4-((Cyclohex-3-en-1-ylmethoxy)methyl)phenyl)boronic acid (3).

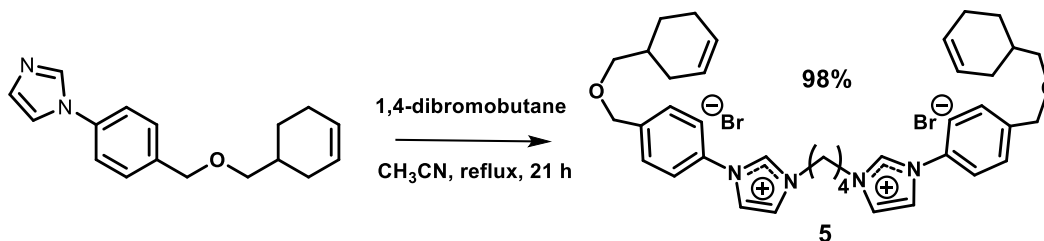
Under Argon atmosphere, the compound **2** (13.85 g, 49.2 mmol) was dissolved in anhydrous THF (129 mL) and mixture was cooled to -78 °C and, subsequently n-BuLi 2.5 M in hexane (23.6 mL, 49.2 mmol) was added dropwise. The mixture was kept stirring at -78 °C for 60 min and then 17 mL (50.5 mmol) of triisopropyl borate was slowly added. The mixture was stirred overnight from -78 °C to room temperature. The reaction was cooled to 0 °C and quenched by adding 50 g of ice cubes followed by the slowly addition of 137 mL of hydrochloric acid (1 M). The yielding mixture was stirred for 30 min. The aqueous layer was extracted by dichloromethane, dried over anhydrous MgSO<sub>4</sub> and concentrated in vacuo. Compound **3** was employed in the next step without further purification since the product degrades in the column. The product was obtained as a off-white crystal compound. **<sup>1</sup>H NMR (500 MHz, Chloroform-d) δ:** 8.21 (d, J = 7.7 Hz, 2H), 7.48 (d, J = 7.7 Hz, 2H), 5.88–5.46 (m, 2H), 4.61 (s, 2H), 3.52–3.32 (m, 2H), 2.28–2.12 (m, 1H), 2.12–2.08 (m, 2H), 2.05–1.95 (m, 1H), 1.95– 1.85 (m, 1H), 1.83–1.72 (m, 1H), 1.35–1.26 (m, 1H). **<sup>13</sup>C NMR (126 MHz, Chloroform-d) δ:** 143.7, 135.9, 133.5, 127.4, 126.4, 126.7, 75.9, 72.8, 34.1, 28.3, 25.5, 24.4.



#### 1-((4-((Cyclohex-3-en-1-ylmethoxy)methyl)phenyl)-1H-imidazole (4).

Initially, imidazole (2.5 g, 37.2 mmol) and copper (I) iodide (236 mg, 1.4 mmol) was stirred for 5 min in 114 mL of methanol. Subsequently, the boronic acid derivative **3** was added and stirred overnight under reflux and bubbling air in the reactional mixture. The solution was cooled to room temperature and filtered using a Celite® pellet and concentrated under reduced pressure. The product was further purified by column chromatography using silica gel and hexane: ethyl acetate (solvent mixture gradient from 70:30 until 0:100) as eluent. Compound **4** was obtained as white crystalline powder. **<sup>1</sup>H NMR (400 MHz, Chloroform-d) δ:** 7.89 (s, 1H), 7.47 (d, J = 8.5 Hz, 2H), 7.36 (d, J = 8.5 Hz, 2H), 7.27 (s,

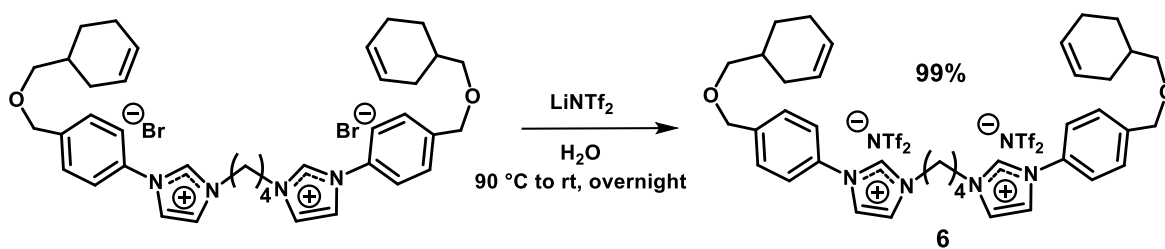
1H), 7.22 (s, 1H), 5.72–5.61 (m, 2H), 4.54 (s, 2H), 3.54–3.22 (m, 2H), 2.18–2.12 (m, 1H), 2.08–2.04 (m, 2H), 2.02–1.94 (m, 1H), 1.89–1.83 (m, 1H), 1.82–1.73 (m, 1H), 1.37–1.29 (m, 1H). **<sup>13</sup>C NMR (400 MHz, Chloroform-d) δ:** 138.5, 136.7, 135.6, 130.5, 128.5, 127.2, 126.2, 121.5, 118.9, 75.6, 72.2, 34.5, 28.4, 25.7, 24.3.



**3,3'-(Butane-1,4-diyl)bis(1-(4-((cyclohex-3-en-1-ylmethoxy)methyl)phenyl)-1H-imidazol-3-ium) bromide (5).**

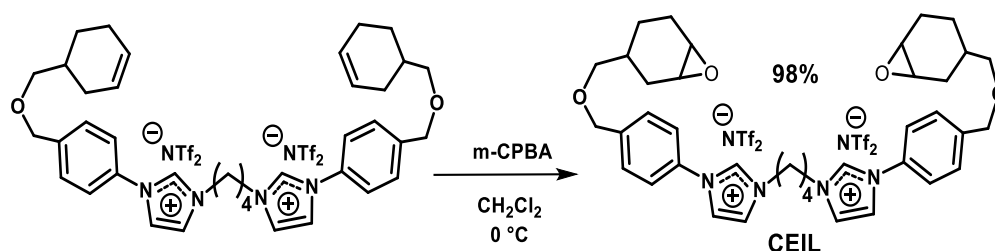
Compound **4** (6.37 g, 23.7 mmol) was solubilized in 33 mL of acetonitrile and 1,4-dibromobutane (2.6 g, 11.87 mmol) was slowly added using a syringe and needle. The reaction was stirred for 21 h at 80 °C. The reaction yielded an off-white precipitate that was washed several times with cold acetonitrile. The product was filtered and dried under vacuum resulting in a white powder. **<sup>1</sup>H NMR (400 MHz, Chloroform-d) δ:** 10.78 (t, J = 1.7 Hz, 2H), 8.44 (t, J = 1.3 Hz, 2H), 7.74 (d, J = 8.5 Hz, 4H), 7.62 (t, J = 1.9 Hz, 2H), 7.52 (d, J = 8.4 Hz, 4H), 5.73–5.54 (m, 4H), 4.82 (t, J = 6.3 Hz, 4H), 4.54 (s, 4H), 3.41–3.35 (m, 4H), 2.37 (t, J = 6.3 Hz, 4H), 2.16–2.08 (m, 2H), 2.08–2.00 (m, 4H), 1.98–1.87 (m, 2H), 1.86–1.77 (m, 2H), 1.79–1.69 (m, 2H), 1.34–1.23 (m, 2H). **<sup>13</sup>C NMR (400 MHz, Chloroform-d) δ:** 141.7, 135.5, 133.7, 129.3, 127.2, 125.8, 124.7, 121.8, 120.2, 75.7, 71.9, 49.3, 34.1, 28.5, 26.6, 25.6, 24.5.





**3,3'-(Butane-1,4-diyl)bis(1-(4-((cyclohex-3-en-1-ylmethoxy)methyl)phenyl)-1H-imidazol-3-ium) bistrifluoromethanesulfonimide (6).**

Compound 5 (21.22 g, 28.28 mmol) was added to 400 mL of dd-water and heated to 85 °C until complete solubilization of the material. Subsequently, a LiNTf<sub>2</sub> (13.52 g, 43 mmol) solution was prepared using 1 mL of dd-water, and it was added to the previous solution. The mixture became cloudy, and this reactional mixture was left to stir for 3h at room temperature. The aqueous layer was extracted by dichloromethane five times, dried over anhydrous MgSO<sub>4</sub> and concentrated in vacuo. The compound 6 was obtained as a colorless oil (32.28 g, 27.99 mmol). **<sup>1</sup>H NMR (400 MHz, Chloroform-d) δ:** 9.07 (t, J = 1.8 Hz, 2H), 7.72 (t, J = 1.8 Hz, 2H), 7.61–7.49 (m, 10H), 5.76–5.57 (m, 4H), 4.59 (s, 4H), 4.44–4.38 (m, 4H), 3.47–3.32 (m, 4H), 2.23–2.12 (m, 6H), 2.10–2.03 (m, 4H), 2.05–1.93 (m, 2H), 1.90–1.88 (m, 4H), 1.38–1.27 (m, 2H). **<sup>13</sup>C NMR (400 MHz, Chloroform-d) δ:** 142.2, 133.8, 133.5, 129.3, 127.2, 125.8, 123.9, 122.5, 121.8, 119.5 (q, J = 321.1 Hz), 75.0, 71.2, 49.3, 34.5, 28.5, 26.5, 24.6, 25.6.

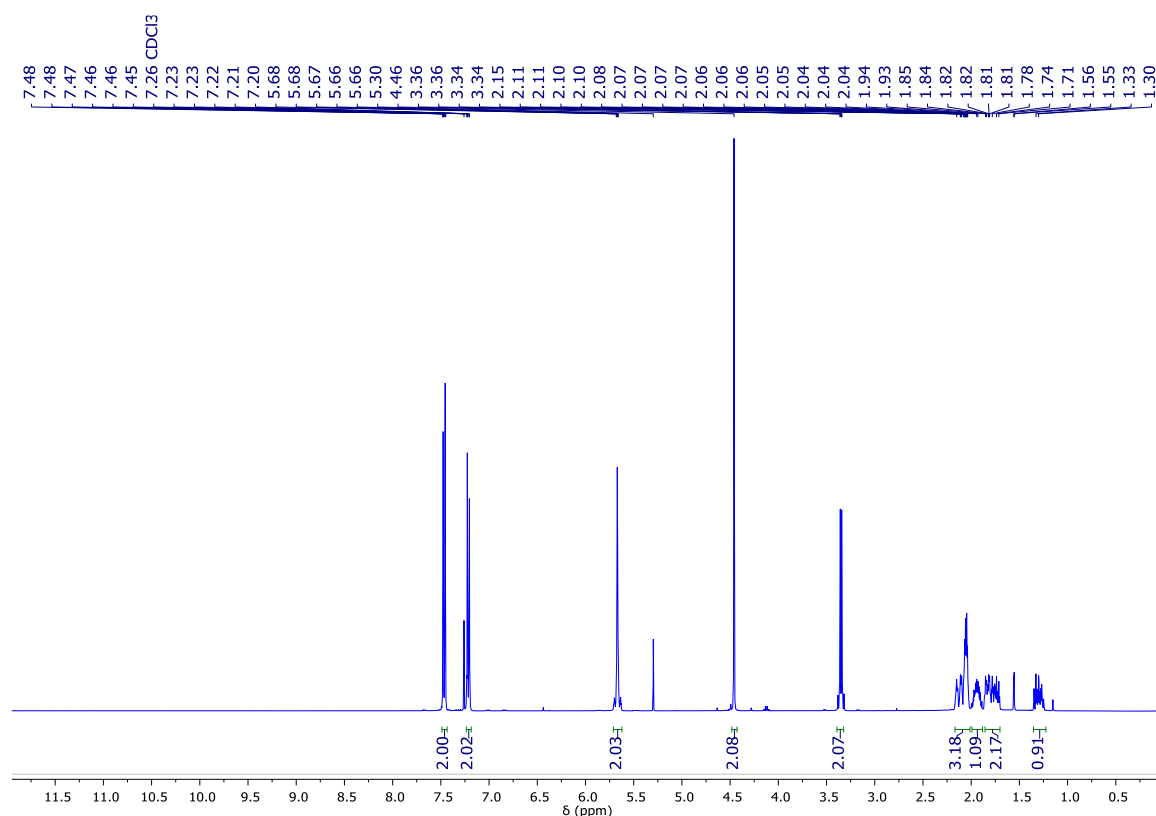


**3,3'-(Butane-1,4-diyl)bis(1-(4-(((7-oxabicyclo[4.1.0]heptan-3-yl)methoxy)methyl)phenyl)-1Himidazol-3-ium) bistrifluoromethanesulfonimide (CEIL).**

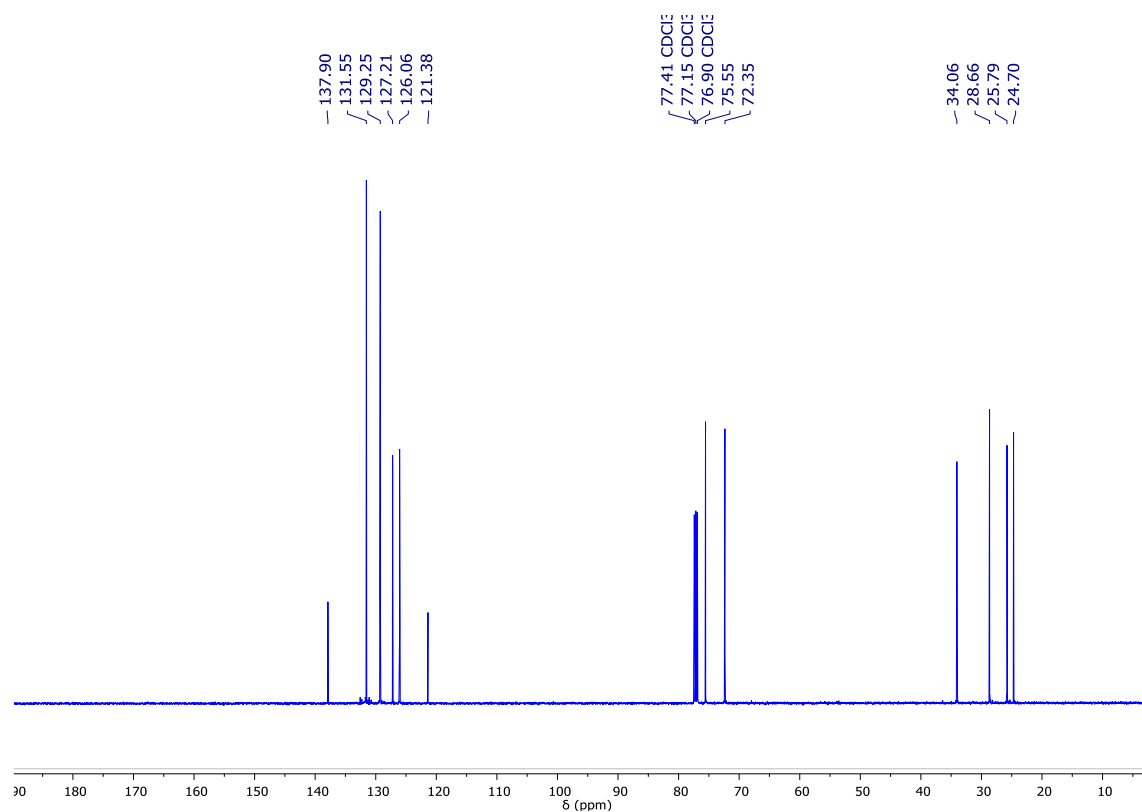
To obtain the final product CEIL, an adaptation of the classical Prilezhaev epoxidation reaction was employed. Compound 6 (9.54 g, 8.31 mmol) was solubilized in anhydrous dichloromethane (54.41 mL) at 0 °C. Next, *m*CPBA (5.97 g, 20.8 mmol) was slowly added. The reaction was stirred at 0 °C for 3 h, and a white precipitate was formed. The reaction mixture was concentrated under reduced pressure and filtered to eliminate the excess of *m*CPBA and its derivatives. The solution obtained from the filtration was poured in diethyl

ether (300 mL). The insoluble part was isolated by decantation and washed three times by diethyl ether. The product was dried under vacuum and resulted in a transparent and colorless viscous oil (9.98 g, 98%). **<sup>1</sup>H NMR (400 MHz, Acetonitrile-d<sub>3</sub>) δ:** 8.92–8.86 (m, 2H), 7.84–7.78 (m, 2H), 7.67–7.58 (m, 10H), 4.62–4.54 (m, 4H), 4.35–4.57 (m, 4H), 3.41–3.29 (m, 4H), 3.19–3.09 (m, 4H), 2.21–1.98 (m, 7H), 1.87–1.38 (m, 9H), 1.21–0.99 (m, 2H). **<sup>13</sup>C NMR (101 MHz, Acetonitrile-d<sub>3</sub>) mixture of stereoisomers δ:** 143.9, 142.9, 135.7, 134.8, 134.9, 130.2, 130.1, 124.3, 123.6, 123.6, 123.1, 120.8 (q, J = 320.8 Hz), 76.7, 76.2, 72.3, 72.2, 53.1, 53.3, 52.2, 51.7, 50.6, 33.10, 31.3, 29.3, 28.2, 27.2, 25.4, 24.8, 23.7, 22.3.

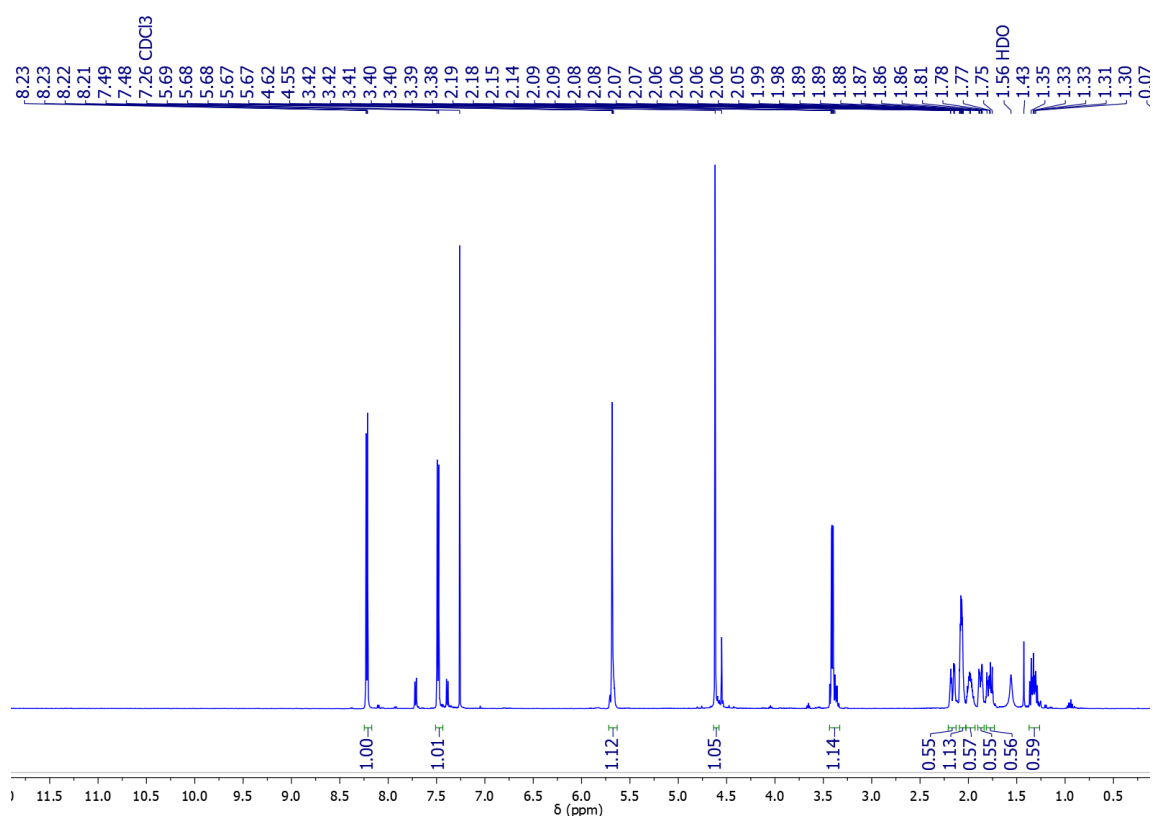
## NMR Spectra



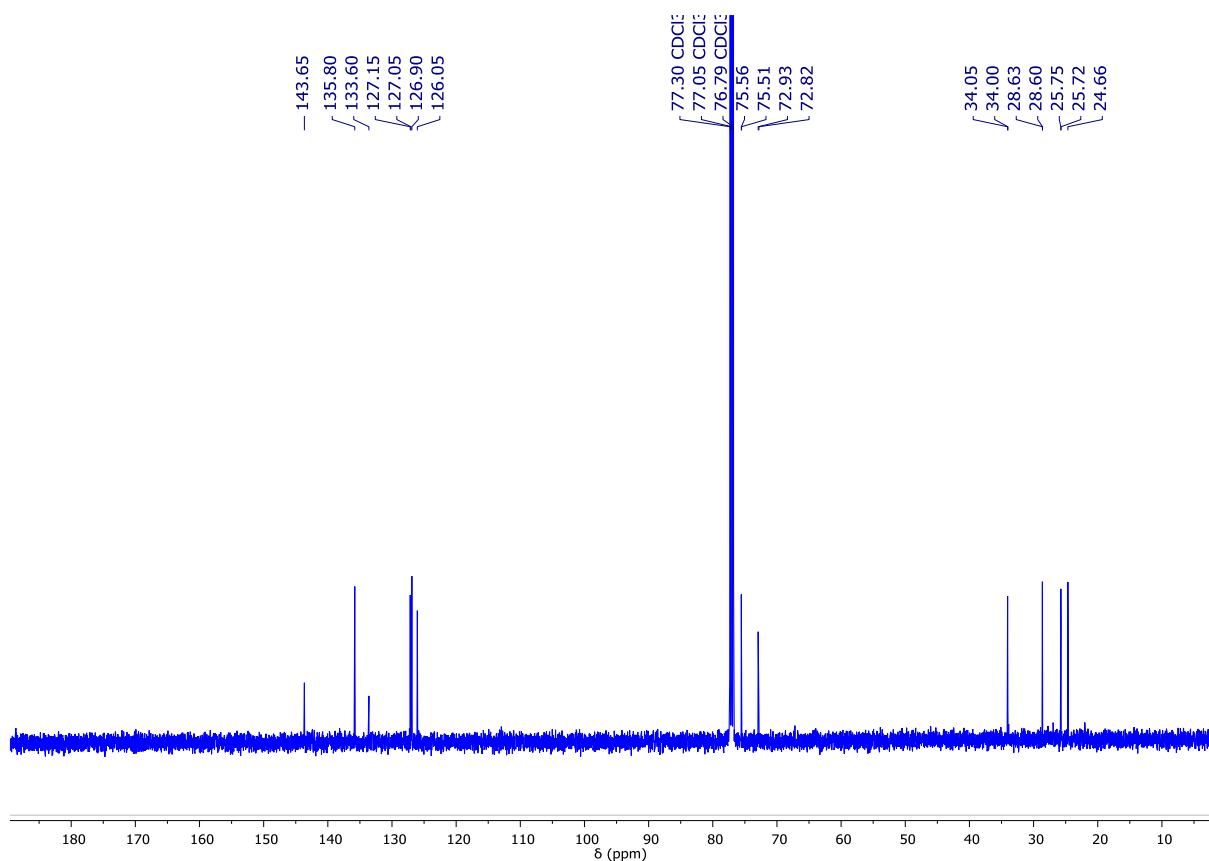
**Figure V-S1.** <sup>1</sup>H NMR spectrum of compound **2** (400 MHz, CDCl<sub>3</sub>, 25 °C).



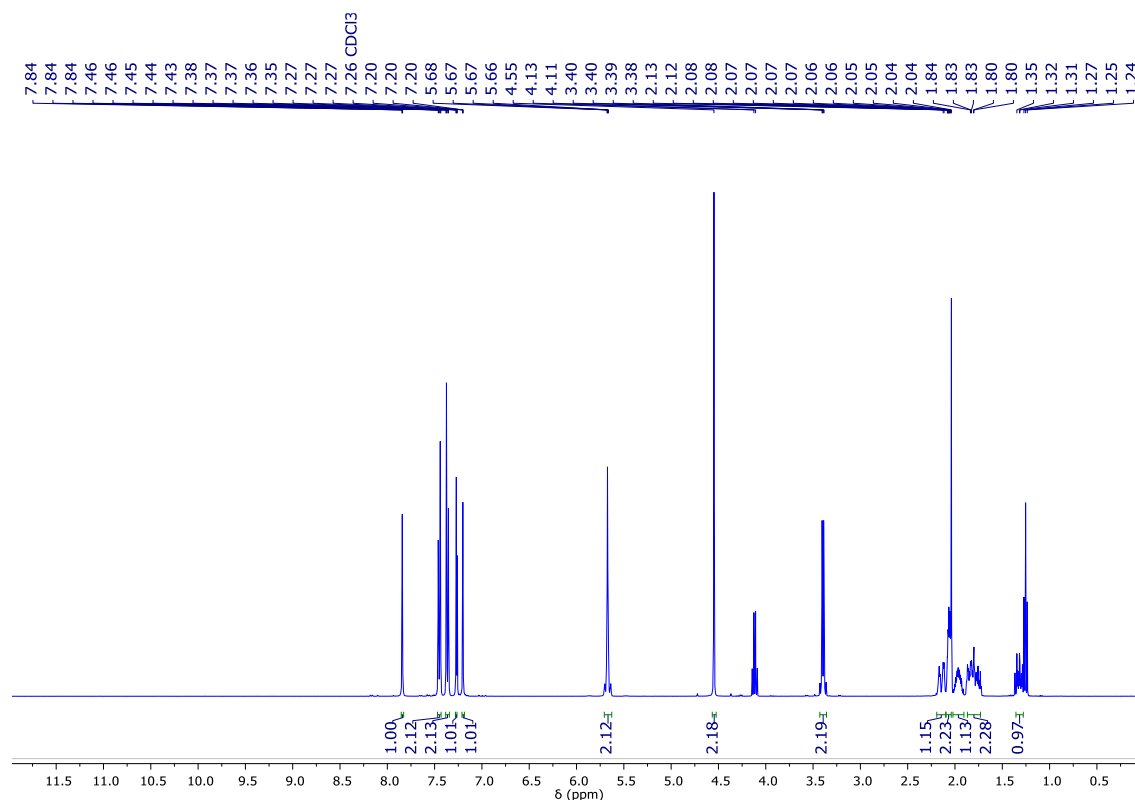
**Figure V-S2.** <sup>13</sup>C NMR spectrum of compound **2** (400 MHz, CDCl<sub>3</sub>, 25 °C).



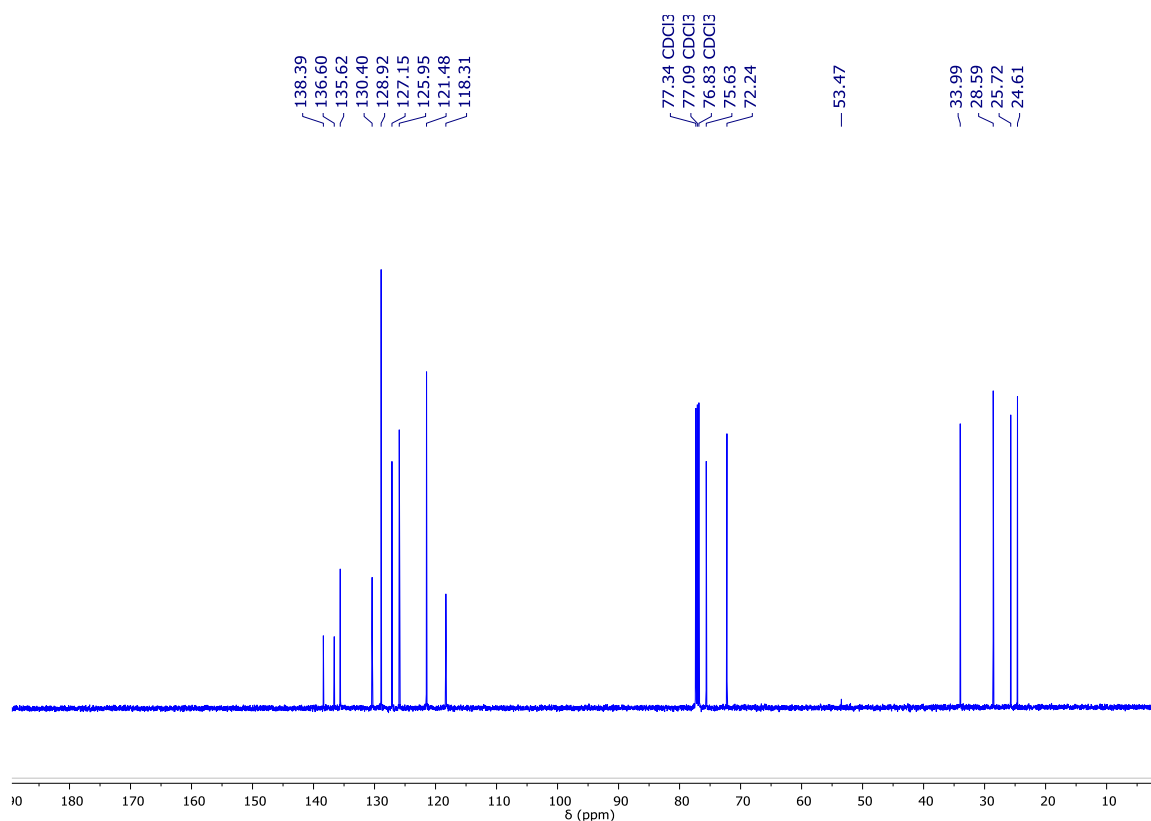
**Figure V-S3.** <sup>1</sup>H NMR spectrum of compound **3** (400 MHz, CDCl<sub>3</sub>, 25 °C).



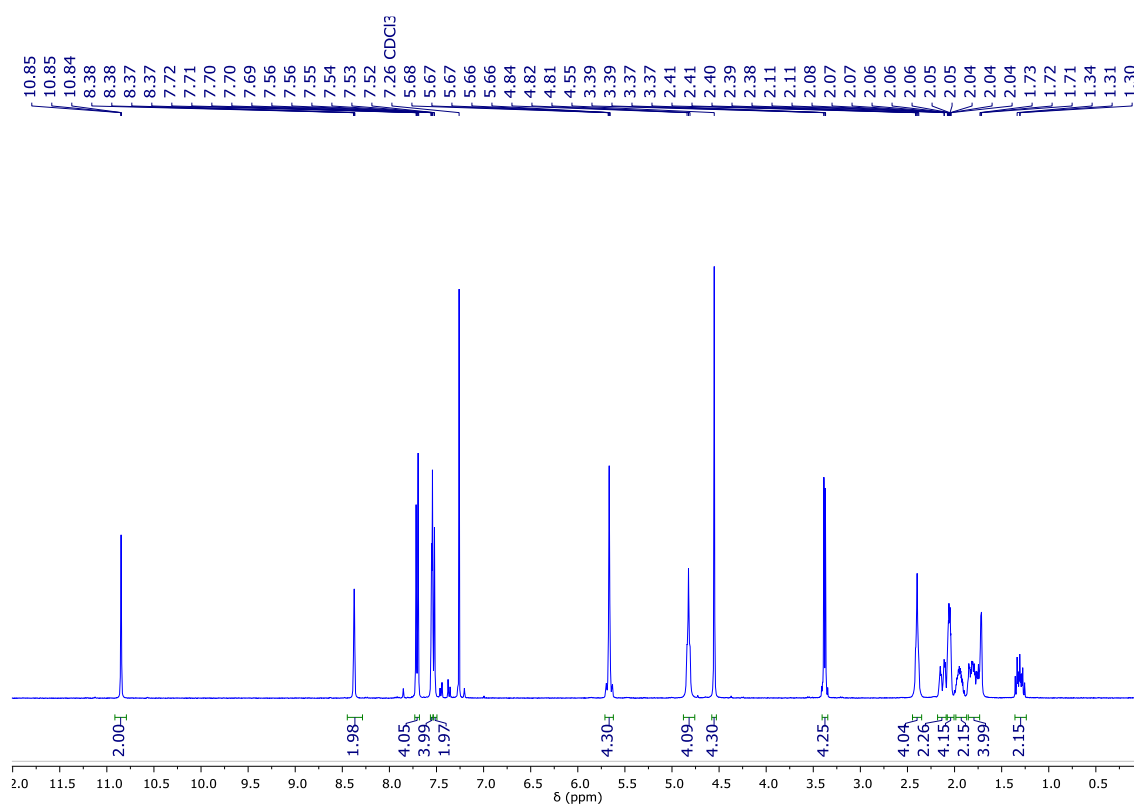
**Figure V-S4.**  $^{13}\text{C}$  NMR spectrum of compound **3** (400 MHz,  $\text{CDCl}_3$ , 25  $^\circ\text{C}$ ).



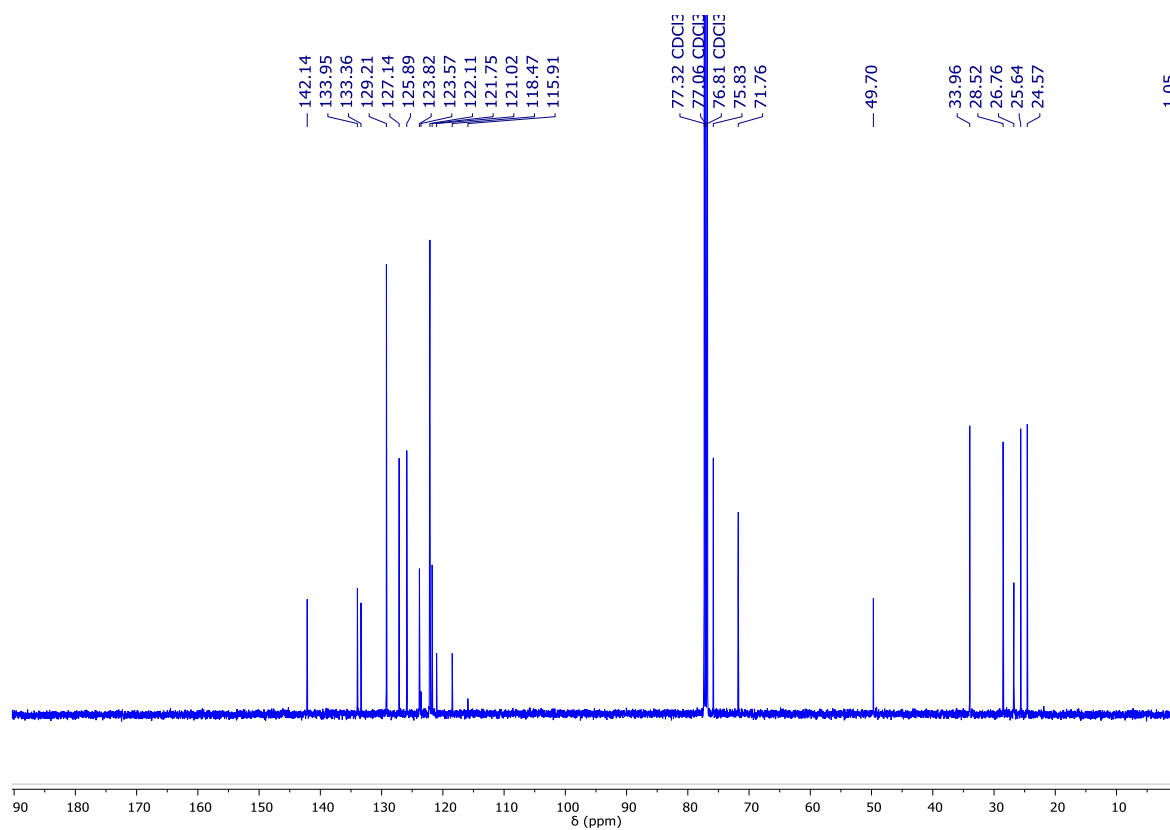
**Figure V-S5.**  $^1\text{H}$  NMR spectrum of compound **4** (400 MHz,  $\text{CDCl}_3$ , 25  $^\circ\text{C}$ ).



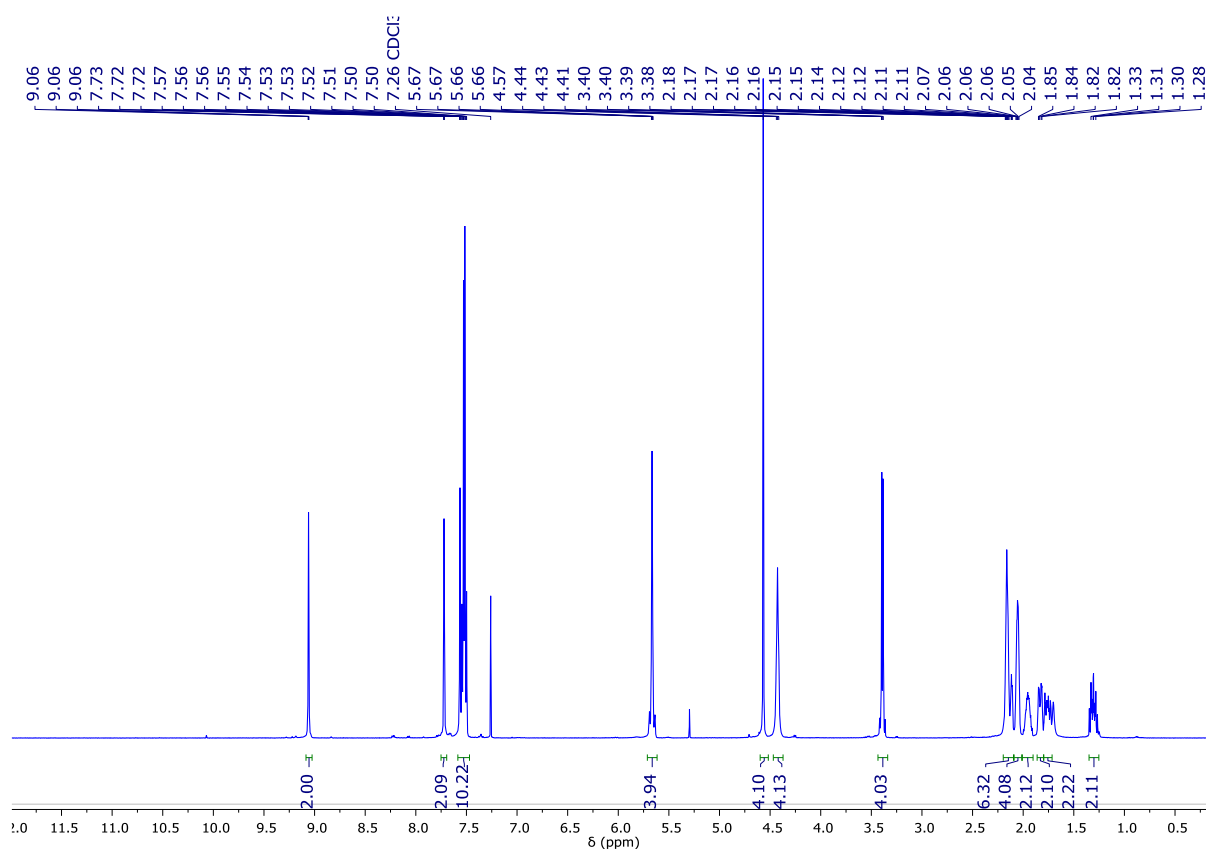
**Figure V-S6.** <sup>13</sup>C NMR spectrum of compound **4** (400 MHz, CDCl<sub>3</sub>, 25 °C).



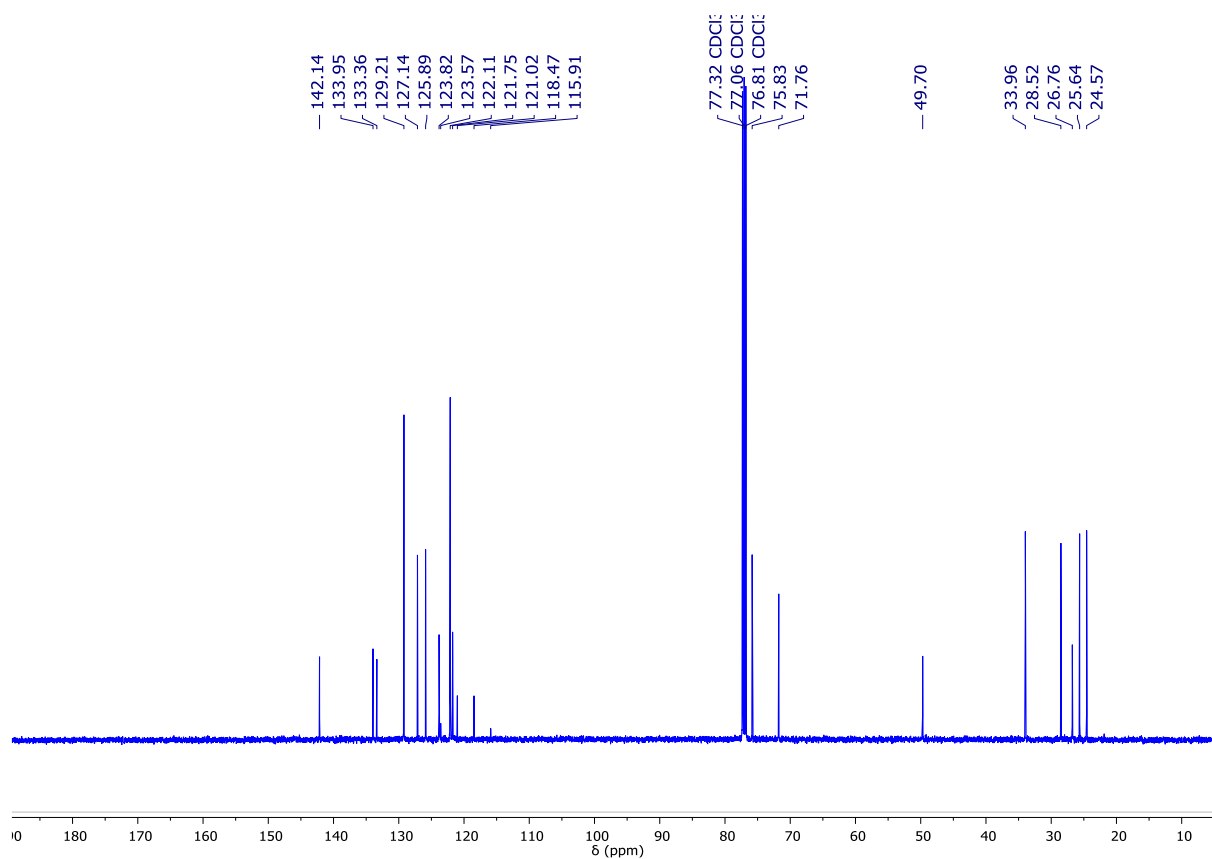
**Figure V-S7.** <sup>1</sup>H NMR spectrum of compound **5** (400 MHz, CDCl<sub>3</sub>, 25 °C).



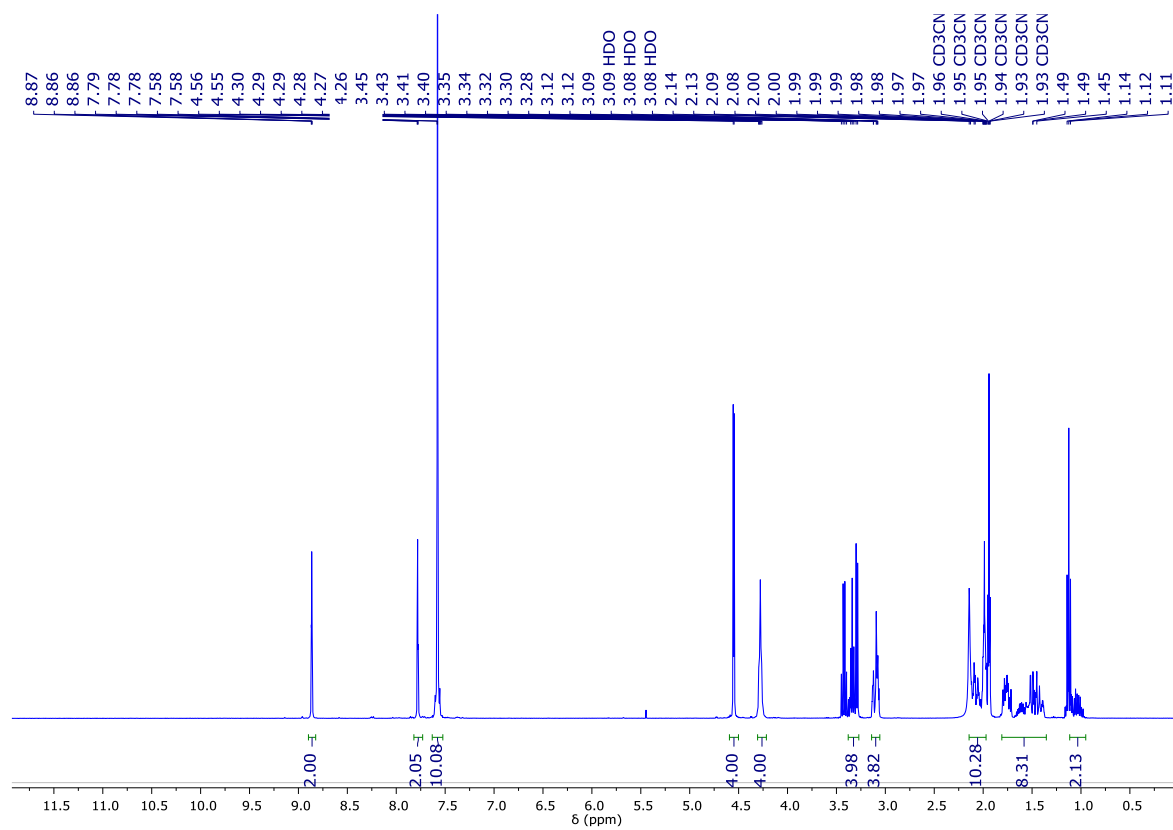
**Figure V-S8.** <sup>13</sup>C NMR spectrum of compound **5** (400 MHz, CDCl<sub>3</sub>, 25 °C).



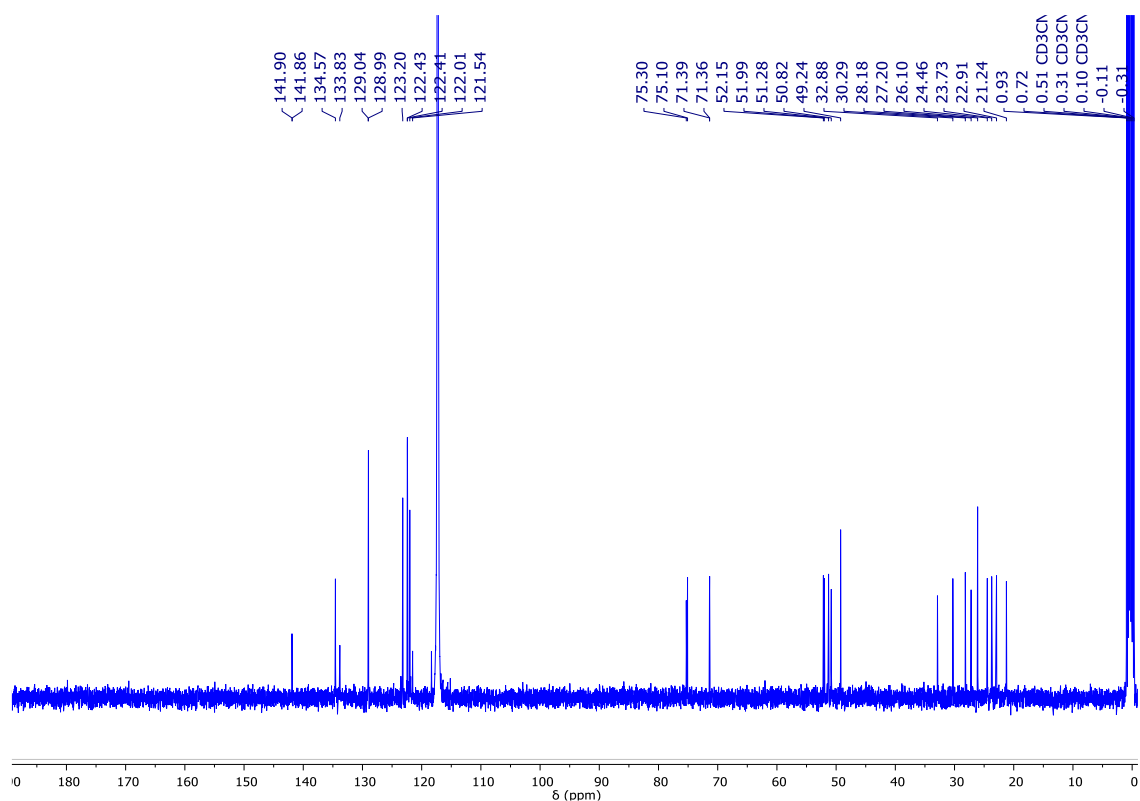
**Figure V-S9.** <sup>1</sup>H NMR spectrum of compound **6** (400 MHz, CDCl<sub>3</sub>, 25 °C).



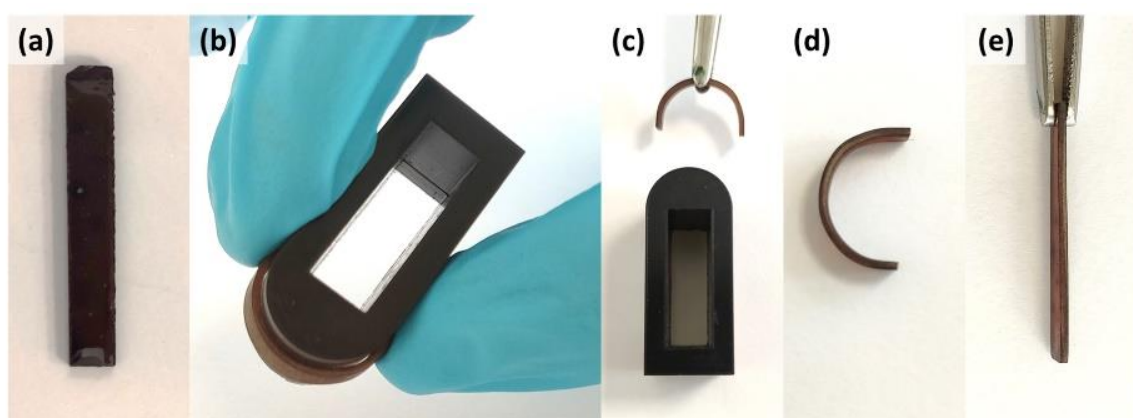
**Figure V-S10.** <sup>13</sup>C NMR spectrum of compound **6** (400 MHz, CDCl<sub>3</sub>, 25 °C).



**Figure V-S11.** <sup>1</sup>H NMR spectrum of compound **7** (400 MHz, CDCl<sub>3</sub>, 25 °C).



**Figure V-S12.**  $^1\text{H}$  NMR spectrum of compound **7** (400 MHz,  $\text{CDCl}_3$ , 25  $^\circ\text{C}$ ).



**Figure V-S13.** Fold-deploy experiment showing the different steps. In **a)** p-CEIL initial shape, **b)** bending process using a mold, **c-d)** folded shape and **e)** the initial shape after the heating process.

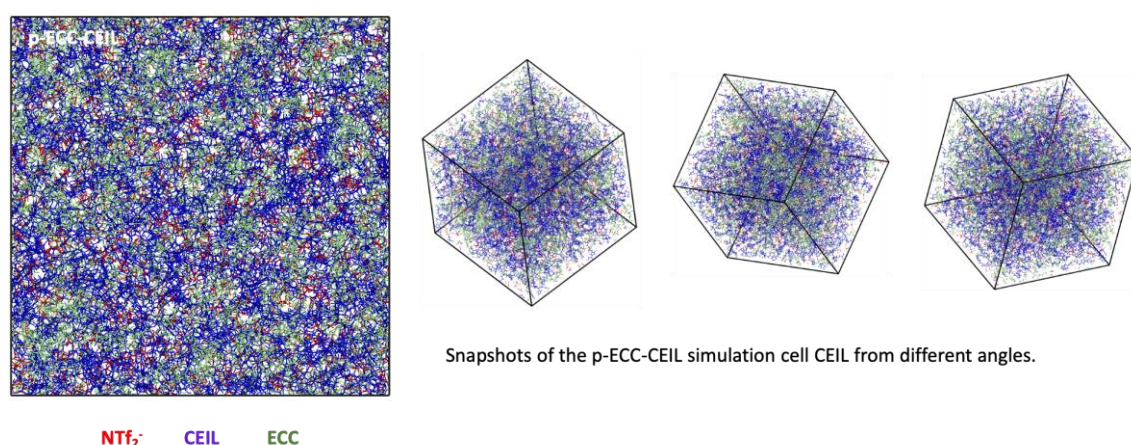


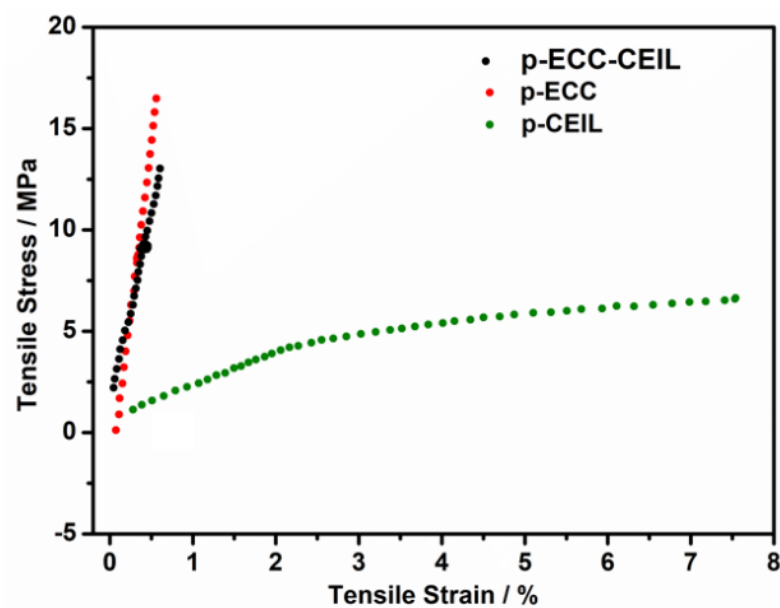
**Table V-S1.** The number of ions/monomers used for each system.

System	CEIL	ECC	TFSI	Total Number of Atoms
p-CEIL-ECC	240	560	480	54240
p-ECC	-	1200	-	50400
p-CEIL	400	-	800	51200

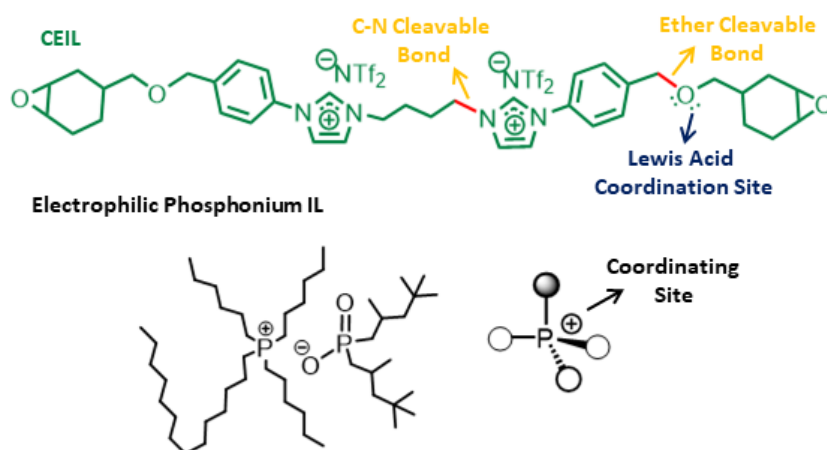
**Table V-S2.** Calculated thermo-mechanical properties of each system.

	p-CEIL-ECC	p-ECC	p-CEIL
Density ( $\text{g cm}^{-3}$ )	1.25	1.08	1.31
Density, std	0.01	0.01	0.00
$T_g$ ( $^{\circ}\text{C}$ )	166.0	215.2	103.0
$T_g$ , std	44.5	18.4	11.6
CVTE, below ( $\text{K}^{-1}$ )	1.99	0.60	4.16
CVTE, below, std	0.14	0.06	0.06
CVTE, above	2.84	1.43	6.45
CVTE, above, std	0.36	0.13	0.14

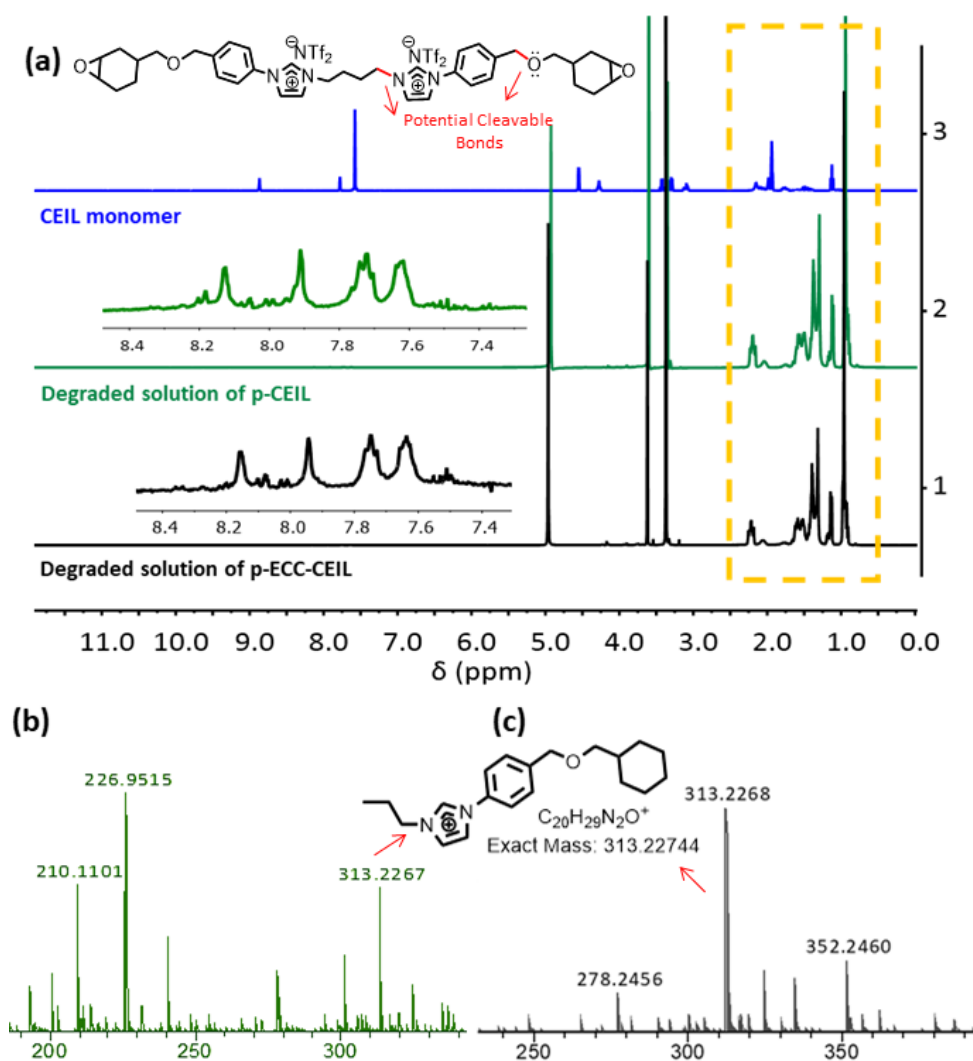
**Figure V-S14.** Snapshots taken from the p-ECC-CEIL system from different angles.



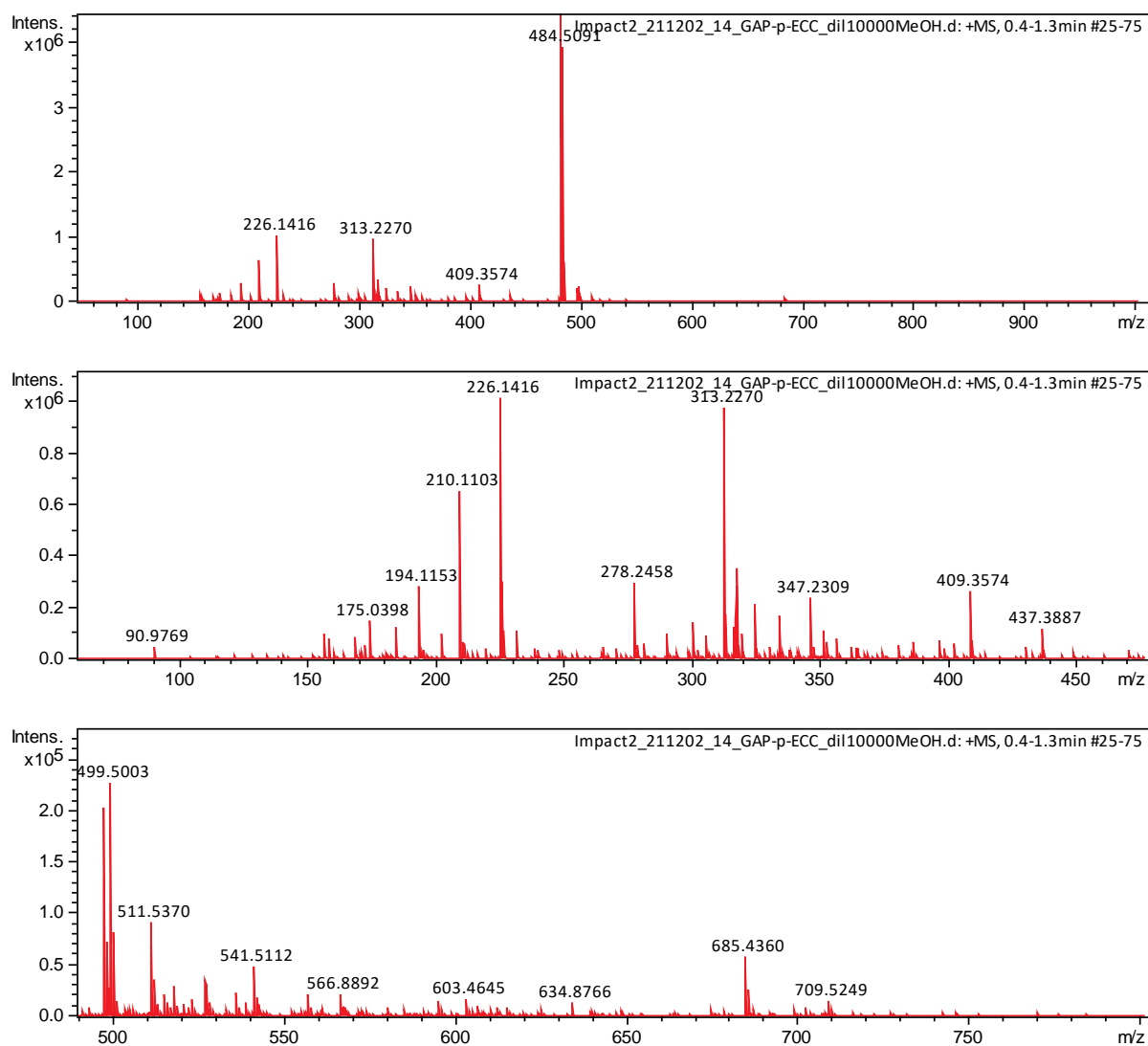
**Figure V-S15.** Stress-strain curves for the three networks prepared by adding 2 wt% of S7MS.



**Figure V-S16.** The CEIL and phosphonium IL104 structures.



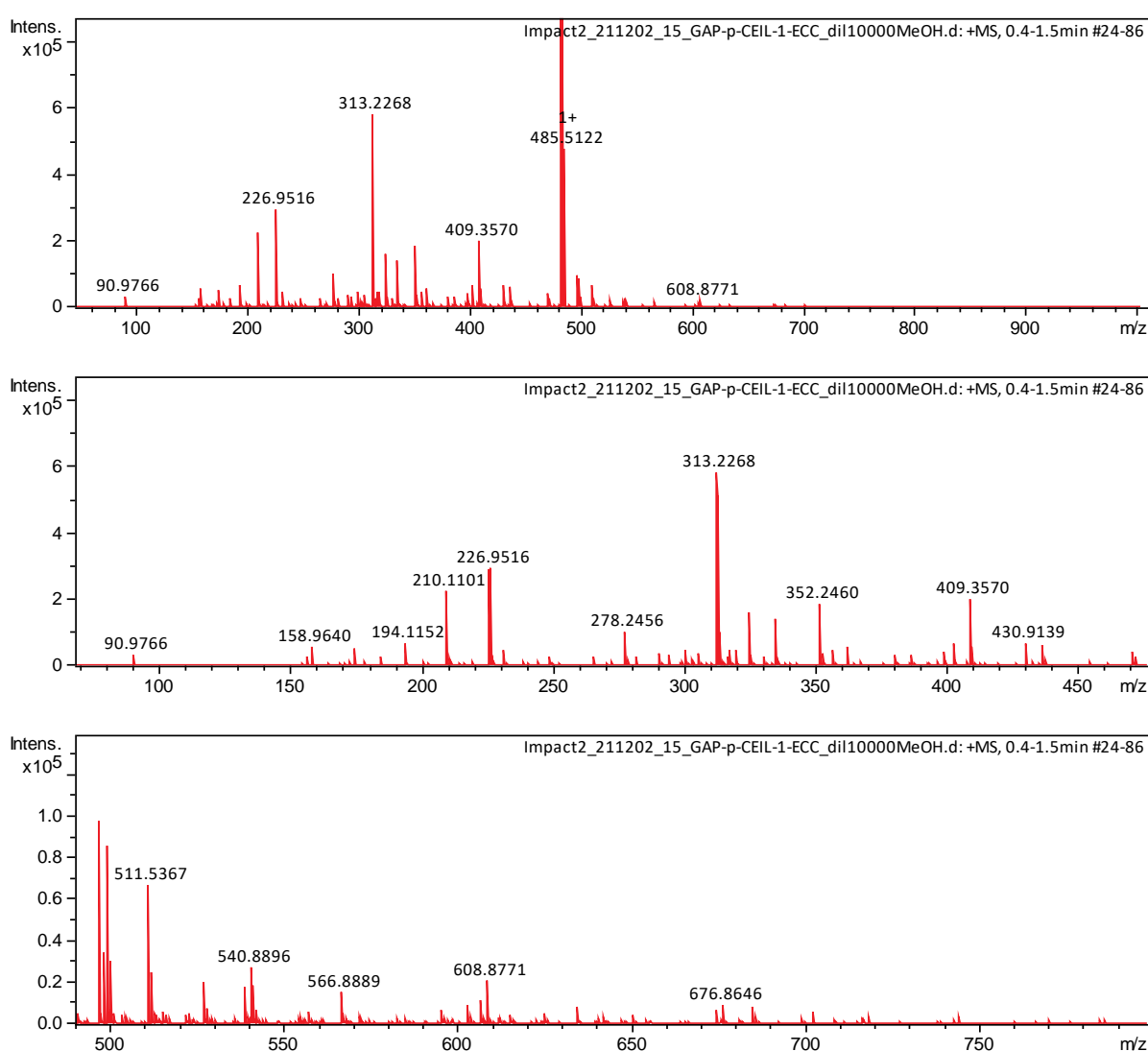
**Figure V-S17.** In **a)** the NMR spectra of CEIL and degraded solutions of p-ECC-CEIL and p-CEIL, and in **b)** the ESI(+)-MS spectra of the degradation products derived from p-CEIL (left) and p-ECC-CEIL (right).



**Figure V-S18.** ESI(+)-QTOF mass spectrum of degradation products of p-ECC.

**Table V-S3.** Molecular ions obtained from ESI(+)-QTOF spectrometry of the degradation products of p-ECC

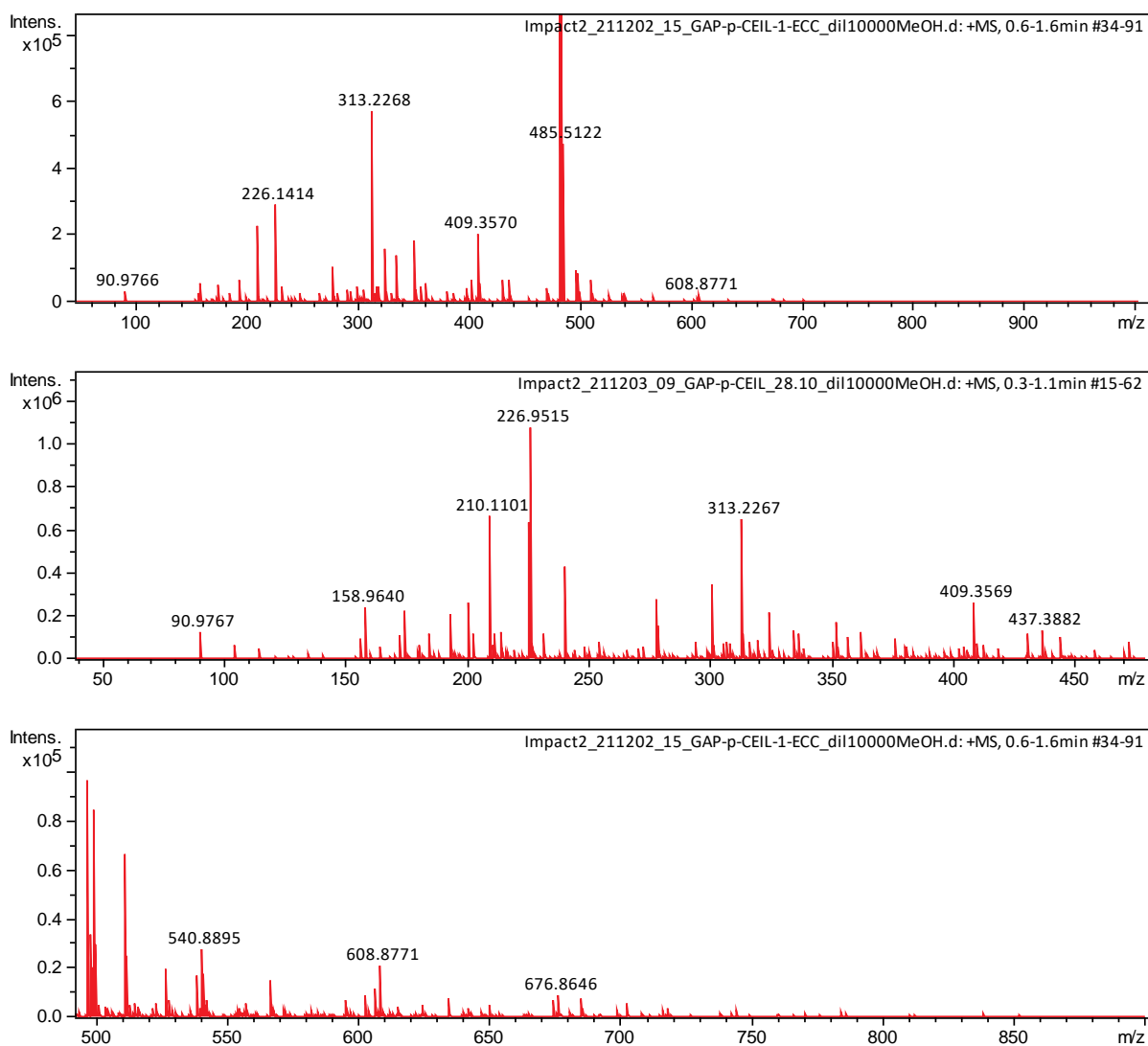
Meas. m/z	Ion Formula	Sum mula	For-	m/z	err [ppm]	mSigma	Ad- duct	z
210.110 3	C <sub>7</sub> H <sub>12</sub> N <sub>7</sub> O	C <sub>7</sub> H <sub>11</sub> N <sub>7</sub> O		210.1098	2.4	4.5	M+H	1+
313.227	C <sub>20</sub> H <sub>29</sub> N <sub>2</sub> O	C <sub>20</sub> H <sub>28</sub> N <sub>2</sub> O		313.2274	1.3	29	M+H	1+
409.357 4	C <sub>28</sub> H <sub>45</sub> N <sub>2</sub>	C <sub>28</sub> H <sub>45</sub> N <sub>2</sub>		409.3577	0.8	34.6	M	1+



**Figure V-S19.** ESI(+)-QTOF mass spectrum of degradation products of p-ECC-CEIL.

**Table V-S4.** Molecular ions obtained from ESI(+)-QTOF spectrometry of the degradation products of p-ECC-CEIL

Meas. m/z	Ion Formula	Sum Formula	m/z	err [ppm]	mSigma	Adduct	z
210.1101	C <sub>7</sub> H <sub>12</sub> N <sub>7</sub> O	C <sub>7</sub> H <sub>11</sub> N <sub>7</sub> O	210.1098	-1.6	4.1	M+H	1+
313.2268	C <sub>20</sub> H <sub>29</sub> N <sub>2</sub> O	C <sub>20</sub> H <sub>28</sub> N <sub>2</sub> O	313.2274	2	29	M+H	1+
409.357	C <sub>28</sub> H <sub>45</sub> N <sub>2</sub>	C <sub>28</sub> H <sub>45</sub> N <sub>2</sub>	409.3577	1.7	35.3	M	1+



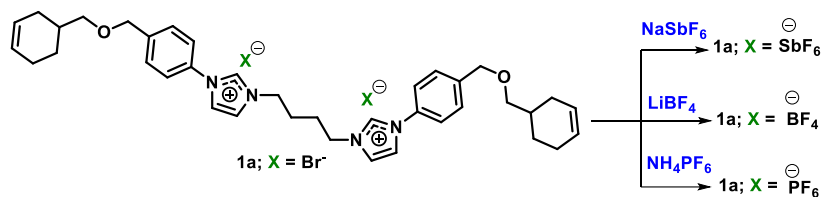
**Figure V-S20.** ESI(+)-QTOF mass spectrum of degradation products of p-CEIL.

**Table V-S5.** Molecular ions obtained from ESI(+)-QTOF spectrometry of the degradation products of p-CEIL

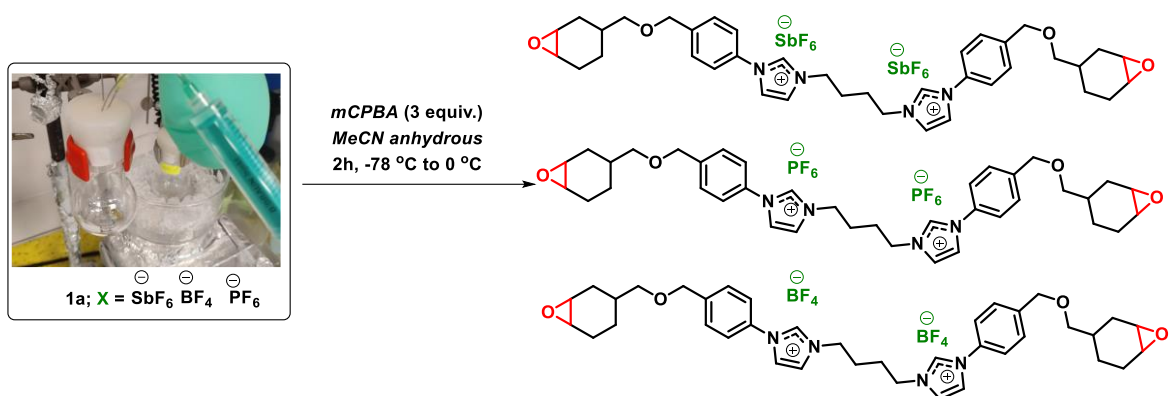
Meas. m/z	Ion Formula	Sum Formula	m/z	err [ppm]	mSigma	Adduct	z
226.1414	C <sub>8</sub> H <sub>16</sub> N <sub>7</sub> O	C <sub>8</sub> H <sub>16</sub> N <sub>7</sub> O	226.1411	-1.6	4.9	M	1+
	C <sub>8</sub> H <sub>16</sub> N <sub>7</sub> O	C <sub>8</sub> H <sub>15</sub> N <sub>7</sub> O	226.1411	-1.6	4.9	M+H	1+
313.2268	C <sub>20</sub> H <sub>29</sub> N <sub>2</sub> O	C <sub>20</sub> H <sub>29</sub> N <sub>2</sub> O	313.2274	2.1	28.8	M	1+
	C <sub>20</sub> H <sub>29</sub> N <sub>2</sub> O	C <sub>20</sub> H <sub>28</sub> N <sub>2</sub> O	313.2274	2.1	28.8	M+H	1+
409.357	C <sub>28</sub> H <sub>45</sub> N <sub>2</sub>	C <sub>28</sub> H <sub>45</sub> N <sub>2</sub>	409.3577	1.8	34.9	M	1+
	C <sub>28</sub> H <sub>45</sub> N <sub>2</sub>	C <sub>28</sub> H <sub>44</sub> N <sub>2</sub>	409.3577	1.8	34.9	M+H	1+
527.4952	C <sub>35</sub> H <sub>63</sub> N <sub>2</sub> O	C <sub>35</sub> H <sub>62</sub> N <sub>2</sub> O	527.4935	-3.3	n.a.	M+H	1+
539.1711	C <sub>33</sub> H <sub>23</sub> N <sub>4</sub> O <sub>4</sub>	C <sub>33</sub> H <sub>22</sub> N <sub>4</sub> O <sub>4</sub>	539.1714	0.5	n.a.	M+H	1+
540.8895	C <sub>2</sub> HN <sub>6</sub> O <sub>27</sub>	C <sub>2</sub> N <sub>6</sub> O <sub>27</sub>	540.8884	-2.1	n.a.	M+H	1+
	C <sub>6</sub> H <sub>5</sub> O <sub>29</sub>	C <sub>6</sub> H <sub>4</sub> O <sub>29</sub>	540.8911	2.9	n.a.	M+H	1+
566.8889	C <sub>4</sub> H <sub>7</sub> O <sub>32</sub>	C <sub>4</sub> H <sub>6</sub> O <sub>32</sub>	566.8915	4.6	n.a.	M+H	1+

## Synthetic Outline

a) Ion-exchange reaction:

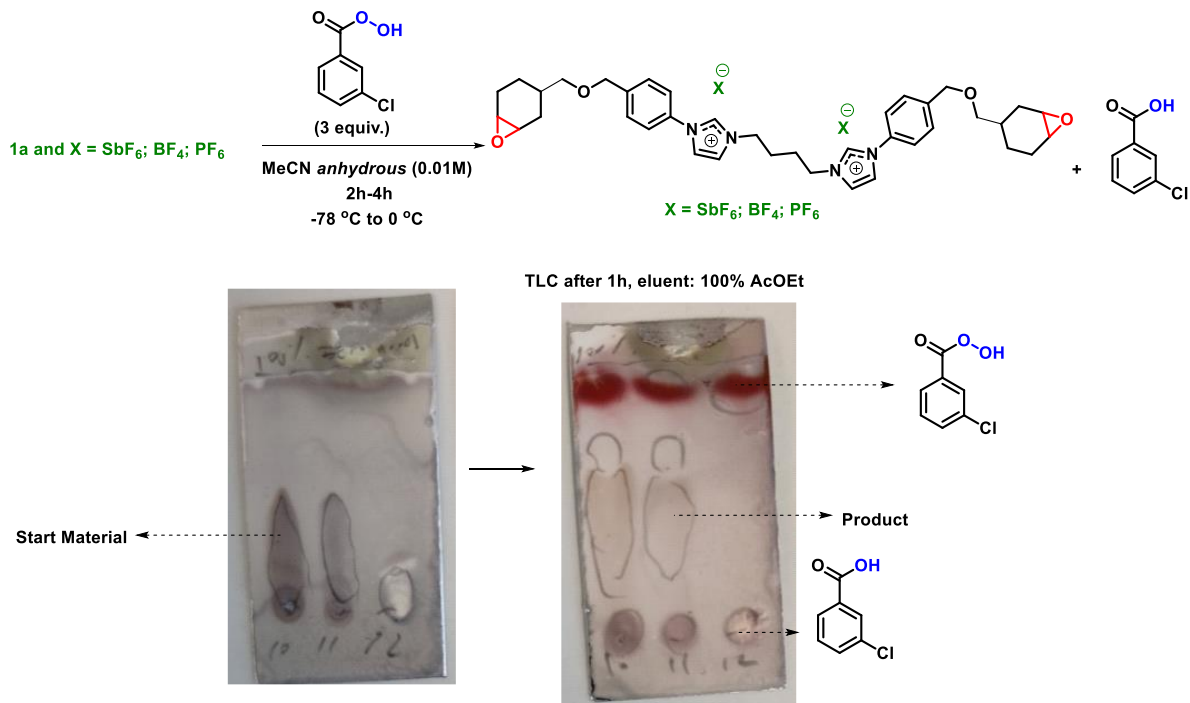


b) Epoxidation reaction



**Scheme V-S1.** Overview of the synthetic route employed.

## Details of Epoxidation Reaction

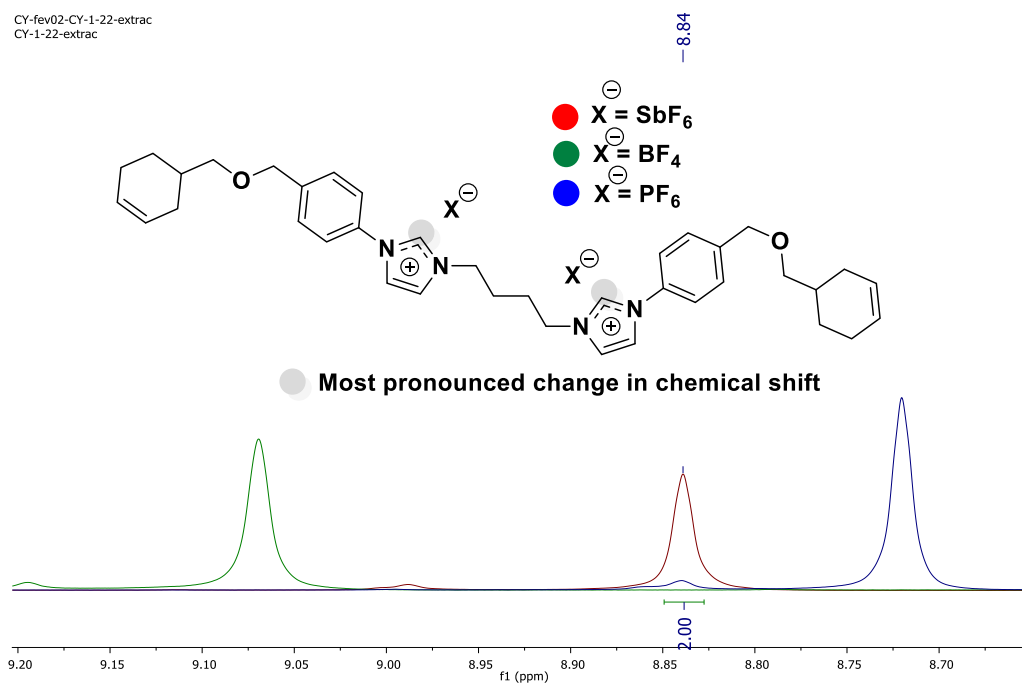


**Scheme V-S2.** TLC and additional details of reactions.

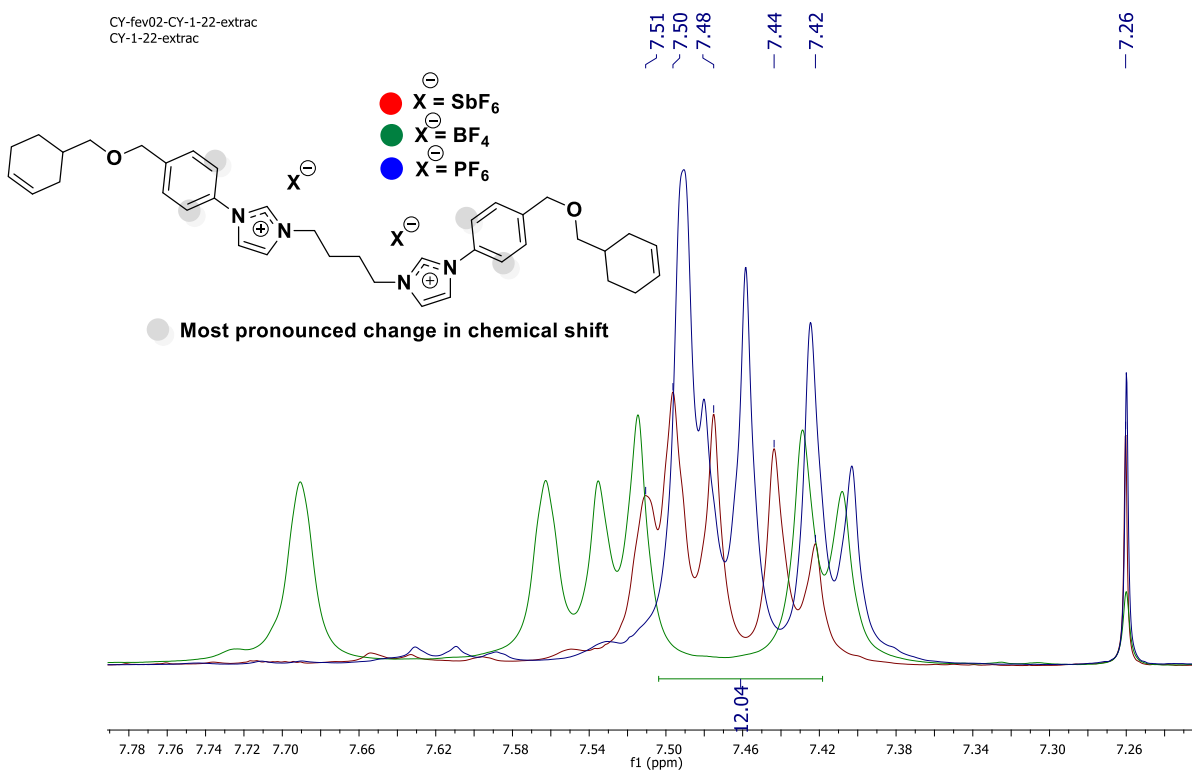


## Comprehensive Investigation by NMR Spectroscopy

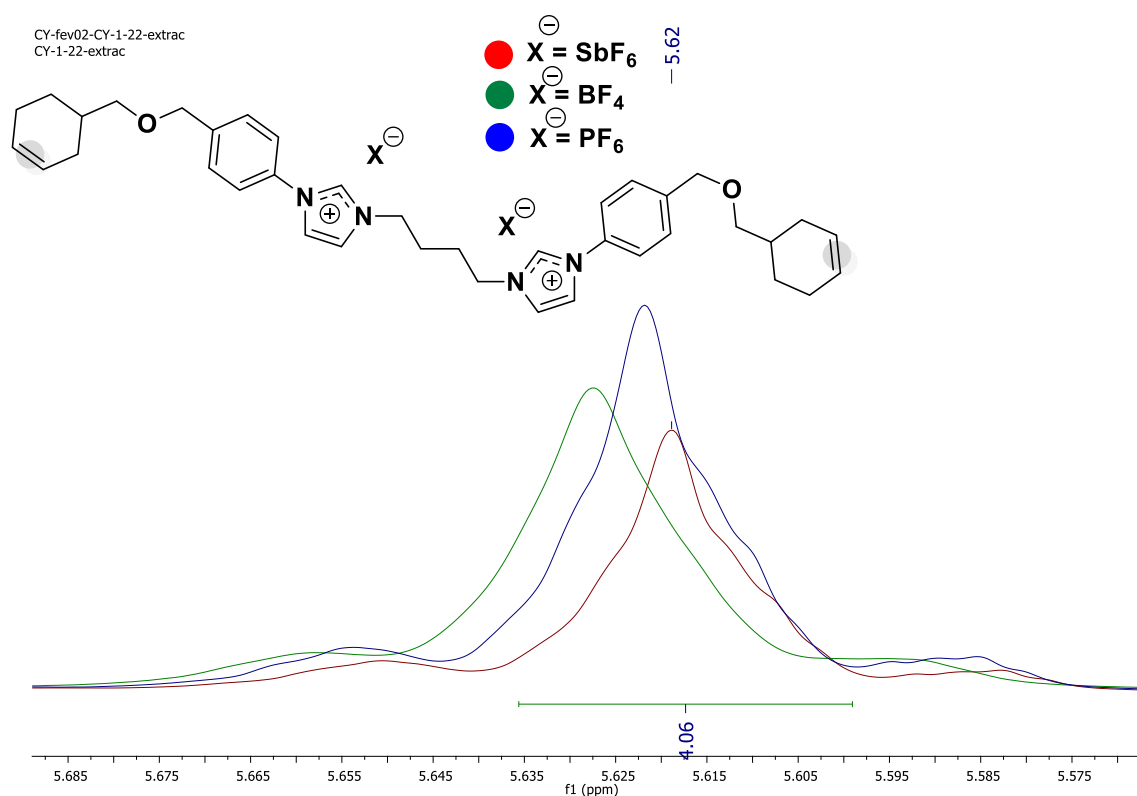
### Comparison of NMR spectra after ion exchange



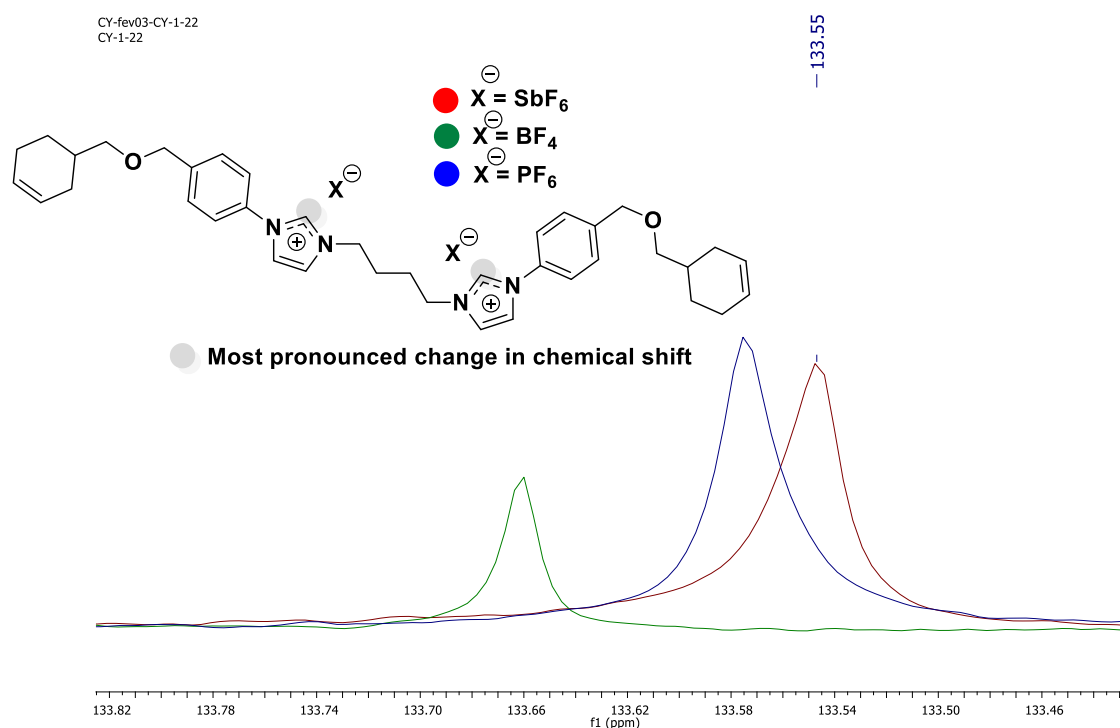
**Figure V-S21.** Overlap in the region between 6-9 ppm of the spectra of hydrogen in chloroform.



**Figure V-S22.** Overlap NMR spectra of ion exchange products.

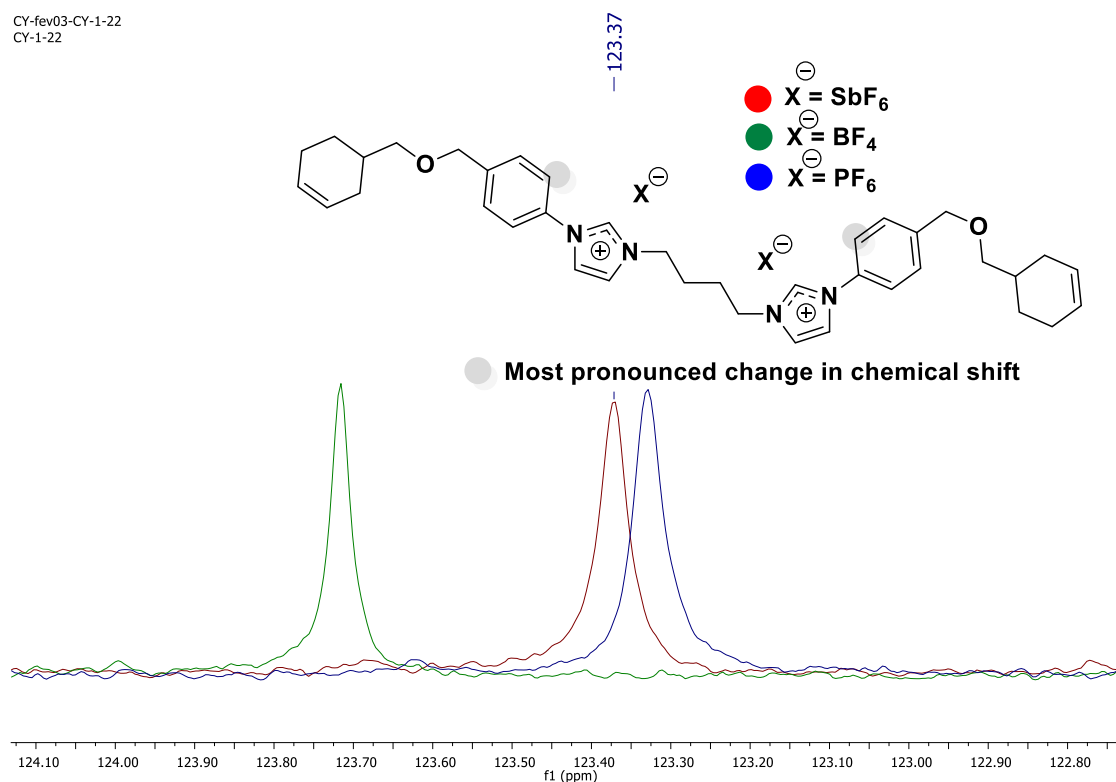


**Figure V-S23.** Overlap NMR spectra of ion exchange products. Focus on the region 5.5-5.9 ppm.



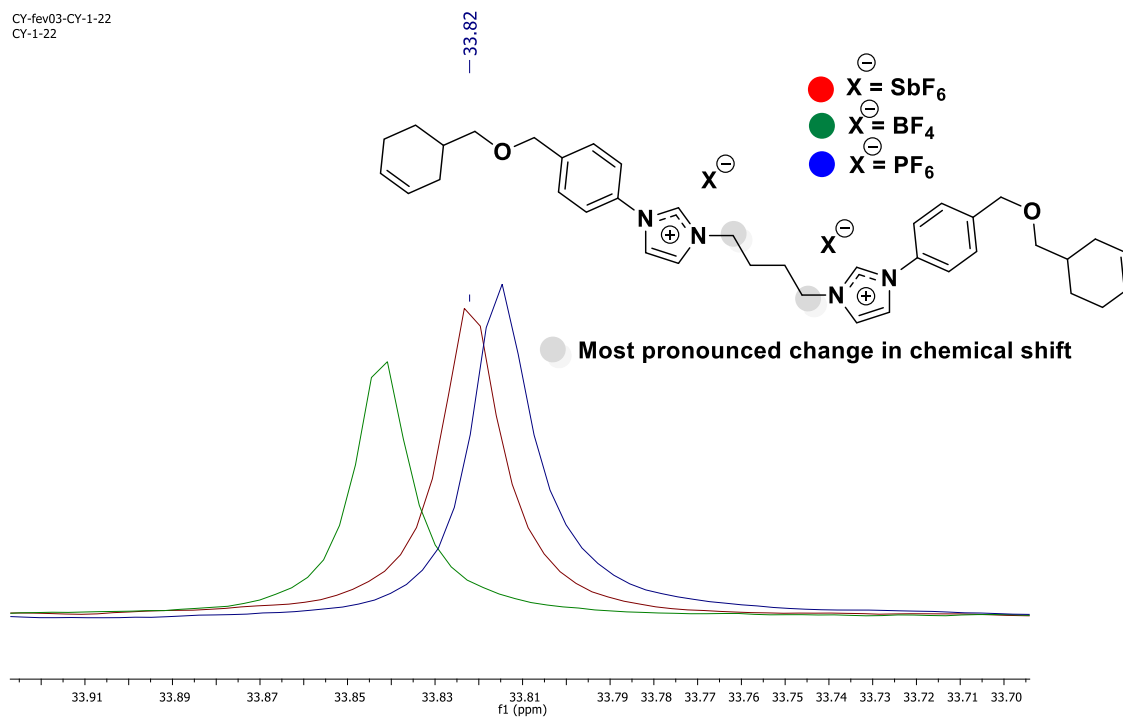
**Figure V-S24.** Overlap of  $^{13}\text{C}$  spectra in chloroform. Region widening between 133-135 ppm.

CY-fev03-CY-1-22  
CY-1-22



**Figure V-S25.** Overlay of  $^{13}\text{C}$  spectra in chloroform. Focus on the region between 122-124 ppm.

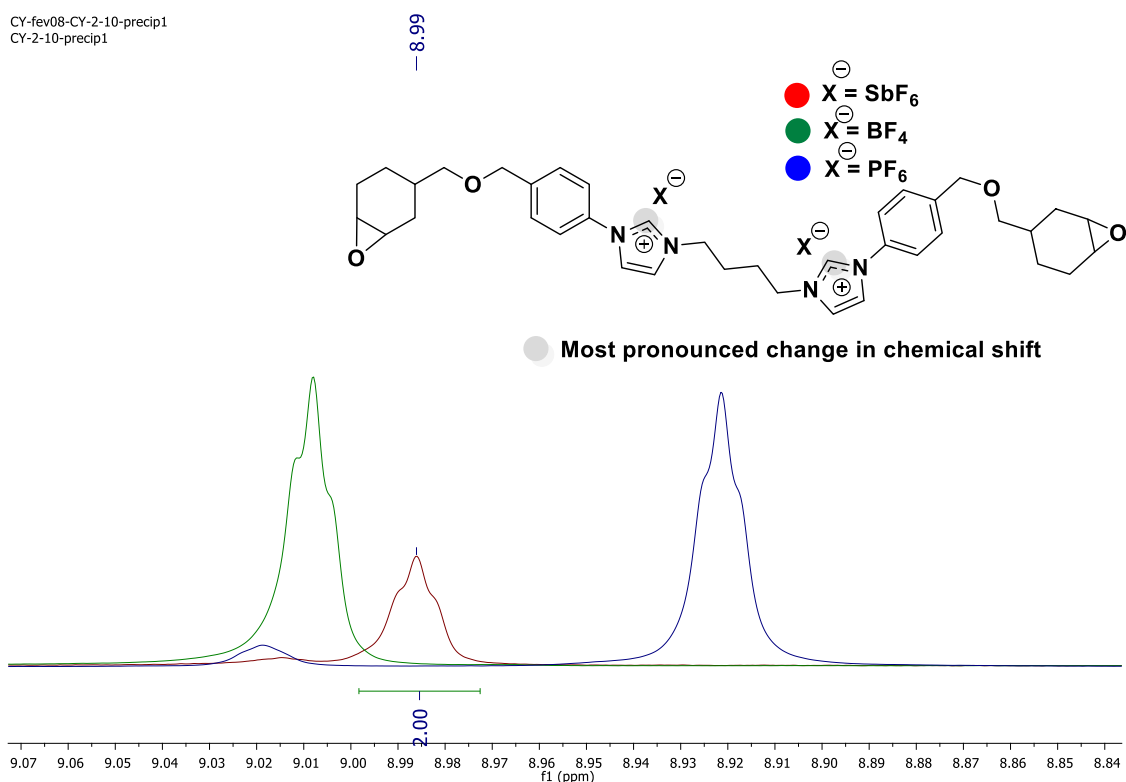
CY-fev03-CY-1-22  
CY-1-22



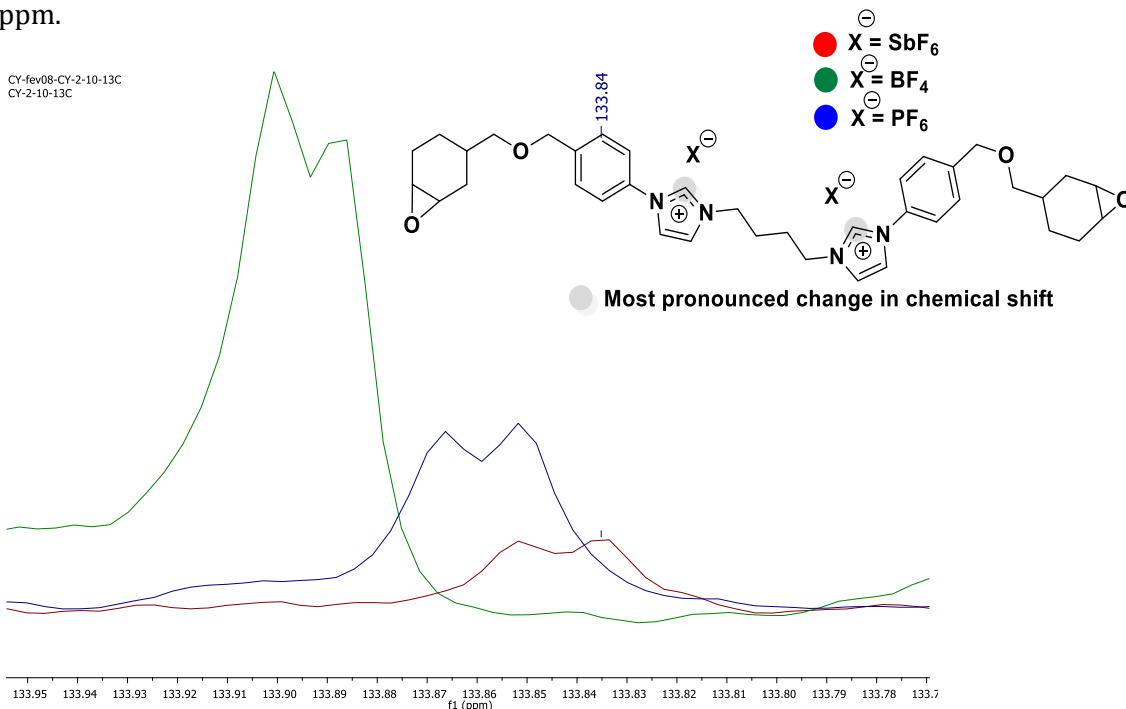
**Figure V-S26.** Overlay of  $^{13}\text{C}$  spectra in chloroform. Focus on the region between 33-35 ppm.

## Comparison of spectra for the epoxidation reaction

CY-fev08-CY-2-10-precip1  
CY-2-10-precip1



**Figure V-S27.** Overlay of  $^1\text{H}$  spectra in chloroform. Focus on the region between 8.84-9.1 ppm.

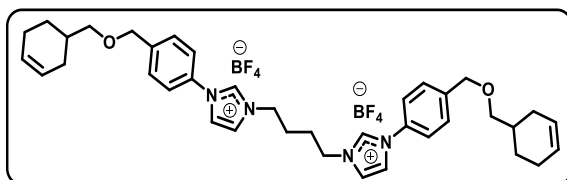


**Figure V-S28.** Overlay of  $^{13}\text{C}$  spectra in chloroform. Focus on the region between 133-135 ppm.

General procedures

Ion-exchange reactions

**3,3'-(butane-1,4-diyl)bis(1-(4-((cyclohex-3-en-1-ylmethoxy)methyl)phenyl)-1H-3l4-imidazol-1-ium) tetrafluoroborate**



In a sealed tube were weighed 3,3'-(butane-1,4-diyl)bis(1-(4-((cyclohex-3-en-1-ylmethoxy)methyl)phenyl)-1H-3l4-imidazol-1-ium) bromide (225.8 mg, 0.3 mmol,

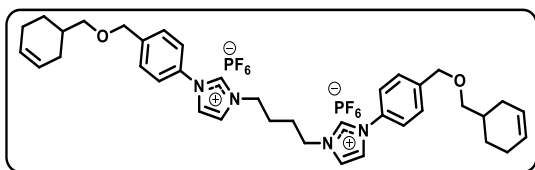
1 equiv.) and lithium tetrafluoroborate (281.2 mg, 3 mmol, 10 equiv.). In sequence, 30 mL of water was added for complete solubilization (**note**: the solubilization is complete at 100 °C). The mixture was stirred at 100 °C during 48 h. The crude product was purified via extraction (**note**: add a little volume of water to avoid loss of the ionic liquid) using water and chloroform to afford the title compound as a slightly yellow oil (156 mg, 68% *yield*).

**TLC:**  $R_f$  = 0.1 (100% EtOAc, *Vanillin stain*).

**$^1\text{H}$  NMR (400 MHz,  $\text{CDCl}_3$ )  $\delta_{\text{H}}$ :** 9.07 (s, 2H), 7.69 (s, 2H), 7.56 - 7.51 (m, 6H), 7.43 – 7.41 (m, 4H), 5.63 (s, 4H), 4.46 (s, 4H), 4.38 (s, 4H), 3.34 (d,  $J$  = 6.4 Hz, 4H), 2.15 – 2.01 (m, 10H), 1.89 – 1.67 (m, 6H), 1.30 – 1.20 (m, 2H) ppm.

**$^{13}\text{C}$  NMR (100 MHz,  $\text{CDCl}_3$ )  $\delta_{\text{C}}$ :** 141.3, 134.1, 133.6, 128.9, 127.0, 125.8, 123.7, 121.9, 121.3, 75.8, 71.7, 49.4, 33.8, 28.4, 26.4, 25.5, 24.5 ppm.

**3,3'-(butane-1,4-diyl)bis(1-(4-((cyclohex-3-en-1-ylmethoxy)methyl)phenyl)-1H-3l4-imidazol-1-ium) hexafluorophosphate(V)**



In a sealed tube were weighed 3,3'-(butane-1,4-diyl)bis(1-(4-((cyclohex-3-en-1-ylmethoxy)methyl)phenyl)-1H-3l4-imidazol-1-ium) bromide (225.8 mg, 0.3 mmol, 1 equiv.)

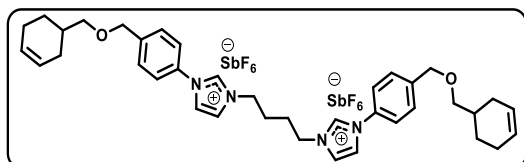
and Ammonium hexafluorophosphate (489 mg, 3 mmol, 10 equiv.). In sequence, 30 mL of water was added for complete solubilization (**note:** the solubilization is complete at 100 °C). The mixture was stirred at 100 °C for 48 h. The crude product was purified via extraction (**note:** add a little quantity of water to avoid loss of the ionic liquid) using water and chloroform to afford the title compound as a title compound as a slightly yellow oil (158 mg, 60% yield).

**TLC:**  $R_f$  = 0.1 (100% EtOAc, Vanillin stain).

**$^1\text{H}$  NMR (400 MHz,  $\text{CDCl}_3$ )**  $\delta_{\text{H}}$ : 8.72 (s, 2H), 7.49 – 7.40 (m, 12H), 5.62 (s, 4H), 4.45 (s, 4H), 4.28 (s, 4H), 3.35 (d,  $J$  = 6.4 Hz, 4H), 2.09 – 2.01 (m, 11H), 1.91 – 1.84 (m, 2H), 1.78 – 1.66 (m, 3H) ppm.

**$^{13}\text{C}$  NMR (100 MHz,  $\text{CDCl}_3$ )**  $\delta_{\text{C}}$ : 141.4, 133.6, 128.8, 127.0, 125.8, 123.3, 122.1, 121.5, 75.8, 71.6, 49.5, 33.8, 28.4, 26.3, 25.5, 24.5 ppm.

**3,3'-(butane-1,4-diyl)bis(1-(4-((cyclohex-3-en-1-ylmethoxy)methyl)phenyl)-1H-3l4-imidazol-1-ium) hexafluorostibate(V)**



In a sealed tube were weighed 3,3'-(butane-1,4-diyl)bis(1-(4-((cyclohex-3-en-1-ylmethoxy)methyl)phenyl)-1H-3l4-imidazol-1-ium) bromide (225.8 mg, 0.3 mmol, 1 equiv.)

and sodium hexafluorostibate(V) (465.7 mg, 1.8 mmol, 6 equiv.). In sequence, 30 mL of water was added for complete solubilization (**note:** the solubilization is complete at 100 °C). The mixture was stirred at 100 °C for 48 h. The crude product was purified via extraction (**note:** add a little quantity of water to avoid loss of the ionic liquid) using water and chloroform to afford the title compound as a title compound as a slightly yellow oil (185 mg, 58% yield).

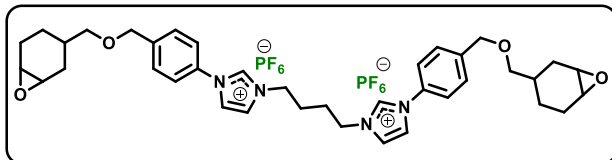
**TLC:**  $R_f$  = 0.1 (100% EtOAc, Vanillin stain).

**$^1\text{H}$  NMR (400 MHz,  $\text{CDCl}_3$ )**  $\delta_{\text{H}}$ : 8.84 (s, 2H), 7.51 – 7.42 (m, 12H), 5.62 (s, 4H), 4.47 (s, 4H), 4.31 (s, 4H), 3.35 (d,  $J$  = 6.4 Hz, 4H), 2.04 – 2.01 (m, 11H), 1.91 – 1.84 – 1.67 (m, 7H) ppm.

**<sup>13</sup>C NMR (100 MHz, CDCl<sub>3</sub>) δ<sub>C</sub>:** 141.6, 133.5, 128.9, 127.0, 125.8, 123.4, 122.2, 121.7, 75.8, 71.6, 49.7, 33.8, 29.6, 28.44, 26.6, 25.5, 24.5 ppm.

### Epoxidation reaction

**1-(4-(((7-oxabicyclo[4.1.0]heptan-3-yl)methoxy)methyl)phenyl)-3-(4-(3-(4-(((7-oxabicyclo[4.1.0]heptan-3-yl)methoxy)methyl)phenyl)-1H-3l4-imidazol-1-ium-1-yl)butyl)-1H-3l4-imidazol-1-ium PF<sub>6</sub>**



Adapted from a procedure by Radchenko and co-workers.<sup>3</sup> Under anhydrous conditions were placed 3,3'-(butane-1,4-diyl)bis(1-(4-((cyclohex-3-en-

1-ylmethoxy)methyl)phenyl)-1H-3l4-imidazol-1-ium) hexafluorophosphate(V) (88.3 mg; 0.1 mmol; 1 equiv.), and MeCN anhydrous (5 mL; 0.01 M). Then, a solution of *m*CPBA (52 mg; 0.3 mmol; 3 equiv.) in 5 mL of MeCN was added drop wise by syringe under Ar. The mixture was stirred at -78 °C for 3 h. The crude product was precipitated in diethyl ether, washed with AcOEt, hexane, acetone, toluene, chloroform, and DCM to afford the title compound as a colorless oil (46 mg, 51 % yield).

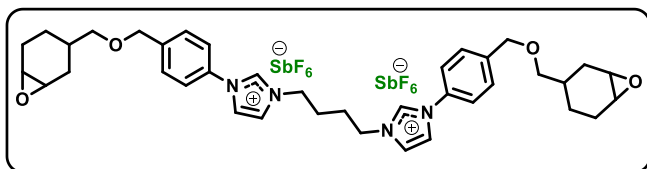
**TLC:** *R<sub>f</sub>* = 0.3 (100% EtOAc, *Vanillin stain*).

**<sup>1</sup>H NMR (400 MHz CD<sub>3</sub>CN) δ<sub>H</sub>:** 8.91 (s, 2H), 7.81 (t, *J* = 1.74 Hz, 2H), 7.63 – 7.61 (m, 10H), 4.58 (d, *J* = 3.5 Hz, 4H), 4.34 (s, 4H), 4.09 (q, *J* = 6.4 Hz, 2H), 3.46 (q, *J* = 6.4 Hz, 2H), 3.36 (t, *J* = 6.4 Hz, 2H), 3.31 (d, *J* = 6.3 Hz, 2H), 3.15 – 3.10 (m, 4H), 2.11 – 1.97 (m, 5H), 1.80 – 1.75 (m, 2H), 1.55 – 1.44 (m, 2H), 1.15 – 1.0 (m, 3H) ppm.

**<sup>13</sup>C NMR (100 MHz, CD<sub>3</sub>CN) δ<sub>C</sub>:** 141.76, 141.73, 134.5, 129.0, 128.9, 123.2, 122.4, 122.3, 121.9, 117.4, 75.3, 75.0, 71.4, 52.2, 52.1, 51.3, 49.3, 32.9, 30.3, 28.1, 27.2, 26.1, 24.5, 23.7, 22.9, 21.2 ppm.

<sup>3</sup> Adapted reaction, see original methodology: **a)** Radchenko, A. V.; Duchet-Rumeau, J.; Gérard, J.; Baudoux, J.; Livi, S. *Polym. Chem.* **2020**, *11*, 5475 – 5485. [\[link\]](#)

**1-(4-(((7-oxabicyclo[4.1.0]heptan-3-yl)methoxy)methyl)phenyl)-3-(4-(3-(4-(((7-oxabicyclo[4.1.0]heptan-3-yl)methoxy)methyl)phenyl)-1H-3l4-imidazol-1-ium-1-yl)butyl)-1H-3l4-imidazol-1-ium SbF<sub>6</sub>**



Adapted from a procedure by Radchenko and co-workers.<sup>4</sup> Under anhydrous conditions were placed 3,3'-(butane-1,4-diyl)bis(1-(4-(cy-

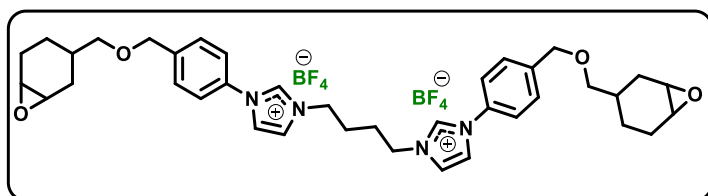
clohex-3-en-1-ylmethoxy)methyl)phenyl)-1H-3l4-imidazol-1-ium) hexafluorostibate(V) (106.4 mg; 0.1 mmol; 1 equiv.), and MeCN anhydrous (5 mL; 0.01 M). Then, a solution of *m*CPBA (52 mg; 0.3 mmol; 3 equiv.) in 5 mL of MeCN was added drop wise by syringe under Ar. The mixture was stirred at -78 °C for 3 h. The crude product was precipitated in diethyl ether, washed with AcOEt, hexane, acetone, toluene, chloroform, and DCM to afford the title compound as a colorless oil (52 mg, 48 % *yield*).

**TLC:**  $R_f = 0.3$  (100% EtOAc, *Vanillin stain*).

**<sup>1</sup>H NMR (400 MHz CD<sub>3</sub>CN) δ<sub>H</sub>:** 8.99 (s, 2H), 7.80 (t, *J* = 1.87 Hz, 2H), 7.62 – 7.60 (m, 10H), 4.58 (d, *J* = 3.5 Hz, 4H), 4.32 (t, *J* = 6.2 Hz, 4H), 3.46 (q, *J* = 7 Hz, 1H), 3.36 (t, *J* = 6 Hz, 1H), 3.31 (d, *J* = 6.3 Hz, 2H), 3.15 – 3.10 (m, 4H), 2.12 – 1.96 (m, 11H), 1.80 – 1.74 (m, 3H), 1.55 – 1.44 (m, 2H), 1.15 – 1.0 (m, 2H) ppm.

**<sup>13</sup>C NMR (100 MHz, CD<sub>3</sub>CN) δ<sub>c</sub>:** 141.82, 141.78, 134.7, 133.8, 129.0, 128.9, 123.2, 122.4, 122.4, 121.9, 117.3, 75.3, 75.0, 71.4, 52.1, 52.0, 51.3, 51.0, 49.2, 32.9, 30.3, 28.2, 27.2, 26.1, 24.5, 23.7, 22.9, 21.2 ppm.

**1-(4-(((7-oxabicyclo[4.1.0]heptan-3-yl)methoxy)methyl)phenyl)-3-(4-(3-(4-(((7-oxabicyclo[4.1.0]heptan-3-yl)methoxy)methyl)phenyl)-1H-3l4-imidazol-1-ium-1-yl)butyl)-1H-3l4-imidazol-1-ium BF<sub>4</sub>**



Adapted from a procedure by Radchenko and co-workers.<sup>5</sup> Under anhydrous conditions were placed 1-(4-((cyclohex-2-en-1-ylmethoxy)methyl)phe-

nyl)-3-(4-(3-(4-((cyclohex-2-en-1-ylmethoxy)methyl)phenyl)-1H-imidazol-3-ium-1-yl)bu-



tyl)-1H-imidazol-3-ium tetrafluoroborate (76.6 mg; 0.1 mmol; 1 equiv.), and MeCN anhydrous (5 mL; 0.01 M). Then, a solution of *m*CPBA (52 mg; 0.3 mmol; 3 equiv.) in 5 mL of MeCN was added drop wise by syringe under Ar. The mixture was stirred at -78 °C for 3 h. The crude product was precipitated in diethyl ether, washed with AcOEt, hexane, acetone, toluene, chloroform, and DCM to afford the title compound as a colorless oil (31.2 mg, 39 % *yield*).

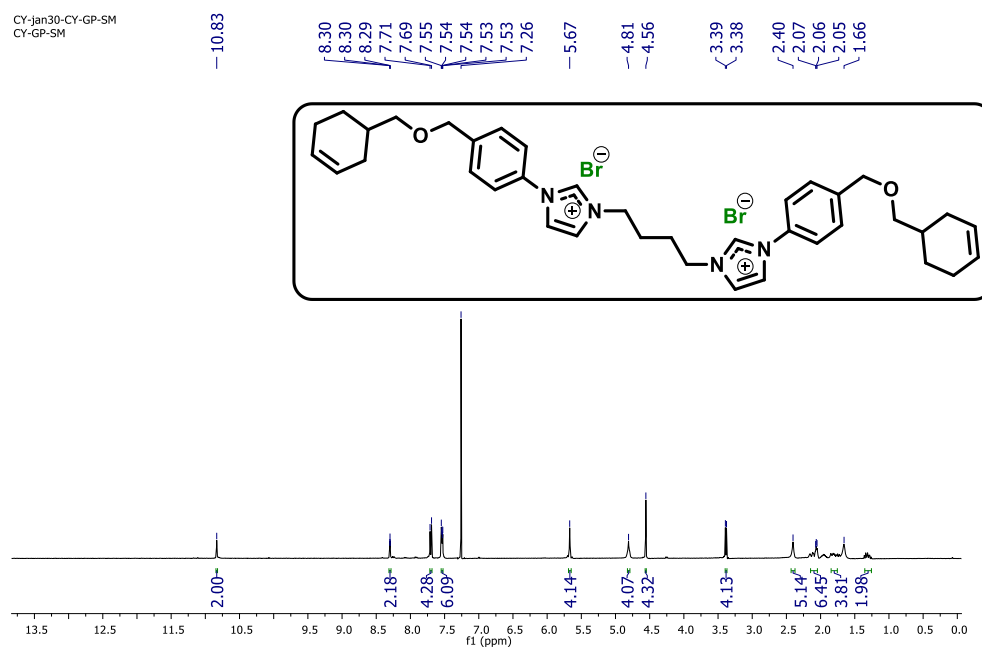
**TLC:**  $R_f$  = 0.3 (100% EtOAc, *Vanillin stain*).

**$^1\text{H}$  NMR (400 MHz,  $\text{CD}_3\text{CN}$ )  $\delta_{\text{H}}$ :** 9.01 (s, 2H), 7.81 (t,  $J$  = 1.74 Hz, 2H), 7.67 – 7.51 (m, 10H), 4.56 (d,  $J$  = 3.5 Hz, 4H), 4.36 (s, 4H), 4.09 (q,  $J$  = 6.4 Hz, 2H), 3.36 (q,  $J$  = 6.4 Hz, 2H), 3.30 (d,  $J$  = 6.3 Hz, 2H), 3.15 – 3.10 (m, 4H), 2.11 – 1.97 (m, 7H), 1.80 – 1.75 (m, 3H), 1.55 – 1.44 (m, 4H), 1.15 – 1.0 (m, 2H) ppm.

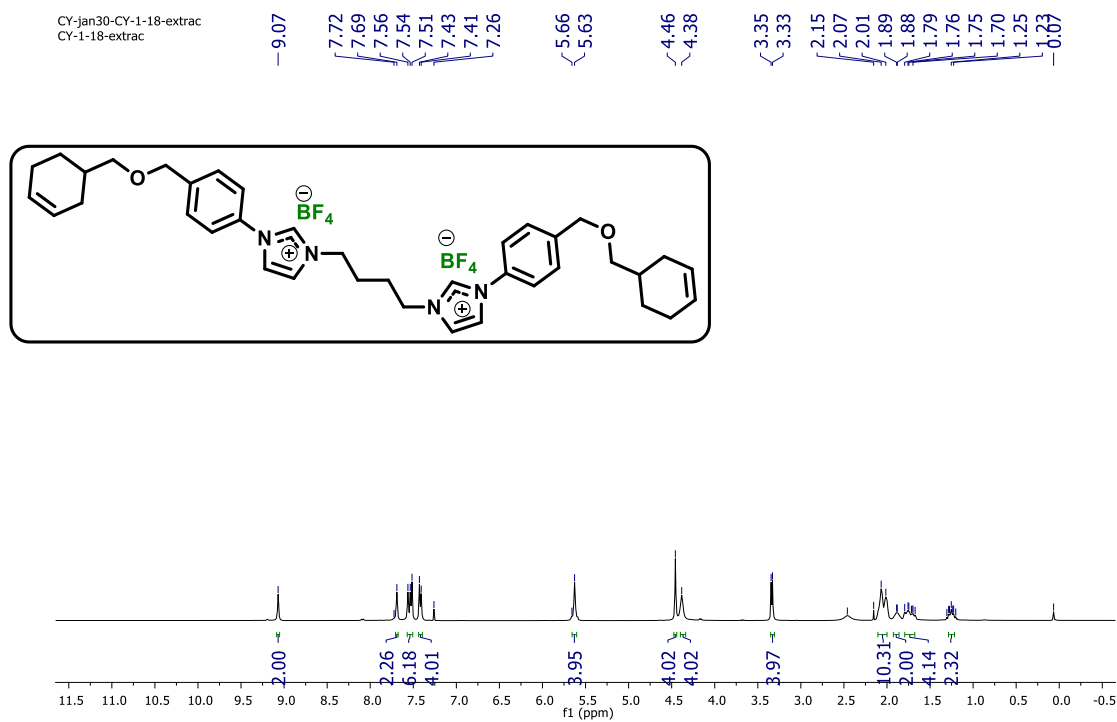
**$^{13}\text{C}$  NMR (100 MHz,  $\text{CD}_3\text{CN}$ )  $\delta_{\text{C}}$ :** 141.67, 141.63, 134.7, 133.9, 129.0, 128.02, 123.2, 122.29, 122.3, 121.8, 117.4, 75.3, 75.0, 71.4, 52.2, 52.0, 51.3, 50.9, 49.2, 32.9, 30.3, 28.1, 27.2, 26.1, 24.5, 23.7, 22.9, 21.2 ppm.

# $^1\text{H}$ , $^{13}\text{C}$ NMR Spectra of Compounds

## $^1\text{H}$ NMR (400 MHz, $\text{CDCl}_3$ )



## $^1\text{H}$ NMR (400 MHz, $\text{CDCl}_3$ )



## <sup>13</sup>C NMR (100 MHz, CDCl<sub>3</sub>)

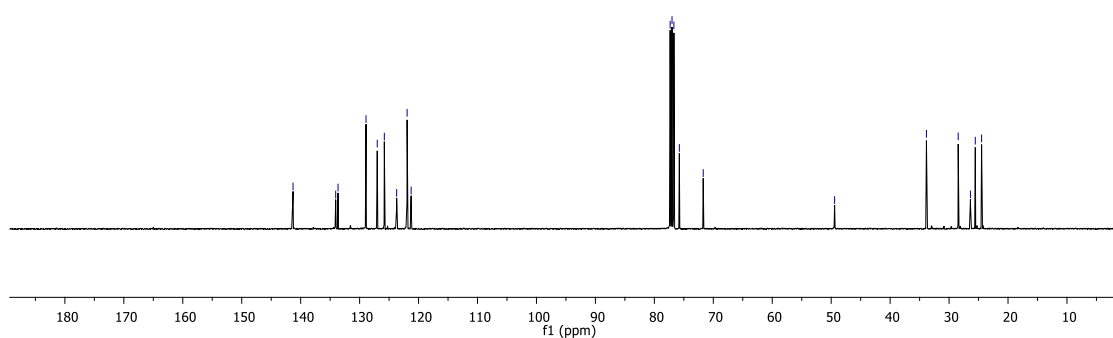
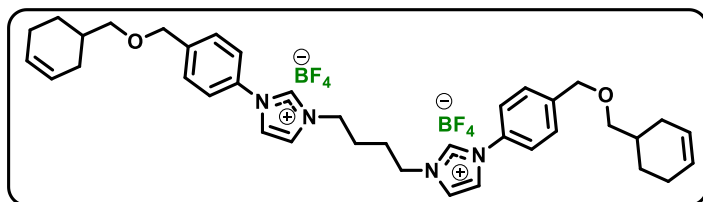
CY-fev01-CY-1-18  
CY-1-18

141.29  
134.06  
133.66  
128.91  
127.01  
125.81  
123.72  
121.94  
121.26

77.32  
77.00  
76.68  
75.76  
71.71

— 49.42

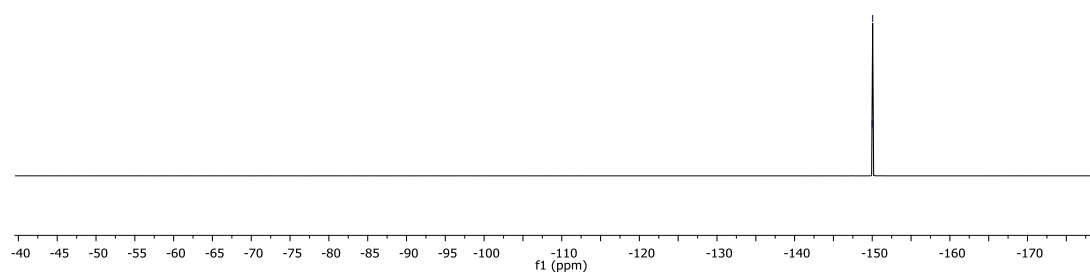
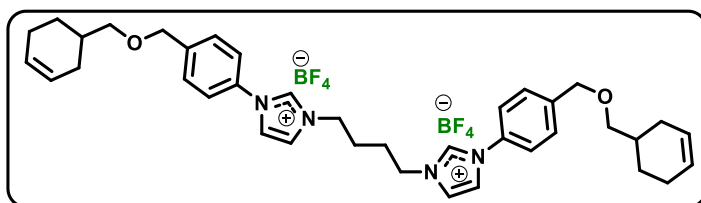
33.84  
28.45  
26.38  
25.55  
24.48



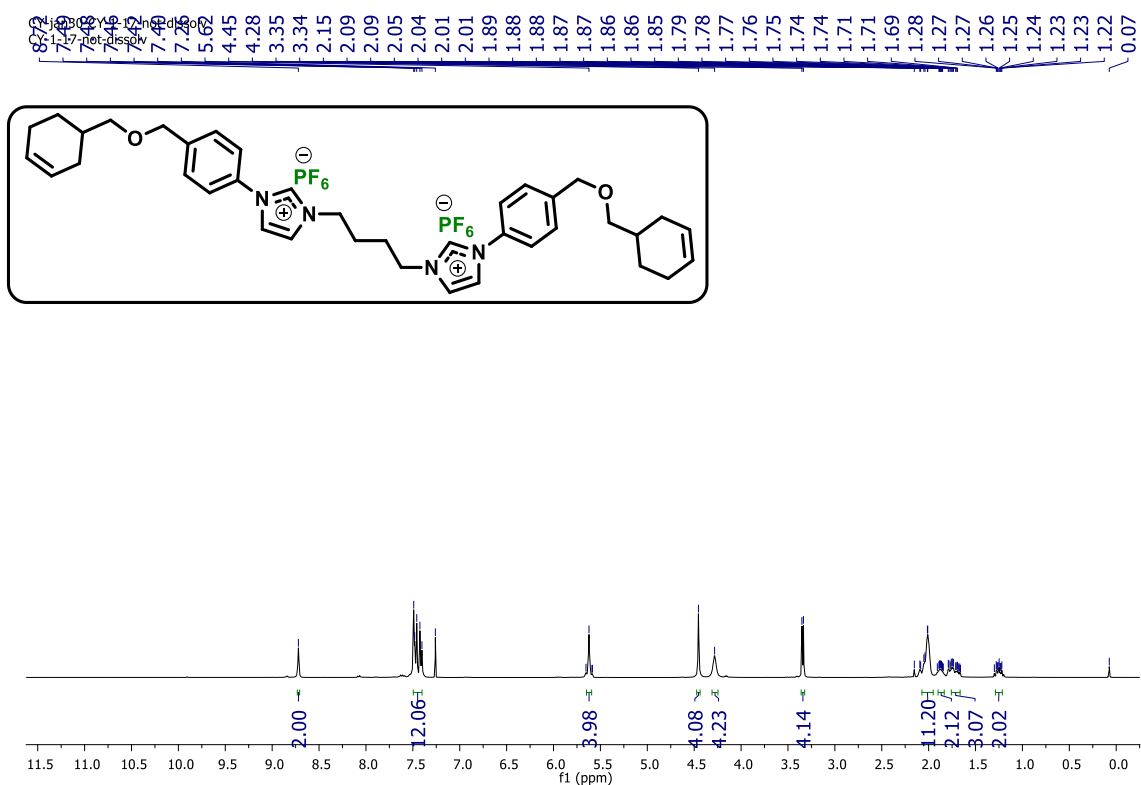
## <sup>19</sup>F NMR (376 MHz, CDCl<sub>3</sub>)

CY-jan31-CY-1-18-extrac  
CY-1-18-extrac

-150.00  
-150.05

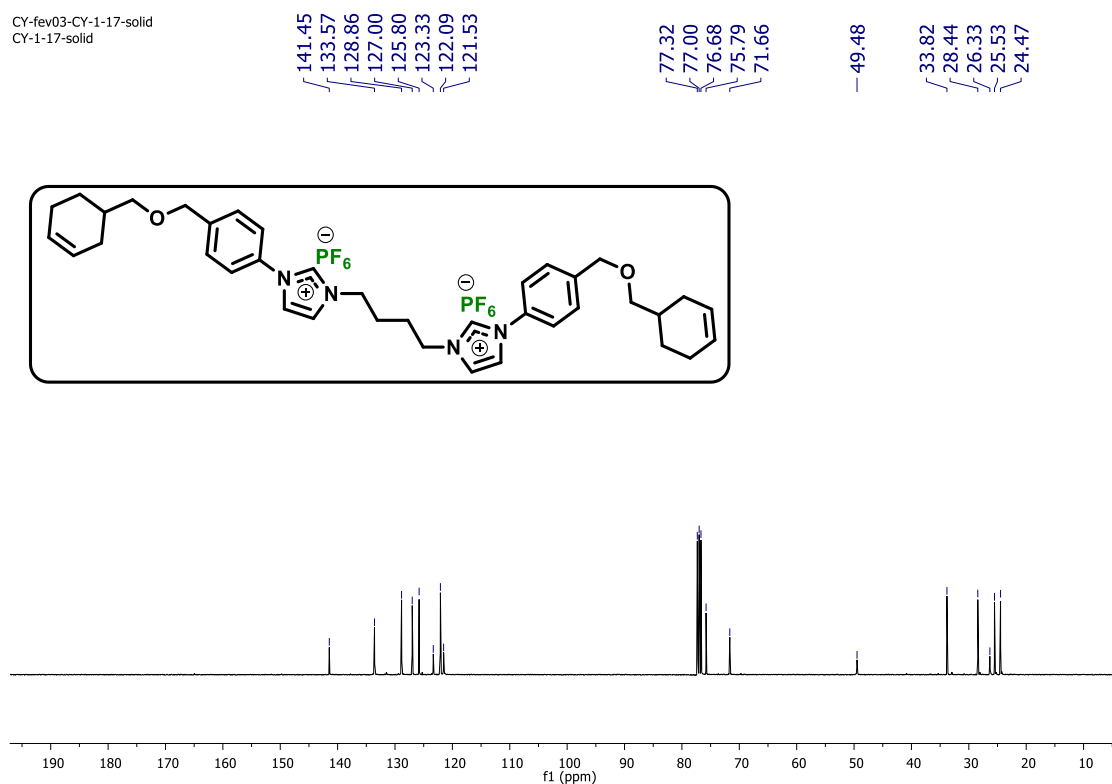


**<sup>1</sup>H NMR (400 MHz, CDCl<sub>3</sub>)**



**<sup>13</sup>C NMR (100 MHz, CDCl<sub>3</sub>)**

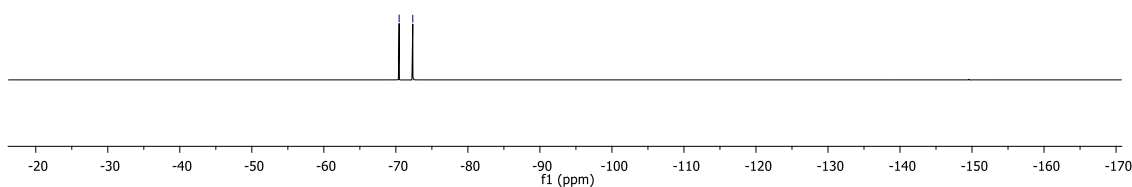
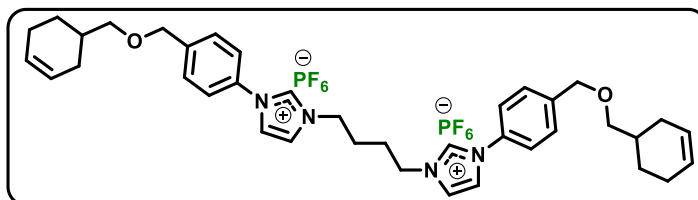
CY-fev03-CY-1-17-solid  
CY-1-17-solid



# **$^{19}\text{F}$ NMR (376 MHz, $\text{CDCl}_3$ )**

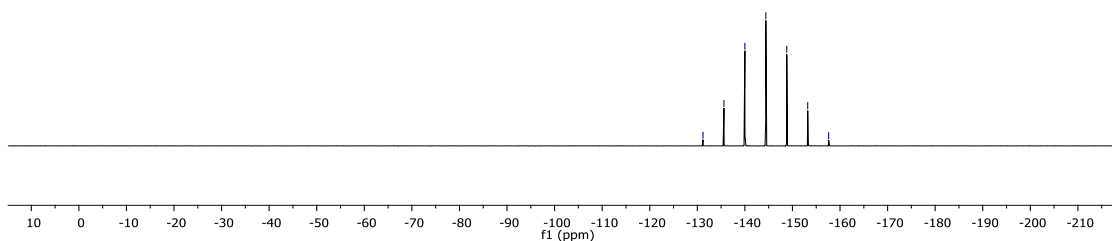
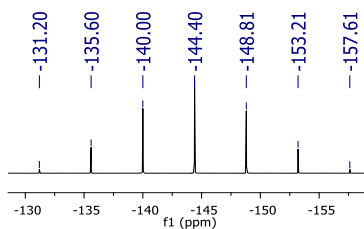
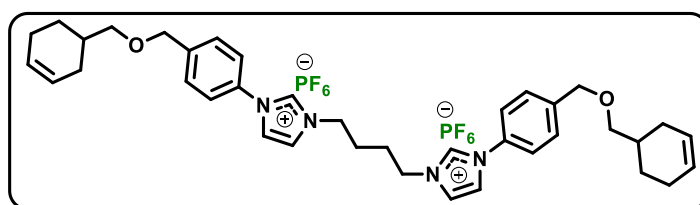
CY-jan31-CY-1-17-solid  
CY-1-17-solid

~ -70.46  
~ -72.35



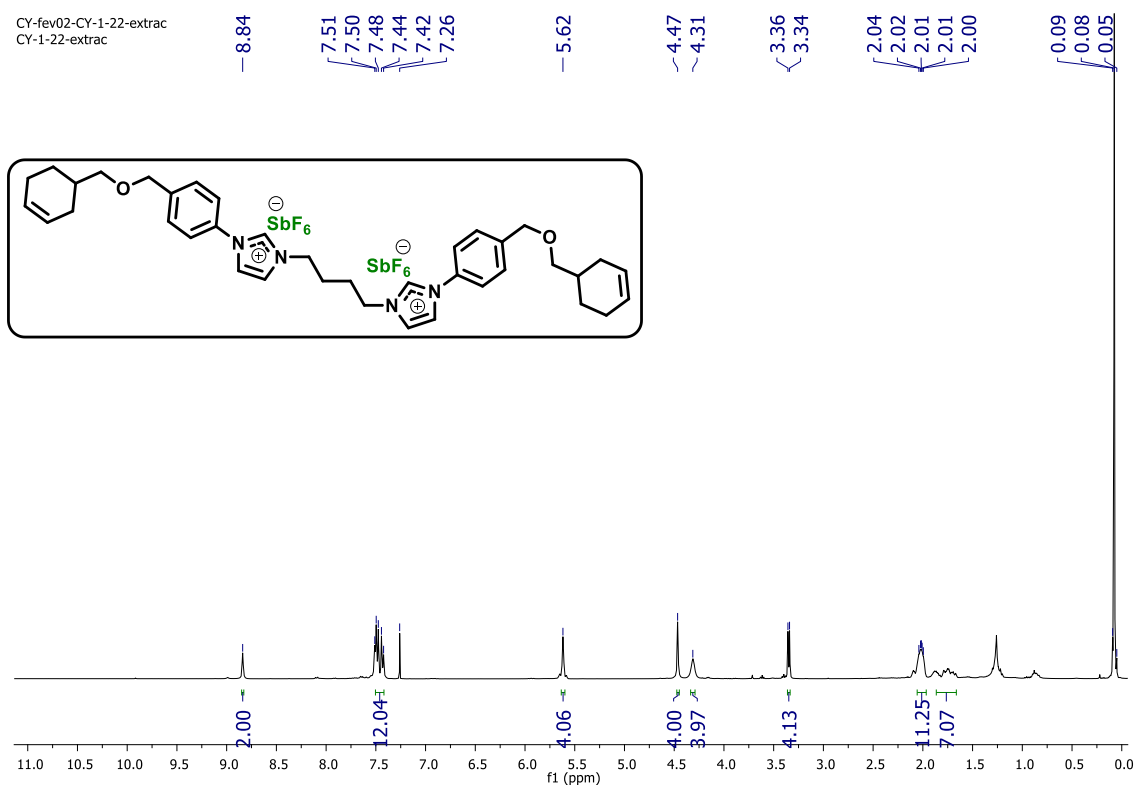
# **$^{31}\text{P}$ NMR (129.6 MHz, $\text{CDCl}_3$ )**

~ -131.20  
~ -135.60  
~ -140.00  
~ -144.40  
~ -148.81  
~ -153.21  
~ -157.61



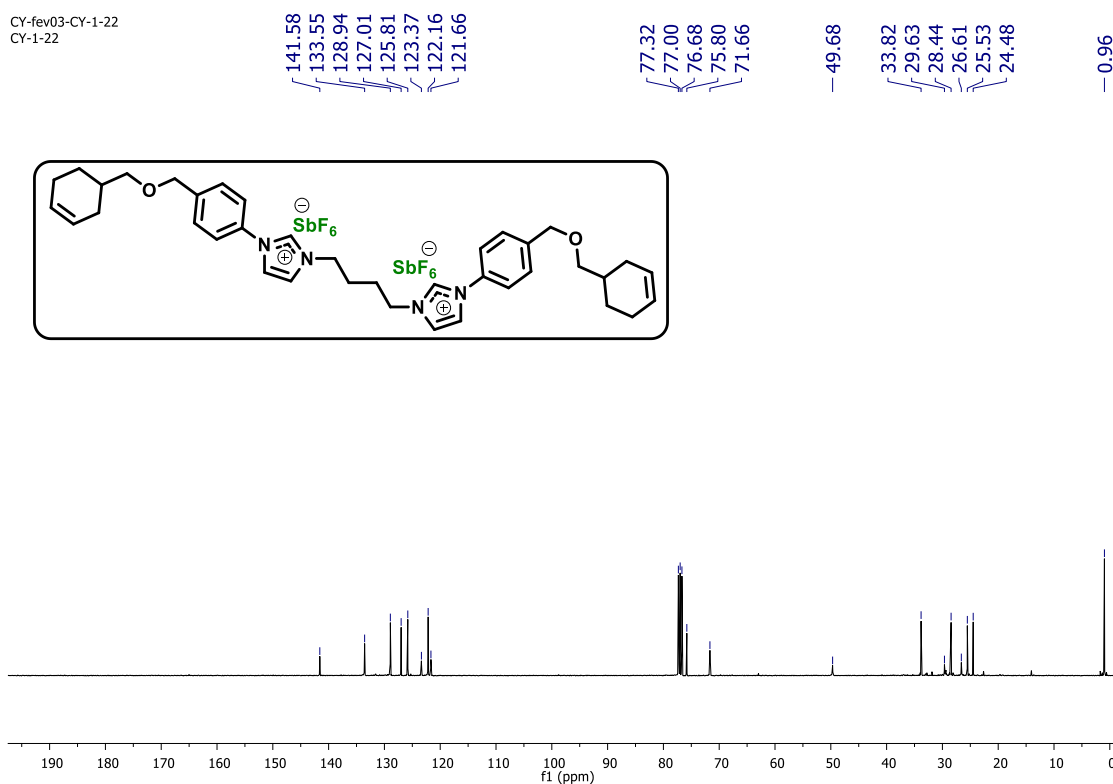
# **<sup>1</sup>H NMR (400 MHz, CDCl<sub>3</sub>)**

CY-fev02-CY-1-22-extrac  
CY-1-22-extrac



# **<sup>13</sup>C NMR (100 MHz, CDCl<sub>3</sub>)**

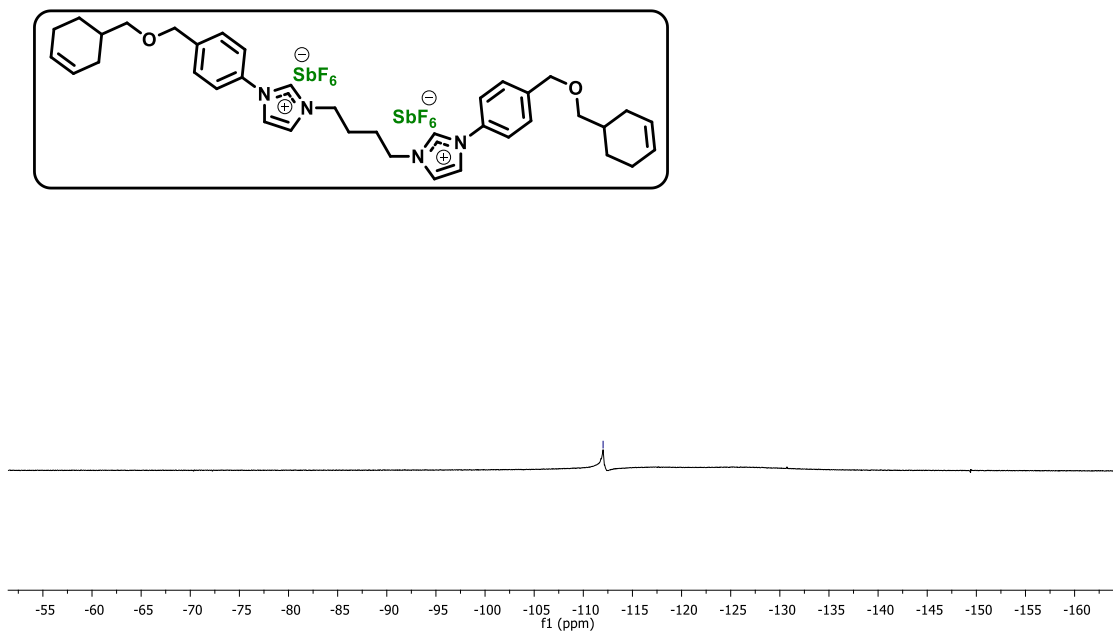
CY-fev03-CY-1-22  
CY-1-22



## $^{19}\text{F}$ NMR (376 MHz, $\text{CDCl}_3$ )

CY-fev02-CY-1-22-extrac  
CY-1-22-extrac

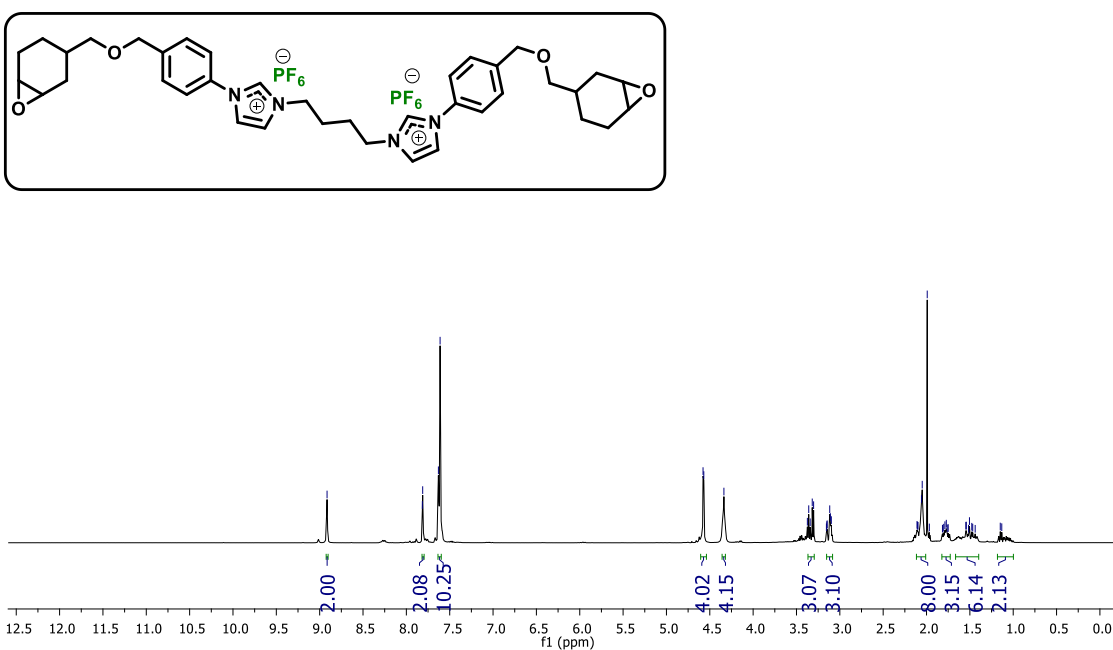
-112.01



## $^1\text{H}$ NMR (400 MHz, $\text{MeCN-d}_3$ )

CY-fev21-CY-2-11-final  
CY-2-11-final

8.91 7.82 7.81 7.63 7.61 4.58 4.57 4.34 3.36 3.32 3.30 3.12 3.11 2.11 2.11 2.06 2.05 1.99 1.79 1.77 1.55 1.54 1.50



### <sup>13</sup>C NMR (100 MHz, MeCN-d<sub>3</sub>)

CY-fev24-CY-2-11-13C  
CY-2-11-13C

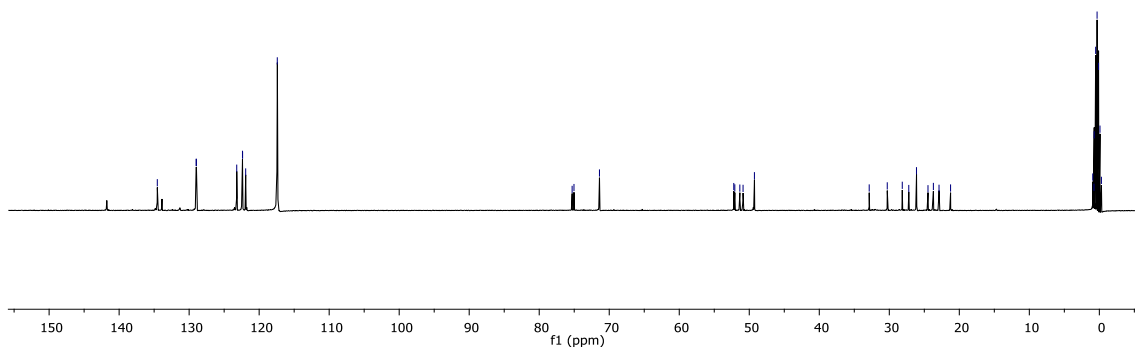
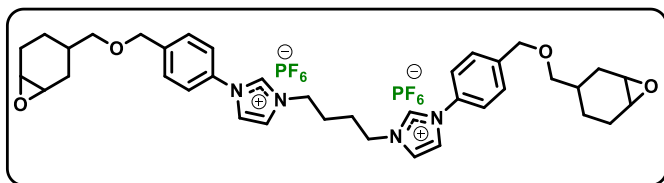
134.59  
129.00  
128.96  
123.20  
122.38  
122.37  
121.93  
117.41

75.30  
75.04  
71.39

52.21  
52.06  
51.35  
50.89  
49.26

32.87  
30.29  
28.15  
27.22  
26.11  
24.47  
23.70  
22.90  
21.25

0.53  
0.32  
0.12  
-0.09



### <sup>1</sup>H NMR (400 MHz, MeCN-d<sub>3</sub>)

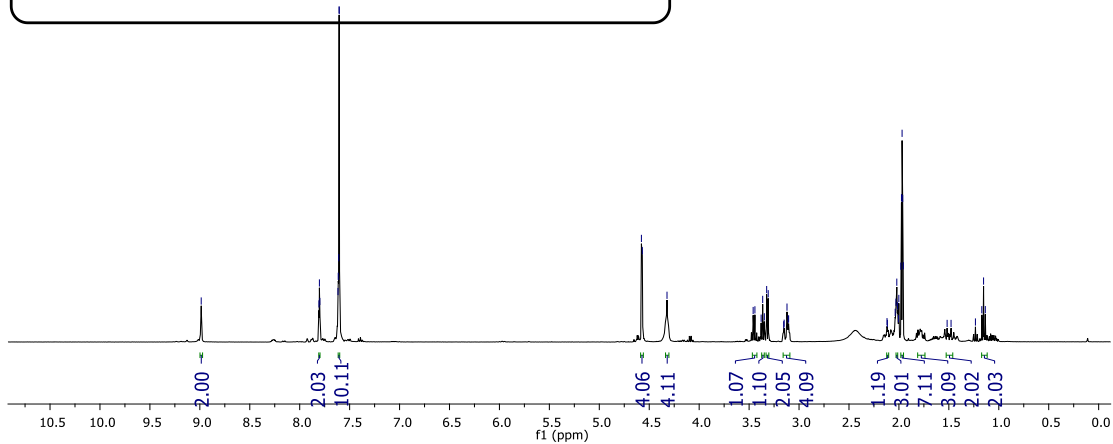
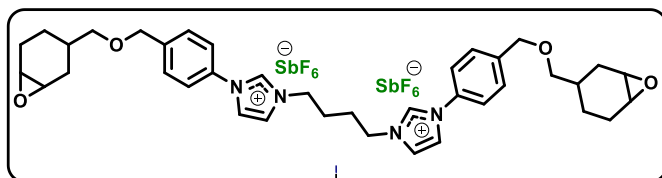
CY-fev08-CY-2-10-precip1  
CY-2-10-precip1

8.99  
7.81  
7.80  
7.80  
7.62  
7.61  
7.61  
7.61  
7.60

4.58  
4.57  
4.32

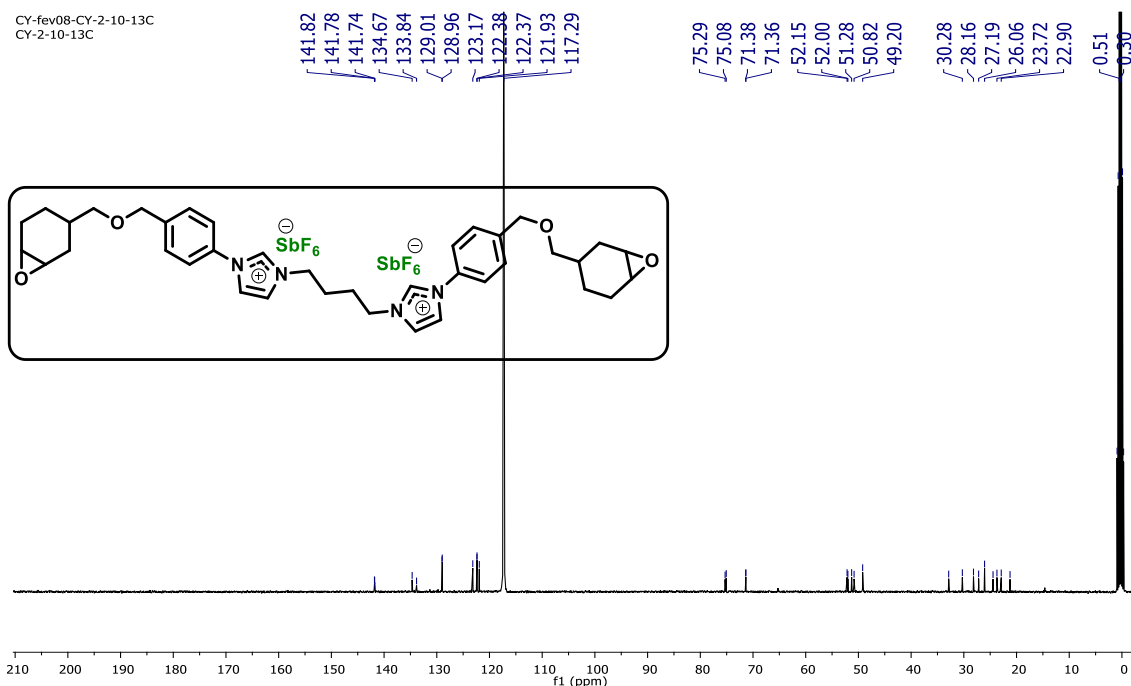
3.46  
3.44  
3.36  
3.32  
3.31  
3.12

2.03  
2.02  
2.01  
2.00  
1.98  
1.97  
1.97  
1.96  
1.15  
1.13

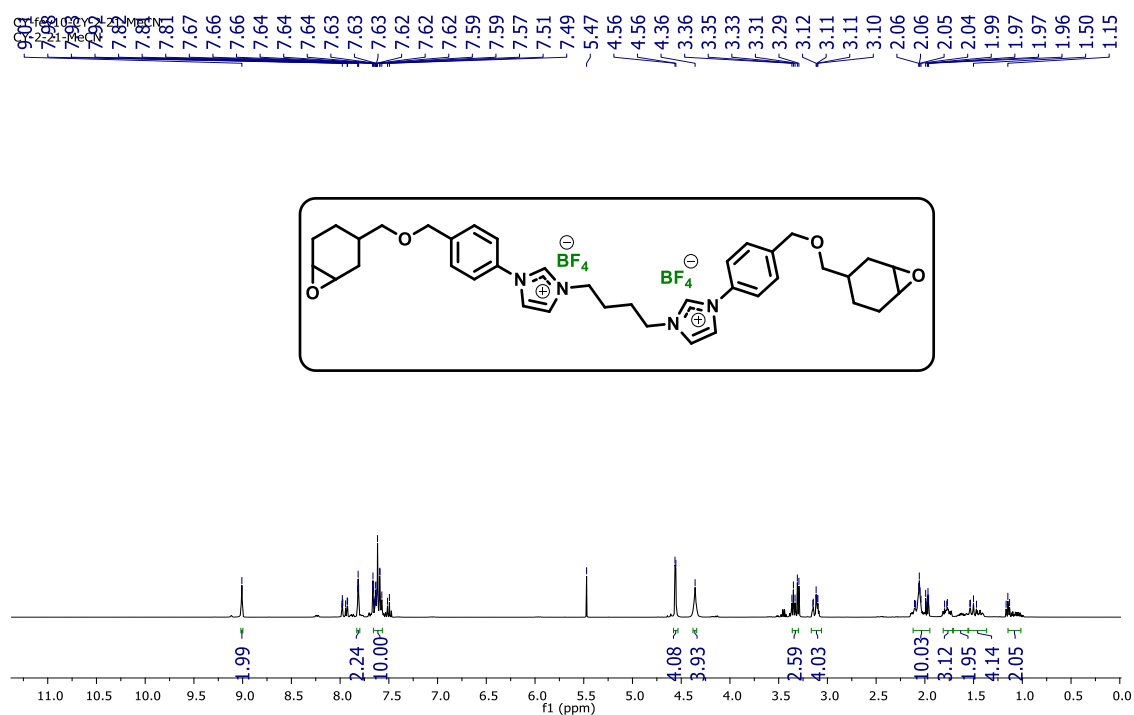




# **$^{13}\text{C}$ NMR (100 MHz, $\text{MeCN-d}_3$ )**



# **$^1\text{H}$ NMR (400 MHz, $\text{MeCN-d}_3$ )**



# <sup>13</sup>C NMR (100, MeCN-d<sub>3</sub>)

CY-fev10-CY-2-21-MeCN  
CY-2-21-MeCN

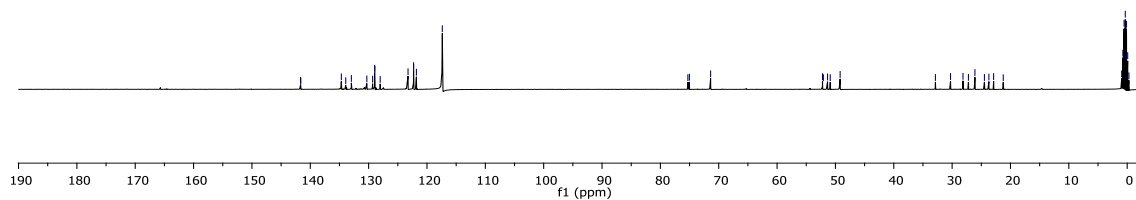
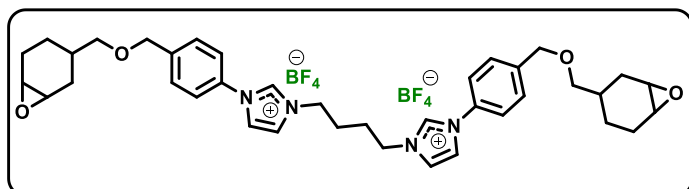
141.67  
141.63  
134.68  
133.92  
132.96  
130.31  
129.32  
128.97  
128.93  
128.02  
123.25  
122.30  
122.29  
121.81  
117.37

75.29  
75.03  
71.39

52.22  
52.07  
51.35  
50.89  
49.19

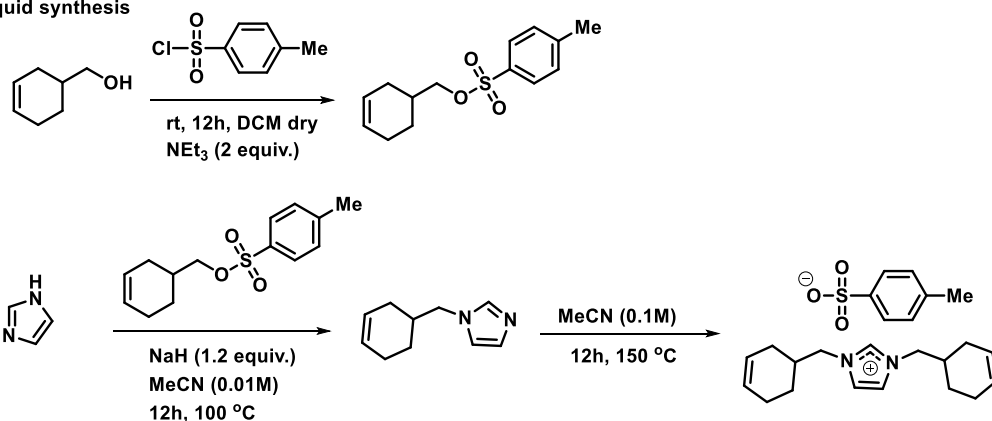
30.28  
28.14  
27.21  
26.09  
24.46  
23.70  
22.89

0.53  
0.32

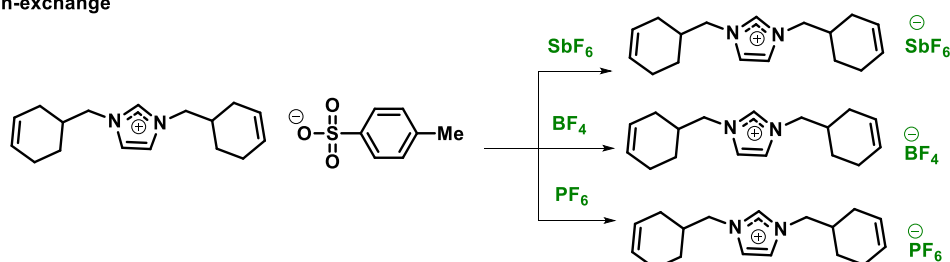


## Synthetic route

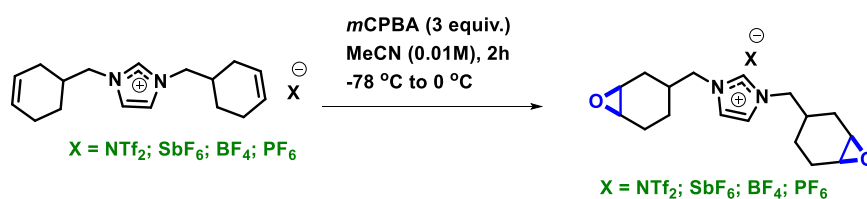
### a) Ionic liquid synthesis



### b) Ion-exchange



### c) Epoxidation



**Figure V-S28.** Overview of the synthetic route employed. **a)** Preparation of ionic liquid via *quaternization*; **b)** reaction of ionic exchange to obtain ionic liquid with appropriate anions not able to catalyze the opening of the epoxide; **c)** *Prilezhaev* epoxidation reaction.<sup>6</sup>

<sup>6</sup> For details of the reaction mechanism, see: Kim, C.; Traylor, T. G.; Perrin, C. L. *J. Am. Chem. Soc.* **1998**, 37, 9513-9515. [\[link\]](#)

## Reaction optimizations

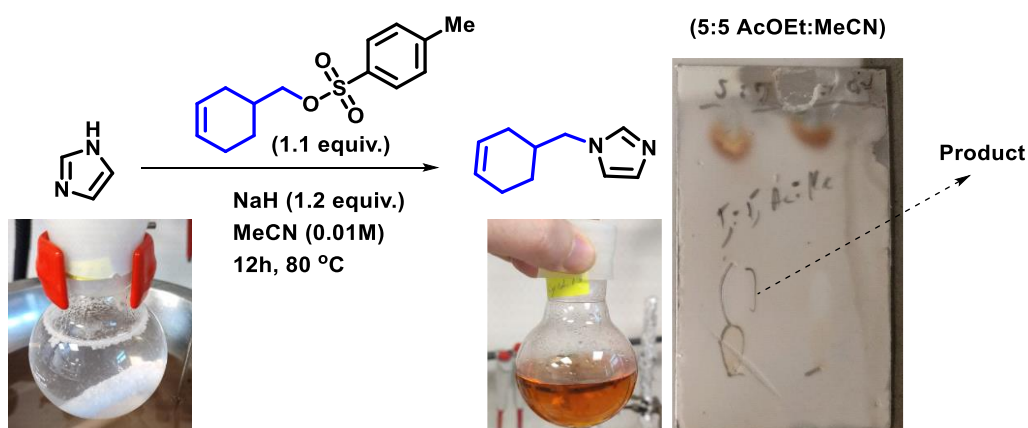
**Table V-S6.** Second reaction for the synthesis of a new family of cycloaliphatic epoxidized ILs

c1cc[nH]c1 + CC1=CC=C(S(=O)(=O)OCC2=CC=CC=C2)C1 (1.1 equiv.)  
 $\xrightarrow[\text{MeCN (0.01M), 12h, } T (^{\circ}\text{C})]{\text{NaH (1.2 equiv.)}}$  CC1=CC=C(S(=O)(=O)OCC2=CC=CC=C2)C1

Entry	T °C)	Yield (%) <sup>[a]</sup>
1	25	trace
2	50	50
3	80	89
4	100	51

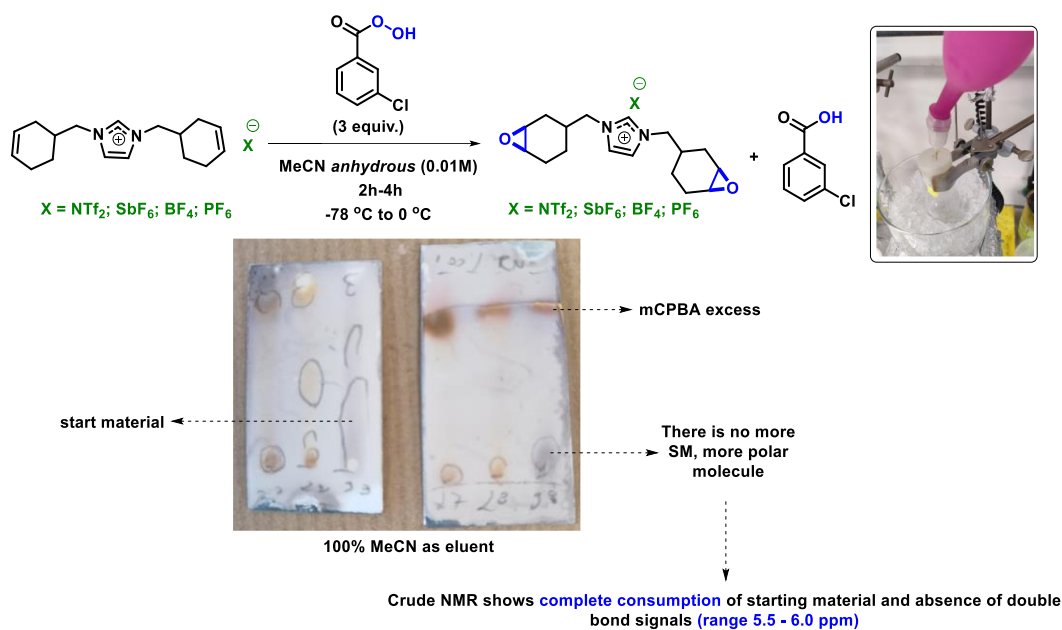
**[a]** Estimated based on the  $^1\text{H}$  NMR crude employing 1,3,5-trimethoxybenzene as internal reference.

### Reaction details:



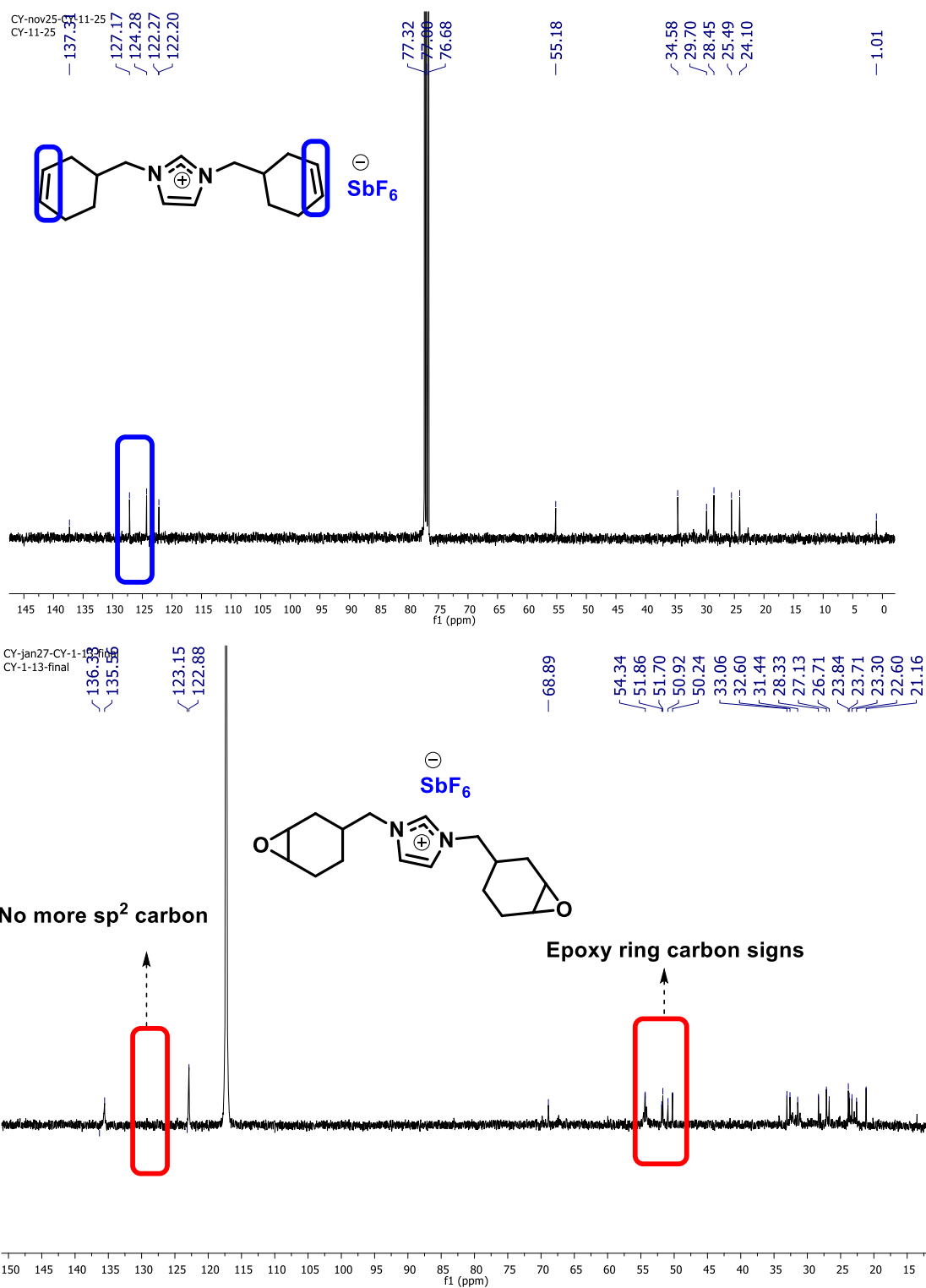
**Figure V-S29.** General Information on the Imidazole Nitrogen Alkylation Reaction.

## Exploring the epoxidation reaction

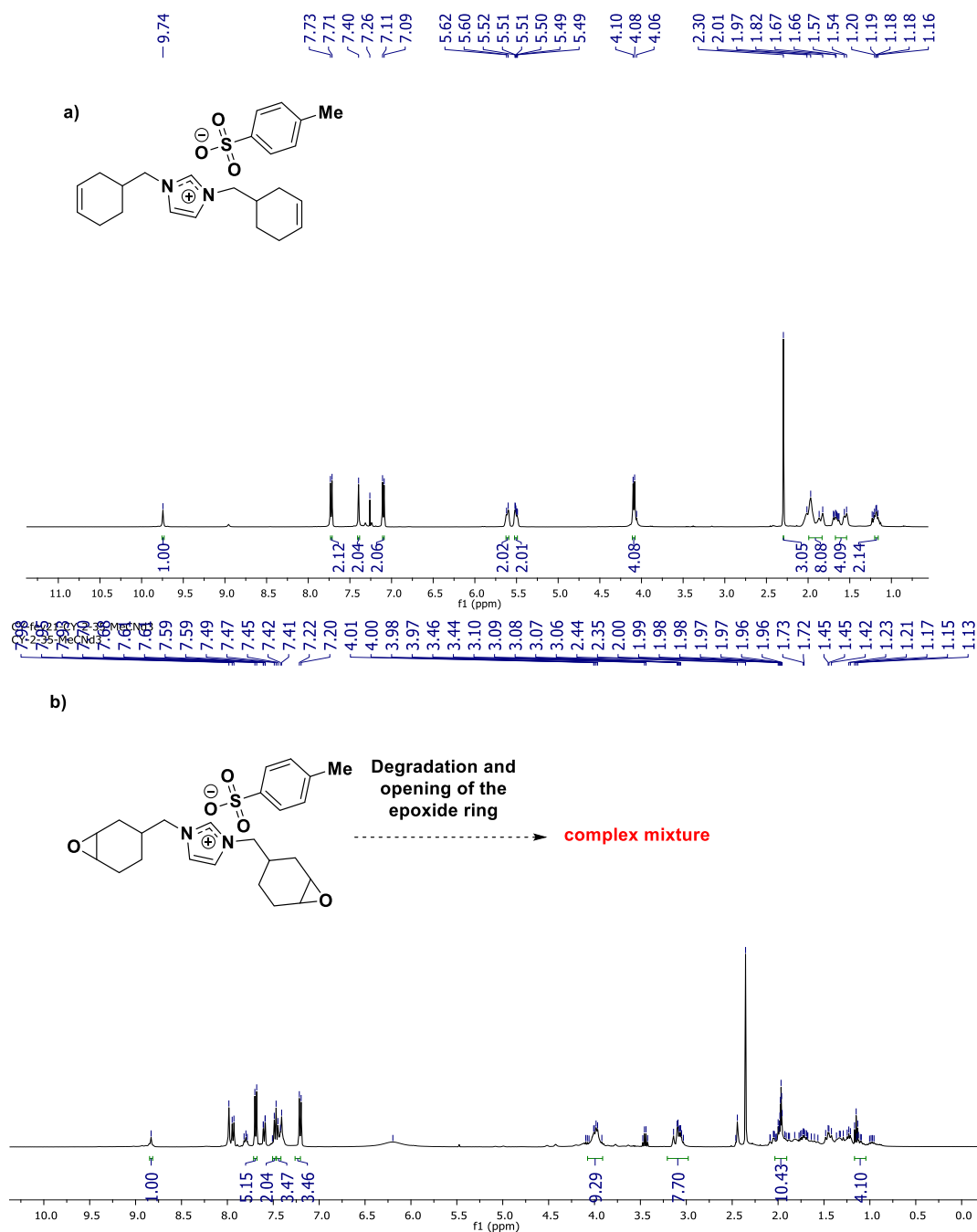


**Figure V-S30.** Synthetic information of the epoxidation reaction using *m*CPBA.





**Figure V-S32.**  $^{13}\text{C}$ -NMR spectrum of reactional mixture for the epoxidation reaction in deuterated acetonitrile after 3 hours of reaction. The spectra comparison corroborates the epoxy groups' formation from the alkenes.



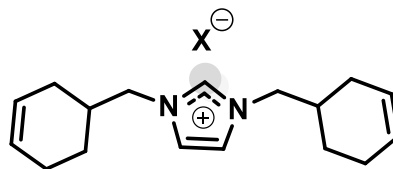
**Figure V-S33. a)** Crude <sup>1</sup>H-NMR spectrum of the reaction in deuterated acetonitrile after 3 hours of reaction; **b)** Spectrum after precipitation in diethyl ether and washing with AcOEt, Hexane, chloroform, and DCM.



## NMR study of synthesized ionic liquids

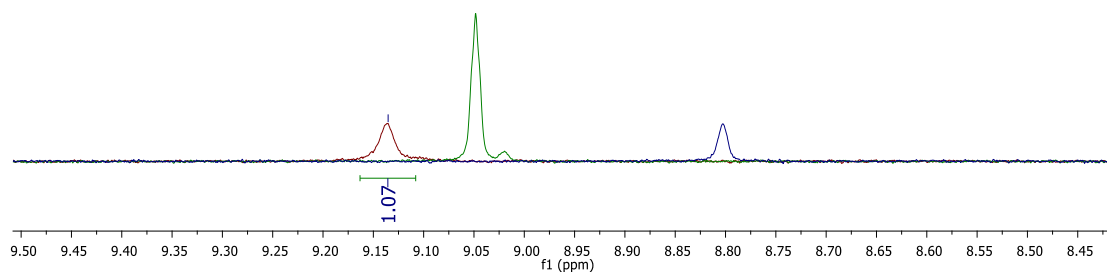
CY-nov29-CY-11-25-washed  
CY-11-25-washed

— 9.14



●  $X^- = \text{SbF}_6^-$   
●  $X^- = \text{BF}_4^-$   
●  $X^- = \text{PF}_6^-$

● Most pronounced change in chemical shift

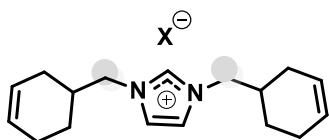


**Figure V-S34.** Overlap of  $^1\text{H}$ -NMR spectra.

CY-nov29-CY-11-25-washed  
CY-11-25-washed

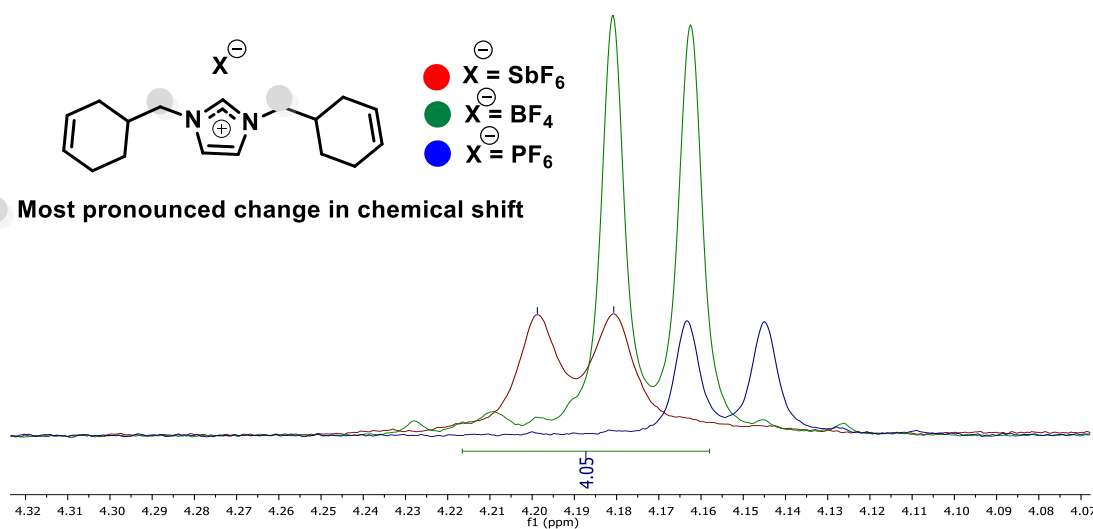
— 4.20

— 4.18



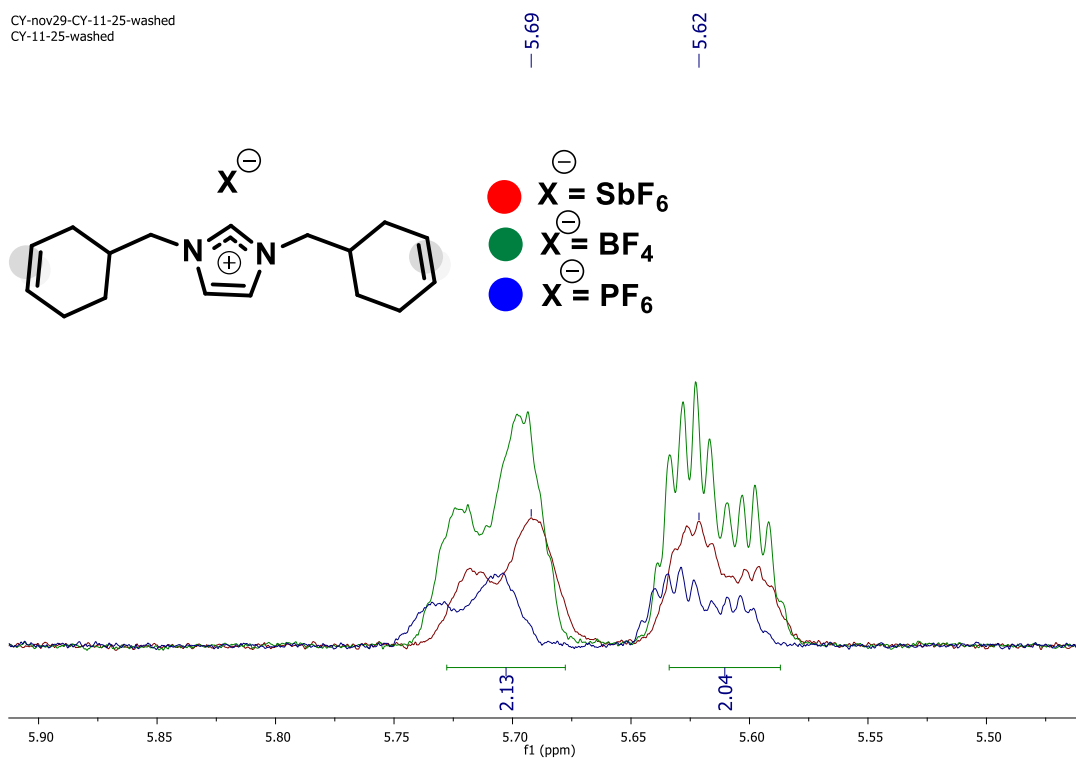
●  $X^- = \text{SbF}_6^-$   
●  $X^- = \text{BF}_4^-$   
●  $X^- = \text{PF}_6^-$

● Most pronounced change in chemical shift



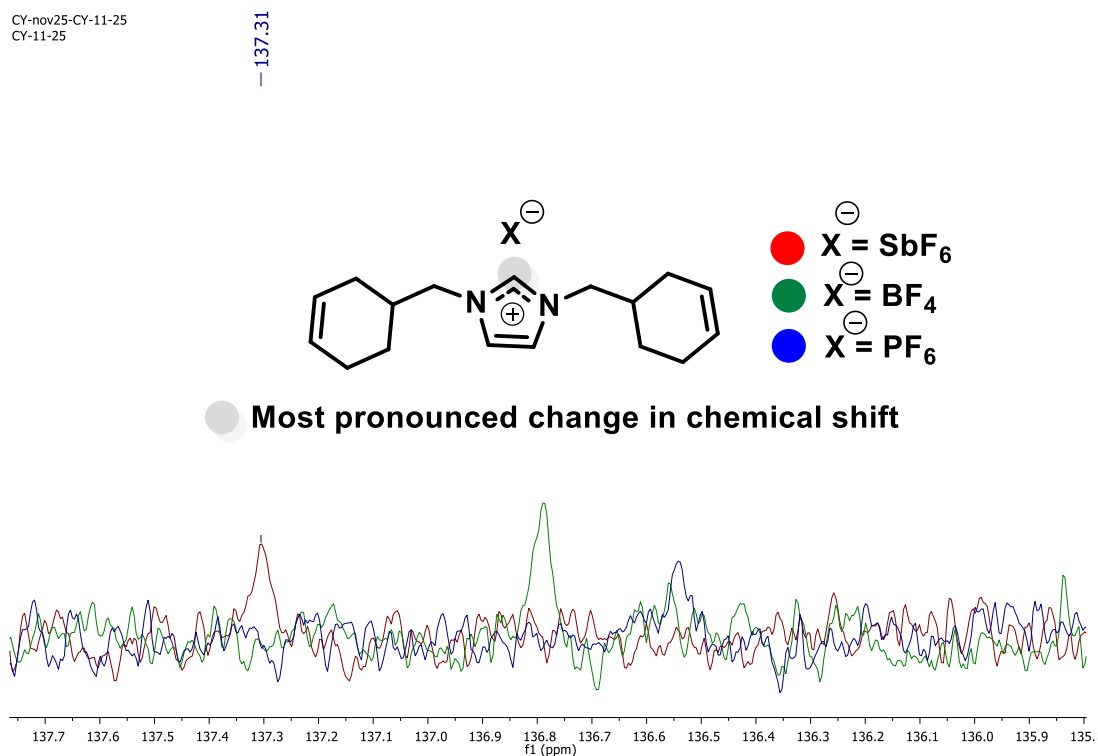
**Figure V-S35.** Overlap of  $^1\text{H}$ -NMR spectra.

CY-nov29-CY-11-25-washed  
CY-11-25-washed

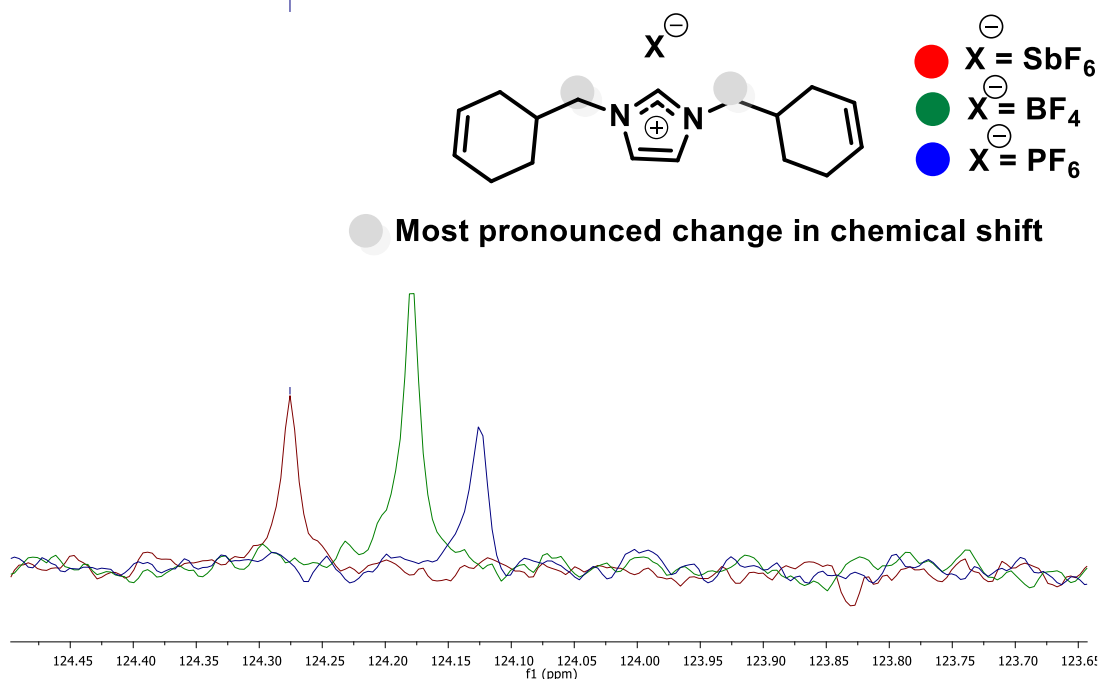


**Figure V-S36.** Overlap of  $^1H$ -NMR spectra.

CY-nov25-CY-11-25  
CY-11-25



**Figure V-S37.** Overlap of  $^{13}C$ -NMR spectra.

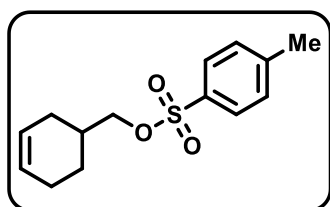


**Figure V-S38.** Overlap of <sup>13</sup>C-NMR spectra.

#### General procedures

##### Step 1 – Alcohol protection

##### *Cyclohex-3-en-1-ylmethyl 4-methylbenzenesulfonate*



Adapted from a procedure reported by Kumar and co-workers.<sup>7</sup> Under anhydrous conditions were placed cyclohex-3-en-1-yl-methanol (1.23 g; 10 mmol; 1 equiv.), triethylamine (4.18 mL; 30 mmol; 3 equiv.) and 4-methylbenzenesulfonyl chloride (5.72 g; 30 mmol; 3 equiv.) under inert atmosphere (N<sub>2</sub>).

Then, the reaction mixture was stirred at 0°C for 10 minutes, in sequence, at *rt* during 12h. The crude product was diluted with DCM and washed with brine. The solvent was removed under reduced pressure, then purified by column chromatography on silica gel (SiO<sub>2</sub>; gradient: 100% Hexane, 9:1 Hex:CHCl<sub>3</sub>, 8:2 Hex:CHCl<sub>3</sub>, 7:3 Hex:CHCl<sub>3</sub> and 5:5 Hex:CHCl<sub>3</sub>) to afford the title compound as a colorless oil (2.48 g, 93% yield).

**TLC:** *R<sub>f</sub>* = 0.5 (8:2 Hex:CHCl<sub>3</sub>, *Vanillin stain*).

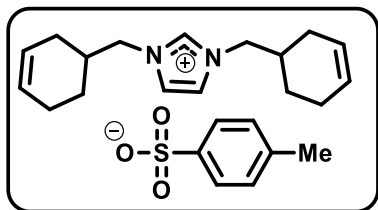
<sup>7</sup> Adapted reaction, see original methodology: Kumar, P.; *et al. J. Org. Chem.* **2011**, 76, 2094-2101. [[link](#)].

**<sup>1</sup>H NMR (400 MHz, CDCl<sub>3</sub>)**  $\delta_{\text{H}}$  7.74 (d,  $J$  = 8 Hz, 2H), 7.31 (d,  $J$  = 8.5, 2H), 5.56 – 5.50 (m, 2H), 3.85 (d,  $J$  = 6.6 Hz, 2H), 2.38 (s, 3H), 1.96 – 1.90 (m, 4H), 1.68 – 1.62 (m, 2H), 1.22 – 1.17 (m, 1H).<sup>8</sup>

Quaternization

**1,3-bis(cyclohex-3-en-1-ylmethyl)-1H-imidazol-1-ium  
4-methylbenzenesulfonate**

**4-**



In a sealed tube were weighed 1-(cyclohex-3-en-1-ylmethyl)-1H-imidazole (48.7 mg, 3 mmol, 1 equiv.), cyclohex-3-en-1-ylmethyl 4-methylbenzenesulfonate (1.60 g, 6 mmol, 2 equiv.). In sequence, MeCN (30 mL; 0.1 M) was added. The mixture was stirred at 150 °C for 18 h.

The crude product was purified via precipitation into hexane and petroleum ether, then washed with diethyl ether 3 times (20 mL) to afford the title compound as a light brown solid (1.09 g, 85% yield).

**TLC:**  $R_f$  = 0.1 (100% EtOAc, *Vanillin stain*).

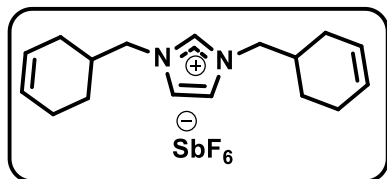
**<sup>1</sup>H NMR (400 MHz, CDCl<sub>3</sub>)**  $\delta_{\text{H}}$ : 9.74 (s, 1H), 7.72 (d,  $J$  = 8.0 Hz, 2H), 7.40 (s, 2H), 7.10 (d,  $J$  = 7.9, 2H), 5.62 – 5.49 (m, 4H), 4.08 (d, 4.7 Hz, 4H), 2.30 (s, 3H), 2.01 – 1.82 (m, 8H), 1.70 – 1.54 (m, 4H), 1.23 – 1.16 (m, 2H) ppm.

**<sup>13</sup>C NMR (100 MHz, CDCl<sub>3</sub>)**  $\delta_{\text{C}}$ : 143.7, 141.6, 131.0, 129.8, 128.9, 128.0, 126.9, 125.6, 124.2, 55.7, 35.8, 29.5, 26.6, 25.2, 21.3 ppm.

<sup>8</sup> In agreement with the literature, see: Zhou, J.; Fu, G. C. *J. Am. Chem. Soc.* **2003**, *41*, 1252712530. [\[link\]](#)

## Ion-exchange reaction

### *1,3-bis(cyclohex-3-en-1-ylmethyl)-1H-3l4-imidazol-1-ium hexafluorostibate(V)*

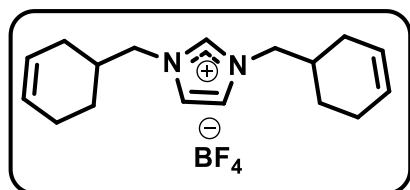


In a sealed tube were weighed 1,3 bis(cyclohex-3-en-1-ylmethyl)-1H-3l4-imidazol-1-ium 4-methylbenzenesulfonate (128.5 mg, 0.3 mmol, 1 equiv.) and sodium hexafluorostibate(V) (465.7 mg, 1.8 mmol, 6 equiv.). In sequence, a 1:1 mixture of acetone and DCE (dichloroethane) was employed for complete solubilization of both solids. The mixture was stirred at 100 °C for 24 h. The crude product was purified via extraction (**note**: add a little quantity of water to avoid loss of the ionic liquid) using water and chloroform to afford the title compound as a slightly yellow oil (128 mg, 87% yield).

**<sup>1</sup>H NMR (400 MHz, CDCl<sub>3</sub>)**  $\delta_{\text{H}}$ : 9.09 (s, 1H), 7.23 (s, 2H), 5.68 – 5.61 (m, 4H), 4.18 (d,  $J$  = 7.3 Hz, 4H), 2.14 – 1.99 (m, 8H), 1.83 – 1.69 (m, 6H) ppm.

**<sup>13</sup>C NMR (100 MHz, CDCl<sub>3</sub>)**  $\delta_{\text{C}}$ : 137.3, 127.2, 124.3, 122.3, 122.2, 55.2, 34.6, 29.7, 28.4, 25.5, 24.1, 1.0 ppm.

### *1,3-bis(cyclohex-3-en-1-ylmethyl)-1H-3l4-imidazol-1-ium tetrafluoroborate*

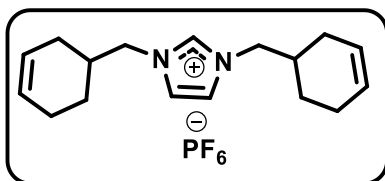


In a sealed tube were weighed 1,3 bis(cyclohex-3-en-1-ylmethyl)-1H-3l4-imidazol-1-ium 4-methylbenzenesulfonate (128.5 mg, 0.3 mmol, 1 equiv.) and lithium tetrafluoroborate (281.2 mg, 3 mmol, 10 equiv.). In sequence, 30 mL of water was added for complete solubilization (**note**: the solubilization is complete at 100 °C). The mixture was stirred at 100 °C for 48 h. The crude product was purified via extraction (**note**: add a little volume of water to avoid loss of the ionic liquid) using water and chloroform to afford the title compound as a slightly yellow oil (89 mg, 88% yield).

**<sup>1</sup>H NMR (400 MHz, CDCl<sub>3</sub>)**  $\delta_{\text{H}}$ : 9.05 (s, 1H), 7.25 (d,  $J$  = 1.5 Hz, 2H), 5.74 – 5.60 (m, 4H), 4.17 (d,  $J$  = 7.3 Hz, 4H), 2.15 – 2.0 (m, 8H), 1.82 – 1.70 (m, 4H), 1.39 – 1.25 (m, 2H) ppm.

**<sup>13</sup>C NMR (100 MHz, CDCl<sub>3</sub>)**  $\delta_{\text{C}}$ : 136.4, 127.1, 124.3, 122.7, 55.0, 34.5, 28.4, 25.4, 24.1 ppm.

### ***1,3-bis(cyclohex-3-en-1-ylmethyl)-1H-3l4-imidazol-1-ium hexafluorophosphate(V)***



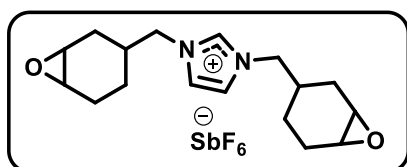
In a sealed tube were weighed 1,3 bis(cyclohex-3-en-1-ylmethyl)-1H-3l4-imidazol-1-ium 4-methylbenzenesulfonate (128.5 mg, 0.3 mmol, 1 equiv.) and Ammonium hexafluorophosphate (489 mg, 3 mmol, 10 equiv.). In sequence, 30 mL of water was added for complete solubilization (**note:** the solubilization is complete at 100 °C). The mixture was stirred at 100 °C for 48 h. The crude product was purified via extraction (**note:** add a little quantity of water to avoid loss of the ionic liquid) using water and chloroform to afford the title compound as a slightly yellow oil (103.8 mg, 86% yield).

**<sup>1</sup>H NMR (400 MHz, CDCl<sub>3</sub>)** δ<sub>H</sub>: 8.80 (s, 1H), 7.23 (s, 2H), 5.72 – 5.61 (m, 4H), 4.17 (d, *J* = 7.3 Hz, 4H), 2.14 – 1.99 (m, 7H), 1.83 – 1.69 (m, 7H).

**<sup>13</sup>C NMR (100 MHz, CDCl<sub>3</sub>)** δ<sub>C</sub>: 136.6, 127.2, 124.2, 122.6, 55.1, 34.5, 28.4, 25.4, 24.0 ppm.

Epoxidation reaction

### ***1,3-bis((7-oxabicyclo[4.1.0]heptan-3-yl)methyl)-1H-3l4-imidazol-1-ium hexafluorostibate(V)***



Adapted from a procedure by Radchenko and co-workers.<sup>9</sup> Under anhydrous conditions were placed 1,3-bis(cyclohex-3-en-1-ylmethyl)-1H-3l4-imidazol-1-ium hexafluorostibate(V) (49 mg; 0.1 mmol; 1 equiv.), and

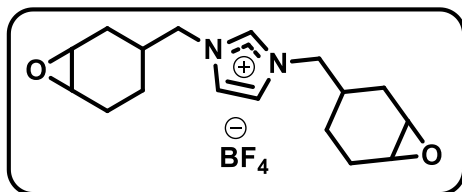
MeCN anhydrous (5 mL; 0.01 M). Then, a solution of *m*CPBA (52 mg; 0.3 mmol; 3 equiv.) in 5 mL of MeCN was added drop wise by syringe under Ar. The mixture was stirred at -78 °C for 3 h. The crude product was precipitated in diethyl ether, washed with AcOEt, hexane, acetone, toluene, chloroform, and DCM to afford the title compound as a colorless oil (*Yield not determined due to impurities*).

**<sup>1</sup>H NMR (400 MHz, CDCl<sub>3</sub>)** δ<sub>H</sub>: 8.44 (s, 1H), 7.39 (m, 2H), 4.01 – 3.96 (m, 4H), 3.14 – 3.11 (m, 2H), 2.10 – 1.98 (m, 2H), 1.92 – 1.75 (m, 4H), 1.52 – 1.36 (m, 10H) ppm.

<sup>9</sup> Adapted reaction, see original methodology: **a)** Radchenko, A. V.; Duchet-Rumeau, J.; Gérard, J.; Baudoux, J.; Livi, S. *Polym. Chem.* **2020**, *11*, 5475 – 5485. [[link](#)]

**1,3-bis((7-oxabicyclo[4.1.0]heptan-3-yl)methyl)-1H-3l4-imidazol-1-ium**

**tetrafluoroborate**



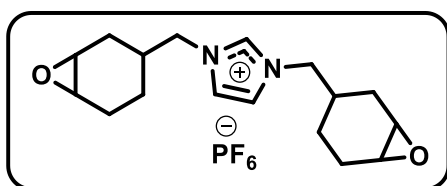
Under anhydrous conditions were placed 1,3-bis(cyclohex-3-en-1-ylmethyl)-1H-3l4-imidazol-1-ium tetrafluoroborate (34.4 mg; 0.1 mmol; 1 equiv.), and MeCN anhydrous (5 mL; 0.01 M). Then, a solu-

tion of *m*CPBA (52 mg; 0.3 mmol; 3 equiv.) in 5 mL of MeCN was added drop wise by syringe under Ar. The mixture was stirred at -78 °C for 3 h. The crude product was precipitated in diethyl ether, washed with AcOEt, hexane, acetone, toluene, chloroform, and DCM to afford the title compound as a colorless oil (*Yield not determined due to impurities*).

**<sup>1</sup>H NMR (400 MHz, CDCl<sub>3</sub>)** δ<sub>H</sub> 9.09 (s, 1H), 7.80 – 7.70 (m, 2H), 4.25 – 4.20 (m, 4H), 3.14 – 3.07 (m, 2H), 2.46 – 2.41 (m, 2H), 1.8 – 1.75 (m, 4H), 1.52 – 1.36 (m, 10H) ppm.

**1,3-bis((7-oxabicyclo[4.1.0]heptan-3-yl)methyl)-1H-3l4-imidazol-1-ium**

**hexafluorophosphate(V)**



Adapted from a procedure by Radchenko and co-workers.<sup>10</sup> Under anhydrous conditions were placed 1,3-bis(cyclohex-3-en-1-ylmethyl)-1H-3l4-imidazol-1-ium hexafluorophosphate(V) (40 mg; 0.1 mmol; 1

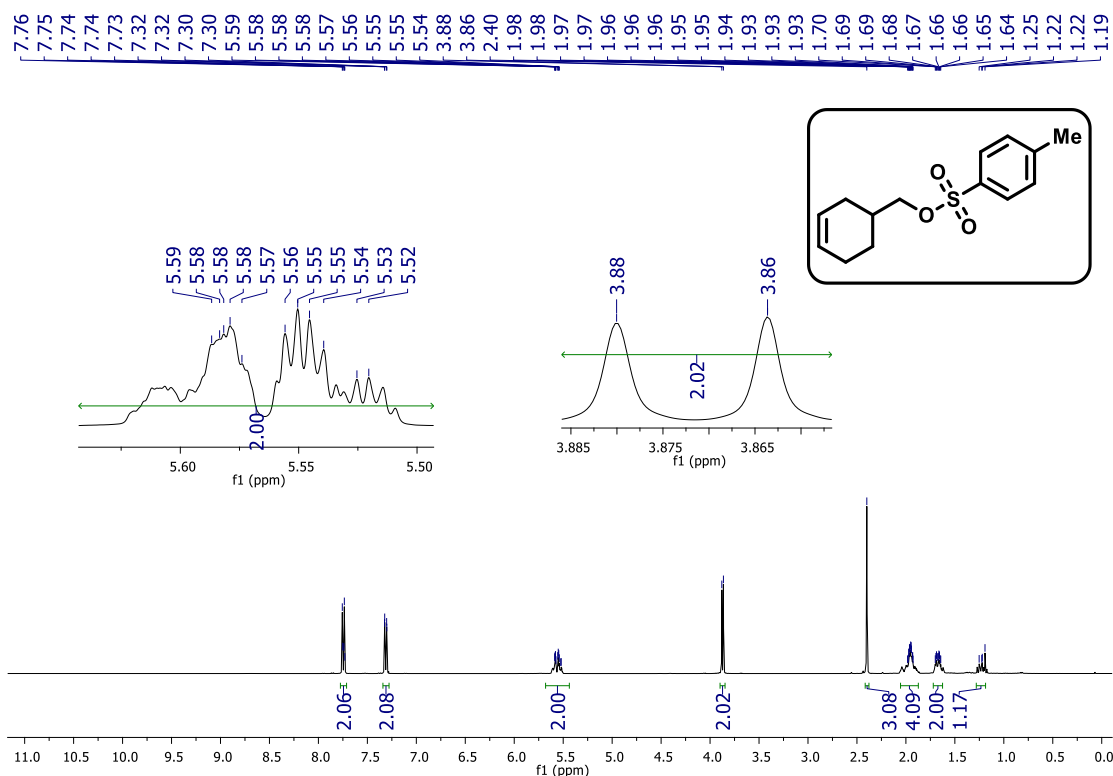
equiv.), and MeCN anhydrous (5 mL; 0.01 M). Then, a solution of *m*CPBA (52 mg; 0.3 mmol; 3 equiv.) in 5 mL of MeCN was added drop wise by syringe under Ar. The mixture was stirred at -78 °C for 3 h. The crude product was precipitated in diethyl ether, washed with AcOEt, hexane, acetone, toluene, chloroform, and DCM to afford the title compound as a colorless oil (*Yield not determined due to impurities*).

**<sup>1</sup>H NMR (400 MHz, CDCl<sub>3</sub>)** δ<sub>H</sub> 8.47 (s, 1H), 7.42- 7.38 (m, 2H), 4.06 – 3.96 (m, 4H), 3.14 – 3.10 (m, 2H), 2.14 – 2.10 (m, 2H), 1.92 – 1.75 (m, 4H), 1.52 – 1.38 (m, 10H) ppm.

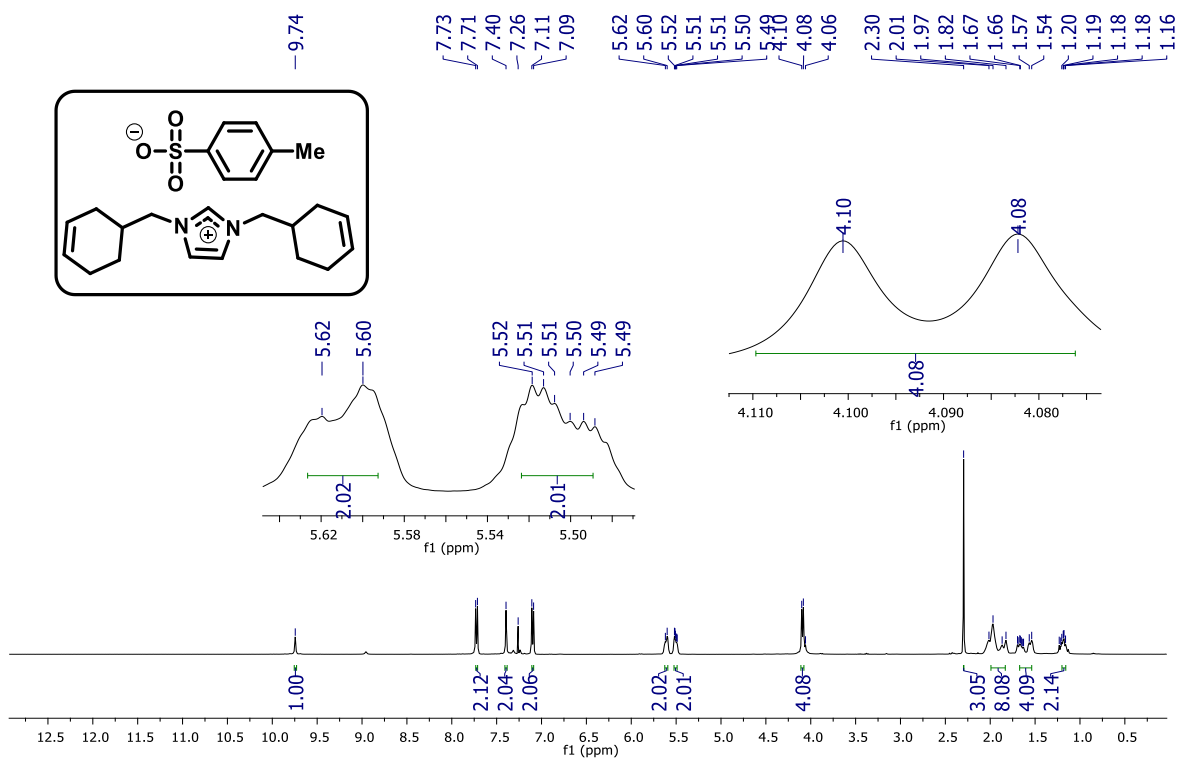
<sup>10</sup> Adapted reaction, see original methodology: **a)** Radchenko, A. V.; Duchet-Rumeau, J.; Gérard, J.; Baudoux, J.; Livi, S. *Polym. Chem.* **2020**, *11*, 5475 – 5485. [[link](#)]

# $^1\text{H}$ , $^{13}\text{C}$ NMR Spectra of Compounds

## $^1\text{H}$ NMR (400 MHz, $\text{CDCl}_3$ )

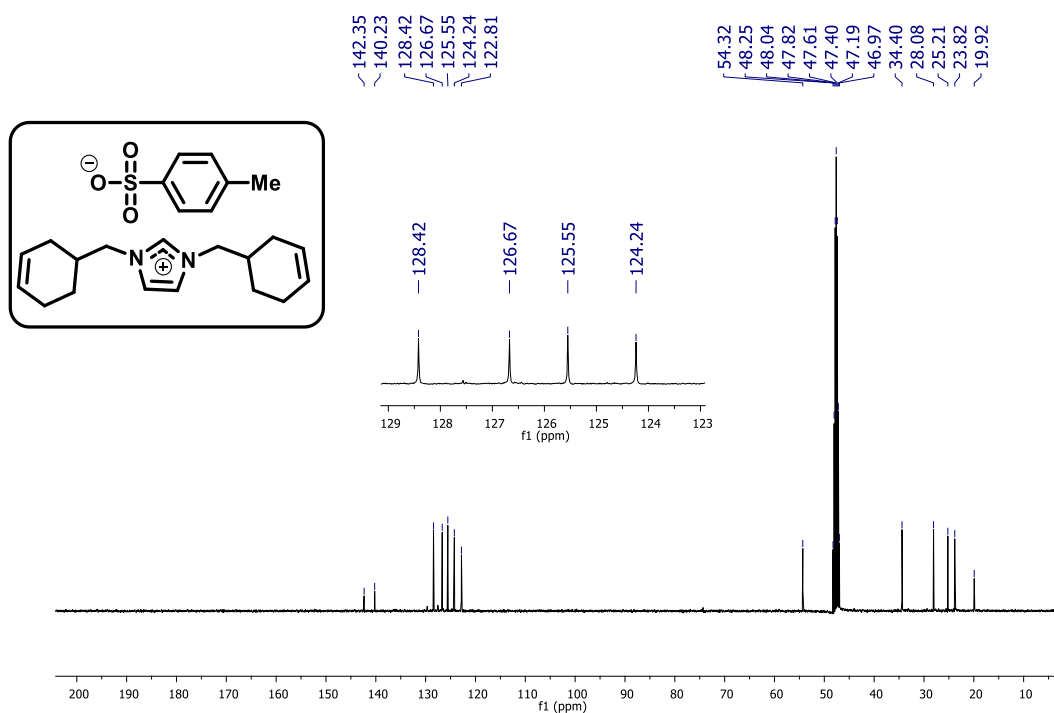


## $^1\text{H}$ NMR (400 MHz, $\text{CDCl}_3$ )

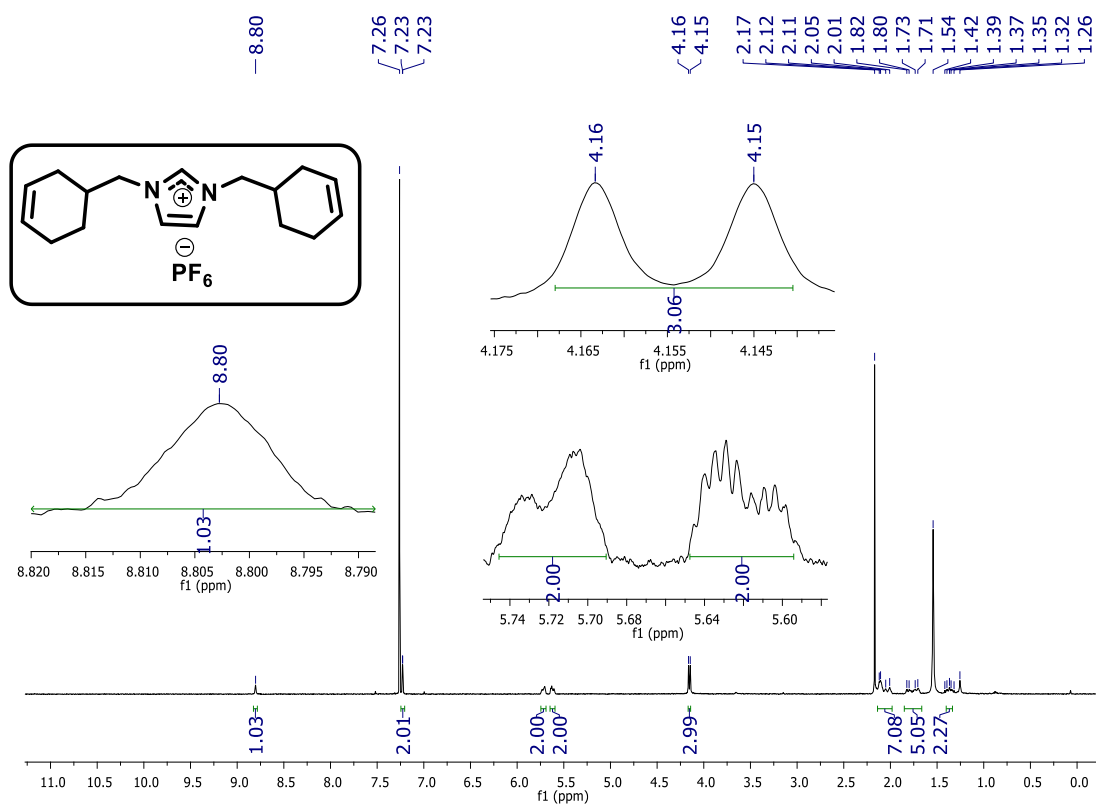




**$^{13}\text{C}$  NMR (100 MHz,  $\text{CDCl}_3$ )**



**$^1\text{H}$  NMR (400 MHz,  $\text{CDCl}_3$ )**



### $^{13}\text{C}$ NMR (100 MHz, $\text{CDCl}_3$ )

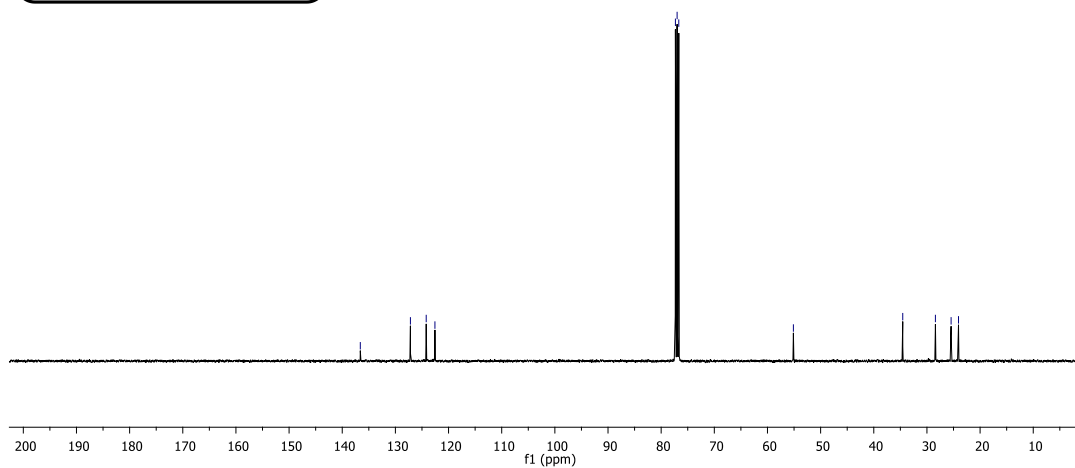
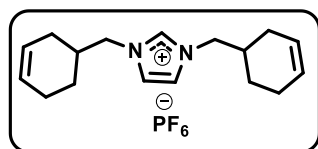
CY-dec09-CY-12-10  
CY-12-10

— 136.60  
/ 127.17  
~ 124.20  
~ 122.56

77.32  
77.00  
76.68

— 55.12

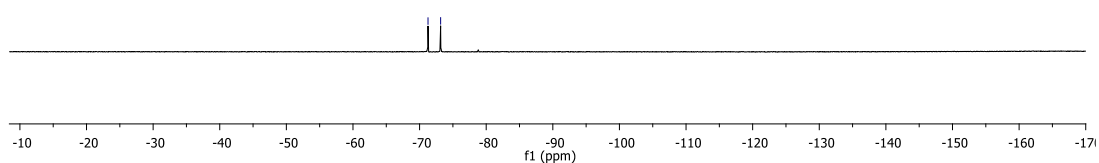
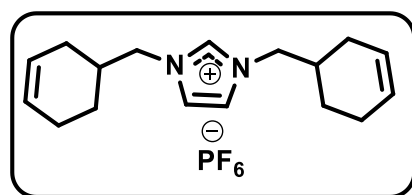
~ 34.55  
/ 28.41  
/ 25.45  
~ 24.06



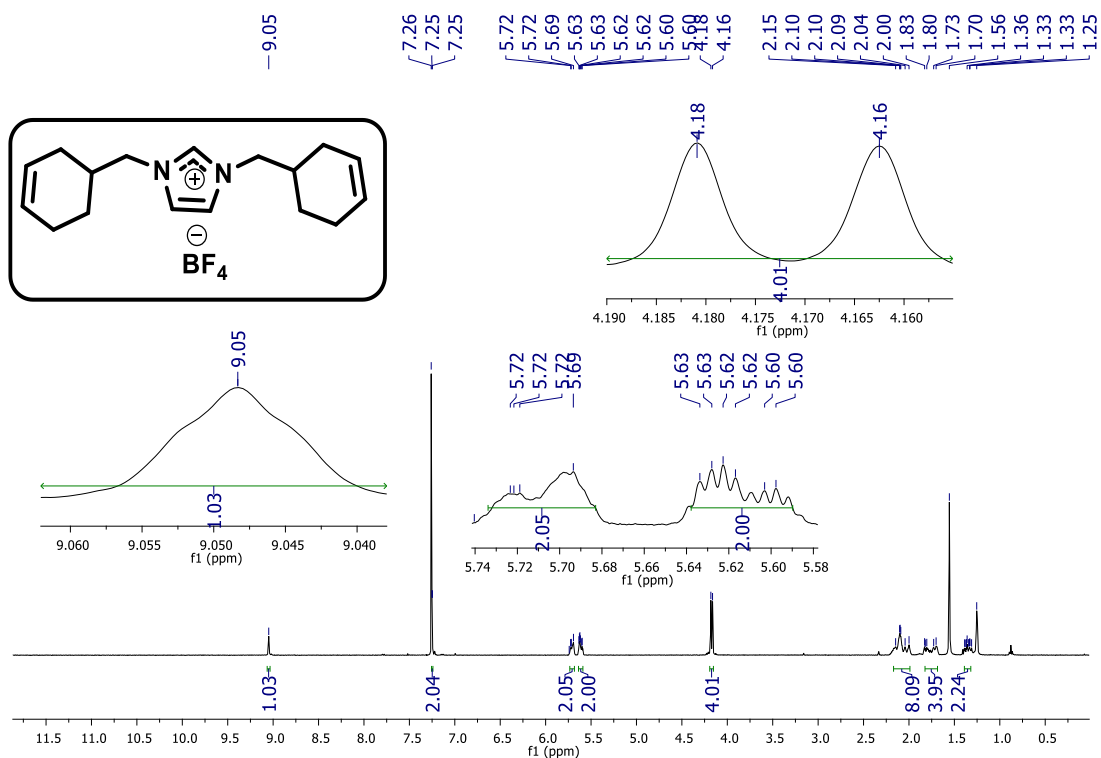
### $^{19}\text{F}$ NMR (376 MHz, $\text{CDCl}_3$ )

CY-nov25-CY-11-27-19F  
CY-11-27-19F

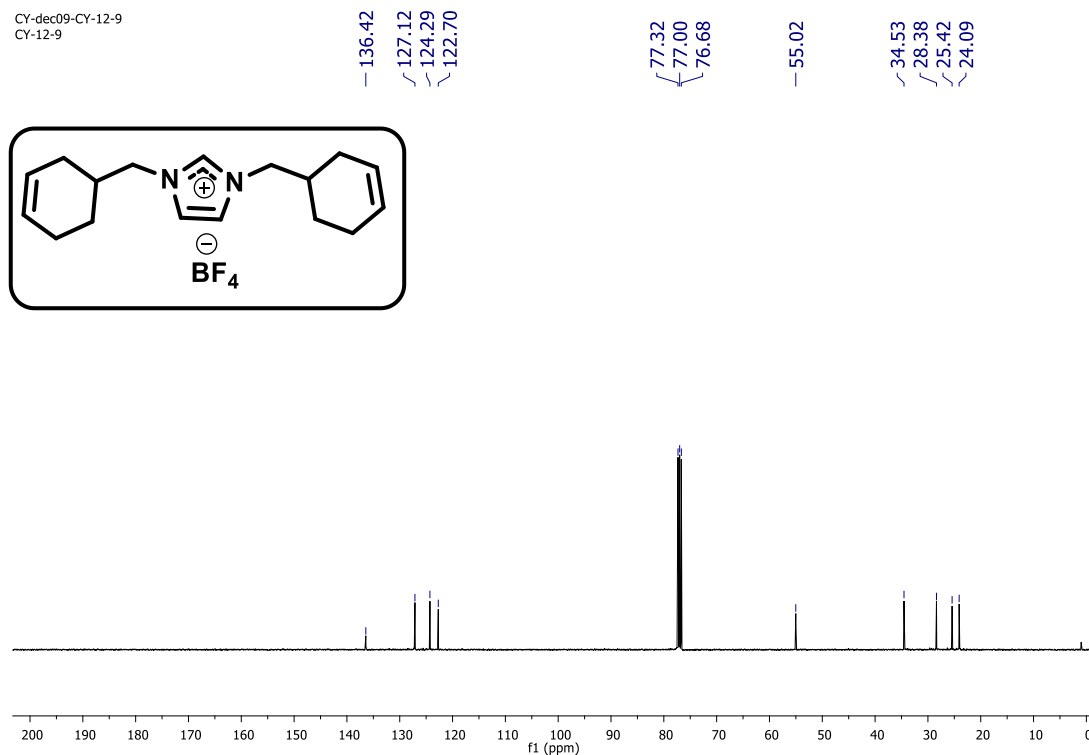
~ -71.26  
~ -73.16



# <sup>1</sup>H NMR (400 MHz, CDCl<sub>3</sub>)

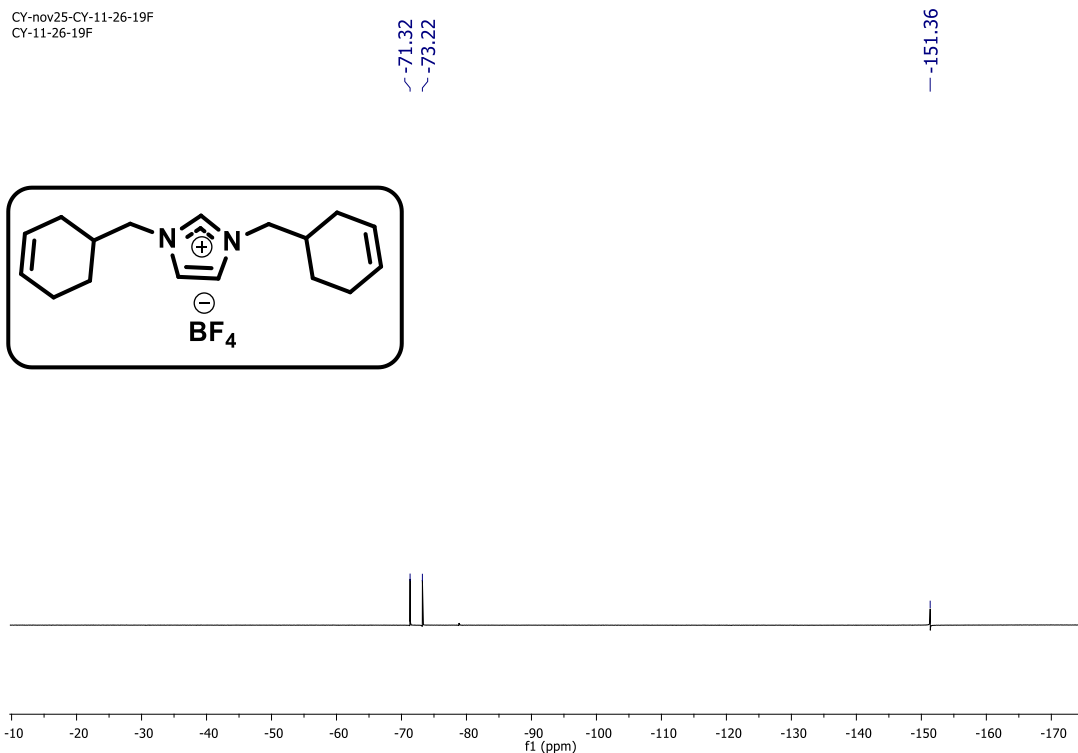


# <sup>13</sup>C NMR (100 MHz, CDCl<sub>3</sub>)

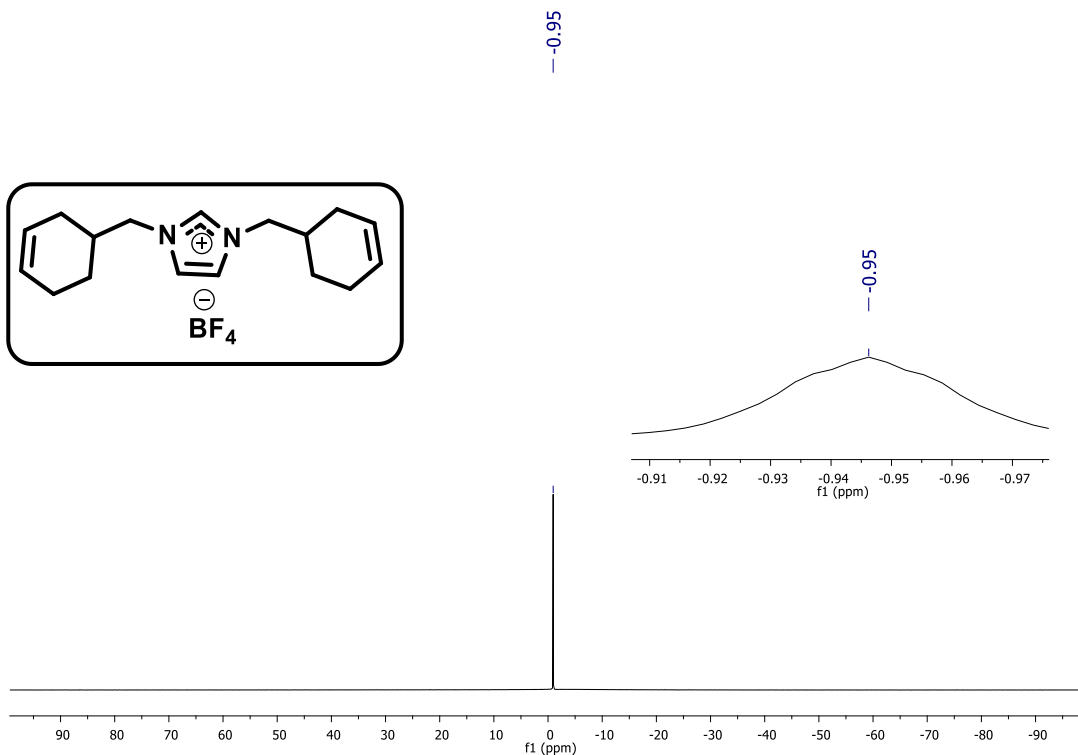


### $^{19}\text{F}$ NMR (376 MHz, $\text{CDCl}_3$ )

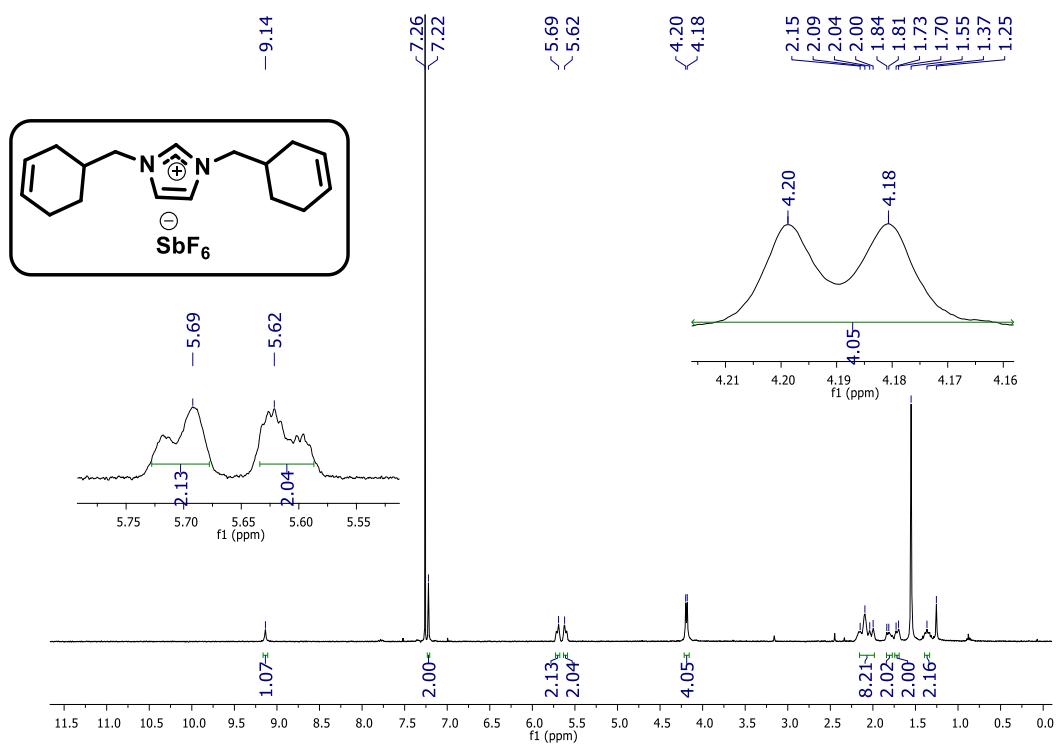
CY-nov25-CY-11-26-19F  
CY-11-26-19F



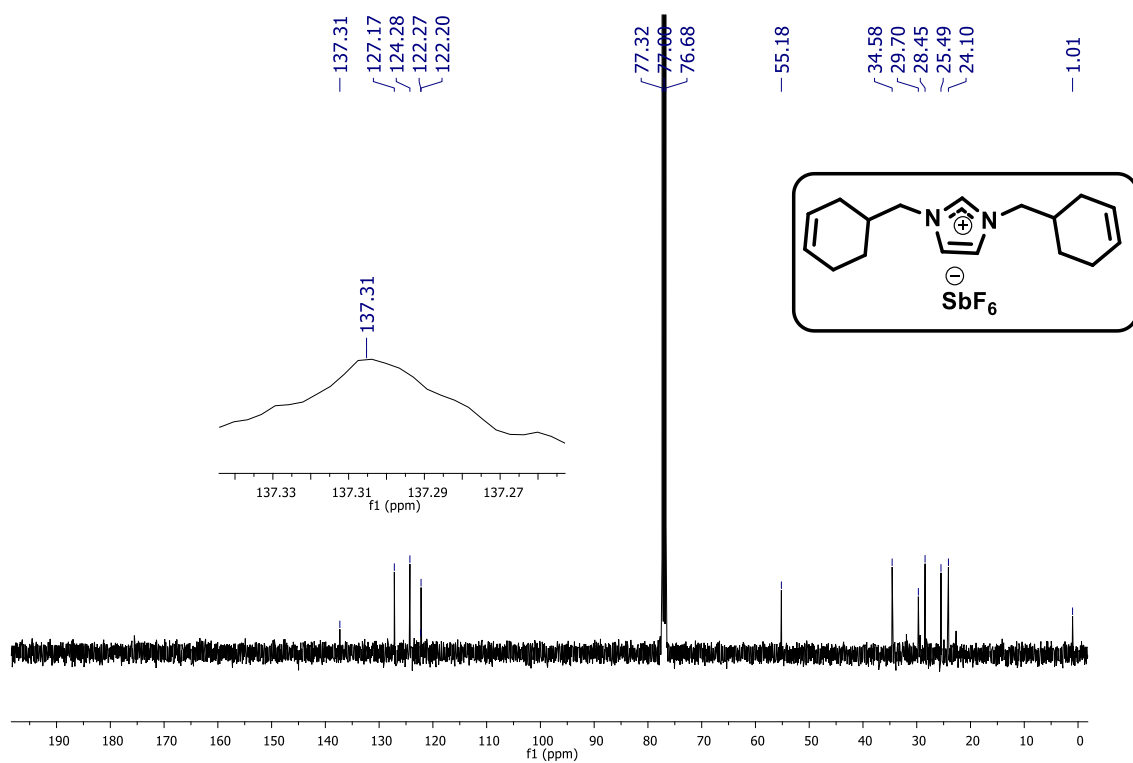
### $^{11}\text{B}$ NMR (102 MHz, $\text{CDCl}_3$ )



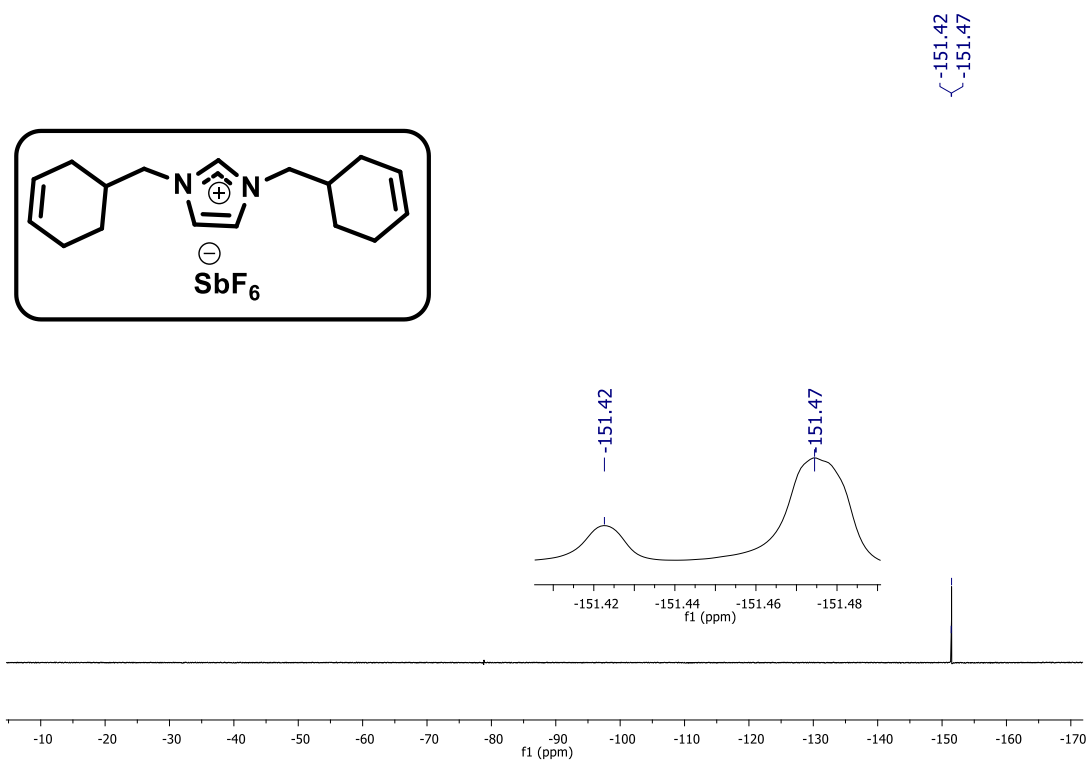
**<sup>1</sup>H NMR (400 MHz, CDCl<sub>3</sub>)**



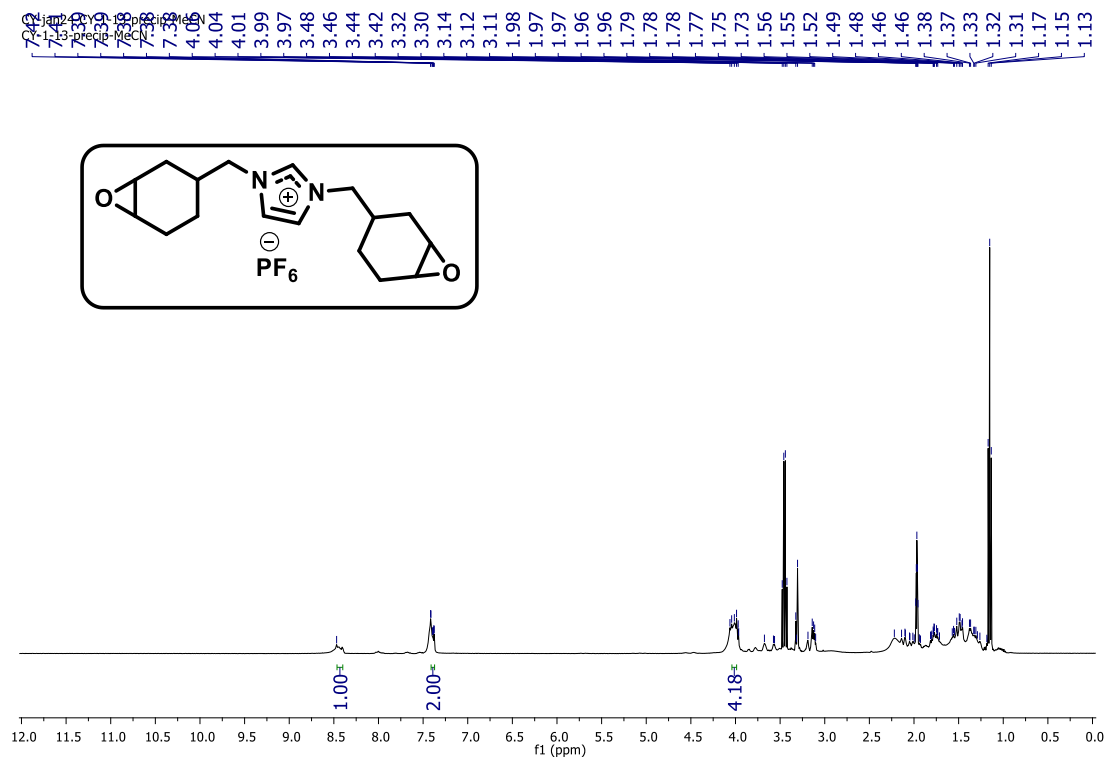
**<sup>13</sup>C NMR (100 MHz, CDCl<sub>3</sub>)**



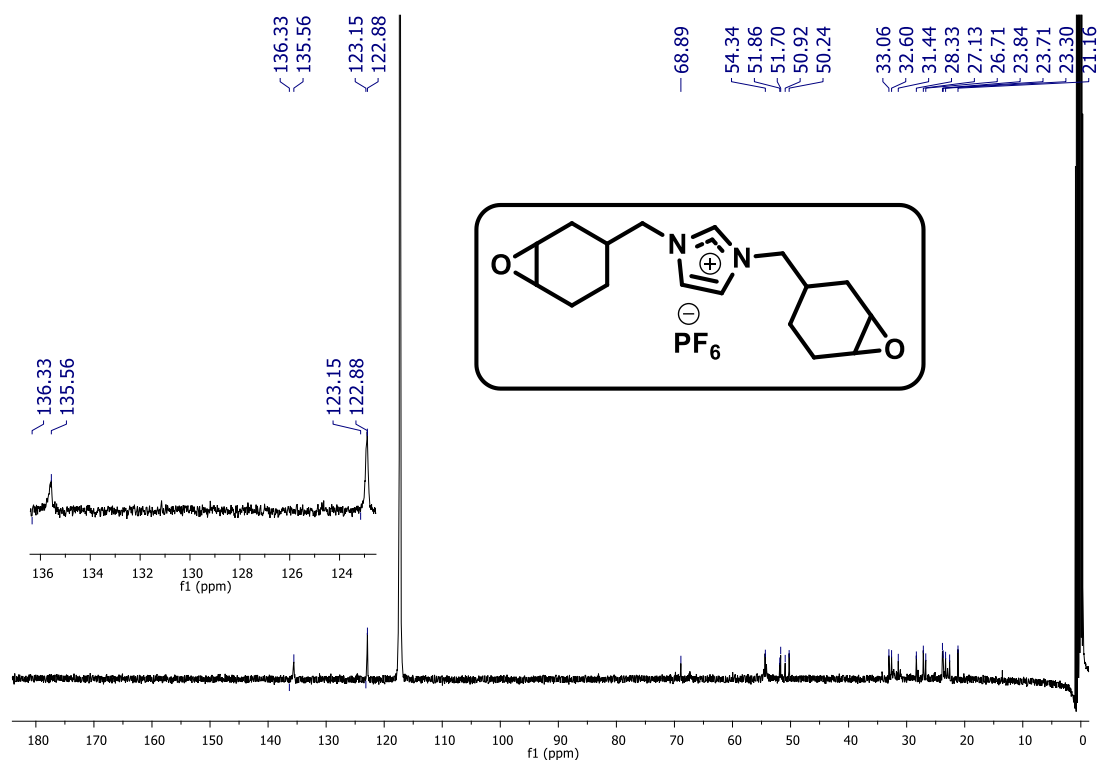
**$^{19}\text{F}$  NMR (376 MHz,  $\text{CDCl}_3$ )**



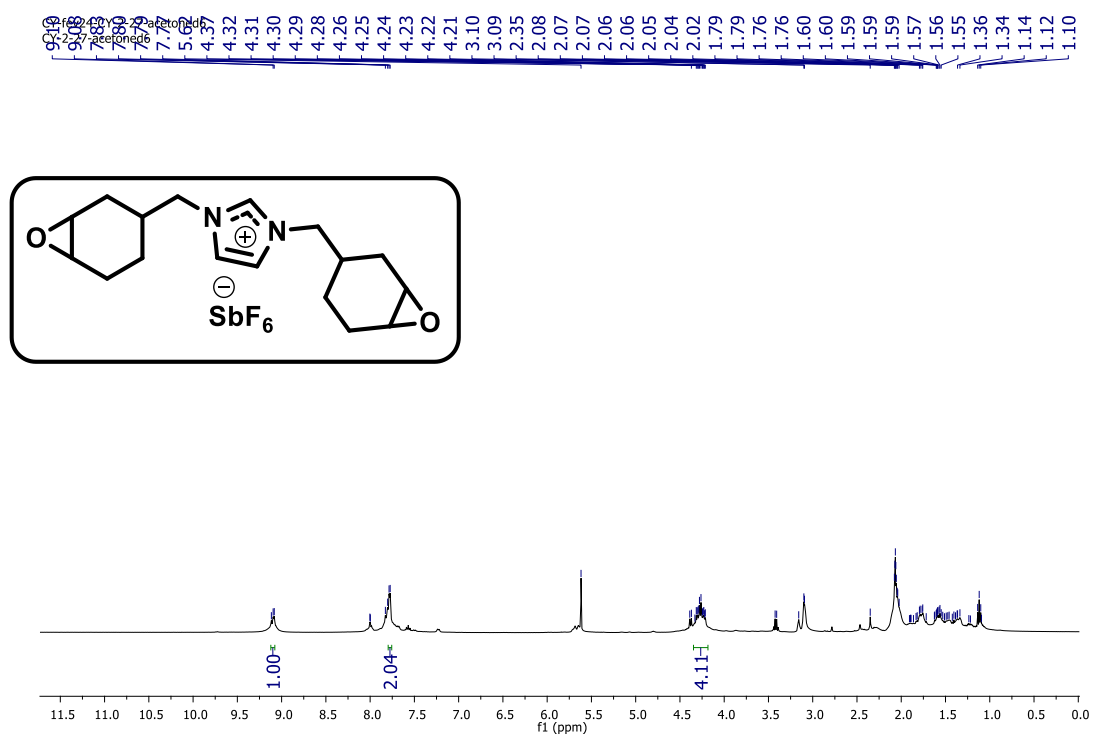
**$^1\text{H}$  NMR (400 MHz,  $\text{CD}_3\text{CN}$ )**



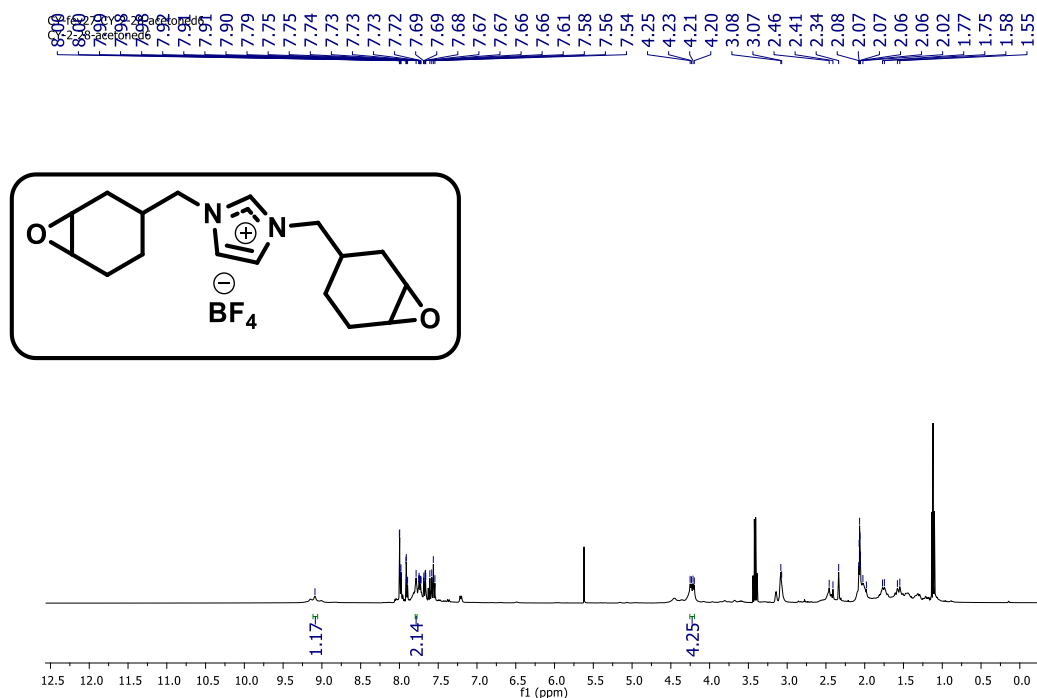
**$^{13}\text{C}$  NMR (100 MHz,  $\text{CDCl}_3$ )**



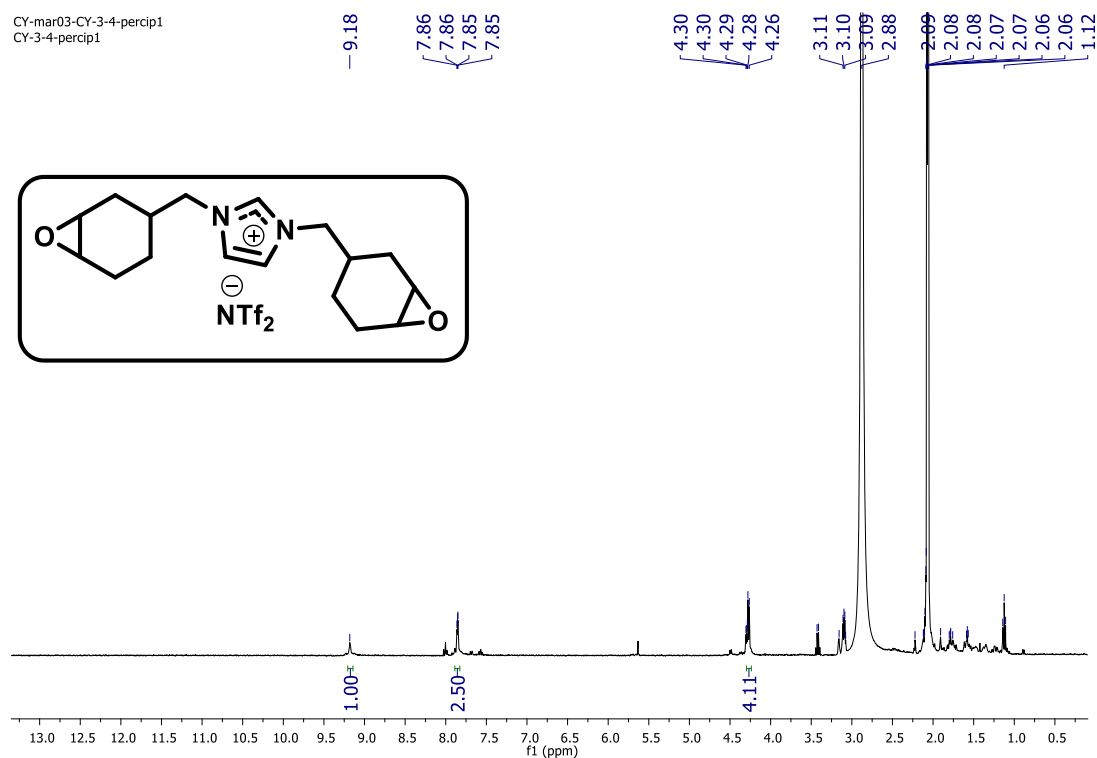
**$^1\text{H}$  NMR (400 MHz,  $\text{CD}_3\text{CN}$ )**



**<sup>1</sup>H NMR (400 MHz, CD<sub>3</sub>CN)**



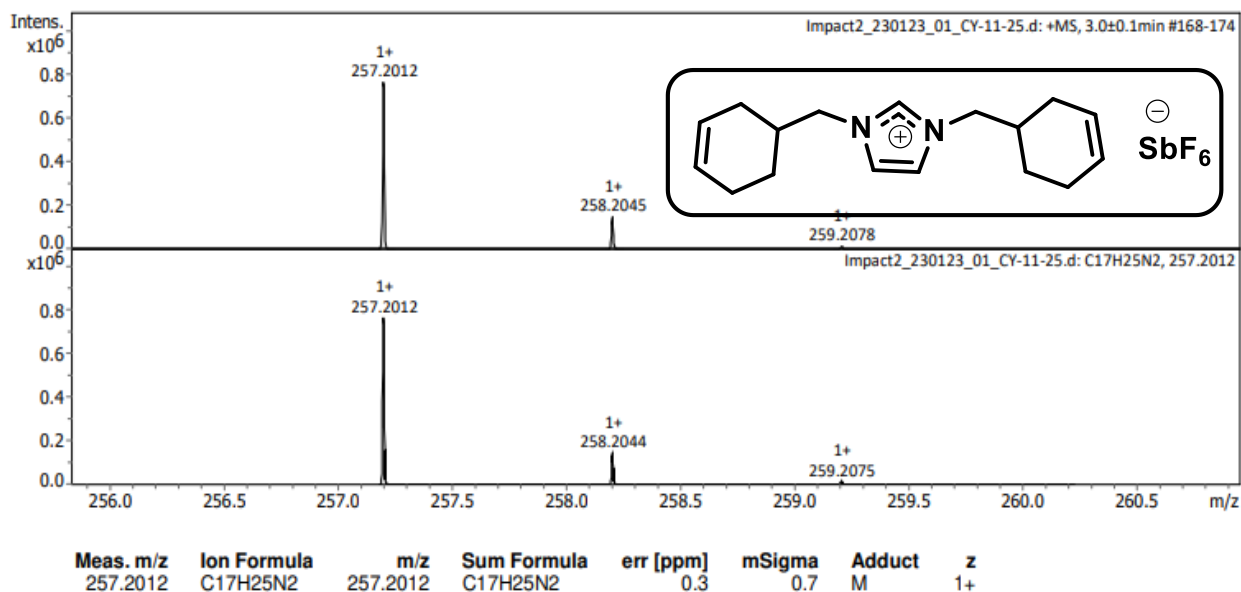
**<sup>1</sup>H NMR (400 MHz, CD<sub>3</sub>CN)**



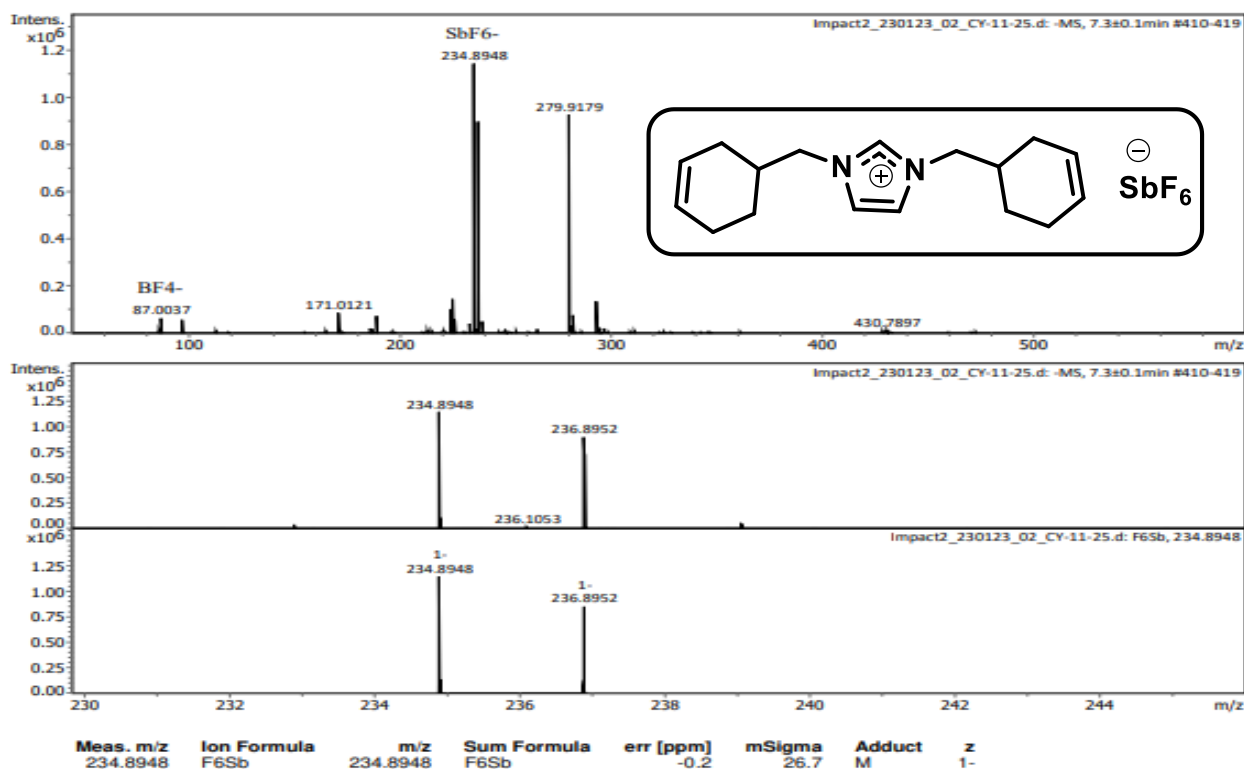


## HRMS analyses

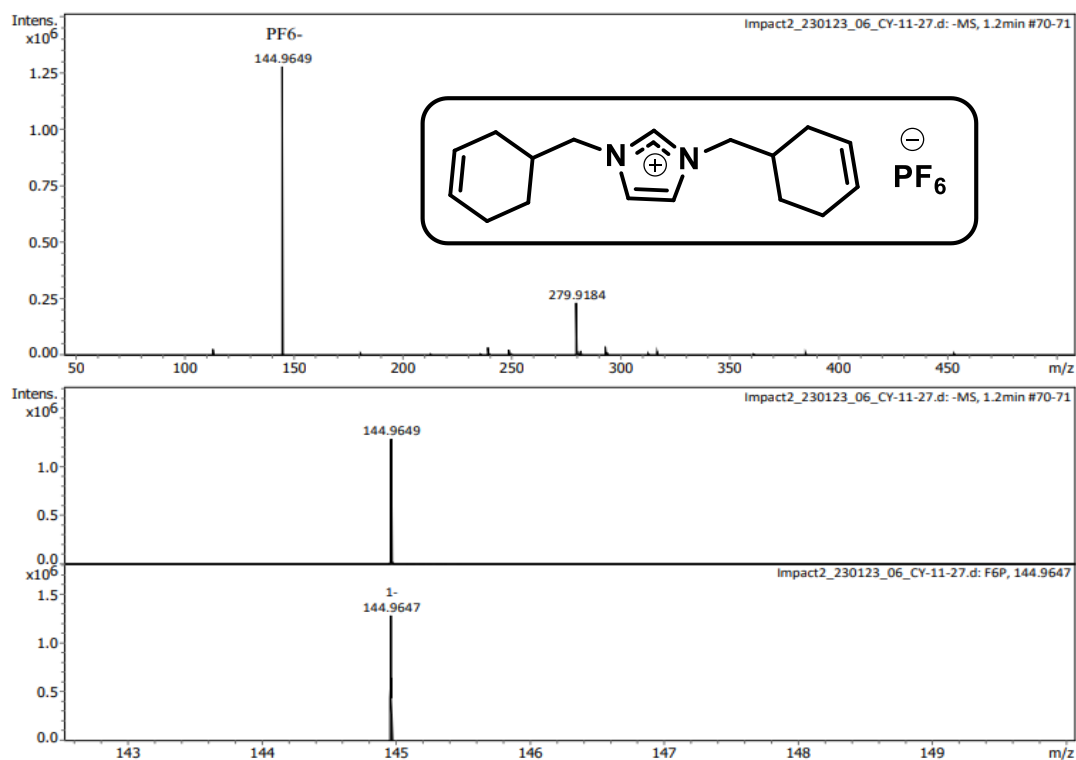
### HRMS positive mode



### HRMS negative mode



HRMS negative mode.



HRMS negative mode.

